

19981014 004

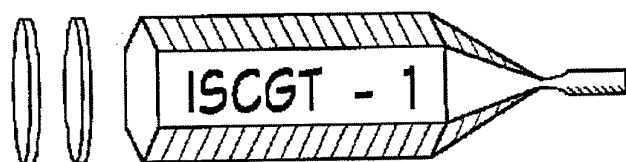
First
International School
on
Crystal Growth Technology

Beatenberg, Switzerland // September 5 - 16, 1998

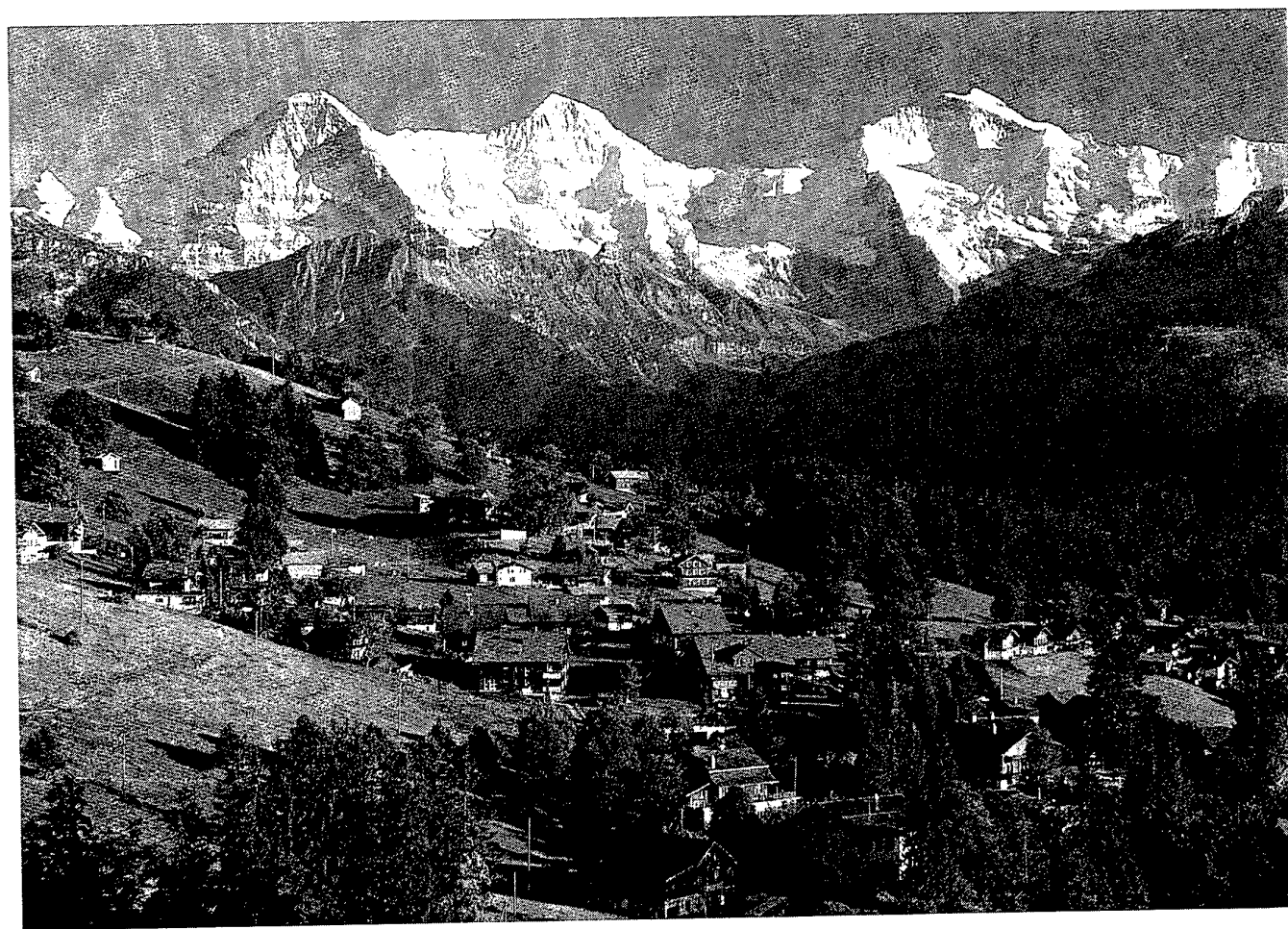
Book of Lecture Notes

Editor: Hans J. Scheel

REPORT DOCUMENTATION PAGE			Form Approved OMB No. 0704-0188	
Public reporting burden for this collection of information is estimated to average 1 hour per response, including the time for reviewing instructions, searching existing data sources, gathering and maintaining the data needed, and completing and reviewing the collection of information. Send comments regarding this burden estimate or any other aspect of this collection of information, including suggestions for reducing this burden, to Washington Headquarters Services, Directorate for Information Operations and Reports, 1215 Jefferson Davis Highway, Suite 1204, Arlington, VA 22202-4302, and to the Office of Management and Budget, Paperwork Reduction Project (0704-0188), Washington, DC 20503.				
1. AGENCY USE ONLY (Leave blank)		2. REPORT DATE September 1998		3. REPORT TYPE AND DATES COVERED Lecture Notes 5 - 16 September 1998
4. TITLE AND SUBTITLE ISCGT-1 First International School on Crystal Growth Technology			5. FUNDING NUMBERS N00014-98-1-1010	
6. AUTHOR(S) Hans J. Scheel, Editor				
7. PERFORMING ORGANIZATION NAME(S) AND ADDRESS(ES) Dr. Hans J. Scheel Swiss Federal Institute of Technology Lausanne Cristallogenese - IMO CH de Bellerive 34, CH 1007 Lausanne, Switzerland			8. PERFORMING ORGANIZATION REPORT NUMBER	
9. SPONSORING/MONITORING AGENCY NAME(S) AND ADDRESS(ES) Technical Director Office of Naval Research International Field Office Europe PSC 802 Box 39 FPO AE 09499-0700			10. SPONSORING/MONITORING AGENCY REPORT NUMBER	
11. SUPPLEMENTARY NOTES				
12a. DISTRIBUTION AVAILABILITY STATEMENT Approved for public release, distribution is unlimited			12b. DISTRIBUTION CODE	
13. ABSTRACT (Maximum 200 words) Compilation of abstracts from the "ISCGT-1" First International School on Crystal Growth Technology Meeting held 5 - 16 September 1998 in Beatenberg, Switzerland				
14. SUBJECT TERMS Key Words: Crystal Growth			15. NUMBER OF PAGES	
			16. PRICE CODE	
17. SECURITY CLASSIFICATION OF REPORT	18. SECURITY CLASSIFICATION OF THIS PAGE	19. SECURITY CLASSIFICATION OF ABSTRACT	20. LIMITATION OF ABSTRACT	



First International School
on
Crystal Growth Technology



Beatenberg, Switzerland // September 5 - 16, 1998

Book of Lecture Notes

DTIC QUALITY INSPECTED 1

Editor: Hans J. Scheel

Schedule ISCGT-1

08.20

12.00 14.00

18.35 20.15

21.40

Saturday	5	Arrival	Registration 10.00-12.30	Arrival	Registration 16.00-19.00	19.00 Reception - 20.30
Sunday	6	Rudolph I	Brandon Klapper	Half-Day Excursion IA & IB		
Monday	7	Abe: General	Scheel Lal	Kimura Terashima	Itsumi Tomzig Ammon	20.30 B. Hofmann: Special Lecture
Tuesday	8	Dupret	Kakimoto Polezhaev	5) Hauser Mori et al.	Lebeau Jensen	Film Session
Wednesday	9	Full-Day Excursion IIA & IIB				Poster Session I
Thursday	10	Falster	Abe Sauter	Yamagishi Ciszek	Kalejs	Folklore Evening
Friday	11	Wenzl	Müller Rudolph II	15.30: Excursion to Banquet Banquet¹⁾ 23.15		
Saturday	12	Full-Day Excursion²⁾ IIIA & IIIB				Discussion: Energy & CGT
Sunday ³⁾	13	Nishida	Weinert Ware	Grant Asahi	Triboulet Derby	Discussion: Future of CGT
Monday	14	Nishizawa	Scheel Nishinaga	Weimann Heuken	Gillesen	Poster Session II ⁴⁾
Tuesday	15	Fukuda	Miyazawa Cochet-Muchy	Osiko Schmid	Bagdasarov Zharikov	
Wednesday	16	Sasaki	Shestakov Balitzky	Korzhik Li	Gektin Lytvynov	Social Discussion Evening
Thursday	17	Departure				

CGT = Crystal Growth Technology incl. Epitaxy Technology

1. Banquet may be shifted to Sept. 14 for weather reasons, in this case the breaks of Sept. 14 will be shortened.
2. Excursion IIIA & IIIB may be shifted to Sept. 13 for weather reason, in this case 3.
3. Sept. 13 program may be shifted to Sept. 12.
4. Poster Session II may be shifted to Sept. 15 in case banquet is shifted to Sept. 14.
5. On Tuesday Sept. 8 from 14.00 to 16.00 there will be 2 introduction lectures by S. Takasu/SEMI Japan: 1. "How to start your crystal growth", 2. "Silicon crystal growth" in lecture room of Guesthouse Bible School/Main Building

Preface

This first international workshop of leading scientists and experts of crystal growth technology (including epitaxy technology) serves to exchange experiences and knowhow on the highest-possible pre-competitive level. The goal is the reduction of development costs by increased scientific understanding of the complex processes where ten or more parameters have to be optimized and compromised. The **multidisciplinary nature of crystal growth technology** demands collaboration of chemical and process engineers, thermodynamicists, hydrodynamicists, electrical and mechanical/machine engineers, material scientists, numerical simulation specialists, physicists, and crystallographers. Thereby, a common language and terminology has to be established which permits multidisciplinary discussions and collaborations.

Progress in crystal growth and epitaxy technology is highly demanded in view of its **essential role for the development** of several important areas such as mass production of high-efficiency photovoltaic cells and detectors for **alternative energy** and **medicine**, and the fabrication of bright long-lifetime light-emitting diodes for **saving energy** by wide use in illumination and traffic lights. Integrated **microelectronics** and **optoelectronics** necessitates improved growth technology for large diameter silicon, GaAs and InP in combination with optimized defect and property control on submicron scale. **High-temperature high-power electronics** demands mastering of growth and processing problems of difficult materials like SiC and GaN. The success of **laser fusion energy** depends on the timely development of high-power laser crystals and radiation-resistant frequency multiplying crystals of oxide compounds. Furthermore, the great and wide potential of **oxide superconductors** with high transition temperatures could not be explored so far because the proper crystal growth and materials technology development was neglected.

Despite its enormous importance and impact is crystal growth technology not widely recognized: it does not yet belong to a specific discipline like chemical engineering or materials science, and there is no curriculum or chair at a technical university for this complex field. Education and long-range planning are required to build up **centers of competence for crystal growth and epitaxy technology**, and existing laboratories in industry should not be finalized by short-term profit thinking. We have to preserve the existing experience in view of the long period of ten or more years to build up a competent crystal growth and crystal machining laboratory.

At ISCGT-1 not only the scientific approaches to complex crystal growth problems will be discussed by leading experts, but also the **future of crystal growth technology**, its role for other sciences and technologies including energy, and necessary steps to increase interest and efforts in the technology of crystal and layer production will be discussed.

With respect to the first initiative of this school the support of the **International Advisory Committee** is highly appreciated. The final program is based on recommendations of the **International Program Committee**, especially of the program co-chairman T. Fukuda, of T. Abe, P. Rudolph and E. Zharikov, to whom all belongs my sincere thanks.

It is very fortunate that the best and competent experts and lecturers of crystal growth and epitaxy technology and of crystal machining and related fields accepted the invitation so that an outstanding program could be established. After a few introductory lectures the silicon and GaAs (including InP, CdTe) technologies are discussed and followed by oxide and scintillator crystals. The heavy program with daily seven hours lectures and a poster, film or discussion evening is interrupted by

excursions on and into mountains and glaciers which at hopefully fine weather provide spectacular views and experiences, besides establishing personal contacts. The accompanying persons hopefully will enjoy the multifaceted **ladies program**.

This extensive program (and the support of several needy lecturers and participants) could not be covered by the modest registration fees: the support of the **main and other sponsors**, listed separately, was absolutely essential: a great "Thank You" to all contributors! A further factor to keep the low costs of ISCGT-1 was the tremendous efforts of the **organizing committee** which handled all matters itself: Dirk Ehrentraut (secretary), Christine Klemenzenz (finances), Ana Maria do Espirito Santo, Ivo Utke, and myself.

It is the first time that experts of crystal growth technology meet on an international scale to discuss production, yield and specification/characterization problems. It is desirable that you really exchange knowledge and experiences so that all participants will return home with ideas to improve the process, the yield and the quality of their products. Hopefully the beautiful village Beatenberg in the Bernese Oberland along with social events and excursions stimulates personal contacts and discussions.

Finally it is hoped that this **Book of Lecture Notes** is useful for all participants. An attempt was made to collect and print the abstracts and copies of the most important transparencies of the lectures (at minimum effort of the extremely busy lecturers) for the maximum benefit for the participants, with sufficient space for making additional notes: Your comments on this approach would be welcome and could be useful for organizers of forthcoming conferences, workshops and schools. For completeness, also the abstracts of the posters are included in the book.

In the name of the advisory, program and organizing committees and of the program co-chairman Prof. T. Fukuda I want to thank all lecturers, participants, and sponsors, but also the many other helpers and the kind people at Beatenberg, including the Tourist Office, for the invaluable contributions to ISCGT-1: hopefully this event will be remembered as most pleasant, interesting and important for the growing field of crystal growth technology.

Lausanne, August 1998

Hans J. Scheel

International Advisory Committee

T. Abe / SEH, Japan
T. Fukuda / Japan
H. Fusstetter / Germany
H. Klapper / Germany
F.A. Kuznetsov / Russia
T. Nishinaga / Japan
J. Nishizawa / Japan
Yu. Ossipyan / Russia
A.M. Prokhorov / Russia
W. Schröder / Germany

International Program Committee

W. von Ammon / Germany
P. Bordui / USA
V. Fratello / USA
T. Fukuda / Japan, co-chairman
P. Lecoq / CERN
L. Lytvynov / Ukraine
S. Miyazawa / Japan
P. Rudolph / Germany
H.J. Scheel / Switzerland, co-chairman
E.V. Zharikov / Russia

PS: On behalf of the sponsor IUCryst it is confirmed herewith that there was no kind of discrimination (sex, race, color, religion etc.): the program and the support for few lecturers and participants were based on excellence and qualification in crystal growth technology, and on actual need.

ISCGT-1 Daily Schedule

Please check Notice Board for exceptions, program changes and excursions

8.02* Bus departs from Hotels Dorint / Beatus / (Gloria)

8.10 Bus arrives at Tourist Office / Congress Center

8.20 - 9.20 Lecture 1

9.20 - 9.45 Coffee break

9.50 - 10.50 Lecture 2

10.50 - 10.55 Short break / stretching

10.55 - 11.55 Lecture 3

12.00 - 13.55 Lunch at Guesthouse Bible School & relax

14.00 - 15.00 Lecture 4

15.00 - 16.00 Lecture 5

16.00 - 16.25 Coffee break

16.30 - 17.30 Lecture 6

17.30 - 17.35 Short break / stretching

17.35 - 18.35 Lecture 7

18.45* Bus to Hotels Dorint / Beatus / (Gloria)

Dinner

20.02 Bus departs from Hotels Dorint / Beatus / (Gloria)
to Tourist Office / Congress Center

20.15 - ~ 21.40 Discussion / Poster / Film Evening

about 21.50** Bus to Hotels Dorint / Beatus / (Gloria)

* official post bus

** 10 minutes after official end of discussion / poster / film evening

Official Excursions and Events ISCGT-1

for all *fully registered* participants and accompanying persons

September 6: After lunch we go by cable-way to the top of Niederhorn (height 1950 m), walk to Burgfeldstand (2063 m), Oberberg - Oberburgfeld - Unterburgfeld - Känzeli - Beatenberg (1200 m): 3 hours.

IA
IB Parallel an easy tour on broad trails where trekking boots or hiking boots are not required: By cable-way to Niederhorn - Flösch - Vorsass (1578 m, possible return by cable-way) - Beatenberg: 2 hours

20.30: **Special Lecture** on Swiss geology and mineralogy (Dr. Beda Hofmann, Museum of Natural History Bern)

September 9: **Full-day excursion** by bus and with hiking: Beatenberg - Innertkirchen (visit of 850 kg stone plate with quartz crystals) - Guttannen (visit crystal museum Rufibach) - Crystal cave Gerstenegg (with "Strahler" Ernst Rufibach) - Water pump power station Grimsel II - Hotel Grimsel Hospiz (lunch) - Ulrichen VS - Lake of Gries (2390 m) - hiking about 2.5 hours over Gries glacier (2620 m) - by bus to Rhone glacier (visit/coffee break) - Furkapass (2431 m) - Wassen - Sustenpass (2250 m) - Stein glacier - Beatenberg (with glaciologist Prof. A. Ohmura/ETH Zurich).

IIA
IIB The parallel easy tour without hiking over glacier: instead visit of the gorge/canyon of Aare.

20.30: **Folklore Evening** at Congress Hall

September 11: Beatenberg 15.30 departure for excursion across Lake of Brienz to Grand Hotel Giessbach for **banquet**, return to hotel about 23.15.

September 12: **Full-day excursion** starting after small or no breakfast by early bus (07.30 a.m.) to Grindelwald, by cable-way to First (2168 m) for brunch, hiking about 2.5 - 3 hours to Bachalpsee (lake 2265 m) and to top of **Faulhorn** (2681 m) for sweet snack and drink, descending about 2 hours to Bussalp (1800 m) for coffee-break, return by bus and train.

IIIA
IIIB The easy parallel tour starts after breakfast and involves a 2 hour walk from Grindelwald-First to Grosse Scheidegg (1962 m) for lunch, with possible extension to the valley of the murmets (2258 m), return by bus to Grindelwald, train to Kleine Scheidegg/coffee break - Wengen - Interlaken.

The costs for these official excursions are included in the registration fees. However, it is recommended to check your health insurance for validity during travel, or to arrange a travel health insurance. Neither the organizers nor the guides can take any responsibility. In case of health / heart problems please contact Hans J. Scheel before the excursion.

A small rucksack suitable for excursion will be provided as conference bag. For the excursions comfortable walking dress with long trousers and a light pullover and raincoat are recommended, also either trekking/hiking boots (for tours IA, IIA, IIIA) or comfortable walking/sports shoes (excursions IB, IIB, IIIB) depending on your choice of excursion type, and sun protection (creme protection factor 10 - 18, hat).

Contents

	<i>Preface</i>	3
	<i>Special Lecture</i>	
S1	<u>B.A. Hofmann</u> : Natural crystals in Switzerland	15
	<i>Lectures</i>	
1	<u>P. Rudolph</u> : Thermodynamic fundamentals of phase transitions applied to crystal growth processes	19
2	<u>Y. Liu, A. Virozub, S. Brandon</u> : Interface kinetics/facetting effects in the growth of large crystals: modeling and real observations	36
3	<u>H. Klapper</u> : Methods of structural characterization for technological important crystals	46
	<i>General Lecture</i>	
4	<u>T. Abe</u> : History and future of silicon crystal growth	66
5	<u>H.J. Scheel</u> : Striations: an intrinsic problem ?	86
6	<u>K. Lal</u> : Role of structural characterization in development of large-diameter silicon	108
7	<u>S. Kimura</u> : Basic properties of silicon melt	120
8	<u>K. Terashima</u> : Influence of boron addition into silicon melts on oxygen atom behavior in CZ pulling system	132
9	<u>M. Itsumi</u> : Structural and chemical characteristics of octahedral void defects found in Czochralski silicon	144
10	<u>E. Tomzig, W. von Ammon</u> : Key issues in the growth of very large diameter silicon single crystals	158
11	<u>F. Dupret, N. Van den Bogaert, R. Assaker, V. Regnier, B. Hoevenaars, S. Kruk</u> : Modeling and simulation of bulk crystal growth considering melt dynamics	161
12	<u>K. Kakimoto</u> : Heat and mass transfer in silicon melt under magnetic fields	172
13	<u>V.I. Polezhaev</u> : Simulation aspects of technologically important hydrodynamics, heat/mass transfer processes during crystal growth	188
14	<u>C. Hauser, P.M. Nasch</u> : Advanced slicing techniques for single crystals	204
15	<u>Y. Mori, K. Yamauchi, K. Yamamura, Y. Sano, H. Kakiuchi</u> : Development of new ultra precision machining methods - plasma CVM and EEM	218

16	<u>M. Lebeau</u> : Residual stress evaluation in bi-refrigent scintillating crystals	230
17	<u>L. Jensen</u> : Float zone silicon	240
18	<u>R. Falster</u> : Intrinsic point defects and reactions in silicon: Advances in defect engineering	258
19	<u>T. Abe</u> : The origin of point defects in FZ and CZ silicon crystals	276
20	<u>B. Sauter</u> : The conversion to 300 mm wafers: Challenges for wafer manufacturing	294
21	<u>H. Yamagishi, M. Kuramoto, Y. Shiraishi, N. Machida, K. Takano, N. Takase, T. Iida, J. Matsubara, K. Takada</u> : Large diameter silicon technology	304
22	<u>T.F. Ciszek</u> : Silicon crystal growth for photovoltaics	314
23	<u>J.P. Kalejs</u> : Shaped silicon crystal growth for solar cells	326
24	<u>H. Wenzl, A. Fattah, E. Kuessel, W.A. Oates, K. Sonnenberg</u> : Evaluation of bulk GaAs melt growth processes: Link between crystal growth research and crystal production	340
25	<u>G. Müller</u> : Growth of low epd - GaAs by the vertical gradient freeze method	354
26	<u>P. Rudolph</u> : Czochralski growth of high-quality GaAs crystals	368
27	<u>Y. Nishida</u> : Growth methods on large diameter GaAs single crystals	380
28	<u>T. Flade, M. Jurisch, A. Kleinwechter, A. Köhler, U. Kretzer, J. Prause, Th. Reinhold, B. Weinert</u> : 6" SI GaAs LEC-crystals	392
29	<u>R. Ware</u> : High pressure liquid encapsulated growth of semi-insulating GaAs	402
30	<u>I.R. Grant</u> : InP crystal and wafer manufacturing	414
31	<u>T. Asahi, K. Kainosho, K. Kohiro, O. Oda</u> : Growth technology of InP and CdTe single crystals	426
32	<u>R. Triboulet</u> : CdTe growth	436
33	<u>J.J. Derby, A. Yeckel</u> : The use of high performance computing for modeling crystal growth from melt and solution	446
34	<u>J. Nishizawa</u> : Comparison of MOCVD, MBE and LPE for performance of optoelectronics devices	460
35	<u>H.J. Scheel</u> : Control of growth modes in epitaxy from the vapor phase and from the liquid phase	480
36	<u>T. Nishinaga</u> : Microchannel epitaxy - A combination of selective area epitaxy and epitaxial lateral overgrowth for high quality heteroepitaxy	496

37	<u>G. Weimann</u> : MBE for the production of III-V devices	508
38	<u>M. Heuken</u> : MOCVD for production of III-V devices	520
39	<u>K. Gillessen</u> : LPE in production	534
40	<u>T. Fukuda</u> : Melt growth of oxide crystals for SAW, piezoelectric, and nonlinear optical applications	546
41	<u>S. Miyazawa</u> : Phase diagram studies necessary for CZ-growth of practical electro-optic single crystals	560
42	<u>D. Cochet-Muchy</u> : Growth technology of LiNbO ₃ and LiTaO ₃	570
43	<u>V.V. Osiko</u> , <u>J.F. Wenckus</u> : Growth of stabilized zirconia crystals by skull melting	580
44	<u>F. Schmid</u> , <u>Ch.P. Khattak</u> : Sapphire crystal growth technology using heat exchanger method (HEM) TM	592
45	<u>Kh.S. Bagdasarov</u> , <u>E.V. Zharikov</u> : Growth of sapphire by horizontal directional crystallization	608
46	<u>M.I. Moussatov</u> , <u>E.V. Zharikov</u> : GOI growth of large perfect sapphire crystals	624
47	<u>T. Sasaki</u> : Growth of nonlinear optical crystals for laser frequency conversion	632
48	<u>A.V. Shestakov</u> , <u>E.V. Zharikov</u> : Growth of oxide crystals for solid-state lasers	646
49	<u>V.S. Balitsky</u> : Crystal growth technology of high-quality quartz	658
50	<u>M. Korzhik</u> : Scintillators on the base of oxide crystals	672
51	<u>P.J. Li</u> , <u>Z.W. Yin</u> , <u>D.S. Yan</u> : Some aspects of growth technology for scintillation crystals	686
52	<u>A. Gektin</u> : Halogenide scintillators. Crystal growth and performance	696
53	<u>L. Lytvynov</u> : Growth of shaped high temperature oxides	712
 <i>Introductory lectures September 8 at 14.00 lecture room Bible School:</i>		
54	<u>S. Takasu</u> : How to start your crystal growth	722
55	<u>S. Takasu</u> : Silicon crystal growth	732

Posters

- 1 K. Kakimoto: Heat and mass transfer in silicon melt under magnetic fields 747
- 2 N. Van den Bogaert, F. Dupret, R. Assaker, V. Regnier, B. Hoevenaars, S. Kruk: Simulation of bulk crystal growth and evolution of point defects and dislocations in the crystal 747
- 3 K. Lal: Role of structural characterization in development of large-diameter silicon 747
- 4 J.J. Derby: The use of high performance computing for modeling crystal growth from melt and solution 749
- 5 A.H. Abgarian: Simulation of temperature and thermoelastic fields in the Al_2O_3 crystal for the set-up wave method CGT 751
- 6 Y. Mori, K. Yamauchi, K. Yamamura, Y. Sano, H. Kakiuchi: Development of new ultra precision machining methods - plasma CVM and EEM 753
- 7 H.J. Scheel: Striations: an intrinsic problem ? 753
- 8 H.J. Scheel: Control of growth modes in epitaxy from the vapor phase and from the liquid phase 753
- 9 M. Lebeau: Mechanical processing of anisotropic scintillating crystals 755
- 10 T. Ogawa: Light scattering tomography for characterization of crystals 757
- 11 N.I. Leonyuk: An example of teaching crystal growth technology for the U.D. and M.Sc. students-crystallographers 761
- 12 N.I. Leonyuk: Crystal growth of borate materials with device potential: Realities and perspectives 763
- 13 Y. Mori, T. Sasaki: Development of CLBO and GdYCOB crystals for UV generation 765
- 14 M. Ishii, K. Imai, N. Tsutsui, I. Yamaga: Crystal growth of LBO ($\text{Li}_2\text{B}_4\text{O}_7$) by modified Bridgman method 767
- 15 A. Yoshikawa, K. Hasegawa, T. Fukuda: Growth of YAG/Sapphire eutectic and YAG single crystal fibers by the micro-pulling-down (μ -PD) method 769
- 16 P.A. Studenikin, Yu.D. Zavartsev, A.I. Zagumennyi: CZ technology and some properties of scandium-gallium garnets and gadolinium orthovanadate crystals as laser media 771
- 17 V. Iov: Growth peculiarities of YAG crystals as revealed by using a scanning electron microscope 773
- 18 M.I. Moussatov: Formation of block structure in sapphire crystals 775

19	<i>S.V. Budakovsky, N.Z. Galunov, V.P. Seminozhenko</i> : Some new approaches to obtain the organic crystals with high quality	777
20	<i>R. Gopalakrishnan, P. Ramasamy</i> : Growth of scintillation and photorefractive single crystals of BGO and BSO and their characterization	779
21	<i>D. Kishimoto, T. Noda, Y. Nakamura, H. Sakaki, T. Nishinaga</i> : Elimination of growth on (111)B side faces by rotating substrate in fabrication of GaAs mesa-structure by MBE	781
22	<i>K. Iizuka, T. Suzuki, H. Okamoto</i> : New surface cleaning method of GaAs or AlGaAs without arsenic flux for molecular beam epitaxy	783
23	<i>O. Parillaud, V. Wagner, H.J. Bühlmann, M. Illegems</i> : Localized epitaxy of GaN by HVPE on patterned substrates	785
24	<i>P. SanthanaRaghavan, P. Ramasamy</i> : Crystal growth of GaAs & InP and their defect investigation	787
25	<i>G.M. Guadalupi, F. Danieli, G. Tolomio, B. Molinas, M. Favaretto, L. Meregalli</i> : III-V semiconductors: A status report on the R&D activities at Centro Ricerche Venezia	789
26	<i>H.-J. Rost, D. Siche, J. Dolle, D. Schulz, J. Wollweber, T. Müller, G. Wagner</i> : Influence of different growth parameters and related conditions on the 6H-SiC crystal growth by modified Lely method	791
27	<i>T. Reichardt, B. Speit</i> : Optical materials for microlithography applications	793
	<i>Addresses of lecturers</i>	794
	<i>List of participants</i>	803

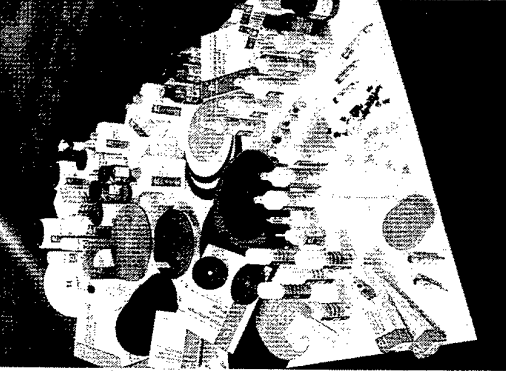
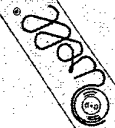
We gratefully acknowledge the support of

Main Sponsors

- **International Union of Crystallography / Commission on Crystal Growth and Characterization / Prof. H. Klapper**
- **Japanese Society for Promotion of Science Committee No. 161 / Prof. T. Fukuda**
- **Shin-Etsu Handotai, Annaka/Gunma, Japan**
- **Swiss Federal Institute of Technology and Group Cristallogenese-IMO, Lausanne, Switzerland**
- **Swiss National Science Foundation**
- **US Air Force, US Army and US Navy through European Offices in London**

Sponsors

- **Aixtron AG**, Aachen, Germany
- **Beatenberg BE**, Gemeinde & Tourist Office, Switzerland
- **N. Bucher AG**, Spreitenbach ZH, Switzerland
- **Comadur**, Le Locle, Switzerland
- **Crystal Technology**, Palo Alto CA, USA
- **Djevahirdjian**, Monthey VS, Switzerland
- **DGKK, German Crystal Growth Society** (Prof. G. Müller)
- **HCT Shaping Systems S.A.**, Cheseaux sur Lausanne, Switzerland
- **Institute of Micro-and Optoelectronics, EPF Lausanne**, Switzerland
- **Wacker Siltronic AG**, Burghausen, Germany
- **WELL-Walter Ebner**, Le Locle, Switzerland
- **ZIRMAT Corp.**, Westford Mass., USA



Well Walter Ebner
Crêt-Vaillant 17, 2400 Le Locle

Alles für die Metallographie
Tout pour la metallographie

Ihr Partner für die Materialprüfung
Votre partenaire pour le contrôle de matériaux

Well Walter Ebner

Crêt-Vaillant 17
2400 Le Locle

Tél. 032 931 17 91
Fax 032 931 23 36

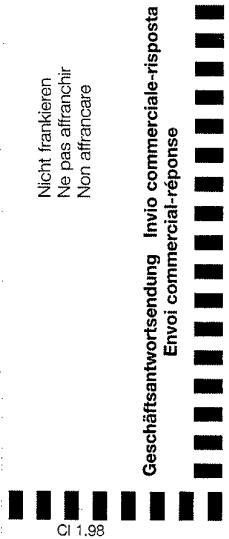
Bitte faxen oder schicken Sie diese Karte an uns.

14

Bitte senden Sie uns Unterlagen über:

- | | |
|--|--|
| <input type="checkbox"/> Diamant-Drahtsägen | <input type="checkbox"/> Scies à fil diamanté |
| <input type="checkbox"/> Trennmaschinen | <input type="checkbox"/> Tronçonneuses |
| <input type="checkbox"/> Polier- und Schleifmaschinen | <input type="checkbox"/> Polisseuses |
| <input type="checkbox"/> Einbettpressen | <input type="checkbox"/> Presses à enrober |
| <input type="checkbox"/> Demotec Kalteinbettmittel | <input type="checkbox"/> Enrobage à froid Demotec |
| <input type="checkbox"/> Hilfsmittel für die Metallographie | <input type="checkbox"/> Produits pour la métallographie |
| <input type="checkbox"/> Bitte setzen Sie sich mit uns in Verbindung | <input type="checkbox"/> S.v.p. prenez contact avec nous |

Nicht frankieren
 Ne pas affranchir
 Non affrancare



Geschäftsantwortsendung **Invio commerciale-risposta**
Envoi commercial-réponse

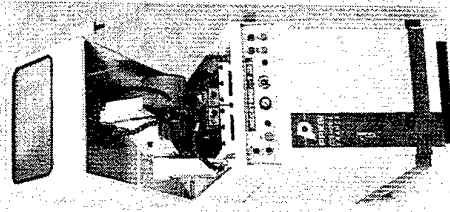
Name/Nom _____

Firma/Maison _____

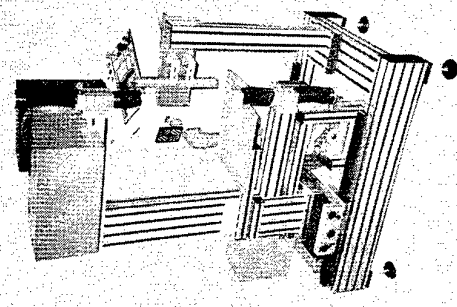
Adresse _____

PLZ/NPA _____ Ort/Lieu _____

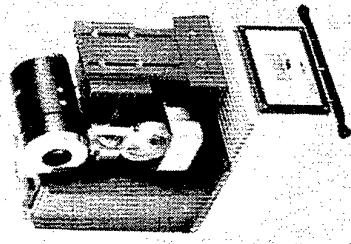
Tel./Tél. _____



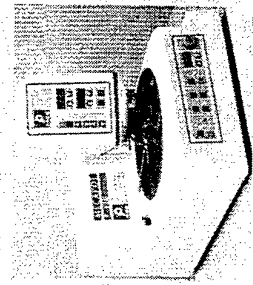
Automatische Trennmaschine
Tronçonneuse automatique



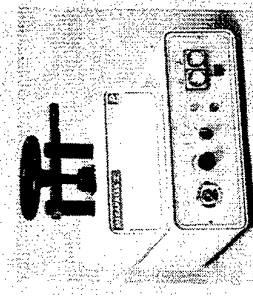
Säge zum Formenschneiden
Scie pour découpe de formes



Diamant-Drahtsägen
Scies à fil diamanté



Polier- und Schleifmaschinen
Polisseuses



Einbettpressen
Presses à enrober

Unsere Drahtsägen erlauben das Schneiden von Produkten in allen Härtegraden,
 z. B. Keramik, Kautschuk, Komposit usw.
Nos scies à fil permettent de scier les produits du plus dur au plus tendre,
 p. ex. céramique, caoutchouc, composite etc.

Natural crystals in Switzerland

Beda A. Hofmann
Natural History Museum
Bernastrasse 15
CH-3005 Bern, Switzerland
beda.hofmann@nmbe.unibe.ch

Natural crystals (or minerals) form virtually all solid parts (rocks) of the earth. Rocks in Switzerland and elsewhere typically consist of crystals 10^{-7} to 10^{-2} m in size. Just about 50 of nearly 4000 known minerals constitute the bulk of the earth's crust. Besides these very common small crystals, there are rare occurrences of much larger and very attractive minerals. Some hydrothermal fissure minerals in the Swiss Alps contain quartz crystals up to 1 m in size with a mass of up to 800 kg.

Geologically, the most interesting part of Switzerland are the Alps, a Tertiary fold belt resulting from the collision of the European and the African continents. The geological processes that resulted in the present-day Alps caused the formation of several types of minerals. In terms of mass, the most abundant alpine minerals are rock-forming metamorphic minerals such as sheet silicates, amphiboles, garnets that were formed as a result of deep burial of rocks and increased pressure and temperature. Two types of outstanding minerals directly related to the formation of the Alps will be dealt with here: Alpine fissure minerals, and rare sulfides formed due to metamorphosis of a sulfidic orebody.

Switzerland has long been known as an area where crystals of quartz ("rock crystal", German "Bergkristall") can be found. Exploration and mining for quartz crystals dates back to pre-Roman times, when quartz was used as local replacement of chert in the fabrication of stone tools. A strong increase in the search for quartz crystals occurred during the 16th to the 18th century, when clear quartz was very sought after for the production of art objects ranging from religious motives to beakers and chandeliers. The art of quartz carving was especially advanced in northern Italy and in Germany. With the advent of relatively cheap glass, the interest in natural quartz crystals for industrial purposes decreased but was replaced by an increase in the scientific interest of natural crystals in the late 18th and

early 19th century. Now the search for crystals continued, based on an increasing demand from collectors. Slowly, an appreciation for other minerals than just quartz developed among collectors. Today, a few full-time and many hobby collectors actively search for minerals in the Alps.

The quartz crystals of the Swiss Alps do occur in so-called alpinotype fissures (German "Zerrklüfte"). These fissures generally are oriented perpendicular to the schistosity and occur in a variety of rocks. Their size ranges from 1 to 20 m lateral extent and a few cm to 2 m in height. The origin of these fissures is due to the enormous stress exerted on the rocks during the African-European continent-continent collision. Fissure formation occurred at depths of 10 to 15 km. With average uplift rates of approximately 1 mm per year, this corresponds to an age of 10 to 15 million years (also determined independently), and a cooling rate of approx. 30°/million years. The fissures were filled by water-dominated fluids (with highly variable contents of CO₂ and NaCl) that were close to chemical equilibrium with the surrounding rocks. During slow uplift and cooling, minerals precipitated from the fluids. Besides slow temperature changes, tectonic movements resulting in fast pressure drops may have been very important factors in mineral precipitation. Temperatures of mineral formation ranged from about 450° to 250 °C. There is evidence that some large quartz crystals (e.g. 1 m length) formed over a period of approximately 5 million years, corresponding to an integrated growth rate of about $2 \cdot 10^{-7}$ m/year. Periods of growth may have been related to short tectonic events, separated by long periods with no growth. Together with dominating quartz many other minerals are found. Common fissure minerals comprise (with typical crystal size): adularia KAlSi₃O₈ (5 cm), albite NaAlSi₃O₈ (2 cm), clinochlore (Mg,Fe)₅Al(Si₃Al)O₁₀(OH)₈ (0.2 mm), calcite CaCO₃ (5 cm), ankerite (Mg,Fe)Ca(CO₃)₂ (1 cm), fluorite CaF₂ (2 cm), the TiO₂-modifications rutile (1 cm), anatase (3 mm) and brookite (3 mm), titanite CaTiSiO₅ (5 mm) and pyrite FeS₂ (5 mm). A large number of very rare minerals is also present, typically they contain less common elements such as REE, Be, As, W, Sb. The relative mass of hydrothermal minerals in a given fissure closely corresponds to the abundance of the constituting elements in the host rocks. Alpine fissure minerals can be regarded as a product of hydrothermal recrystallization of host rock minerals in the immediate surroundings of the fissures over long periods of time. Alpinotype fissure minerals are not only known from the Alps, but also from other major mountain belts such as the Urals and the

Himalaya. Alpine fissure minerals are quite widespread in the Swiss and adjoining Austrian, French and Italian Alps, but the abundance is locally highly variable.

Alpine fissure minerals are not just a mineralogical curiosity. They do contain a wealth of information about the geological history of the Alps, especially about the fluid circulation over a very long period of time. Information is hidden in trace element contents, stable isotopes, and, most prominently, in small inclusions of the fluid from which the minerals crystallized.

Another well-known Swiss mineral locality which shows some resemblance to alpine fissures, but is mineralogically very distinct, is the Lengenbach mineral quarry in the Binn Valley. Here, a Triassic-aged (230 million years old) sedimentary sulfide deposit of probable exhalative origin in a dolomite host rock was affected by alpine metamorphism with peak temperatures of approximately 450°C. High concentrations of As(III), Tl, Pb, Ag and S(-II and +VI)) aided the formation of a sulfide melt coexisting with an aqueous fluid under metamorphic conditions. Slow cooling of this mixture of minerals, sulfide melt and aqueous fluid at roughly 20°/million years resulted in the precipitation of a complex suite of rare sulfide minerals of Pb, As, Sb, Cu, Tl, Ag, Sn. Close to 100 minerals have been identified in this small locality, about 25 of which have been discovered here for the first time. The unique mineral association at Lengenbach indicates that a rare combination of conditions existed there, basically an unusual chemical composition subjected to extremely slow cooling during alpine uplift. The Lengenbach quarry has been exploited in several phases in the early 19th century, around 1900, from 1958-1997. Beginning 1998, a new consortium is working there with the aim to maintain access to the unique locality for future investigations.

The Swiss Alps are a special environment of natural crystal growth leading to unusually large and extremely rare minerals, mainly due to the very slow cooling ranging from temperatures of 400 to 550°C to ambient over 10 to 20 million years, combined with fast pressure changes associated with tectonic activity.

Thermodynamic fundamentals of phase transitions applied to crystal growth processes

Peter Rudolph

Institute of Crystal Growth, Rudower Chaussee 6, 12489 Berlin, Germany

1. Introduction

The thermodynamics is of enormous practical use for the crystal growth. For instance, it helps to understand (i) existence regions and stability behaviour of crystalline materials under growth and application conditions, (ii) optimal growth conditions (temperature, pressure, solubility) and finding of the most effective phase transition i.e. growth method, (iii) driving (and inhibitory) forces of crystallization, and (iv) measures of in-situ control of the crystal composition during the growth. Hence, thermodynamics belongs to the basic knowledge of each crystal grower.

The *classic thermodynamics* is concerned with macroscopic equilibrium states of quasi-closed systems and helps to understand the near-equilibrium conditions between starting (fluid) phase, crystalline phase and separating interface, their mutual influence and variations as function of small deviation from equilibrium. In order to describe nonequilibrium processes of quasi-open crystallization systems, characterized by continuous in- and output of energy and intrinsic flows of heat and matter, one uses the *linear nonequilibrium thermodynamics*.

2. Perfect and real structure of crystals to be grown

The basic trend of thermodynamic processes in a given system is the *minimization of free energy*. Hence, the single crystalline state is a normal one because the free thermodynamic potential of Gibbs G is minimal if the "crystal growth units" (atoms, molecules) are arranged perfectly in a three dimensional ordered crystal structure, i.e. the atomic bonds are saturated regularly. This *process of ordering* is characterized by the minimization of enthalpy ($H \rightarrow \min$). On the other side an ideally ordered crystalline state would imply an impossible minimal entropy S and, thus, the opposite directed process of increasing entropy causes the force of *disordering* ($S \rightarrow \max$) gaining in energetical relevance with increasing temperature T . That's the point of basic equation of the thermodynamic potential of Gibbs $G = H - TS$ with $H = U + PV$ (U - internal energy, P - pressure, V - volume). Thus, in reality, no ideal but only optimal crystals with characteristic *equilibrium point defect concentration* can be grown. In comparison to that dislocations, grain boundaries and precipitates are not in thermodynamic equilibrium state and are de facto avoidable.

3. Thermodynamics of phase equilibrium

The crystal growth process is characterized by a first-order phase transition consisting of two contacting phases separated by an interface. In equilibrium the Gibbs potentials of both phases are equal and $\Delta G = 0$. In the case of melt-solid phase transition one uses the *free Helmholtz potential* $\Delta F = \Delta H - T\Delta S$ due to $\Delta V \approx 0$. At the melting point T_m becomes $\Delta H = T_m \Delta S$, the value of which is continuously liberated during growth as *latent heat of fusion*. In the case of discontinuous growth modes, however, it releases as thermal impulses $I_T = (\Delta H/c_p)\Delta z$, with c_p the heat capacity and Δz the crystallizing step width.

In a system consisting of two (or more) components the free potential of Gibbs is also determined by the component quantity n_i . At fixed T , P and V Euler's Theorem can be applied and the molar free Gibbs potential $G/n_i = g$ equals the sum of *chemical potentials* $\sum \mu_i x_i$ with *mole fraction* x_i . It is convenient to write the chemical potential as $\mu_i = \mu_i^\circ + RT \ln \gamma_i x_i$ with μ_i° the chemical *standard potential*, R the universal gas constant and γ_i the *activity coefficient*. The

criterion for *phase equilibrium* is that the chemical potential of any given component i must be the same in every phase ($\mu_i^I = \mu_i^J$). In the case of *ideal mixing* there is no interaction between the particles of the different constituting components ($\gamma = 1$), i.e. there is no mixing enthalpy ($\Delta h_M^{id} = 0$). The thermodynamic derivation of the equilibrium distribution coefficient and melt growth specifics of near ideal mixed crystals, like $\text{Ge}_{1-x}\text{Si}_x$, will be discussed.

For *real solutions* ($\gamma_i \neq 1$) the term Δh_M is not more zero and deforms the $g(x)$ course leading to extremes of formation of intermediate compounds ($\Delta h_M < 0$) or clustering and decomposition ($\Delta h_M > 0$). In order to specify γ different models (QRS, DLP, Hume-Rothery) are used for prediction of the interaction parameter ω between the substituting components. These considerations play an increasing role in advanced epitaxial processes of super-thin semiconductor ternary systems where the acting lattice strain can reduce the free energy by atomic ordering effects (superlattice arrangements of PtCu or AuAg types) rather than clustering.

The thermodynamically stable atomic arrangement near crystal and thin film surfaces is qualitatively different from the thermodynamically stable arrangement in a infinite bulk crystals. The force which minimizes the dangling bonds and surface area A is called *free interface energy* $\sigma = \partial G / \partial A$. Especially, at nucleation processes, including the two-dimensional nucleation growth of interfaces, when the cluster size approaches molecular dimensions, the surface contribution turns into an essential energetical part of the free potential leading in ternary semiconductor thin films to bandgap anomaly which has important consequences for the optical and electrical properties. Further, the equilibrium between the three interface energies σ^{sv} , σ^{sl} and σ^{lv} controls the capillary (meniscus) conditions at pulling methods from the melt (Czochralski, FZ, EFG).

4. Systems with compounds and nonstoichiometry related growth effects

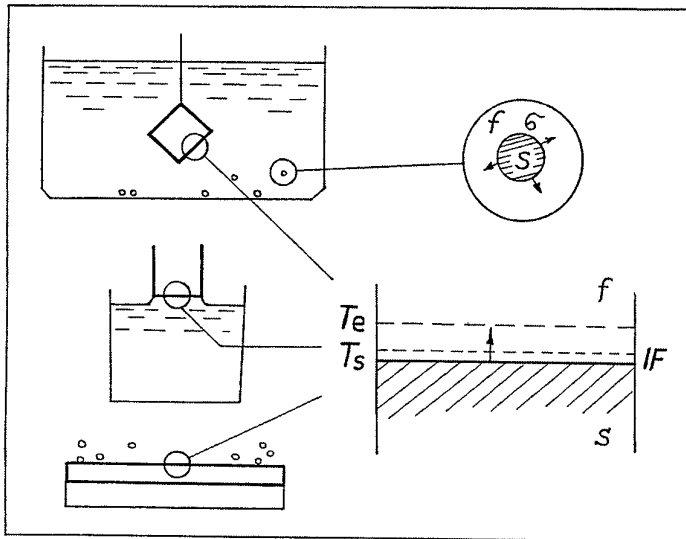
The growth of *binary compounds*, like AIII-BV and AII-BVI semiconductors, is of increasing role for numerous advanced applications. Of essential methodical significance is the width and deviation of the homogeneity region from stoichiometry affecting the as-grown crystal quality considerable (point defect generation and clustering, morphological instability, inclusions of the excess component). In general, the existence of second phase particles is one of the fundamental defects in melt grown compound crystals typically for semiconductors and oxides. A preventive measure is the in-situ vapour pressure control of stoichiometry already applied to the melt growth of semiconductors but, paradoxically, not to oxide crystals yet. Selected results of stoichiometry-controlled growth of CdTe, ZnSe, GaAs and PbMoO_4 will be shown.

5. Deviation from equilibrium

The precondition for crystallization of a solid phase within a metastable fluid phase is the *deviation from the thermodynamic equilibrium*. The difference of the chemical potentials of the metastable (1) and stable (2) phases $\Delta\mu = \mu^1 - \mu^2$ denotes the *driving force of crystallization* which can be quantified by the *supersaturation* and *supercooling* as $\Delta\mu = kT \ln(P/P^e)$ and $\Delta\mu = (\Delta h/T_m) \Delta T$, respectively. Comparing the various methods of epitaxy the supersaturation $\ln(P/P^e)$ differs considerably between 0.1 (LPE) and 10-100 (MBE, MOCVD). At bulk growth of silicon from melt ΔT yields about 1 - 4 K at the {111} facet.

Small deviations from equilibrium are considered by the *linear nonequilibrium thermodynamics* which implies irreversible processes of continuous transport of heat, mass and momentum. The basic principle is the *production of entropy* $P_s = dS/dt$. According the *Glansdorff-Prigogine Evolution Criterion* such state, quite related to realistic crystal growth processes, is able to generate high ordered *dissipative structures*, like convection patterns, cellular interfaces, solvent stratifications etc. which can exist in stable stationary forms.

The importance of thermodynamics for the crystal growth



Crystal growth deals with *first-order phase transitions*

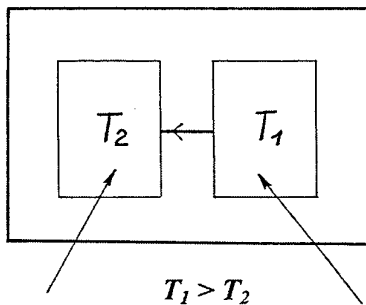
1. - coexistence of two distinct uniform phases which are stable at equilibrium point and separated by a *phase boundary*, i.e. surface; since the surface does not have a thermodynamically favourable structure, it tends to be thin and small;
2. - close to the equilibrium point the phases can still exist, one as the thermodynamically stable, the other as the thermodynamically metastable phase; the metastable phase is *supersaturated* with respect to the stable (equilibrium) phase; there is a *driving force* for transition to the stable phase;
3. - there is a *nucleation barrier* due to the competition between the thermodynamic driving force and surface free-energy effects hindering the outgrowth of small crystals; nuclei may be formed by spontaneous fluctuations or providing of a *seed (substrate)*.

To understand the fundamentals of crystal growth one has to study three equilibrium structures - mother phase, crystal and interface-, their mutual influence, and variations of their properties in dependence of deviations from equilibrium.

P. Rudolph, IKZ Berlin Elements of Thermodynamics for Crystal Growth 1. Introduction

Equilibrium (reversible) thermodynamics

closed systems



Q/T_2

$-Q/T_1$

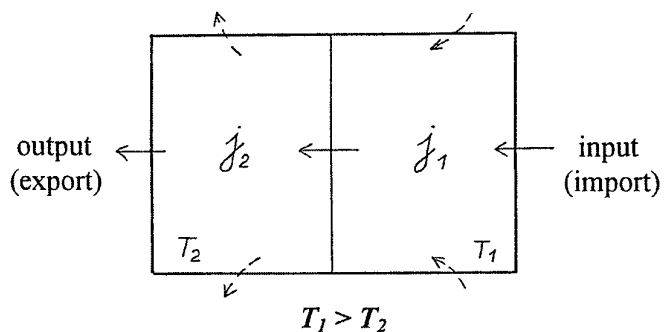
$$\Delta S \geq \frac{Q}{T_1} + \frac{Q}{T_2} = Q \left(\frac{1}{T_2} - \frac{1}{T_1} \right) = Q \frac{T_1 - T_2}{T_1 T_2} \geq 0$$

if $T_1 = T_2$ reversibility

$S \rightarrow \max, dS = 0 \Rightarrow$ highest degree of disorder

Nonequilibrium (irreversible) thermodynamics

open systems



$$\text{change of entropy } dS = dS^{\text{ext}} + dS^{\text{int}} > 0$$

$dS > 0, S < S_{\max} (!) \Rightarrow$ higher order
entropy production $P = dS/dt > 0$

P. Rudolph, IKZ Berlin Elements of Thermodynamics for Crystal Growth 1. Introduction

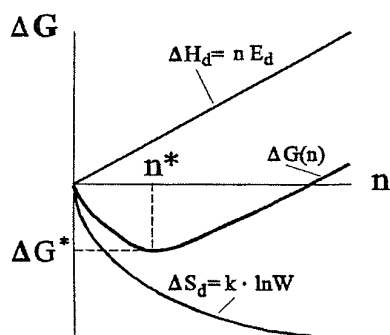
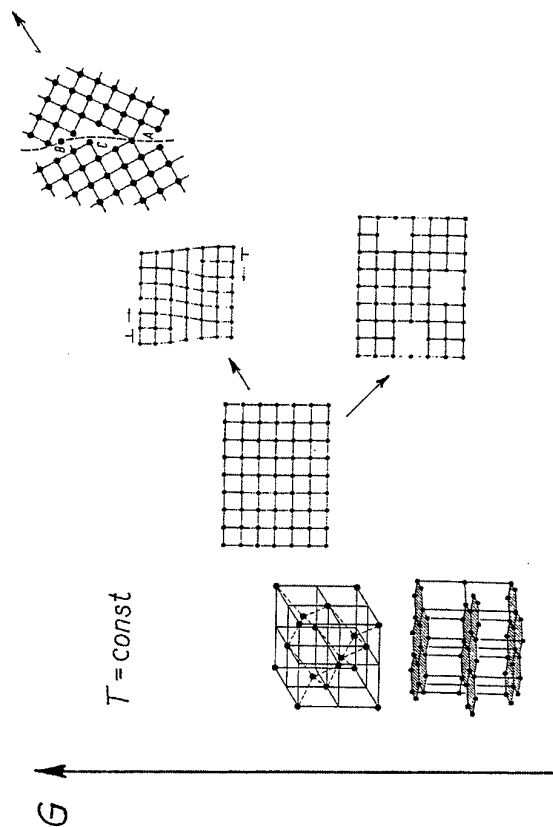
Gibbs potential and phenomena of order and disorder

minimization of the free energy

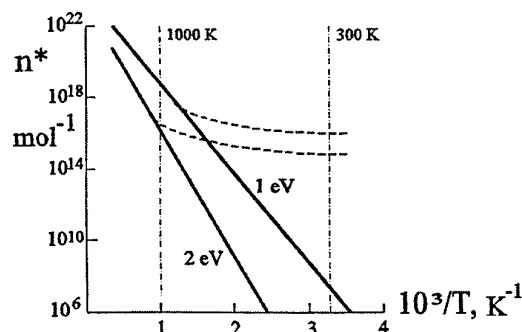
$$G = U + PV - TS = H - TS \rightarrow \min$$

process of ordering $H \rightarrow \min$

force of disordering $S \rightarrow \max$



Schematic illustration of the equilibrium defect concentration ("perfection limit") n^* obtained by superposition of defect enthalpy ΔH_d and entropy ΔS_d



Defect concentration vs. temperature at $E_d = 1 \text{ eV}$ (1) and 2 eV (2). Dashed lines: the "freezing" courses of high temperature defects

One phase and one component system

First Law

$$dU = dQ + dW$$

Second Law

$$dQ/T = k \ln W = dS$$

$$G = U + PV - TS$$

$$dG = dU + PdV + VdP - TdS - SdT$$

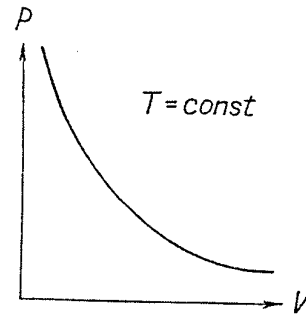
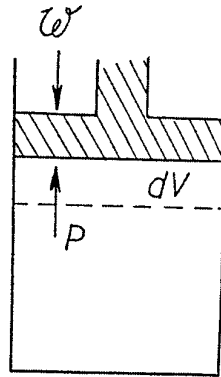
$$= TdS + VdP - TdS - SdT$$

$$dG = VdP - SdT$$

$$dT = 0: \partial G / \partial P = V$$

$$dP = 0: \partial G / \partial T = -S$$

$$dW = -PdV$$



differential of Gibbs potential :

$$dG = \left. \frac{\partial G}{\partial P} \right|_T dP - \left. \frac{\partial G}{\partial T} \right|_P dT$$

Gibbs' Phase Rule

$$f = C - \phi + 2 = 2$$

$\underset{1}{\parallel}$ $\underset{1}{\parallel}$

P. Rudolph, IKZ Berlin Elements of Thermodynamics for Crystal Growth 3. Thermodynamics of phase equilibrium 3.1. One phase and one component system

Equilibrium between two phases in a one component system

$$G^1 = U^1 - TS^1 + PV^1$$

$$G^2 = U^2 - TS^2 + PV^2$$

phase equilibrium:

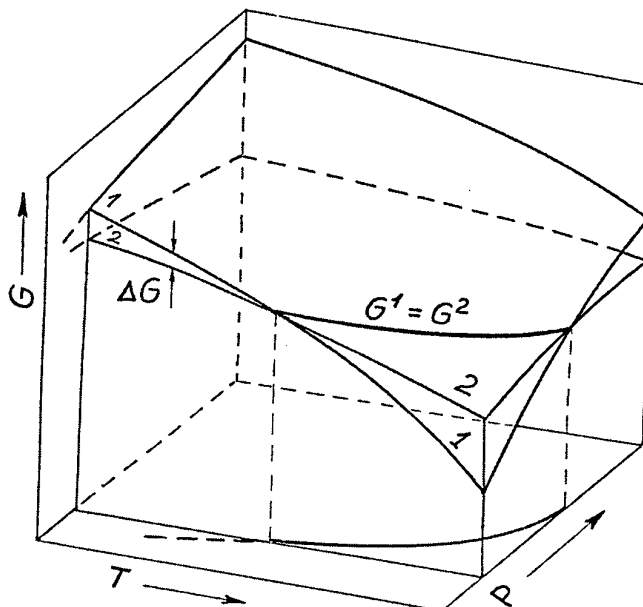
$$G^1 - G^2 = \Delta G = \Delta U - T\Delta S + P\Delta V = 0$$

melt-solid phase transition:

$$\Delta V \approx 0$$

free Helmholtz potential F

$$\Delta F \equiv \Delta G|_{V,P} = \Delta H - T\Delta S = 0$$



$$f = C - \phi + 2 = 1$$

Real solutions

(enlarged attracting or repulsing forces between A and B atoms)

$$\Delta h_M \neq 0$$

$$g(x)^{real} = g(x)^{id} + g(x)^{exc}$$

$$(g^o + RT \ln \gamma x) = (g^o + RT \ln x) + g(x)^{exc}$$

$$g(x)^{exc} = g(x)^{real} - g(x)^{id} = RT \ln \gamma x - RT \ln x = RT \ln \gamma$$

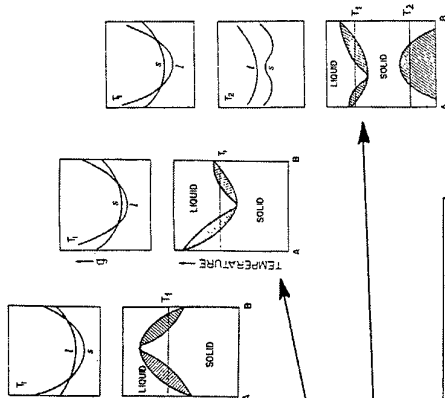
Model of regular solutions

excess term $\Delta h_M^{exc} = T \Delta s_M^{exc}$
ideal mixture of molten state ($\Delta s_M^{exc} = 0$)

$$\Delta g(x)^{exc} = \Delta h_M^{exc} = RT \ln \gamma = \omega x (1-x)$$

ω - (adjustable) interaction parameter

$$\begin{array}{l} \gamma < 1 \quad \Delta h^{exc} < 0 \quad \Delta g(x)^i < \Delta g(x)^j \\ \gamma > 1 \quad \Delta h^{exc} > 0 \quad \Delta g(x)^i > \Delta g(x)^j \end{array}$$



P. Rudolph, IKZ Berlin Elements of Thermodynamics for Crystal Growth 4. Phase diagrams 4.2. Two component systems

Two phases and two (or more) components

$$G = f(T, V, P, n_i)$$

total differential of the free Gibbs potential

$$dG = - \left. \frac{\partial G}{\partial T} \right|_{P, n_i} dT + \left. \frac{\partial G}{\partial P} \right|_{T, n_i} dP + \sum_{i=1}^C \left. \frac{\partial G}{\partial n_i} \right|_{P, T} dn_i$$

chemical potential

$$\partial G / \partial n_i = \mu_i$$

$$\mu_i = \mu_i^o(T, P) + RT \ln(\gamma_i x_i)$$

mole fraction x_i $x_A = n_A / (n_A + n_B)$; $x_B = (1 - x_A)$

intensive (molar) values $g = G/n$, $h = H/n$, $s = S/n$

$$\begin{array}{l} \mu_i = \left(\frac{\partial G}{\partial n_i} \right)_{T, P} \\ d\mu_i = RT \frac{dP}{P} = RT d \ln P_i \\ \mu_i = \mu_i^o(T, P) + RT \ln P_i \\ P_i = \gamma_i x_i P \\ \mu_i = \mu_i^o(T, P) + RT \ln(\gamma_i x_i) \end{array}$$

P. Rudolph, IKZ Berlin Elements of Thermodynamics for Crystal Growth 3. Thermodynamics of phase equilibrium 3.3. Two phases and two (or more) components

Phase diagrams of two-component systems

equilibrium between solid and liquid phases

$$\begin{array}{l} \mu_B^s(x_B^s, T) = \mu_B^l(x_B^l, T) \\ \mu_B^o + RT \ln x_B^s \gamma_B^s = \mu_B^o + RT \ln x_B^l \gamma_B^l \\ RT \ln \left(\frac{x_B^s \gamma_B^s}{x_B^l \gamma_B^l} \right) = -\Delta \mu_B^o = -(\Delta h_B^o - T \Delta s_B^o) = 0 \end{array}$$

$$\Delta s_B^o = \Delta h_B^o / T_{mB}$$

$$\ln \left(\frac{x_B^s \gamma_B^s}{x_B^l \gamma_B^l} \right) = - \frac{\Delta h_B^o}{R} \left(\frac{1}{T} - \frac{1}{T_{mB}} \right)$$

Ideal and nearly ideal (liquid) solutions ($\gamma^{s,l} \approx 1$)

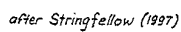
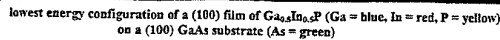
van Laar equation:

$$\frac{x_B^s}{x_B^l} = k_o^B = \exp \left[- \frac{\Delta h_B^o}{R} \left(\frac{1}{T} - \frac{1}{T_{mB}} \right) \right]$$

with k_o^B the (thermodynamic) equilibrium distribution coefficient

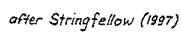
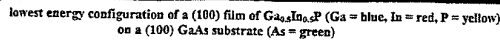
P. Rudolph, IKZ Berlin Elements of Thermodynamics for Crystal Growth 4. Phase diagrams 4.2. Two component systems

Compositional Modulation and Ordering in Semiconductors



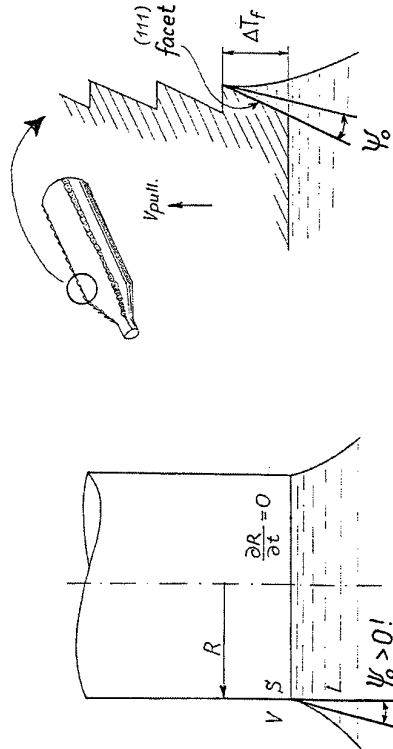
P. Rudolph, IKZ Berlin	Elements of Thermodynamics... for Crystal Growth	3. Thermodynamics of phase equilibrium 3.4. Phase boundaries and surfaces
------------------------	---	--

Compositional Modulation and Ordering in Semiconductors



P. Rudolph, IKZ Berlin	Elements of Thermodynamics... for Crystal Growth	3. Thermodynamics of phase equilibrium 3.4. Phase boundaries and surfaces
------------------------	---	--

diameter control

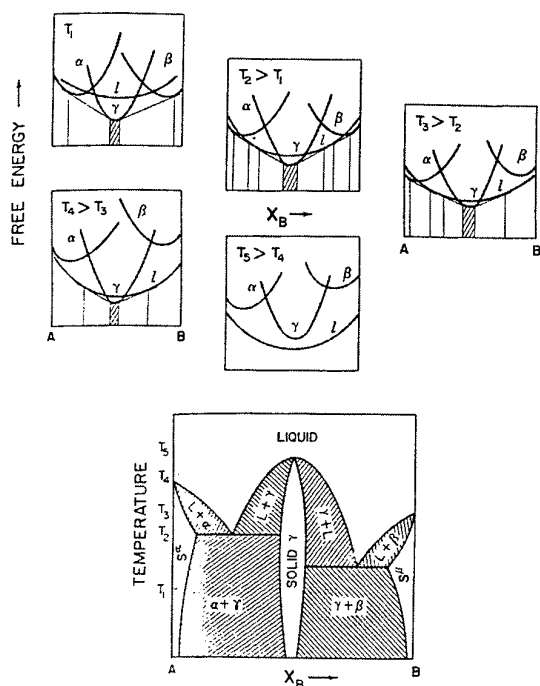


equilibrium condition at the three-phase interface line

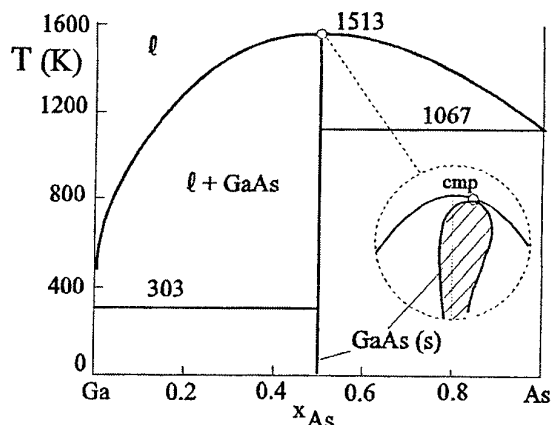
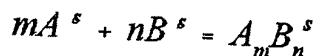
$$\psi_0 = \arccos[(\sigma_{Lv}^2 + \sigma_{sv}^2 - \sigma_{sl}^2)/2\sigma_{lv}\sigma_{sv}]$$

 $11^\circ \pm 1^\circ$ for silicon $12^\circ \pm 1^\circ$ for germanium $25^{\circ} \pm 1^{\circ}$ for indium antimonide

P. Rudolph, IKZ Berlin



attractive forces between unlike atoms
ionic or covalent character



P. Rudolph, IKZ Berlin Elements of Thermodynamics for Crystal Growth 4. Phase diagrams
4.2. Two component systems



INSTITUT FÜR KRISTALLZÜCHTUNG BERLIN

At $T > 0K$ the Gibbs energy is minimal if the defect entropy tends towards maximum.

$$G_d = H_d - TS_d$$

$$H_d = n g$$

$$S_d = k \ln W \approx k \ln(N-n) - \ln n$$

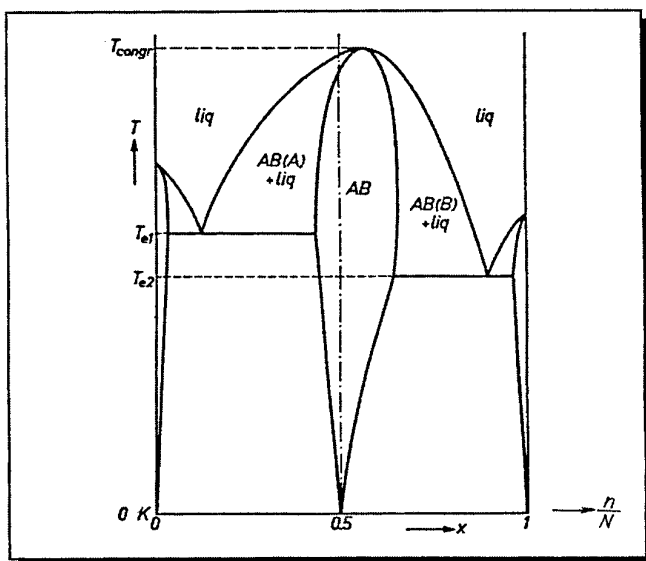
$$\delta G / \delta n = g - kT [\ln(N-n) - \ln n]$$

$$N \gg n$$

$$n/N = \exp(-g/kT)$$

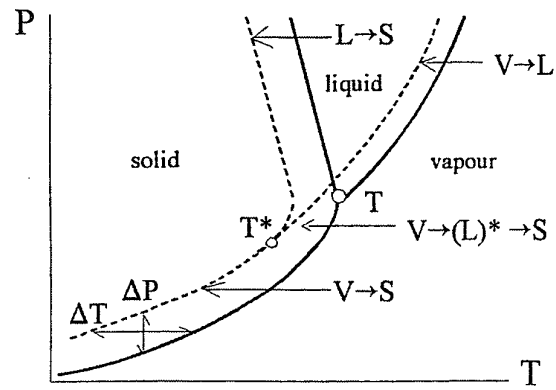
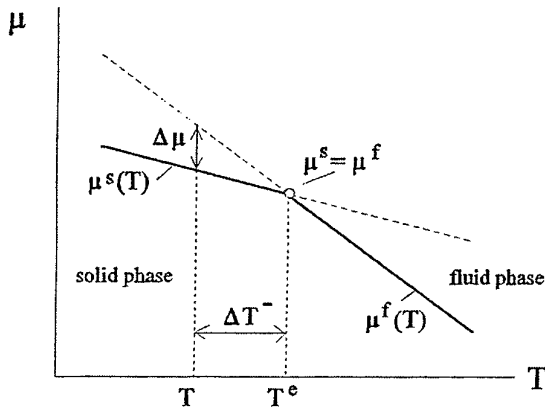
n - number of point defects
(deviation from stoichiometry)

N - total number of sites
 g - defect enthalpy



P. Rudolph, IKZ Berlin Elements of Thermodynamics for Crystal Growth 5. Existence region and nonstoichiometry
5.1. Stoichiometry and nonstoichiometry

Driving force of crystallization



deviation from the thermodynamic equilibrium

$$\Delta\mu = \mu^f - \mu^s$$

P. Rudolph, IKZ Berlin	Elements of Thermodynamics for Crystal Growth	6. Deviation from equilibrium 6.1. Driving force
------------------------	--	---

supercooling:

$$\Delta T = (T_m - T),$$

$$\Delta\mu^{l \rightarrow s} = \Delta h - T\Delta s = \Delta h - T(\Delta h/T_m) = (\Delta h/T_m)(T_m - T) = (\Delta h/T_m)\Delta T$$

supersaturation:

$$\Delta\mu/kT = \ln(P/P^e) \approx \sigma^*$$

liquid phase epitaxy

vapour phase epitaxy

molecular beam epitaxy

metal organic chemical vapour deposition

σ_{LPE}^*	≈ 0.1
σ_{VPE}^*	$\approx 0.5 - 2$
σ_{MBE}^*	$\approx 10 - 100$
σ_{MOCVD}^*	≈ 40

P. Rudolph, IKZ Berlin	Elements of Thermodynamics for Crystal Growth	6. Deviation from equilibrium 6.1. Driving force
------------------------	--	---

Interface kinetics/faceting effects in the growth of large crystals: modeling and real observations

Y. Liu, A. Virozub, and S. Brandon

Department of Chemical Engineering, Technion-Israel Institute of Technology,
Haifa 32000, Israel

Anisotropy of material properties and growth parameters may lead to a wide variety of phenomena occurring during the directional growth of single crystals from the melt. One of the most important phenomena caused by anisotropy is facet formation, which in itself is associated with a number of problems in the quality of the crystal obtained after growth. These include the "facet effect" by which a dopant, trapped by the rapid motion of steps along a facet, is incorporated into the crystalline phase at a concentration which is different than that predicted by equilibrium segregation (see e.g. [1] and [2] for this effect during the growth garnets and semiconductors respectively). Another problem of interest involves the nucleation of twins on facets located at the three-phase-boundary during the Czochralski growth of certain semiconductor materials (see e.g. [3]).

Facets are known to appear on crystalline faces with large values of Jackson's α parameter, which can be thought of as a dimensionless entropy of fusion [4]. Examples of these faces include the {111} surfaces of germanium and silicon and the {211} and {110} surfaces of yttrium aluminum garnet (YAG). Once a facet is formed, its evolution (during the growth process) is governed by a combination of transport phenomena and non-equilibrium (kinetic) effects. Traditionally, facet formation on the melt/crystal interface during directional growth has been understood through an analysis based on simplifications of the thermal field in the vicinity of the melting point isotherm. These ideas, which are presented in a number of references (e.g. [5, 6]), give rough predictions for the facet size as a function of the maximum undercooling at the facet center, the curvature of the melting-point isotherm, and the thermal gradient in the vicinity of the melt/crystal interface. Obtaining accurate predictions of facet formation requires large-scale, detailed modeling of transport phenomena taking place during the growth process.

It is well recognized that large-scale numerical analysis of transport limited crystal growth is a useful tool for the understanding and improvement of melt-growth techniques. Such analyses have been successfully used to complement and guide experimental studies. In particular, they can provide detail which is very difficult or even impossible to obtain

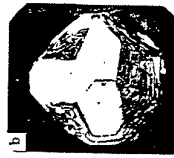
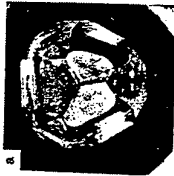
from experiments. Important information gleaned from these studies includes the time-dependent distribution of temperature and solute in the crystalline and melt phases, as well as the evolving melt/crystal interface shape. However, it should be understood that successful quantitative or even semi-quantitative predictions of these quantities are reported only in the case of materials whose growth is controlled by heat transport through the system; the growth of materials which exhibit faceting (associated with anisotropic kinetic effects) cannot be accurately simulated using standard techniques.

In this contribution an extensive overview of the phenomenon of faceting in melt growth systems will be given. Our work (presented in part in [7, 8]), involving a newly developed technique for Finite Element modeling of facet formation during melt growth, will be discussed. The application of this technique in the analysis of the confined growth of oxides will be described in detail. Particular issues to be discussed include the effect of parameters such as crystal growth rate and furnace temperature gradient on facet formation and characteristics, as well the interaction between transport phenomena (such as melt convection and radiative heat transfer) and facet formation.

References

- [1] B. Cockayne, J. M. Roslington and A. R. Vere, *J. Mater. Sci* **8** (1973) 382.
- [2] W. Bardsley, J. B. Mullin and D. T. J. Hurle, *Iron Steel Inst.* **1967**(110) (1968) 93.
- [3] D. T. J. Hurle, in: *Sir Charles Frank, OBE, FRS: An 80th Birthday Tribute*, Eds. R. G. Chambers, J. E. Enderby, A. Keller, A. R. Lang and J. W. Steeds, (Adam Hilger, 1991) 533.
- [4] K. A. Jackson, in: *Liquid Metals and Solidification*, A seminar on liquid metals and solidification held during the Thirty-Ninth National Metal Congress and Exposition, Chicago, November 2 to 8, 1957 (Published by the American Society for Metals) 174.
- [5] J. C. Brice, *J. Crystal Growth* **6** (1970) 205.
- [6] A. A. Chernov, *Ann. Rev. Mater. Sci* **3** (1973) 397.
- [7] Y. Liu, The Effect of Anisotropic Kinetics on Crystal Growth From the Melt, D.Sc. Thesis, Technion (1997).
- [8] Y. Liu, A. Virozub and S. Brandon, *J. Crystal Growth* submitted.

Experimental Evidence of Faceted Interfaces:



Petrosyan and Bagdasarov
(JCG 34 110, 1976)

Xuewu et al
(JCG 133 267, 1993)

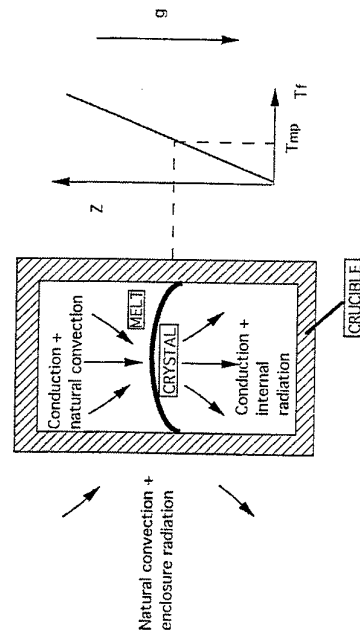
Interface kinetics/faceting effects in the growth of large crystals: modeling and real observations

S. Brandon, Y. Liu and A. Virozub

Dept. of Chem. Eng., Technion, Haifa 32000, Israel

Beatenberg - September 1998

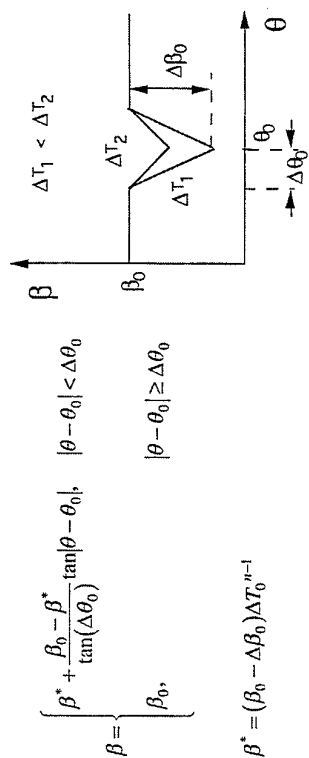
Heat Transport in an Idealized Vertical System



Outline

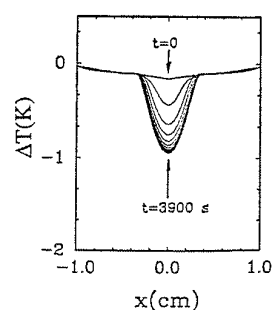
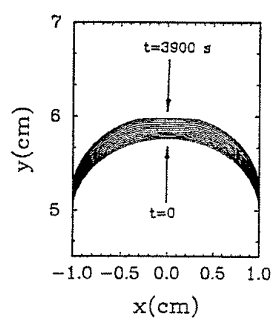
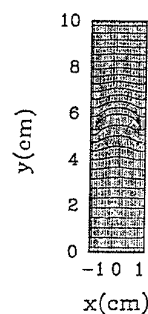
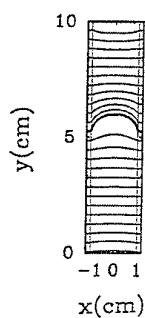
- Experimental observations
- Traditional approach to modeling
- Modeling of crystal growth from the melt in systems with faceted melt/crystal interfaces
- Results:
 - Effect of model parameters
 - Sensitivity to operating parameters
 - Effects of melt convection and radiative heat transport

Model Kinetic Coefficient



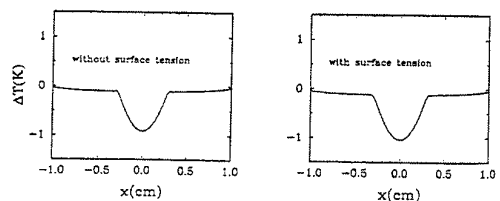
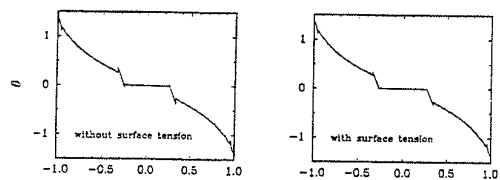
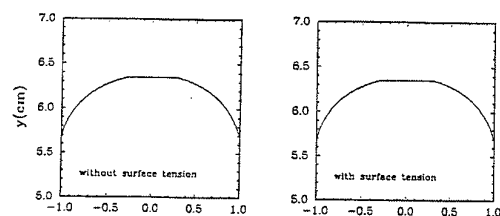
Sample Transient Result

($n=1$, $V=2\text{mm/hr}$, $\theta_0=0$, $G=50\text{ K/cm}$, $\Delta\theta_0=0.05$, $\Gamma=0.005\text{ cmK}$)



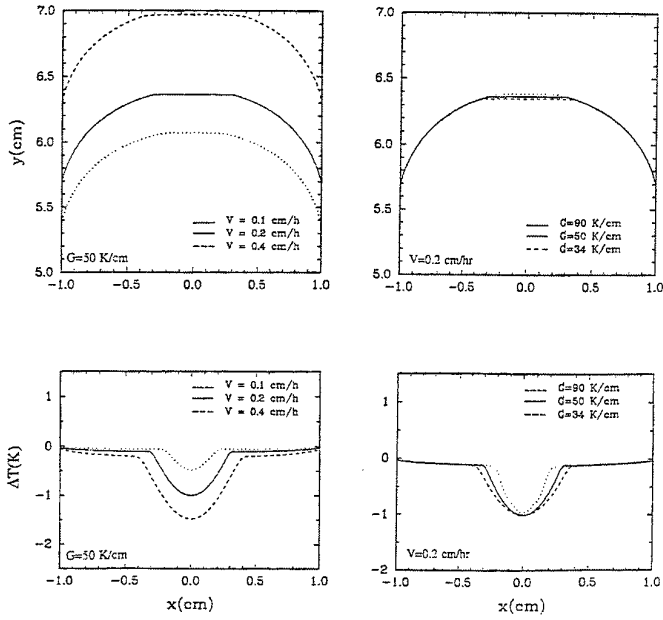
Effects of Artificial Surface Tension

($n=1$, $V=2\text{mm/hr}$, $\theta_0=0$, $\Delta\theta_0=0.05$, $G=50\text{ K/cm}$, $32 \times 28\text{ mesh}$)



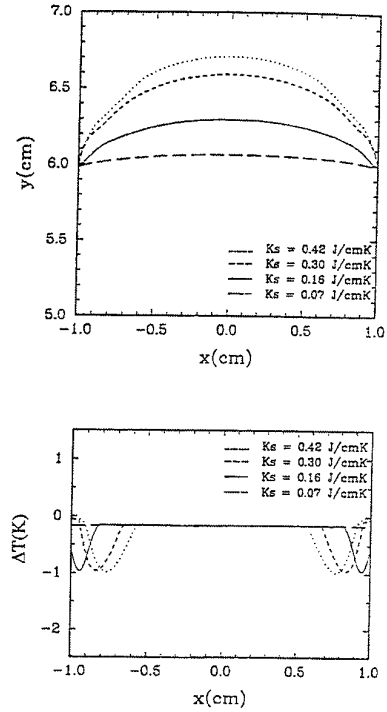
Effects of Growth Rate and Furnace Gradient on Facet Size and on Undercooling

($n=2$, $\theta_0=0$, $\Delta\theta_0=0.05$, $\Gamma=0.005$ cmK)



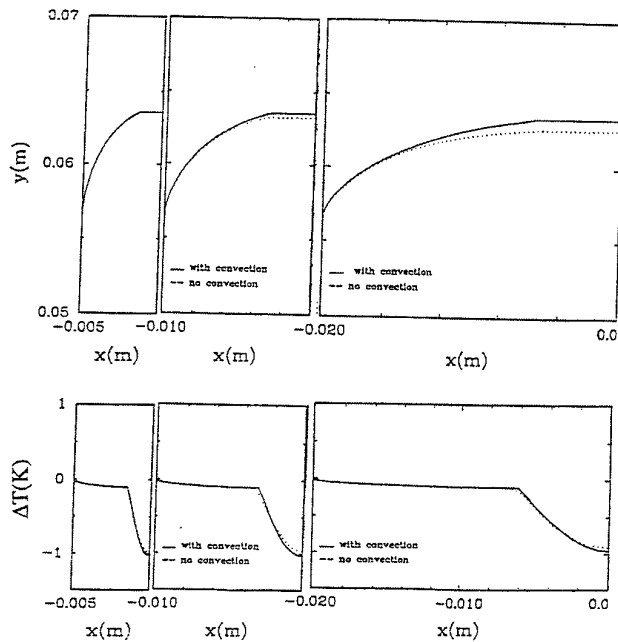
Effect of Varying Effective Solid Conductivity on Facet Size and Position

($n=2$, $\theta_0=\pi/4$, $\Delta\theta_0=0.05$, $\Gamma=0.005$ cmK, $G=50$ K/cm, $V=0.3$ cm/h)



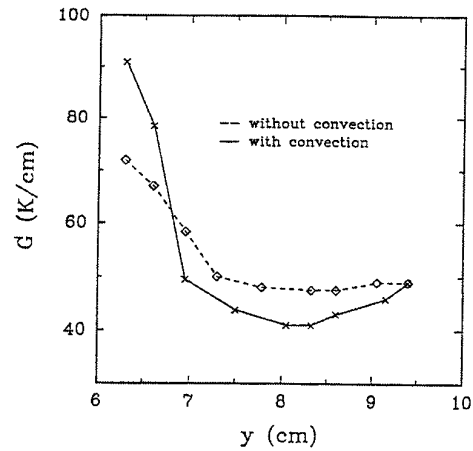
Influence of Melt Flow on Facet size and Shape and on Undercooling

($n=1$, $\theta_0=0$, $\Delta\theta_0=0.05$, $\Gamma=0.005$ cmK, $G=50$ K/cm, $V=0.2$ cm/hr)



Effect of Melt Convection on Vertical Gradient in the Melt

($n=1$, $\theta_0=0$, $\Delta\theta_0=0.05$, $\Gamma=0.005$ cmK, $G=50$ K/cm, $V=0.2$ cm/hr, $d=2$ cm)

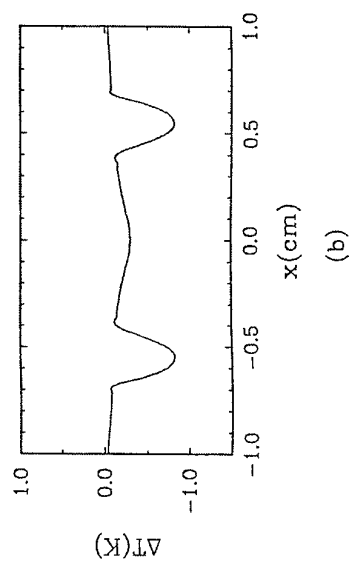
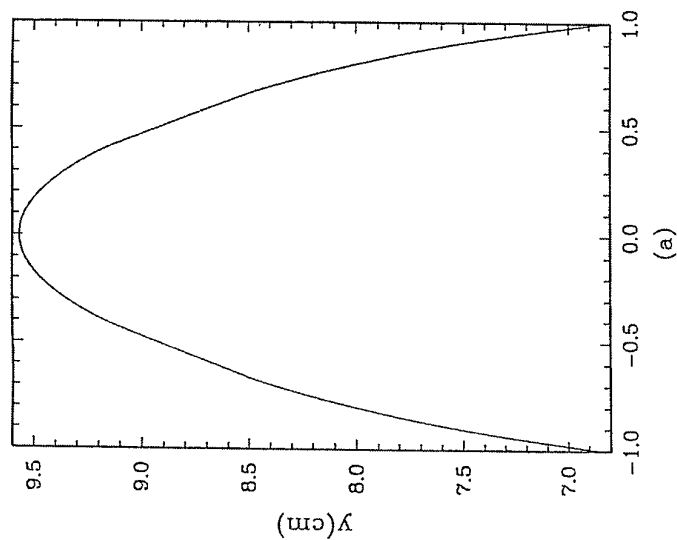
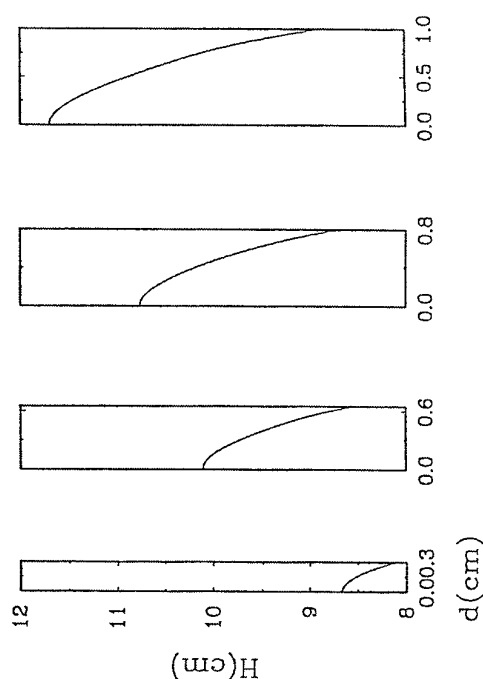
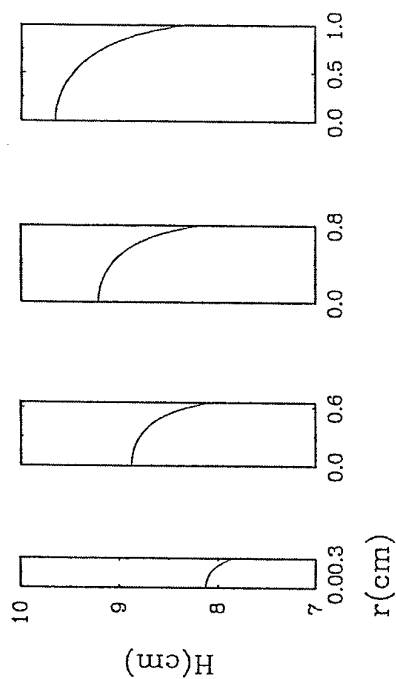


Faceting of curved interfaces associated with internal radiative heat transport

($n=2$, $V=5.5$ mm/hr, $\theta_0=1.2$, $\Delta\theta_0=0.05$, $\Gamma=0.005$, $G=50$ K/cm)

Geometric effects:

cylinders versus slabs



Methods of Structural Characterization for Technologically Important Crystals

Helmut Klapper

Mineralogisches Institut der Universität Bonn

The aims of the structural characterization of technologically important crystals are

- to analyse the crystal defects generated during growth, sample preparation and device processing and to find out optimal methods and conditions to avoid them;
- to assess and certify the structural perfection of crystals provided for technical applications.

In this lecture the following three methods to characterize the structural perfection of large technological important crystals are treated: **Etching**, **polarization optics**, and - with particular emphasis - **X-ray diffraction topography**.

Etching [1] is the oldest and still most frequently applied method to reveal structural defects outcropping at the surface of crystals. Dislocations, all kinds of striations, growth-sector boundaries, twin domains and twin boundaries can easily be detected if a suitable etchant selectively attacking the strained regions surrounding the defects is available. Etching is the most wide-spread routine technique for the structural characterization of semiconductor crystals such as Si, Ge, GaAs, CdTe, etc.. The etch-pit density on the surface of a crystal is a commonly used measure for the dislocation density in the bulk of the crystal.

Polarization optics (stress birefringence microscopy) widely is used for crystals transparent in the range of visible light and infrared and reveals all defects accompanied by stress birefringence. It is particularly suitable for cubic (i.e. optically isotropic) crystals and is very effective for crystals with large refractive index and strong elasto-optical effect, such as garnets (visible [2,3]) and - in the infrared range,

Si and Ge [4]). In these crystals even single dislocations can be revealed by stress birefringence.

X-ray diffraction topography [5] in its various techniques is one of the most powerful methods for the imaging and characterization of individual defects in large and nearly perfect crystals. Classic fields of application are crystal growth [6,7] and semiconductor processing for device production [8].

All X-ray diffraction topographic techniques are based on the reflection of X-ray by a set of lattice planes (hkl). Two diffraction geometries, the Bragg or „reflection“ geometry and the Laue or „transmission“ geometry are applied. Defects embedded in an undisturbed crystal are imaged by a locally changed diffracted intensity („contrast“). The contrast arises from the lattice deformations surrounding the defect, not from the defect itself.

X-ray topography is a non-magnifying method with poor spatial resolution. Due to its high sensitivity to lattice strain, the contrast widths of defects is rather wide (e.g. image width of dislocations $> 15 \mu\text{m}$). Therefore, X-ray topography is suitable only for crystals with low defect density.

The following frequently used X-ray topographic techniques are presented:

White-Radiation methods: Laue technique with conventional x-ray and with synchrotron radiation.

Monochromatic-radiation methods: Berg-Barret technique, the Lang projection and section topography and the double-crystal technique.

X-ray topography allows the imaging and the characterization of dislocations, stacking faults, antiphase boundaries, growth striations, growth-sector and vicinal-sector boundaries, facet regions, twin domains and twin boundaries, inclusions. Burgers vectors and characters of dislocations (screw, edge, mixed) can be determined as well as fault vectors of stacking faults and antiphase boundaries. Growth defects, post-growth defects and defects introduced during processing or by

improper sample preparation (e.g. „mechanical damages“) are easily distinguished. Moreover, threading dislocations in high-perfection substrate crystals and misfit dislocations in epitaxial layers can be imaged and analysed.

Among others, the following examples will be presented:

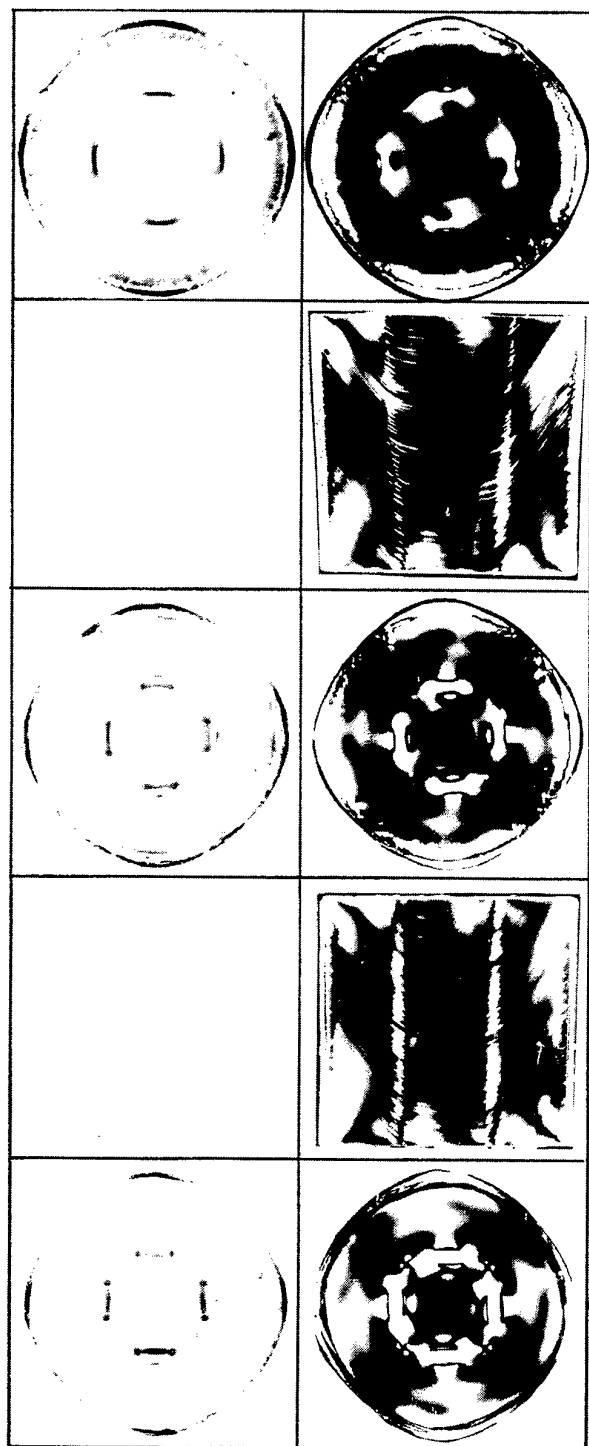
Etch patterns of LiF, birefringence patterns of GGG, scattered-light laser tomograph of KDP.

Synchrotron Laue topograph of beryll, Lang projection topographs of synthetic quartz, KTP, GaPO_4 , LiNbO_3 , YAlO_3 , GaAs substrate with Ga(In)As epilayers, and of slowly and rapidly grown KDP and ADP.

Section topographs of natural and synthetic tool diamonds and of oxygen precipitations in Silicon.

References

- [1] S. Amelinckx, Direct Observations of Dislocations, Solid State Physics, Suppl. 6, Academic Press, New York and London, 1964.
- [2] J.W. Matthews, T.S. Plaskett and J. Ahn, Phil. Mag. **33** (1976)73.
- [3] W. Schmidt and R. Weiss, J. Crystal Growth **43** (1978)515.
- [4] W.L. Bond and J. Andrus, Phys. Rev. **101**(1956)1211.
- [5] A.R. Lang, Techniques and Interpretation in X-Ray Topography. In: *Diffraction and Imaging Techniques in Materials Science*. S. Amelinckx , R. Gevers and J. Van Landuyt. eds. North-Holland , Amsterdam 1977.
- [6] A. Authier, X-Ray and Neutron Topography of Solution-grown Crystals. In: *1976 Crystal Growth and Materials* (Current Topics in Materials Science, Vol 2), p. 515. E. Kaldis and H.J. Scheel, eds., North-Holland, Amsterdam 1977.
- [7] H. Klapper, Structural Defects in Crystals and Techniques for Their Detection. Materials Science Forum 276/277 (1998) p.291-306.
- [8] A.J.R. de Kock, Effect of Growth Conditions of Semiconductor Quality. In: *1976 Crystal Growth and Materials* (Current Topics in Materials Science, Vol. 2), p. 661. E. Kaldis and H.J. Scheel, eds., North-Holland, Amsterdam 1977.



4000

4000

4500

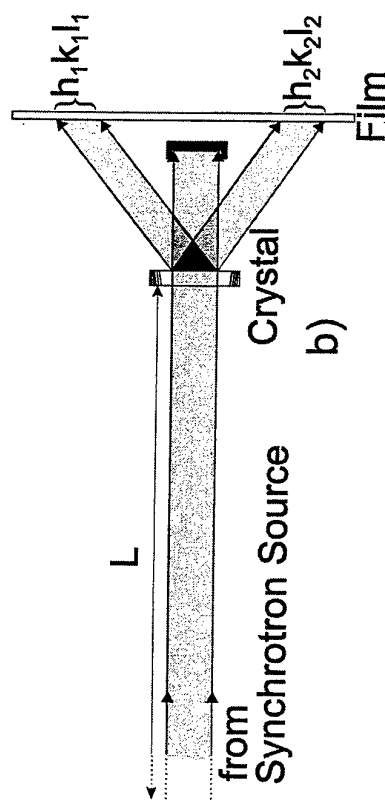
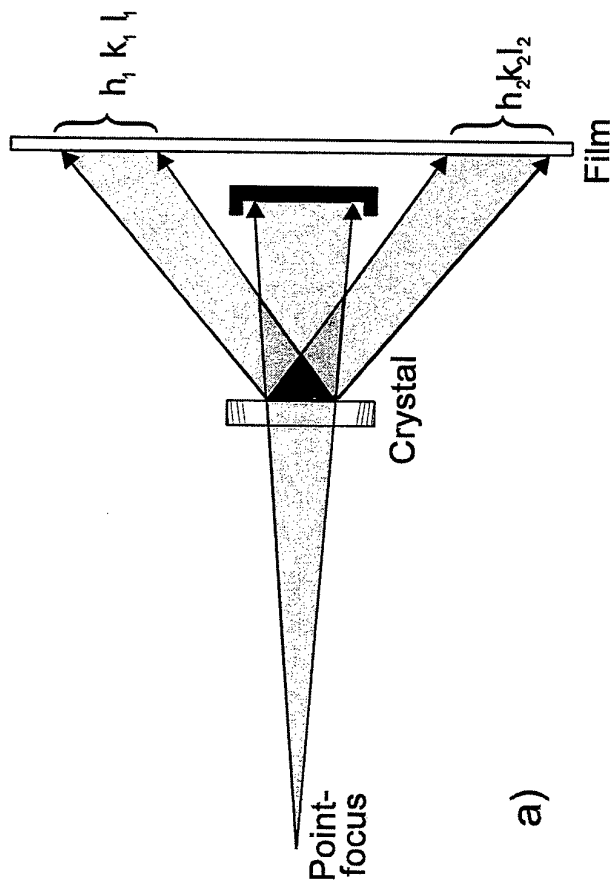
4000

4000

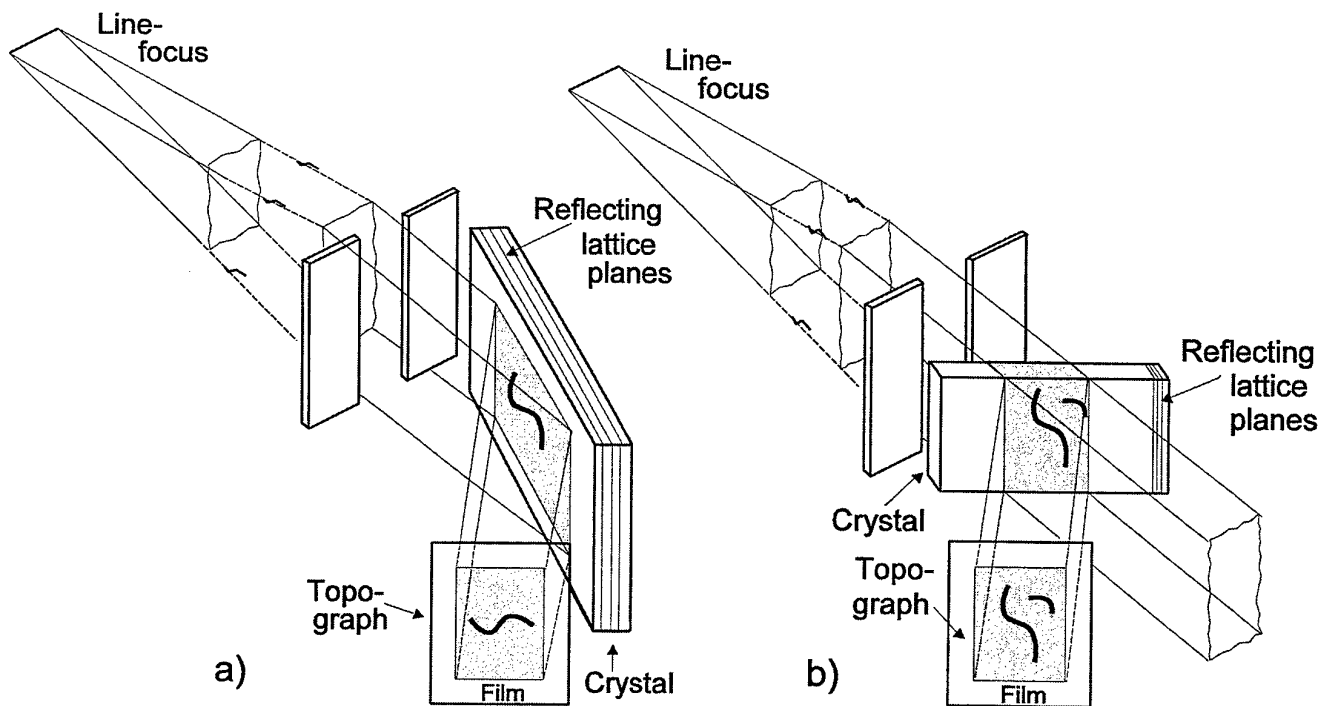
4000

→ < 110 >

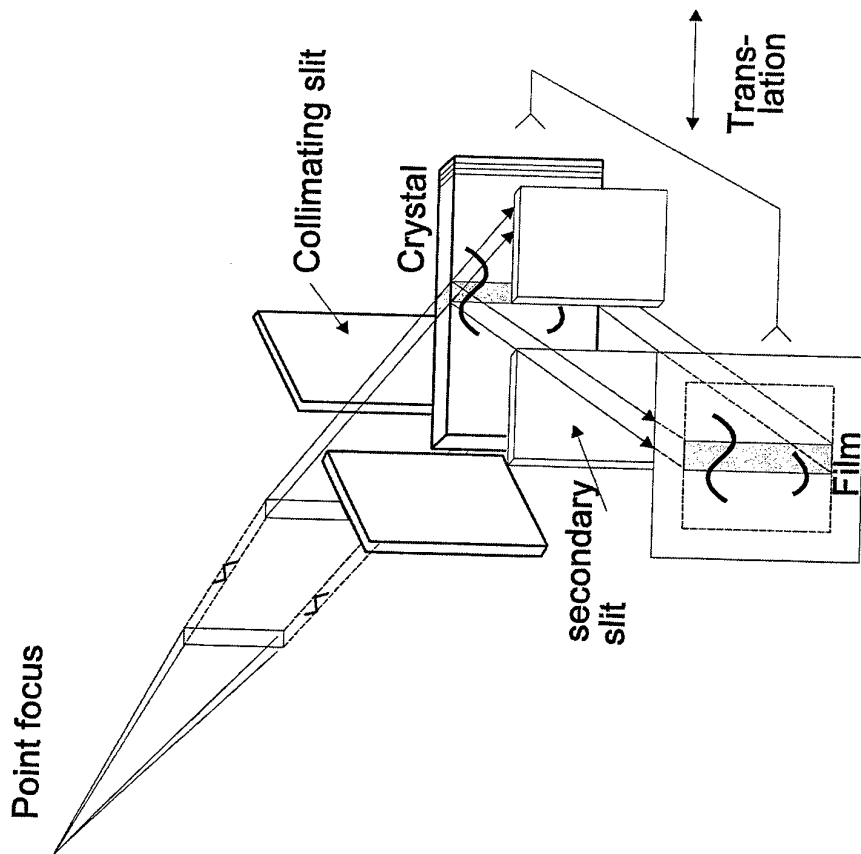
Stress birefringence study of FZ GGG



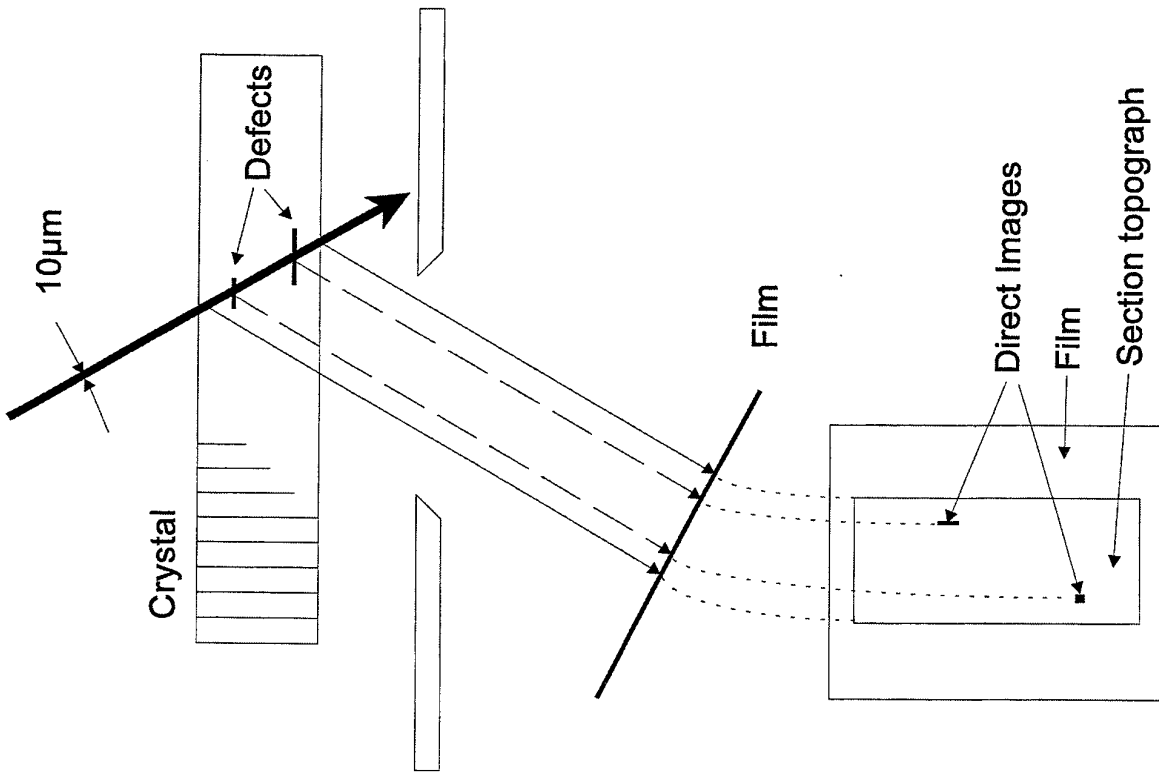
(a) Laue method with conventional X-ray source.
 (b) Laue technique with white Synchrotron radiation.



(a),(b) Berg-Barrett technique in reflection (Bragg case) and transmission (Laue case) with film normal to the diffracted beam.



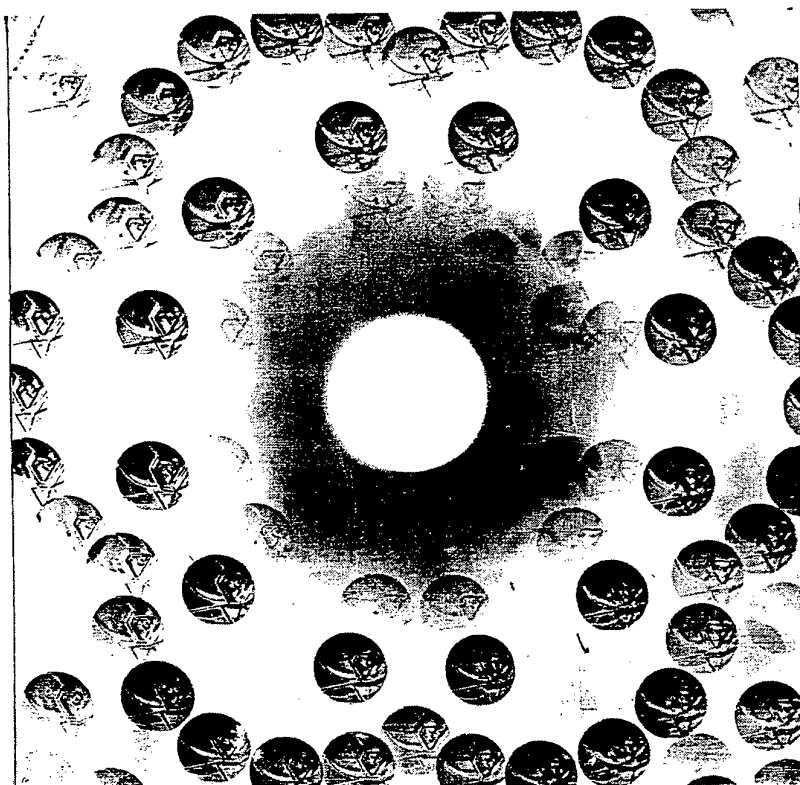
Lang projection method, permitting high spatial resolution by reflection of the $K\alpha_1$ -line alone. A secondary slit shields the film against the primary beam and the background radiation. By coupled translation of crystal and film the whole crystal is scanned and imaged on the film.



Location of defects in the depths of the crystal plate, derived from the position of the direct images within the width of the section topograph.

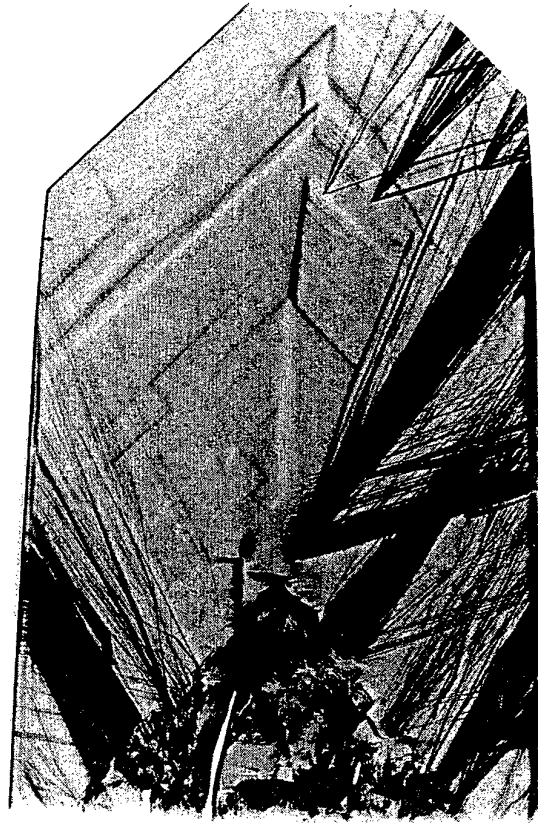
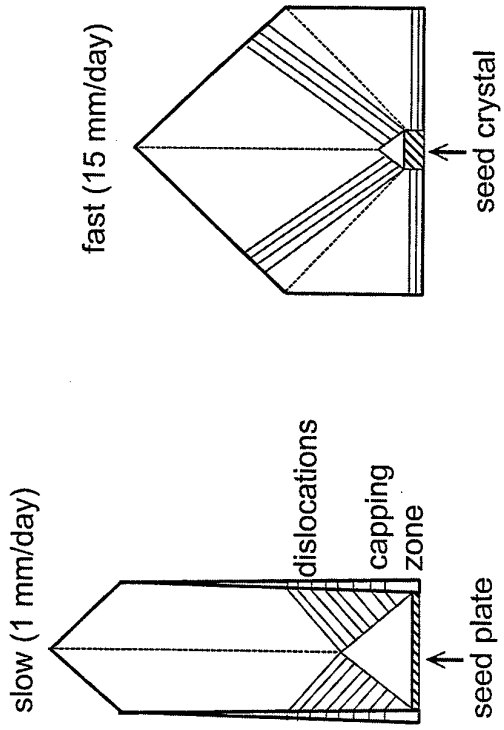


Verneuil Sapphire (30 mm diameter)

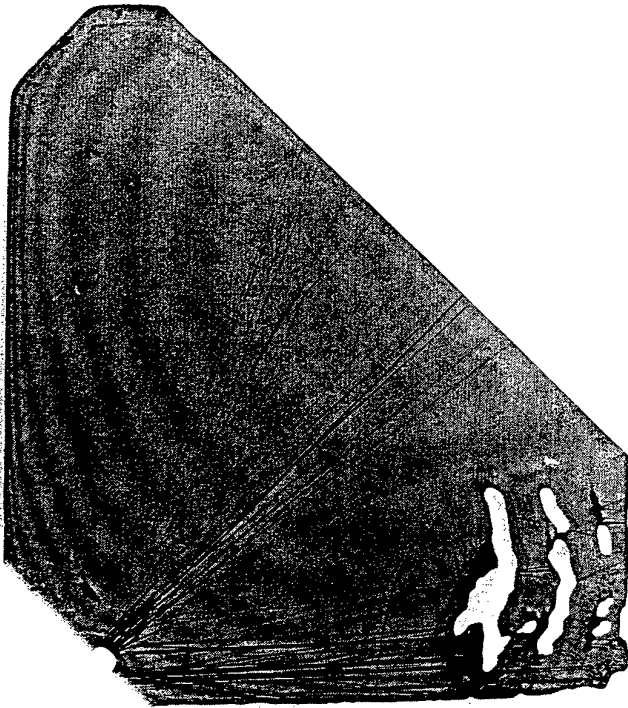


Synchrotron Laue topograph of beryll
(N. Herres and A.R. Lang)

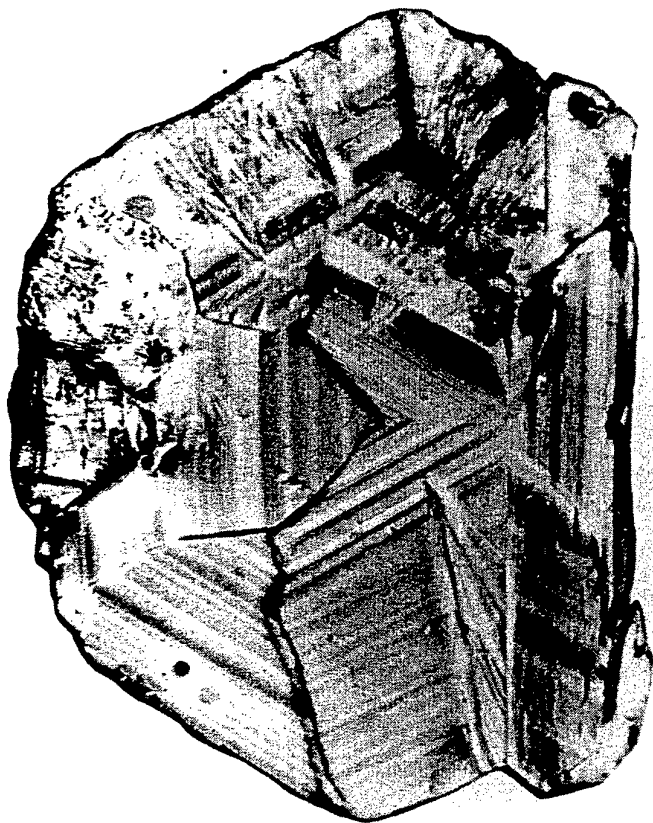
Morphology KDP/ADP



KDP (28 x 42 mm²)



ADP (60 mm horizontal diameter)

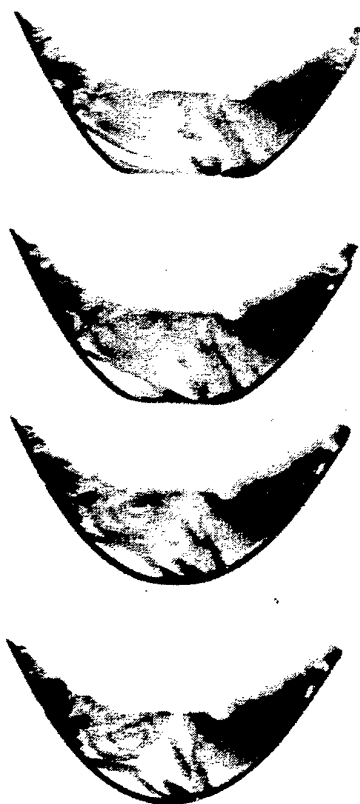
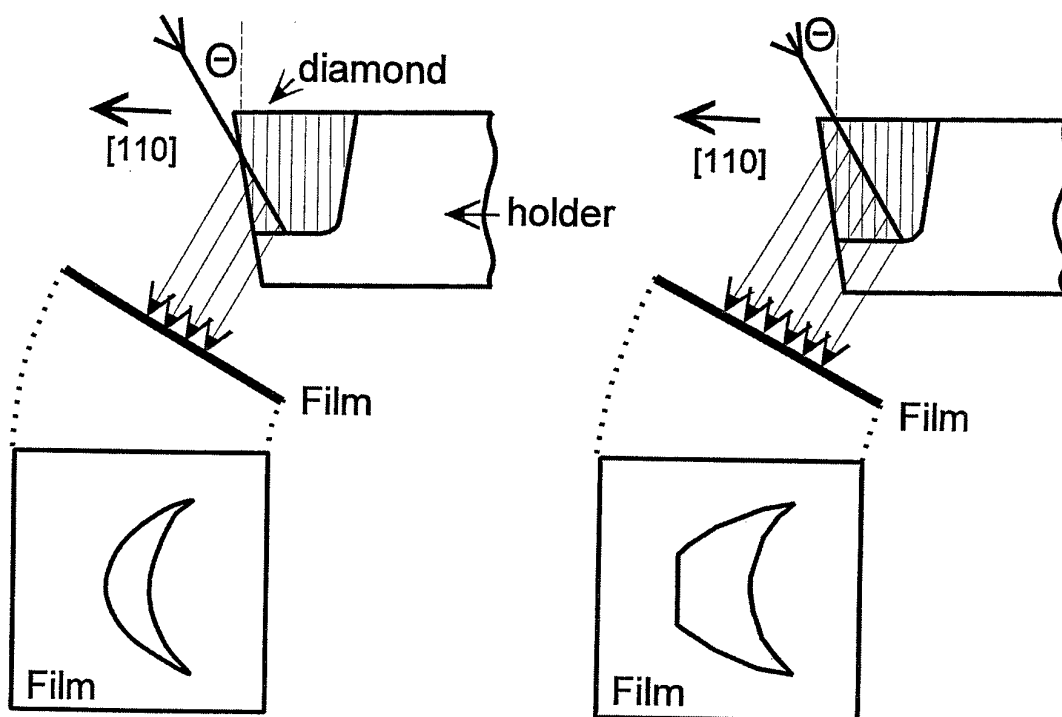


GaPO₄ (0001) plate, 8mm diameter

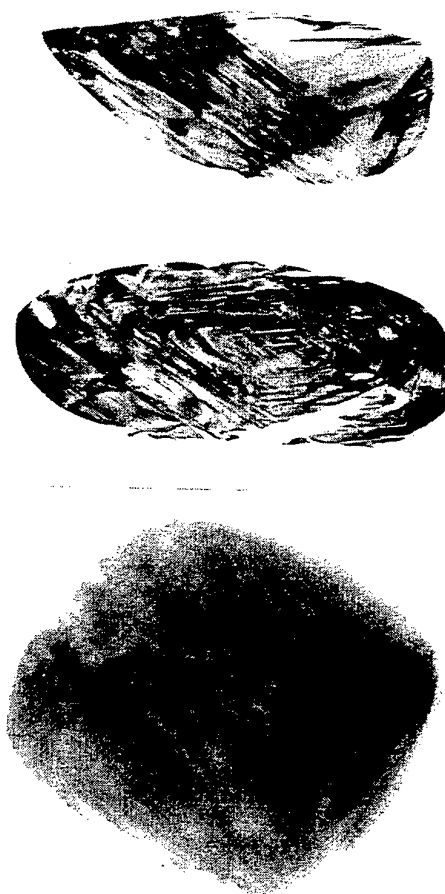


Fault surfaces in synthetic quartz

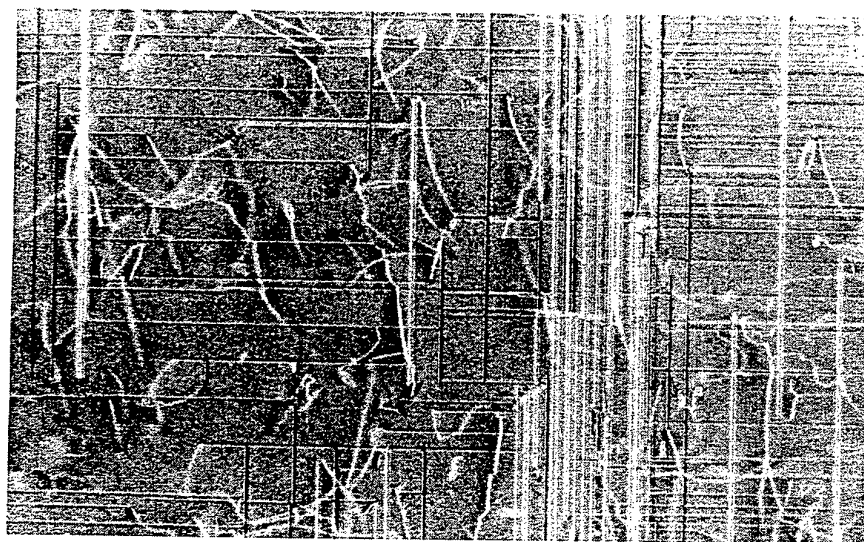
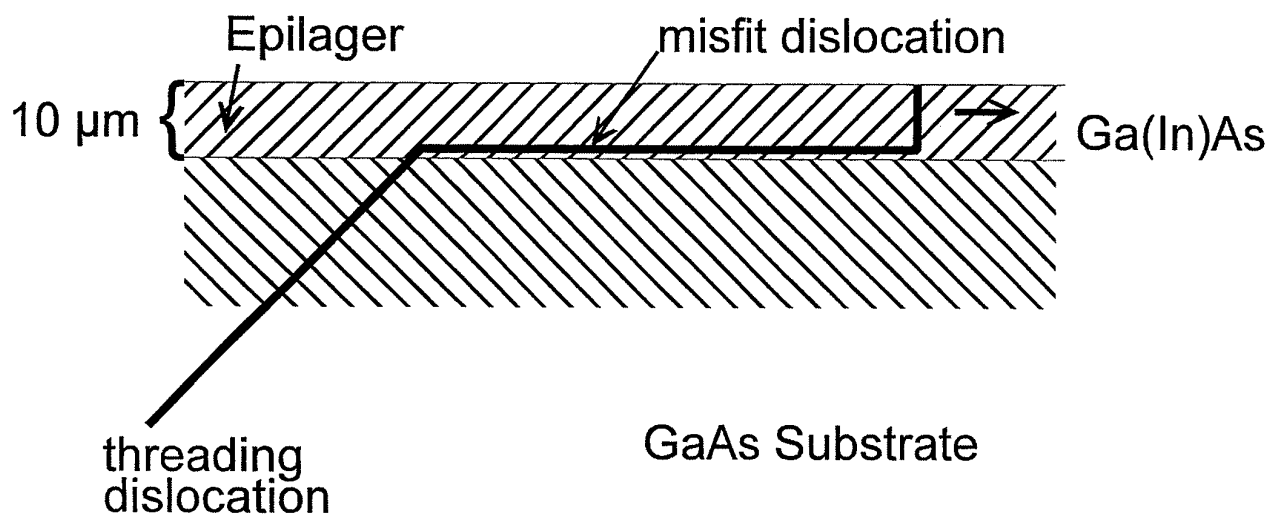
Section topography of tool diamond



Section topographs of tool diamond



Projection + section topographs of natural diamond for tools



Threading and misfit dislocations
10 μm Ga(In)As Epilayer on GaAs
substrate

HISTORY AND FUTURE OF SILICON CRYSTAL GROWTH

Takao Abe
Shin-Etsu Handotai
Isobe, Annaka, Gunma 379-0196, Japan

INTRODUCTION

By anticipating transformation from germanium to silicon, in 1950s Bell Telephone Laboratories and General Electric groups had finished most of the basic research focused on crystal growth methods (FZ, CZ and epitaxial), segregation and diffusion of every important impurities and finally variety of evaluation. It is surprising that their data are still useful without any correction. It is interesting to mention, that while the basic research on silicon had been completed in the United States, the starting point of silicon industry was at Siemens in Europe where the present mass production methods of poly silicon and FZ were developed. The rectifiers, diodes, transistors and thyristors produced by FZ single crystals were used for color TV, controllers of ShinKan-Sen etc. in Japan. From the invention of IC in 1970, the CZ method innovated by some inventors in the United States became the foundation of the present Japanese mass productions. 1 which have been brushed up by high level of quality controls.

It is widely recognized that the largest contribution to the present mass production of silicon is the Dash's necking process¹⁾ for dislocation-free crystals. With this process it is possible to grow larger diameter crystal without limitation and with higher growth rate compared to the dislocated growth. Another important factor in silicon, it was elimination of undesired light elements such as carbon, oxygen and heavy metal impurities. Oxygen was considered as a poison, but it has changed to a medicine since the emergence of the so called IG (intrinsic gettering) concept²⁾. Finally, after development of control method for these impurities, the grown-in defects consisting of point defects still remain in the present CZ crystals. These grown-in defects can be denoted as the fourth impurity.

In this paper, in addition to the main events of FZ and CZ crystal growth technologies the recent progresses of understanding on point defects and the new result of the annihilation experiment are introduced. Instead of the traditional bulk wafer, the hydrogen induced delamination (HID) technology³⁾ which may enable to realize the SOI Era is described together with two kinds of applications.

FZ ERA (1960s)

In early 1960's Siemens used vacuum in FZ process as an ambient for obtaining ultra high resistivity (over $1,000 \Omega \text{ cm}$) by boron evaporation effect for 25mm diameter. Then for resistivity control of several $10 \Omega \text{ cm}$, the core-doping method was applied where high concentration dopants such as boron or phosphorous are introduced in a slim

rod (~ 6mm) centered in a CVD polycrystal. The vacuum FZ method had been used for dislocated crystals up to 40mm in diameters. However, this method was not successful to grow dislocation-free crystals due to evaporated silicon particles spited back from RF coil surfaces to the floating melt zone. An argon ambient instead of vacuum was possible to do gas doping so that both problems of the long process time core-doping method and the spited back particles were solved. Dislocation-free technique by Dash's necking brought about 50mm diameter crystal growth. Variety of brand names of dislocation-free crystals such as Lopex, Perfex and Waso were supplied from several crystal growers. However, at the beginning dislocation-free crystals had two kinds of problems. One was the slippage lines in device processes which makes visible step lines. Second was the degraded device yields compared to that of the dislocated crystals. Afterward, it was found that the reason is due to lack of dislocations as gettering sites of point defects ⁴⁾ or/and heavy metals.

CZ ERA (1970~)

The CZ growth started in the United States at the same time where IC industry emerged. The CZ process is independent of the shape of poly crystals and does not need special skills for crystal growth comparing to the FZ process. The CZ pullers which included many innovative ideas were proposed. One of the most innovating things was the applications of a tungsten wire instead of a stainless steel shaft to pull a crystal. The wire system give always a right angle to the melt surface, no leakage of air, a machine simplification etc., which have seemed to overwhelm that of the shaft system. However, the author learned recently that in some European CZ pullers the shaft systems are still in use. That indicates that new technology is not always the only factor to be considered in production. In very near future, crystal weight increases very much. It is evident that Dash's necking with 3mm in diameter cannot support safely over a 150kg heavy ingot. New supporting system is required. Presently two systems are proposed. One system is necessary a bulge portion after Dash's necking to support large weight by some mechanical arms. Another is a dislocation free seeding process ⁵⁾. A dislocation and damage-free seed having pencil like shape tip is prepared. When the tip of seed contacts with melt, thermal shock is small due to small heat capacity and remelting of the seed starts. When desired diameter is reached, crystal diameter increases by lowering melt temperature. In principle we cannot find any other limitations for larger diameter crystal growth at present.

SOI ERA (2000~)

Discrete devices made by FZ crystal has been used as cut or lapped surfaces. IC devices have required mirror polished surfaces since 1970. However, the basic wafering process from slicing to final CMP (chemical mechanical polishing) has not been changed over last 25 years, although the diameter increased and quality controls such as oxygen concentration, flatness, particles etc. were progressed. Epitaxial wafers which had been used only for some discrete and bipolar devices are now substituting CZ wafers for the mainstream C-MOS technology. This is because the grown-in defects in CZ crystals as described in the previous section cannot be annihilated completely at

present. Accordingly, if the elimination of latch up effect by high boron doped epitaxial substrates is not considered, the epitaxial wafers do not offer a big advantage compared with the CZ wafers. However, the SOI wafers will give many advantages such as high speed, high density, high and low voltage, low power and radiation hardness. This is because the device active layer is completely isolated by an insulator. This concept of the SOI is opposite to that of the traditional bulk wafer. The HID technology³⁾ is the promising technology in this field.

SUMMARY

Depending on the customer's requests driven for example by expansion of multimedia world, diameter of CZ crystals will be increased and perfection of crystals improved. The former is according to the principle of economy and the latter is due to technology requirement. Device chip fabrications become already so-called equipment industry following the national roadmap. However, discrepancies from the roadmap are highly expected. The SOI technology is a kind of the off-roadmap technology.

REFERENCE

1. W. C. Dash, E. E. Gardner and W. K. Tice, : J. Appl. Phys., 29, 736 (1958)
2. T. Y. Tan, : Appl. Phys. Lett., 30, 175 (1977)
3. M. Bruel : Electronics Letters, 31, 1201 (1995)
4. N. J. Queisser, Solid State Electron., 5, 1 (1962)
5. T. Abe

A HISTORY AND FUTURE OF SILICON CRYSTAL GROWTH

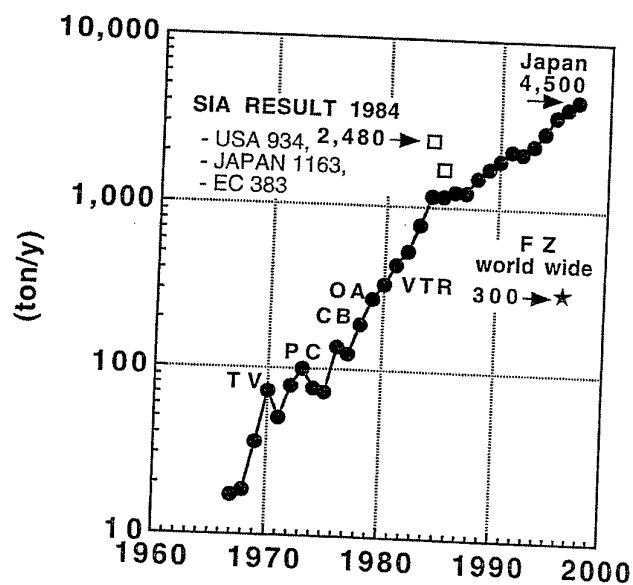
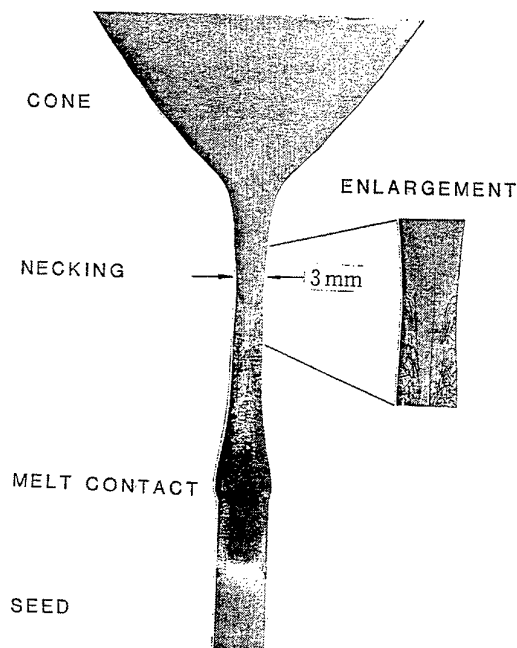
Takao ABE
Shin-Etsu Handotai

[CONTENTS]

1. FZ ERA *opened the history*
2. CZ ERA *has grown with IC*
3. SOI ERA *will go to fields*

ISCGT-1 '98

SILICON MASS PRODUCTION BY DASH NECKING



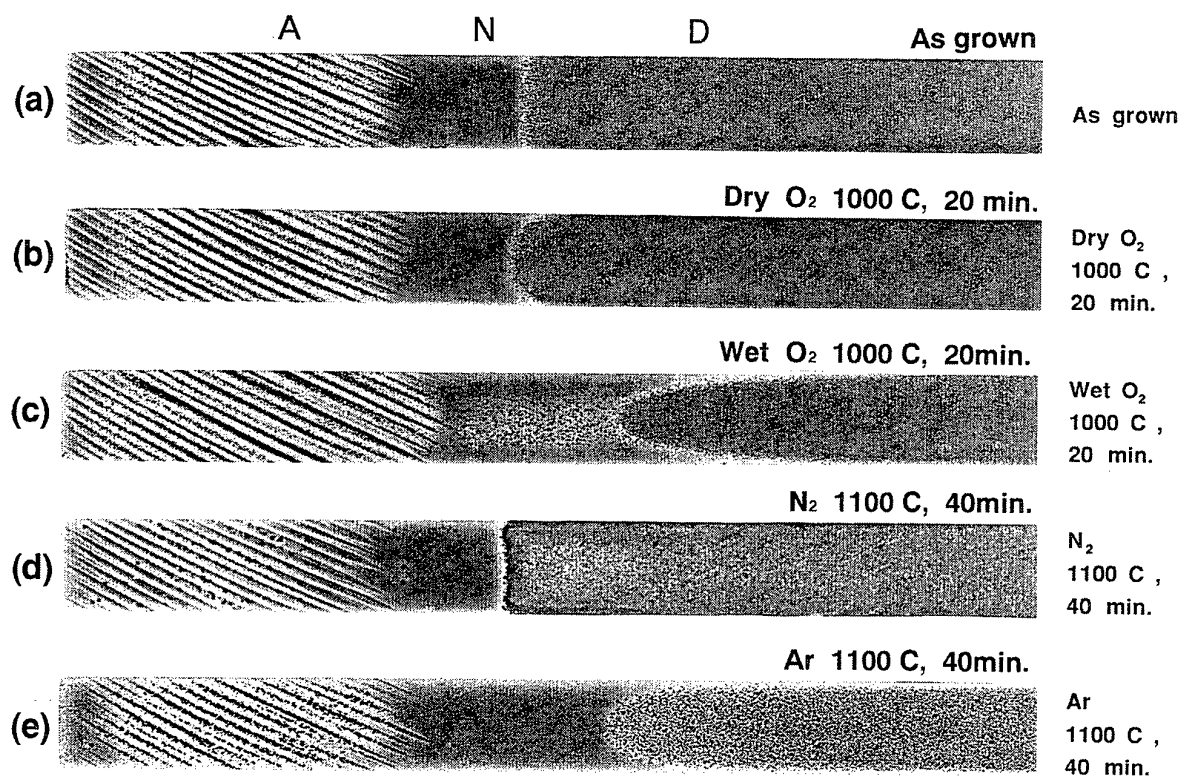
ISCGT-1 '98

FLOAT ZONE ERA

	1960s	1970s	1980s	1990s
Dia. (mm)	10 ~ 25	40	~	max 150
Ambient	Vacuum	Ar	→	N ₂ in Ar
Perfection	Dislocated	Dislocation - Free		
	Lineage/Twin	<ul style="list-style-type: none"> • A and D Defects → Defects - Free • Slippage → Tough Crystal 		
		<ul style="list-style-type: none"> • Striations (Phos.) → NTD (n, γ) reaction 		

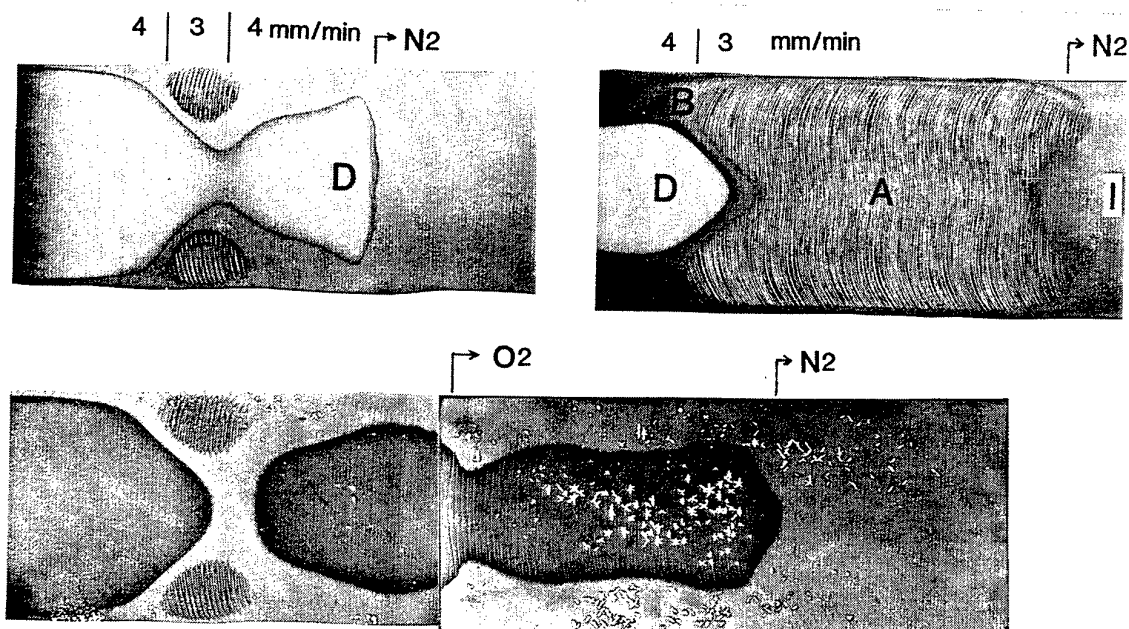
ISCGT-1 '98

GENERATION AND ANNIHILATION OF A- AND D-DEFECTS

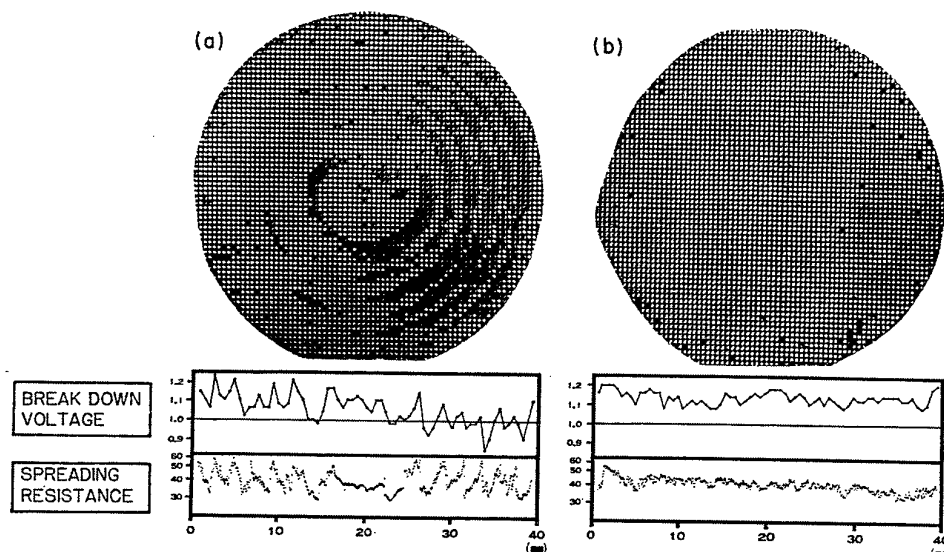


X-ray topographs of specimens after copper decoration. These specimens with thickness of 3 mm were annealed in various ambients and cut vertical to surface with thickness of 1 mm.

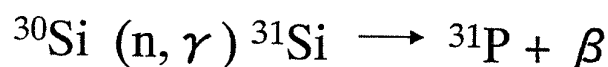
NITROGEN : SUPPRESSION ON SWIRLS / D-DEFECTS



TRANSISTOR YIELD / STRIATIONS



Neutron Transmutation Doping (NTD)



ISCGT-1 '98

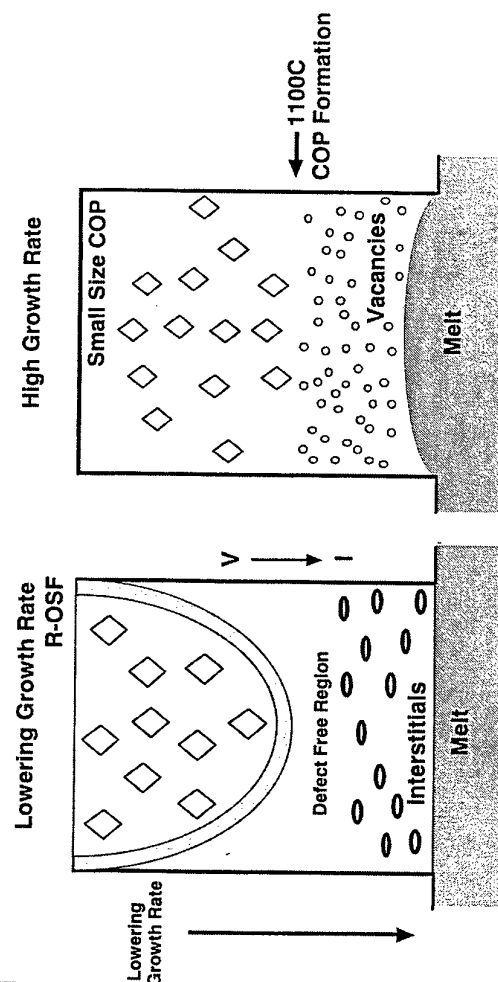
CZOCHEKRALSKI ERA

	1970s	1980s	1990s	2000s
Dia. (mm)	50 ~		~ 300	450
Modifications of Puller	Atmos. Press ↓ <i>Low Press.</i>	Shaft ↓ <i>Wire</i>	Melt Flow ↓ <i>Magnet</i>	Dash Neck ↓ <i>> DFS</i>
Subjects	• Carbon • Oxygen	• Heavy Metals ↓ OSF	• Point Defects ↓ <i>Ryuta et al. (1990)</i> COP / Void	LD × HGR ↓ <i>Mass Prod.</i>
Solutions	Intrinsic Gettering + Cleaning <i>Tan et al. (1977)</i>		HGR + RTA <i>COP /</i> <i>Roughness Free</i>	Low Cost + Thin Wafer <i>Sollar Cell</i>

DFS : Dislocation Free Seeding, NGR : high growth rate, LD : large diameter

ISCGT-1 '98

GROWTH RATE AND RELATED DEFECTS



Cryst. Dia. (mm)	Charged Weight (kg)	Crucible Size (inch)
200	100 ~ 150	22 ~ 24
300	300 ~ 400	32 ~ 36
400	600 ~ 800	40 ~ 48

Crystal Length is 1.2m

Silicon Symposium '98

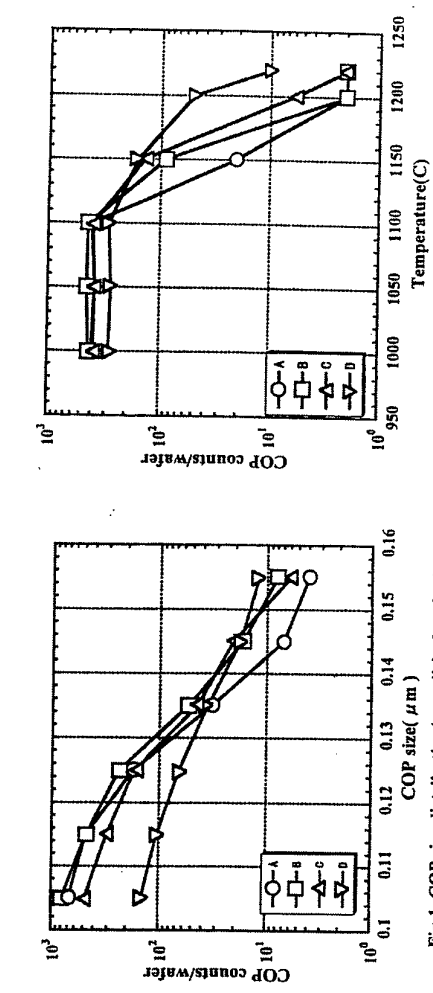


Fig.1 COP size distribution (as-polished wafers) depending on growth rate and oxygen concentration.

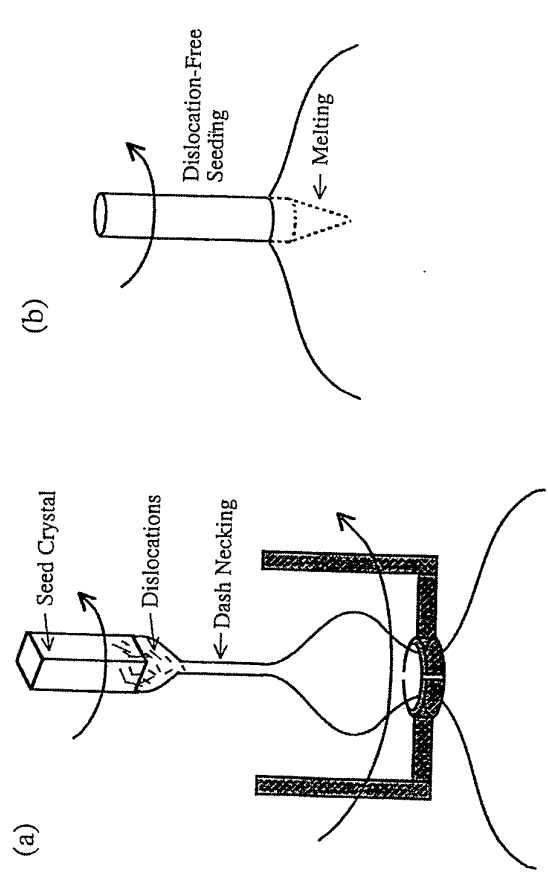
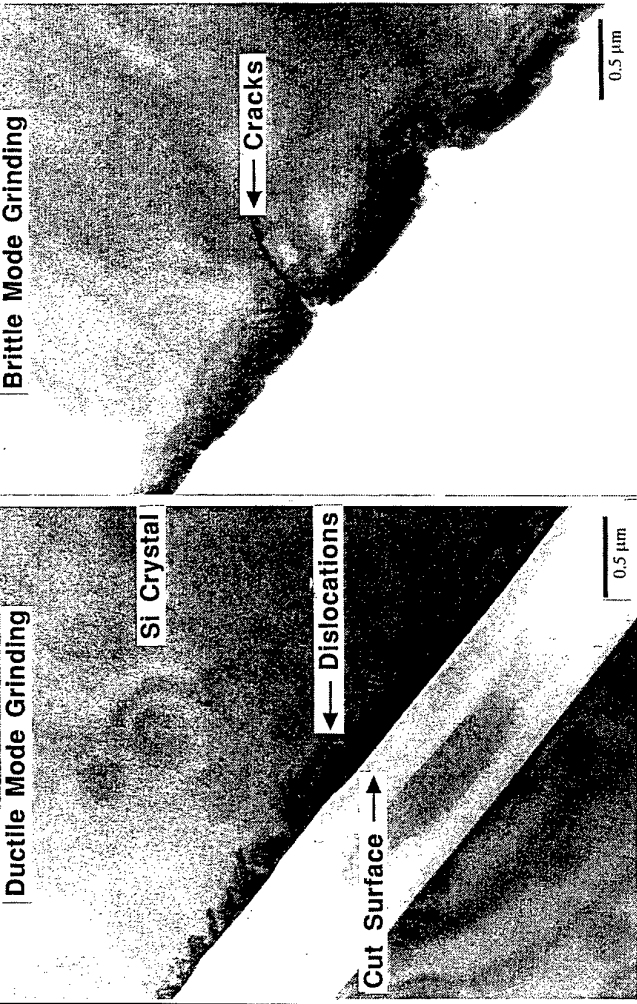


Fig.3 COP annihilation by RTA in H₂/Ar for 10sec COP counts means total COPs in the range of 0.1-0.2μm.

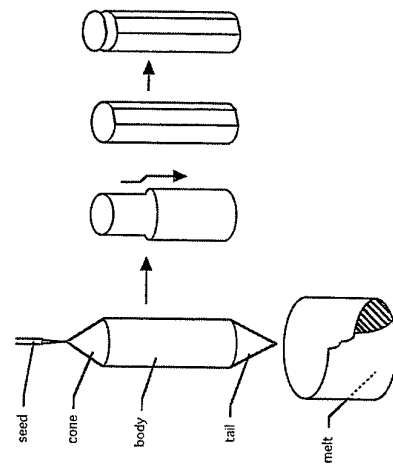


ISSUES ON WAFERING SOLUTIONS

1. SLICING	<ul style="list-style-type: none"> • ID saw → Wire saw • <i>to be innovated</i>
2. LAPPING	<ul style="list-style-type: none"> • Enlargement • Enlargement • Elimination
3. ETCHING	<ul style="list-style-type: none"> • <i>Surface Grinder (DMG)</i>
4. POLISHING	<ul style="list-style-type: none"> • DSP, Single Wafer • <i>PACE</i>

ISCGT-1 '98

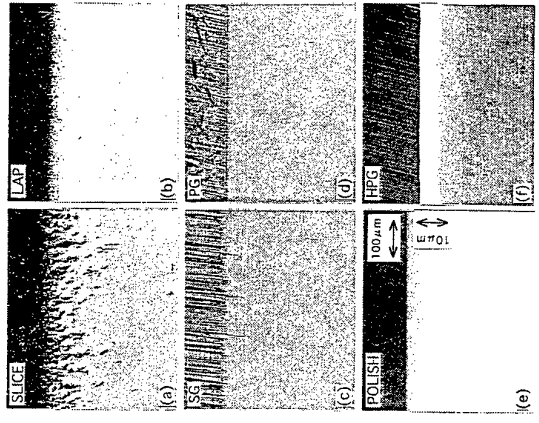
Material Loss in Growth Process



Material Loss in Wafering Process

Slice	Lap, Etch	Inspect,	Wafer
270-350 μm	Polish	100 μm	625 μm (dia. 150mm)
Material Loss			

Damage Depth Profiles : Angle Polishing and Etching

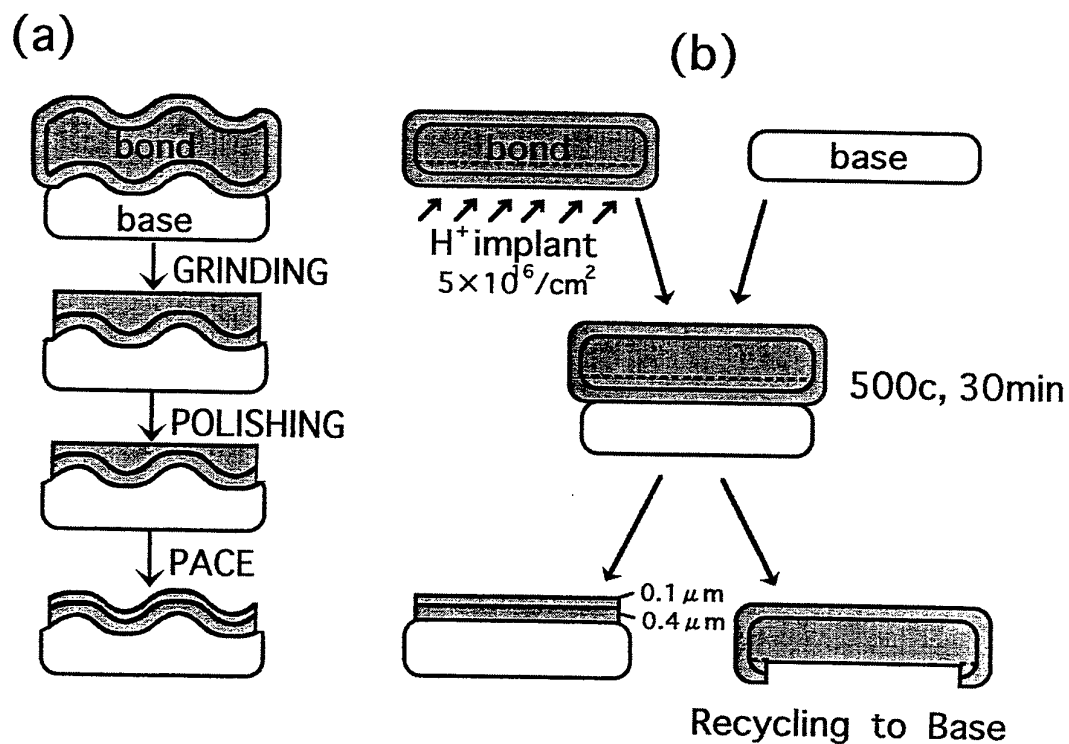


SOI ERA

	1960s	1970s	1980s	1990s	2000s
<u>SOS</u>	<i>Manasevit et al.</i> (1964)	Heteroepi on C-Zirconia, Spinel and CaF ₂			
<u>ZMR</u>	<i>Fa and Jew</i> (1966)	G-Heater, E-Beam and Laser		TFT-LCD a- /poly Si	
<u>SIMOX</u>		<i>Izumi et al.</i> (1978) ————— Itox —→			
<u>BSOI</u>	<i>Nakamura</i> (1961)	<i>Ikeda et al.</i> (1975)	<i>Lasky</i> (1986)	PACE (1992) →	Thick SOI for Power Devices
				Smart Cut® <i>Bruehl</i> (1995) →	All Electron Devices, TFT-LCD, 3D and Silicon Photonics

ISCGT-1 '98

PACE AND SMART CUT® PROCESSES

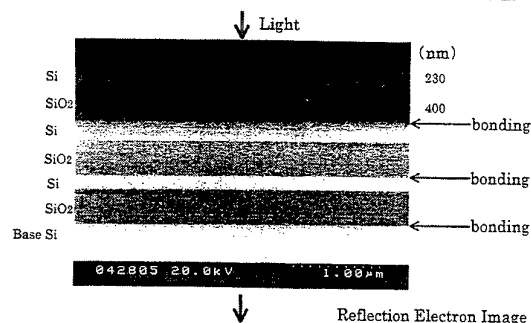


SUMMARY

1. FZ opened Silicon History and still increases Production.
2. CZ Diameter may have no Limit. Productivity becomes so Large. Not only LSI but Photovoltaic Use are also Possible.
3. SOI by Smart-Cut[®] will create New Fields. High Frequency with Low Power, TFT-LCD, 3D and Silicon Photonics.

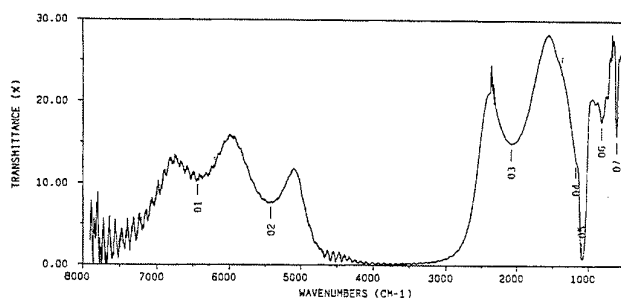
ISCGT-1 '98

PHOTONIC BAND GAP STRUCTURE BY SMART CUT[®]



Silicon Symposium '98

PHOTONIC BAND GAP BY THREE LAYERS BY SMART CUT[®]



Silicon Symposium '98

Striations: an intrinsic problem?

Hans J. Scheel

Cristallogenèse - IMO

Swiss Federal Institute of Technology

Chemin de Bellerive 34, CH-1007 Lausanne, Switzerland

Phone +41-21-693-4452; FAX +41-21-693-4750; e-mail Hans.Scheel@epfl.ch

Striations are defined as growth-induced inhomogeneities in the crystal which are either aligned along the growth surface, or which are related to the traces of macrosteps in case of faceted growth (1).

The detection limit of striations depends on the analytical method respectively on the application of the crystal. "Striation-free" may thus be defined in a specific case as not detectable by analytical or optical methods, or by the inhomogeneity being below the limit of being deleterious for the specific application. In a strict sense there are no absolutely striation-free crystals.

Striations have long been regarded as an intrinsic problem of crystal growth so that promising materials could not be developed for nonlinear-optic and electrooptic applications (2) and as substrates for optoelectronic devices based on III-V compounds (3). Since these growth bands were related to convective instabilities, efforts have concentrated to **reduce** buoyancy-driven convection by microgravity, and in case of semiconductors by application of magnetic fields, first 1980 at SONY to silicon, then by Terashima and Fukuda to Czochralski growth of gallium arsenide (4).

Striations are caused by differences of growth rates, either by growth rates fluctuating with time, or by lateral growth-rate differences along the growth interface.

The second cause of striations can be eliminated in the majority of growth situations by control of the interface shape, either by achieving a continuous curvature, or by achieving transition to faceting (5,6) thereby preventing macrosteps and growth instability.

In this talk we shall concentrate on the origin of striations due to temporal growth-rate fluctuations and their relation to the temperature distribution and to the hydrodynamic scene within the growth system. The critical parameters in designing growth processes for achieving striation-free crystals will be discussed and demonstrated by growth of homogeneous crystals of solid solutions, using **forced convection** and ultra-precise temperature control.

- (1) T. Kajimura, K. Aiki and J. Umeda, Appl. Phys. Lett. 30 (1977) 526-528.
- (2) H.J. Scheel and P. Günter, Ch. 12 in Crystal Growth of Electronic Materials, ed. E. Kaldis, Elsevier, Amsterdam 1985, 149-157.
- (3) K. Nakajima, J. Crystal Growth 125 (1992) 127-134.
- (4) K. Terashima and T. Fukuda, J. Crystal Growth 63 (1983) 423-425.
- (5) H.J. Scheel, Appl. Phys. Lett. 27 (1980) 70-72.
- (6) A.A. Chernov and H.J. Scheel, J. Crystal Growth 149 (1995) 187-195.

Striations: an intrinsic problem?

Hans J. Scheel

Cristallogénèse - IMO

Swiss Federal Institute of Technology

ch. de Bellerive 34, CH-1007 Lausanne, Switzerland

Introduction

Types of striations, inherent problem.

Segregation Phenomena

in melt solutions.

Approaches to solve striation problem by reduced convection and by forced convection.

Example: $\text{KTa}_{1-x}\text{Nb}_x\text{O}_3$ "KTN"

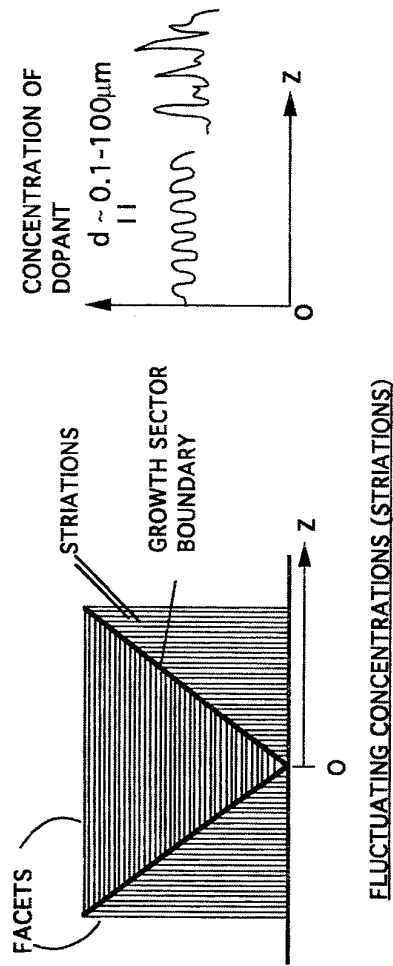
Theoretical analysis.

Technological approach (Forced convection & precise temperature control).

→ "Striations-free" KTN crystals.

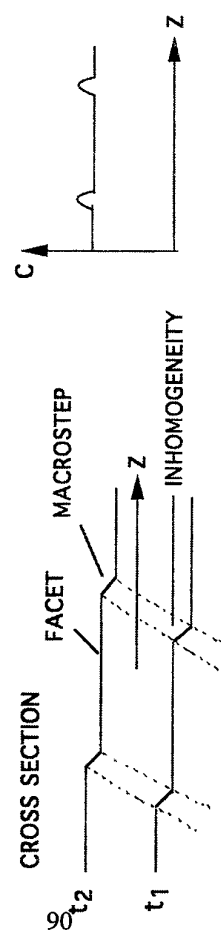
Conclusions / Striations Rules

CHEMICAL INHOMOGENEITIES IN DOPED CRYSTALS AND IN SOLID SOLUTIONS



FLUCTUATING CONCENTRATIONS (STRIATIONS)

ORIGIN • $k_{eff} \neq 1$ AND GROWTH RATE FLUCTUATIONS



LOCAL INHOMOGENEITIES AT SURFACE CORRUGATIONS AND MACROSTEPS

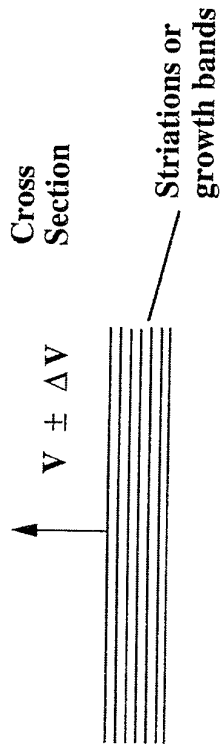
- ORIGIN
- DIFFERENT GROWTH MECHANISMS (GROWTH RATES) OF FACET AND OF MACROSTEPS
 - ACHIEVEMENT OF SINGLE GROWTH MECHANISM (e.g. REDUCE STEP BUNCHING BY APPLYING LOW SUPERSATURATION)
 - GROWTH ON FACETS

TRANSITION TO FACETING : APPL.PHYS.LETT. 3Z (1980) 70
 ATOMIC FLATNESS & STM : J. CRYSTAL GROWTH 60 (1982) 199

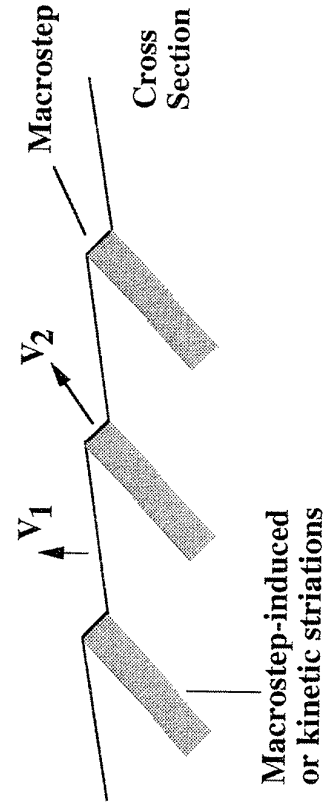
Definitions of Striations

Growth-induced inhomogeneities caused by

- temporal growth-rate variations



- lateral growth-rate differences due to macrosteps or partial faceting



Detection of striations :

- Optical absorption
- Refractive-index variation
- Strain birefringence (polarized light)
- Interferometry
- Etching & microscopy
- Electron microprobe
- X-ray topography
- Photoluminescence, cathodoluminescence

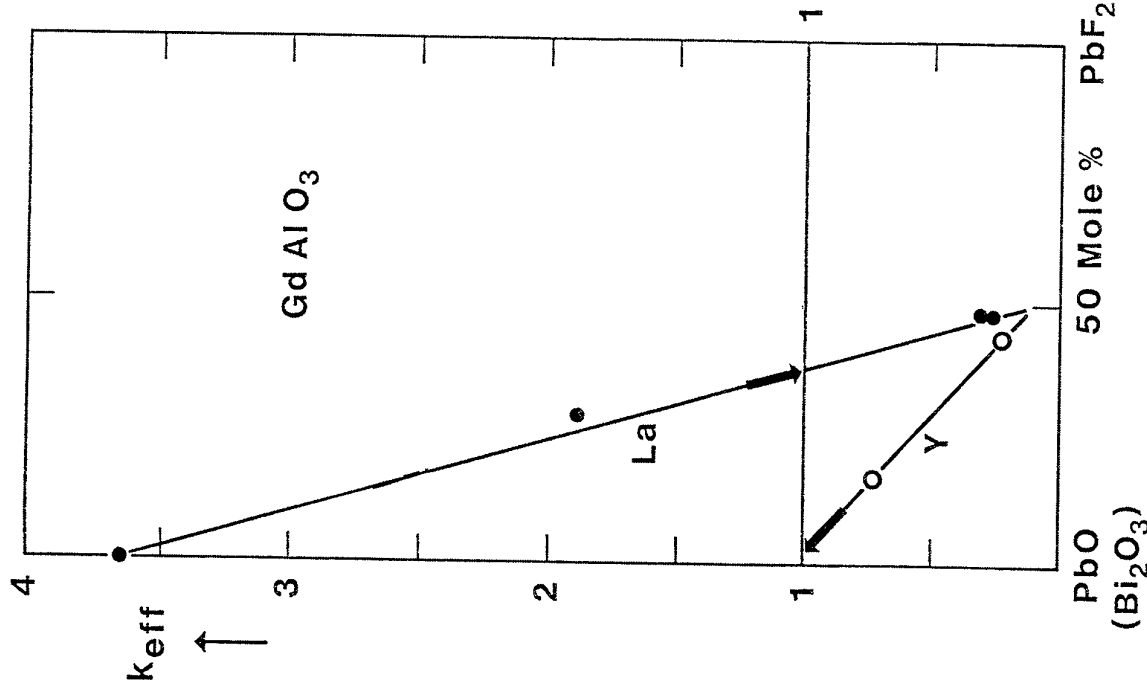
STRIATION PROBLEM

"Striations are present in all crystals of KTN"
H. Fay : Mat. Res. Bull. 2 (1967) 499.

.... "Inherent Striations in Ba₂Nb₅O₁₅ Crystals"
"Serious attempts to grow striation-free
Ba₂Nb₅O₁₅ crystals have not been successful so
that the use of this material is not widespread"
R.L. Byer: Ann. Rev. Mater. Sci. 4 (1974) 147.

"Because of the difficulties in growing very
homogeneous crystals, the availability of this material
(Ba₂Nb₅O₁₅) remains a problem....
Crystal growth is still harder with Sr_{1-x}Ba_xNb₂O₆.
The main problem is growth striations which can
hardly be avoided"
A. Räuber in 'Current Topics in Materials Science' vol. 1
(North-Holland 1978) 481.

"Growth striations are a more 'intrinsic' phenomenon
of the growth process itself. Consequently they cannot
be avoided completely"
P. Reiche, R. Schalge, J. Böhm, D. Schultze : Kristall
und Technik 15 (1980) 23.



$$k_{\text{eff.}} = \frac{k_0}{k_0 + (1 - k_0) \exp. \left(- \frac{v\delta}{D} \right)}$$

1

k_0 EQUILIBRIUM DISTRIBUTION COEFFICIENT (C_S/C_L)

v CRYSTAL GROWTH RATE

δ DIFFUSION BOUNDARY LAYER

D DIFFUSION COEFFICIENT

BURTON, PRIM, SLICHTER: J. CHEM. PHYS. 21 (1953) 1987

TEMPERATURE

HYDRODYNAMICS

(ROTATING DISC)

$$V \propto \frac{(n_\infty - n_e) \cdot D}{\rho_c \cdot \delta} \quad (2) \quad \delta = 1.6 D^{1/3} v^{1/6} \omega^{-1/2} \quad (3)$$

(FOR DIFFUSION-LIMITED GROWTH) $\delta = \left[0.463 \left(\frac{\eta}{\rho_D} \right)^{1/3} \left(\frac{\mu_D}{\eta x} \right)^{1/2} \right]^{-1} \quad (4)$

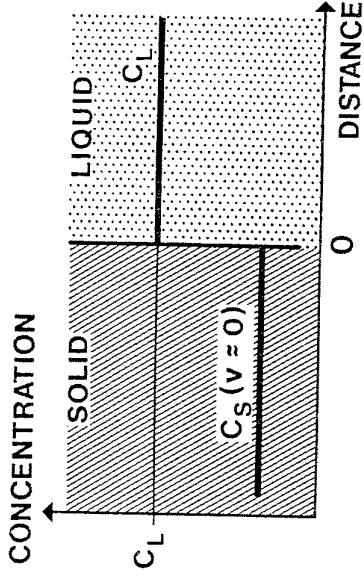
$(2) + (3) \quad (2) + (4)$

$V \propto \omega^{1/2}; \quad V \propto u^{1/2}$

($\Delta T \sim 1 - 5^\circ \text{C}$; $0.1 - 100^\circ \text{C}$ IN EXTREME CASES)

(2) inserted in (1) : $k_{\text{eff.}} \propto \frac{k_0}{k_0 + (1 - k_0) \exp. \left(- \frac{n_\infty - n_e}{\rho_c} \right)} \quad (5)$

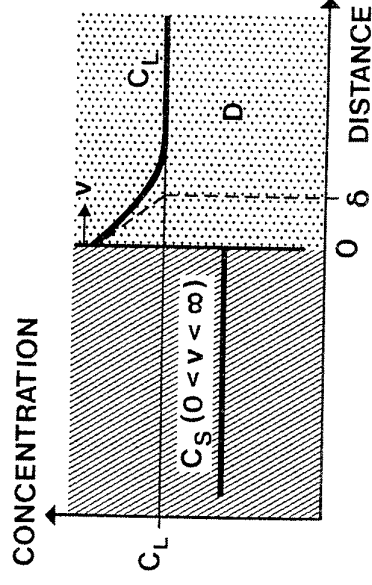
$k_{\text{eff.}} \propto \frac{k_0}{k_0 + (1 - k_0) \exp. (-\Delta T)} \quad (6)$



$k_0 < 1$
 $C_S/C_L \equiv k_0$
EQUILIBRIUM
 ($v \rightarrow 0$, OR
 COMPLETE MIXING)

$k_{\text{eff}} \rightarrow k_0$

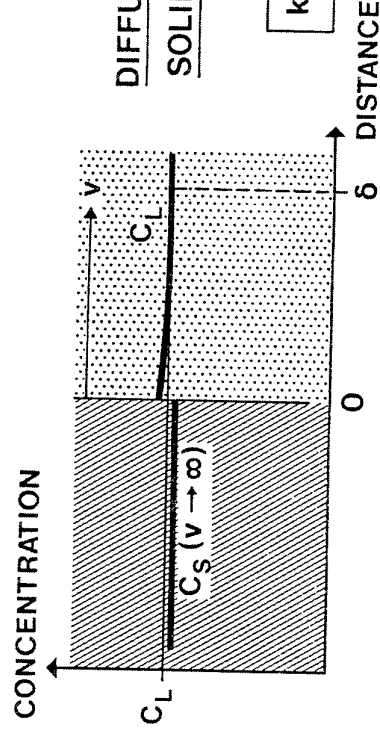
STEADY STATE



$k_0 < k_{\text{eff}} < 1$

DIFFUSION - LESS

SOLIDIFICATION



$k_{\text{eff}} \rightarrow 1$

Forced Convection to Suppress Striations

1. Continuous Flow

- Along a plate or crystal face
- Towards a rotating disc (Cochran or Ekman flow)

2. Alternating Flow Direction or Velocity

- Reciprocating crystals in growth from aqueous solutions
- Accelerated crucible rotation technique ACRT in growth from high-temperature solutions (H.J. Scheel, E.O. Schulz-DuBois 1971, 1972) in Bridgman growth A. Horowitz et al. 1983 in hydrothermal growth for AlPO_4 1983 ICCG-7

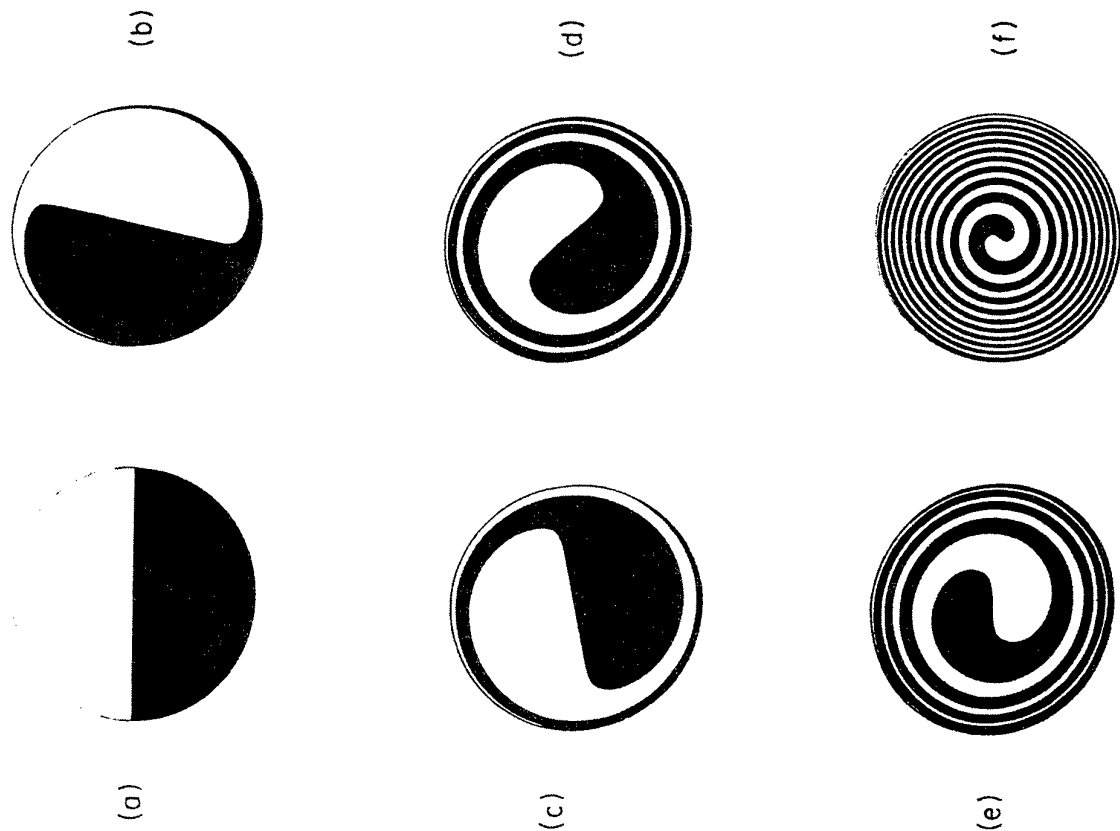
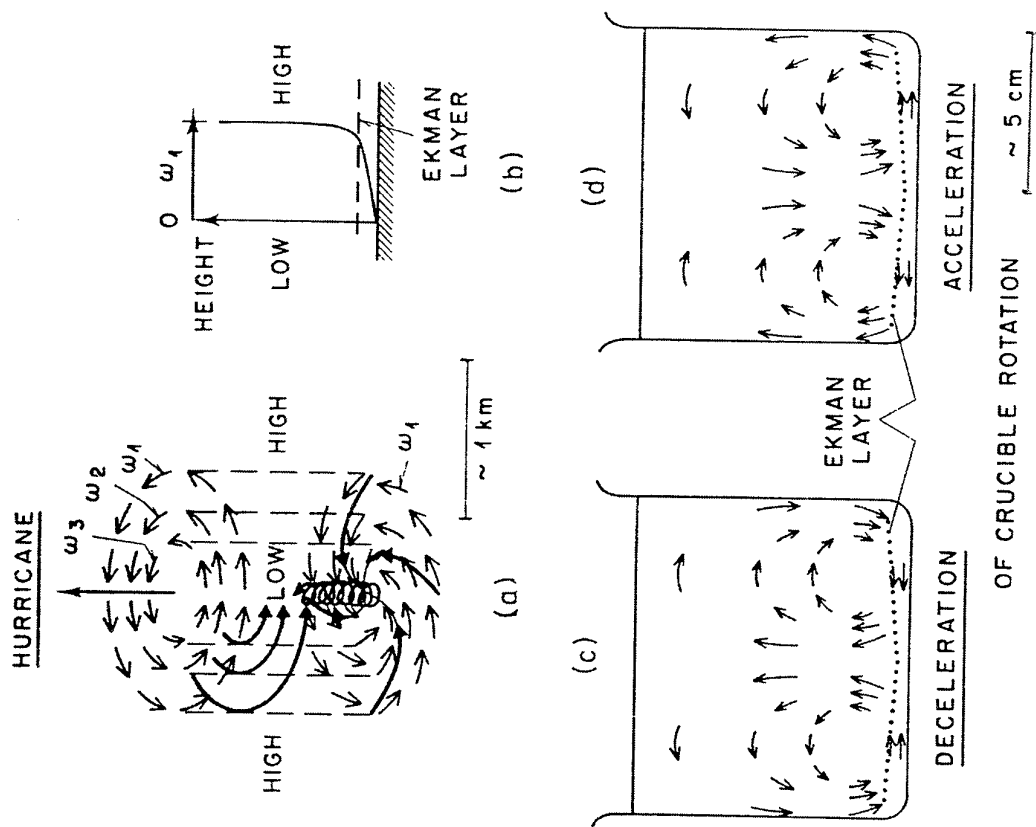
3. Vibrations : R. Feigelson et al. 1987; E. V. Zharikov 1995.

Striations are caused by fluctuations of the growth rate which originate from temperature fluctuations.

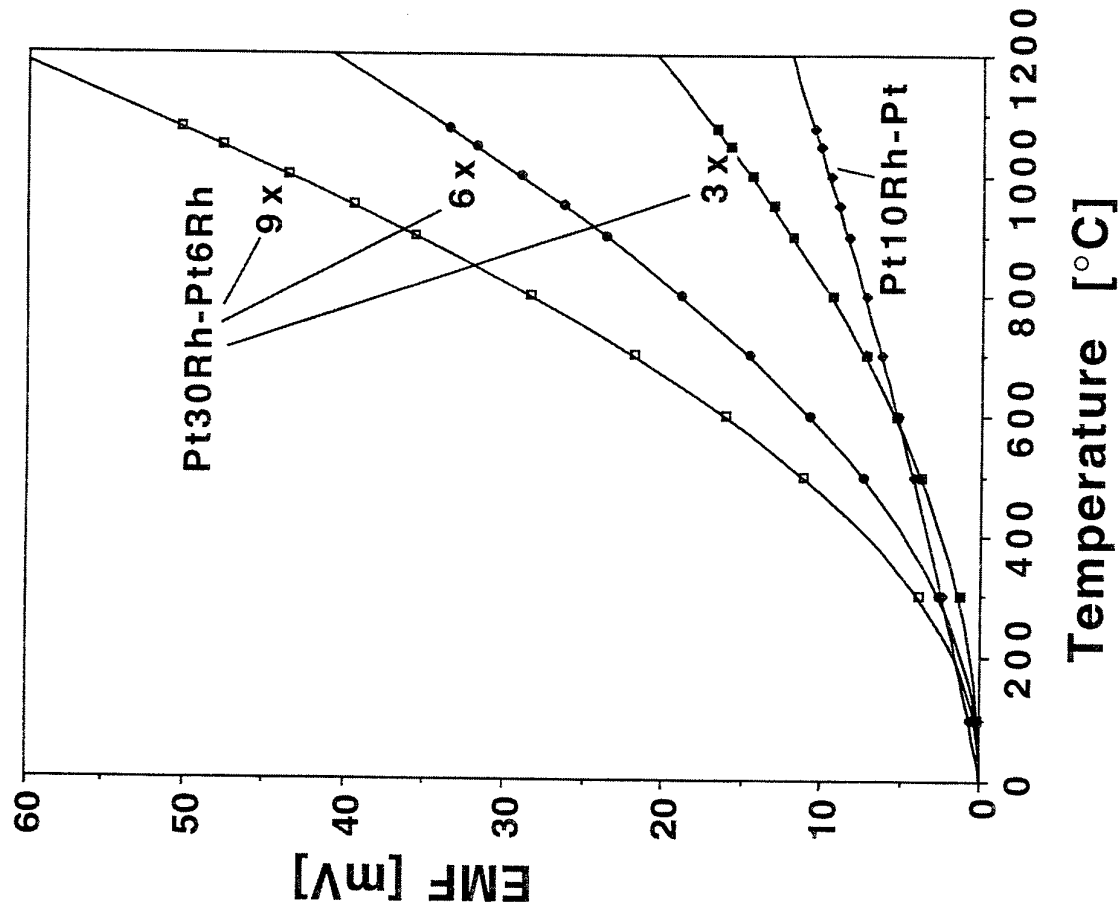
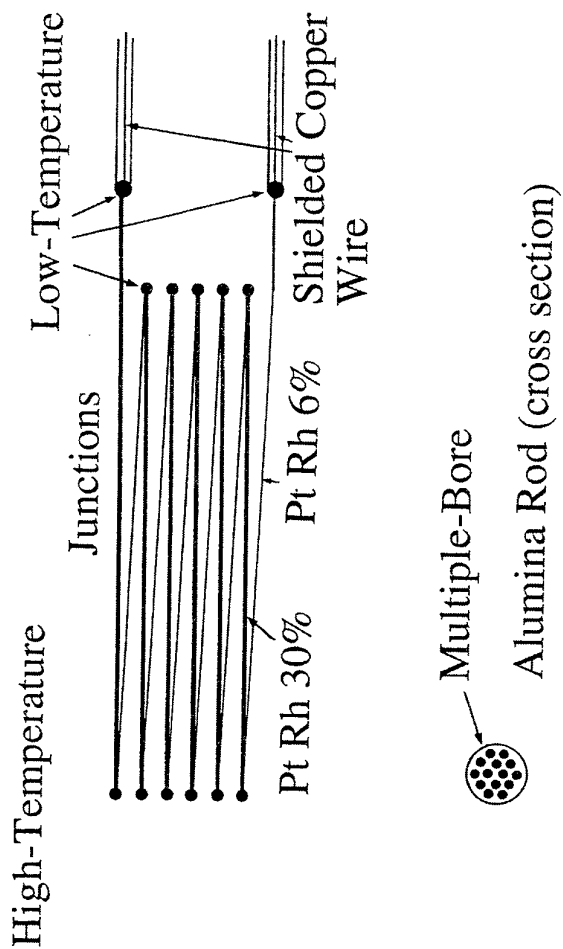
Note: Hydrodynamic fluctuations of isothermal melts or solutions do not cause striations!

Ekman layer flow in hurricanes, in ACRT, and in a glass of tea with tealeaves

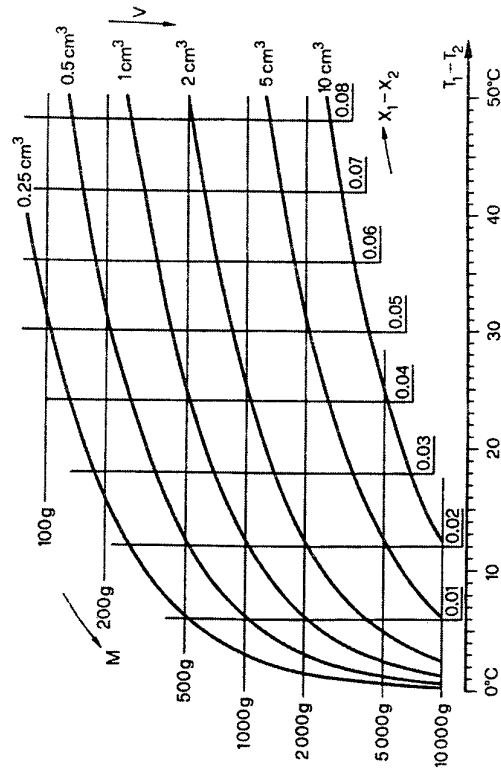
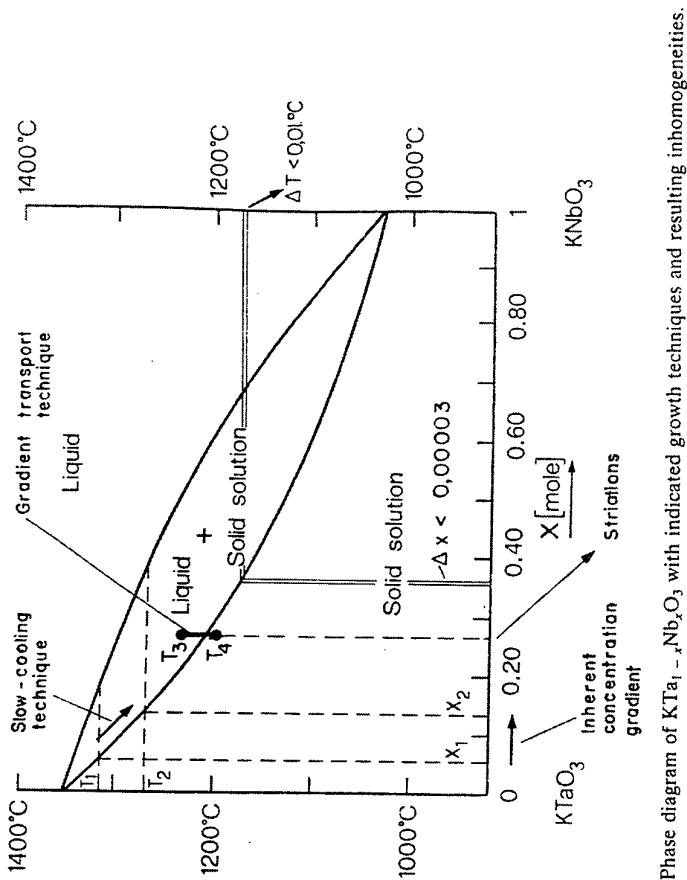
Accelerated crucible rotation technique ACRT



Thermocouples



Temperature Control



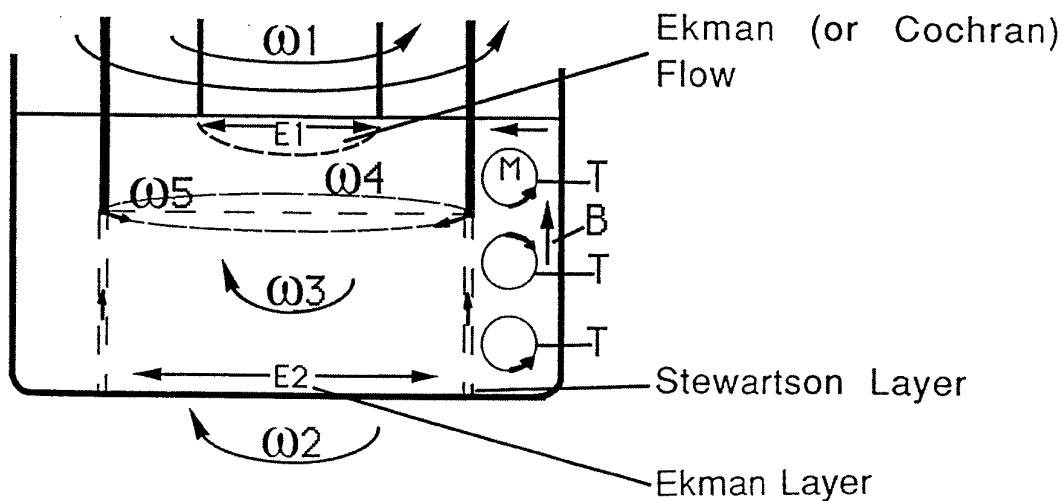
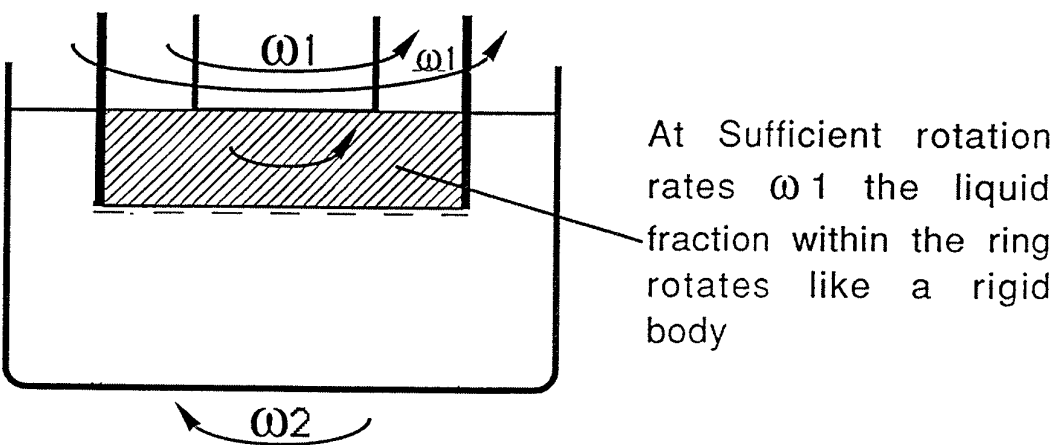
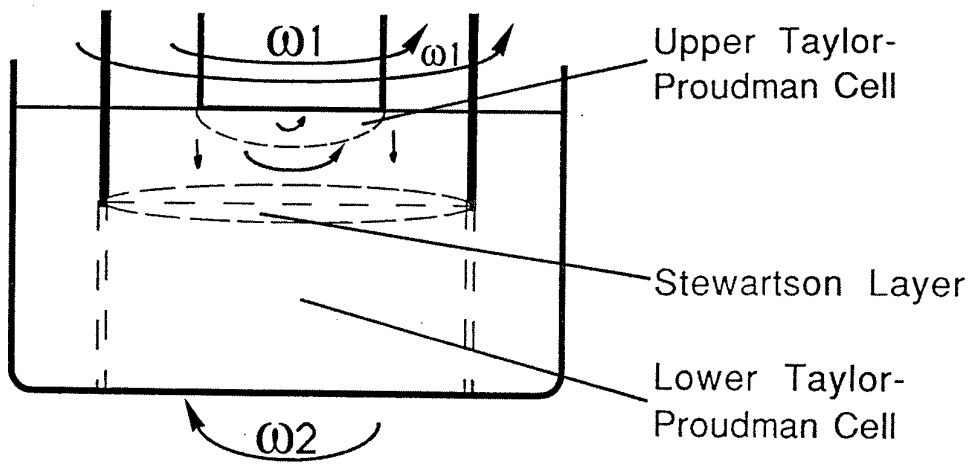
Plot of crystal size V and inhomogeneity $x_1 - x_2$ as a function of experimental parameters (mass of melt M and cooling interval $T_1 - T_2$). A numerical example is detailed in the text.

Sensitivity [$\mu\text{V}/^\circ\text{C}$] of Thermocouples	at 25°C	at 1400°C	$\Delta T/T$
Pt - Pt90Rh10	6	12.0	$\sim 10^{-4}$
Pt94Rh6 - Pt70Rh30	< 0.07	10.5	$\sim 10^{-5}$
Thermopile of 10 Pt94Rh6 - Pt70Rh30 Thermocouples*	< 0.6	105	$\sim 10^{-6}$

*H.J. Scheel, C.H. West : J. Phys. E: Scientif. Instr. **6** (1973) 1178.
D. Elwell, H.J. Scheel : Crystal Growth from High-Temperature Solutions, ch. 7.
Academic Press, London-New York 1975, reprint by Dover, New York 1997.

Co-rotating ring Czochralski

CRCZ



Conclusions

The precise conditions for growth of specific solid solutions have to be derived theoretically.

Efficient / economic growth of homogeneous crystals requires forced convection & extremely precise temperature control.

The striation problem is resolvable.

Conditions for Growth of Striation-Free Crystals

1. Flat (smooth) Growth Surface
 2. Isothermal Growth Surface
 3. Homogeneous Melt or Solution
 4. Constant Growth Rate
-

Hydrodynamic Fluctuations are not harmful.

Forced Convection and ACRT can Assist to Homogenize the Melt or Solution.

ROLE OF STRUCTURAL CHARACTERIZATION IN DEVELOPMENT OF LARGE-DIAMETER SILICON

Krishan Lal

*National Physical Laboratory,
New Delhi - 110012, India.*

Structural Characterization of Large-Diameter Silicon: The size of important semiconductor crystals like silicon is continuously increasing due to technical as well as economic considerations. The increase in sizes calls for suitable changes in techniques of crystal growth, special handling of large mass boules and wafers, and modifications in wafer cutting as well as surface preparation technology. It is expected that for advanced applications more stringent conditions may be imposed on orientations of wafers. Due to changes in thermal parameters in growth chambers, a detailed evaluation of structural perfection and particularly characterization of residual point defects and their clusters would be desirable. Also, the residual stresses would lead to bending of wafers and general degradation of perfection. Structural characterization techniques have to meet these challenges and provide requisite information to those involved in production as well as the user community. There are a series of structural techniques available to serve this purpose including electron optical methods (TEM and SEM), scanning tunnelling microscopy, atomic force microscopy and high resolution X-ray diffraction techniques. Due to their non-destructive nature and capacity to directly investigate large volumes of crystals high resolution X-ray diffraction techniques find wide-ranging applications. In this lecture applications of these techniques will be discussed.

High Resolution X-ray Diffraction Techniques: These are extensively used for evaluation of crystalline perfection of single crystals (bulk as well as thin films); accurate determination of crystallographic orientation of flat surfaces and straight edges (flats); accurate measurement of lattice parameter; measurement of curvature or bending of crystal wafers; biaxial stress and strain in thin films; and lattice mismatch and orientational mismatch between epitaxial films and their single crystal substrates.

Multi-crystal X-ray Diffractometers: By using dynamical theory of X-ray diffraction from perfect crystals, diffraction curves (rocking curves) can be conveniently calculated for parallel and monochromatic exploring X-ray beams. To realise a nearly perfect exploring X-ray beam ($\Delta\lambda \cong 0$; $\Delta\theta \cong 0$), combinations of high brilliance small focus sources, mechanical collimation, and a series of diffraction from selected lattice planes of nearly perfect crystals are employed in multicrystal X-ray diffractometers. In author's laboratory a series of multicrystal diffractometers have been developed. The most advanced among these is a Five Crystal X-ray Diffractometer, with state of the art level resolution. The first three crystals of this diffractometer are collimator-

monochromators. The specimen is generally the fourth crystal. The fifth crystal is used as an analyser crystal. Diffraction curves recorded with this system have shapes and half widths very close to those expected theoretically. Therefore, this system enables observation and characterization of all types of crystal defects. Following experiments can be performed on this system: diffractometry, topography, diffuse X-ray scattering measurements, measurement of curvature of crystal wafers and determination of biaxial stress in thin films, accurate determination of lattice parameter, lattice mismatch and orientational mismatch between epitaxial films and their substrates, accurate determination of crystallographic orientation (crystal surfaces, and straight edges) and measurement of absorption coefficient of crystals for X-rays (normal and anomalous). Applications of multicrystal diffractometers will be described.

Evaluation of Crystalline Perfection and Characterization of Crystal Defects:

Boundaries in a crystal manifest as multiple peaks in diffraction curves, each peak representing a separate grain/subgrain. The angular separation between peaks directly gives the tilt angles, characterizing the boundaries. Recently, it has been observed that multicrystal diffractometers can reveal subgrain boundaries with tilt angles of less than a arc min. High resolution equipment enables direct observation of these very low angle boundaries. Dislocations in nearly perfect crystals (densities $\leq 10^6 \text{ cm}^{-2}$) can be directly imaged in X-ray diffraction topographs (traverse and section). By recording topographs with different diffraction vectors the nature of dislocations (edge, screw, or mixed) can be determined. Even those dislocations, which do not intersect the surface of the crystal, are imaged. It is possible to simulate images of dislocations in section topography. With multicrystal X-ray diffractometers even small disturbance produced by dislocations at large distances (~1 mm) from dislocation core can be imaged directly. Examples of dislocations in technologically important materials like GaAs, diamond, sapphire, garnets etc will be discussed. Presently, large quantities of single crystals are being prepared which are free of dislocations (e.g. Si). Even these crystals are not ideally perfect as at all finite temperatures there are point defects and their aggregates, a thermodynamical requirement. Characterization of point defects and their aggregates in otherwise perfect crystals is a challenging task as their concentrations are low and these produce very small disturbances in the lattice. High resolution diffuse X-ray scattering measurements have been extensively used to characterize point defects in as grown heat-treated and implanted silicon crystals. It is possible to differentiate between predominant defects in silicon crystals grown by the float zone and the Czochralski methods. In recent times an extended version of this method, named as reciprocal lattice imaging is being widely used.

Determination of Crystallographic Orientation: For most applications of single crystals it is necessary to specify the tolerable angle between the visible surface and the desired set of lattice planes. For single crystal wafers, additional information about orientation of straight edges or flats is necessary. With high resolution X-ray diffraction techniques it is possible to determine orientation of flat surfaces with unprecedented level of accuracy of ± 6 arc sec. An X-ray diffraction topographic method enables determination of orientation of straight edges with accuracy of a few arc min. Both these techniques are expected to play a significant role in preparation of large size crystals of silicon with well defined orientation.

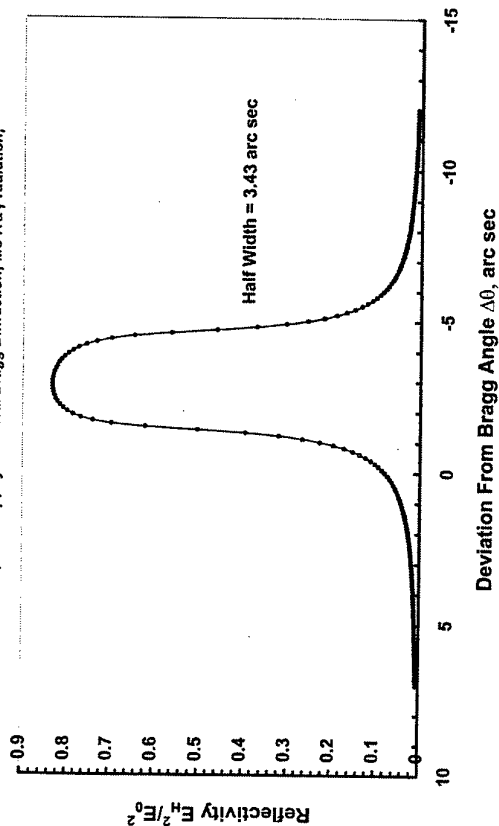
Determination of Lattice Parameter: Accurate value of lattice parameter can be determined by using the Bond method. Nearly parallel and monochromatic exploring beam of multicrystal X-ray diffractometers is of great value for accurate determination of lattice parameter. It is possible to reduce measurement uncertainty to ppm level or less. Generally, control of temperature and vibrations in the ambience are the parameters, which limit the accuracy of these measurements.

Bending or Curvature Measurements: Wafers of large diameter silicon crystal will have fairly large masses and this will cause bending of wafers under their own weight and other complications associated with mounting or fixing these at different locations for device fabrication. In addition, there is bending due to residual stresses, which has to be kept at low acceptable levels. Oxygen is an important impurity, which produces stress. High resolution X-ray diffraction techniques can be employed to accurately measure curvature of single crystal wafers. Essentially a traverse topography arrangement is utilised. The variation in orientation of diffraction vector is measured as a function of the linear position of the specimen across the exploring X-ray beam, which yields the value of the radius of curvature. Very large radii of curvature of ~30 km can be measured by using advanced diffractometers.

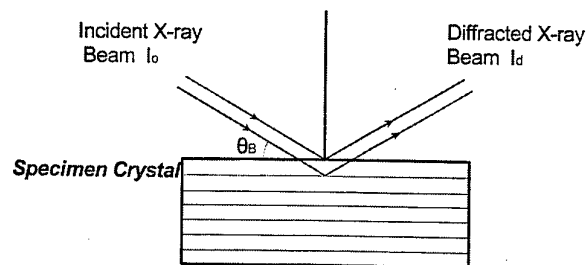
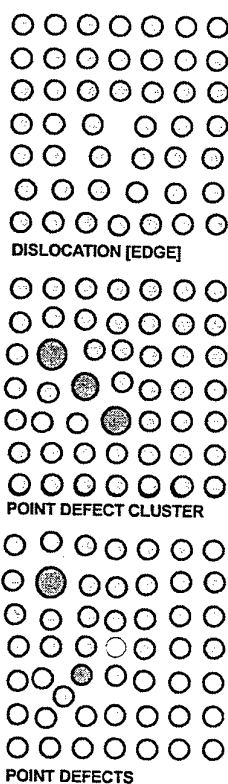
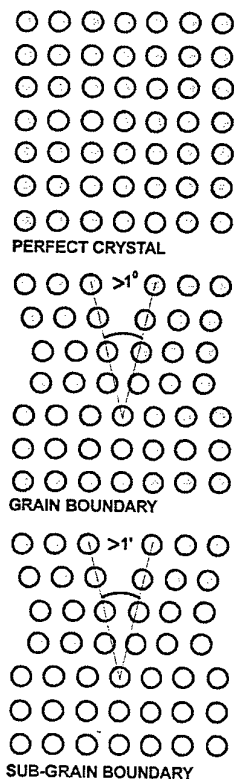
References:

1. H. R. Huff and R. K. Goodall, *Solid State Phenomena* **47-48**, 65 (1996)
2. W. M. Bullis and W. C. O'Mara, *Solid State Technology* April, 59 (1993)
3. W. v. Ammon, *Solid State Phenomena* **47-48**, 97 (1996).
4. B. W. Batterman and H. Cole, *Rev. Mod. Phys.* **36**, 681 (1964).
5. N. Kato, *J. Acta Cryst.* **A48**, 834-841 (1992).
6. A. R. Lang, *J. Appl. Phys.*, **29**, 597 (1958); and in *Modern Diffraction and Imaging Techniques in Materials Science*, S. Amelinckx, R. Gevers, G. Remant and L. Landyut (Eds.), North-Holland, Amsterdam, p. 407.
7. B.K. Tanner, *X-ray Diffraction Topography*, Pergamon Press, Oxford (1976).
8. Krishan Lal in *Crystalline Materials : Growth and Characterization*, R. Rodriguez -Clemente and C. Paorici (Eds.), Trans. Tech. Pub., Zurich, (1991), p. 205.
9. Krishan Lal, *Bull. Mater. Sci.*, **16**, 617 (1993).
10. M. A. Krivoglaz, *Theory of X-ray and Thermal Neutron Scattering by Real Crystals*, Plenum Press, New York (1969).
11. P.H. Dederichs, *J. Phys. F* **3**, 471 (1973); *Phys. Rev.* **B4** 1041 (1971).
12. R. R. Ramanan, G. Bhagavannarayana and Krishan Lal, *J. Crystal Growth*, **156**, 377 (1995).
13. Krishan Lal in *Semiconductor Devices*, Krishan Lal (Ed.), Narosa Publishers, New Delhi, p.243. (1996).
14. Krishan Lal and S. Niranjana N. Goswami, *Rev. Sci. Instr.* **59**, 1409 (1988).
15. Krishan Lal, G. Bhagavannarayana, Vijay Kumar and S.K. Halder, *Meas. Sci. and Tech.*, **1**, 793 (1990).
16. Krishan Lal, S. Niranjana N. Goswami, J. Wurfl and H. L. Hartnagel, *J. Appl. Phys.* **67**, 4105 (1990).

Theoretical Diffraction Curve
Silicon, 111 Refl; Symmetrical Bragg Diffraction; Mo K α_1 radiation;



Page 1

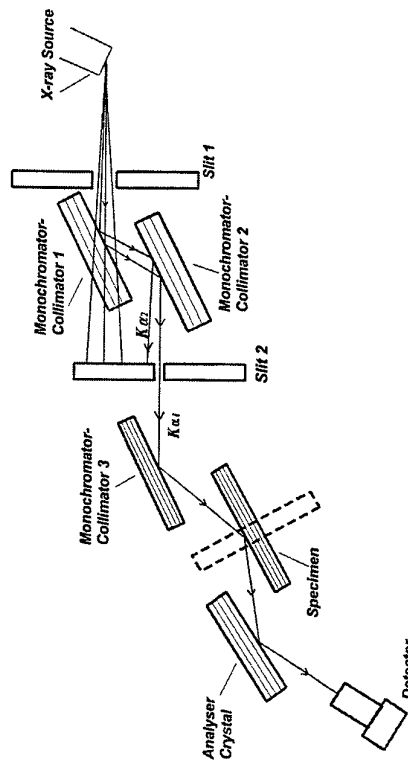


$$2d \sin \theta_B = n\lambda$$

Incident X-ray Beam:
Parallel $\Delta \theta = 0$;
Monochromatic $\Delta \lambda = 0$.

$$I_0/I_d = ?$$

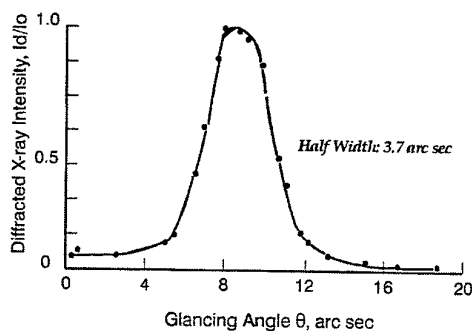
Angular range of diffraction = ?



FIVE CRYSTAL X-RAY DIFFRACTOMETER

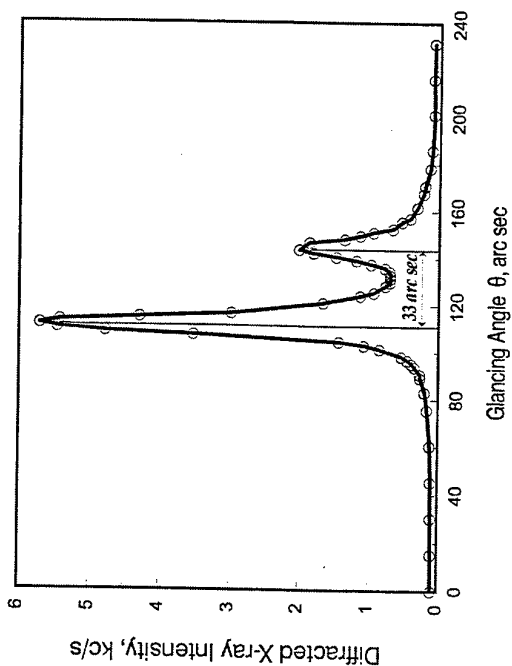
HIGH RESOLUTION X-RAY DIFFRACTION CURVE RECORDED WITH THE FIVE CRYSTAL X-RAY DIFFRACTOMETER

(111) Silicon Crystal Specimen; (111)
Diffracting Planes;
MoK α Radiation;
(+,+,+,+,+) Configuration.



Characterization of Very Low Angle Boundaries High Resolution X-ray Diffractometry

(100) Bismuth Germanate Crystal; Double Crystal X-ray Diffractometer; 400 relp; (+,-) configuration ; MoK α_1 radiation; Symm. Bragg geometry.



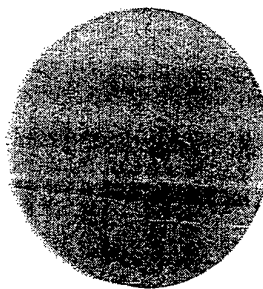
CHARACTERIZATION OF DISLOCATIONS

High Resolution X-ray Diffraction Topography
Nearly Perfect Gallium Arsenide Crystal

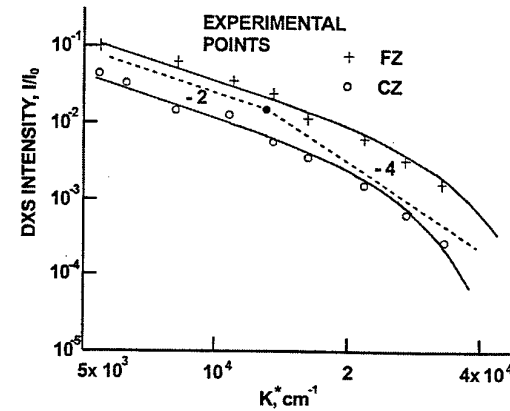


CHARACTERIZATION OF NEARLY PERFECT SINGLE CRYSTALS

High Resolution X-ray Diffraction Topography
Dislocation Free Silicon Crystal



Characterization of Point Defects and Their Aggregates in Nearly Perfect High Purity Silicon Crystals Grown by Czochralski and Float zone Techniques



Ramanan, Bhagavannarayana and Lal, *J. Crystal Growth* 156, 377(1995)

CHARACTERIZATION OF POINT DEFECTS AND THEIR CLUSTERS BY DIFFUSE X-RAY SCATTERING MEASUREMENTS

High Purity (10 kΩ) Nearly Perfect Crystals of Silicon Grown by the Czochralski (Cz) and the Float Zone (FZ) Methods

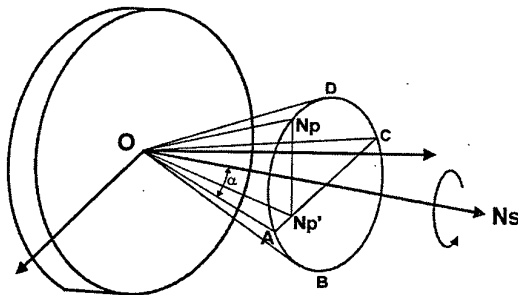
Values of Radius of Cluster R_{cl} , Volume per Cluster A_{cl} , and Number of Defects per Cluster N_{cl}

Specimen	Cluster Radius R_{cl} (μm)	Volume of Cluster A_{cl} (cm^3)	Number of Defects per Cluster N_{cl}	Nature of Defect
Cz	0.8	2.02×10^{-16}	1.26×10^6	Interstitial
FZ	0.6	1.32×10^{-16}	8.3×10^6	Vacancy

Ramanan, Bhagavannarayana and Krishan Lal, *J. Cryst. Growth*, 156 (1995) 377-382.

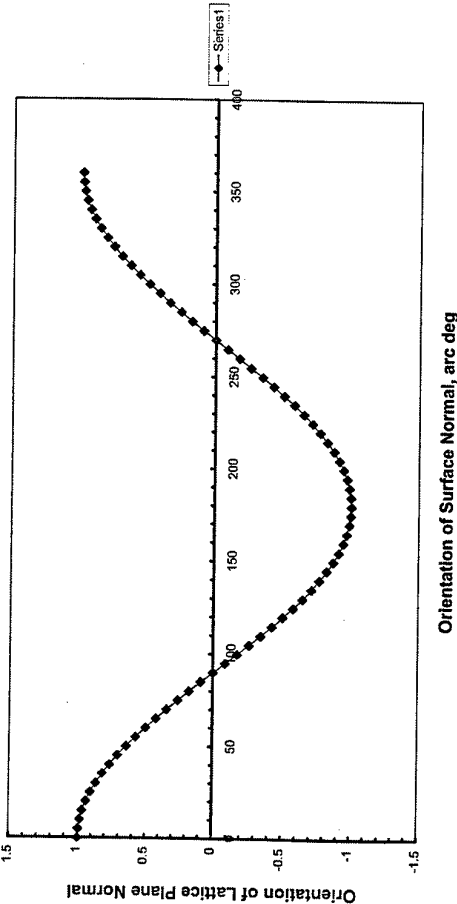
DETERMINATION OF ORIENTATION - FLAT SURFACES

High Resolution X-ray Diffraction Method

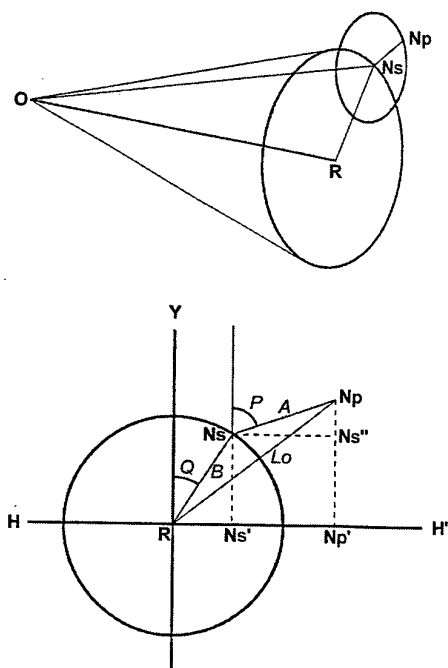


Lal et al, *Meas. Sci. Tech.* 1, 793(1990)

Orientation of Normal to Lattice Planes as a Function of Orientation of Surface Normal



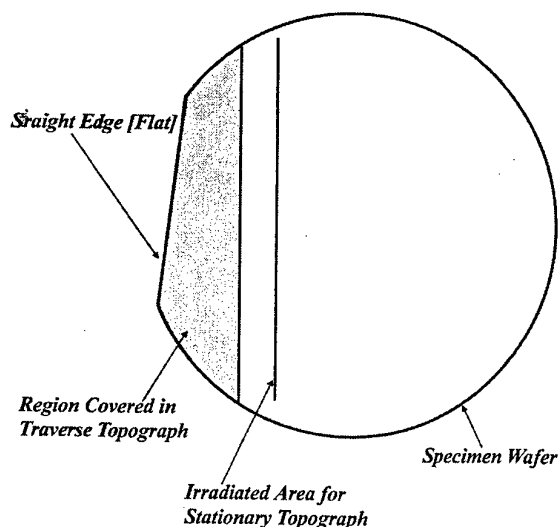
**DETERMINATION OF ORIENTATION
- FLAT SURFACES**
High Resolution X-ray Diffraction Method



Lal et al, Meas. Sci. Tech. 1, 793(1990)

**DETERMINATION OF ORIENTATION
- STRAIGHT EDGES [FLATS]**

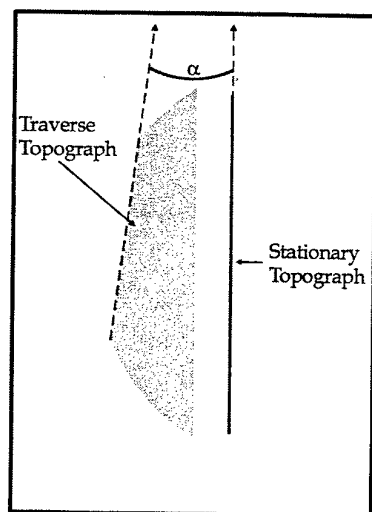
X-ray Diffraction Topographic Method



Lal and Goswami, Rev. Sci. Instr. 59, 1409(1988)

**DETERMINATION OF ORIENTATION
- STRAIGHT EDGES [FLATS]**

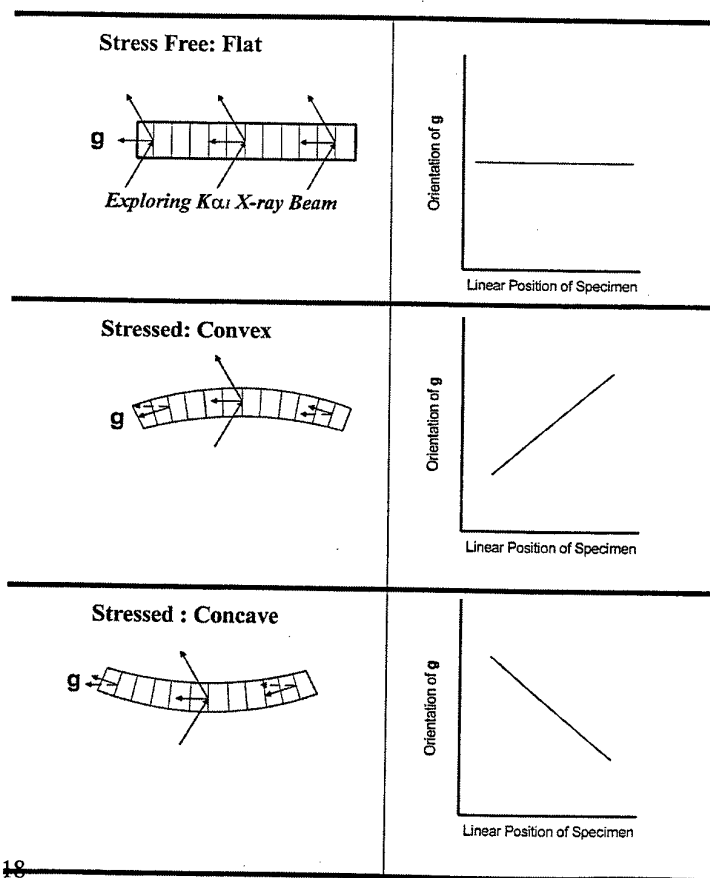
X-ray Diffraction Topographic Method



Photographic Film/Plate

Lal and Goswami, Rev. Sci. Instr. 59, 1409(1988)

Measurement of Curvature (Bending) of Crystal Wafers



Basic Properties of Silicon Melt

Shigeyuki Kimura

National Institute for Research in Inorganic Materials

1-1, Namiki, Tsukuba 305-0044, Japan

Introduction

Single crystal silicon is one of the most important fundamental materials in modern semiconductor industry. More than 90 % of the source crystals for wafers is grown by the Czochralski method and the rest is supplied almost entirely by the floating zone method. In both cases the melt is a bridging state for producing silicon crystals and a good care is necessary for growth of high quality crystals.

A substantial amount of data on basic physical properties of silicon melt were obtained during 1950th [1]. Some sporadical works followed afterwards, but the data reliability remained problematic. Computer simulation of crystal growth operation based on the fluid dynamics started in late 1960th [2] and the development of the algorithm is steadily getting momentum. The calculation results do not necessarily agree with the experimental observation, for the main cause apparently comes from the employed thermophysical data.

In this report, published results of such basic properties of silicon melt as density, surface tension, viscosity, electrical resistivity, thermal emissivity, and thermal diffusivity are reviewed for better understanding of silicon crystal growth.

Density

It was a general understanding that the density was 2.53 g/cm^3 at the melting temperature and the volume thermal expansion coefficient was $1.2 \times 10^{-4} \text{ K}^{-1}$. An excellent review was made available by Glazov et al. [1]

The result of density measurement of the silicon melt in SiC and SiO₂ crucibles by Sasaki et al. [3] indicated 2-3 % larger density values than the previous literature values. The notable feature of their data is the anomalous temperature dependence in the region close to the melting point. The volume expansion coefficient is nearly an order of magnitude steeper than in the higher temperature region. Rhim et al. [4] carried out an experiment by measuring the diameter of a levitated silicon melt sphere and found no anomalous temperature dependence, while their data agreeing well with the previous literature values.

Sasaki et al. also studied the influence of boron and gallium addition (0.1 atom %). Boron somewhat enhanced the anomaly, while gallium addition not only wiped out the anomaly but caused a negative temperature coefficient in volume expansion.

Surface tension

The literature data for surface tension of silicon melt are of much variety. It is not easy to find out which are reliable. However, there are some common features which indicate the basic nature of surface tension of silicon melt. Hardy [5] made a pioneering work by the sessile drop method and showed the fact that surface tension of silicon melt decreased with oxygen content. Mukai et al. [6] reported the result of

their surface tension measurement, showed dependence of surface tension on oxygen pressure in the atmosphere and gave a semi-quantitative explanation on the Hardy's experiment. Sasaki et al. [7] measured surface tension of silicon melt as contained in an either SiC or SiO₂ crucible by the ring method. Their results indicated possible occurrence of near-melting-temperature anomaly.

Viscosity

Experimental results from three different sources [1,8,9], all employing the oscillation dumping method, showed that viscosity was about 0.9 cP at the melting temperature. The temperature dependence was different and so were the high temperature viscosity values. Glazov et al.[1] used an alumina container. Alumina reacts with Si melt easily. Their data may have been influenced by aluminum contamination and cup wall roughness caused by the dissolution. Kakimoto et al. [8] showed the plotted data without describing details of the experimental method. According to the private communication, they used a BN cup. Out of two sets of the data reported by Sasaki et al. [9], one using SiC as the cup material, showed 0.20 eV as the activation energy of viscous flow. SiC wall becomes wet with silicon melt but BN wall does not. Si melt in the BN cup may, under oscillating condition, slip along the cup wall. Thus the data obtained using the SiC cup seems most reliable.

Electrical resistivity

The value 8.1×10^{-4} ohm cm was reported by Mokrovsky et al.[10] A similar result was obtained by both the four probe method and an electrodeless method by Glazov et al.[1] with small positive temperature dependence up to 1600°C. The values reported by Sasaki et al.[11] by the four probe method using a graphite container were almost independent on temperature. Their value of $7.17 \pm 0.03 \times 10^{-4}$ ohm cm, remarkably constant up to 1630°C, is about 8 % smaller than the value shown above. The former two reports were on the experiments using a corundum container and the difference may be explained in terms of impurity effect. An interesting point of the data by Sasaki et al. is the temperature dependence which has a minimum at somewhere between 1450 and 1500 °C.

Normal spectral emissivity

Shvarev et al. [12] reported the value of 0.27 at 0.65 μ m at the melting temperature. Recent report by Takasuka et al.[13] showed the values, 0.27 for all through the visible wavelengths and 0.21 for the infrared region up to 3 μ m, in good agreement with the previous ones obtained under monochromatic conditions by Krishnan et al. [14] and Shvarev et al. [12]. The reported values by the latter authors did not include the dependence on wavelength, but it could be deduced from the optical constants of Si melt as determined by Jellison and Lowndes [15] and by Shvarev et al. [16]. The result by Takasuka et al. also agreed relatively well with the deduced values for the dependence on wavelength. The dependence on the wavelength agrees well with the free electron model, or Drude model, for the optical properties of Si melt.

Thermal diffusivity

Shashkov and Grishin[17] determined the thermal conductivity of silicon melt, $0.67 \text{ W cm}^{-1} \text{ K}^{-1}$, which corresponded to the thermal diffusivity of $0.27 \text{ cm}^2/\text{sec}$, on the basis of the heat balance at the crystallization front in the CZ method. The thermal diffusivity of silicon melt has also been measured by the laser flash method. Yamamoto et al. [18] gave $0.228 \text{ cm}^2/\text{sec}$. Takasuka et al.[19] reported a value close to that of Yamamoto et al.

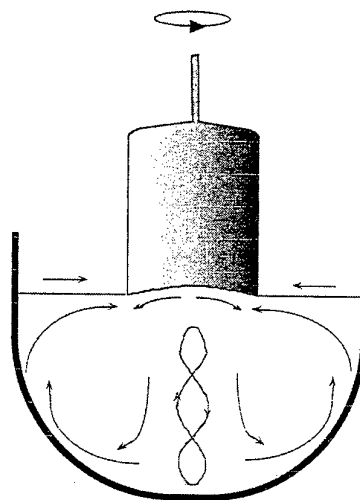
References

- [1] V. M. Glazov, S. N. Chizhevskaya and N. N. Glagoleva, *Liquid Semiconductors* (Plenum Press, New York, 1969)
- [2] N. Kobayashi and T. Arizumi, *Jpn. J. Appl. Phys.* 9 (1970) 361
- [3] H. Sasaki, E. Tokizaki, K. Terashima and S. Kimura, *Jpn. J. Appl. Phys.* 33 (1994) 3803
- [4] W.-K. Rhim, S. K. Chung, A. J. Rulison and R. E. Spjut, *Proceedings of the 4th Asian Thermophysical Properties Conference, C2a1, Tokyo, September 1995*
- [5] S. C. Hardy, *J. Crystal Growth* 69 (1984) 465
- [6] K. Mukai, Z. G. Niu, Y. Shiraishi, T. Hibiya, and K. Kakimoto, *J. Japn. Assoc. Crystal Growth* 22 (1995) 149 (in Japanese)
- [7] H. Sasaki, E. Tokizaki, X.-M. Huang, K. Terashima and S. Kimura, *Jpn. J. Appl. Phys.* 34 (1995) 414
- [8] K. Kakimoto, M. Eguchi, H. Watanabe and T. Hibiya, *J. Crystal Growth* 94 (1989) 412
- [9] H. Sasaki, E. Tokizaki, X.-M. Huang, K. Terashima and S. Kimura, *Jpn. J. Appl. Phys.* 34 (1995) 3432
- [10] N. P. Mokrovsky and A. R. Regel, *Zh. Tekh. Fiz.* 23 (1953) 779
- [11] H. Sasaki, A. Ikari, K. Terashima and S. Kimura, *Jpn. J. App. Phys.* 81 (1997) 6384
- [12] K. M. Shvarev, B. A. Baum and P. V. Gel'd, *Sov. Phys. Solid State*, 16 (1975) 2111
- [13] E. Takasuka, E. Tokizaki, K. Terashima and S. Kimura, *J. Appl. Phys.* 81 (1997) 6384
- [14] S. Krishnan, J. K. R. Weber, P. C. Nordine, R. A. Schiffman, R. H. Hauge and J. L. Margrave, *High Temp. Sci.*, 30 (1991) 137
- [15] G. E. Jellison, Jr. and D. H. Lowndes, *Appl. Phys. Lett.* 51 (1987) 352
- [16] K. M. Shvarev, B. A. Baum and P. V. Gel'd, *High Temp.* 15 (1977) 548
- [17] Y. M. Shashkov and V. P. Grishin, *Sov. Phys. Solid State* 8 (1966) 447
- [18] K. Yamamoto, T. Abe and S. Takasu, *Jpn. J. Appl. Phys.* 30 (1991) 2423
- [19] E. Takasuka, E. Tokizaki, K. Terashima and S. Kimura, *Proc. 4th Asian Thermophys. Properties Conference, (Tokyo, 1995) B1d4.*

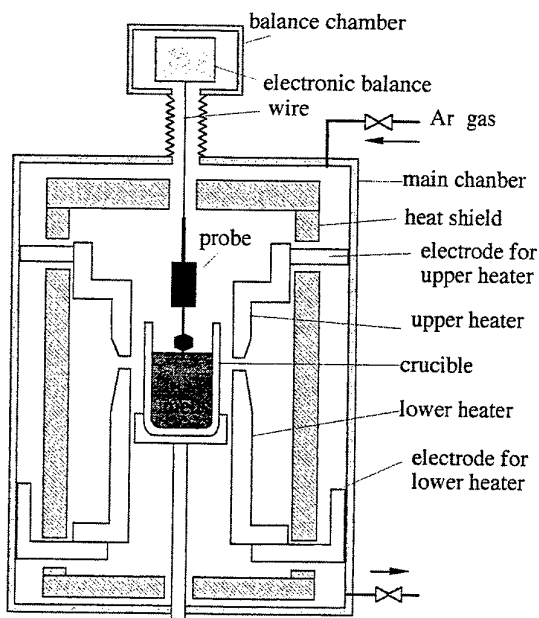
Basic Properties of Silicon Melt

Shigeyuki Kimura
National Institute for Research in Inorganic Materials
Science and Technology Agency, Japan

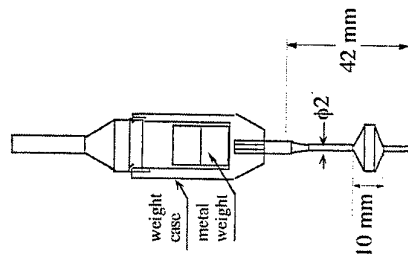
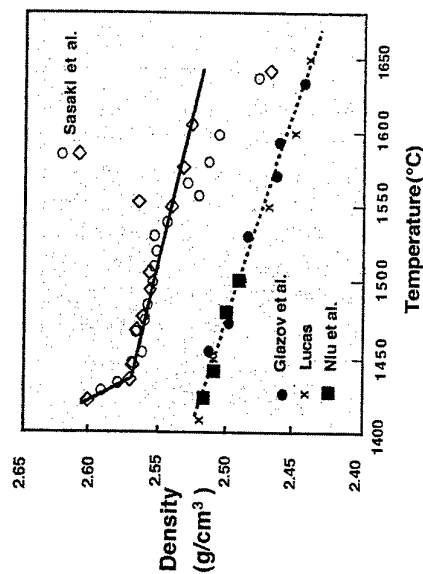
Basic flow of silicon melt during CZ growth

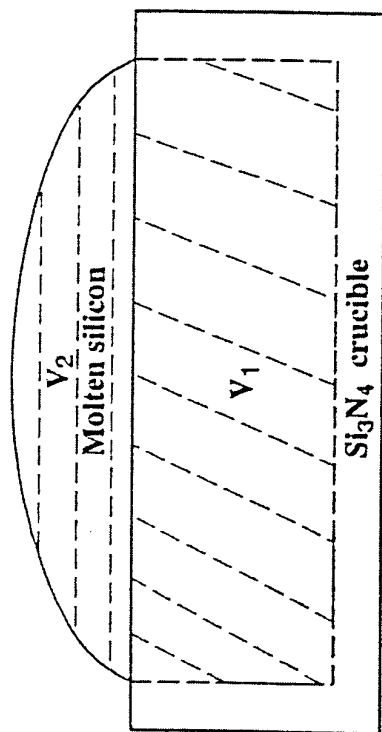


Density measurement

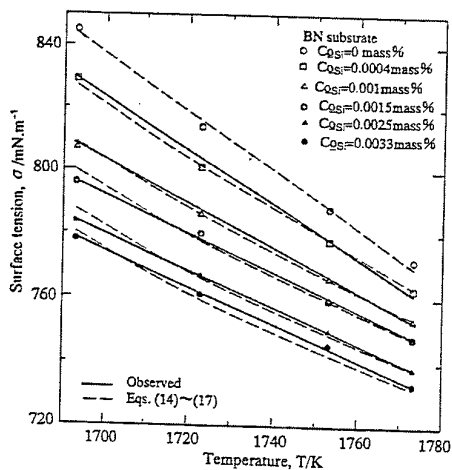


Density of silicon melt

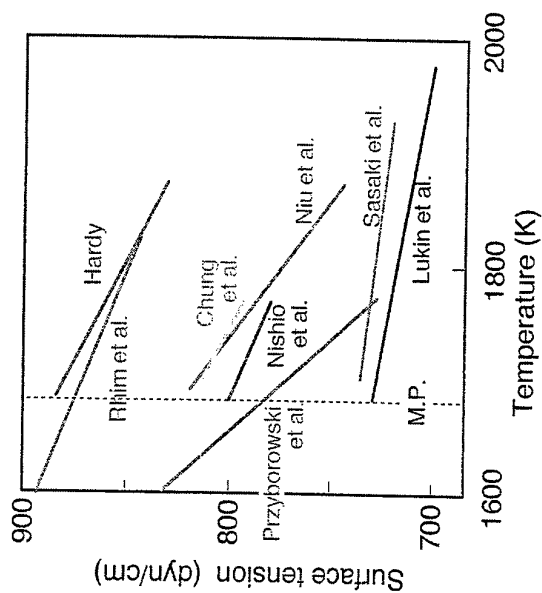




Shape of molten silicon in crucible.

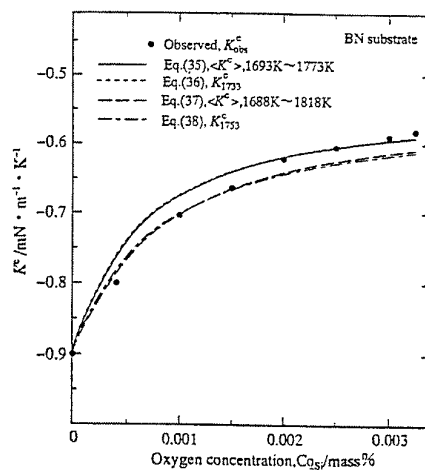


Temperature dependence of surface tension of molten silicon.



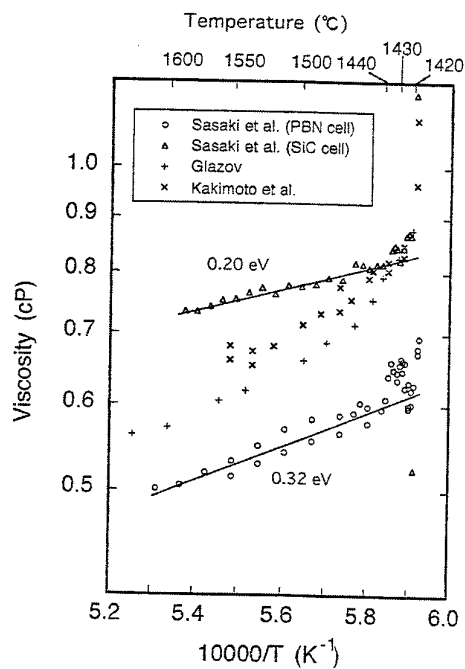
Surface Tension of Si Melt

after Mukai et al.,
J. Jpn. Assoc.
Crystal Growth,
23(1996)93

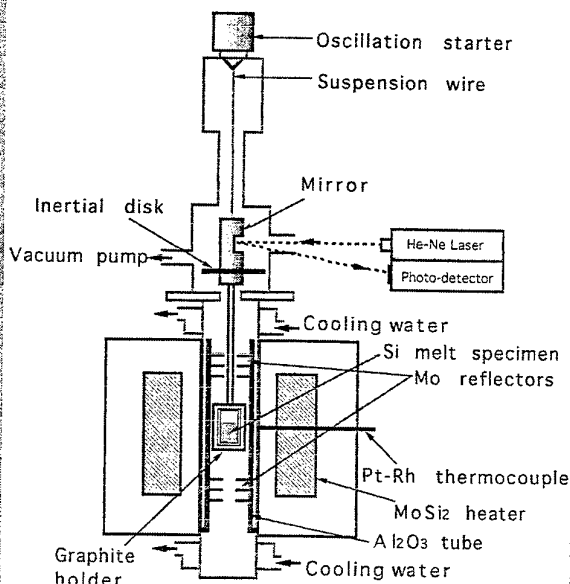


Relation between temperature coefficient of surface tension and oxygen concentration at 1693 K ~ 1773 K.

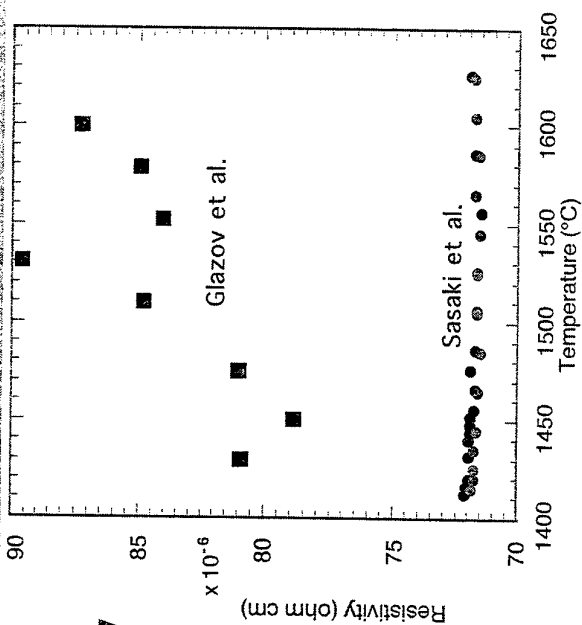
Viscosity of Si melt



Apparatus for viscosity measurement

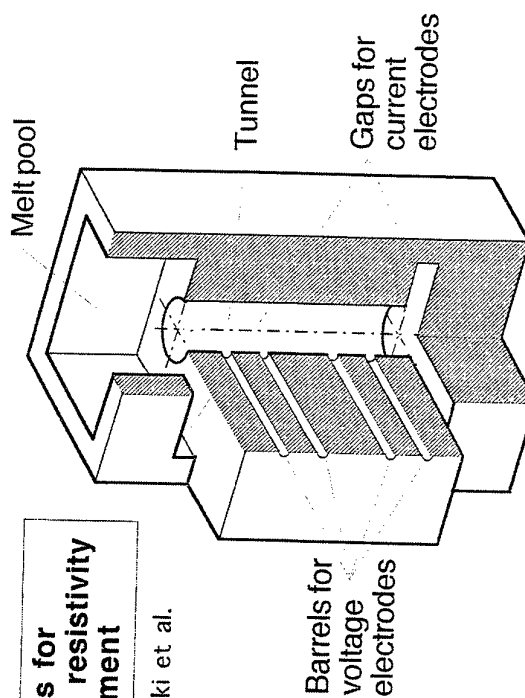


Electrical Resistivity of Si Melt

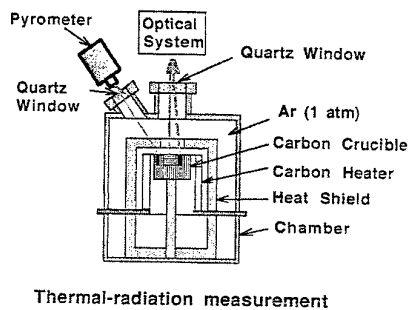
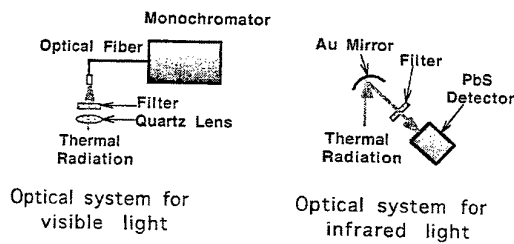


Apparatus for electrical resistivity measurement

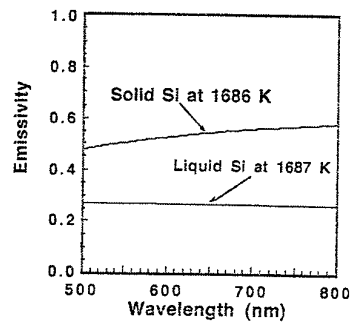
After Sasaki et al.



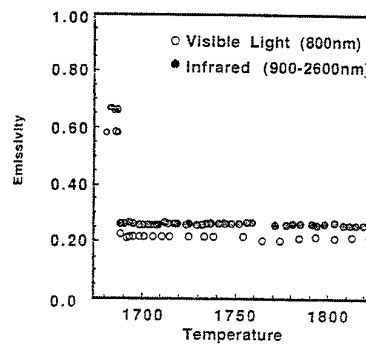
Experimental setup for emissivity measurement after Takasuka et al.



After Takasuka et al.

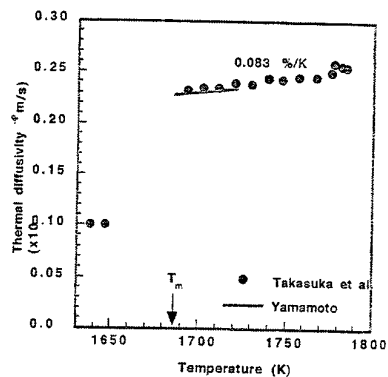


Spectral emissivity of liquid and solid Si around the melting point



Temperature dependence of emissivity of liquid Si

Temperature dependence of thermal diffusivity

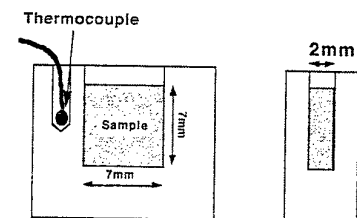


Thermal conductivity: $\lambda = \alpha \rho C_p = 62 \text{ W/mK}$ (at T_m)

Lorenz number: $L = \lambda / \sigma T = 2.8 \times 10^{-8} \Omega \text{W/K}$ (at T_m)

(Theoretical Lorenz number: $L_0 = 2.45 \times 10^{-8} \Omega \text{W/K}$)

Experimental setup for measurement of thermal diffusivity After Takasuka et al.



INFLUENCE OF BORON ADDITION INTO SILICON MELTS ON OXYGEN ATOM BEHAVIOR IN CZ PULLING SYSTEM

Kazutaka Terashima

**Silicon Melt Advanced Project, Shonan Institute of Technology
1-1-25 Tsujido-nishikaigan, Fujisawa, Kanagawa 251, Japan**

The solubility of oxygen atom into boron doped silicon melt increases with increasing boron concentration. The dissolution rate of fused quartz also increases with increasing boron concentration. It has been found that the fraction of cristobalite area grown on fused quartz rod surface varies the fused quartz dissolution rate. The evaporation rate of silicon mono oxide has a tendency to increase with increasing boron concentration. The importance of silicon melt understanding will be discussed. The strategy to grow well controlled silicon crystals and recent advanced results are described.

Contents

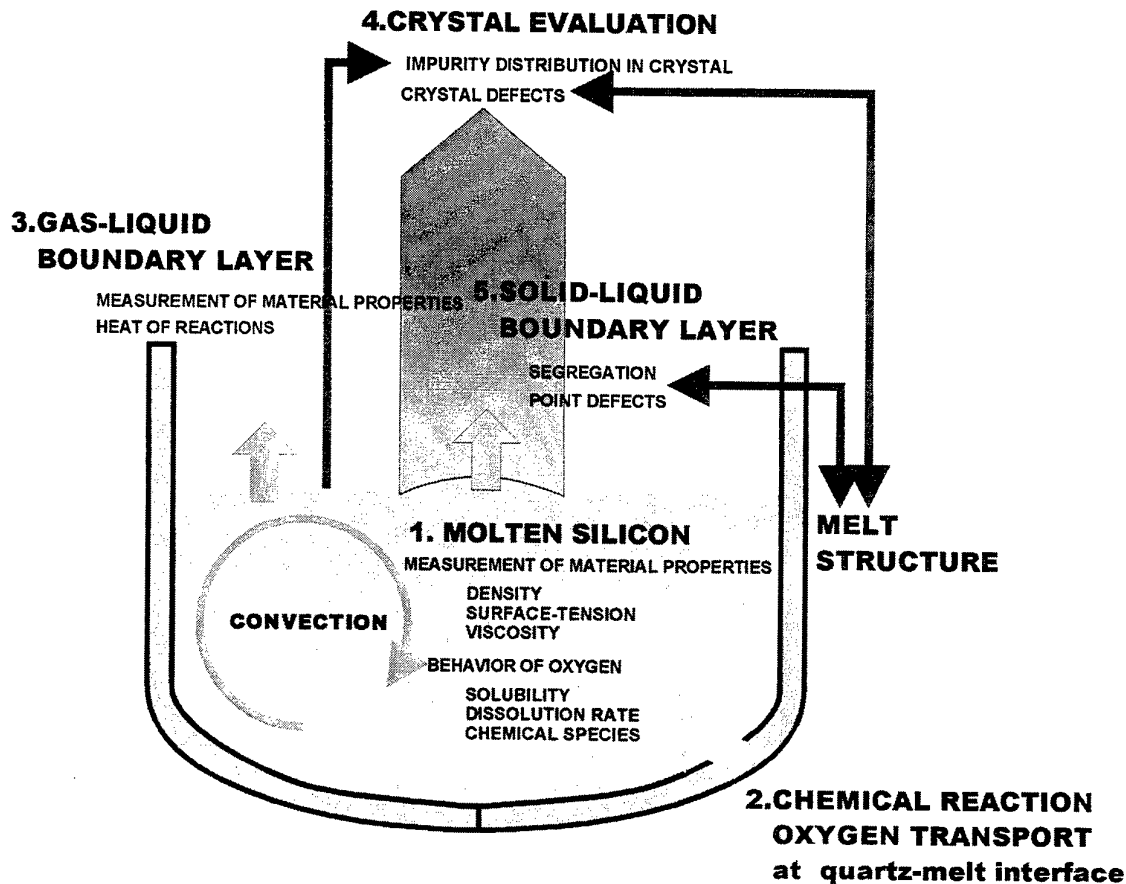
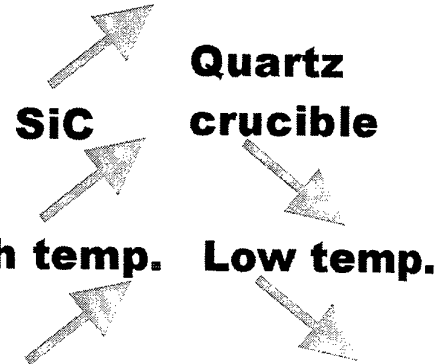
- 1.Introduction**
- 2.Solubility of Oxygen**
- 3.Dissolution Rate of Fused Quartz**
- 4.Evaporation From Melt Surface**
- 5.Crystal Uniformity**

Introduction

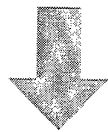
Influence of B addition on
Oxygen solubility

Dissolution rate of quartz

Evaporation rate



What happen in B-doped silicon melt?



Crystal pulling with various diameter
Numerical simulation of melt convection

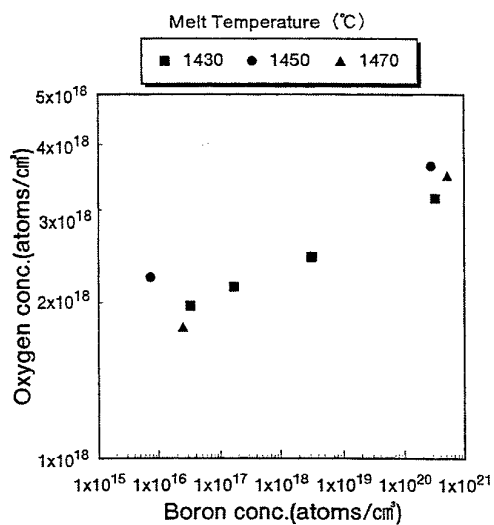


Fig. Dependence of the oxygen concentration on the boron concentration

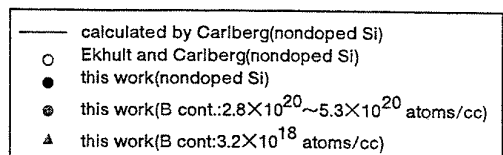


Fig. Relationship between oxygen concentration and temperature .

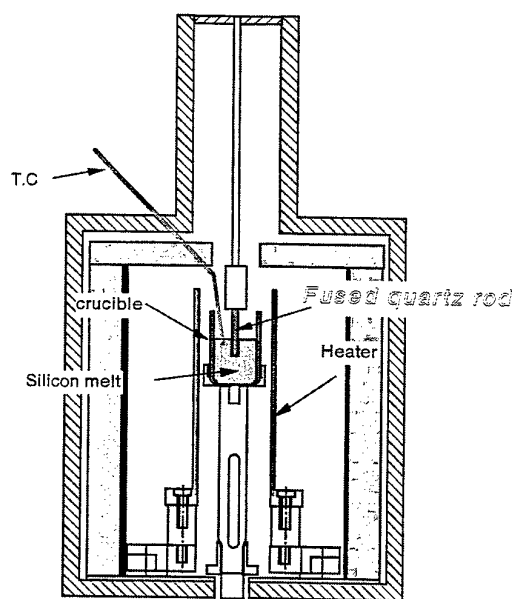


Fig. Furnace of fused quartz dissolution rate experiment

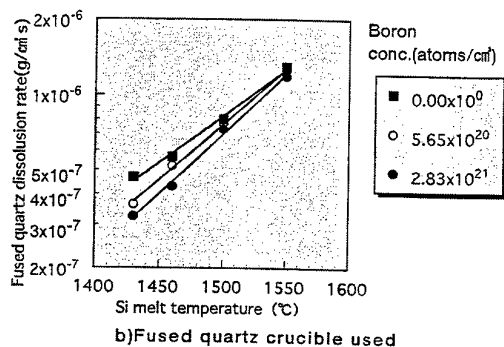
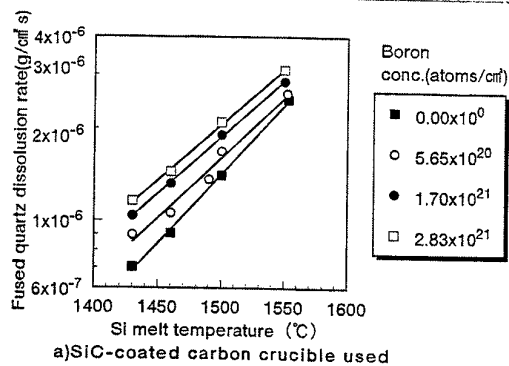


Fig. Dependence of the quartz dissolution rate on the silicon melt temperature in a boron doped silicon melt



$$\text{Dissolution rate} = A_0 \exp\left(\frac{-\Delta E}{RT}\right)$$

A_0 : Frequencies and modes of molecules collisions
 ΔE : ctivation energy of the quartz dissolution rates

calculated activation energy: ΔE and pre-exponential factor: A_0

Boron conc.(atoms/cm ³)	Crucible	ΔE (kcal/mol)	A_0
0	SiC-coated carbon	151	172
6×10^{20}		128	11.6
2×10^{21}		121	5.54
3×10^{21}		119	4.73
0	fused quartz	122	2.82
6×10^{20}		145	46.4
3×10^{21}		157	180

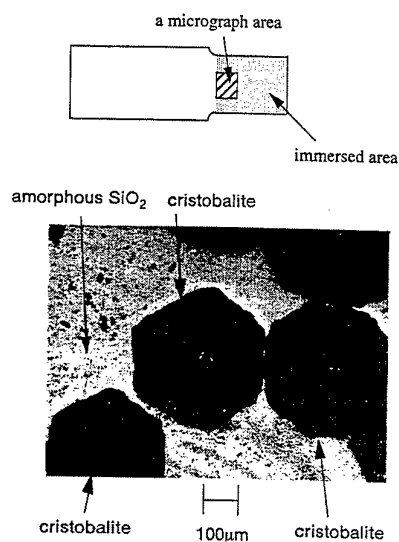
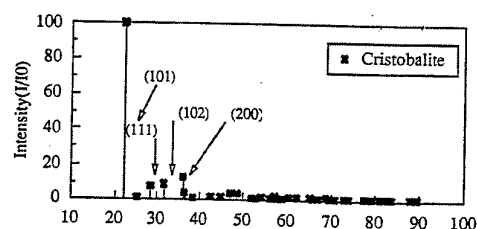
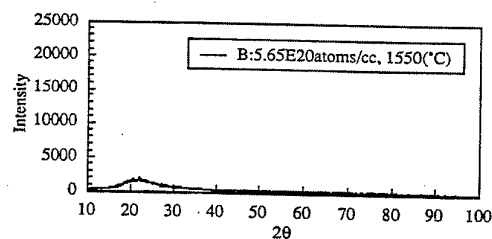
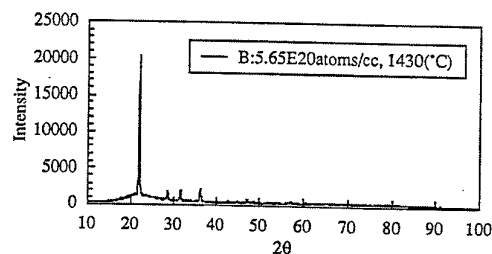


Fig. A micrograph of fused quartz rod surface immersed in boron doped silicon melt (5.65×10^{20} atoms/cm³) : Silicon melt temperature:1430°C

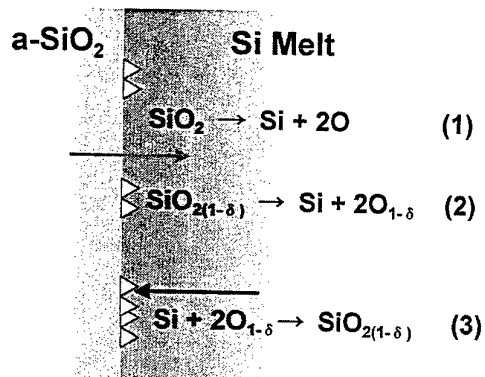


cristobalite (1500°C)



cristobalite (1550°C)

Fig. micrographs of sample surface



(1) dissolution of amorphous SiO_2

(2) dissolution of cristobalite

(3) growth of cristobalite

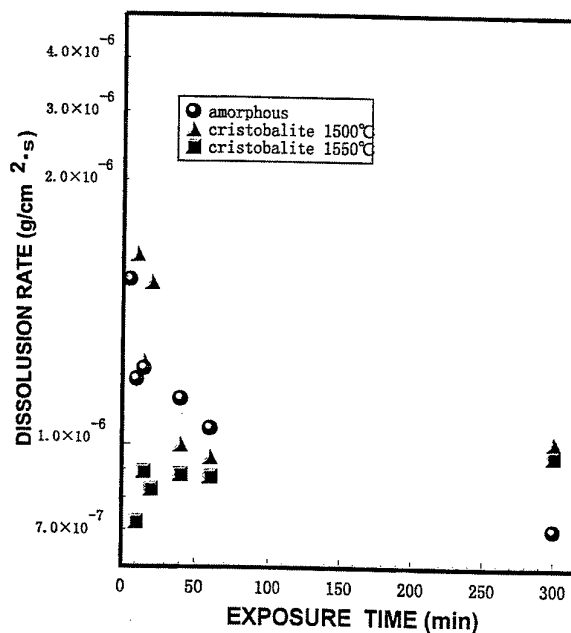
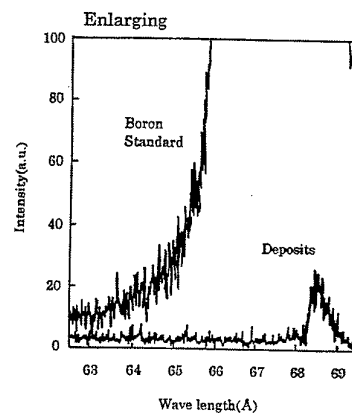
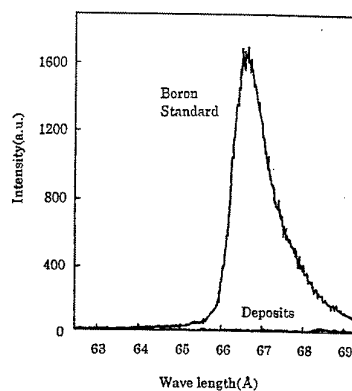
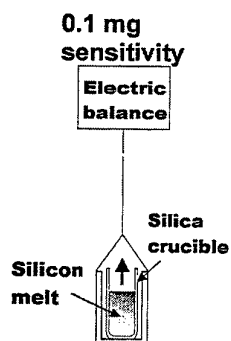
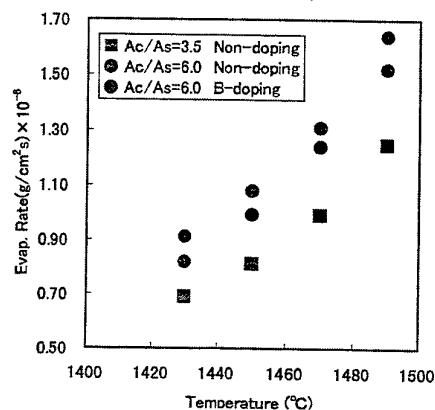
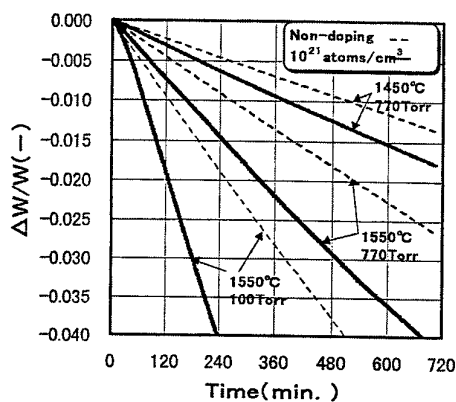


Fig. Dissolution rate vs. Exposure time

Weight variations of silicon melts doped with boron due to evaporation of oxide species



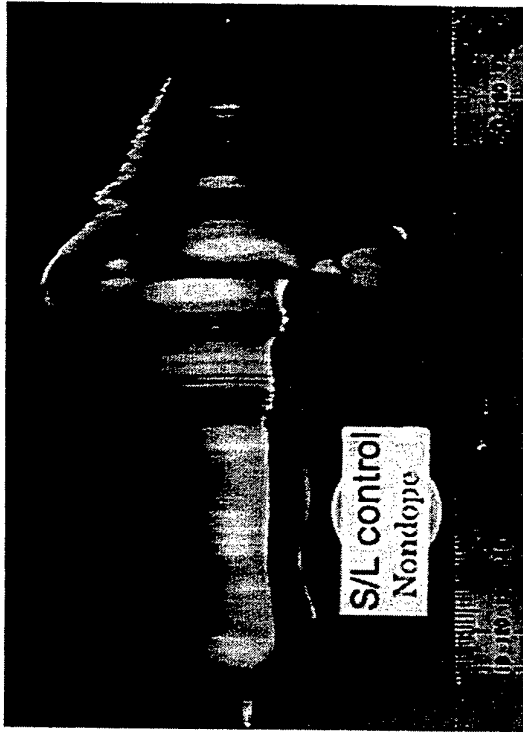


Fig. Typical crystal with various diameter

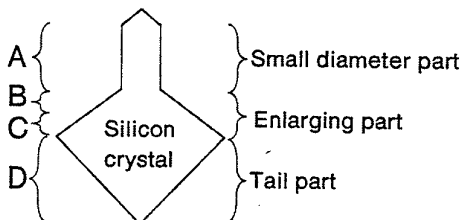
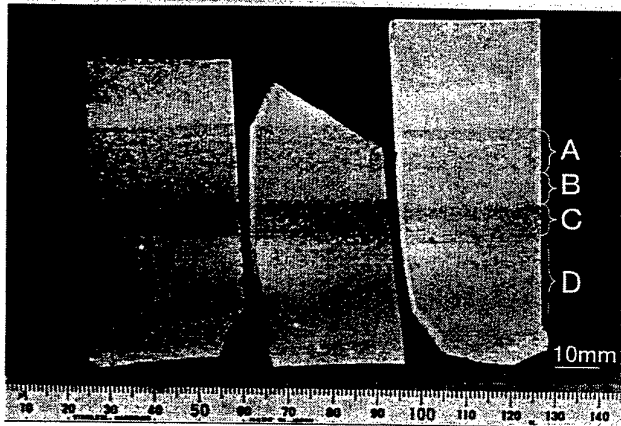
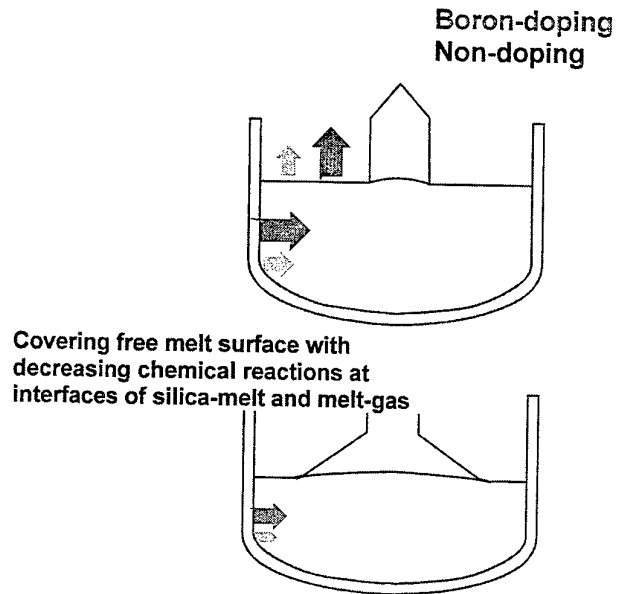
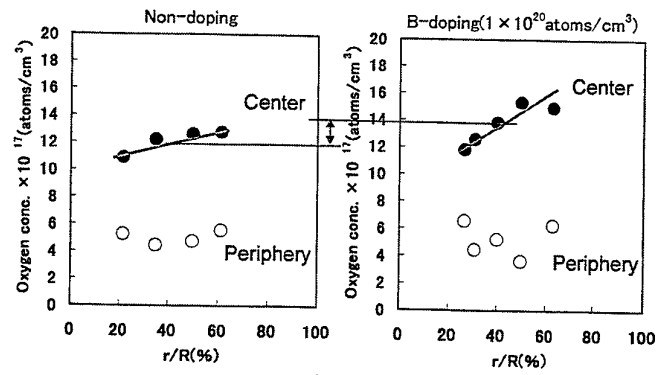


Fig.2

Structural and chemical characteristics of octahedral void defects found in Czochralski silicon

Manabu Itsumi

NTT System Electronics Laboratories,
3-1 Morinosato Wakamiya, Atsugi-Shi, Kanagawa, 243-0198 Japan
e-mail: itsumi@aecl.ntt.jp

In the past 20 years there have been several breakthroughs in the research on grown-in defects in Czochralski silicon (CZ-Si) for commercial use. Around 1982 the presence of oxide defects originating in CZ-Si was reported [1]. In 1990, crystal originated particles (COPs) were reported [2]. A few years later, in 1995, octahedral void defects were found just under oxide defects [3-4] (Fig. 1), and in 1996 octahedral void defects were also found in bulk CZ-Si [5-7]. As a result, it was widely recognized that the octahedral void defects are a cause of oxide defects, and of COPs [8-10].

Octahedral void defects are composed of eight (111) subplanes (Fig. 2). But, we often observe an incomplete octahedral structure that is partially truncated by a (100) subplane and furthermore two incomplete octahedral defects convoluting each other (dual-type void defects)(Fig. 3). The size of the defects is about 0.1 microns, defect density per unit volume is about 10^5 - 10^6 /cm³, and defect density per unit area is about 1-10/cm². Octahedral defects are basically void defects, and the inner walls of the void defects are covered with a 2-4-nm thick oxide (Fig. 4). These features are common for prominent Si vendors, partly because the Si crystal growth rate is almost the same (about 1 mm/min). Two voids of dual-type defects either overlap each other, or are situated close to each other (that is, a 2-3-nm thick oxide is located between the two voids)[11].

The formation of octahedral void defects is related to the behavior of point defects during a Si crystal growth process. A model is as follows. First, vacancies and oxygen atoms were incorporated into the Si crystal from the melting Si. In the cooling process of Si crystal, vacancy supersaturation was followed by vacancy agglomeration at some nucleation sites and at about 1100°C, void structures begin to form. Oxygen agglomeration was followed by oxide growth on the inner walls of the void structures.

Prominent manufacturers of Si large-scale integrated circuits (LSIs) began to attach importance to the problem and to find these defects in the failure chips of the actual mega-bit level dynamic random access memories they manufactured. Investigations of the octahedral void defects are expanding.

References [1] M. Itsumi and F. Kiyosumi, Appl. Phys. Lett., 40 (6), 496 (1982). [2] J. Ryuta et al., Jpn. J. Appl. Phys., Vol. 29, No. 11, L1947 (1990). [3] M. Itsumi et al., J. Appl. Phys., 78(10), 5984 (1995). [4] M. Miyazaki et al., Jpn. J. Appl. Phys., 34, 6303 (1995). [5] T. Ueki et al., 1996 Int. Conf. on Solid State Devices and Materials, Yokohama, LA-1, 862 (1996). [6] M. Kato et al., Jpn. J. Appl. Phys., 35, 5597 (1996). [7] M. Nishimura et al., J. Electrochem. Soc., 143, 243 (1996). [8] N. Inoue, Proc. of The Kazusa Akademia Park Forum on The Sci. and Technol. of Si Materials, Nov., Chiba, edited by K. Sumino, 135 (1997). [9] G. Rozgonyi et al., ibid., 215 (1997). [10] D. Graf et al., J. Electrochem. Soc., Vol. 145, No.1, 275 (1998). [11] T. Ueki et al., Jpn. J. Appl. Phys., Vol. 37, Part 1, No. 4A, 1667 (1998).

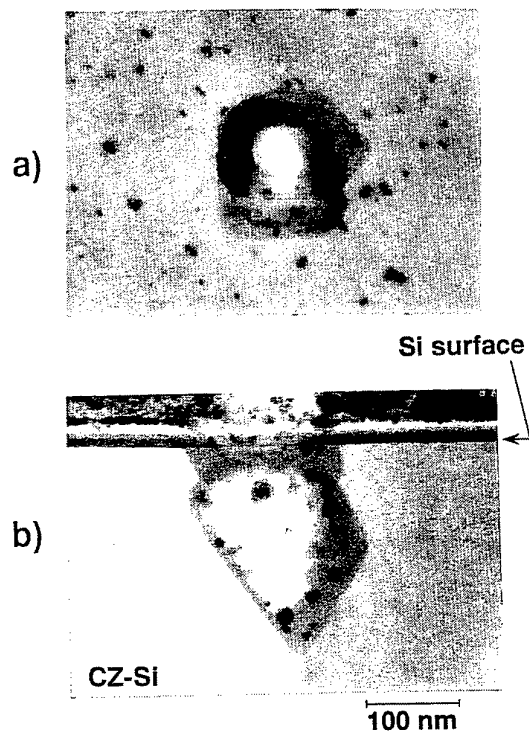


Fig. 1. Octahedral-structured defects found just under the oxide defects on a Si surface.
 (a) plan view
 (b) cross section

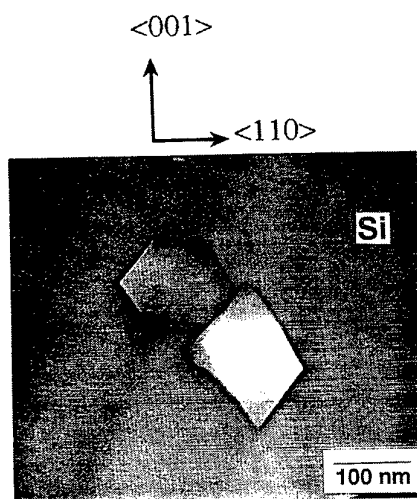


Fig. 3. Cross-sectional TEM micrograph.
 (two voids overlapping)

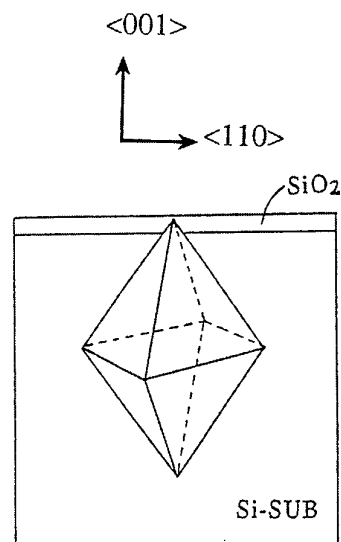


Fig. 2. A schematic illustration of octahedral structure.

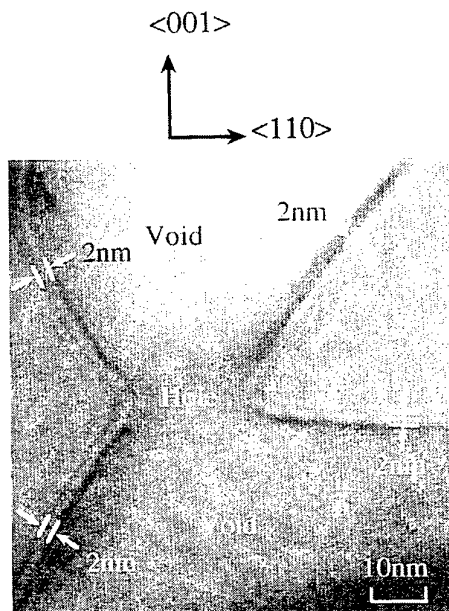
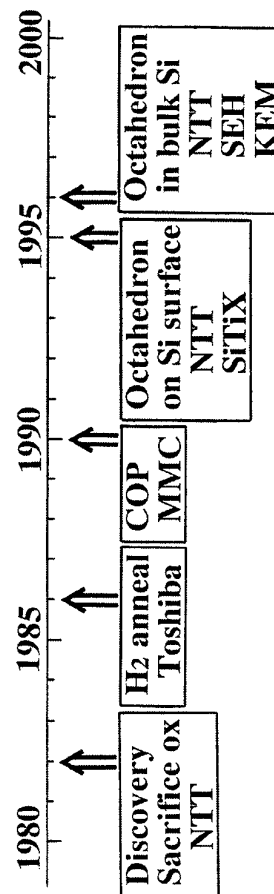


Fig. 4. Cross-sectional TEM micrograph.
 (two voids overlapping)

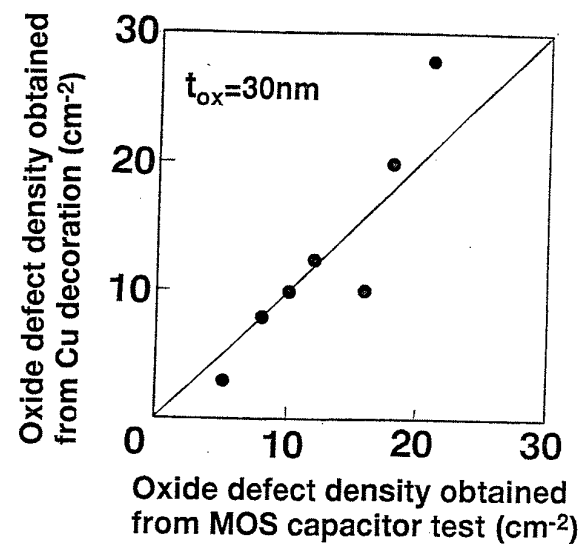
OUTLINE

1. History of research on grown-in defects in Czochralski Si
2. Observation methods
3. Characterization of octahedral void defects
4. Generation and elimination of octahedral void defects
5. Effects on oxide defect generation

History of research on grown-in defects in Czochralski Si

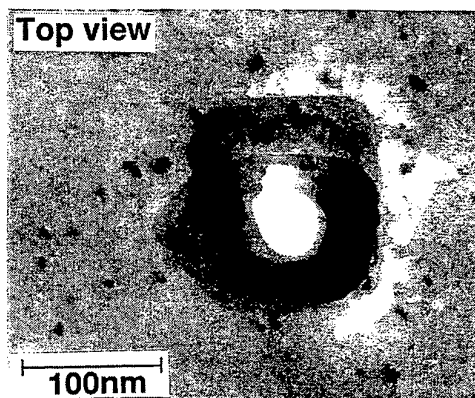
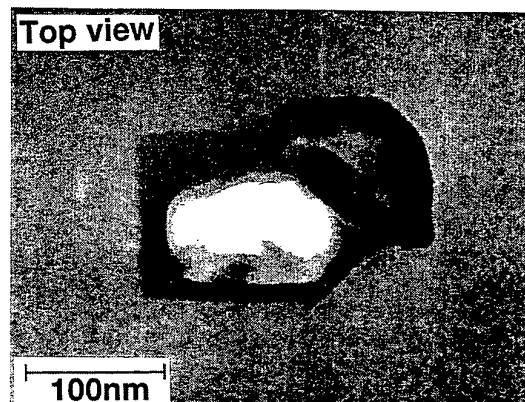


Comparison of Cu Decoration and MOS Capacitor Test

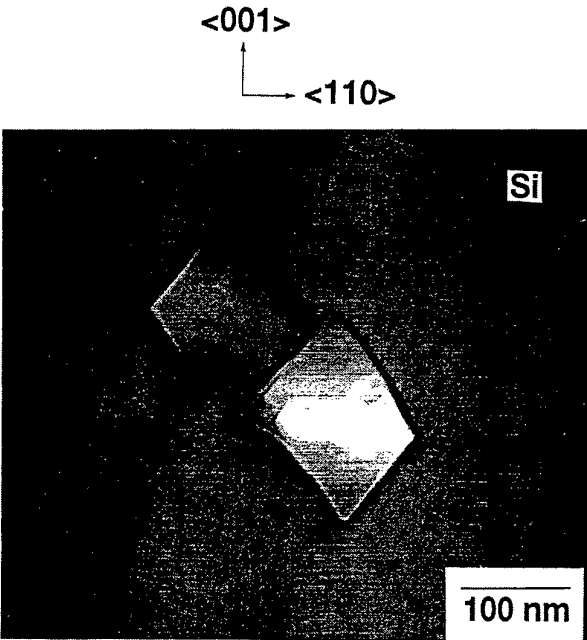
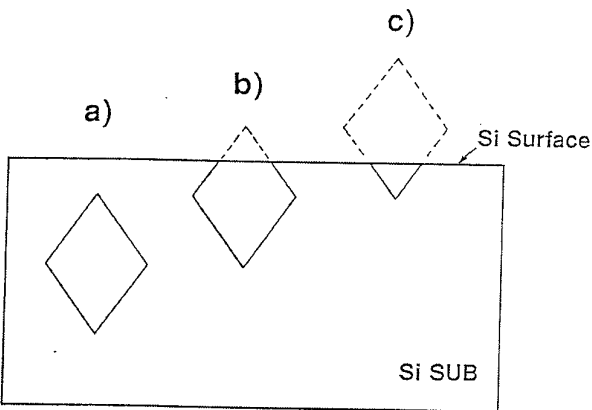
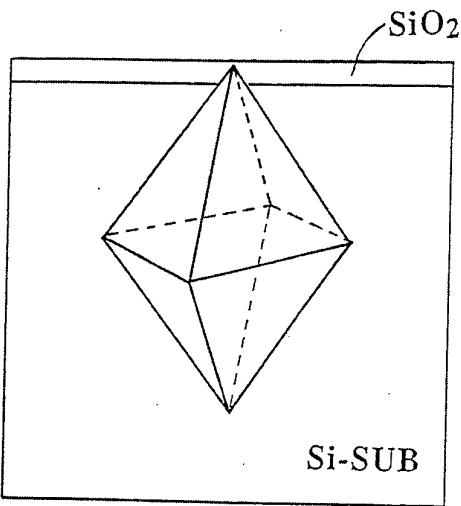
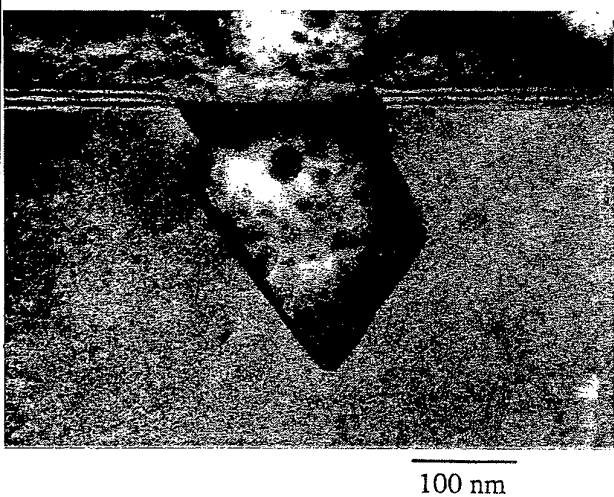


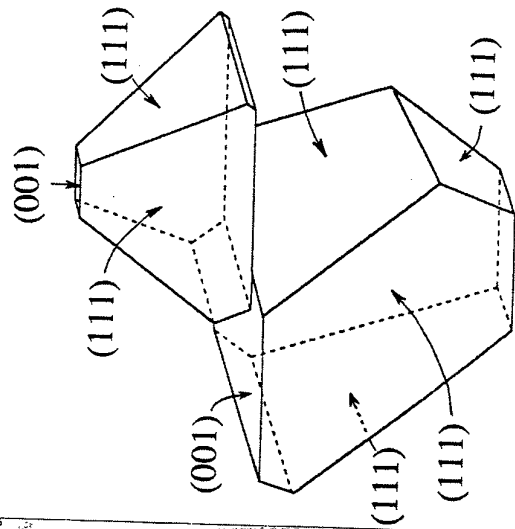
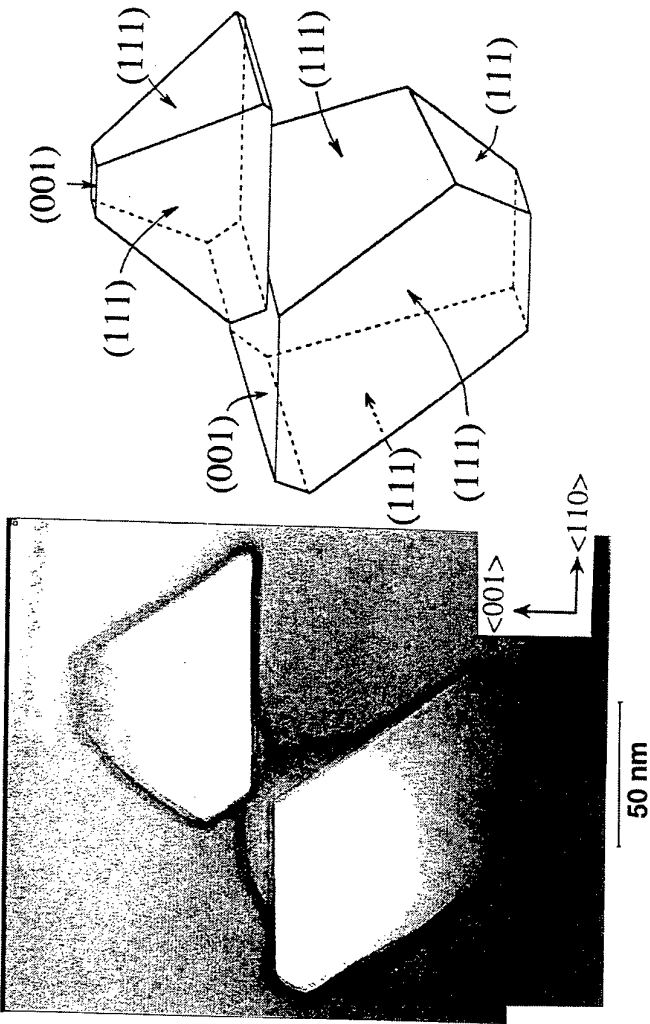
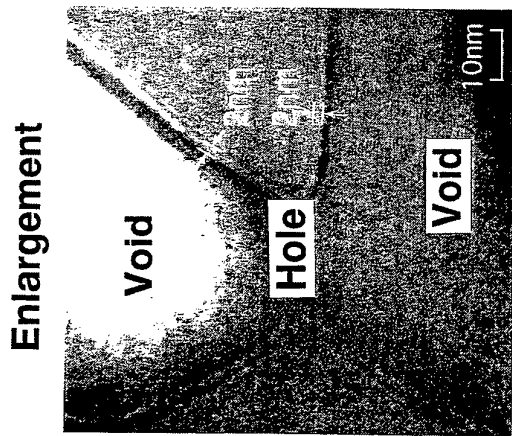
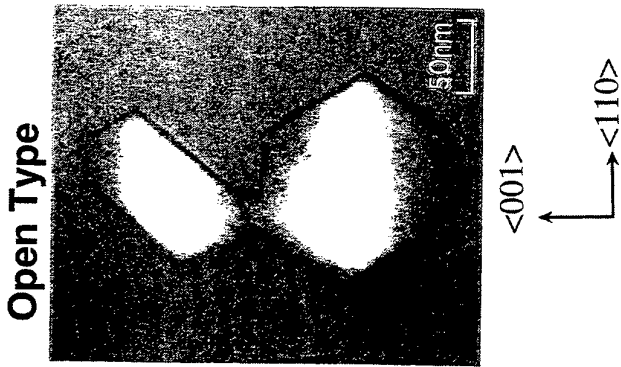
Octahedron Detected by Cu Decoration

($t_{ox} = 30\text{nm}$, decoration time: 1-2min)



Octahedron Detcted by Cu Decoration

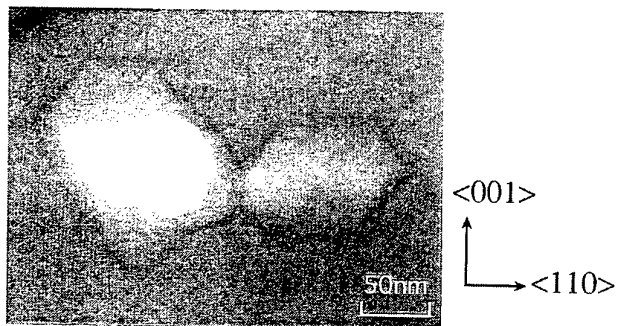




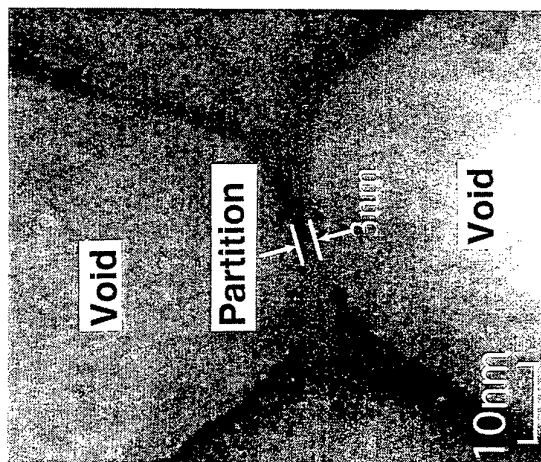
Features of the grown-in defects in CZ-Si

1. Structure	Dual-type octahedral void defects + incomplete, truncated by (100) subplane + 2-4-nm thick oxide on side walls of defects
2. Dimension	0.1-0.15 microns
3. Density	$\sim 10^5$ - 10^6 /cm ³ (per unit volume) ~ 1 - 10 /cm ² (per unit area)

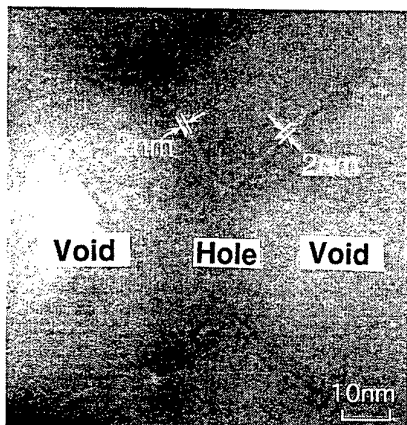
Open Type



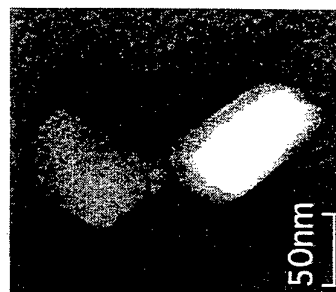
Enlargement



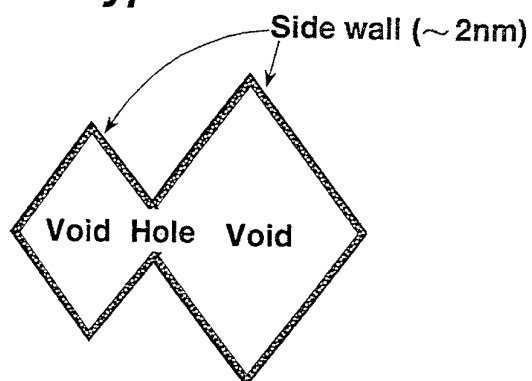
Enlargement



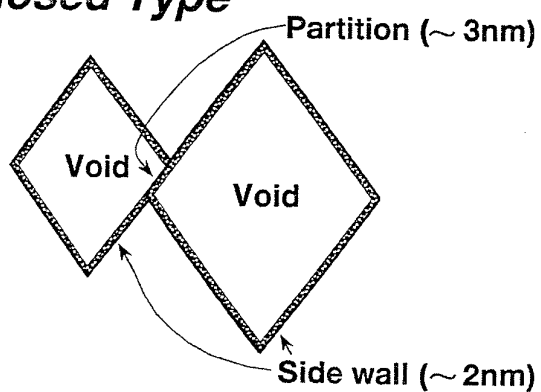
Closed Type



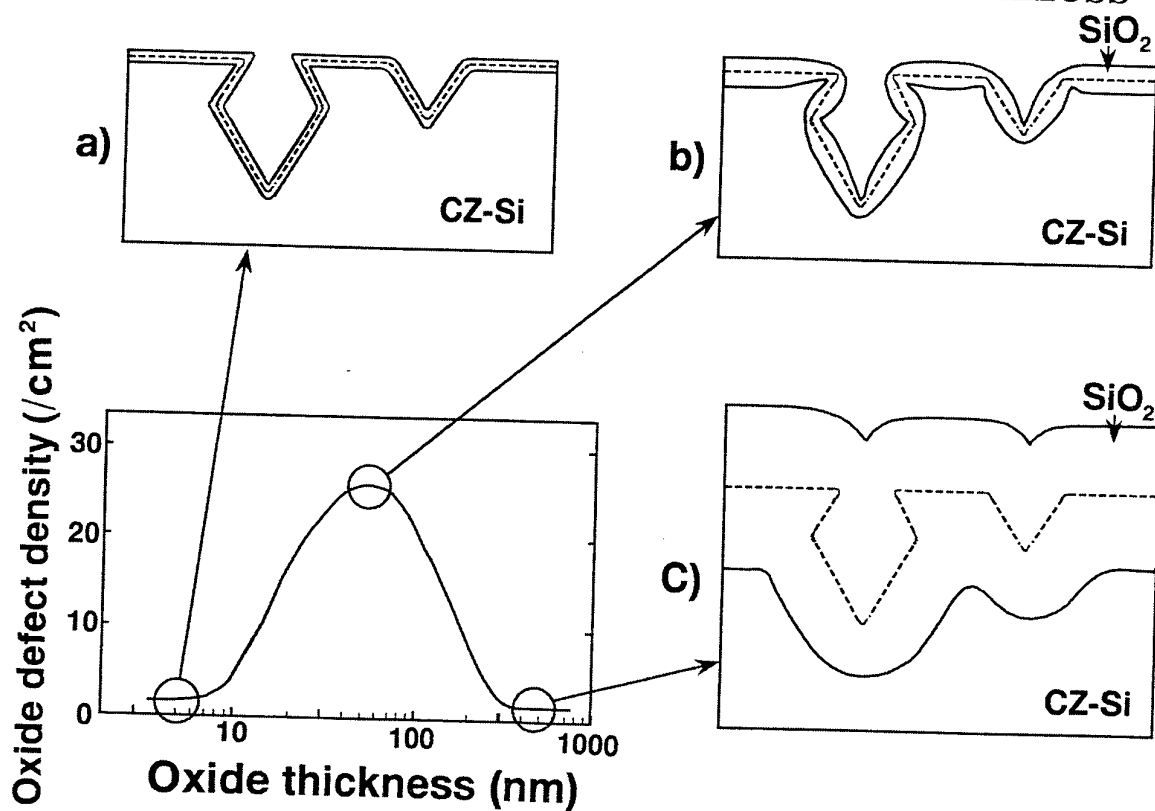
Open Type



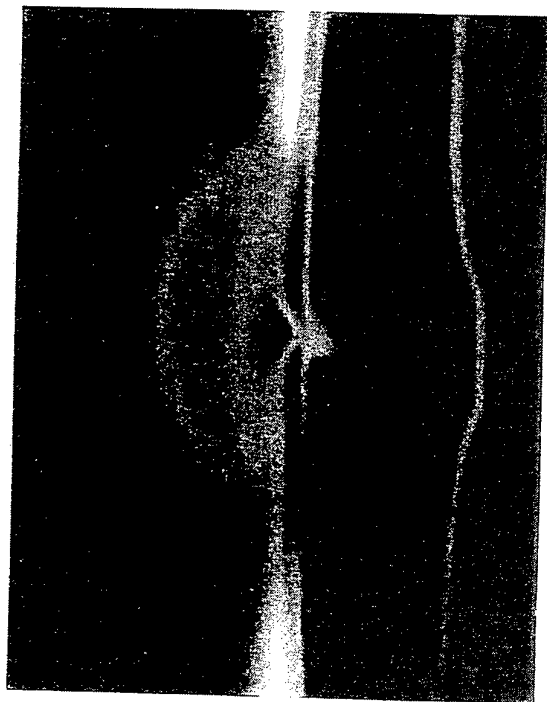
Closed Type



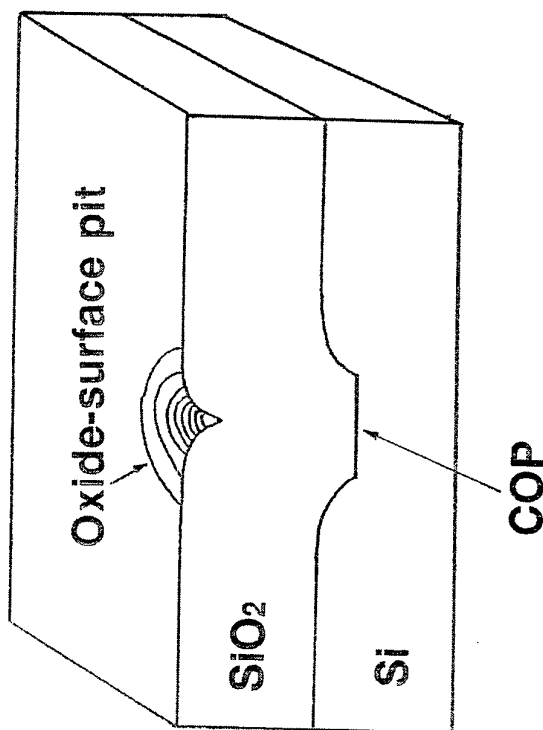
Oxide defect density vs. Oxide thickness



Octahedron after Oxidation



500 nm



KEY ISSUES IN THE GROWTH OF VERY LARGE DIAMETER SILICON SINGLE CRYSTALS

E. Tomzig / W.v.Ammon

Wacker Siltronic AG, D-84479 Burghausen, P.O.Box 1140, Germany

1. Introduction

The semiconductor industry is currently preparing the step to the next larger wafer diameter, i.e. from 200 mm to 300 mm. The driving forces are mainly the potential of cost reduction, but also the larger capacity per device fab. However, the exact timing for the changeover to 300 mm is not yet clear, as the recent progress in photolithography allows to shrink the design rule faster than originally expected which, in turn, lowers the cost per chip without the need to build new and expensive 300 mm fab's. With the recent downturn of the semiconductor market, most device manufacturers cannot afford the huge investments for 300 mm fab's. Nevertheless, the wafer suppliers continue their 300 mm R+D activities, as the technological challenges, particularly in crystal growth, are tremendous and require real breakthrough innovations in some cases (1).

2. Key issues in growth technology

The main technological issues in very large diameter crystal growth have already been described a few years ago (2). Most of them are related to the large charge size of poly silicon (>250 kg as compared to ca. 120 kg for 200 mm crystal growth) necessary to grow very large diameter crystals of economical length. Accordingly, the size of the hot zone characterized by the silica crucible diameter will increase from 24" (200 mm crystals) to 32" - 40" (300 mm and 400 mm crystals) (3). For some of the earlier identified key issues, solutions have become conceivable.

- The seed neck stability may be increased by applying a special seeding technique which allows to grow significantly thicker seed necks (4). Another technique to support the seed neck is a mechanical cramp which can be fixed underneath a small subsidiary cone when the growing crystal exceeds more than 150 kg in weight (3).

- The higher temperature fluctuations can be successfully suppressed by the application of magnetic fields (MCZ) which dampen the melt convection and, hence, the temperature fluctuations.

- The application of the MCZ technology may also help to reduce the risk of structure loss resulting from the enhanced corrosion of the silica crucible. Due to the strong suppression of the melt convection, the small silica particles washed into the melt from the corroded silica surface are dissolved before they reach the growth interface of the crystal and generate dislocations.

The disadvantage of MCZ, however, are additional costs and safety issues as the operators may get exposed to large stray fields. In addition, the required high field strengths also lower the oxygen content to values where oxygen precipitation in the device processes may no longer occur. Thus, the wafer bulk loses its internal gettering capability for metallic contaminants. Moreover, 300 mm wafers will be double side polished which makes it difficult to integrate the deposition of a gelling backside layer in the wafer manufacturing process. This could cause a severe problem as many device manufacturers cannot live without gettering in their production lines up to now. Furthermore, the observed higher susceptibility of very large wafers to slippage during thermal wafer processing calls for higher oxygen contents, too. It is therefore questionable whether most devices manufacturers will accept low oxygen material.

- The risk of structure loss is also increased by the considerable longer time constants for the process control owing to the large thermal budget. This requires new intelligent control systems which are able to predict the time dependent behavior of growth parameters several hours in advance. A solution to this problem may be fuzzy logic control algorithms or online realtime process simulations.

As dislocations generated during the growth process propagate back into already dislocation free grown material by a distance of about one diameter, a higher risk of structure loss entails huge material losses with increasing crystal diameter. Hence, the economical production of 300 mm and larger diameter crystals requires an almost perfect growth process which, in view of the above challenges, will be difficult to achieve.

It has also previously been pointed out that the economy of very large diameter growth processes is additionally challenged by the reduction of the maximum pull rate with increasing crystal diameter. It was found that, due to the considerable generated latent heat, the lateral temperature gradient on the melt surface becomes too small to facilitate a stable growth process. Meanwhile, however, it appears that the increasing thermal stress in the growing crystal with larger diameter may limit the pull rate even more. In contrast to 200 mm or smaller diameter crystals, 300 mm crystals crack, if they are pulled too fast. Thus, the reduction of the thermal stress by a proper hot zone design has become a key issue in current R+D activities. Up to now, no solution to the pull rate problem has been indicated and it is rather questionable whether or not significant improvements will be possible.

3. Key issues of the bulk quality

The lower pull rate has also a negative impact on the defect behavior in the crystal bulk. From computer simulations it is predicted that the Voronkov parameter $V/G(r)$ (V =pull rate, G =axial temperature gradient at the growth interface, r =radial position) which determines the type of defect that develops in the growing crystal, will drop below the critical value of $1.34 \times 10^{-3} \text{ cm}^2 \text{ K}^{-1} \text{ min}^{-1}$ over the entire crystal volume for crystal diameters larger than 300 mm. So far, all crystals produced for the semiconductor industry have been grown with V/G above the critical value. As a result, the defect aggregation is now dominated by excess Si interstitials instead of vacancies and, hence, L-pits (dislocation loops) should be observed instead of microvoids for very large diameter crystals. In case of 300 mm, it may be still possible to grow entirely vacancy rich crystals, but it remains to be seen, whether or not this will be possible on a production scale. As L-pits severely deteriorate the performance of semiconductor devices, the use of polished wafers in very large diameter device manufacturing lines is seriously questioned unless new methods for the suppression of L-pits can be developed. Very recently, it has been shown that, in contrast to microvoids, L-pits near the epi substrate surface grow into epi layers and generate defects there. Hence, p-p- epi wafers are probably no solution for device manufacturers who have developed their cell design on polished wafers.

3. Conclusions

Up to now, the p+p- epi wafer seems to be the 300 mm wafer of choice as the high boron content of the substrate suppresses L-pits as well as microvoids and offers superior internal gettering capability, as the higher solubility of Fe in the p+ substrate depletes residual Fe atoms in the epi layer and traps them in the p+ substrate.

References

- 1) W.v.Ammon, Solid state Phenomena Vols. 47-48 (1996) 97
- 2) W.v.Ammon,
- 3) K.Takada, H.Yamagishi, H.Minami, M.Imai, Semiconductor Silicon 1998, The Electrochem. Soc. Proceedings Volume 98-1, (1998) 376
- 4) T.Abe, ULSI Sci. and Tech./1997, H.Z.Massoud, H.Iwai, C.Claeys and R.B.Fai, Editors, PV 97-3, p.123, The electrochem.Soc. Proceeding Series, (1997)

No copies of transparencies received

Modeling and Simulation of Bulk Crystal Growth Considering Melt Dynamics

F. Dupret, N. Van den Bogaert, R. Assaker, V. Regnier, B. Hoevenaars, S. Kruk

CESAME, Université catholique de Louvain, 4 avenue G. Lemaître,
B-1348 Louvain-la-Neuve, BELGIUM

Major progress has been observed during the last 15 years in the numerical simulation of bulk crystal growth. The constant and extraordinarily fast increase of computer power has opened the door to accurate, process-oriented, crystal growth simulation programs (1-3). It is worth observing that this software development activity was, and remains, strongly driven by industrial use, since the principal companies producing single crystals (and especially the silicon growers in view of the silicon market size) can afford to purchase and use large scale software in the frame of their R&D effort. Today, numerical modeling therefore represents an indispensable tool, which combines with experimental methods in order to help design new furnaces and determine optimal processing conditions (4).

Off-line, simulation assisted, control of the growth process aims at four basic objectives. First, one wishes to estimate the relation(s) linking the processing conditions (heater power, pull rate, crystal and crucible or feed-rod rotation rates, magnetic field intensity if any ...) in order to grow a crystal of the desired shape (1, 5). Secondly, the evolution of the temperature field in the grown crystal must be accurately predicted, as a function of the processing conditions and taking into account the effect of heat shields and other constituents (including the encapsulant in LEC growth), since dislocation and defect formation in the solid phase is directly affected by the crystal thermal history (6-12). Thirdly, the shape of the solidification front must be exactly determined, as a function of time, since several critical phenomena take place in its vicinity and, in general, the solid-liquid interface is a mathematical boundary for dislocation and defect calculation (6, 9). Fourthly, the evolution of the melt flow must be well understood and correctly calculated, in view of the direct influence of the flow pattern and regime on striations and crystal composition (from segregation effects), and on the transfer of dopes and impurities (such as oxygen in silicon growth) to the solidification front. From these basic results, additional decoupled simulations can be performed to predict the evolution of dislocations, defects, precipitates ... within the crystal, as long as the governing physics is known (6-12).

The four basic simulation objectives (namely, to link the processing conditions and to determine the crystal thermal history, the interface shape and the melt flow) pose a *coupled, global, non-linear and dynamic inverse problem* (1, 5). The problem is coupled and global, since the heat transfer in the crystal and the melt and the solidification front deformation interact and are linked by radiation transfer in the overall furnace. Non-linearity results from the physics of radiation, convection and solidification. Dynamic effects must be considered in

critical process stages (principally, the seeding and tail-end stages). Finally, the problem is inverse because a natural output (the crystal shape) is prescribed, while a natural input (very often the heater power, but possibly the pull rate) is calculated.

The market demand to continually increase the wafer size results from economical and technological considerations. In silicon growth, the shift from 8" to 12" wafers is accelerating, and the 16" era might even start in the beginning of the next millenary (13). Growing crystals of a larger diameter, however, generally increases the complexity of the melt flow and modifies the balance between the system time constants (14, 19). In Czochralski growth, from small to large diameter crucibles, the melt flow regime changes from steady laminar to laminar periodic or quasi-periodic, and finally weakly turbulent, with in this latter case a complex behavior which is not fully chaotic, but exhibits spatial and temporal organization (15-19). Also, the flow pattern becomes rapidly three-dimensional. On the other hand, the thermal inertia of the different constituents and the solidification front increases with larger furnaces, and this results in longer thermal transients, and thus more significant dynamic effects at the growth time scale (14), while the impact of the much shorter flow transients is more and more pronounced. The tremendous difficulty of the basic simulation problem should therefore be emphasized. Nevertheless, solving this problem is a requirement to grow large single crystals, in view of the many technological difficulties resulting from crystal size increase (13, 14).

There are several ways to act either on the melt flow, or on the crystal thermal history, or on the solid-liquid interface shape. Magnetic fields can be used to damp out the flow turbulence in semi-conductor growth (20-24). Additional heaters and/or water-cooled components can be introduced to better design the heat transfer in the hot zone. All these methods, however, result in an increased number of geometrical and process parameters, and thus in more difficulties to determine the optimal furnace design and operational window for the input conditions. The need to resort to numerical simulation is therefore enhanced.

The objective of the talk will be to present the quasi-steady/time-dependent numerical model that has been developed by the CESAME research center of UCL in order to predict the global temperature field in Czochralski (1, 5, 14, 25), vertical Bridgman and floating zone (23) furnaces. The FEMAG software is based on this work. Calculations are axisymmetric. Radiation transfer is accurately modeled. All the dynamic effects induced by crystal lengthening and crucible lift are considered, together with the heat capacity of each constituent, the motion and thermal inertia of the solid-liquid interface, the deformation of the melt-gas meniscus, and the varying interface radius. The effect of melt convection is taken into account by means of a general axisymmetric flow model, able to represent the mixing effect of the azimuthal and temporal flow oscillations on the global heat transfer (14, 19, 23, 24).

This research is currently supported by the Belgian Program on Inter-university Poles of Attraction and several industrial contracts.

REFERENCES

- 1 – F. Dupret and N. Van den Bogaert, in Handbook of Crystal Growth, D.T.J. Hurle, Editor, Vol. 2B, Chapter 15, p. 875, Elsevier Science, the Netherlands (1994).
- 2 – E. Dornberger, E. Tomzig, A. Seidl, S. Schmitt, H.-J. Leister, Ch. Schmitt and G. Müller, J. Crystal Growth, 180, 461 (1997).
- 3 – K. Takano, M. Iida, E. Iino, M. Kimura and H. Yamagishi, J. Crystal Growth, 180, 363 (1997).

- 4 – T. Duffar and J.Ph. Nabot, *J. Crystal Growth*, 180, 711 (1997).
- 5 – N. Van den Bogaert and F. Dupret, *J. Crystal Growth*, 171, 65 (1997); 171, 77 (1997).
- 6 – E. Dornberger, D. Gräf, M. Suhren, U. Lambert, P. Wagner, F. Dupret and W. von Ammon, *J. Crystal Growth*, 180, 343 (1997).
- 7 – J. Vanhellemont, S. Senkader, G. Kissinger, V. Higgs, M.-A. Trauwaert, D. Gräf, U. Lambert and P. Wagner, *J. Crystal Growth*, 180, 353 (1997).
- 8 – S. Kobayashi, *J. Crystal Growth*, 180, 334 (1997).
- 9 – T. Sinno, R.A. Brown, E. Dornberger and W. von Ammon, *Appl. Phys. Lett.*, 70, 2250 (1997).
- 10 – S. Gondet, Th. Duffar, G. Jacob, N. Van den Bogaert and F. Louchet, submitted to *J. Crystal Growth*.
- 11 – J. Völkl, in *Handbook of Crystal Growth*, Vol. 2B, Chapter 14, D.T.J. Hurle, Editor, p. 821, Elsevier Science, the Netherlands (1994).
- 12 – E. Dornberger, J. Esfandyari, J. Vanhellemont, D. Gräf, U. Lambert, F. Dupret and W. von Ammon, *Proc. 8th Int. Symp. on Silicon Materials Sci. and Technol.*, Electrochem. Soc. Proc., 98-1, 490 (1996).
- 13 – K. Takada, H. Yamagishi, H. Minami and M. Imai, *Proc. 8th Int. Symp. on Silicon Materials Sci. and Technol.*, Electrochem. Soc. Proc., 98-1, 376 (1996).
- 14 – R. Assaker, N. Van den Bogaert and F. Dupret, *J. Cryst Growth*, 180, 450 (1997).
- 15 – G. Müller and A. Ostrogorsky, in *Handbook of Crystal Growth*, Vol. 2B, Chapter 13, D.T.J. Hurle, Editor, p. 709, Elsevier Science, the Netherlands (1994).
- 16 – S. Kimura and K. Terashima, *J. Crystal Growth*, 180, 323 (1997).
- 17 – M. Tanaka, M. Hasebe and N. Saito, *J. Crystal Growth*, 180, 487 (1997).
- 18 – A. Seidl, G. Müller, E. Dornberger, E. Tomzig, B. Rexer and W. von Ammon, *Proc. 8th Int. Symp. on Silicon Materials Sci. and Technol.*, Electrochem. Soc. Proc., 98-1, 417 (1996).
- 19 – F. Dupret, N. Van den Bogaert, R. Assaker and V. Regnier, *Proc. 8th Int. Symp. on Silicon Materials Sci. and Technol.*, Electrochem. Soc. Proc., 98-1, 396 (1996).
- 20 – D.T.J. Hurle and R.W. Series, in *Handbook of Crystal Growth*, Vol. 2A, Chapter 5, D.T.J. Hurle, Editor, p. 259, Elsevier Science, the Netherlands (1994).
- 21 – K. Kakimoto, M. Eguchi and H. Ozoe, *J. Crystal Growth*, 180, 442 (1997).
- 22 – R. Assaker, N. Van den Bogaert and F. Dupret, *Magnetohydrodynamics*, 31, 254 (1995).
- 23 – R. Assaker, PhD thesis, Université catholique de Louvain, Louvain-la-Neuve, 1998.
- 24 – R. Assaker, N. Van den Bogaert and F. Dupret, *Proc 8th Int. Seminar on MHD-Flows and Turbulence*, Jerusalem, 1996, to be published in Progress Series of the AIAA Journal.
- 25 – F. Dupret, P. Nicodème, Y. Ryckmans, P. Wouters and M.J. Crochet, *Int. J. Heat Mass Transfer*, 33, 1849 (1990).

3. To determine the evolution of the solidification front position
 → in view of the critical effect of the interface shape
 on the solidification process
 (→ diffusion, defect, radiation, ... boundary layers).

4. To understand and calculate the melt flow

- in view of the direct effect of the flow pattern/regime
 on crystal striations,
 oxygen and impurity transfer to the crystal,
 ...

Principal aspects of the problem

1. Coupled global problem

- interaction between
 | heat transfer within the crystal
 | deformation of the solidification front
 | overall radiation transfer

2. Nonlinear problem

- effects of
 | radiation
 | melt convection
 | solidification

Modelling and Simulation of Bulk Crystal Growth Considering Melt Dynamics

F. Dupret
 N. Van den Bogaert
 R. Assaker
 V. Regnier
 B. Hoevenaars
 S. Kruk

Off-line bulk crystal growth control Basic objectives of numerical simulation

1. To provide a link between the processing conditions (heater power, pull rate, crystal and crucible rotation rates, magnetic field intensity, ...)
 → in order to grow a crystal of the desired shape.
2. To predict the temperature evolution in the crystal, taking into account the overall furnace geometry
 → in order to understand/predict the formation of defects in the crystal.

2. Dynamic model

- Vertical motion of crystal, crucible ...
→ evolution of view factors
- Crystal, melt, solidification front and meniscus shape evolutions
- Heat capacity of all the constituents
+ interface thermal inertia
- Direct or inverse calculations
(+ quasi-steady analysis)

3. Dynamic problem

→ critical process stages

seeding
shouldering
tail-end
post-growth

4. Inverse problem

→ with

prescribed natural output (crystal shape)
calculated natural input (heater power or ...)

Basic aspects of the FEMAG software

1. Global model

- Subdivision of the furnace into macro-elements
(radiative, conductive, shell, ... + crystal-melt)
- Assembly of macro-elements
| temperature continuity and heat flux balance
| solidification heat
| outer boundary conditions
- Accurate radiation calculations
(axisymmetric view factors)

3. Melt flow

- Axisymmetric and quasi-steady
- Laminar or turbulent (mixing length or k-l models)
- Axisymmetric rigid magnetic fields (axial or cusp)
- Marangoni convection
- Simplified evolution model

Principal modeling difficulties

1. Melt flow problem

- 3D, time-dependent physics (with short time constants)
Quasi-steady flow model ? (required for global simulations)

- Turbulence

2. Geometrical problem

- Objective : automatic prediction of the entire growth process
- Complex unknown evolution of the geometry, with large deformations and topological changes

Physical hypotheses

1. Radiation transfer
 - Diffuse surface radiation
 - Band-energy method
(wavelength-dependent properties; semi-transparent media)
2. Fourier heat conduction
 - Temperature dependent material properties

Melt flow

Physical model

Hypotheses : Incompressible Newtonian fluid
Boussinesq approximation
Steady, turbulent or laminar flow

Reynolds equations :

$$\rho_0 \left(\frac{\partial \mathbf{v}}{\partial t} + (\mathbf{v} \cdot \nabla) \mathbf{v} \right) = -\nabla p + \nabla \cdot ((\mu + \mu_r)(\nabla \mathbf{v} + \nabla^T \mathbf{v})) - \rho_0 \beta (T - T_0) \mathbf{g} + \mathbf{J} \times \mathbf{B}$$

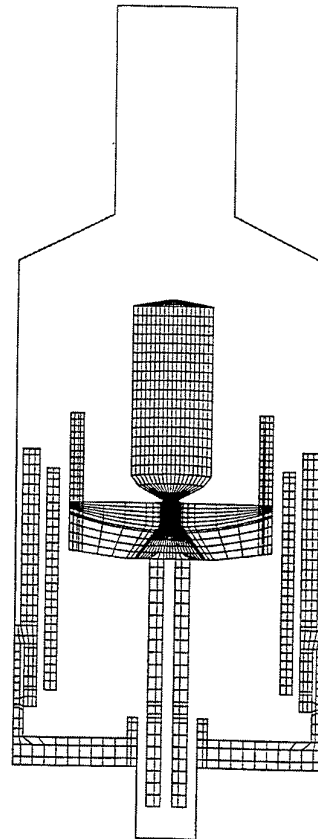
$$\nabla \cdot \mathbf{v} = 0$$

β : volumetric expansion coefficient
 μ_r : turbulent viscosity
 \mathbf{B} : magnetic induction
 \mathbf{J} : current density

Impact of crystal diameter increase

1. Change of melt flow regime
 - steady laminar \longrightarrow laminar periodic \longrightarrow
 \longrightarrow laminar quasi-periodic \longrightarrow weakly turbulent
 - chaotic, with however spatial/temporal organization
 - three-dimensional
2. Increase of thermal inertia of
 - the furnace constituents
 - the solidification front
 - longer thermal transients
 - more significant dynamic effects at the growth time scale
 - enhanced effect of flow transients

- Objective : to perform the time-dependent simulation of the whole Czochralski (or Bridgman or float zone) process including all growth stages.
- Develop a completely automatic algorithm in order to easily switch between different geometrical configurations.
- Compute heat and mass transfer on any geometry.
- Analyze the physics of the critical stages of the process.



$R_{\text{CRYSTAL}} = 10 \text{ cm}$
 $R_{\text{CRUCIBLE}} = 22 \text{ cm}$

PULL RATE = 2.4 cm/h.
 CONE ANGLE = 60°
 (← VERTICAL DIRECTION)

Hypothesis : Diffuse surface radiation

Energy equation

$$\rho c \left(\frac{\partial T}{\partial t} + (\mathbf{v} \cdot \nabla) T \right) = \nabla \cdot ((k + k_t) \nabla T) + w$$

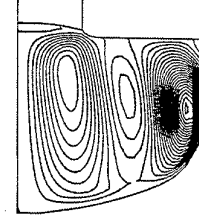
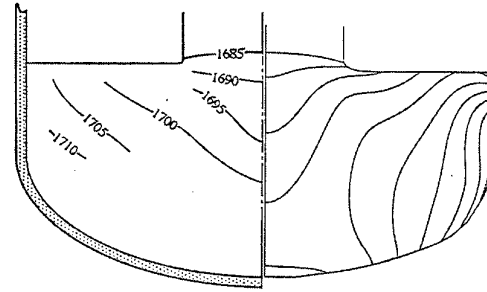
Interface equation

$$T = T_{\text{tp}}$$

T_{tp} : Triple point temperature
 k_t : Turbulent conductivity
 w : Heat source

EXPERIMENTS

MIRROR FREE-SURFACE
CONDITIONS



k-l model c1=0.3 Prt=1 Galerkin method

Heat and mass transfer in silicon melt under magnetic fields

Direct observation and numerical simulation of molten silicon flow during crystal growth under magnetic fields by X-ray radiography and large-scale computation

Kakimoto Koichi

Institute of Advanced Material Study, Kyushu University,
6-1, Kasuga-Koen, Kasuga, 816-8580 Fukuoka, JAPAN

1. Introduction

This lecture introduces how several kinds of magnetic fields modify melt flow of silicon during crystal growth in a Czochralski growth furnace. The first part of this lecture is how to visualize melt flow under magnetic fields. Subsequently, three-dimensional time-dependent calculations of melt flow under several types of magnetic fields. Finally, video films on melt flow under magnetic field visualized by X-ray radiography [1] and numerical simulation [2] will be introduced.

2. Magnetic fields

Magnetic fields have not been utilized for controlling melt flow except some specific production of silicon so far, although several kinds of magnetic fields have been reported. Diameter of growing crystals is increasing due to requirement of chip size, therefore, melt flow becomes turbulent. Since melt flow should be more quiescent use of magnetic field to control melt flow is opening up a new fields to control flow of silicon melt in a large crucible. This lecture focused on how magnetic fields such as cusp-shaped, vertical and horizontal magnetic fields affect melt flow.

3. Visualization by X-ray

The visualization system shown in Fig.1 is based on X-ray radiography and on a solid tracer method. In order to adopt this method for observation of molten silicon flow under the magnetic fields, it is necessary to protect an X-ray source and an X-ray camera from leakage of magnetic fields from magnets because magnetic fields modulated X-ray

radiograph image. In this lecture, apparatus for crystal growth under the magnetic fields such as VMF and CMF, and an improved observation system for molten silicon flow are introduced. Reduction of flow velocity in the melt is also introduced under a VMF using this system.

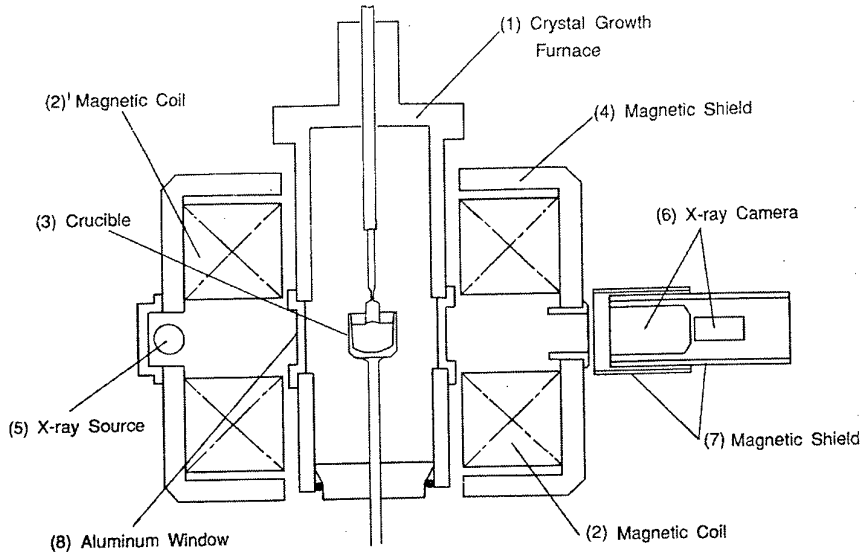


Fig. 1 Schematic diagram of the magnetic field applied CZ crystal growth furnace with X-ray radiography system.

4. Three-dimensional time-dependent calculation

Control volume method was used for discretizing the governing equations such as continuity, Navier-Stokes, energy, and impurity transfer equations in the present calculation. Using Alternating Directional Implicit (ADI) method as a matrix solver carried out time-dependent calculation with three-dimensional geometry. Governing equations of continuity, Navier-Stokes, energy and impurity transfers are expressed in eqs. (1-3).

$$\frac{\partial \rho}{\partial t} + \nabla \rho u = 0, (1), \quad \rho \frac{\partial \Phi}{\partial t} + u(\rho \nabla \Phi) = \nabla(\Gamma \nabla \Phi) + S_{\Phi}, (\Phi = u, T, c) (2), \quad S_{\Phi} = -\nabla p + F (= \rho g) + f, (3)$$

where, ρ , T , Γ are density, temperature and diffusivity for the variables such as velocity, temperature and impurity concentration. p , f and g are pressure, an external forces such as Lorenz and viscous forces, and gravitational acceleration, respectively. u , T and c are velocity, temperature and impurity concentration, respectively. S is a source term of each valuables of velocity, temperature and impurity concentration.

When the effect of magnetic fields was taken into account, Lorenz force (f_L) expressed by eq. (4) was included in eq. (3) as an external force,

$$f = J \times B, \quad (4) \quad J = \sigma(-\nabla\Psi + u \times B), \quad (5)$$

where J , Ψ , σ and B are electric current, scalar potential, electric conductivity and magnetic field, respectively. When effects of cusp-shaped magnetic fields (CMF) was calculated the following equation based on Biot and Savart's law was used by taking into account electric current which was distributed in the solenoids with a finite volume,

$$dH = \frac{1}{4\pi\mu_0} \left(\frac{Idl \times r}{r^3} \right) dV, \quad (6)$$

where H , μ , J are the magnetic field strength, permeability, and current in solenoids, respectively. r and V are the distance and volume, respectively. Equation (6) was numerically integrated to obtain magnetic field at specific points.

5. Time dependent flow

Figure 2 shows temperature and velocity distributions under a cusp-shaped magnetic field [3]. Asymmetric temperature and velocity distributions can be observed, although symmetric temperature distribution was imposed around a crucible wall.

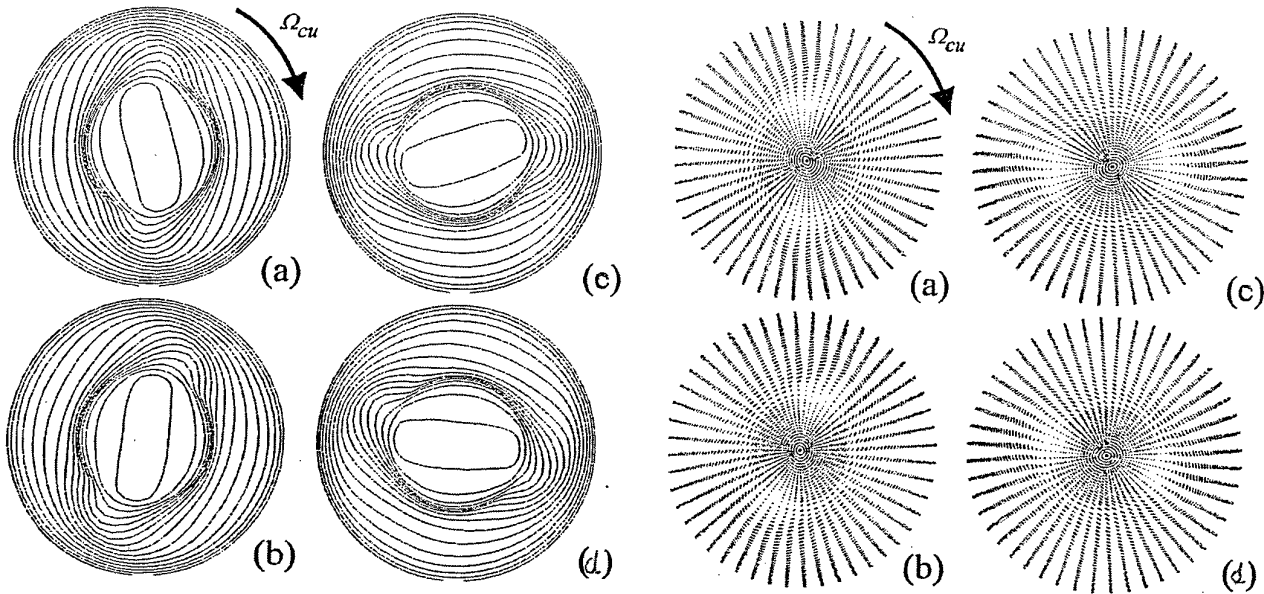


Fig. 2 Temperature and velocity distributions in the top of silicon melt.

Ref. 1) K. Kakimoto, Prog. Crystal Growth and Charact., 30 (1995) 191.

2) K.-W. Yi, et al., Jpn. J. Appl.Phys., 33 (1994) L487.

3) Y-C Won, et al., ICCG-12 Proceedings.

Heat and mass transfer in silicon melt under magnetic fields

K. Kakimoto

Institute of advanced material study
Kyushu university
6-1, Kasuga-Koen, Kasuga 816
Japan

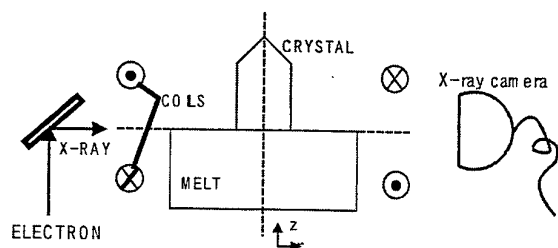
Outline

1. Flow visualization
& numerical simulation
2. Crucible & crystal rotation effects
3. Magnetic field effects

Outline

- Flow visualization of liquid metal of silicon (X-ray)
- Numerical technique
- Benard and baroclinic instabilities
- Magnetic field effects
- Oxygen sensors
- Thermo-physical propertied by molecular dynamics
- Summary

Experimental system



Schematic of a cusp-shaped magnetic field

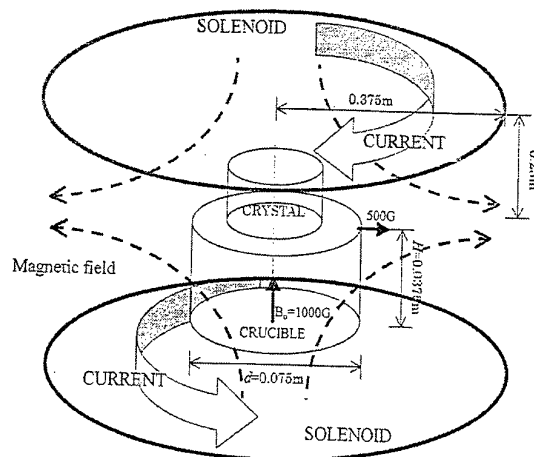
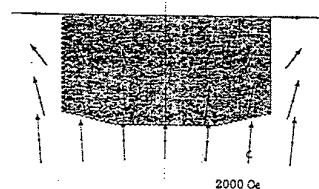


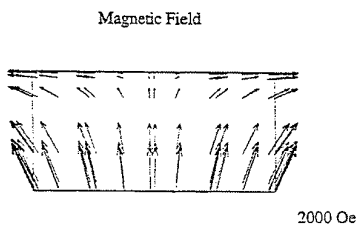
Figure 2. Dimension of magnetic field B.

Magnetic Fields



Experimental

After Hoshikawa
Et al.



Calculated

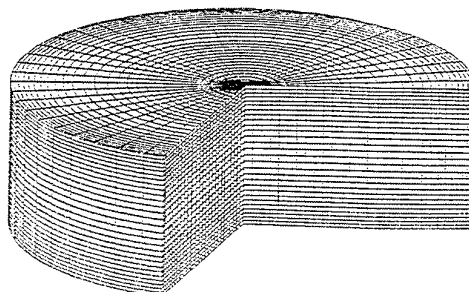
Calculation Method

$$\rho \left[\frac{\partial \phi}{\partial t} + \frac{1}{r} \frac{\partial u \phi}{\partial r} + \frac{1}{r} \frac{\partial v \phi}{\partial \theta} + \frac{\partial w \phi}{\partial z} \right] =$$

$$\frac{1}{r} \frac{\partial}{\partial r} \left[r \Gamma_{\phi} \frac{\partial \phi}{\partial r} \right] + \frac{1}{r^2} \frac{\partial}{\partial \theta} \left[\Gamma_{\phi} \frac{\partial \phi}{\partial \theta} \right]$$

$$+ \frac{\partial}{\partial z} \left[\Gamma_{\phi} \frac{\partial \phi}{\partial z} \right] + S_{\phi} \quad (2)$$

$$\vec{F} = \vec{J} \times \vec{B}, J = \sigma(E + u \times B) \quad (3)$$

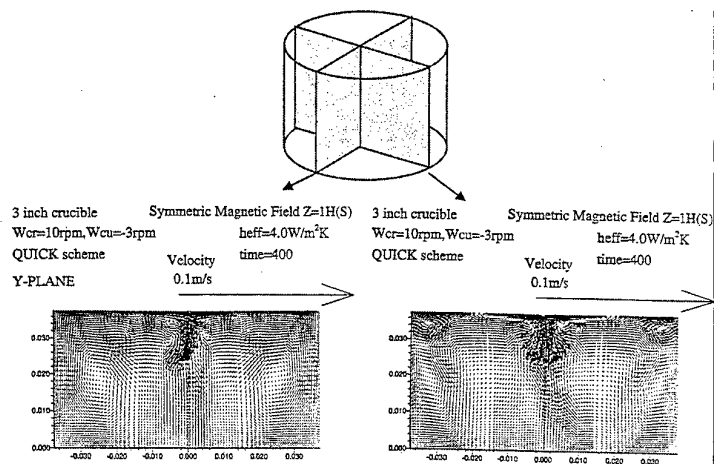


Questionnaire

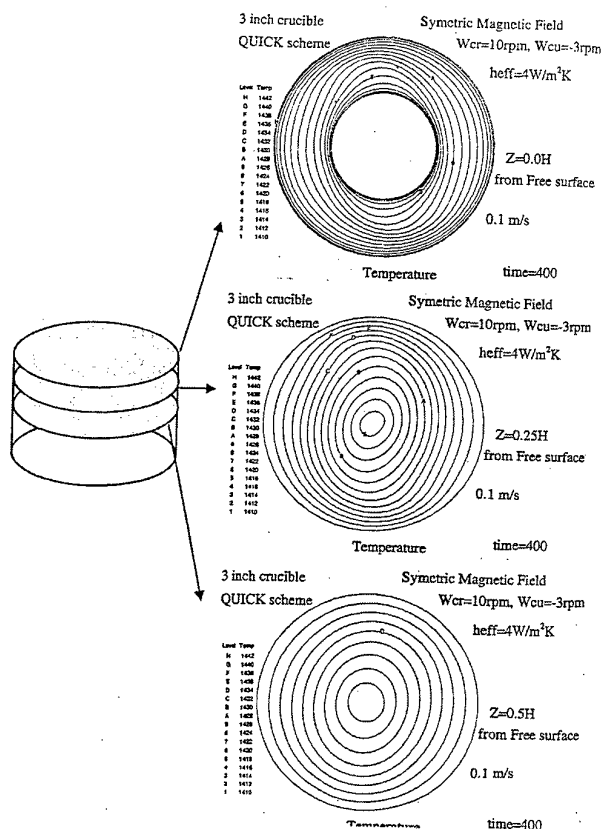
- ◆ Magnetic fields really suppress flow velocity of metallic melt ?

→
No, Some parts are enhanced

Three-dimensional Velocity Vectors



Three-dimensional Temperature Distribution



Sequential Temperature Contours

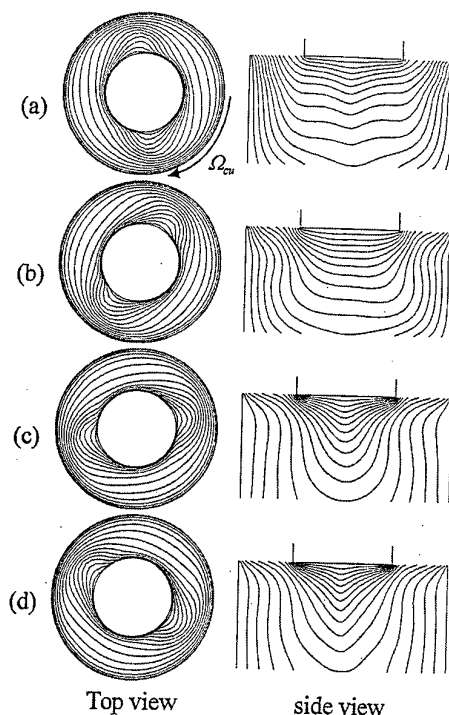
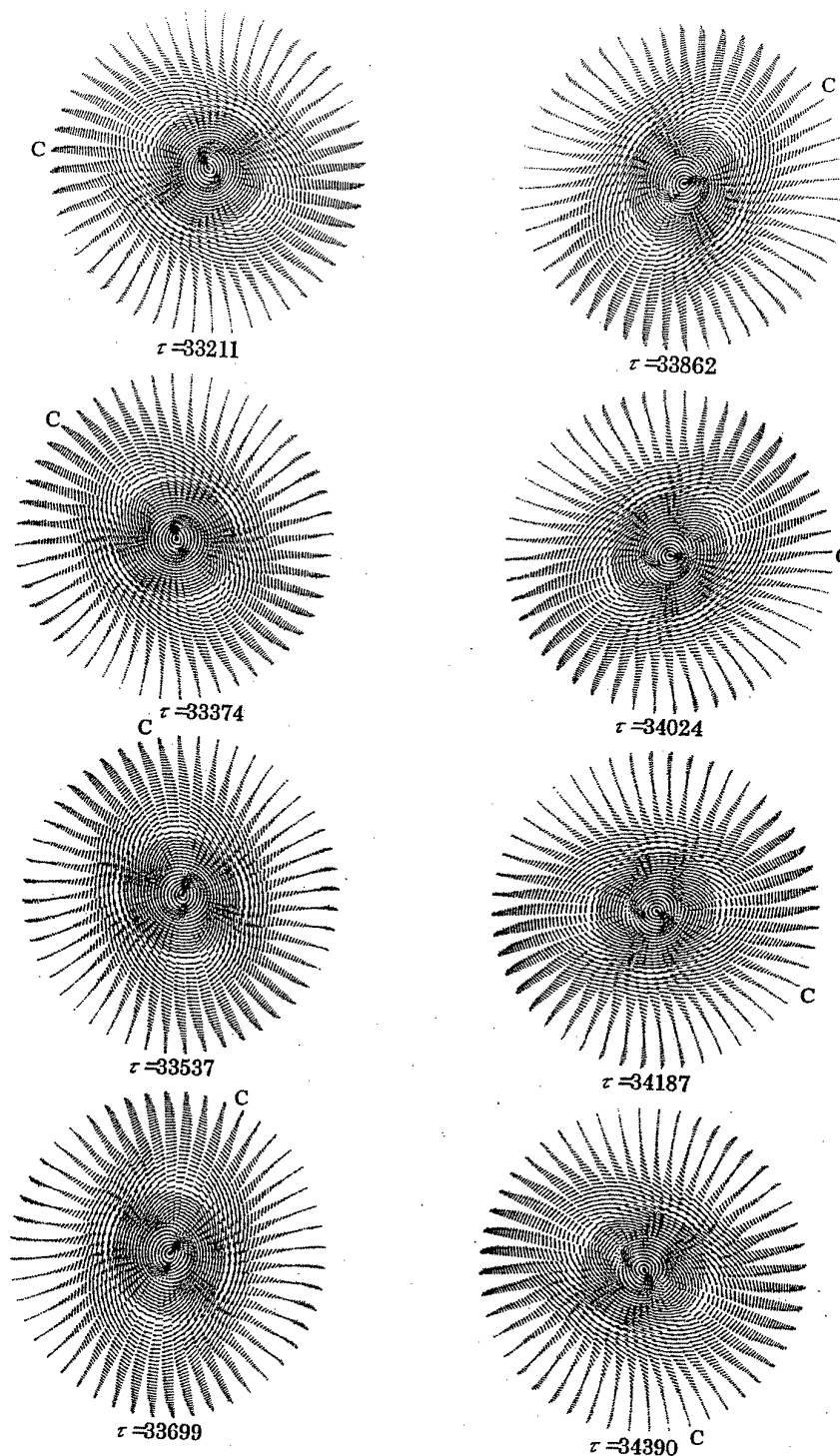


Figure 12. A series of instantaneous contours of temperature at the top of silicon melt ($Z=1H$) and in a vertical cross section $SX-SX'$ from $r=47480$ to $r=48455$ and $Ha=161$.
(a) $t=7480$ (b) $t=7800$ (c) $t=8120$ (d) $t=8440$

Velocity vectors



Velocity vector from rotating coordinate at 0.25H from the top of silicon melt ($z=0.75H$) from $\tau = 33211$ to $\tau = 34390$.

Temperature distribution

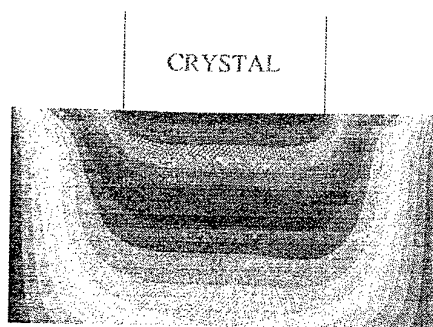


Figure 20. Temperature at SX-SX' section

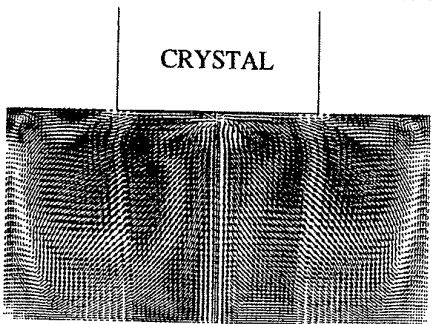


Figure 21. Velocity profile at SX-SX' section

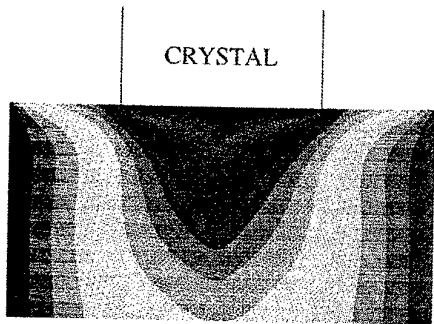


Figure 22. Temperature at SY-SY' section

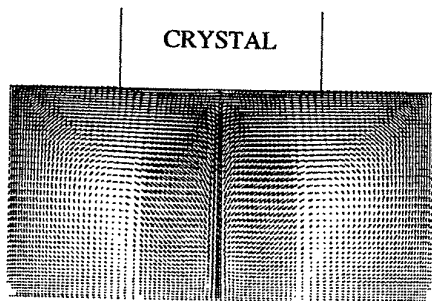
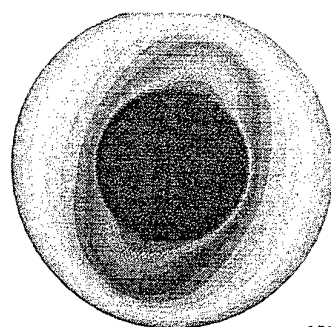
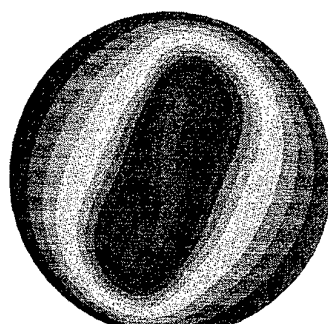


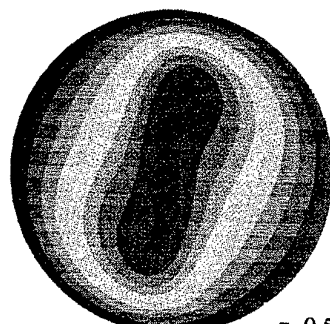
Figure 23. Velocity profile at SX-SX' section



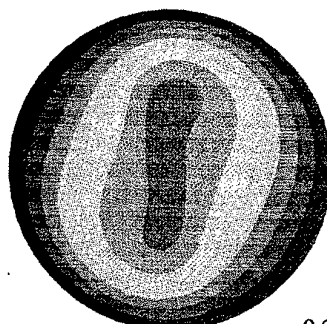
$z=1H$



$z=0.75H$



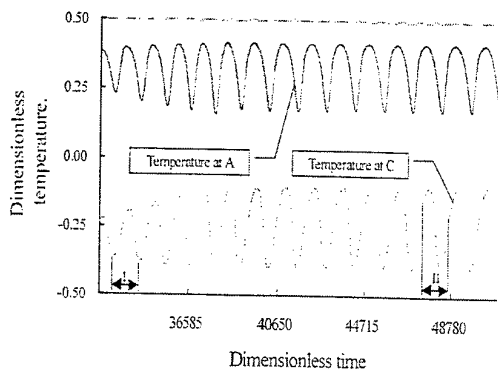
$z=0.5H$



$z=0.25H$

Figure 24. Temperature distribution of each horizontal cross section at $\tau=47724$.

Temperature Fluctuation



Temperature variation along time at point A and point C.

Period I is for $\tau = 33211$ to $\tau = 34390$.

Period II is for $\tau = 47480$ to $\tau = 48699$.

Oxygen concentration

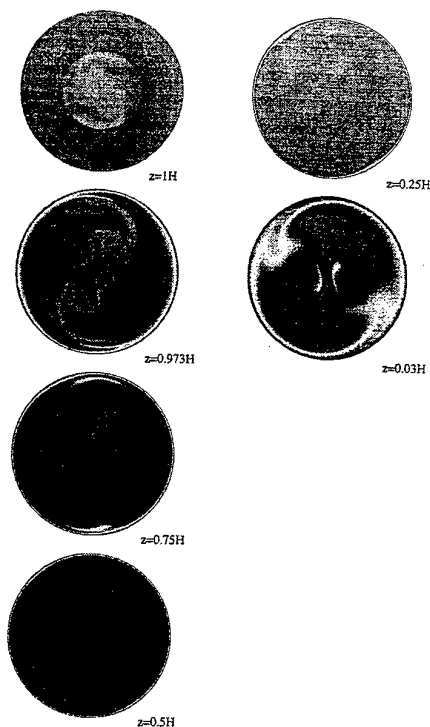
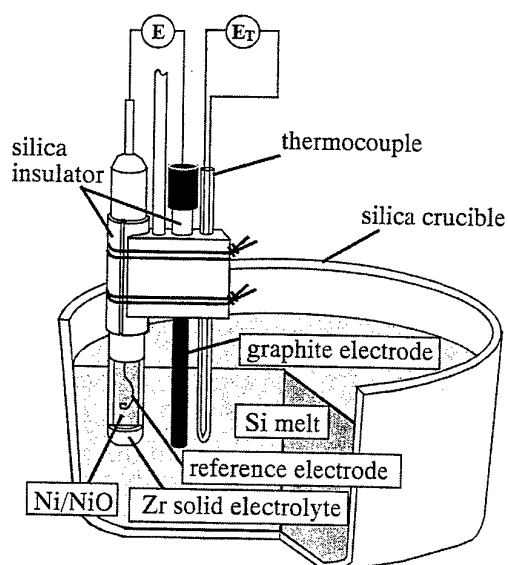
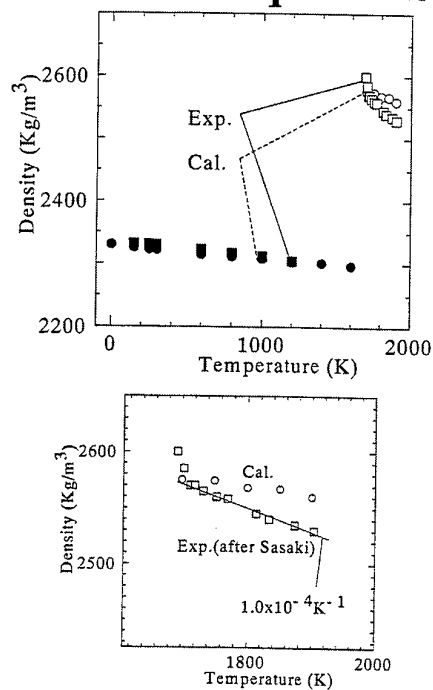


Figure 8. Oxygen concentration profile of each cross section at $\tau = 47724$

Oxygen sensor for silicon melt



Density temperature dependence of solid and liquid silicon



SIMULATION ASPECTS OF TECHNOLOGICALLY IMPORTANT HYDRODYNAMICS, HEAT/MASS TRANSFER PROCESSES DURING CRYSTAL GROWTH

V.I. POLEZHAEV

Institute for Problems in Mechanics, Russian Academy of Sciences
117526 Moscow, Prospect Vernadskogo 101

Extended Abstract

Lecture contains description of ideas, strategy and concrete results of Technological Hydrodynamics, using mathematical models for study of forced and natural convection, heat and mass transfer processes for crystal growth with the aim of improvement of technology and quality of crystals [1-4] (see also [5-9]). The way for realization of this conception is to combine the numerical methods for hydrodynamics processes with the knowledge of technology and connection of physical modelling, data of material properties and industry setups.

Classification of the technologically important hydrodynamics, heat/mass transfer processes during crystal growth by the principle of driven forces includes mechanical (forced) convection, gravitational (natural) convection, surface - driven (natural nongravitation) convection and electromagnetic. However each of these groups consists from several elementary processes. For instance, gravitational-type of convection in binary double - diffusion system consists from a number of cases for different mutual directions of heat and mass fluxes and gravity vector. Similar situation exists for surface-driven convection in binary system .

Different types of convection may be positive or negative for materials perfection and technology processes productivity and working not only in earth, but also in microgravity. Each of mentioned motions have complex: inner structure with boundary layers near solid walls, hydrodynamic "core" inside the crucible and very often secondary flows.

Development of the special hierarchy of the models and tools for simulation of the hydrodynamics, heat transfer and impurity distribution on the basis of general equations of fluid mechanics (Navier-Stokes equations) are discussed in the first part of the lecture [2, 3, 10-12].

Temperature oscillations of fluid flow induced by instability and nonlinear interaction in Czochralski system are studied in second part of the lecture using direct computer simulation and stability analysis on the basis of unsteady Navier-Stokes equations for axisymmetry and three- dimensional approaches. Different

kinds of control actions: a) dynamic (mechanical) (ratio, values and the sign of rotation of crystal and crucible are varied in numbers as well as time), b) heat (local distribution of the total heat flux supplied to the crucible, thermal boundary conditions, c) geometry (the shape of crucible and the values, H/R_c , R_c/R_s as well as portions inside the crucible are variable) and d) gravity (varying the value and direction to control the gravitational mechanism of convection).

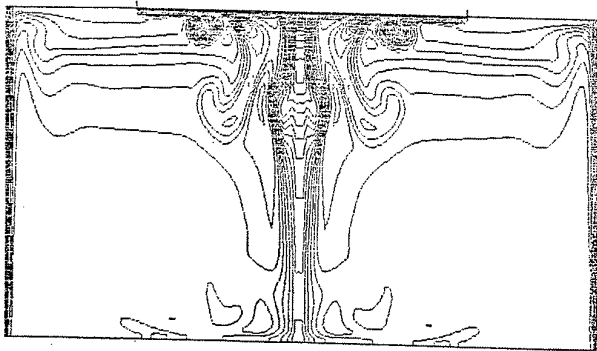
The talk is focused on the results of parametrical analysis of nonlinear coupling fluid flows. It makes use of new mathematical modelling technique and includes comparison with experimental data and analysis of the microgravity alternatives to avoid instability and temperature oscillations in the melt [11-13]. Analysis makes use of the parameters of international benchmark for the prescribed temperatures on the seed and crucible wall, thermal isolation of the crucible bottom and linear temperature distribution on the free melt surface [14, 15].

Nature of oscillations and damping of oscillations using adiabatic melt surface is discussed. Parametrical analysis of ground-based regime of semiisolating GaAs crystal growth with counterrotation will also be presented. Oscillation's mechanism for the case of zero rotation and for the coupled nonlinear flows case are presented in axisymmetrical and three dimensional approaches. Two types of gravity - driven convection: the due to cooling above of the disk and side heating of crucible will be discussed. Validation of computational solutions is discussed using comparison with new experimental data of temperature oscillation for transparent liquid as well as GaAs encapsulation growth [16, 17]. Computer simulation and video visualization of the unsteady convective processes are done on the basis of special version of PC-based system "COMGA" and computer laboratory [11]. Development of optimized growth process and growth parameters, the requirements of crystal growth equipment, crucibles, process control are discussed on the basis of the presented here and published results [17-22].

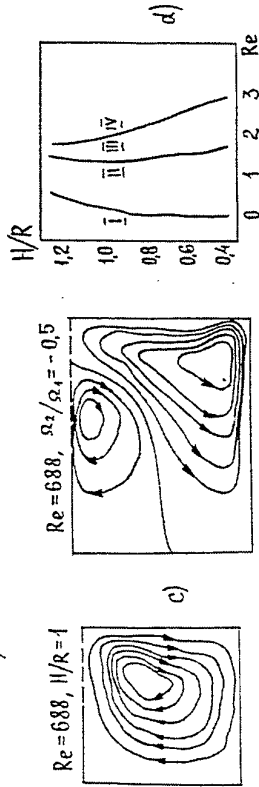
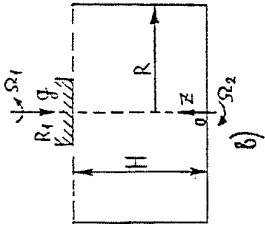
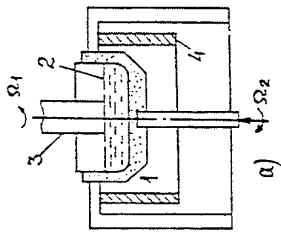
REFERENCES

1. Hydrodynamics heat and mass transfer during material processing (eds.) S. Avduevsky, V.I. Polezhaev. Nauka, Moscow, 1990, 275 p., (in Russian).
2. V.I. Polezhaev, A.V. Bune, N.A. Veresub et al. Mathematical modelling of the convective heat and mass transfer on the basis of Navier-Stokes equations. Nauka, Moscow, 1987, 271 p., (in Russian).
3. Polezhaev V.I., Comput. Methods Appl. Mech. Engr., Vol. 115, 1994, P. 79-92.
4. V.I. Polezhaev, In: Crystals growth, properties and applications. V.I.O. Springer-Verlag, 1983, 87 p.

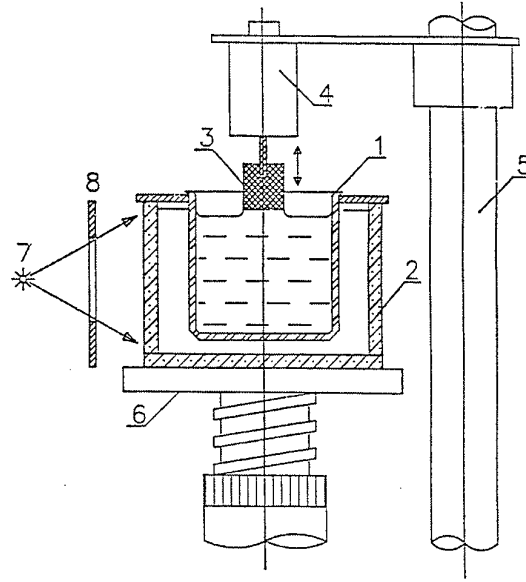
5. Carruthers J.R., In: Preparation and Properties of Solid State Materials (Eds. W.R.Wilcox, R.A. Lefever), V.3, P. 1-121, Marcel Dekker, Inc. New York and Basel, 1977.
6. G.Müller, In: Crystals, growth, properties and applications. V.12. Crystal growth from the melts. Springer-Verlag, 1988.
7. Hurle D.T.J. Crystal pulling from the melt. Springer, 1993.
8. Dupret F., Van Den Bogaert N., In: Handbook of Crystal Growth, ed. D.T.J. Hurle, Vol. 2, P. 875-1010, 1994.
9. Müller, G. and Ostrogorsky, A., In: Handbook of Crystal Growth, Vol. 2, P. 711-819, 1994.
10. L.D.Landau, E.M.Lifshitz. Fluid mechanics. Pergamon Press, 1959.
11. M.K.Ermakov, S.A.Nikitin, V.I.Polezhaev, Fluid Dynamics, Vol.32, No.3, 1997, P. 338-350.
12. V.I. Polezhaev, M.K Ermakov, S.A. Nikitin et al., In: Proceedings of Int. Symposium on Advances in Computational Heat Transfer 26 - 30 May, 1997 Cesme, Turkey, Advances in Computational Heat Transfer, Begel House, 1998, P. 492-499.
13. Nikitin N.V., Polezhaev V.I., Fluid Dynamics, 1998 (in press).
14. Wheeler A.A., J. Crystal Growth 102, 1991, 691.
15. Bückle, U. and Schäfer, M., J. Crystal Growth, Vol. 126, P. 682-694, 1993.
16. Polezhaev V.I., Prostomolotov A.I., Verezub N.A. et al., Symp. on heat and mass transfer processes and single crystal growth. Obninsk, Russia, 22-24 September 1997, In: Cristallgrafiya, 1998 (in press).
17. Kosushkin V.G., Polezhaev V.I. Zakharov B.G. In.: Proceedings of the Microgravity Science and Applications Session. International Aerospace Congress, Moscow, (Eds.) R.K.Crouch, V.I. Polezhaev, 1995, P. 141-146.
18. Rappl H.O., Matteo Ferraz L.F., Scheel H.J., et al. Journal of Crystal Growth. (North-Holland Physics Publishing Division), Amsterdam, V.70, 1984, P. 49-55.
19. Ristorcelli J.R., Lumely J.L., J. Crystal Growth 116, 1992, P. 447-460.
20. Qiang Xiao, Jeffrey J.Derby, Journal of Crystal Growth 152, 1995, P. 169-181.
21. Seidi A., McCord G., Muller G., Leister H.-J., Journal of Crystal Growth 137, 1994, P. 326-334.
22. Wagner C., Friedrich R., In: New results in numerical and experimental fluid mechanics: Braunschweig, Germany, 1996 / ed. by Horst Korner and Reingard Hilbig.- Braunschweig: Vieweg, 1997, P. 367-380.



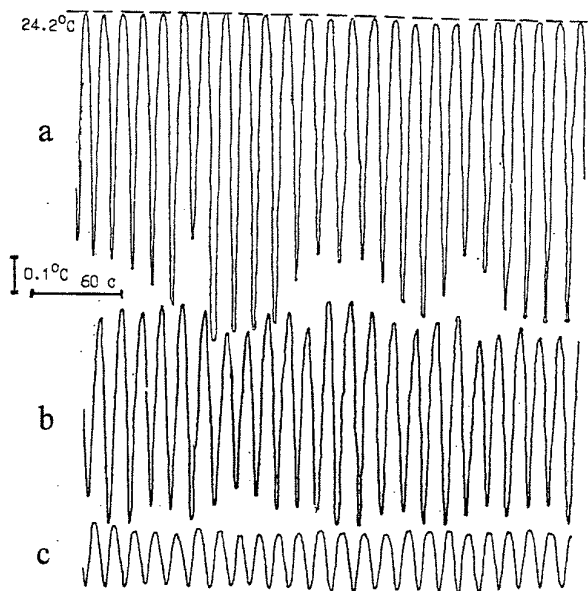
Isotherms of thermals under crystal, induced by thermal gravity-driven convection.
Simulation, axisymmetrical case, 81×81 ,
 $Pr=6.5$, $Gr=4.5 \cdot 10^7$, $Re_s=Re_c=0$



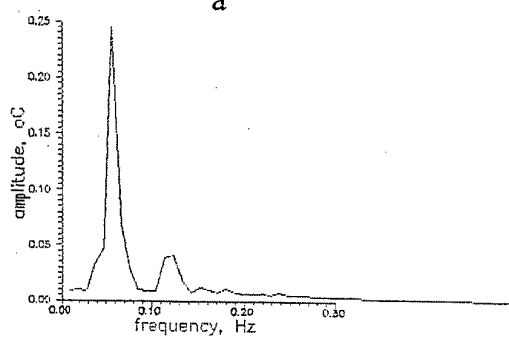
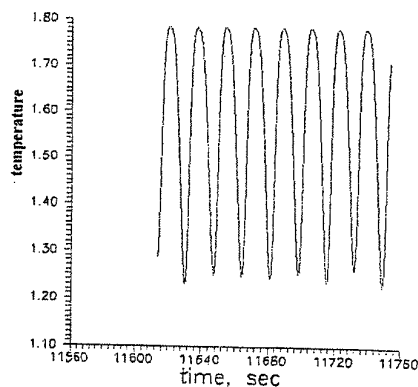
Scheme of Czochralski growth (a) and mathematical model (b).
Modelling results: structure (c) and regimes (d) of isothermal flow



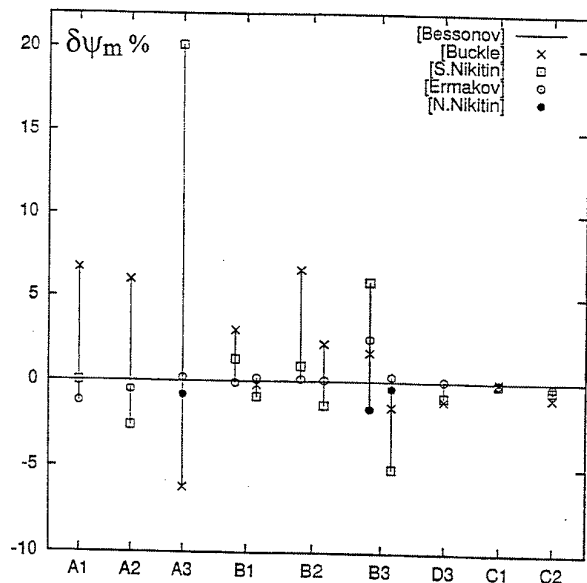
Scheme of Czochralski modelling with the use of transparent liquids: 1 - crucible, 3 - model of the crystal, 4 - vibrator, 5 - support, 6 - table with vertical transport, 7 - light



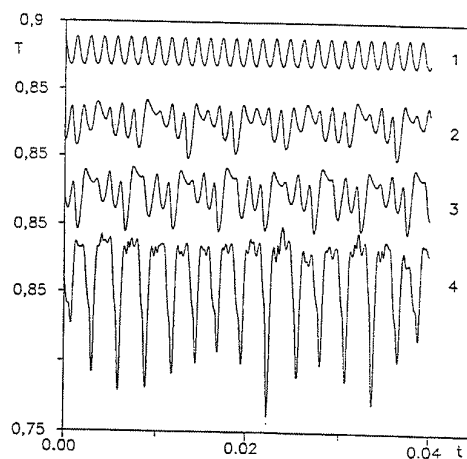
Temperature oscillations, induced by convective instability in Czocharlski model $Gr = 2 \cdot 10^6$, $Pr = 6.5$, $\Delta T = 2$ grad, $H/Rc = 1.0$, $Rc/Rs = 2.0$, $h = 2$ mm. Measurement's results:
a) - $r = 0.5$, $z = 1.86$, b) - $r = 0.5$, $z = 1.94$,
c) - $r = 0.5$, $z = 1.98$



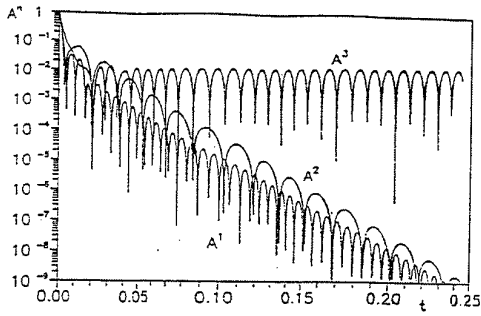
Temperature oscillations (a) and spectrum of oscillations (b) in a water. Simulation $Pr = 6.5$, $Gr = 2 \cdot 10^6$, $Re_s = Re_c = 0$, $r = 0.5$, $z = 1.86$, (Calcul. period - 16 sec, Measur. - 13 sec)



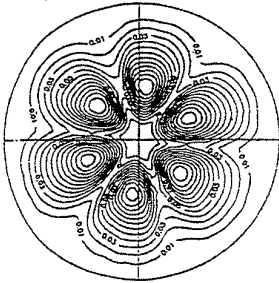
Comparison of the numerical results for benchmark problem (A.Wheeler, 1991).
% Deviation:
A1, A2, A3, B1, B2, B3 - Min. values of ψ ,
B1, B2, B3, D3, C1, C2 - Max. values of ψ



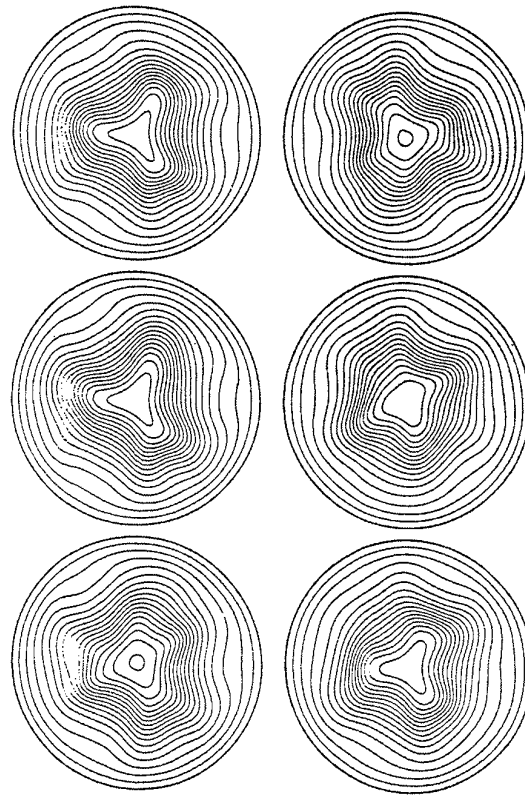
Temperature oscillations for benchmark problem, $Re_s = Re_c = 0$ (point $r = 0.64$, $z = 0.5$); transition to chaos; Gr numbers:
1 - $6 \cdot 10^6$, 2 - $7 \cdot 10^6$, 3 - $7.5 \cdot 10^6$, 4 - 10^7



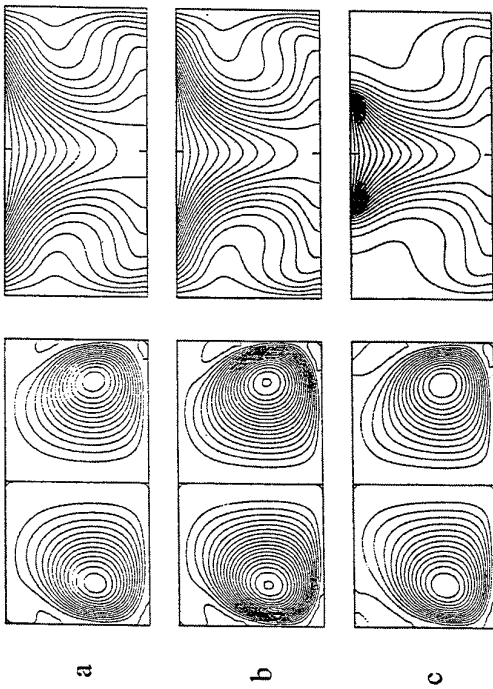
Three dimensional instability: temporal behavior of the function for different modes as illustration critical Grashof value for benchmark problem C ($Gr_c = 5\ 105$)



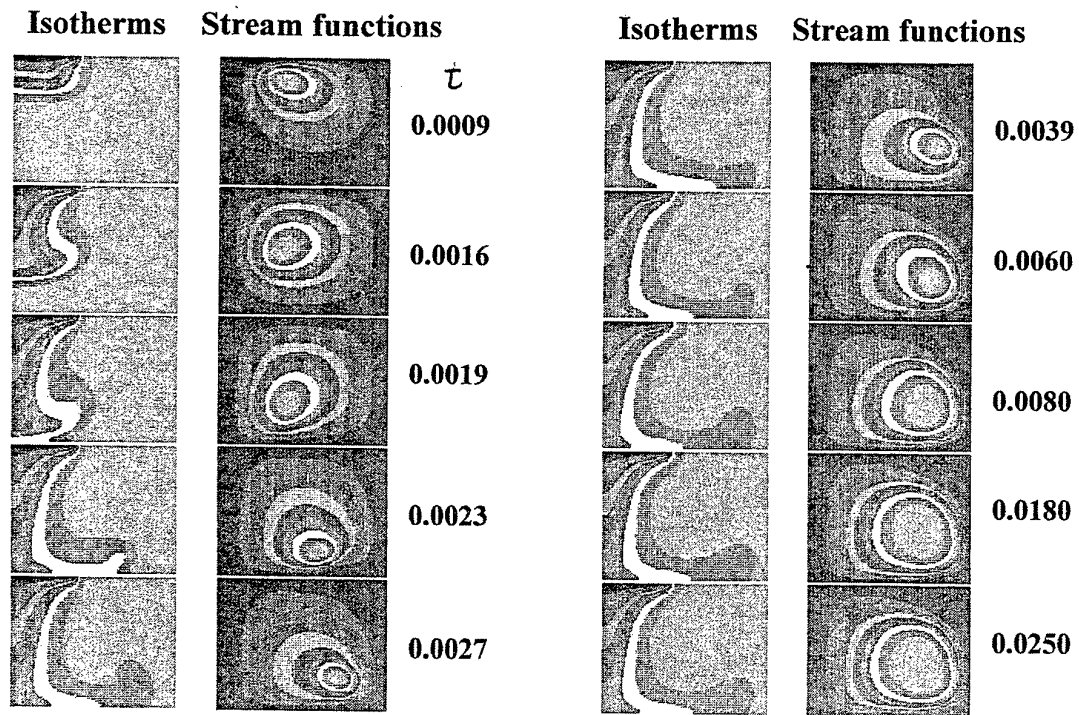
Three dimensional instability: isolines of the mean square of temperature oscillations, $z = 0.85$, C2 problem ($Gr = 106$)



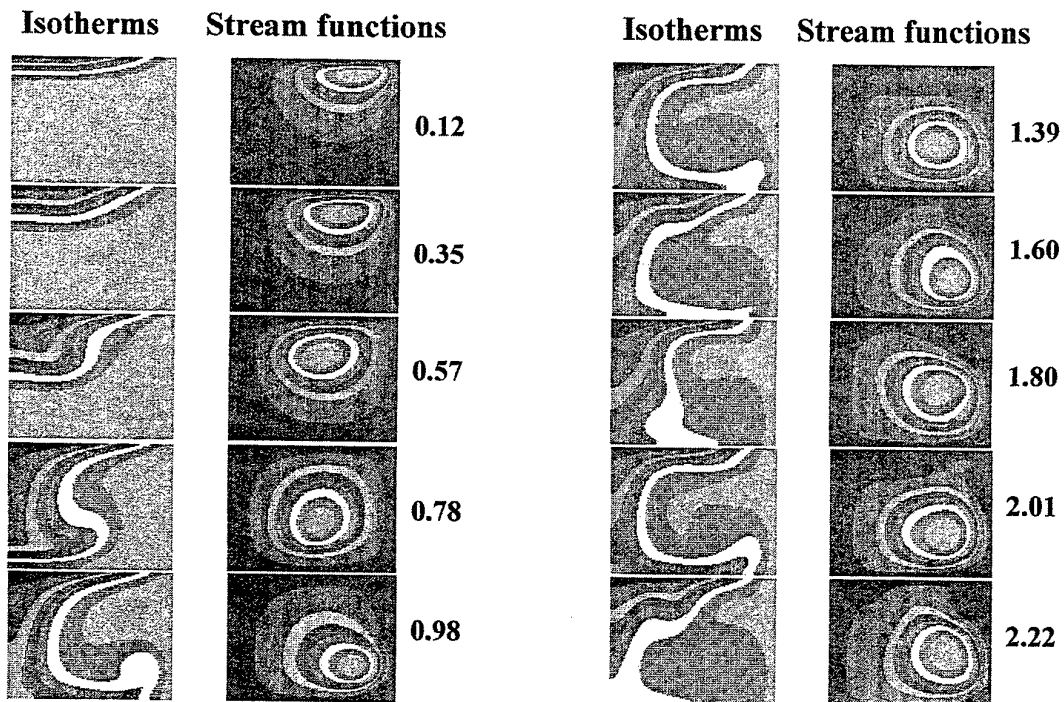
Three dimensional approach: Temporal behavior of isotherms for $Gr = 106$, $z = 0.86$ (linear profile on the free surface of the melt)



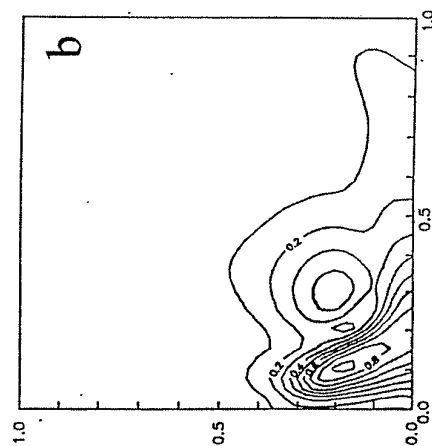
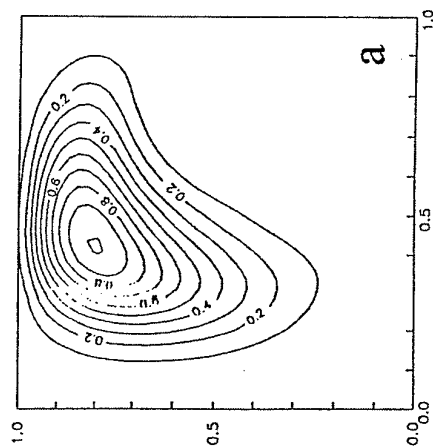
Stream function isolines (left) and isotherms (right), different boundary condit. on free surface of melt:
a) 5 105, b) 106 - linear temperature profile, c) 106 - adiabatic



**Benchmark C2 with thermal isolations of the crucible surface ,
 $Gr = 6 \cdot 10^6$, $Ws = 0$, $Wc = 0$. Isotherms and Stream functions.**



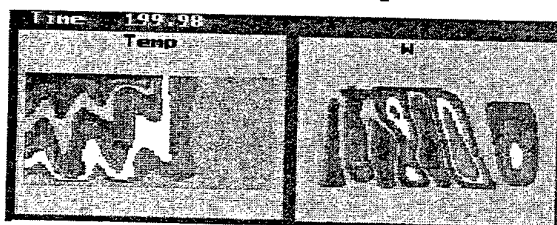
**Benchmark C2 , $Gr = 6 \cdot 10^6$, $Ws = 0$, $Wc = 0$
 Isotherms and Stream functions.**



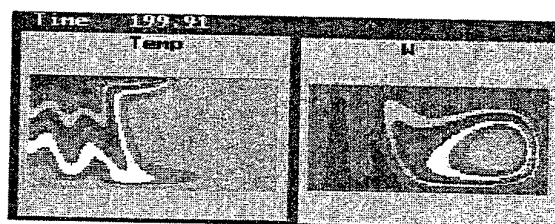
Instability of the axsymmetrical flows.
Fields of the eigenfunction's amplitudes
a) $n = 3$, $Res = 0$, b) $n = 1$, $Res = 103$

$$Gr = 7.8 \cdot 10^7, Ws = 0$$

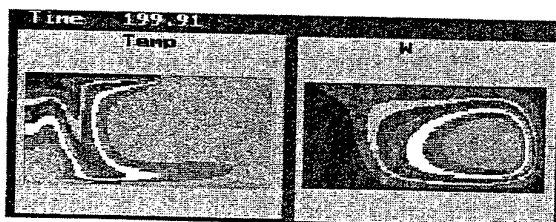
$Wc = 10$ rpm



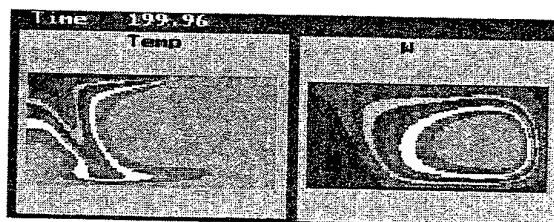
$Wc = 3$ rpm



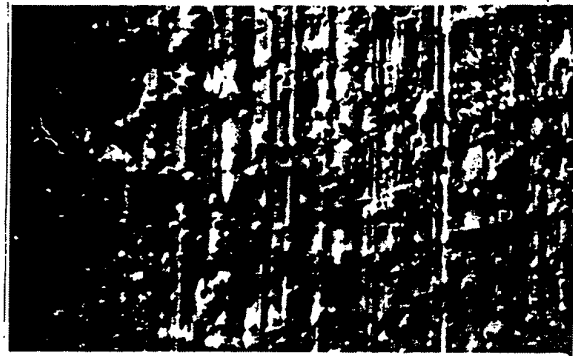
$Wc = 2$ rpm



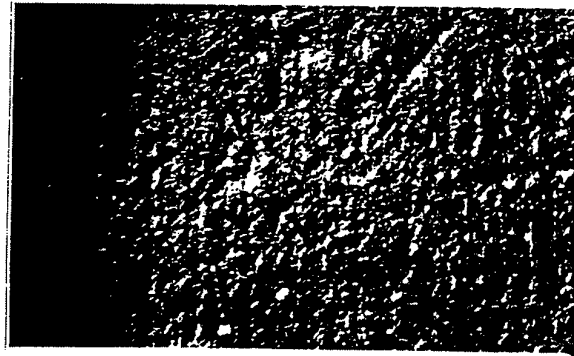
$Wc = 1.5$ rpm



**Damping of the W-type structure of temperature oscillations
using reduction of the crucible speed rotation**



a



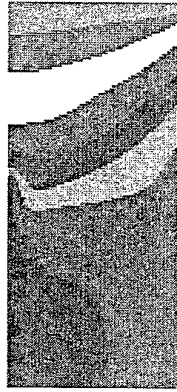
b

Metallographic pictures of the crystal section grown (a) without and (b) with oscillations of the heater's temperature

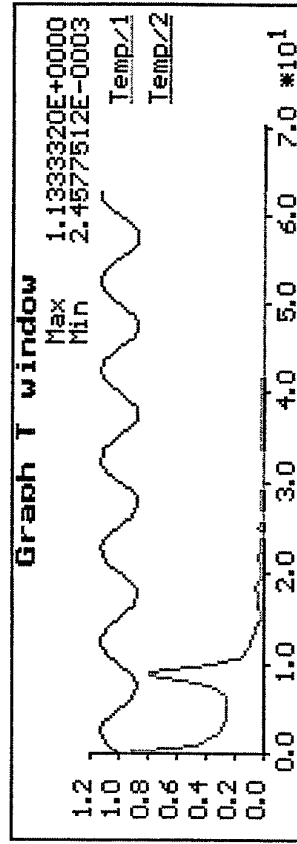
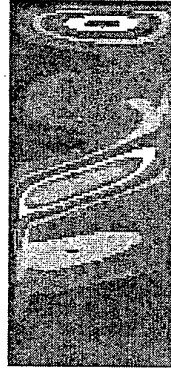
Control of convection due to oscillation of the side wall and bottom temperature

$$T_W = T_{W0} + A \sin\left(\frac{2\pi t}{p}\right)$$

Temperature



Stream function



$$A = 4^0, \quad p = 10s$$

Advanced Slicing Techniques for Single Crystals

C. Hauser and P. M. Nasch
HCT Shaping Systems SA
CH-1033 Cheseaux

Abstract

Generally, monocrystalline materials of industrial applications such as silicon, GaAs, YAG, InP, III-V compounds, quartz, ceramics and other exotic crystals are considerably hard material (few tens of GPa) with an elevated rigidity (brittle) rendering their machining and slicing particularly difficult. For low cost production of single-crystal slices, manufacturing problems are complex primarily because of the requirements of minimum kerf loss (high raw material cost), minimum surface damage, minimum warpage and thickness variation, high production rates and yields, and their impacts on down-stream processes.

The difficulty in large scale production of high-precision slicing single-crystal for electronic applications is further illustrated by the little number of existing methods.

- Internal Diameter (ID)
- Fixed Abrasive Multi-Blade sawing (MBF)
- Fixed Abrasive Multi-Wire Slicing Technique(MWF/FAST)
- Multi-Blade Slurry sawing (MBS)
- Multi-Wire Slurry sawing (MWS)

The ID sawing unit employs a stainless steel blade core with the cutting edge on the inner diameter of a centered hole in the blade. Very critical to the proper functioning of the saw is the uniform tensioning of the blade within the clamping head in order to assure adequate axial rigidity.

In the multi-blade/wire saw, a wire/blade sheet is stretched between two bladeheads mounted onto a reciprocating frame. The single crystal ingot is placed in a feed mechanism perpendicular to the wire-blade sheet.

The wire saw consists of a thin wire moving, either uni-directionally or bi-directionally, on the surface of the workpiece (e.g., silicon ingot). The single wire is wound on wire-guides carefully grooved with constant pitch forming thus a horizontal wire-web. The wire-guides are rotated by a pair of powerful master-slave drives, causing the entire wire-web to move at a relatively high speed (5-15 m/s). A couple of high flow-rate nozzles are feeding the cutting zone with abrasive slurry. The workpiece (or the wire-web) is moved vertically. The wire tension is maintained constant during the cutting process. A wire feed reel provides the length of new wire and a wire takeup reel stores the used wire.

The various slicing methods can be categorized according to their material removal process. In the case of fixed abrasive techniques (ID, MBF, MWF/FAST), material is removed by diamond grains or clads which are firmly bonded on the tool cutting rim or wire by electroplating methods. The plunge grinding cutting action is essentially that of conventional single-edge cutting tool which consists of a

ploughing mechanism characterized by high cutting speeds and a comparatively high total contact zone between tool and workpiece.

In the case of free abrasive techniques (MBS, MWS), material is removed by third-party free abrasive grains transported in a liquid media (slurry). The cutting action in the case of free abrasive machining is essentially that of a fast three-body lapping process essentially characterized by a *rolling & indenting* cutting mechanism. The larger abrasive grains are occasionally trapped by the asperities of the surfaces of the specimen and the tool and are then forced to rotate by the parallel shear motion of these two bodies. During this rotation the abrasive grains transmit part of the applied compressive load from one surface to the other resulting in both surfaces being indented. The rotation of the particules enables indentation but not scratching to occur on the surfaces. The relative penetration depths into each surface will be determined by the hardness of the two materials. Material removal results from the formation of lateral cracking where the abrasives indent. The removal rate of matter (or wear rate) \dot{Q} is proportional to the product of the contact load pressure P times the relative sliding speed v .

Because of the tight technical, physical, chemical, and geometrical requirements imposed on substrates for highly complex microelectronic components, microstructural defects can lead to altered characteristics of the substrate, in particular the near-surface layer. Abrasive processing essentially induces mechanical and thermal effects at the locus of kerf generation. The overall depth of penetration of these damages is dependent upon the dynamics of material removal process. Reduction of the depth of damage can in principle be achieved by reducing the grit size of abrasive. Surface damage in MWS silicon wafers are reduced by as much as 50-60% compared to that in wafers produced by ID sawing. The depth of damage in MWS is empirically found to be about 1.5 times the abrasive grain diameter, and is in the range 5-15 μm which has to be compared with 15-50 μm in ID methods.

The use of single crystals for optical or semiconductor applications often requires to slice the crystals with a very precise orientation relatively to the crystal lattice. On one hand, since the crystal growth process does not allow perfect crystal orientation with respect to the geometrical axis, it is necessary to correct for growth error in order for the cut to meet precise orientation. On another hand, it is sometimes required to slice the crystals with a crystal orientation slightly modified compared to the natural crystalline orientation of the grown ingot. In both cases, one needs to precisely measure or know the actual crystal axis orientation and to position and maintain the geometrical ingot in space such that the displacement of the cutting device is parallel to the targeted cutting plane of the single crystal. There are an infinite number of such possible positions, but among these, only four positions exists that allow simultaneously the geometrical axis of the ingot to be horizontal. This property is of pristine importance in wire saw because the ingot is then parallel to the horizontal wire-web, which reduces cutting time and allows optimized (multi-ingots) loading of the machine.

References

Buijs, M., and K. Korpel-van Houten, A Model for Three-Body Abrasion of Brittle materials, *Wear* 162-164, 954-956, 1993.

Helmreich, D., R. M. Knobel, and W. Ermer, Experiences with a Pilot System for Preparing Multicrystalline Silicon Wafers, *IEEE*, 1390-1394, 1988.

Oishi, H., K. Asakawa, and J. Matsuzaki, Design Concept of Multi-Wire Saw for 400mm Diameter Silicon Ingot Slicing, *Proceedings of « Silicon Machining », 1998 Spring Topical Meeting*, Vol. 17, pp. 109-112, The American Society for Precision Engineering (ASPE), April 13-16, 1998, Carmel-By-The-Sea, California.

Phillips, K., G. M., Crimes, and T. R. Wilshaw, On the Mechanism of Material Removal by Free Abrasive Grinding of Glass and Fused Silica, *Wear* 41, 327-350, 1977.

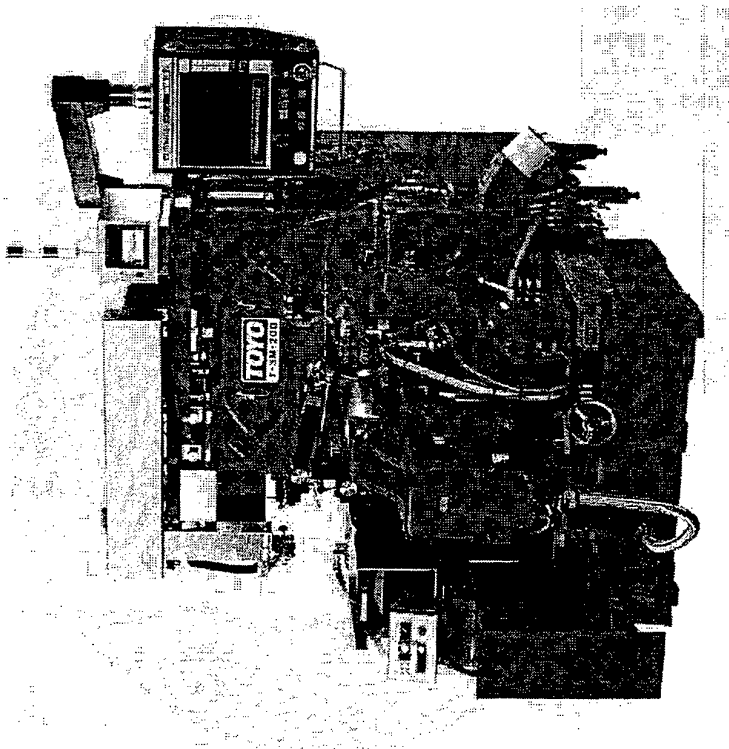
Tabata, K., M. Geshi, K. Kaneko, M. Takatani, K. Hashimoto, and M. Fujisaki, Silicon Slicing for Solar Cell, *Technical Digest of the International PVSEC-1*, Kobe Japan, 809-812.

Tönshoff, H. K., M., Hartmann, R. Przywara, and M. Klein, Defects in Silicon-Wafers – Characterisation and Prevention, *Advancement of Intelligent Production*, Elsevier Science B.V. / Jap. Soc. Prec. Eng., 627-632, 1994.

Tönshoff, H. K., W. v. Schmieden, I. Inasaki, W. König, G. Spur, Abrasive Machining of Silicon, *Annals of the CIRP*, vol. 39/2, 621-633, 1990.

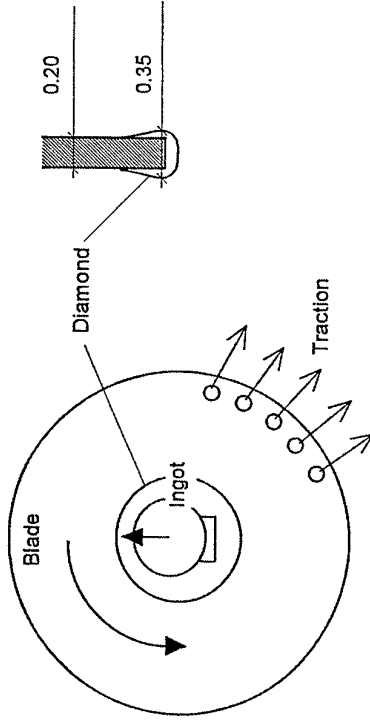
Werner, P. G., and I. M. Kenter, Comparative Study of Advanced Slicing Techniques for Silicon, 1988 Inter-Society Symposium *Machining of Ceramic Materials and Components – 2nd International Symposium Chicago-Illinois 11/28-12/2, 1988*.

Typical ID saw



ID SAW

Principle



Productivity

ID Saw

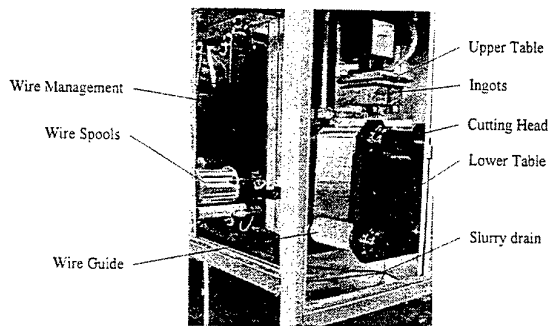
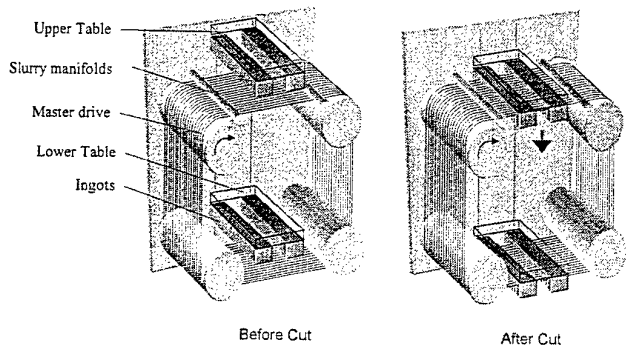
~ 20 wafer / h 4"

~ 10 wafer / h 8"

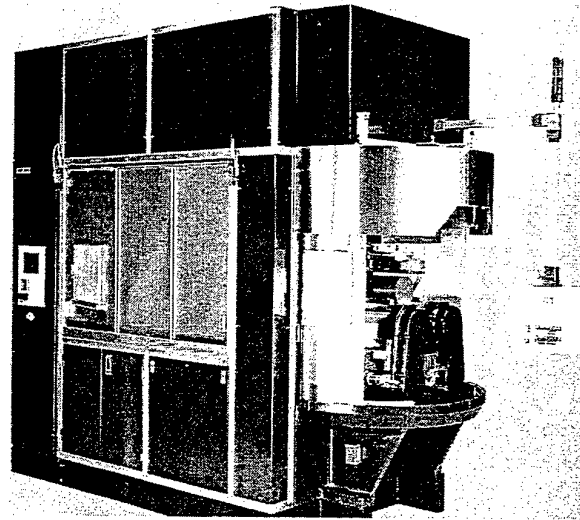
Production problems

- Blade dressing
- Exit chipping
- Minimal thickness 300 μm
- Kerf loss > 300 μm
- Throughput
- Manpower assistance

Multiwire Saw



Typical wire saw



Fixed Abrasive Material Removal Process

Methods: ID, MBF, MWF/FAST

Cutting action: *Ploughing*

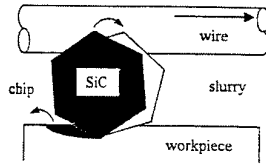
Characteristics:

- $v_{\text{abrasive}} = v_{\text{tool}}$ (~25 m/s)
- single-edge cutting tool
- high cutting speed (thermal shock → recrystallisation)
- high total contact zone between tool and workpiece
- large penetration of surface damage

Free Abrasive Material Removal Process

Methods: MWS, MBS

Cutting action: Rolling & Indenting



Removal rate: $\dot{Q} = b P v$

Characteristics:

- $v_{\text{abrasive}} < v_{\text{tool}}$ (~10-15 m/s)
- multiple-edge cutting tool
- low cutting speed
- low depth of surface damage penetration

Surface Damages

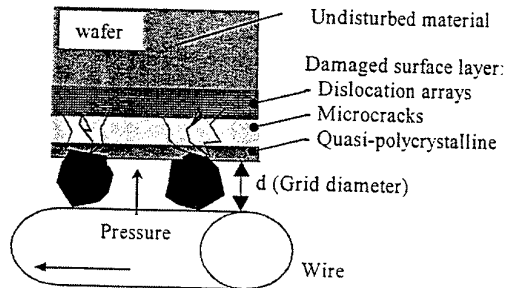
Surface damages are generated by the cutting process and vary with the mechanism of material removal. They can be generated by

1. Local pressure (plastic deformation, cracking)
2. Chip removal type with diamond wheel
3. Thermal shock during material removal

In MWS sawing, the case 1 is probably most responsible for the surface damage.

Depth of Damages $\cong 1.5 \times$ grid diameter (d)

In ID sawing, cases 2 and 3 are predominant leading to a depth of damages 50-60% greater than in MWS.



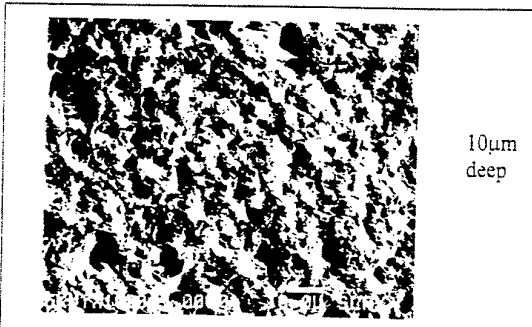
Scanning Electron Micrographs
magnification x1000

10μm ●—●

ID

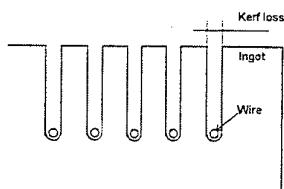


MWS



Kerf Loss

Wire Saw



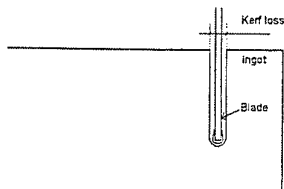
$$D(\text{wire}) \approx 180 \mu\text{m}$$

$$K_{ws} = D + 2,5 d$$

$$K_{ws} \approx 220 \mu\text{m}$$



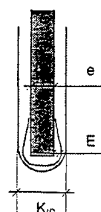
ID Saw



$$\text{Blade} \approx 250 \mu\text{m}$$

$$K_{ID} = e + E + 10 \mu\text{m}$$

$$K_{ID} \approx 350 \mu\text{m}$$



Production

Wire Saw

4": E400SD

8": E500ED

ID Saw

Productivity

~ 436 wafer / h (4")

~ 100 wafer / h (8")

~ 20 wafer / h (4")

~ 10 wafer / h (8")

Material usage (1 kg) thickness = 350 μm

76 wafer / kg

61 wafer / kg (4")

Yield

95 %

90 %

Throughput

72 wafer / kg

55 wafer / kg

← 31 %

Production of 2 millions wafers per year

1 Wire Saw

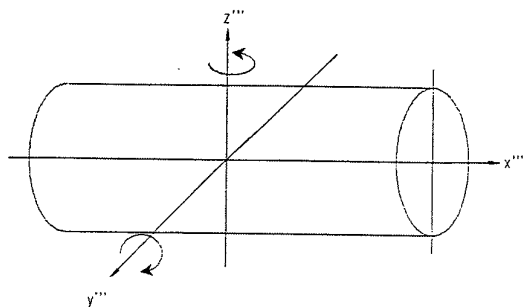
21 ID Saws (Photovoltaic)

1 Wire Saw

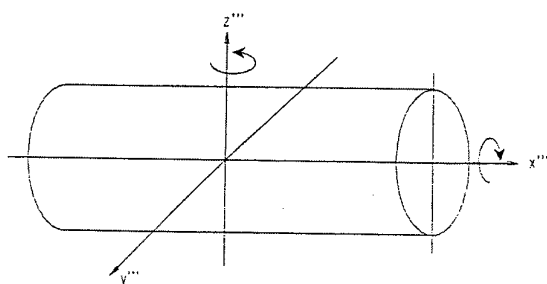
10 ID Saws (Electronic)

ORIENTATION

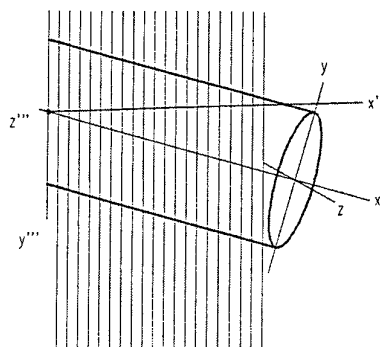
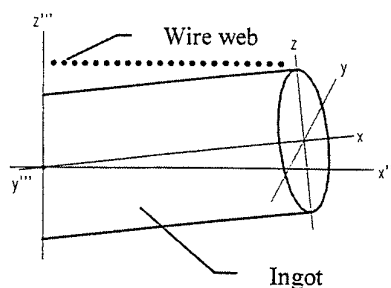
Conventional orientation



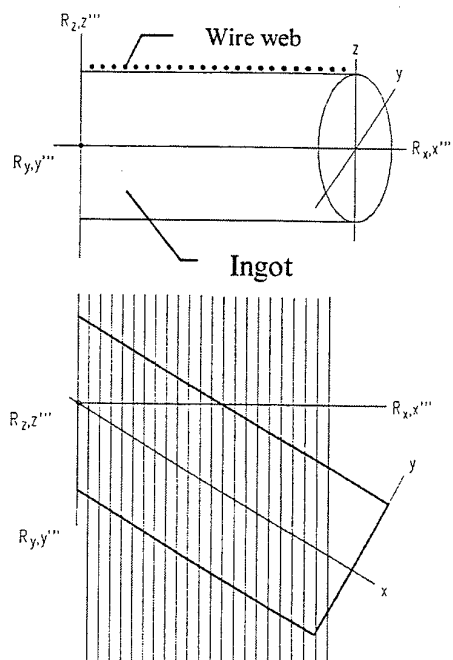
HCT orientation axis



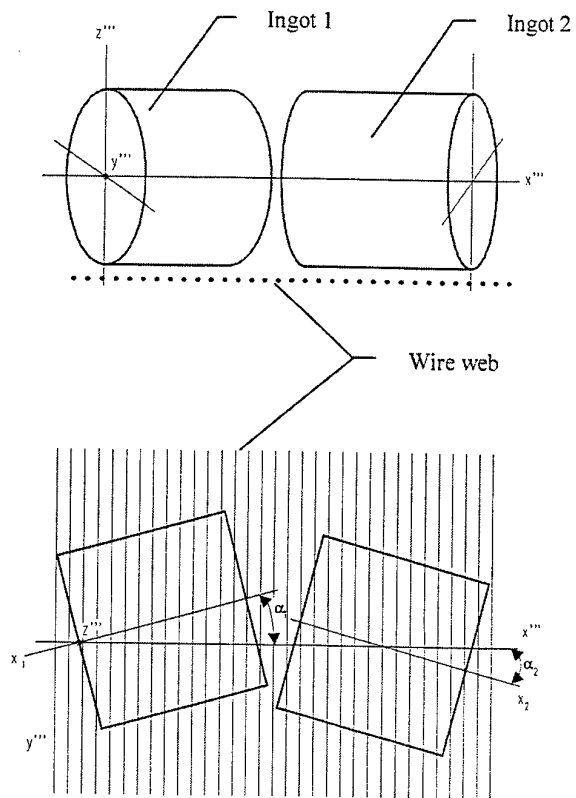
Conventional orientation
(x,y,z) ingot referential
(x'',y'',z'') machine referential



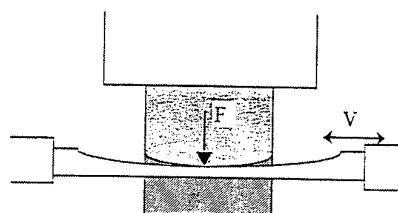
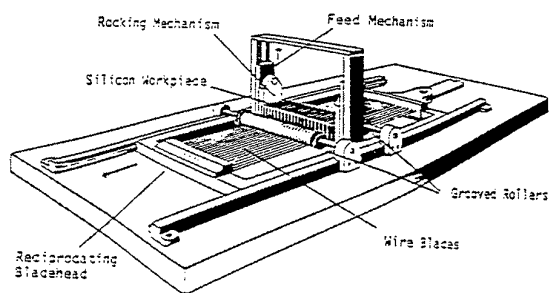
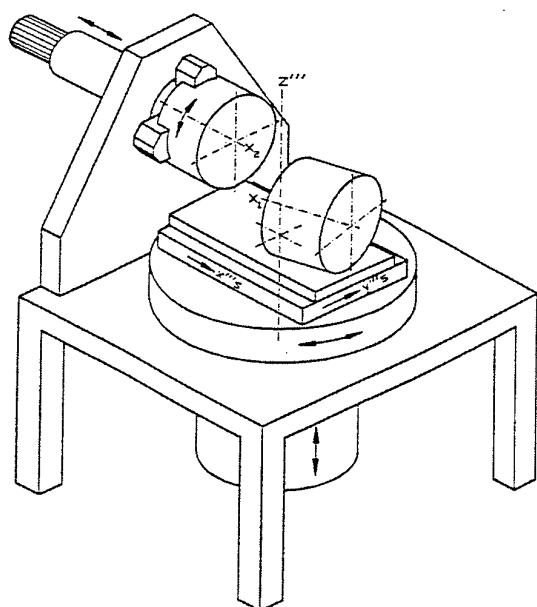
HCT ingot orientation procedure



Multiple ingots mounting



FAST



Development of New Ultra Precision Machining Methods -Plasma CVM and EEM-

Yuzo Mori, Kazuto Yamauchi, Kazuya Yamamura, and Yasuhisa Sano
Department of Precision Science & Technology
Graduate School of Engineering
Osaka University, 2-1 Yamada-oka, Suita, Osaka 565-0871, Japan
Phone & Fax +81-6-879-7286

1. Introduction

Next Si technology would require the Si wafer with atomically smooth and crystallographically perfect surfaces. However, conventional machining processes cannot fabricate such perfect surfaces due to the deformation of surface layers caused by mechanical effects. Authors have proposed EEM (Elastic Emission Machining) and plasma CVM (Chemical Vaporization Machining) as new ultraprecision atomic order removal processes based on chemical reaction.

2. Plasma CVM(Chemical Vaporization Machining)

Plasma CVM is a new chemical machining method with high removal rate. In plasma CVM, high density radicals for the removal reaction are generated in the atmospheric pressure plasma by employing rotary electrode. Stable supply of the reactive gases, effective ejection of reaction products, and cooling of the electrode surface are realized by the viscous flow induced by the rotation of the electrode. Furthermore, in the atmospheric pressure, generated plasma is localized in close proximity to the electrode. Those effects realize high removal rate and high spatial resolution equivalent to conventional machining methods. (such as grinding and lapping)

In this study, new Si wafer fabrication processes using the plasma CVM have been proposed and are expected to apply to slicing of the Si ingot, polishing of the Si wafer, and thinning of the SOI wafer. To realize those applications, three pieces of experimental apparatus have been developed. Those apparatus have various shapes of the rotary electrode, for example, blade shape for the slicing, cylindrical shape for the polishing, and spherical shape for the numerically controlled machining. For those pieces of experimental apparatus, following ultraclean technology is applied.

- (1) Hydrostatic bearing systems using process gas for supporting the rotary electrodes and the sample stages.
- (2) Process gas purifying system by adsorption of reaction products and trapping of particles.

From those developments, ultraclean environment for machining will be achieved so that the sample surface is prevented from contaminating with particle and organic compound.

3. EEM(Elastic Emission Machining)

EEM is an ultraprecision machining process utilizing surface chemical activities of the ultrafine powders of metal oxide compounds such as SiO_2 or ZrO_2 . The ultrafine powders are mixed into the ultrapure water and transported to the work surface along the streamlines. When they contact to the work surface, chemical reactions between the surfaces of the ultrafine powder and the work are induced. And when they are separated by the viscous drag from the flow of the ultrapure water, the surface atoms are removed from the work with atomic unit.

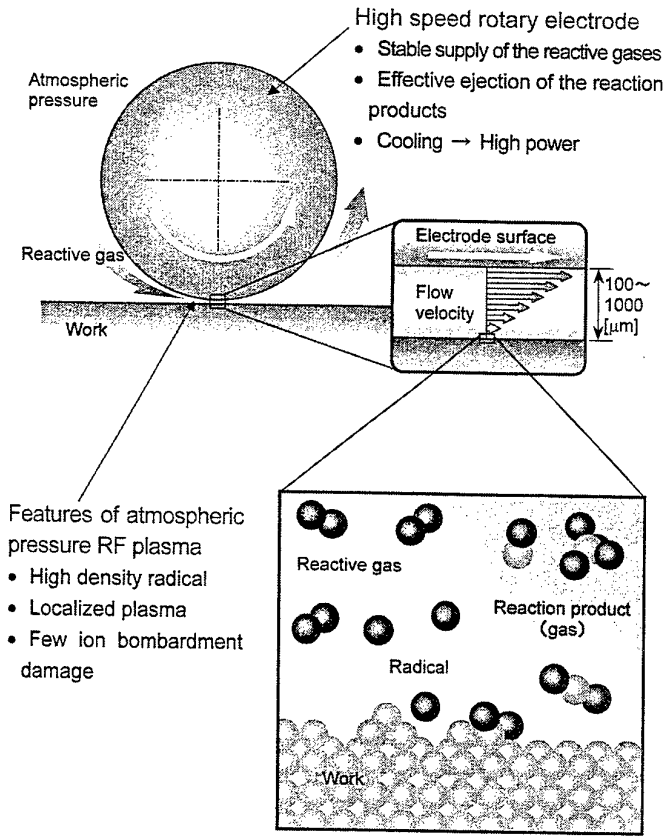
EEM has been recognized as a very effective technique to make surfaces with the atomic order smoothness without any distortions of the crystallographical configurations of the surface atoms. This technique has been successfully applied to polish the mirrors of the laser gyroscope which has been employed as an orbit controller of Japanese H-II rocket.

Numerically controlled EEM system to be applied for the final polishing of semiconductor wafer is now under construction, and partially tested. The most important motivation of the development of the new EEM system is the application of the ultraclean technology same as to the new plasma CVM systems. EEM properties strongly depend on the chemical reactions between the surfaces of the ultrafine powder and the work, so that the impurities in the ultrapure water bring many bad influences to the finished surface quality. As examples, the organic impurity acts as a mask to block the chemical reactions between the surfaces, and the oxygen molecule dissolved in the ultrapure water oxidizes the work surface. Those are the causes of the microroughness of the finished wafer surfaces. The features of the newly developed EEM system are as follows:

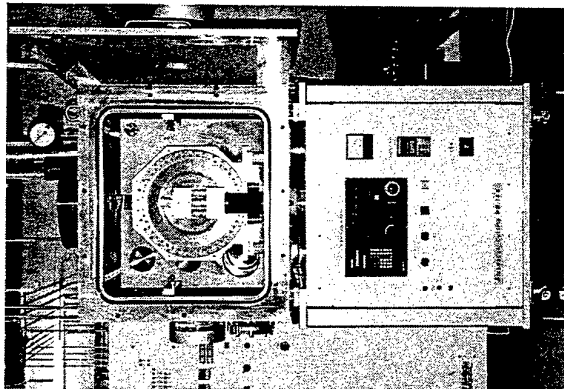
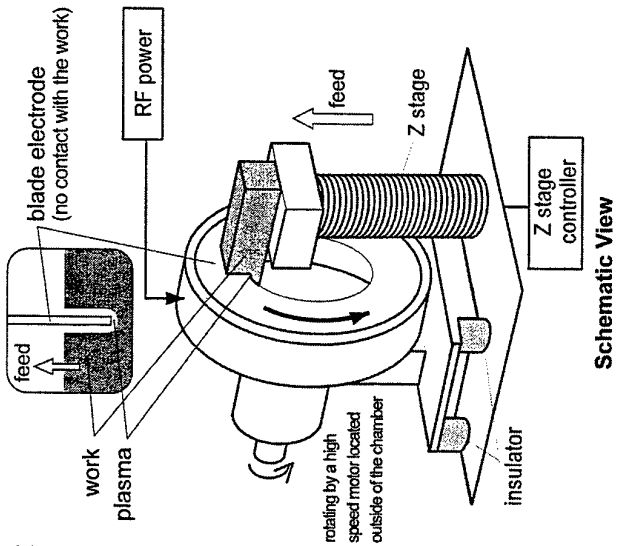
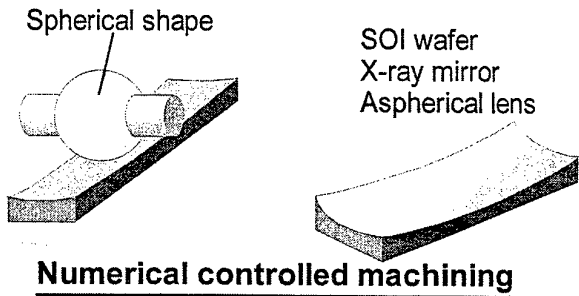
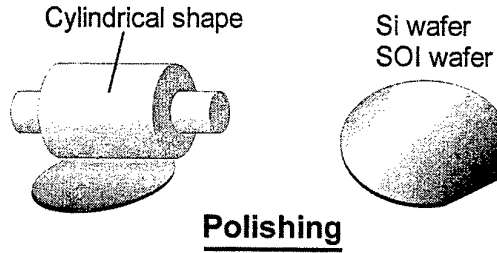
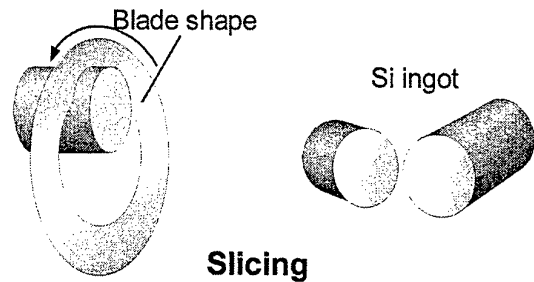
- (1) Processing area is completely isolated from the atmosphere.
- (2) In-process purifier of ultrafine powders and ultrapure water has been developed and employed.
- (3) Numerically controlled sample stage employing ultrapure water hydrostatic supporting system has been developed and employed.
- (4) Diamond nozzle type flow generator of the ultrapure water for the transportation of ultrafine powders has been developed and employed.

Newly developed plasma CVM and EEM systems with ultraclean technology are expected to be advanced fabrication processes for the next generation Si wafer.

PLASMA CVM (CHEMICAL VAPORIZATION MACHINING)

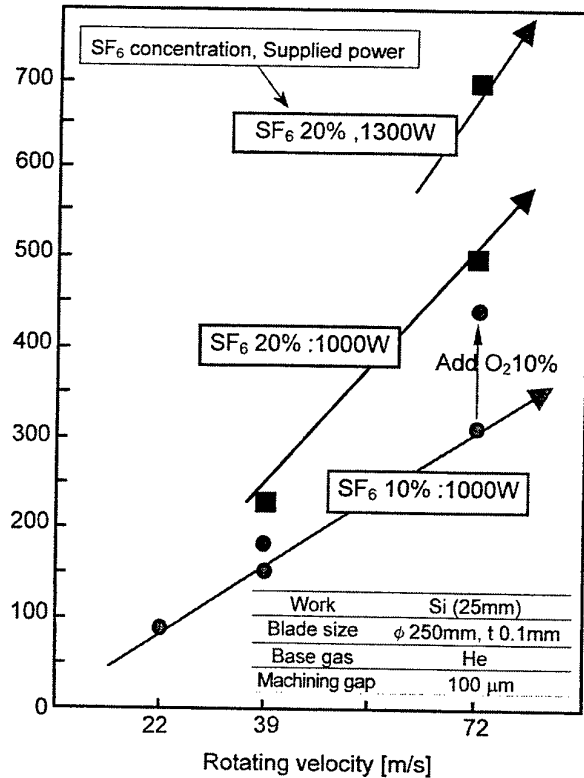


APPLICATIONS OF PLASMA CVM

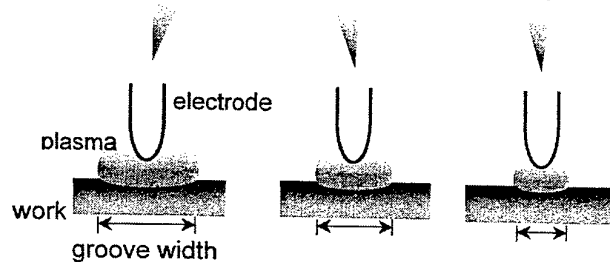
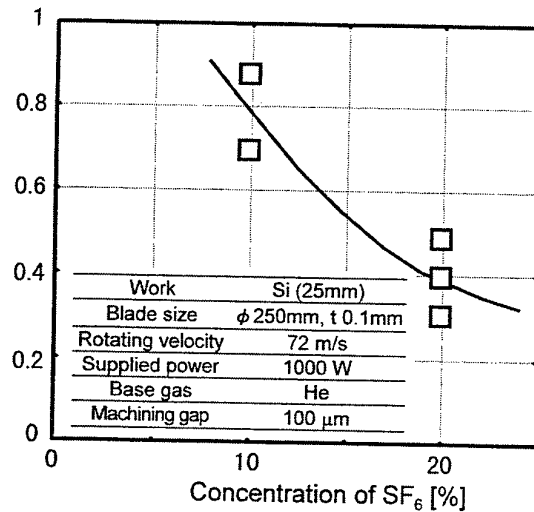


REMOVAL RATE AND GROOVE WIDTH

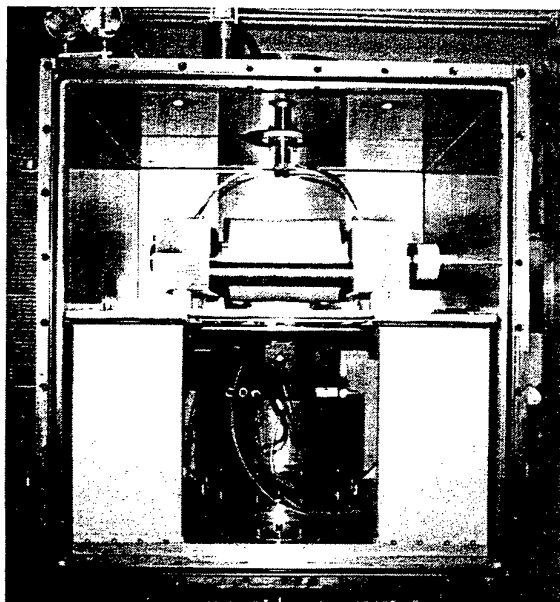
Removal rate [$\mu\text{m}/\text{min}$]



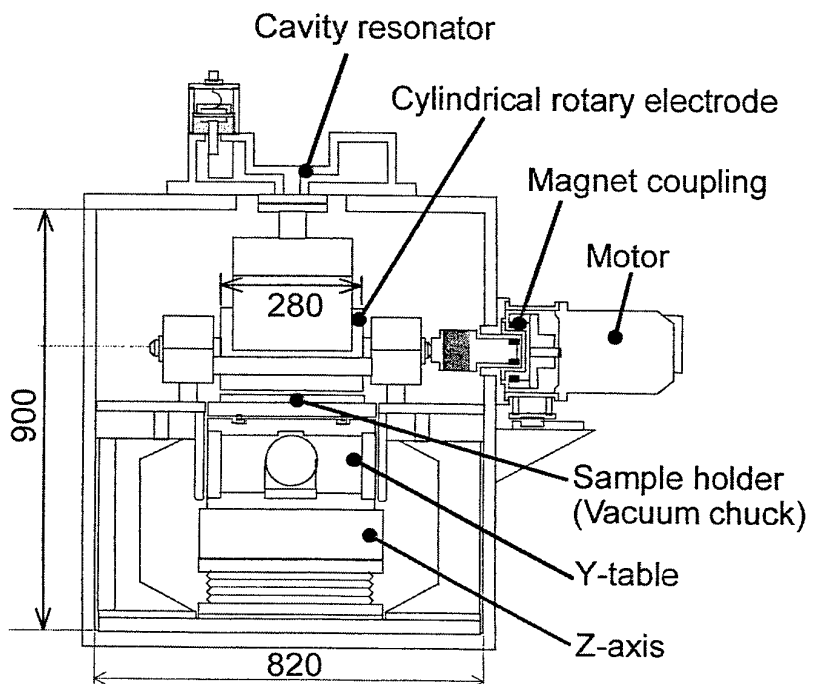
Groove width [mm]



POLISHING MACHINE

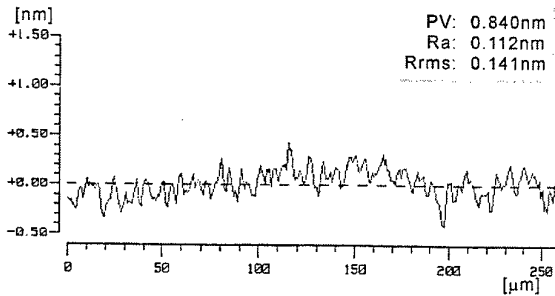


Photograph

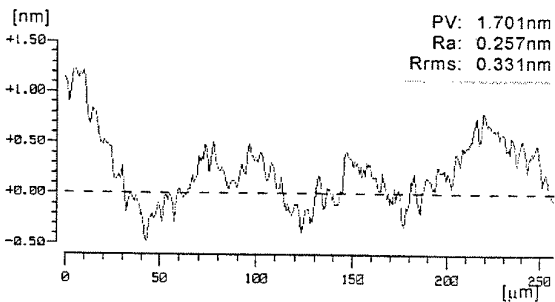


Schematic View

EVALUATION OF SURFACE ROUGHNESS

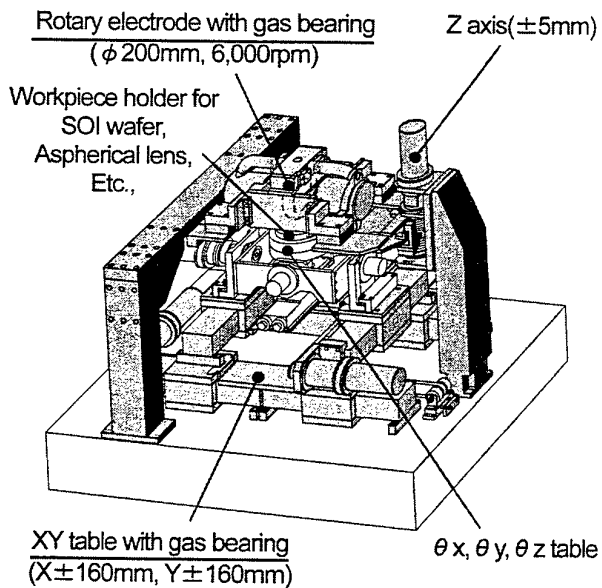


Si wafer machined by plasma CVM



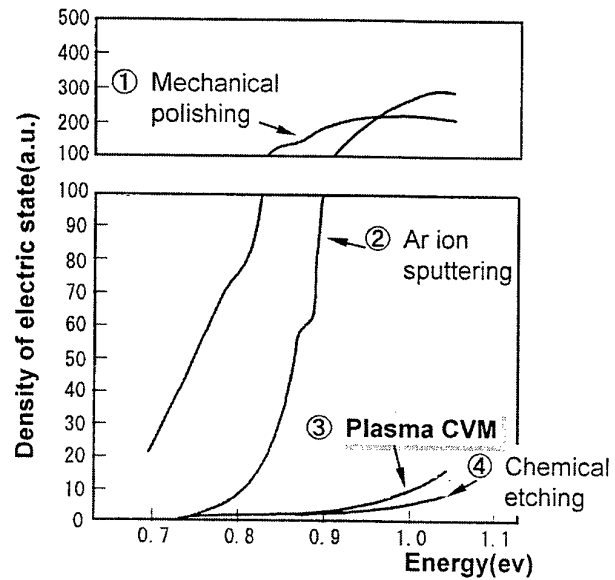
Si wafer for ULSI device

PLASMA CVM MACHINE FOR NUMERICAL CONTROLLED MACHINING



**Contamination (particle, organic compounds)
- free system is constructed by using
hydrostatic bearing with process gas.**

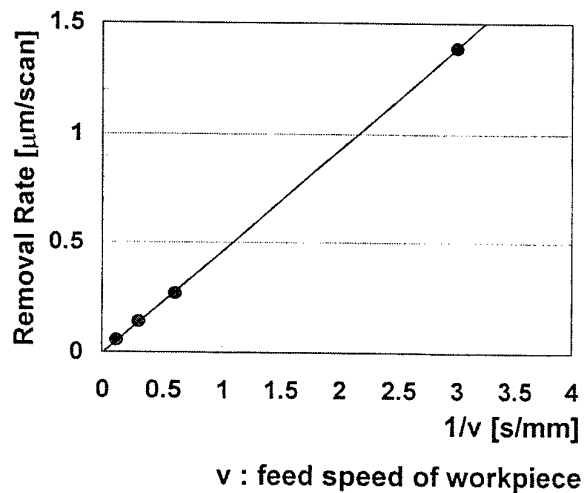
DENSITY OF ELECTRIC STATE



Experimental Conditions :

- ① **Mechanical polishing**
Slurry: SiO_2 (ϕ 0.1 μm), Load: 150gf/cm²
- ② **Ar ion sputtering**
Vacc.=1KV, I=5 $\mu\text{A/cm}^2$
- ③ **Plasma CVM**
Gas: He+ SF_6 1%, P=100W
- ④ **Chemical etching**
HF: HNO_3 : H_2O =1:6:8

CONTROLLABILITY OF REMOVAL RATE

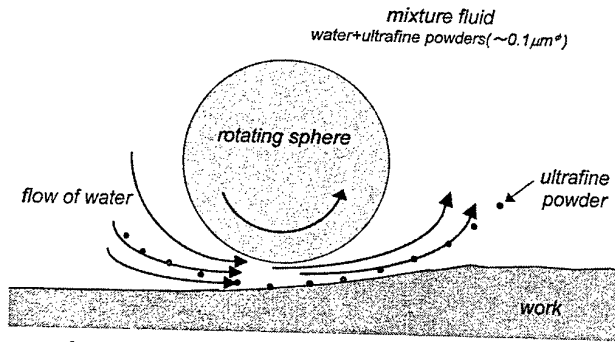


Experimental Conditions :

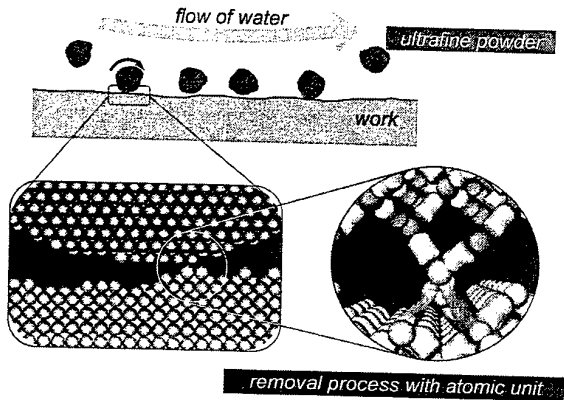
Gas : He: CF_4 : O_2 =99.8:0.1:0.1
Power : 500W
Rotation speed : 31.4m/s
Machining gap : 1mm

EEM (Elastic Emission Machining)

An ultraprecision machining process utilizing chemical reaction between surfaces of work and ultrafine powder

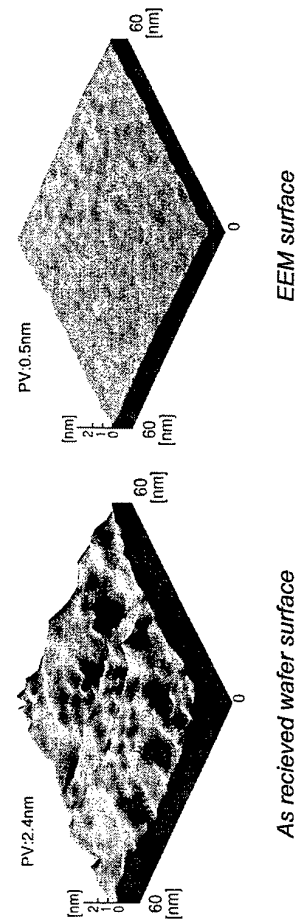


A method to transport ultrafine powders to work surface utilizing flow of water.



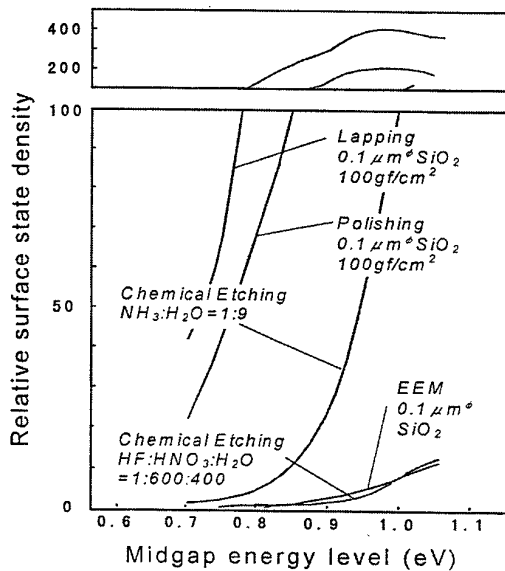
Extremely flat surfaces can be obtained in EEM

STM(Scanning Tunneling Microscopy) observations

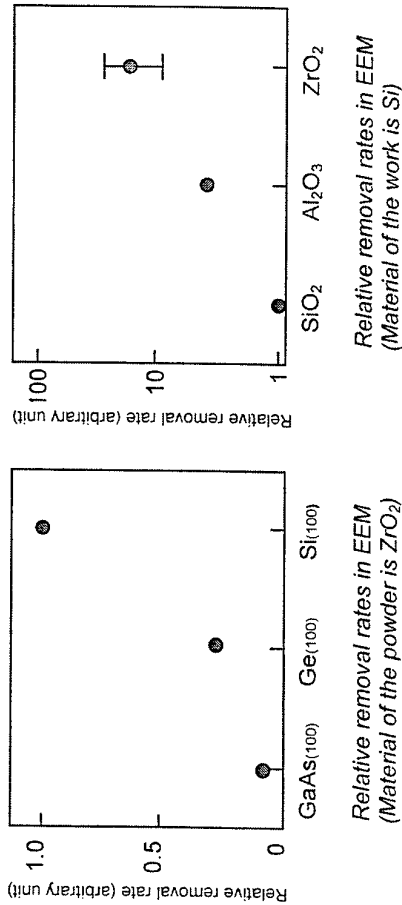


Finished surfaces has no crystallographical damage.

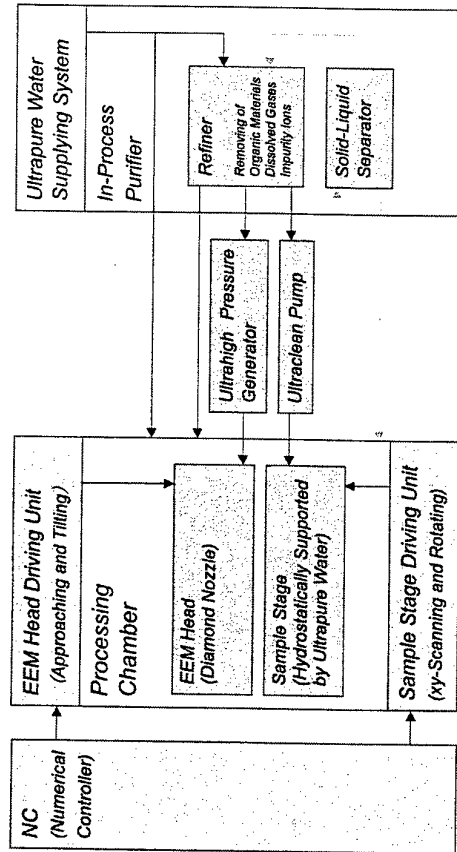
Surface state densities of finely prepared Si(100) surfaces. Observed by surface photo-voltage spectroscopy.



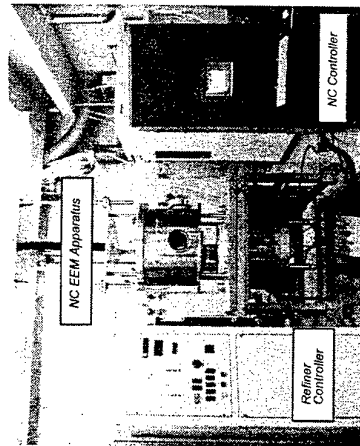
Removal rates strongly depend on combinations between materials of powders and works



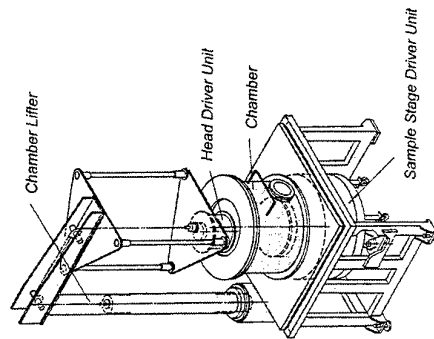
Numerically Controlled EEM System Adopting UCT (Ultraclean Technology)



Si Wafer Polishing System

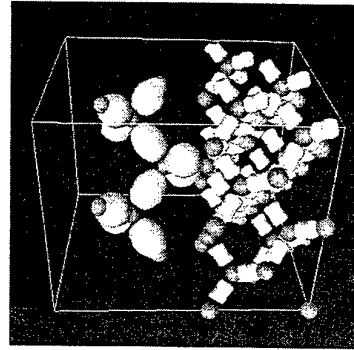


Photograph

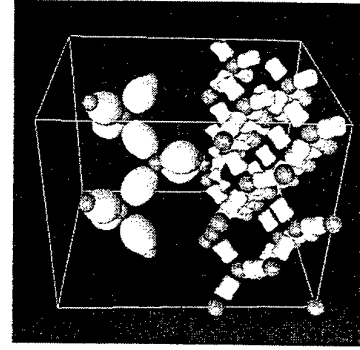


Schematic View

First Principles Molecular Dynamics Simulations Snap Shots of EEM Process



Chemisorption between Si(001) surface and SiO₂ cluster



after 0.1nm lifting of SiO₂ cluster

Michel Lebeau

CERN 1211 Geneva 23 Switzerland

tel. 00 41 22 767 2044

fax 00 41 22 767 8930

First International School on Crystal Growth Technology ISCGT-1

Beatenberg, Interlaken, Switzerland September 5-16, 1998

Abstract of lecture

Title: Residual Stress Evaluation in Bi-refrigent Scintillating Crystals

The mass production of the 82000 PbWO_4 crystals for the CMS Electromagnetic Calorimeter at CERN-LHC complies with tight quality inspection standards. Built-in mechanical tensions -detrimental for the mechanical processing, handling during assembly and long term reliability of the calorimeter- can be revealed by photoelasticimetry as transparent birefringent monoaxial crystals become optically biaxial under mechanical stresses.

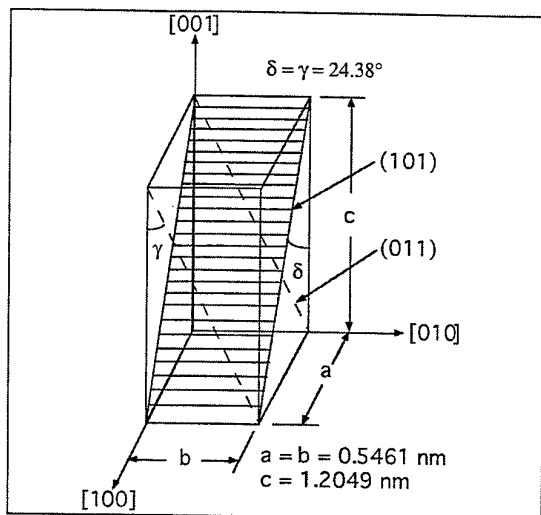
The application of photoelasticity to the inspection of internal tensions in transparent media is well established, in particular for materials with isotropic optical properties, for which the observed fringe pattern is in a linear relation with the stress gradient. We previously applied this method to determine the photoelastic constant of BGO, a scintillating crystal with a cubic lattice. More generally, the fact that finished scintillators are polished to a good optical grade renders the method attractive as a simple observation in polarised light reveals internal stresses, provided the fringe order is high enough for a stress level below the breaking point. This depends on the value of the photoelastic constant. The procedure can be part of the quality inspection protocol, and the information fed back to the crystal growth or annealing conditions.

The lead tungstate (PbWO_4) scintillating crystal chosen for the construction of the CMS Electromagnetic Calorimeter has a tetragonal lattice. It is naturally birefringent, uniaxial. In sodium light the values of ordinary and extraordinary indices are $n_{\text{ord}} = 2.30$, $n_{\text{ext}} = 1.98$. In the stress-free state a circular symmetrical fringe pattern is visible in polarised convergent light when the crystal is observed along its \mathbf{c} axis. Concentric rings representing loci of constant phase difference are visible between the two normal directions \mathbf{a} and \mathbf{b} (cross pattern). Stresses applied or induced in the crystal break this symmetry, the crystal becomes biaxial and the circular pattern deforms into a figure with two apparent centres. They correspond to the two optical axes N1 and N2 derived from the original \mathbf{c} axis. The growing method developed in Russia produces crystals with the \mathbf{c} axis across two planar side faces, rendering the observation of fringes very easy.

Preliminary observations are presented and prove that for PbWO_4 :

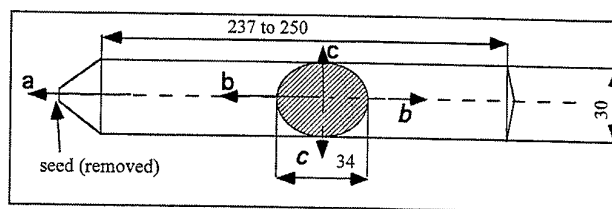
- 1) with loading increasing, the observed fringe system clearly evolves from a symmetrical pattern to a distorted pattern with features predicted by the theory
- 2) the fringe pattern distortion is clearly visible for stress levels far below the yield stress
- 3) different regions of a given sample can be observed with significantly different fringe patterns, depending on the intensity and also on the sign of the stress, resulting from outside loads or from built-in stresses.
- 4) scintillating crystals with the real size of the CMS calorimeter building elements can be directly observed in a very simple set-up

This work is continued and deepened at the Department of Mechanics, University of Ancona, Italy, as a Diploma work, with a participation of CERN for the construction of the experimental set-ups. The elastic constants will first be determined on selected samples, using an existing calibration loading bench. A special set-up will be built to maintain good observation conditions in spite of \mathbf{c} axis orientation errors up to 5° . Corrections will be applied for the 17 different crystal shapes and side face angles. At a further stage a simple set-up for the inspection of the mass-produced 82000 crystals is envisaged.



Lead Tungstate (PbWO_4) Crystal Lattice (after Ishii et al)

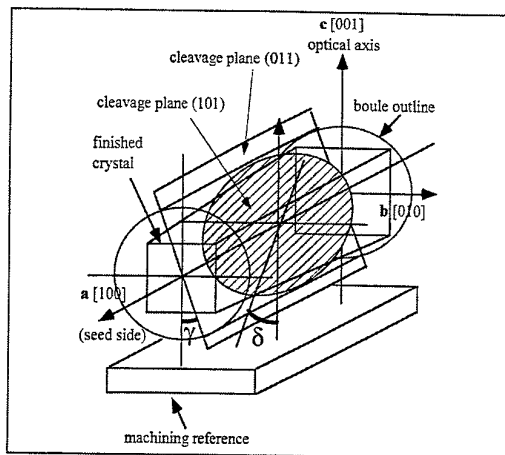
2



Typical size and crystal lattice orientation of a PbWO_4 Czochevski boule.

The oval section results from the epitaxial conditions, it is a clear indication of the lattice orientation.

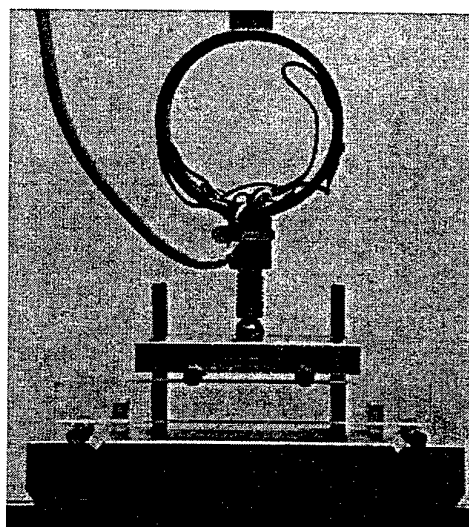
3



PbWO_4 crystal lattice orientation with respect to finished shape

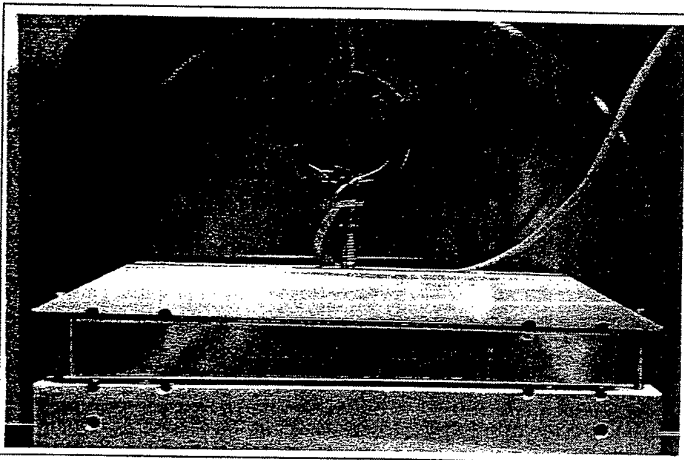
The oval section of the raw boule is used to position the crystal on its machining reference.

4

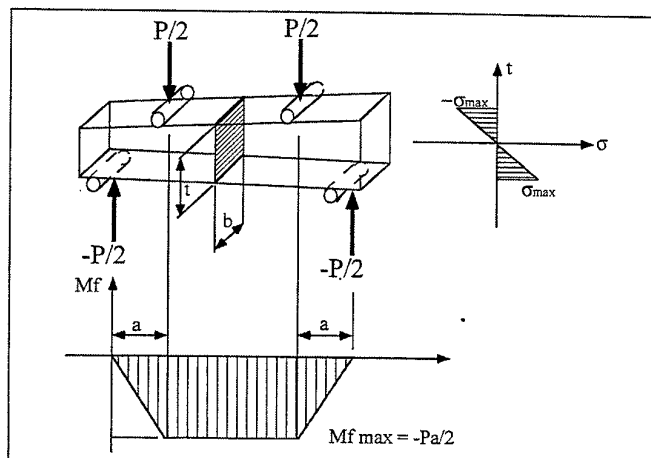


BGO crystal sample in the loading cell

6

PWO₄ crystal sample in the new loading cell

7



Four-point bending principle

The load P is applied to the upper beam. It produces at its bearings two equal forces $P/2$ which are reacted by the lower beam bearings as $-P/2$. The resulting bending moment is $M_f = -(P/2) \cdot a$ with a the projected distance between the upper and lower bearings. This moment is constant on the distance d between the two lower bearings. The bending moment produces a stress gradient from $+\sigma_{\max}$ (tension on the sample lower face) to

$-\sigma_{\max}$ (compression on the sample upper face) which is expressed as:

$$|\sigma_{\max}| = M_f \cdot t / 2 \cdot I_x$$

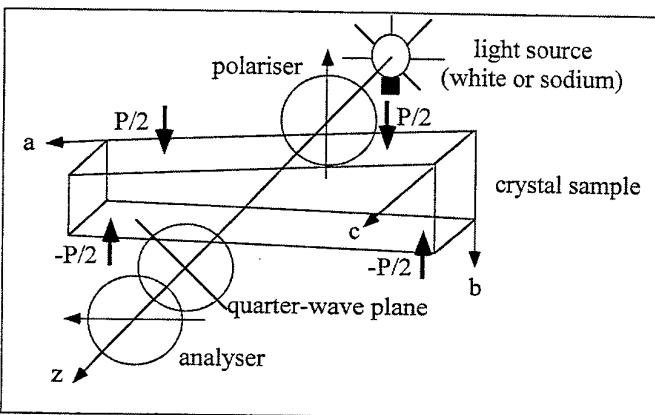
t is the sample height, I_x is its flexural inertia $= (b \cdot t^3) / 12$

With the sample width $b = t$ the expression of the maximal stress is:

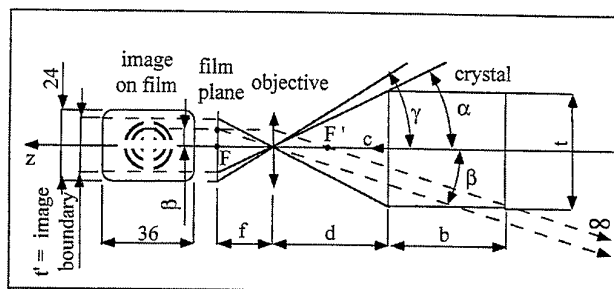
$$\sigma_{\max} = 3 \cdot P \cdot a / b^2$$

In the set-up $a = 30$ mm. With the sample tapered shape, $b_{\text{left-hand}} = 21.1$ and $b_{\text{right-hand}} = 23.2$, for a loading of 800 N the maximal stress is $\sigma_{\max} = 7.66$ Mpa at left-hand and 5.77 Mpa at right-hand.

8



Polariscope scheme



Position of camera vs. crystal sample

The photographic camera is aligned on the c axis and placed as near as possible to the sample (distance d on figure) to produce the largest possible observation angle α through the crystal front face acting as a window. The front of the camera cannot come closer than the analyser plane. An objective with long focus has been chosen for the camera to obtain the best details on the fringes of first orders.

The set-up conditions are $t = 22.5$, $f = 80$ and film format 24×36 mm².

The interferogram is observed with the camera focused to infinite.

The camera angular vertical half-aperture limit is:

$$\gamma = \text{Atan}(12/f) = 8.53^\circ$$

Conversely, the horizontal half-aperture is

$$\delta = \text{Atan}(18/f) = 12.68^\circ$$

From the distance d of the objective to the sample and the focal distance f , the picture scale can be computed in angular value. The interferogram vertical half-aperture limit is

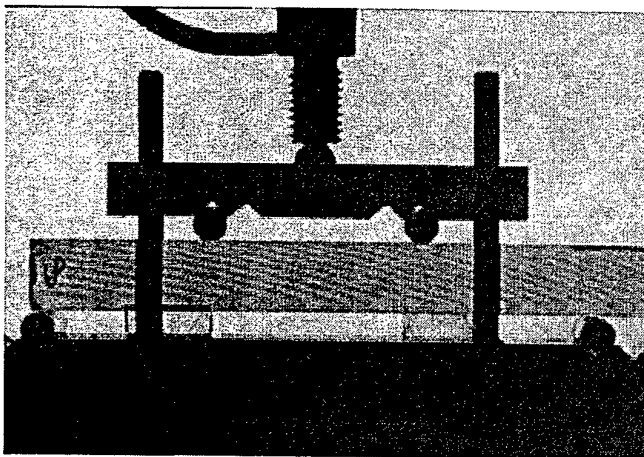
$$\alpha = \text{Atan}(t/(2 \cdot d)) = 4.29^\circ \quad (\alpha < \gamma) \text{ with } d = 150$$

Dimensions in the interferogram will therefore be expressed in degrees (e.g. β as the position of a given point of the interferogram scheme on figure).

The image of the crystal height t on the film has a dimension

$$t' = t \cdot f / d = 12$$

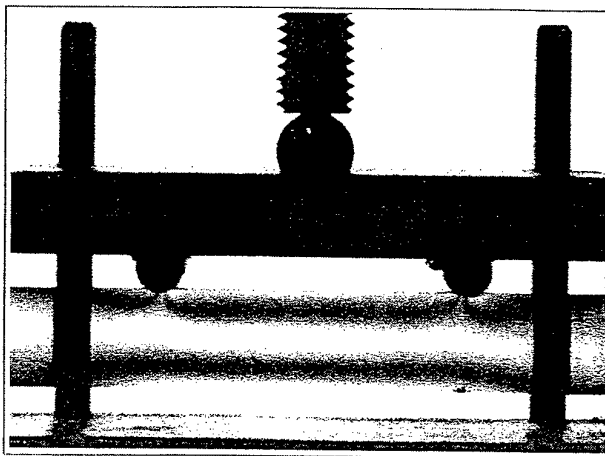
Because of the accuracy of positioning of the boule on the mechanical processing reference, the c axis may not be exactly across the observed crystal face: error angle θ . The z axis of the system has therefore to be inclined to the face normal at an angle $\theta' = 2.30 \cdot \theta$. If the error θ is large it may reduce the observation aperture $2 \cdot \alpha$ such that the observation is impossible.



Loaded CeF_3 crystal observed in light background

A part of a circular fringe pattern typical of a uniaxial crystal is visible. The centre of the pattern is out of the observation field, because of the too large angle of the c axis to the crystal sample face.

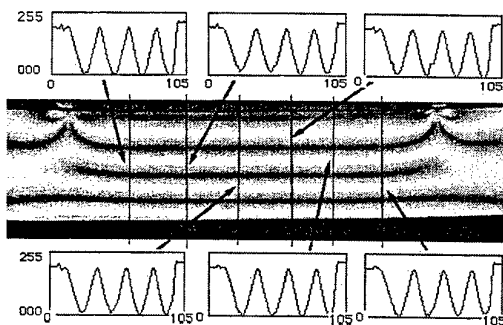
11



Interference pattern of a BGO sample under pure bending.

The system of parallel fringes is typical of mono-refracting media, becoming bi-refracting under stress.
Crystal section $10 \times 10 \text{ mm}^2$, $P = 110 \text{ N}$, $\sigma_{\text{max}} = 3.3 \text{ MPa}$, light background.

12



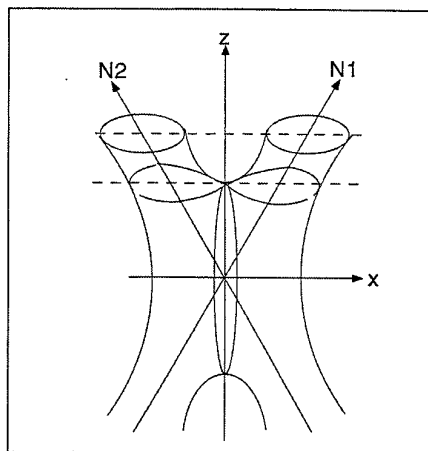
Conversion of interferogram into numerical data

The fringe pattern picture (*) is treated by a computer software (**), for instance to measure the fringe distances. In this instance a Plexiglass calibration sample.

(*) if on film, converted into numerical data to CD-ROM by KODAK Photo-CD®

(*) NIH-Image® v.1.45 for Macintosh

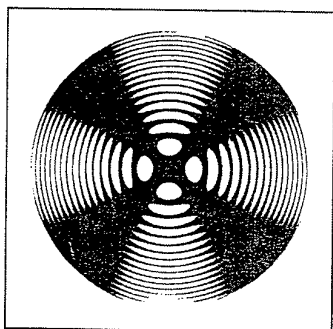
13



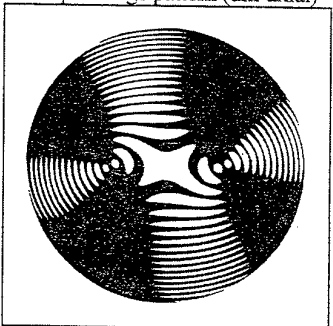
Surface of constant phase difference in a bi-axial crystal

Uni-axial crystals become bi-axial under stress. The fringe pattern reveals two pseudo-centres corresponding to the axes N1 and N2. The phase difference and therefore the fringe density, depends on the indices of the medium. The distance between the centres -or the angle N1;N2- depends on the photo-elastic constant, and on the amount of stress. The effect is more visible on the fringes of the first orders, fringes of larger orders tend to become closer to circles.

14



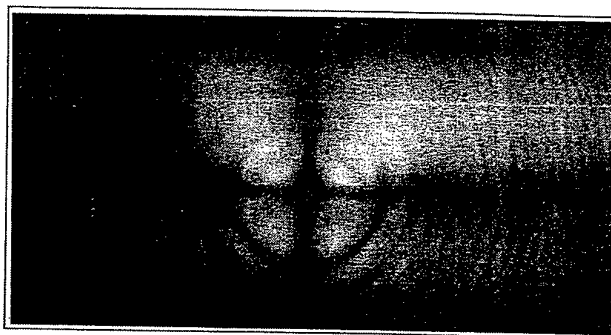
Fluorspar fringe pattern (uni-axial)



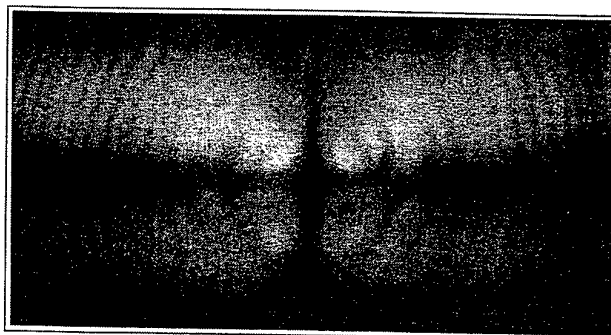
Topaz fringe pattern (bi-axial)

The literature [] mentions fringe patterns typical of uni- and bi-axial optical properties in natural crystalline structures

15

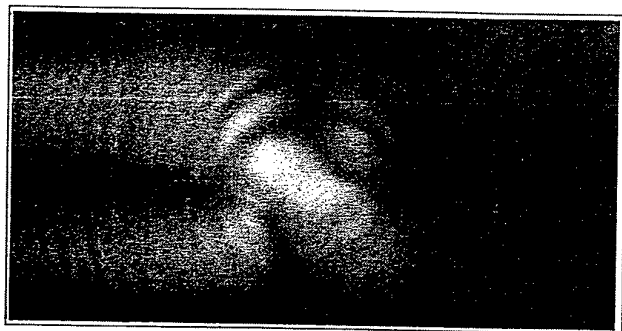


Typical symmetry of the fringe pattern of an unloaded, stress-free PbWO_4 crystal sample



Fringe pattern of an unloaded PbWO_4 crystal sample with built-in stresses showing a distortion of the cross pattern.

16



Fringe pattern of a loaded PbWO_4 crystal sample. The cross pattern is distorted and two centres appear.

17

Load Max stress	Loaded crystal observed in polarised light with dark background
12 N 0.1 MPa	
275 N 2.3 MPa	
447 N 3.8 MPa	
626 N 5.3 MPa	
813 N 6.8 MPa	

PbWO_4 crystal fringe pattern evolution with increasing loading

The two centres of the bi-axial fringe pattern are visible on the three first pictures. In the first picture, with the very low loading, the dissymmetry is probably to be attributed to built-in stresses and not to the loading proper. In the fourth and fifth pictures the pattern tends to leave the center of the crystal face. This could be explained as the first optical axis stays along the c axis and the second optical axis progressively sets apart. The elastic deformation of the side faces resulting from the bending is negligible and cannot produce any visible optical distortion (prism or lens) by itself. In any case the very clear modification of the fringe pattern happens far below the crystal yield stress (between 10 and 20 MPa depending on crystal quality) and indicates the possibility to compute the photo-elastic constant, and to calibrate a test jig.

18

Float Zone Silicon

Jensen, Leif

Topsil Semiconductor Materials A/S
Linderupvej 4
DK-3600 Frederikssund

The float zone silicon crystal has become an important product, which is widely used as substrate in electronic components. There are three important goals: For one thing, to make a dislocation free crystal with a low defect density. Second, to make an accurate axial and radial distributed doping profile with no other contaminating elements. Third, it is important to have a high yield.

It is a complex process to make a single crystal, that meets these goals, so it is important to look at all parameters involved. The parameters are built into the mechanical and electrical design of the float zone puller. Other parameters are connected to the chemical parameters of polysilicon and protection gas. Finally, it is very important to look at the molten zone, and how the zone is influenced by the magnetic field.

The segregation in the float zone process has been used as zone refining process to raise the quality of the polysilicon rods. But today the contamination level of silane or trichlorsilane is very low, and it is possible to make a crystal from a single pass process. In the single pass process it is necessary to look at the crystalline structure of polysilicon and the surface of the rod.

As grown polysilicon rods have a rough surface, and it may be necessary to make an axial grinding to smoothe the surface, and as grown polysilicon rods must have mechanical dimensions suitable to the float zone process. It is important to look at new data like warp and bow. A cleaning of the polysilicon surfaces is necessary, and a combination of ultrasonic bath, etching, and rinse by DI water is most efficient.

Crystal growth is started by heating the polysilicon rod by inducing current into the surface of the polysilicon rod. A single turn coil is used to make the magnetic field. A small droplet of molten silicon is formed in the centre hole of the coil. In addition a seed crystal is pushed into the droplet. The dislocation free single crystal is obtained by neckpulling. A narrow (6 mm) and long (40 mm) crystal is formed out of the droplet. After neckpulling the crystal and polysilicon speed is adjusted to make a crystal outwards angle of solidification. Measuring tools and computer control support the operator in making the single crystal. At the final diameter the process parameters are adjusted according to a optimized process to make a controlled melt convection and an accurate radial doping profile.

The silicon melt motion and solidification of the crystal can be controlled in a number of ways. Heat balance can be adjusted with pre- and after heating systems. Coil design and frequency used as heating sources have a huge influence, and the coil is one of the most important parameters to optimize. Silicon can be heated by inducing heat from frequency in the MHz range, and the RF generator design must be an integrated part of the float zone process. The RF generator can be a self-oscillating design based on vacuum tube or semiconductor power FET design.

Two different techniques are used to dope a crystal. One is Neutron Transmutation Doping (NTD), where silicon is irradiated with neutrons in a nuclear reactor. In this process small parts of the silicon atoms are transformed into phosphorus. Accurate doping can be achieved by controlling the neutron dose.

Doping in the float zone process can be performed by a gas phase process, which is less expensive than Neutron Transmutation Doping. A carrier gas and a doping gas are mixed and subsequently blown out close to the silicon melt, whereby doping elements are transferred into the melt. Having a known polysilicon doping concentration and a constant melt volume, it is possible to calculate the concentration of doping atoms in the carrier gas. Gas phase doping can be influenced by many parameters from the float zone process, among which the oxygen concentration, and the distance from the melt surface to the nozzle are critical parameters.

The mechanical design of a float zone puller is optimized to be equipment without vibrating parts. All parts of a float zone puller, such as the process chamber, shafts and coil must be water-cooled. The water-cooling is necessary to prevent heating and out-diffusion of metal ions into the process. To avoid atmospheric contamination of the process the process chamber must be leak tight for vacuum and pressure.

New ideas are introduced to reduce defect density, raise single crystal weight, and reduce resistivity variation. Computer modelling is important in optimizing the crystal growth. Modelling can reduce development costs of large diameter crystals.

To control the melt, new tools are brought into the process. Magnetic fields can be used as melt breaks, and a rotating magnetic field can be used as stirring elements. Other trends are moving towards adding more active heating elements like LASER preheating of polysilicon rods, to make a more homogeneous surface prior to melting in the floating zone.

The challenge in silicon FZ crystal growth is to make even bigger crystals, with even better doping distribution. And after more than 40 years of achievements, it is still possible to add knowledge on top of the teoretical and experimental work allready done.

References

1. R.U. Barz, G. Gabeth, U. Wunderwald, E. Buhrig, and Yu. M. Gelfgat. Modelling of the isothermal melt flow due to rotating magnetic fields in crystal growth. *Journal of Crystal Growth*, 180:410-421, 1997.
2. D.T.J. Hurle, editor. *Bulk crystal growth*, volume 2A of *Handbook of Crystal growth*. North-Holland, 1994.
3. W. Keller and A. Mühlbauer. *Float-zone silicon*. Marcel Dekker, 1981. Vol. 5 in Preparation and properties of solid state materials.
4. N. De Leon, J. Guldberg, and J. Salling. Growth of homogeneous high resistivity FZ silicon crystals under magnetic field bias. *Journal of Crystal Growth*, 55:406-408, 1981.
5. K.H. Lie, D.N. Riahi, and J.S. Walker. Buoyancy and surface tension driven flows in float zone crystal growth with a strong axial magnetic field. *International Journal of Heat and Mass Transfer*, 32(12):2409-2420, 1989.
6. D.V. Lyubimov, T.P. Lyubimova, S. Meradji, and B. Roux. Vibrational control of crystal growth from liquid phase. *Journal of Crystal Growth*, 180:648-659, 1997.
7. A. Mühlbauer, A. Muiznieks, and J. Virbulis. Analysis of the dopant segregation effects at the floating zone growth of large silicon crystals. *Journal of Crystal Growth*, 180:372-380, 1997.
8. A. Mühlbauer, A. Muiznieks, J. Virbulis, A. Ludge, and H. Riemann. Interface shape, heat transfer and fluid flow in the floating zone growth of large silicon crystals with the needle-eye technique. *Journal of Crystal Growth*, 151:66-79, 1995.
9. H. Riemann, A. Ludge, K. Böttcher, H. Rost, B. Hallmann, W. Schröder, W. Hensel, and B. Schleusener. Silicon floating zone process: Numerical modelling of RF field, heat transfer, thermal stress and experimental proof for 4" crystal. In *Semiconductor silicon, seventh international symposium on silicon materials science and technology*. Electrochemical Society, 1994.
10. G.H. Yeoh, A. de Vahl Davis, E. Leonardi, H.C. de Groh III, and M. Yao. A numerical and experimental study of natural convection and interface shape in crystal growth. *Journal of Crystal Growth*, 173:492-502, 1997.
11. G.W. Young and A. Chait. Surface tension driven heat, mass and momentum transport in a two-dimensional float-zone. *Journal of Crystal Growth*, 106:445-466, 1990.

ISCGT-1

Float Zone Silicon

Outline

- 1. Brief description of the FZ process**
- 2. Goal in single crystal growth**
- 3. History**
- 4. Poly silicon rod**
- 5. Heating sources**
- 6. Single crystal process**
- 7. Melt flow**
- 8. Doping systems**
- 9. Mechanical design**
- 10. New Ideas**

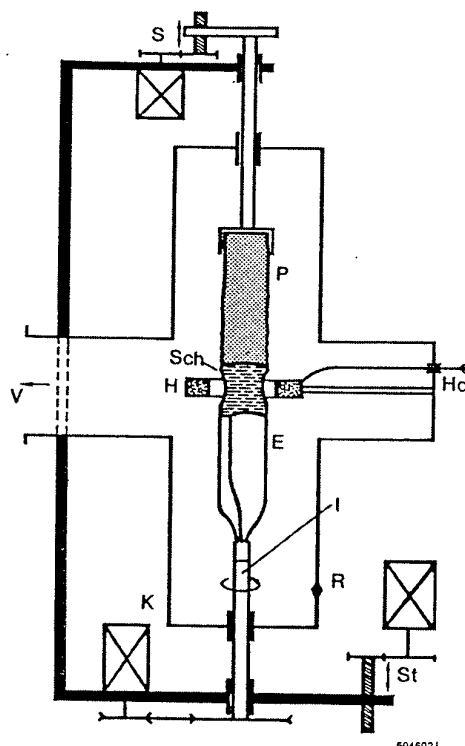
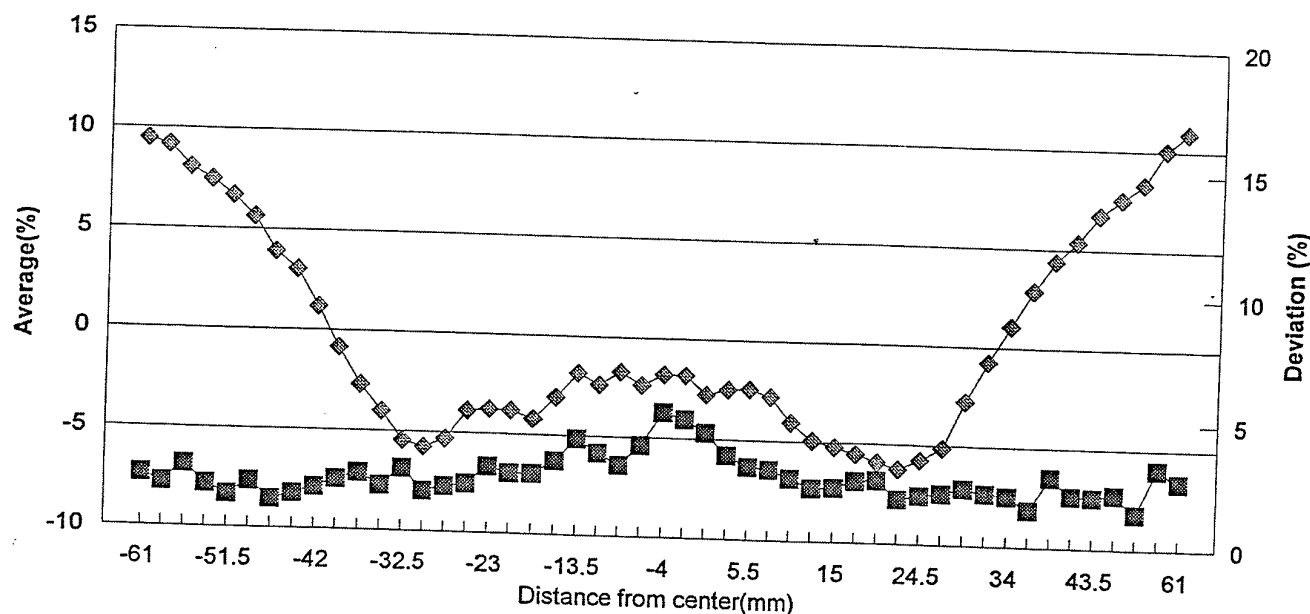


Bild 12:

Das Zonenziehen von Silizium (als Ausgangsmaterial für Halbleiterbauelemente) ist ein wichtiges Einsatzgebiet von HF-Generatoren.
 S = Streck-Stauch-Antrieb; P = Polystab; Sch = Schmelzzone; H = HF-Spule; Ho = Hochfrequenzleitung; E = Einkristall; V = Vakuumpumpe; I = Impfkristall; R = Rezipient; K = Kristalldrehung; St = Stabantrieb.

CFZ 5", P-type <1-0-0>: 127 Ωcm

Radial resistivity profile



■ STD ◆ AVG

As Grown Mechanical Data

Bow (outside bend) - the distance between the flat bar and the end of the rod (measured at the bridge end).

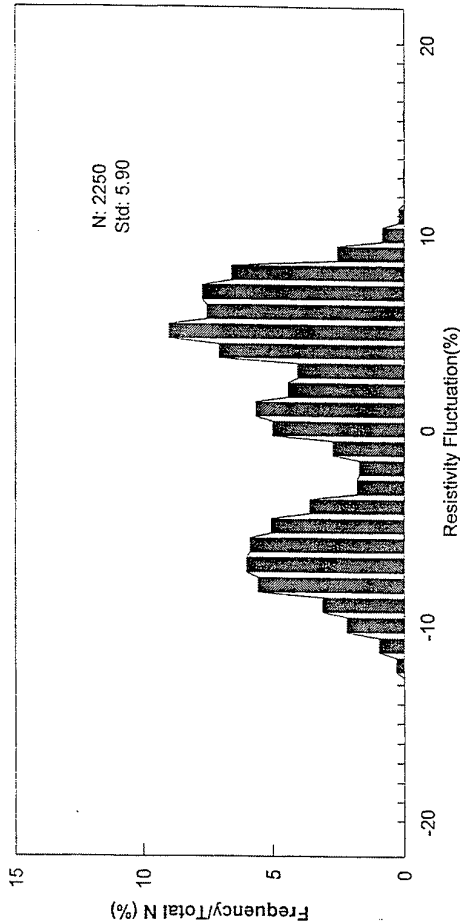


Ellipticity - the greatest diameter variation of the three measured locations.

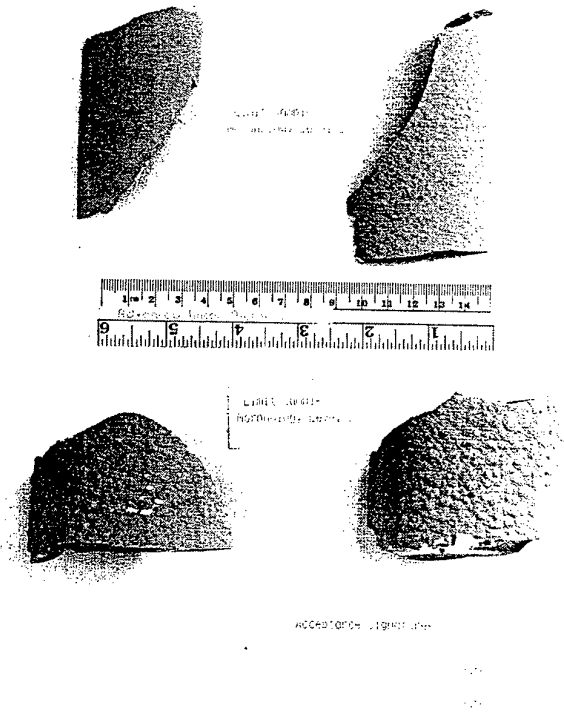
Taper - the difference between the largest diameter measurement on the rod and smallest diameter measurement.

Rod diameter measurements are taken within 50 mm of both ends of the rod and at the center of the rod.

CFZ 5", P-type <1-0-0>: 127 Ω cm
Resistivity Fluctuation

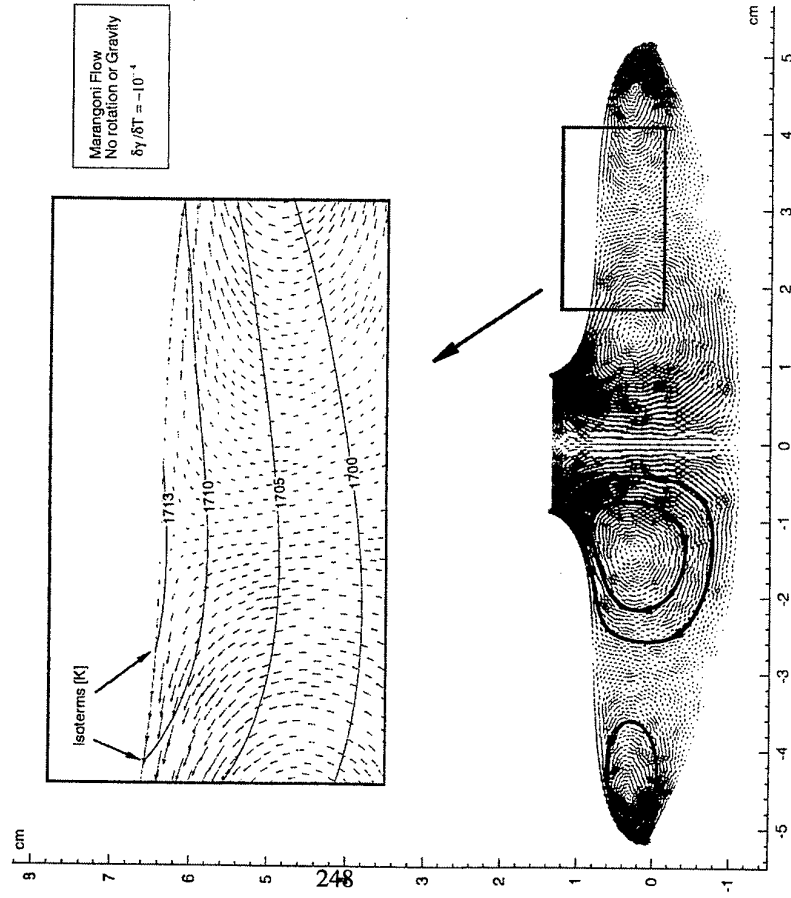


Poly Silicon Surface
as Grown



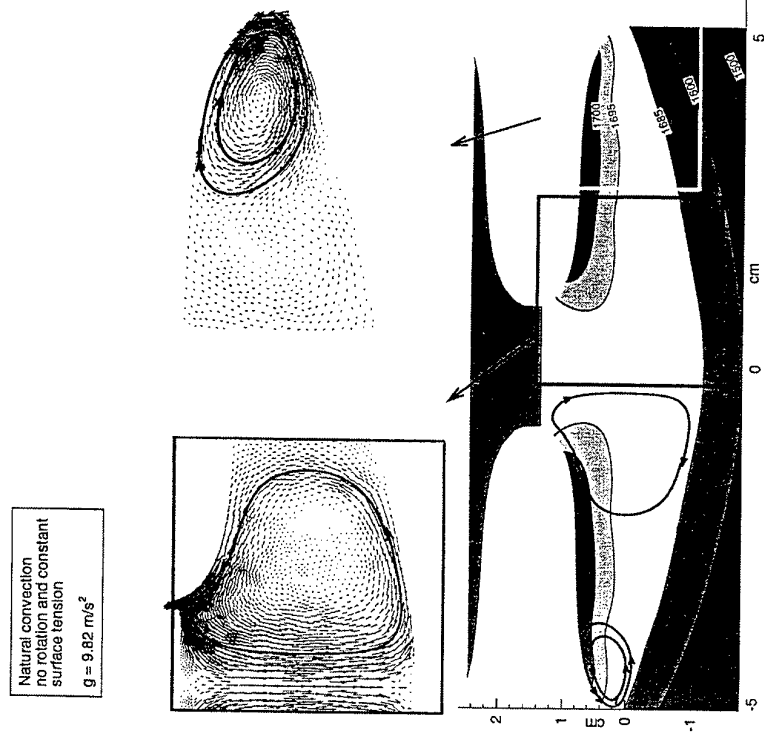
Marangoni Convection

Surface Tension Driven Flow



Buoyancy Driven Convection

Natural Convection



FZ Crystal Diameter Measuring

Optimized filter, CCD camera and software to measure accurate diameter and other visible FZ-data.

- 1. Filter system
- 2. CCD camera
- 3. Frame grabber
- 4. Sub pixels edge measuring

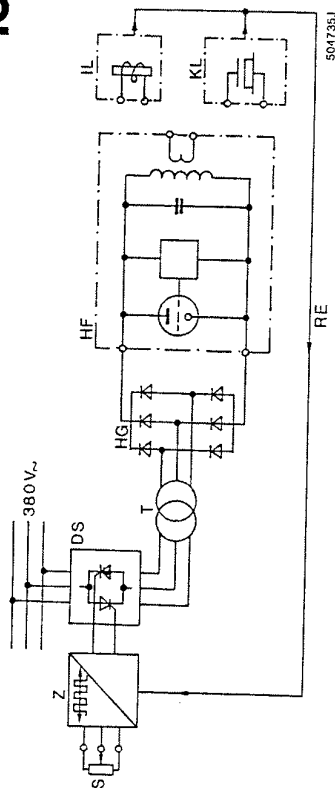


Bild 175:

Leistungsregelung eines modernen HF-Generators

- S = Sollwert
- Z = Zündbaustein
- DS = Primärsteller
- T = Transformator
- RE = Regelgröße
- HG = Hochspannungs-Gleichrichter
- HF = Hochfrequenzteil
- IL = Induktive Last
- KL = Kapazitive Last

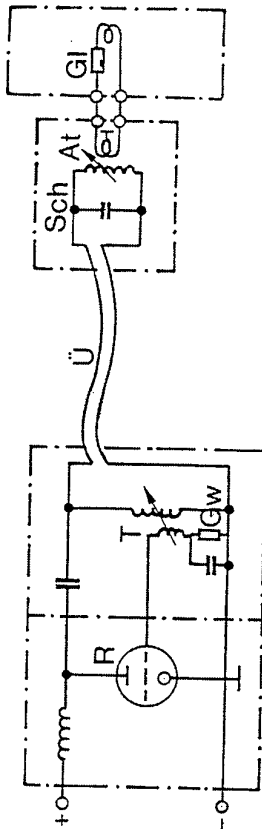
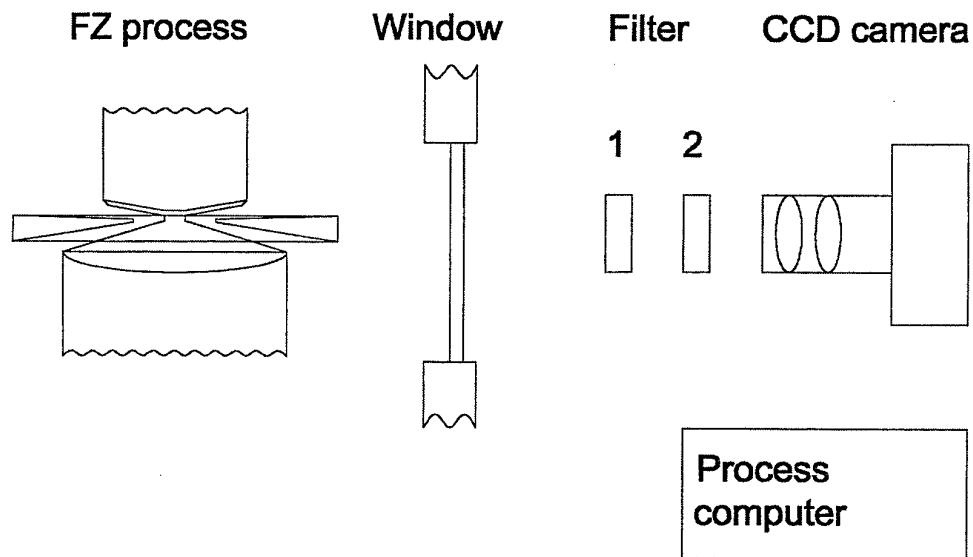


Bild 7:

Prinzipschaltbild des Oszillators der induktiven HF-Generatoren

- R = Oszillatorröhre
- T = Rückkopplungstransformator
- GW = Gitterwiderstand
- Ü = HF-Übertragungsleitung (flexibel)
- Sch = HF-Schwingkreis
- At = HF-Auskopplungstransformator
- GI = Elektrisches Ersatzschaltbild der Generatorlast

Measuring setup



Filter System

Examples:

1.

Filter 1: Short pass 690 nm

Filter 2: Band pass 548 nm +/- 12 nm

2.

Filter 1: Short pass 690 nm

Filter 2: Band pass 455 nm - 490 nm

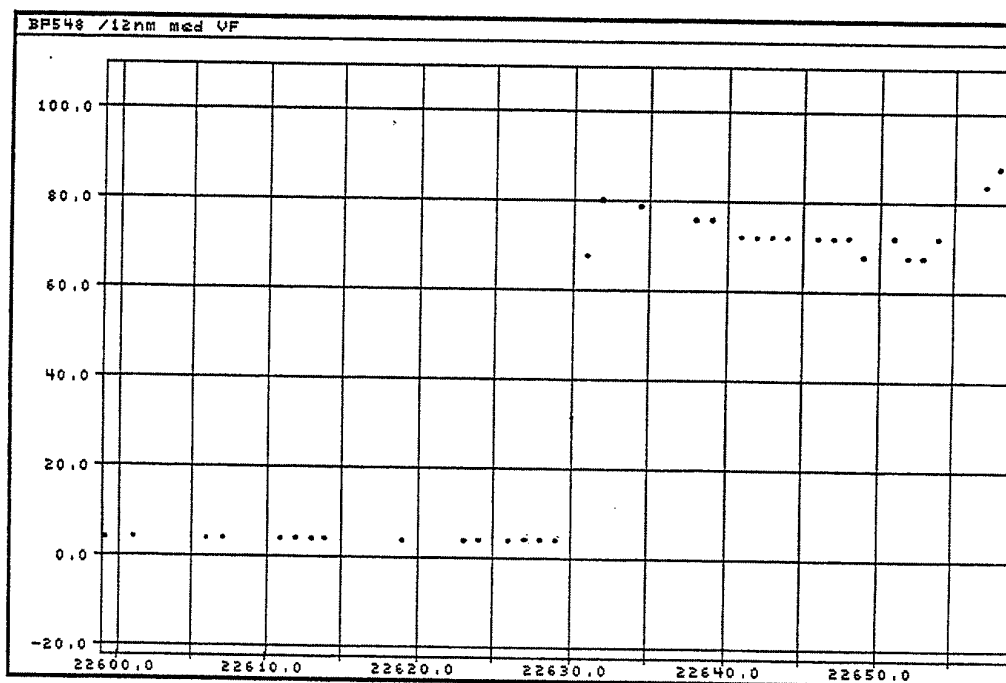
Filter

TOPSiL

Example 1.

Short pass 690 nm

Band pass 548 nm \pm 12 nm



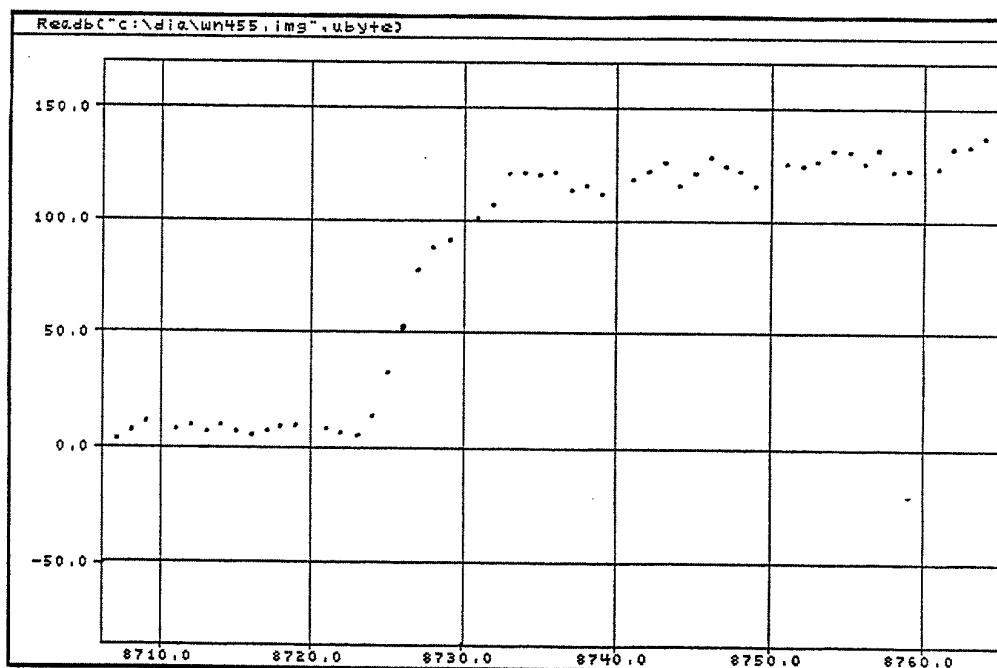
Filter

TOPSiL

Example 2.

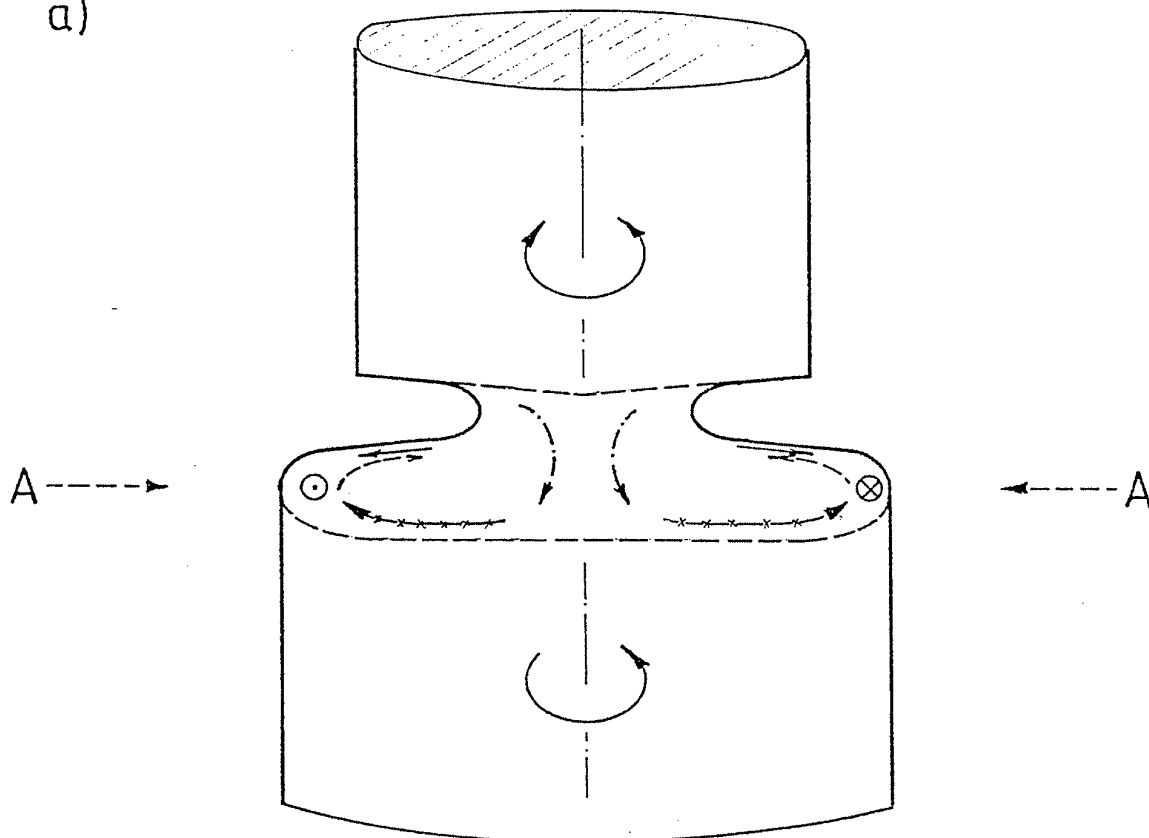
Short pass 690 nm

Band pass 455 nm - 490 nm

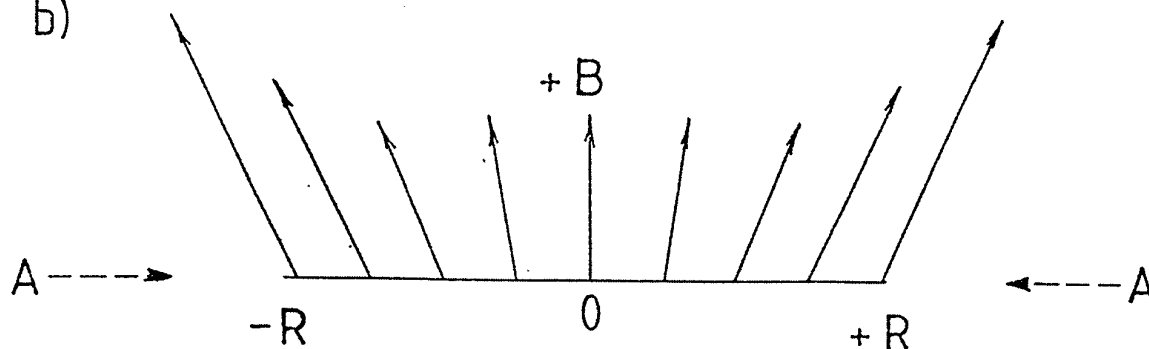


FZ Silicon Crystal under Magnetic Field Bias

a)



b)



INTRINSIC POINT DEFECTS AND REACTIONS IN SILICON: ADVANCES IN DEFECT ENGINEERING

R. Falster

MEMC Electronic Materials SpA,
Viale Gherzi 31
28100 Novara, Italy.

EXTENDED ABSTRACT

Perhaps the most pressing materials problem facing the future of Czochraski-grown silicon today is the control and engineering of defects and defect performance. In this regard there are two important defect classes in silicon today: (1) the agglomeration supersaturated intrinsic point defects – vacancies or self-interstitials – during the cooling of silicon ingots following the crystallization from the liquid phase and (2) the behavior of oxygen during IC processing - the control of its precipitation and its reliable use as a highly effective gettering system for unintentional metal contamination during subsequent wafer processing .

The intrinsic point defect issue is of particular relevance today. Products of the reactions of intrinsic point defects, in particular low-density voids and dislocation clusters from vacancy and self-interstitial reactions respectively, can limit the yield potential of a polished silicon wafer in certain advanced applications such as 256M DRAMs. In this talk we discuss the incorporation of excess vacancies or self-interstitials into silicon near the growth temperature, the reactions which nucleate the agglomerated defects important to device yield, and the effects of potential unconsumed residual point defects on the subsequent clustering of oxygen at later stages of the cooling of the crystal. It is through this link of residual vacancy concentration that the two main defect related issues in CZ silicon – intrinsic point defect agglomerates and oxygen precipitation – are coupled. Excess residual point defect concentrations following the main reactions can and often do have a profound effect on the subsequent behavior of oxygen in the cooling crystals. Essentially all ring-like phenomena in silicon wafers (OISF bands, oxygen precipitation rings, etc.) can be traced back to intrinsic point defect reactions.

Techniques have been developed which can reduce the density and size of potentially yield killing intrinsic point defect agglomerates produced during crystal growth, but it is unclear whether or not such methods will produce material of sufficient quality for future generations of IC products. If this cannot be resolved in a cost effective way, then it may be that many classes of future generations of ICs will have to be manufactured in epitaxial silicon wafers for defect control reasons. The conditions which result in these reactions in CZ silicon (sufficiently high supersaturated concentrations of vacancies or self-interstitials) are not reached in CVD-epitaxial silicon and hence such defects are not found in thin epitaxial films and device yields in such material cannot be limited by such

defects. Epitaxial silicon, however, contains other types of defects and is significantly more costly than polished CZ silicon as a rule.

Advances in crystal growth technique have, however, resulted in methods for the production of large diameter silicon ingots in which the reactions which produces these defects are completely suppressed rather than just controlled. Such material, called "Perfect Silicon" is completely free of intrinsic point defect agglomerates and thus may offer a cost effective path to the future for CZ grown silicon in advanced IC applications. Such material is already in production at 150 and 200 mm diameters.

Insight into the interaction of intrinsic point defects and oxygen has led to the development of an entirely new class of silicon wafer and material engineering tool. This novel approach tackles and robustly solves the other CZ silicon related defects issue: that of the control of the behavior of oxygen during its processing into an integrated circuit. The core of this new process involves the engineering - not of the oxygen concentration profiles, as is done conventionally - but of the concentration profile of vacancies throughout the thickness of the silicon wafer by rapid thermal annealing techniques. These treatments insure that the final defect behavior of the wafer is ideal and, importantly, completely decoupled from the details of the crystal growth process. Such a wafer is effectively *pre-programmed* by the rapid treatment to behave in a well-defined and ideal way. These wafers produce ideal defect performance characteristics: robust denuded zones (defect-free surface layers) and internal gettering performance - independent of all material and process parameters. These (in conventional silicon, strongly coupled) parameters include all those which have rendered the control of the behavior of oxygen something of a black art in the past: the concentration of oxygen, the wafer's "thermal history" and details of the crystal growth process, and even the details of the application to which the wafer is submitted. Taken together, these two inventions represent a large step toward the complete resolution of defect related problems associated with polished silicon wafers, ultimately would greatly simplify their manufacture and use.

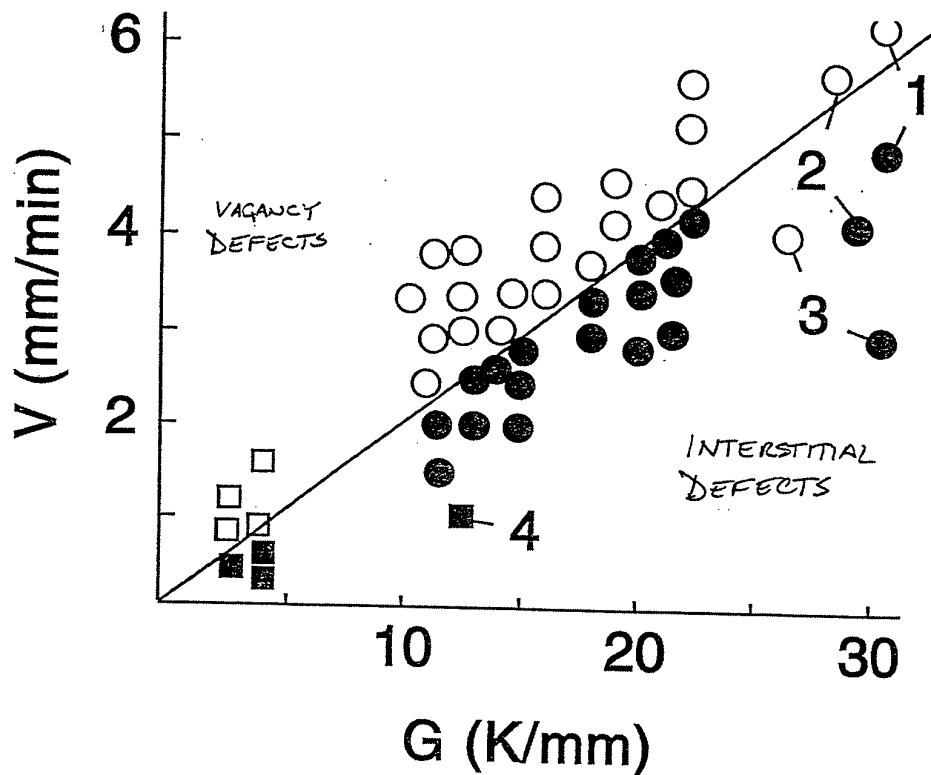
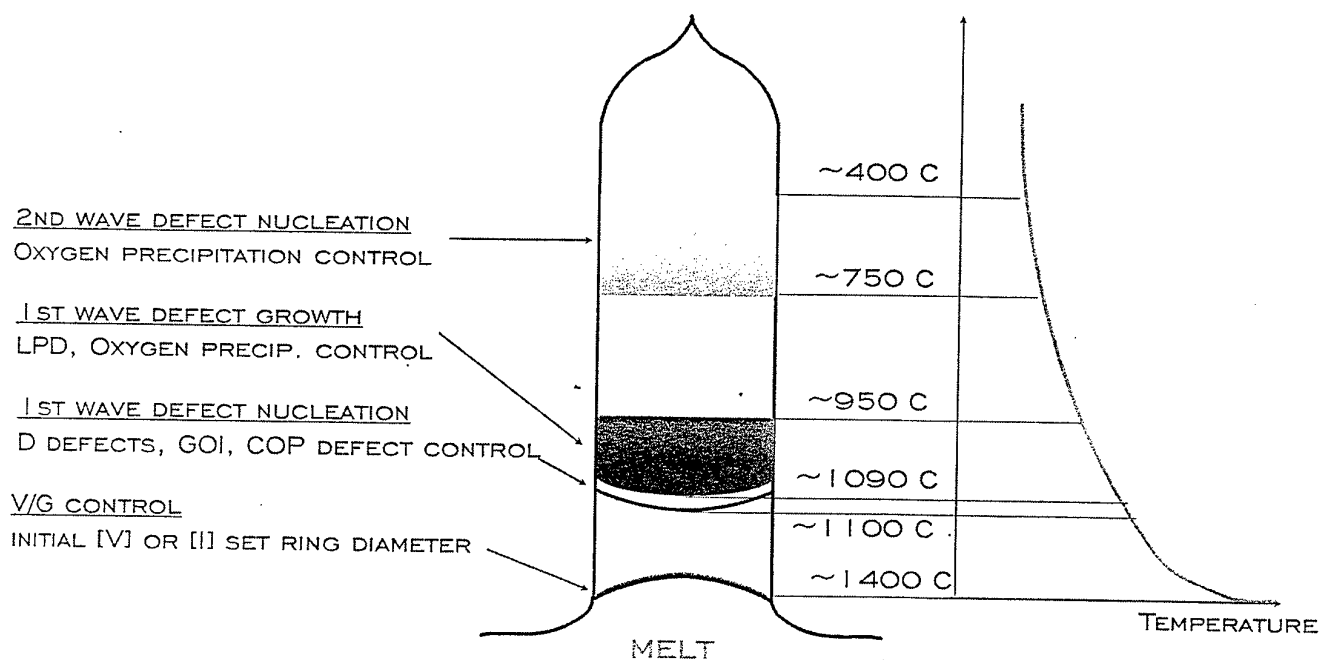
INTRINSIC POINT DEFECTS AND REACTIONS IN SILICON: ADVANCES IN DEFECT ENGINEERING

Robert Falster
MEMC Electronic Materials
Novara, Italy

INTRINSIC POINT DEFECTS AND REACTIONS IN SILICON

- How do excess intrinsic point defect arise?
- The intrinsic point defect reactions
- The oxygen problem
- New solutions to old problems
 - “Perfect Silicon”
 - “Magic Denuded Zones”

DEFECT REACTIONS DURING CZ CRYSTAL GROWTH

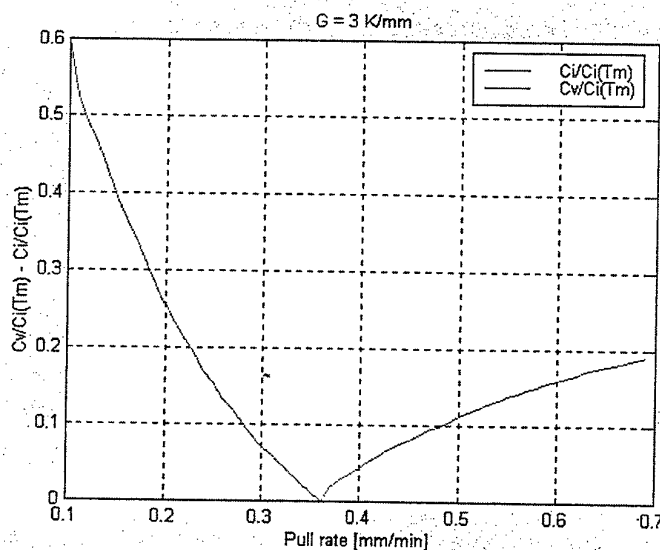


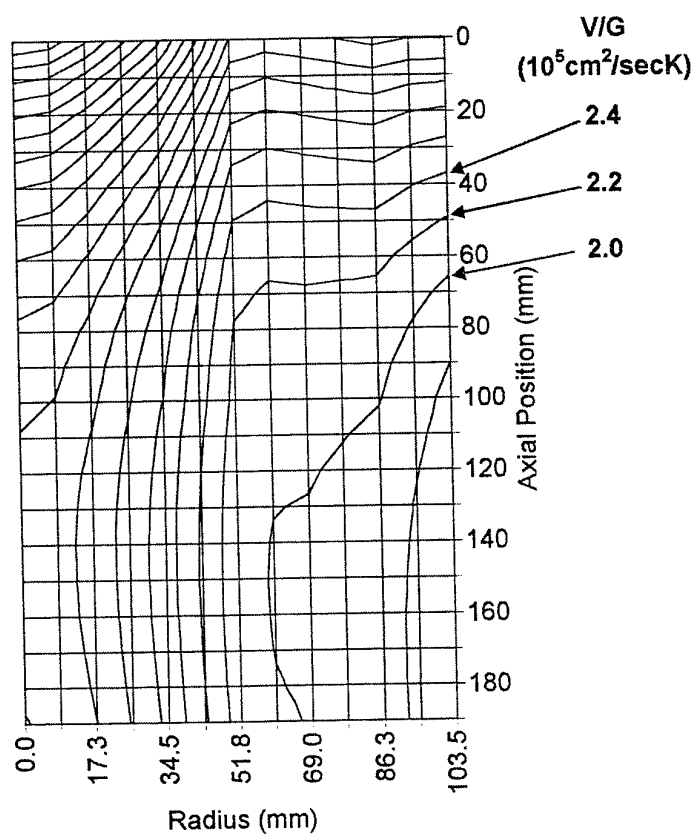
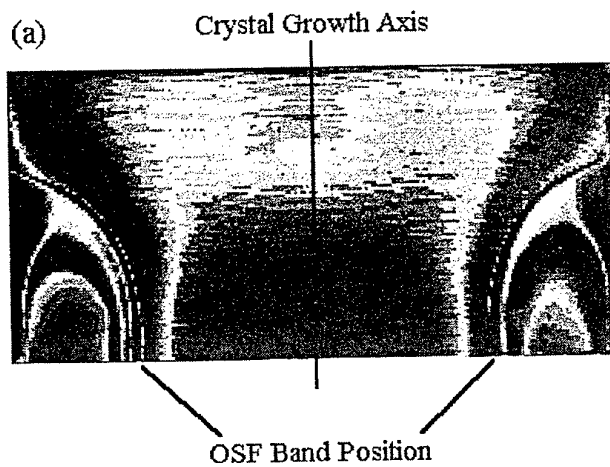
V.V. Voronkov, R. Falster, "Vacancy-type microdefects..."

How excess vacancies or interstitials get incorporated in growing silicon crystals: Voronkov model

- Equilibrium at melt interface
- Rapid V-I recombination
- Transport through temperature field creates concentration gradients through recombination
- Flux competition:
 - Vacancies (convection: pull rate)
 - Interstitials (diffusion: temperature gradient)
- Larger flux becomes supersaturated species

Vacancy & Interstitial Incorporation in Silicon Crystals





Vacancy reactions: two paths

The source of banding in vacancy regions

- 1) Vacancy only agglomerates (voids)

Important at “normal” vacancy concentrations

$$\mu_V = kT \ln (C_V/C_{Ve})$$

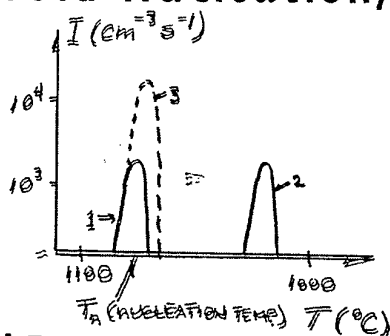
- 2) Joint vacancy/oxygen agglomeration (oxide particles)

Important at “low” vacancy concentrations

$$\mu_P = \mu_{ox} + 0.5\mu_V$$

MEMC Silicon Materials Research

Void Nucleation/Growth kinetics



1: “standard”

2: with lower C_{V0} ($= C_V^{\text{survived}}$)

3: with higher q ($= dT/dt$) $_{T_n}$

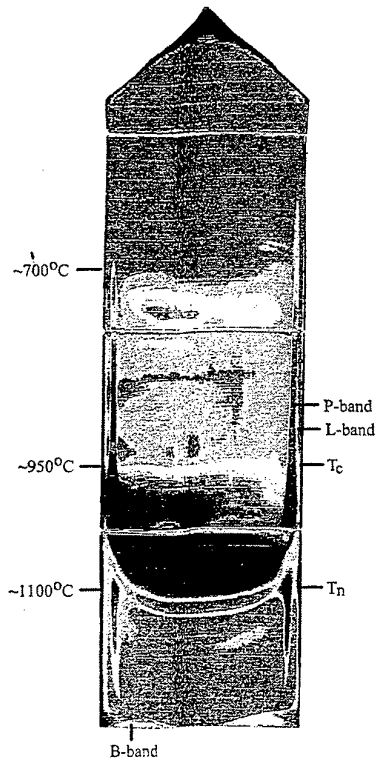
$$\Delta T_n \approx 5K, T_n \approx 3 \text{ min}$$

$$N_V \approx q^{3/2} C_{V0}^{-1/2} \quad (\text{And } \approx D_V^{-3/2})$$

(Similar relation is true for the i-mode)

$$D_V \approx 2 \times 10^{-5} \text{ cm}^2/\text{s}, D_I \approx 3 \times 10^{-4} \text{ cm}^2/\text{s}$$

VOID DENSITY



$$N = (1.72/4\pi m^*) (qE^* / DkT^2)^{3/2} (2C_o / \rho)^{-1/2}$$

Q = COOLING RATE AT T_N

C_o = VACANCY CONCENTRATION AT T_N

MEMC Silicon Materials Research

DEFECTS IN SILICON

Vacancy region of the crystal - predominant defects - voids which can cause failure of the gate oxide



Perfect region of crystal - NO extended defects.



Interstitial-rich region of the crystal - predominant defects interstitial loops which cause catastrophic device failure.

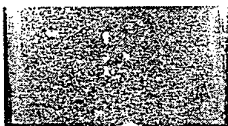
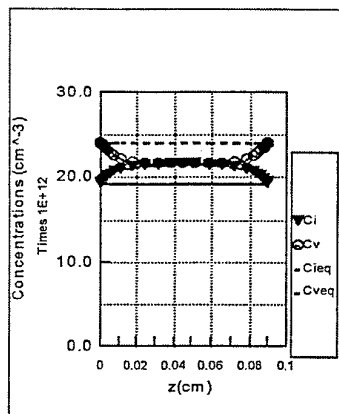


Image of a silicon crystal cross-section after etching. The defects in the crystal appear as etch pits.

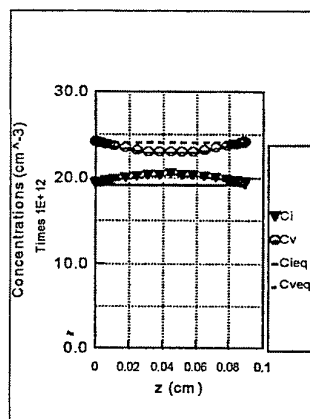
MDZ: Principles

- Vacancies can greatly accelerate oxygen clustering rates
- Vacancy concentration can be tailored in thin silicon wafers
- They may be added: *thermal generation + injection*
- They may be removed: *direct recombination + surface recombination*

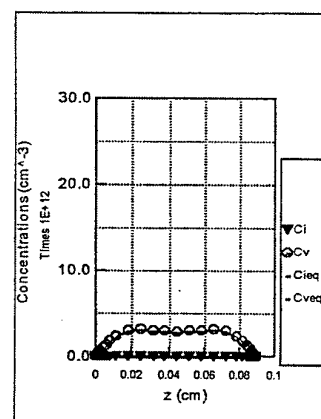
Evolution of point defect concentration profiles



Heat to 1200°C



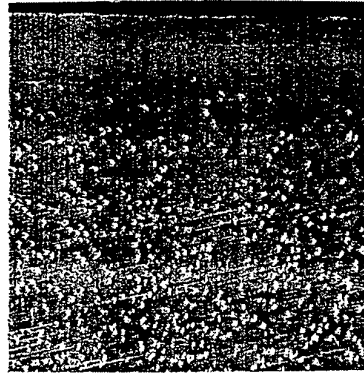
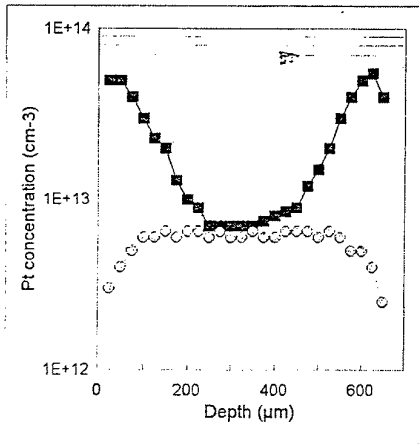
Soak at 1200°C



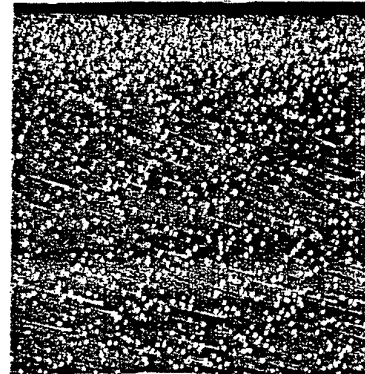
Cool at 100 C°/s

Magic Denuded Zones:

Basic Principles: Vacancy profiles and Precipitate Profiles-Examples



MDZ



HTP



MEMC Silicon Materials Research

MDZ: Summary

- Vacancy concentration profiles can be engineered by RTP techniques to create the MDZ effect
- Robust, ideal, programmable oxygen precipitate distributions created
- *Generic high tech*: independence of all parameters: oxygen concentration, crystal growth, application

The Origin of Point Defects in FZ and CZ Silicon Crystals

Takao ABE

Shin-Etsu Handotai

Isobe, Annaka, Gunma 379-0196

1. Introduction

Since the conversion period (~ 1966) from dislocated crystals to dislocation-free crystals, the research history of point defects¹⁾ in melt-grown silicon crystals has continued. On the opportunity of COPs (crystal originated particles) observation²⁾ (1991) and COP related GOI (gate oxide integrity)³⁾ issue, many researchers have joined to this field. They have used the Voronkov's theory⁴⁾ to explain their experimental results.

In this paper, we propose the different model⁵⁾ from that of the Voronkov's theory and discusses the origin of point defects.

2. Voronkov's theory

The Voronkov's theory was originally proposed to explain the experimental results by Roksnoer et al.⁶⁾ using 26mm diameter crystals by pedestal pulling method. The basic parameters are the growth rate V and the thermal gradient G at the growth interface. The simplified explanation of the theory is as follows.

$V / G < C_{crit}$: Interstitial rich

$V / G > C_{crit}$: Vacancy rich

3. G Effects

We measured the temperature distributions of growing crystal surface along the growth direction by using a two-color thermometer to estimate G .⁵⁾ The parameters were crystal diameters and G . The obtained relationships of G to V and to crystal diameters are following,

1. G of the crystal grown with 4mm / min is smaller than that of the crystal with 0 mm / min. Generally, higher growth rate induces lower temperature gradient. The reverse is also true.
2. G of the crystal with larger diameter is smaller than that of the crystal with smaller diameter.

The present results suggest that the following equation would be not valid :

Latent heat (q_f) + heat (q_m) transferred to crystal from melt = heat (q_c) conducted away from the interface by the crystal,

$$q_f + q_m = q_c \quad (1)$$

Although the equation is most frequently used to explain the experimental data, the previous reports based on the equation should be reconsidered.

4. Our model

Here, we propose that critical value of thermal gradient G_{crit} for special species of point defects instead of the balanced values of $V / G = C_{crit}$. In other words, vacancies are dominant when $G > G_{crit}$, while interstitials are dominant when $G < G_{crit}$.

5. Interpretation to the previous results

The result of Roksnoer et al.⁶⁾ can be explained as follows. In order to become vacancy rich in a small diameter crystal with large G , ultra high V over 6 mm / min is necessary to lower such high G .

The recent experimental results by Dornberger et al.⁷⁾ are beautifully accorded with the Voronkov's theory. They obtained the G depending on V for the different hot zones and different diameters. This is a contradiction to which the present author describes here. Their calculated G seems to be right. That is, even the same hot zone, if the crystal diameter is small, its thermal gradient is large. To this extent their results are true. Due to using the uncorrected equation (1), however, the whole logic of the interpretation is wrong. It should be thought that increasing V affects to decrease G . For example, if a small diameter crystal grows in a hot zone with large G and with high V , the G of the crystal must be a too high value but the reality shows a moderate G . This is because the high V brings the small G . Therefore, we can interpret the results of Dornberger et al.⁷⁾ as follows. For the given hot zone and diameter, a proper V is chosen to get a critical value G_{crit} .

There are two reasons to reach such misinterpretation as the Voronkov's theory. One is the lack of measurements of the real thermal gradients depending on growth rate. Another is the traditional heat balance equation noted above. This equation means that the latent heat produced by high V has to be transferred by increasing the G in the solid, which is contradictory to the present results. A new heat balance equation including heat transfer by mass transfer may be a clue to explain whole experimental data. In other words, heat transferred by high temperature silicon material should be considered for the real thermal gradient.

6. V and diameter effects in CZ crystals⁸⁾

In order to show the same mechanisms in CZ crystals as that in FZ crystals on

point defect generations, 6 CZ crystals were grown with different V and different diameters from one crucible. If the diameter is small, interstitials are dominant but diameter is large, vacancies are dominant. On the other hand, small V induces excess interstitials and large V produces vacancies. These are the exactly same features in FZ crystals and the species of point defects are determined only by the G by not the V . It is, however, showed that the G does not follow spontaneously when V is changed. It is newly found that the R-OSF rings distribute like an egg shape in center region which is spreading both the sides of the lowered V region in small diameter crystals.

7. Discussion

The present author has already point out the following problems ⁶⁾ in the Voronkov's theory. Since G is dependent on V the criterion based on V / G should be written only by G . Due to coexistence of self-interstitials and vacancies in the same interface layer, V is not a substantial parameter. When $V=0$ and $G=0$, point defects cannot be defined but they still exist. For example, if $G=0$, the crystal may be filled with vacancies over 1200C.

8. Conclusions

The species of point defects are determined by the degree of G near the interface during growth. Dynamic changes of species and their concentrations happen by the the change of the G_{crit} . This fact excludes the equilibrium concentration models during growth, which postulates equal concentrations of interstitials and vacancies at growth interface. However, in non-thermal gradient state, vacancies are dominant. From the fact that the G determines the species and their concentrations, it is suggested that stress compensation be attributed to point defect generation.

Reference

1. T. Abe, T. Samizo and S. Maruyama, Jpn. J. Appl. Phys., 5, (1966) 458
2. J. Ryuta, E. Morita, T. Tanaka and Y. Shimanuki, Jpn. J. Appl. Phys. 29 (1990) L1947
3. K. Tachimori, T. Sakon and T. Kanaka, 7th Crystal Engineering Symposium 1990, JSAP Catalog Number : AP 902217 p.31 (in Japanese)
4. V. V. Voronkov, J. Cryst. Growth, 59 (1982) 625
5. P. J. Roksnoer and M. M. B. Van Den Boom, J. Cryst. Growth, 53 (1981) 563
6. T. Abe, H. Harada and J. Chikawa, Physica 116B (1983) 139
7. E. Dornberger and A. V. Ammon, J. Electrochem. Soc., 143, 1648 (1996)
8. T. Abe and K. Hagimoto, Solid State Phenomena, 47-48, (1996) 107

THE ORIGIN OF POINT DEFECTS IN FZ AND CZ SILICON CRYSTALS

Takao ABE
Shin-Etsu Handotai

【CONTENTS】

1. Thermal Gradient Effects
 2. Voronkov's Theory and Heat Balance Equation
 3. Summary
-

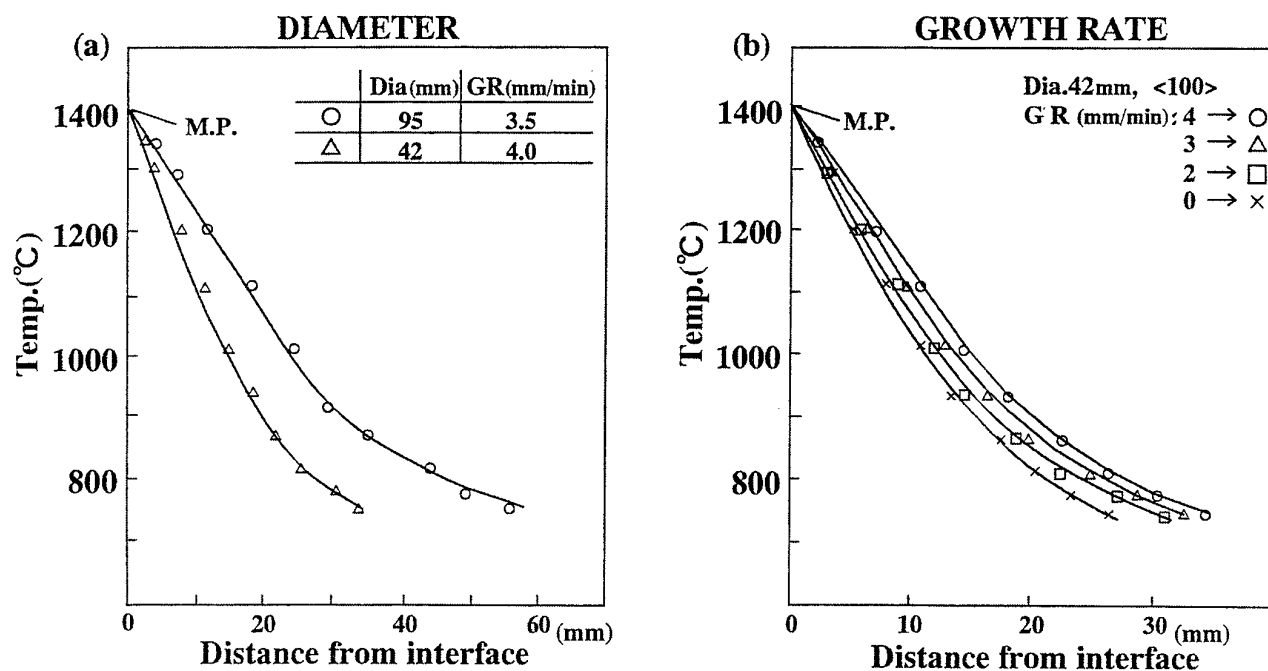
ISCGT-1 '98

RELATION OF G TO V AND DIAMETERS FROM OUR RESULTS

1. Big diameter reduces G and vice versa.
 2. G with 4 mm / min is small compared with G with 0 mm / min. It is concluded that larger V induces lower G. The reverse is also true.
 3. Heat transferred by high temperature silicon mass should be considered.
-

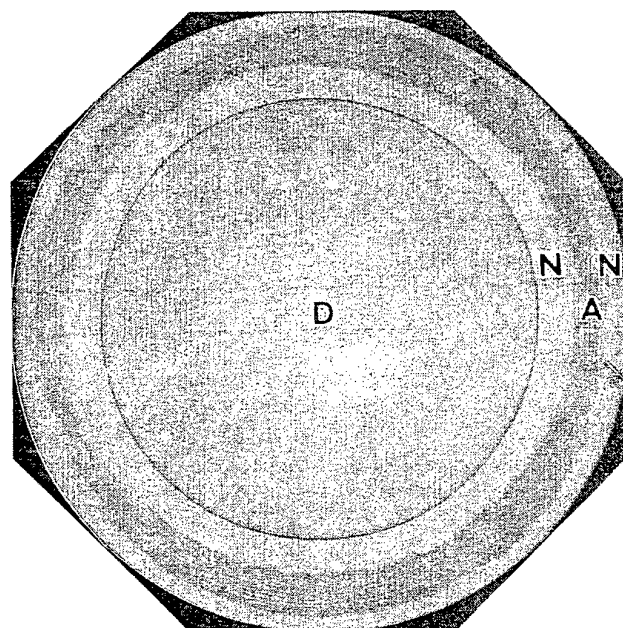
ISCGT-1 '98

TEMPERATURE GRADIENTS ON SURFACE OF GROWING FZ CRYSTALS

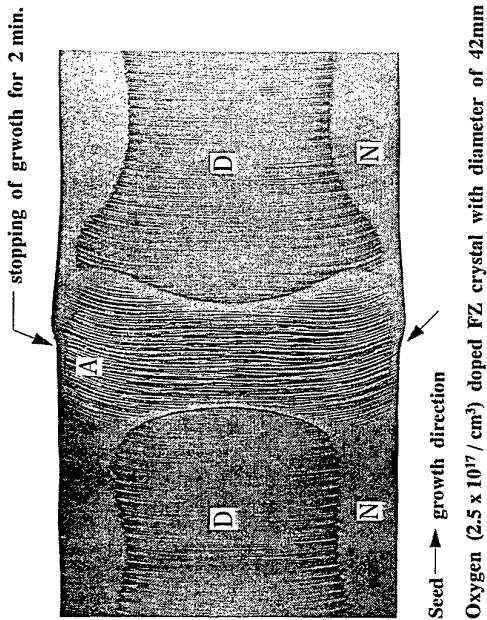


COEXISTENCE OF INTERSTITIALS AND VACACIES

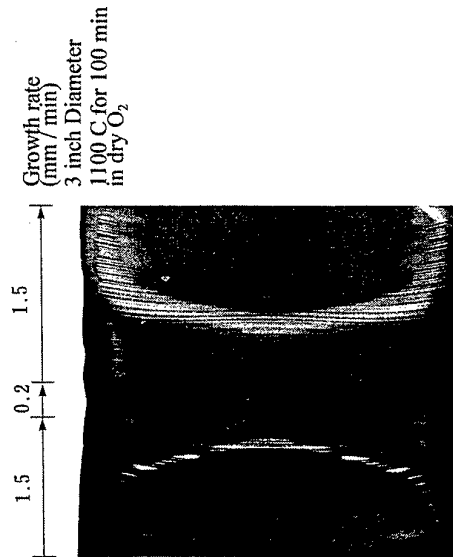
X-ray Topo. After Cu decoration . 100mm diameter



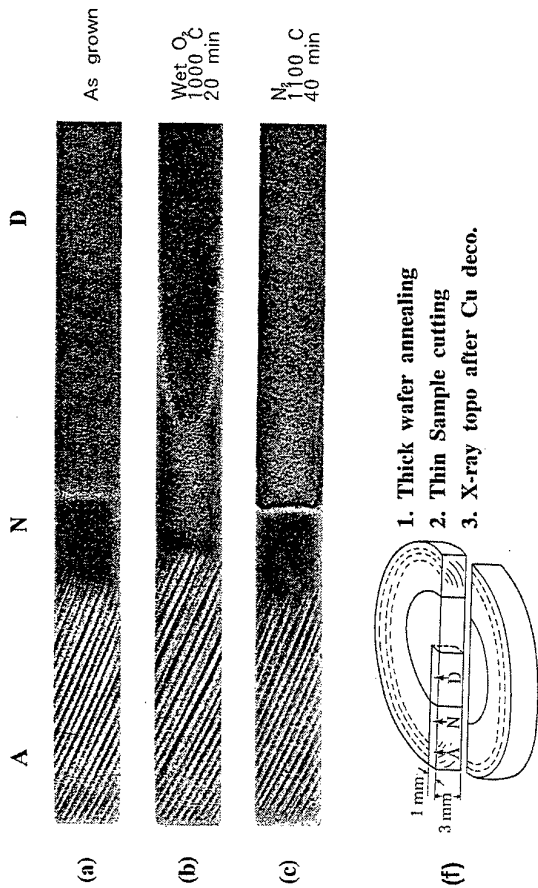
A DEFECTS GENERATED BY *IN SITU* ANNEALING



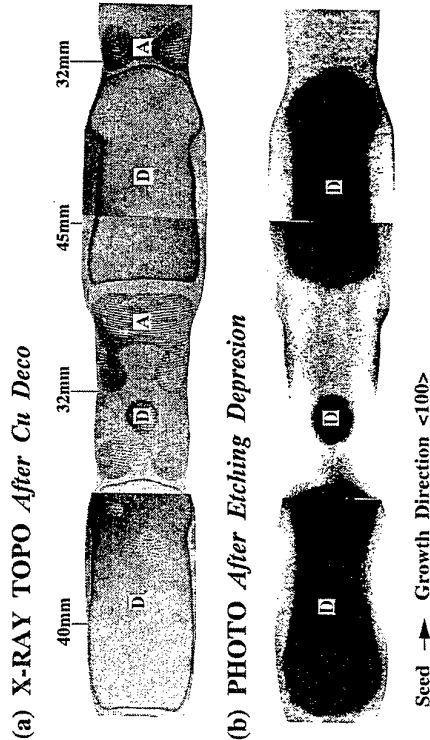
X-RAY TOPOGRAPH OF CZ CRYSTAL WITH R-OSF REGION (SYMMETRICAL U-SHAPED)



IN-DIFFUSION OF INTERSTITIALS AND VACANCIES



DIAMETER EFFECTS ON A AND D DEFECTS IN FZ CRYSTAL



DEFECT GENERATION ON GROWTH RATE AND DIAMETER

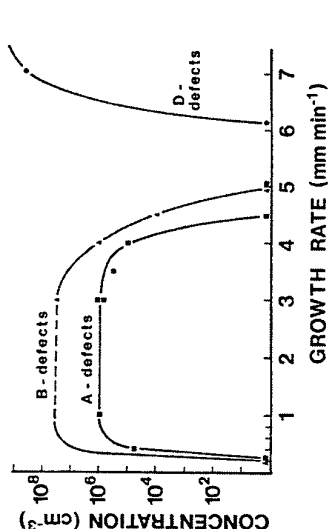
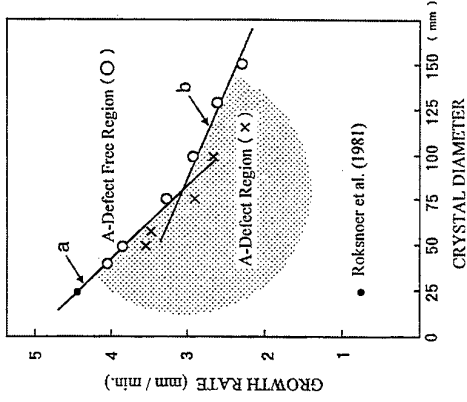


Fig. 6. The concentration of A-, B- and D-type defects as a function of growth rate in 23 mm thick pedestal-pulled silicon crystals. Atmosphere pure argon.



ISCGT-I '98

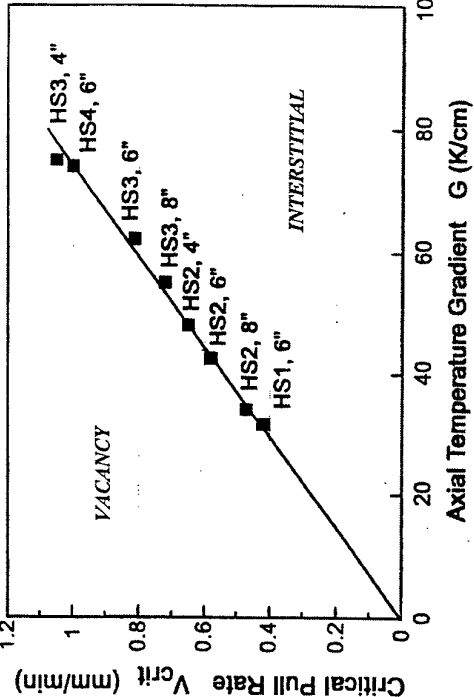


Fig. 2. Functional dependence of V_{crit} on the axial temperature gradient at the solid/liquid interface in the center of the growing crystal, for crystals from 4 to 8 in. and heat shields HS1-HS4.¹³

Erich Dornberger and Wilfried von Ammon J. Electrochem. Soc., Vol. 143, 1648 1996

PROBLEMS OF VORONKOV'S THEORY

Latent heat + heat transferred to crystal from melt = heat conducted away from the interface by the crystal (4-1)

$$L \frac{dm}{dt} + k_1 \frac{dT}{dx_1} A_1 = k_s \frac{dT}{dx_2} A_2 \quad (4-2)$$

where L = latent heat of fusion
 dm/dt = amount freezing per unit time
 T = temperature
 k_1 = thermal conductivity of the liquid
 dT/dx_1 = thermal gradient in the liquid at some point x_1 close to the interface
 A_1 = area of the isotherm which goes through x_1
 k_s = thermal conductivity of the solid
 dT/dx_2 = thermal gradient in the solid near the interface
 A_2 = area of the isotherm through x_2 , which will be approximately the area of the crystal (exactly, if the isotherm is planar and perpendicular to the growth direction)

$V / G < C_{crit}$: Interstitial rich
 $V / G > C_{crit}$: Vacancy rich

1. Due to coexistence of Interstitials and Vacancies with the same V , V is not substantial .
2. When $V = 0$ and $G = 0$, point defects cannot be discussed but they still exist. If $G = 0$, a crystal may be filled with vacancies over 1200C. Even when $V = 0$, if G is small, vacancy is rich.

ISCGT-I '98

EXPERIMENTS

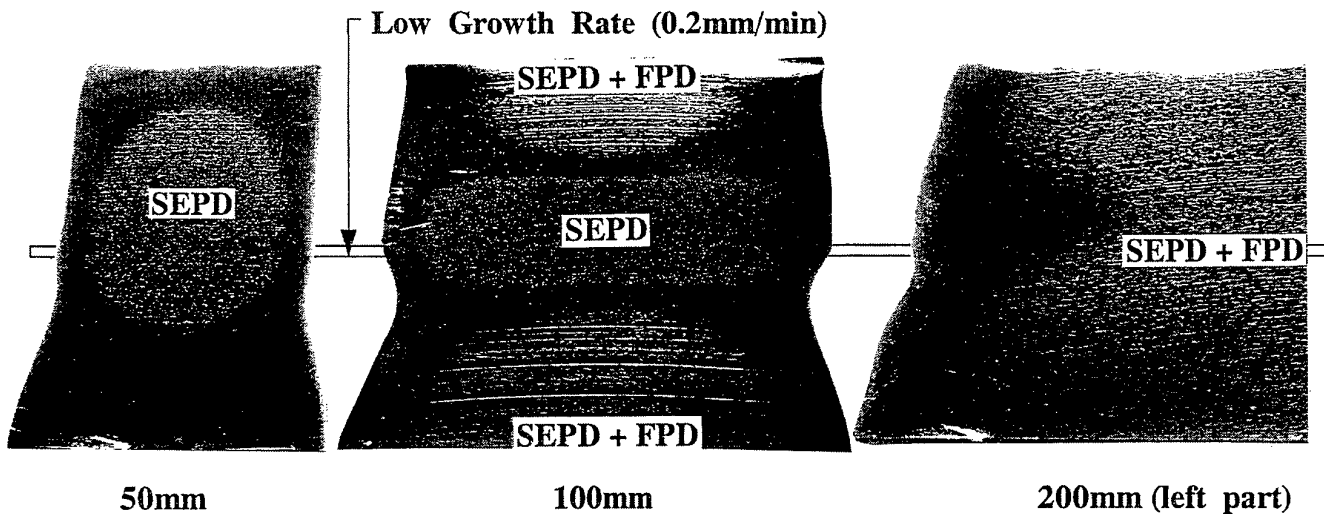
1. Conventional CZ Furnace with 70kg Charge
2. Constant Growth Rate : 1mm/min except for 30min with 0.2mm/min
3. Crystal weights (= recharged weights) of each diameter crystal

Diameter (mm)	200	150	125	100	75	50
Weight (kg)	39.3	18.6	12.4	8.0	4.6	2.5

Longitudinal Cut Wafers to Growth Direction with 15cm in Length

4. Secco Etch, Dark Field Photo, X-ray Topo, Wafer Lifetime (SEMILAB), Cu Depo, RTA (PROTECH)

DARK FIELD PHOTO AFTER SECCO ETCH



COP SIZE AND ANNIHILATION BY RTA

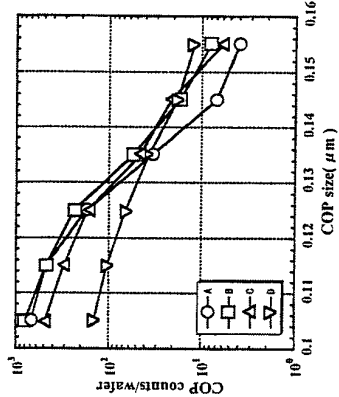


Fig.1 COP size distribution(as-polished wafers) depending on growth rate and oxygen concentration.

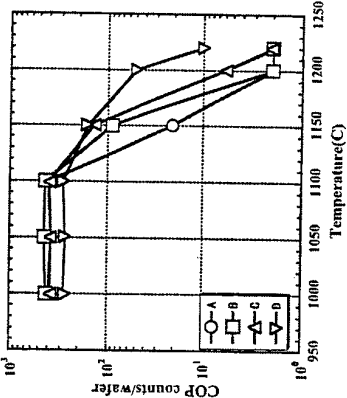


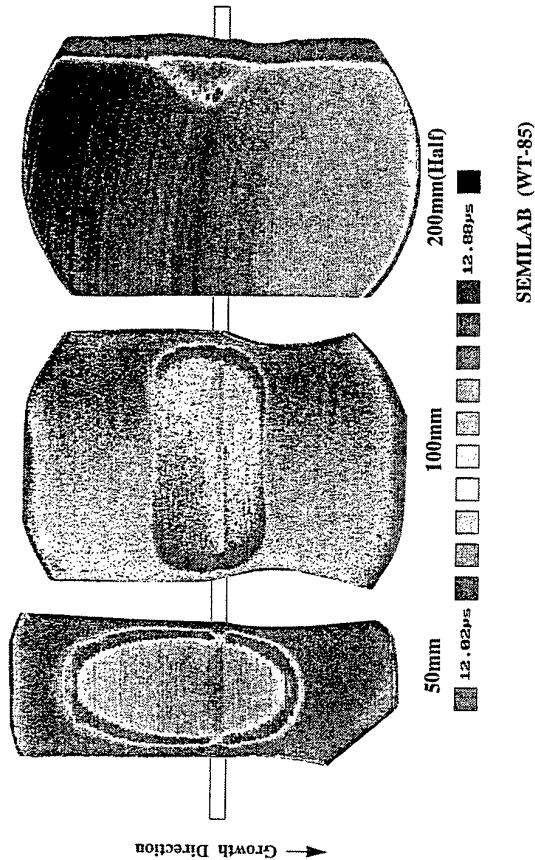
Fig.3 COP annihilation by RTA in H₂/Ar for 10sec
COP counts means total COPs in the range of 0.1-0.2μm.

Table 1 Sample wafers and annihilation rate

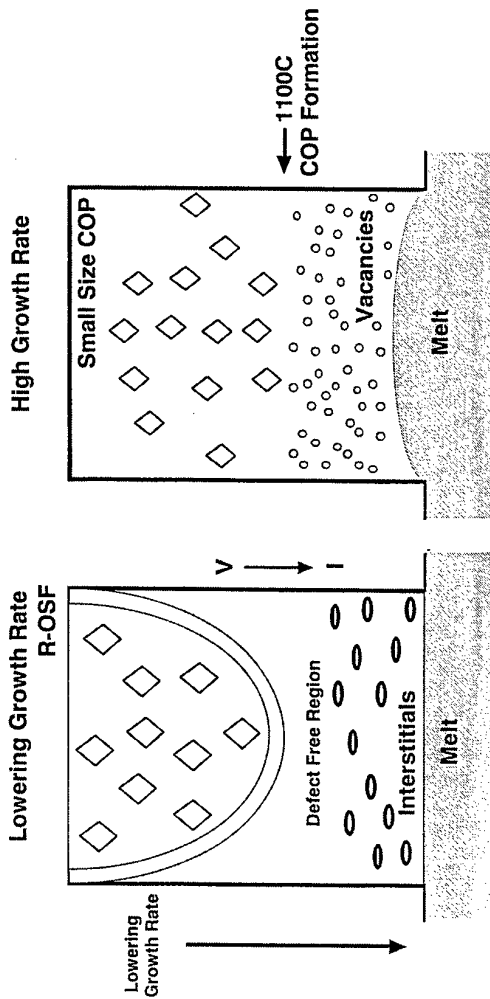
Sample	Growth rate (mm/min.)	Oxygen conc. (ppm)	Annihilation Rate(%)
A	1.6	9	70.9
B	1.6	16	66.0
C	0.9	16	61.4
D	0.6	16	60.4

ISCGT-1 '98

WAFER LIFETIME DISTRIBUTION



GROWTH RATE AND RELATED DEFECTS



SUMMARY III

IDENTIFICATION OF SECONDARY DEFECTS

species	FZ		CZ	
	as grown		as grown	annealed
Interstitial	A defect* ¹	SEPD / DL	R-OSF	
Vacancy	D defect* ²	FPD / COP	AOP	

SEPD : Secco Etch Pit Defect, DL : Dislocation Loop

FPD : Flow Pattern Defect, COP : Crystal Originated Particle

R-OSF : Ring like distributed Oxidation Induced Stacking Fault

AOP : Anomalous oxidation precipitation, *1 : Swirl defect *2 : Etching Depression

ISCGT-I '98

ISCGT-I '98

CONCLUSION

1. The species of point Defects are determined by the degree of thermal gradient during growth.
2. Dynamic changes of species and their concentrations happen near growth interface. This denies the equilibrium concentration models at interface.
3. The unified understanding between point defects in FZ and CZ crystals is possible.
4. From both the thermal gradient effects, the stress compensation may be suggested to point defect generations.

ISCGT-I '98

ISCGT-I '98

SUMMARY I

VERIFICATION OF VORONKOV THEORY

1. Voronkov's theory is not applicable.
2. Traditional heat balance equation is clearly wrong for real growth.
3. Simulation works using 1 and 2 are not true.

SUMMARY II

POINT DEFECTS AT HIGH TEMPERATURE

1. Large G : Interstitials
2. Small G : Vacancies
3. Equilibrium : Vacancies (Rapid Cooling)
(No G)

The Conversion to 300mm Wafers: Challenges for Wafer Manufacturing

Bernd Sauter

Wacker Siltronic AG, P.O. Box 1140, 84479 Burghausen, Germany

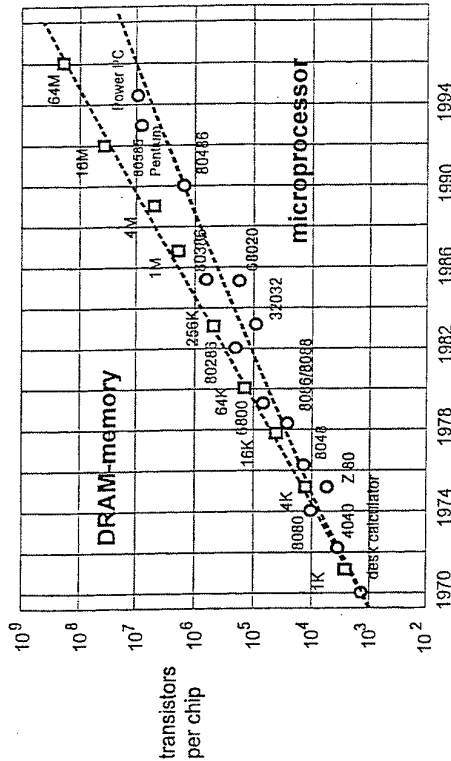
The conversion to 300mm silicon wafers is characterized by many challenges and uncertainties, yet offers big opportunities for the semiconductor and electronics industry. Since the birth of the integrated circuit in 1959 by Jack Kilby, the semiconductor industry lives to fulfill Moore's Law: the number of devices in a single integrated circuit doubles every 18 months. This rapid technological progress is the necessary basis for the growth of the semiconductor business, which is only possible as long as the cost per electronic function continues to decrease. In parallel to the increase in device density the wafer size evolved from 2 inches in 1970 to 200mm in the late 80's and now even to 300mm. The driving forces behind each conversion are the economic advantages obtained by using larger substrates for manufacturing ICs and in order to limit capital investments for new fabs. Despite the obvious economical advantages, only very few IC manufacturers are currently building 300mm pilot or production lines. This is due to several reasons: Some IC houses plan to use 200mm wafers for one or two future design rule generations beyond 0.25 μ m, a complete tool set for IC manufacturing was not available until 1998, and the revenues of the industry are decreasing making heavy capital investments difficult. On the other hand, all market forecasts predict growth rates well above 10% in the years 1999 to 2002. The challenge is the right timing for 300mm to minimize the risks and maximize the opportunities.

Wafer manufacturers face similar and additional challenges. Whereas only very few IC companies started to construct 300mm lines by mid of 1998, all major wafer manufacturers already produce 300mm wafers in their pilot lines to allow for the development of a complete and functional tool set for device lines and to feed the pilot device lines with engineering samples. Moreover, wafer manufacturers need to solve a new type of a technological challenge. From past experience, the device community was determined not to convert to a larger diameter and to the next smaller design rule at the same time, but rather convert at one design rule with processes driven to high yields. For 300mm, the conversion

was planned for 0.25 μ m design rule originally. It now looks like that it is going to be "smeared" out from 0.25 through 0.18 μ m to 0.13 μ m design rule. So, capability requirements for 300mm silicon wafers are toughening during the development work. With the availability of the 1997 version of the SIA Roadmap silicon manufacturers have a generic set of goals clearly lined out. Among the most challenging requirements for 300mm silicon are the number and size of local light scatterers, wafer geometry, bulk and surface metals. The requirements are aggravated for 300mm by the 2.25 fold wafer area compared to a 200mm wafer. Analysis of particle transfer probability and of lattice slip susceptibility during thermal stress created a global consensus, that the back surface of the wafer has to be polished, too. This also requires new technologies and/or a specific combination of manufacturing processes not common in 200mm wafering. Applying a simultaneous double side polishing method can achieve this efficiently and with the same excellent potential for local flatness as the more traditional and mature single side polishing. Multiple wire sawing for slicing a grown silicon ingot into wafers offers the prospect of minimum taper, bow and warpage to the wafer while minimizing kerf loss compared to ID sawing. A big challenge posed by the requirements of sub-quarter micron design rules is the crystalline perfection. In the area of metrology, the main challenges were to provide early equipment for wafer geometry measurement, for detection of local light scatterers and for surface metals, and at the same time challenges that came with the request not to touch the polished back side of the wafers, the requirement for better resolution and less edge exclusion.

In order to make the transition to 300mm successful, apart from solving technological issues minimizing the cost of wafer manufacturing is crucial to obtain lower die cost than with 200mm wafers. Using standardized equipment and standardized wafer specifications like wafer dimensions, backsurface glossiness, and 100% ID marking will further decrease cost. Beyond that the conversion to 300mm is strongly coupled to numerous cooperations between silicon suppliers and IC houses including the consortia Selete and I300I to facilitate total cost minimization. Open communication on pre-competitive fields among the industry partners help to make rapid progress on the learning curve while avoiding costly dead ends. Although the industry faces many challenges, it is believed that 300mm will open opportunities to gain market share and create new business for existing and new players and will sustain long term growth for the semiconductor industry.

Historical development of memories and microprocessors



WACKER

ISCGT-1, Beatenberg Wacker Siltronic AG

The Conversion to 300mm Wafers: Challenges for Wafer Manufacturing

First International School on Crystal Growth Technology - Beatenberg, September 1998

Bernd Sauter, Wacker Siltronic AG

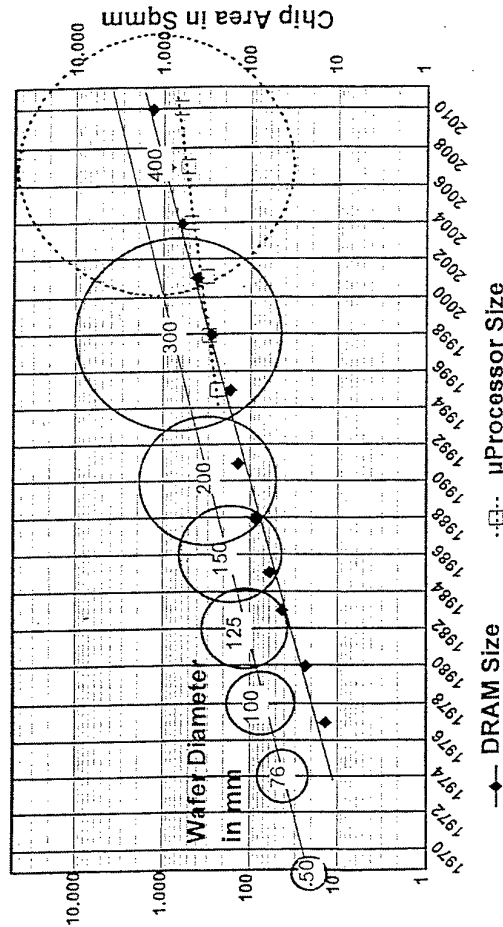
Outline

1. Introduction: Historical Development and Silicon Market
2. Technological Challenges
 - Crystal Growing
 - Wafer Shaping
 - Metrology
3. Non-Technological Challenges
4. Summary

WACKER

ISCGT-1, Beatenberg Wacker Siltronic AG

Silicon Wafer Trends: Wafer Diameter and Chip Size



WACKER

ISCGT-1, Beatenberg Wacker Siltronic AG

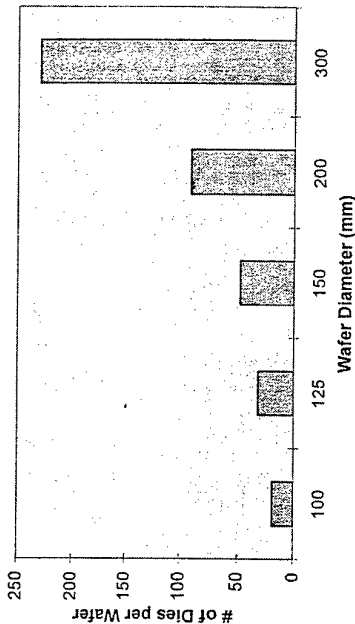
1. Introduction: Historical Development and Silicon Market

- Historical development of memories and microprocessors (Moore's law)
 - 1970: 10^3 transistors per chip (desk calculator)
 - 1998: 10^8 transistors per chip (256 M)
- Silicon wafer trends
 - 1970: 2 inches (20 cm^2)
 - 1998: 300mm (706 cm^2)

WACKER

ISCGT-1, Beatenberg Wacker Siltronic AG

Productivity and Wafer Size (256M DRAW)



⇒ Productivity Increase: 2.5 (300mm compared to 200mm)

WACKER

ISCGT-1cd.W-EWIDr. B. Sauter/July 5, 1998, Page 7/20

2. Technological Challenges

Industry Requirements

NTRS Roadmap 1997 (Extract)

Year of First Product Shipment	1997	1999	2001	2003
Technology Generation (nm)	250	180	150	130
Wafer Diameter (mm)	200	300	300	300
Site Flatness (SFQR) (nm)	≤250	≤180	≤150	≤130
Site Size (mm x mm)	22 x 22	25 x 32	25 x 34	25 x 36
Edge Exclusion (mm)	3	2	2	2
Critical Surface Metals (cm ²)	≤2.5E10	≤1.3E10	≤1.0E10	≤7.5E9
Minimum LLS Size (nm)	125	90	75	65
Number of Particles per wafer	≤41	≤60	≤47	≤38
Number of LLS per wafer	≤172	≤192	≤178	≤96
Gate Oxide Defects DRAM (cm ²)	≤0.06	≤0.029	≤0.026	≤0.014
Structural Defects in Epi Layers (# per Wafer)	≤1	≤2	≤1.8	≤1.6
Frontside Roughness (nm)	≤0.15	≤0.1	≤0.1	≤0.1

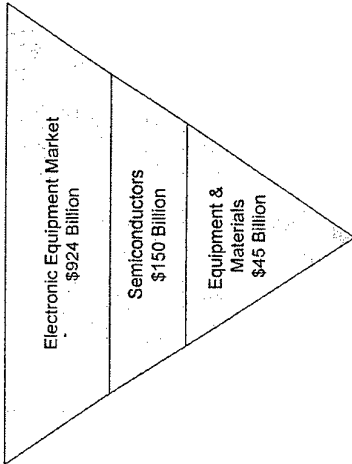
WACKER

ISCGT-1cd.W-EWIDr. B. Sauter/July 5, 1998, Page 9/20

The Silicon Wafer Market

- Silicon wafers are the basis of the electronics industry (1997: total market > \$1000 Billion)

1997



Source: Dataquest

- Wafer area generation model: 10% CAGR in silicon area

WACKER

ISCGT-1cd.W-EWIDr. B. Sauter/July 5, 1998, Page 5/20

Why 300mm?

- Industry decision in 1995 after evaluating risks and benefits of 300, 350, and 400mm wafers
- Cost reduction per die relative to 200mm (30% to 40%)
- World-wide increase of electronics market (communication, internet)
- Constraint of resources (e.g. invest)

WACKER

ISCGT-1cd.W-EWIDr. B. Sauter/July 5, 1998, Page 6/20

– lower bow and warpage

– waviness: more work required

Wafer Grinding

- Wafer grinding combined with simultaneous double side polishing is now most important for wafer geometry, replaces lapping combined with single side polishing
- improved process control (single wafer vs. batch process)
- improved wafer geometry compared to lapping (GBIR, SFQR)
- improved wafer thickness control
- less sub-surface damage (ca. 0.5-15µm): reduced material removal in succeeding steps
- automated equipment

WACKER

ISCGT-1cdLW-EWDr. B. Sauer/July 5, 1998, Page 1320

300

Polishing

- Double-side Polishing
 - analysis of particle transfer probability, lattice slip susceptibility during thermal stress created consensus on polished wafer back side
 - simultaneous polishing of both wafer sides with wafers not mounted to a carrier plate gives very good, uniform wafer geometry (local flatness)
 - less experience compared to single side polishing

WACKER

ISCGT-1cdLW-EWDr. B. Sauer/July 5, 1998, Page 1420

Crystal Growing

>>> Economic crystal growing: large cylindrical crystal length required <<<

Requirements (examples):

- crystalline perfection: smaller radial uniformities of resistivity and O_1 for a 50% increased diameter compared to 200mm crystals
- large melt volumes → convection currents, thermal fluctuations
 - 200mm: 100kg
 - 300mm: 300kg
- large silica crucibles → manufacturability, cost, cleanliness, mechanical stability
 - 200mm: 22' to 24'
 - 300mm: 32' to 36'
- limited strength of seed crystal → new methods required for heavy crystals

WACKER

ISCGT-1cdLW-EWDr. B. Sauer/July 5, 1998, Page 1020

Wafer Shaping

>>> New Wafer Manufacturing Technologies are Required for 300mm and Larger Wafers and 0.18 µm and Smaller Technology Generations <<<<

Wire Sawing

- Multiple Wire Sawing replaces ID sawing
 - 300mm is technological limit for ID sawing (sawing blade availability, size of sawing head etc.)
 - less kerf loss due to thin wire (diameter typical 180µm, length: 100km or more): ID saw: 350-400µm; wire saw: 200-250µm
 - less sub-surface damage (SIRD) (ID saw: 30 to 40 µm; wire saw: ca. 20µm): reduced material removal in succeeding steps

WACKER

ISCGT-1cdLW-EWDr. B. Sauer/July 5, 1998, Page 1220

3. Non-Technological Challenges

- Challenge: Right timing
 - Dependent on availability of complete, tested tool set for IC manufacturing for 0.25µm and smaller design rules
 - Dependent on general semiconductor market
- Challenge: Limit cost
 - Huge upfront invest needed, benefit later
 - Limit cost of silicon: processes with lower silicon and kerf losses, eliminate process steps, new technologies
 - More equipment standardization, shared development
 - Global standards for materials (e.g. backsurface glossiness, standard edge profile, 100% ID marking), carriers, metrology
 - strategic partnerships and cooperations with customers and suppliers

WACKER

ISCGT-1&LW-EWIDr. B. Sauter/July 5, 1998, Page 18/20

302

4. Summary

Challenges

- o 300mm wafer manufacturing for 0.18 µm technology is feasible, no show stoppers
- o costs need close attention, standards are very important

Opportunities

- o new ideas/innovations will facilitate transition → generate new business
 - o gain market share by early development
- ⇒ opportunities for materials, equipment and IC manufacturers

WACKER

ISCGT-1&LW-EWIDr. B. Sauter/July 5, 1998, Page 19/20

Metrology

>>>> You can only improve what you can measure <<<<

- Key metrology equipment: geometry measurement, detection of local light scatterers, surface metal measurement
- Main challenges:
 - larger wafer diameter
 - better resolution
 - edge exclusion: 2mm
 - edge-gripping (polished back side)
- Geometry measurement:
 - tools based on capacitive sensors approach resolution limit → new tools based on optical interferometry are required

WACKER

ISCGT-1&LW-EWIDr. B. Sauter/July 5, 1998, Page 15/20

Surface inspection system:

- high threshold sensitivity required: <0.1µm LSE
- multiple dark and bright field channels required for distinction between particles and pits/COPS

WACKER

ISCGT-1&LW-EWIDr. B. Sauter/July 5, 1998, Page 16/20

LARGE DIAMETER SILICON TECHNOLOGY

H. Yamagishi, M. Kuramoto, Y. Shiraishi, N. Machida, K. Takano,

N. Takase, T. Iida, J. Matsubara and K. Takada

Super Silicon Crystal Research Institute Corp.

Nakanoya 555-1, Annaka, Gunma 379-0125, Japan

1. INTRODUCTION

Super Silicon Crystal Research Institute Corporation (SSi) was established in 1996. SSi will develop the key technologies of silicon wafers with a super large-diameter of 400 mm by 2001. 400 mm silicon wafers were expected to be used in 2008. It seems a little early to develop such 400 mm wafers. However we believe that our developing technologies will be useful even for 300 mm wafers fabrication since the platform of 400 mm wafer technology is almost common to every wafer fabrication with a diameter larger than 200 mm. SSi has three laboratories, CZ crystal growth, wafer shaping and epitaxial growth.

In this paper, we mainly focus on fundamental concept for large diameter crystal growth.

2. DEVELOPED KEY TECHNOLOGIES FOR CZ CRYSTAL GROWTH

We have to develop the following key technologies for 400 mm CZ crystal growth; CZ crystal growing furnaces with a crystal suspending system, large hot zone parts, handling and transportation system for heavy hot zone parts, retrieving system for a grown crystal from the CZ furnace, spherical grinding machine on a grown crystal and ingot cutting band saw. We also develop an anti-steam-explosion safety in CZ furnace and consider crystalline quality. These targets are described in details in [1-3].

SSi installed first huge CZ crystal growing furnace, made by collaboration with Leybold Systems Corp. in Germany, in the end of 1997 and started crystal growing in the beginning of March in 1998. Its total height from the ground level and total weight

are about 12 m and heavier than 30 metric ton respectively. A super conductive cusp type magnet made by Mitsubishi Electric Co. is provided surrounding the first CZ furnace to suppress silicon melt convection and to control interstitial oxygen concentration. The maximum magnetic field at the 36 inch quartz wall is 3000 gauss.

We control the furnace from an isolated operating room to avoid steam explosion and straying magnetic field. Its present status is alternate improvement for initial troubles and crystal growing by using 36 inch hot zone.

Isotropic graphite material and carbon composites (CC) are available for hot zone size of 102 cm (40 inch) in diameter. We are now using hot zone size of 91.4 cm (36 inch) in diameter without any problems. Quartz crucibles with a diameter of 36 inch are used. Slight deformation of quartz crucible is observed after CZ crystal growth. It is not obvious whether the corrosion of quartz crucible's surface induces the structure loss during CZ crystal growth.

The weight of a grown 400 mm silicon single crystal becomes heavier than 400 kg. So We need a minimum necking diameter of 6 mm for the crystal weight of 400 kg. Recently Chandrasekhar reported a success of necking with a diameter larger than 10 mm in high boron doped silicon crystal growth [4]. However we believe that it is not easy to grow such a necking in heavily charged silicon melt since we have to control the melt temperature to maintain the curvature of the growth interface. Moreover we have to consider a safety factor larger than 2 to grow a single crystal safely and creep phenomena at high temperature around 800 C.

Therefore we have to invent a suspending system of growing silicon single crystals instead of necking [1-3]. During necking process, its diameter is kept around 3mm to achieve dislocation free and then a subsidiary cone is made, by increasing the diameter up to a few tens mm and decreasing again up to about 10 mm. The diameter is kept until the beginning of the following cone process. A mechanical cramp is attached to the beneath of subsidiary cone when the growing crystal weight increases to about 150 kg.

Moreover, we will present a handling and transportation system for heavy hot

zone parts and crystals.

References

- [1] H. Yamagishi, M. Kuramoto, Y. Shiraishi, N. Machida, K. Takano, N. Takase, T. Iida, J. Matsubara and K. Takada, "CZ crystal growth development in super silicon project", *Proceedings of The 2nd International Symposium on Advanced Science and Technology of Silicon Materials*, M. Umeno, Editor, The 145th Committee of The Japan Society for The Promotion of Science, Tokyo, 1996, p.59.
- [2] H. Yamagishi, M. Kuramoto, Y. Shiraishi, N. Machida, K. Takano, N. Takase, T. Iida, J. Matsubara and k. Takada, "CZ crystal growth development in super silicon project", *Gettering and Defect Engineering in Semiconductor Technology 1997*, C. Claeys, J. Vanhellemont, H. Richter aand M. Kittler, Editors, V57-58 of Solid State Phenomena, Scitec Publications, Switzerland, 1997, p.37.
- [3] K. Takada, H. Yamagishi, H. Minami and M. Imai, "Research and development of super silicon wafers", *Semiconductor Silicon 1988*, H. R. Huff, H. Tsuya and U. Gosele, Editors, PV-98-1, The Electrochemical Proceeding Series, New York, 1998, p.376.
- [4] S. Chandrasekhar and K. M. Kim, "Growth of large diameter (>10mm) necks for large size CZ silicon", *ibid 4.*, p.411.

DEVELOPED KEY TECHNOLOGIES FOR CZ CRYSTAL GROWTH

1. CZ crystal growing furnace with a crystal suspending system.
2. Large hot zone.
3. Handling and transportation system for heavy hot zone parts.
4. Retrieving system for a grown crystal from the CZ furnace.
5. Grinding machine on a grown crystal and ingot cutting band saw.
6. An anti-explosion safety system due to steam in CZ furnace.
7. Crystalline quality.

Here we focus on our installed equipment.



CZ crystal growing furnace

1. Made by collaboration with Leybold System Corp. in Germany, in the end of 1997.
2. Started crystal growing in the beginning of March in 1998.
3. Its total height from the ground level is about 12 m and total weight is heavier than 30 metric ton.
4. A super conductive cusp type magnet made by Mitsubishi Electric Co. is provided surrounding the first CZ furnace to suppress silicon melt convection and to control interstitial oxygen concentration.

Its outer diameter, inner diameter and height are about 3 m, 2 m and 3 m respectively.

5. The maximum magnetic field at the 36 inch quartz wall is 3000 gauss.
6. Its storage energy is 9 MegaJ, which is very higher than ordinary used super conductive magnet of 1 MegaJ.
7. We control it from an isolated operating room to avoid steam explosion and straying magnetic field.

Its present status is alternate improvement for initial troubles and crystal growing by using 36 inch hot zone.



Hot zone parts and quartz crucible

Graphite & CC:

1. Isotropic graphite material and carbon composites (CC) are supplied by Toyotanso Co. and Nihon Carbon Co., respectively.
2. Their size is available for hot zone size of 102 cm (40 inch) in diameter.
3. We are now using hot zone of 91.4 cm (36 inch) in diameter without any problems.

Quartz Crucible:

1. Quartz crucibles with a diameter of 36 inch were supplied by Shin-Etsu Quartz Products Corp. and Mitsubishi Material Corp..
2. Slight deformation of quartz crucible is observed after CZ crystal growth.
3. It is not obvious whether corrosion of quartz crucible's surface induces the structure loss during CZ crystal growth.

By numerically global heat transfer simulation.

the heater power and maximum temperature on the quartz crucible:

≅24 inch hot zone for silicon crystal with a diameter of 200 mm.

Dislocation free crystal growth is observed even after re-melting.

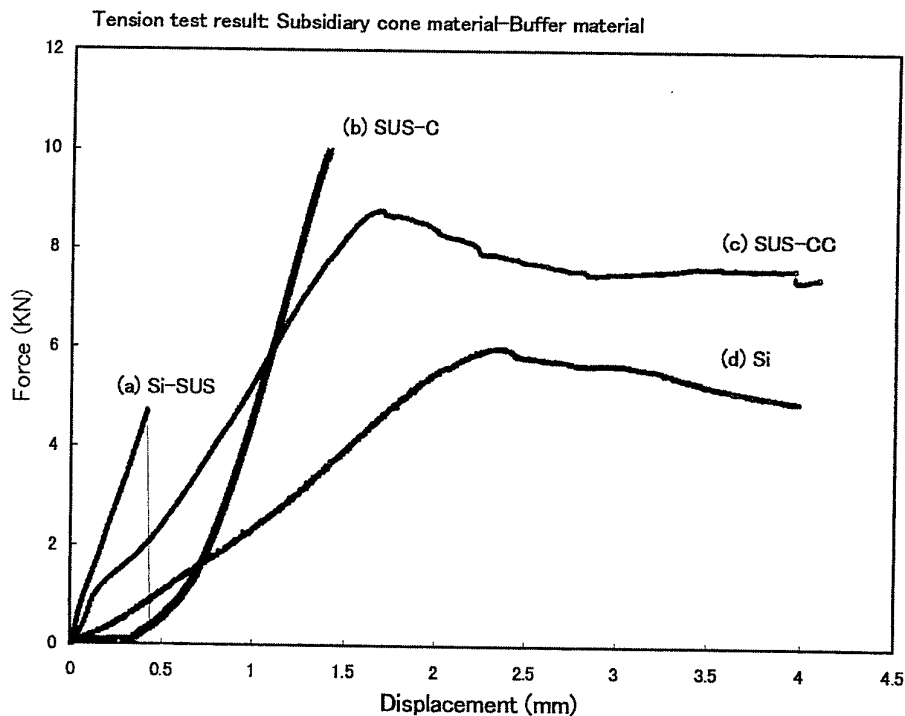
We believe 36 inch quartz crucible is sufficient for 400 mm crystal growth.

 **Super Silicon Crystal Research Institute Corp.**

Crystal suspending system

1. The maximum tensile stress with a diameter of 15 mm: 2.7 kgf/mm²
The crystal weight: 400 kg.
The calculated maximum temperature on the necking: 600 C
2. The mechanical strength between 700 C and 500 C :
increasing from 10 kgf/mm² to 64 kgf/mm². (after Yasutake)
3. Theoretically able to suspend the crystal weight of 400 kg :
in the safety factor of about 4.

 **Super Silicon Crystal Research Institute Corp.**



SSI Super Silicon Crystal Research Institute Corp.

Handling and transportation system for heavy hot zone parts and crystals

Quartz crucible in the weight of 70 kg.

Graphite parts: 300 kg.

Charging Poly Si: 500 kg.

Grown crystal: 400 kg.

↓

Precharging.

Graphite handling.

Retrieving system for a grown crystal.

Transportation system.

SSI Super Silicon Crystal Research Institute Corp.

Silicon Crystal Growth for Photovoltaics

Ted F. Ciszek

National Renewable Energy Laboratory
1617 Cole Boulevard
Golden, CO 80401 USA



The major crystal growth techniques used in the silicon electronics industry, Czochralski (CZ) growth and float-zone (FZ) growth, focus on uniformity, high purity, and low defect concentrations. The cost of crystal growth is not a major determining factor for the end-use device products. In the silicon photovoltaics (PV) industry, uniformity, high purity, and low defect concentrations are also desirable attributes because the solar cell efficiency η is directly related to the minority charge-carrier lifetime τ . Lifetime is strongly affected by impurities and defects. But the Si PV industry is extremely cost conscious. A solar cell is a large-area device and costs cannot be decreased by increasing the density of devices on a chip as they are in the semiconductor industry. Cost reductions are achievable through automation and economies of scale, and crystalline silicon has maintained a dominant role in the commercial PV power systems market by addressing these issues. Of the ~150 megawatts now being produced yearly, crystalline silicon supplies about 95%. The cost of the silicon substrate is a substantial fraction (about 1/3) of the total cost of a PV system. The focus of Si crystal growth technology development for PV use is on low-cost, high-throughput methods with somewhat relaxed quality requirements.

CZ and FZ growth produce single, dislocation-free crystals. Many alternative methods have been explored in hopes of reducing costs, and most of these result in multicrystalline ingots or sheets. Float zoning is used very little for PV, but it does make the highest efficiency cells (23%). CZ growth is used by one of the largest Si PV companies. Other ingot technologies developed especially for PV applications include

directional solidification or batch casting of large multicrystalline ingots and cold crucible electromagnetic semicontinuous casting. Most of these methods are simpler than CZ or FZ growth and produce large (30 to 190 kg) ingots. The throughput of cold-crucible casting, 20 kg/h (equivalent to about 3,000 cm²/min of wafer area) is more than 10 times that of CZ growth. Because of the grain boundaries and dislocations, cell efficiencies are only about 85-90% as large as those obtained with CZ wafers.

Maximizing the throughput and wafer yield per unit length of ingot are important considerations in wafering processes. Modern SiC-slurry wire saws have increased the throughput by a factor of 20 over older inside diameter (I.D.) saw technology, and have doubled the yield per unit length.

The objective of ribbon or sheet growth is to eliminate the cost and material waste of the wafering process. More than 20 approaches have been explored over the past 25 years. Most were abandoned for technological, financial, or strategic reasons. There are currently four methods being pursued commercially. Three of these pull ribbons vertically with a solid-liquid interface that has the same cross-section as the ribbon (100 to 300 μ m thick by 60 to 800 mm wide). In order of increasing width, these are:

- (1) dendritic web growth (a 40- to 80-mm-wide ribbon solidifies between two bounding dendrites propagating into supercooled melt regions at the ribbon edges),
- (2) edge-supported meniscus growth which is similar but continuously incorporates foreign filaments into the edges of a 50- to 100-mm-wide ribbon, and
- (3) growth from a meniscus atop a graphite capillary-shaping die that has 8 sides, each 100-mm wide.

The vertical pulling rates are similar at about 20 mm/min, so the range of throughputs from ~10 to ~160 cm²/min is primarily a function of total width.

The forth method utilizes a large-area solid-liquid interface and growth in a direction nearly perpendicular to the pulling direction. A number of variants have been explored. Commercial activities involve solidifying sheet silicon onto a moving, reusable substrate that separates easily from the sheet upon cool down. This is the fastest melt-grown ribbon approach, with a throughput of $10^3 \text{ cm}^2/\text{min}$ or higher. Grain sizes are small, however, and cell efficiencies are on the order of 12%.

Considerable R&D activity is focused toward Si thin-layer growth on substrates by liquid-phase epitaxy (LPE), chemical vapor deposition (CVD) and other methods. Clear leaders are not yet identifiable. In principle, 85% of useful photons can be absorbed in a 30- μm -thick Si layer (even thinner if light-trapping schemes are employed). A major hurdle is finding an adequate substrate.

The approaches to PV Si crystal growth will be discussed in detail, along with considerations of crucibles, auxiliary materials, properties, and characterization methods. A summary of the various growth methods is given below.

Method	Size, weight (mm, kg)	Growth rate (mm/min)	Throughput (cm^2/min)	Energy Use (kWh/kg)	Efficiency typical (best)%
Czochralski (single)	200, 75	0.8 - 1.6	700	60 - 80	<15 (20)
Float-zone (single)	150, 80	2 - 4	1800	30	<18 (23)
EM continuous casting	220, 190	2 - 4	3000	30	<13 (16)
Directional solidification	440, 125	0.1 - 0.6	1700	8 - 15	<15 (17)
Dendritic web (single)	75, --	1 - 2	10	—	<15 (17)
Edge- supported	100, --	2	20	—	<14 (15)
Capillary Die	800, --	2	200	—	<14 (16)
Substrate melt shaping	200, --	Fast	>1000	—	<12 (16)
Thin Layer on substrate	—	$10^{-3} \perp$	—	—	—

Silicon Crystal Growth for Photovoltaics

lecture presented at the

First International School on Crystal Growth Technology (ISCGT-1)

Beatenberg, Switzerland
September 5-16, 1998

by

Ted F. Cizek
National Renewable Energy Laboratory
1617 Cole Boulevard
Golden, Colorado, 80401 USA



Outline:

- ♦ Introduction and fundamentals:
 - Properties of Si for PV
 - Silicon source materials
 - Purity issues
 - Si growth from the melt
- ♦ Experimental foundations:
 - Heating/melting techniques
 - Crucibles
 - Auxiliary materials
 - Wafer preparation
- ♦ Growth techniques:
 - Czochralski growth (CZ)
 - Float-zone growth (FZ)
 - FZ and CZ comparisons
 - Cold crucible methods
 - Directional solidification (DS)
 - Sheet and ribbon growth
 - Si layer growth on substrates
 - Comparison of the methods
- ♦ Characterization:
 - Crystal defects
 - Impurities
 - Electrical properties
 - Diagnostic solar cells
- ♦ Summary

Silicon source materials:

- Essentially all silicon originates in an arc furnace (MG-Si) process:
 - Coke reduction of quartzite: $\text{SiO}_2 + \text{C} \rightarrow \text{Si} + \text{CO}$, CO_2 , SiC, etc.
 - Purity is ~ 98-99% (mostly Fe, Al, C); cost is ~ \$1-2/kg
- MG Si is converted into SiHCl_3 , SiH_4 , etc. and purified for
 - Siemens process \Rightarrow Si rods; Fluidized bed process \Rightarrow Si pellets
 - E.g. $\text{SiHCl}_3 + \text{H}_2 \rightarrow \text{Si} + 3\text{HCl}$ (1100°C, weeks, \$30-\$80/kg)
- Off-grade or remelt silicon
 - Discards of the semiconductor industry
 - This is currently one of the largest sources of feed stock for cost-effective PV silicon crystal growth
 - Not a sustainable feed stock source for future PV production

ISCGT-1, Switzerland, 1998

Lecture: Si Crystal Growth for PV

T. Ciszek



Purity issues

- Threshold levels of various metal impurities that cause a drop in PV performance were determined by Davis et. al.
 - 10^{11} - 10^{13} atoms/cm³: Ta, Mo, Nb, Zr, W, Ti, V
 - 10^{14} - 10^{16} atoms/cm³: Cr, Mn, Fe, Co, Al, Ni
 - 10^{17} - 10^{18} atoms/cm³: Cu, P
- O, C, N show smaller, effects at $\sim 10^{18}$, 10^{17} , 10^{16} atoms/cm³
- H passivation enhances the performance of low-quality Si
- Impurity sources
 - Sand: 98-99% SiO_2 ; <1% Al_2O_3 , <0.3% MgO, <0.15% Fe_2O_3
 - MG Si: 98-99% Si; Fe & Al are major impurities (many others)
 - $\text{SiH}_x\text{Cl}_{4-x}$: < 5ppm hydrocarbons, <0.3 ppb B, <1.5 ppb P
 - Polycrystalline CVD Si has negligible impurity levels for PV.
 - It is difficult to quantify impurity content in scrap/remelt Si.

ISCGT-1, Switzerland, 1998

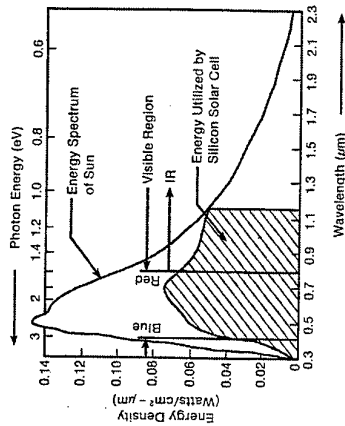
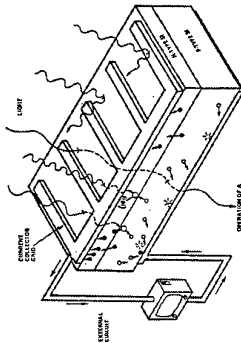
Lecture: Si Crystal Growth for PV

T. Ciszek



Properties of silicon as a PV material:

- Advantages of c-Si for PV
 - abundance
 - salubrity
 - excellent technology base
 - high PV efficiency (23%)
 - easy SiO_2 passivation
 - low basic materials cost
- Disadvantages of c-Si for PV
 - low absorption coefficient
 - escalation of materials costs with processing



ISCGT-1, Switzerland, 1998

Lecture: Si Crystal Growth for PV

T. Ciszek



Physical Properties of Silicon

- Band gap (indirect, \Rightarrow poor absorption): 1.1 eV
- Mobility (electrons, holes): 1900, 500 cm²/V-s
- Index of refraction: 3.49
- Boiling point: 2628 K (2355°C)
- Density of liquid at the melting temperature: 2.53 g/cm³
- Density of solid at the melting temperature: 2.29 g/cm³
- Latent heat of fusion: 12.1 kcal/mole
- Liquid/solid contact angle: 11° for (111)
- Melting temperature, T_m : 1685 K (1412°C)
- Molecular weight: 28.0855
- Solid/liquid surface tension: 720 dyn/cm
- Specific heat: 702 J/kg-K
- Spectral emissivity at 0.65 μm and 1685°C: 0.46
- Thermal conductivity of solid at T_m : 0.287 W/cm²°K
- Thermal expansion coef. (linear value): $4.7 \times 10^{-6}/^\circ\text{C}$

ISCGT-1, Switzerland, 1998

Lecture: Si Crystal Growth for PV

T. Ciszek



Silicon wafer preparation

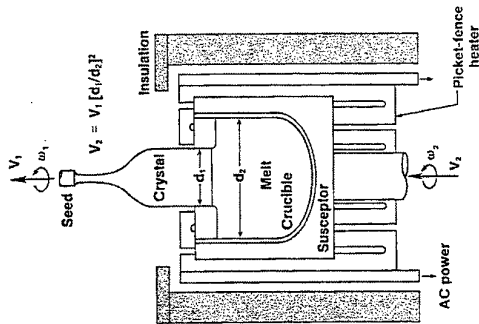
- Ribbons, sheets, and thin layers on substrates require no wafering, but scribing, dicing, or laser cutting may be used for sectioning.
- The large ingot growth methods require cropping, slabbing into blocks (typically done with a diamond band saw), and wafering.
- There are two main wafering approaches:

Method:	I.D. Saw	Wire Saw
Kerf loss (µm)	300-400	~200
Thickness (µm)	>300	>100
Damage depth (µm)	~30	~10
Maximum Yield (wafers/cm)	16	33
Throughput (wafers/hour)	20-30	Up to 500

ISCGT-1, Switzerland, 1998
Lecture: Si Crystal Growth for PV
T. Ciszek

Czochralski growth (CZ): J. Czochralski, Z. Physik. Chem. 92 (1918) 219.

- Standard semiconductor industry method for ~85% of Si growth
- Experimental details are given in a separate lecture.
- Relevant parameters for PV use
 - Si feed material can be remelt/ Pot-scrap Si or virgin poly Si.
 - Pulling speed: ~1-2 mm/min
 - Diameter: 125 - 200 mm for PV
 - Major Impurities: O, C
 - Minority charge carrier lifetime ~100 µs (varies with impurities)



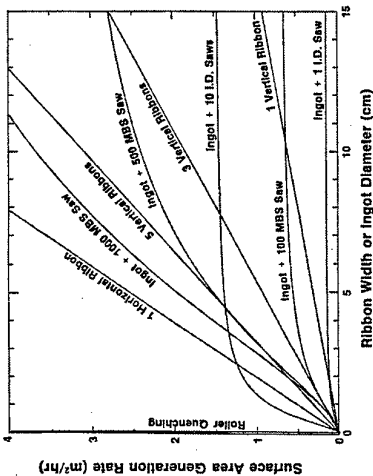
ISCGT-1, Switzerland, 1998
Lecture: Si Crystal Growth for PV
T. Ciszek

Crystallization from the melt – maximum growth rates

- Ingots: $(1/L\rho_m)(\sigma\varepsilon K_m T_m)^{5/12}[1/r]^{1/2}$
- Ribbons (\perp to melt surface): $(1/L\rho_m)(\sigma\varepsilon K_m T_m)^{5/12}[(W+t)/Wt]^{1/2}$,

T_m = melting temp., K_m = thermal conductivity at T_m , ρ_m = density at T_m , σ = Stefan-Boltzmann constant, ε = emissivity, r = ingot radius, W = ribbon width, and t = ribbon thickness.

- Actual growth rates are typically < 25% of above values.



ISCGT-1, Switzerland, 1998
Lecture: Si Crystal Growth for PV
T. Ciszek

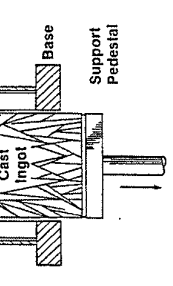
Experimental foundations

- Minimum energy for melting Si
 - Theoretical: 0.8 kWh/kg
 - Technically feasible (radiation/conduction losses): 3.0 kWh/kg
- Main methods of heating
 - Resistance heating: Heat generated in a graphite or other resistor (simple, efficient, but there are potential contamination problems)
 - Induction heating: Heat generated in the molten Si or a susceptor (very clean if direct, lower efficiency, strong stirring for > 1 kg)
 - Optical: Si is good absorber for UV. Sometimes used for thin Si.
- Crucibles
 - Quartz (for single-crystal CZ growth)
 - Quartz, Si₃N₄, cold crucibles, graphite, vitreous carbon, and SiC (for multicrystalline ingot solidification, sheet/ribbon growth, LPE)
- Other materials: graphite heaters, susceptors, preheaters, dies, meniscus support strings, and insulation; copper induction coils, quartz insulation, SS or quartz chambers, argon purge gas

ISCGT-1, Switzerland, 1998
Lecture: Si Crystal Growth for PV
T. Ciszek

Cold-crucible electromagnetic casting:

- Biot & Savart-law repulsion between currents induced in "fingers" and in melt
- A variety of feed silicon can be used (melts, rods, pellets, scrap, etc.).
- Interface is submerged, away from slag
- Various cross-section shapes are possible.

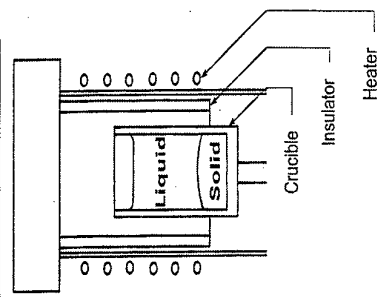


- Growth parameters:
 - Pull speed: ~1 - 3 mm/min
 - Size: 22 x 22 x 170 cm (192 kg)
 - Power consumption: ~30 kWh/kg
- Crystal characteristics:
 - Grain size: 1.5 mm avg
 - Diffusion length: 75 μ m avg
 - Impurities: O - $< 6 \times 10^{15}$;
 - Solar cell efficiency: Best - 16%; Typical - 85% of CZ.
 - C - $< 8 \times 10^{16}$ atoms/cm³

ISCGT-1, Switzerland, 1998
Lecture: Si Crystal Growth for PV
T. Ciszek
NREL

Directional solidification of Si block-shaped ingots

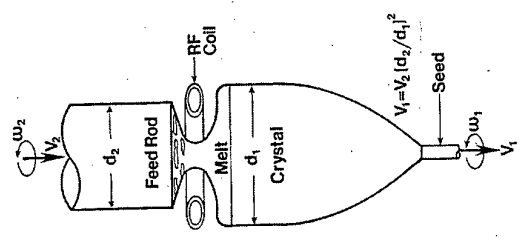
- Two main approaches:
 - Melt and solidify in the same container
 - simple process, no melt pouring
 - long reaction times at high temp.
 - long turn around times
 - Melt in one container/pour into another for controlled solidification
 - more complex process and equipment
 - melting & solidification are decoupled
 - higher throughput is possible
- Growth parameters
 - Growth rate: .1 - .6 mm/min
 - Energy use: 8-15 kWh/kg
 - Weight: <150 kg
 - Throughput: 3-15 kg/h
- Ingot characteristics
 - Grain size: mm to cm
 - Cell efficiency: 14 -16%
 - Diffusion length: <300 μ m
 - Impurities: C, O, N



ISCGT-1, Switzerland, 1998
Lecture: Si Crystal Growth for PV
T. Ciszek
NREL

Float-zone growth (FZ):

- Highest purity & lifetime (applications: power devices, IR detectors, high η PV)
- Experimental description
 - Si feed is crack-free CVD polyrods)
 - Water-cooled induction coil (~2-3 MHz)
 - "Cold" environment
 - Graphite "pre-heater"
 - No crucible
- Growth parameters
 - Pulling speed: 2-5 mm/min
 - Diameter: up to 150 mm
- Crystal characteristics
 - Uniform axial dopant distribution
 - Minority charge carrier lifetime, τ : 500-10,000 μ s (varies with microdefects)



ISCGT-1, Switzerland, 1998
Lecture: Si Crystal Growth for PV
T. Ciszek
NREL

A COMPARISON OF THE CZ AND FZ GROWTH METHODS

Characteristic	CZ	FZ
Growth Speed (mm/min)	1 to 2	3 to 5
Dislocation-Free?	yes	yes
Crucible?	yes	no
Consumable Material Cost	high	low
Heat-Up/Cool-Down Times	large	small
Axial Resistivity Uniformity	poor	good
Oxygen Content (atoms/cm ³)	$> 1 \times 10^{18}$	$< 1 \times 10^{16}$
Carbon Content (atoms/cm ³)	$> 1 \times 10^{17}$	$< 1 \times 10^{16}$
Metallic Impurity Content	high	low
Bulk Minority Charge Carrier Lifetime (μ s)	50-100	1,000-20,000
Mechanical Strengthening	10^{18} O	10^{16} N
Production Diameter (mm)	150-200	100-150
Degree of Sophistication	less	more
Polycrystalline Si Feed Form	any	crack-free rod
Typical No. of Pulls/Crystal	1	2

Summary comparison:

Method	Size, weight (mm, kg)	Growth rate (mm/min)	Throughput (cm ² /min)	Energy Use (kWh/kg)	Efficiency typ (best)%
Czochralski (single)	200, 75	0.8 - 1.6	700	60 - 80	<15 (20)
Float-zone (single)	150, 80	2 - 4	1800	30	<18 (23)
EM contin- ous casting	220, 190	2 - 4	3000	30	<13 (16)
Directional solidification	440, 125	0.1 - 0.6	1700	8 - 15	<15 (17)
Dendritic web (single)	75, --	1 - 2	10	—	<15 (17)
Edge- supported	100, --	2	20	—	<14 (15)
Capillary Die	800, --	2	200	—	<14 (16)
Substrate melt shaping	200, --	Fast	>1000	—	<12 (16)
Thin Layer on substrate	—	10 ⁻³ L	—	—	—

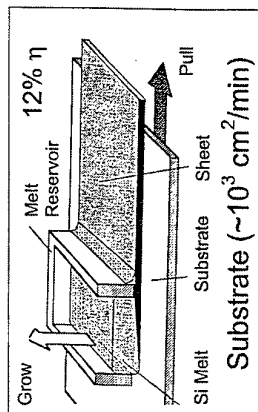
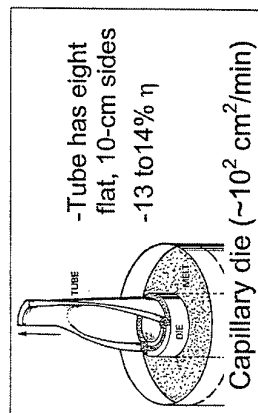
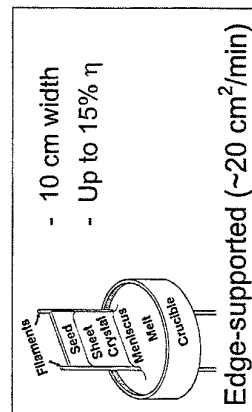
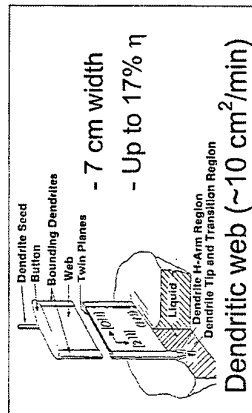
ISCGT-1, Switzerland, 1998

Lecture: Si Crystal Growth for PV

T. Ciszek
NREL

Ribbon/sheet growth from the melt

Of over a dozen methods, only ~4 are active today:



ISCGT-1, Switzerland, 1998

Lecture: Si Crystal Growth for PV

T. Ciszek
NREL

Crystalline Si thin-layer growth on substrates:

- ♦ Thin-layer Si growth on a substrate can utilize less material
 - 5-50-μm vs. 100-400-μm thickness for conventional PV cells
 - A 30-μm-thick Si layer absorbs 85% of the useable photons
- ♦ Thin cells have less stringent material quality requirements
 - Light generated carriers have a shorter path to the surfaces
 - Lifetime τ or diffusion length L can have lower value
- ♦ For very thin layers, light trapping structures may be necessary
- ♦ Several layer growth approaches may be promising (LPE, CVD)
- ♦ A common problem is a suitable substrate that is:
 - Low in cost
 - Useable at high temperature
 - Electrically conductive
 - Conductive to large-grains
 - Lattice matched to Si
 - Optically reflective
 - Thermal expansion matched to silicon
 - Non-contaminating
 - Available in large areas

ISCGT-1, Switzerland, 1998

Lecture: Si Crystal Growth for PV

T. Ciszek
NREL

Shaped Silicon Crystal Growth for Solar Cells

J. P. Kalejs

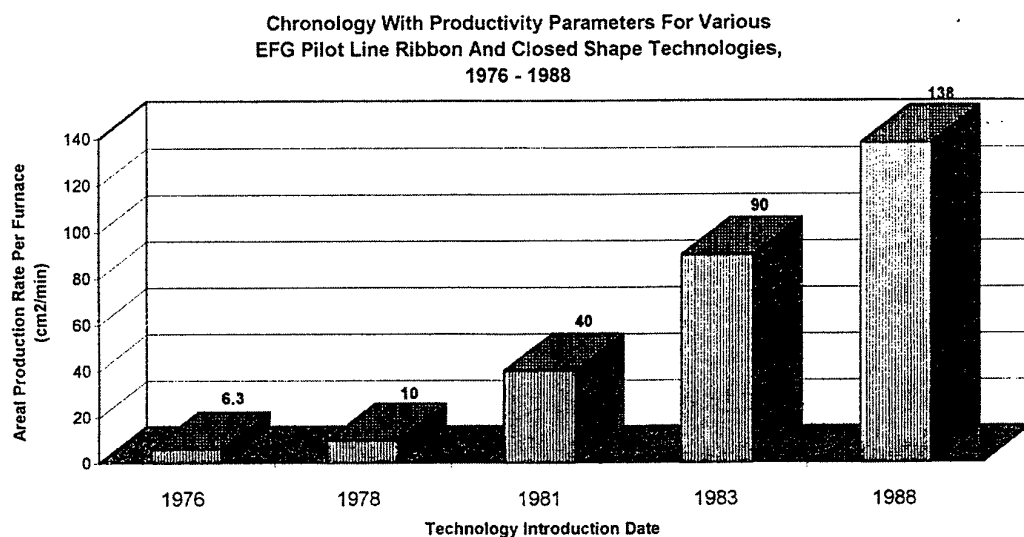
ASE Americas, 4 Suburban Park Drive, Billerica, MA, 01821, USA
tel: 978-667-5900, ext. 293; fax: 978-663-7555; email: jpkasepv@aol.com

Shaped growth of crystals from the melt has been practiced for over a half century. The Stepanov technique was first conceived in 1938 [1]. It utilized “dies” or “shapers” made from materials which were predominantly not wetted by the melt, e.g., quartz dies for silicon growth, to produce crystals of various semiconductor and dielectric crystals. The die constrains the crystallization front to a predetermined set of geometries and generally separates, and may isolate, the growth interface from the bulk melt. The genesis of the present Edge-defined Film-fed Growth (EFG) technique practiced for silicon wafers for solar cells, and the subject of this lecture, was the technique invented for sapphire in 1967 at Tyco Laboratories, which used dies made of a wetting material, molybdenum [2].

The growth characteristics and interface conditions are very different for wetting and non-wetting die materials. Out of the concept to work with dies wetted by the silicon melt came the first silicon “ribbon” or filament, in 1971, a few mm wide produced from a graphite die and designated the EFG technique. The main motivation for growth of silicon crystals in the form of sheet has been to dramatically lower the silicon feedstock utilization by avoiding the kerf loss which arises from wafering from conventional CZ and ingot crystals by sawing. The development of EFG technology culminated in 1994 with a full-fledged manufacturing line based on EFG wafer technology which can supply 3 million wafers to produce 4 MW of solar cells and modules annually. This manufacturing line is continuing to grow rapidly, with an expansion just being completed up to 11 MW, and plans to further expand to 20 MW beyond the year 2000. This rapid commercialization will then reach a production of 15 million 10 cm square EFG wafers consuming about 90 tons of silicon annually. This lecture will examine the fundamental principles behind the EFG silicon crystal technology being practiced for the photovoltaics industry, and present the elements of crystal growth required to achieve high volume manufacturing targets for crystal quality, uniformity and productivity. The three main areas covered will be on the theoretical principles of shaped growth, growth factors affecting EFG silicon material characteristics and how they impact on solar cells, and manufacturing system aspects and limitations on growth speed and process control.

Currently, the EFG technique is used to produce a silicon crystal in the form of a 5 meter long hollow octagonal tube, with each octagon face having a 10 cm width. The octagon is thus equivalent to 8 ribbons each 10 cm wide being grown simultaneously from a single crucible. The wall thickness of each tube is approximately 300 microns and the full length tube weighs 3 kg. It is grown with continuous melt replenishment over its full length at a growth speed of 1.73 cm/min. The octagons are cut into 10 cm x 10 cm or 10 cm x 15 cm wafers by high speed lasers.

The productivity gains for EFG technology are shown in the figure below. The main areas of crystal growth or research and development which have contributed in progress in understanding of the growth process and equipment over these years will be covered in the lecture, and are: 1) the push toward larger tube diameters in order to improve productivity per crystal growth station; 2) continued reduction of wall thickness to improve silicon utilization; 3) the presence of supersaturated carbon levels in the melt and in the crystal arising from the graphite crucible used to contain the melt; and 4) the development of a detailed understanding of the elements of process control to facilitate a high level of automation.



Wafer Parameter				
Width(cm)	2.5	5.0	5.0	10.0
Growth Rate (cm/min)	2.5	2.0	2.0	1.63
Number/Furnace	1	1	4	8
Thickness(um)	300	400	400	300
			(nonagon)	(octagon)

[1] A. V. Stepanov, Bulletin of the Academy of Sciences of the USSR, Physical Series, **33** (1969)1775.

[2] H. E. LaBelle and A. I. Mlavsky, Nature **216** (1967)5115.

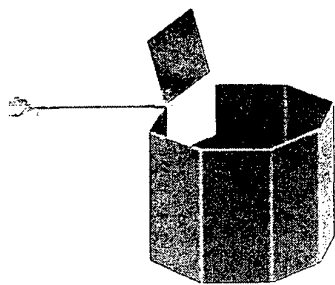
Shaped Silicon Crystal Growth for Solar Cells

J. P. Kalejs

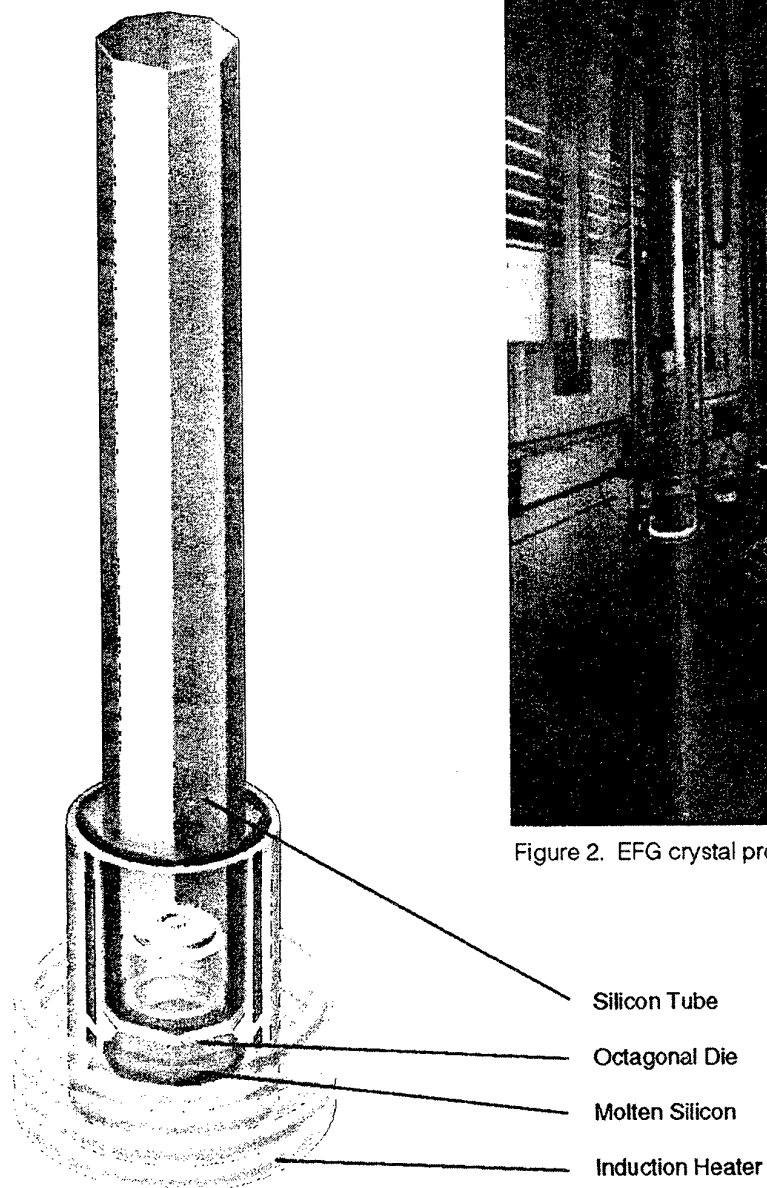
ASE Americas, 4 Suburban Park Drive, Billerica, MA, 01821, USA
tel: 978-667-5900, ext. 293; fax: 978-663-7555; email: jpkasepv@aol.com

First International School on Crystal Growth Technology
ISCGT-1

September 5-16, 1998
Beatenberg, Switzerland



b. Laser cuts wafers



a. Octagon crystal growth



Figure 2. EFG crystal production facility

Figure 1. Multicrystalline silicon wafers are produced by Edge-defined Film-fed Growth (EFG) of octagons and cut into wafers 10 cm x 10 cm, 300 microns thick with high-speed lasers.

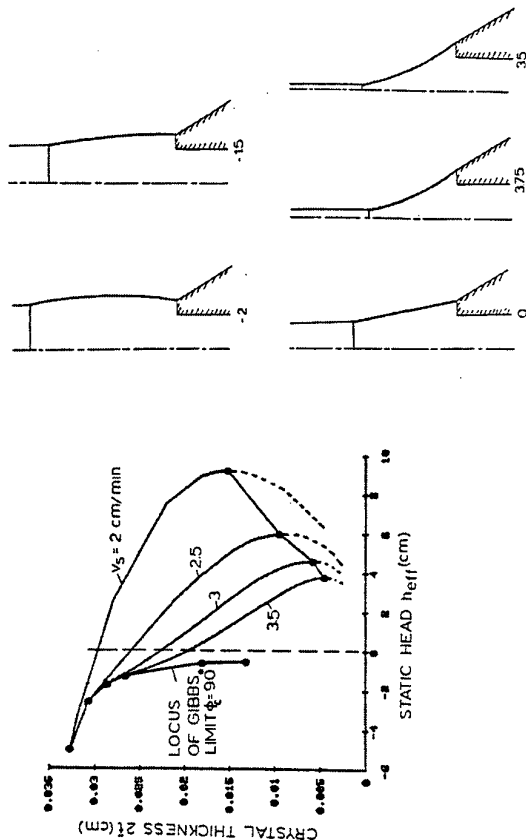
Process Limits - Heat Transfer

Thermocapillary Instability

- * Maximum stable growth rate reduced below radiation limit
- * Die tip-bulk melt distance (static head - h_{eff}), radiation boundary conditions provide additional restrictions

6/28/98ISCCT.DOC

Interaction between capillarity and heat transfer causes loss of stable solutions in equations beyond limiting values of static head (h_{eff}) and limits pulling (growth) speed (v_s)



- * Fundamentals of shaped growth and theory for EFG Si wafer manufacturing
- * Material properties and characteristics; bulk lifetime requirements for solar cells
- * Low cost EFG wafers: manufacturing with high productivity, yield and effective silicon utilization

6/28/98ISCCT.DOC

EFG Process Fundamentals, Control, and Growth Limits

Area	Physical concepts	Technology variable
Stability - operating variable diagrams - growth termination - growth initiation	Heat transfer/capillarity	Productivity (duty cycle)
Stress - buckling - residual stress - dislocations	Thermoelasticity/plasticity	Productivity (speed)
		Yield
		Solar cell efficiency
Impurities - carbon and oxygen - metallic impurities		Solar Cell Efficiency
	Crucible, ambient impurities Interface shape, segregation	

6/28/98ISCCT.DOC

EFG Crystalline Silicon Wafer Material Characteristics

Comparison of Growth Variables Affecting Material Properties to Those for CZ and Ingot Cast Silicon

Variable	CZ Silicon	Ingot Cast Silicon	EFG Silicon
Growth Speed V_s	0.1 cm/min	0.1-0.5 cm/min	2 cm/min
Interface Temp. Gradient G	200°C/cm	200°C/cm	1000°C/cm
Interface Cooling Rate ($V_s G$)	20°C/min	20-100°C/min	2000°C/min
V_s/G	5×10^{-4} cm ² /°C-min	5×10^{-4} - 2.5×10^{-3} cm ² /°C-min	1×10^{-3} cm ² /°C-min
Cooling time $\sim (V_s G)^{-1}$	500 mins	100-500 mins	5 mins
Substitutional Carbon C_s	$\leq 1 \times 10^{17}$ at/cc	$\sim 1.5 \times 10^{17}$ at/cc	$\sim 1 \times 10^{18}$ at/cc
Interstitial Oxygen O_i	$\sim 1 \times 10^{18}$ at/cc	$\sim 5 \times 10^{17}$ at/cc	$\leq 1 \times 10^{17}$ at/cc
C_s/O_i Ratio	≤ 0.1	0.1-1	≥ 10
Metallic Impurities k_{eff}	$< 10^{14}$ at/cc	10^{14} - 10^{16} at/cc	$\sim 10^{16}$ at/cc
	≤ 0.01	0.01-1	< 1

DEFECTS - WHAT CAN BE OBSERVED ?

EFG CRYSTALLINE SILICON

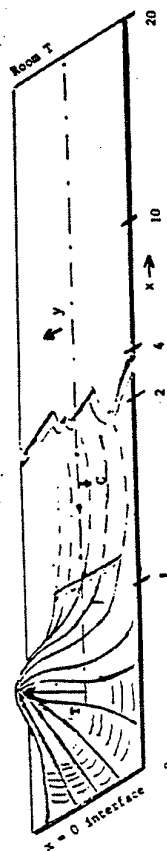
- * HIGH INTERFACE COOLING RATES (1000 C/CM)
 - DISLOCATIONS (UP TO $10^9/\text{CM}^2$)
 - FEW GRAIN BOUNDARIES
 - COHERENT TWINS, TWIN BUNDLES
 - TRANSITION METALS
- * GROWN FROM CARBON CRUCIBLES WITH $C \sim 10^{19}/\text{CM}^3$
 - NO SiC OR SiO₂ PRECIPITATES
- * ADDITIONAL INHOMOGENEITIES/VARIABLES
 - ASYMMETRIC AMBIENT EXPOSURE TO CARBON MONOXIDE ON SHEET (WAVER) SURFACES DURING GROWTH
 - LOW OXYGEN LEVELS ($3\text{-}6 \times 10^{16}/\text{CM}^3$)

Process Limits - Thermoelastic Stress and Plasticity

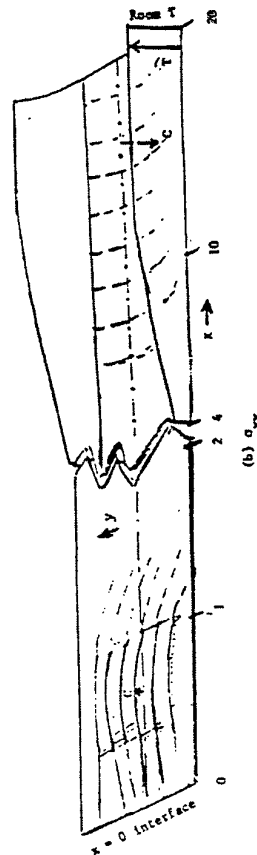
- * Linerization of cooling profile most important in thermoelastic model
- * Plasticity (creep) fixes limit to pulling (growth) speed well below radiation limit in practice
- * Low stress system design variables:
 - residual stress/dislocations
 - horizontal gradients
 - buckling (nonflatness) product tolerances

62899MSCCT.DOC

Stress components in sheet with tensile stress (T) shown upward, compressive (C) downward.



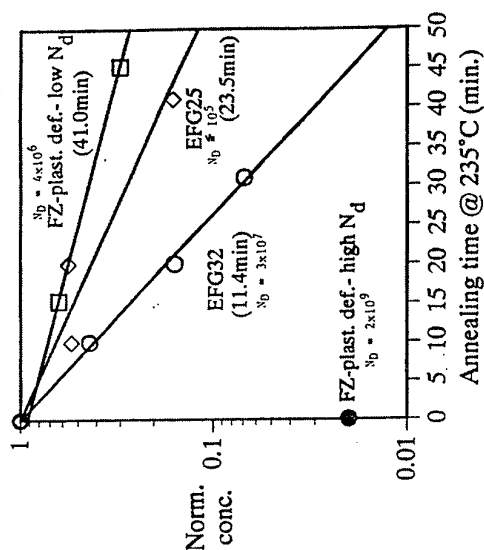
(a) σ_{yy}



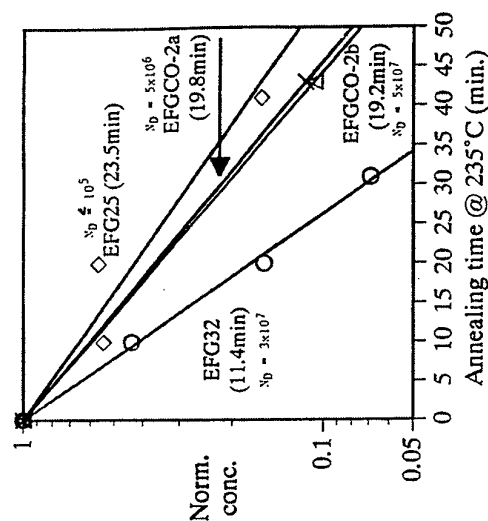
(b) σ_{xx}

FE PRECIPITATION STUDIES IN EFG CRYSTALS
(E. WEBER ET AL: UC-BERKELEY)

LOW DISLOCATION EFG HAS FE PRECIPITATION RATES GREATER THAN
COMPARABLE DISLOCATION DENSITY FZ SILICON



OXYGEN ADDITION VIA CARBON MONOXIDE AMBIENT OPERATES ON FE
PRECIPITATION SITES AND DECREASES THEIR PRECIPITATION RATE



EFG TECHNOLOGY MILESTONES: 1976-1996

SOLAR CELL EFFICIENCY

DATE	TECHNOLOGY	CELL EFFICIENCY	QUALITY LIMITATION	TECHNOLOGY ADVANCE
1976	2.5 CM RIBBON	8%	METALLIC IMPURITIES DISLOCATIONS	
1978	5 CM RIBBON	10%	DISLOCATIONS SiC	GRAPHITE PURIFICATION; OXYGEN
1983	NONAGON	11%	DISLOCATIONS SiC	NONAGON REDUCED SiC
1992	OCTAGON	12.5%	METALLIC IMPURITIES	HYDROGEN PASSIVATION; SHORT DIE
1996	OCTAGON	14%	METALLIC IMPURITIES CELL DESIGN	GRAPHITE PURIFICATION; BSF; FINGER SHADOWING

Manufacturing Issues Scale EFG Crystalline Silicon Wafer Production at ASE Americas

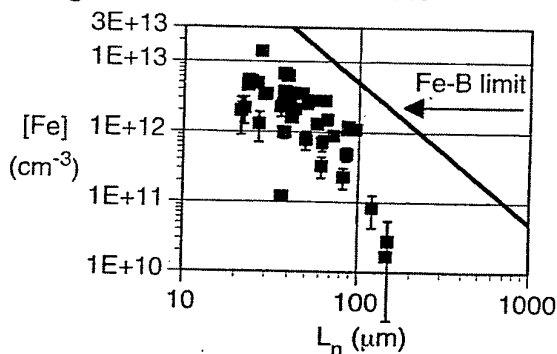
* Currently at 3 million 10 cm square wafers annual capacity;
installing equipment for 8 million by YE 1998; plan to go to
13 million wafers capacity by the year 2000

* Productivity/cost element parameters under development:

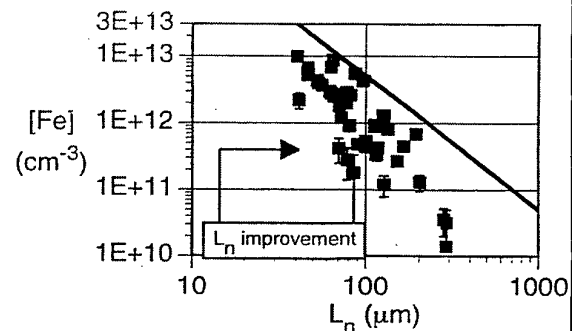
- diameter \uparrow (30 cm \rightarrow 100 cm)
- run length \uparrow (> 50 tubes from one crucible)
- thickness \downarrow (300 μm \rightarrow 100 μm)
- cell efficiency \uparrow (14% \rightarrow $>15\%$)
- yield (flatness, laser cutting)

6/28/98ISCGT.DOC

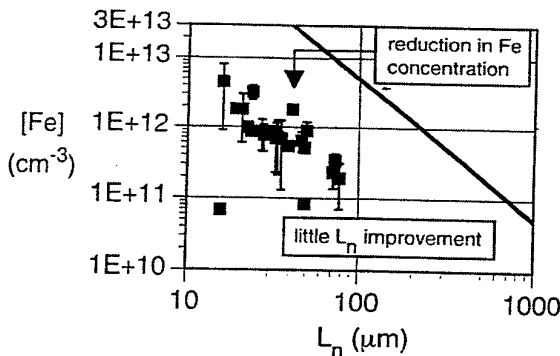
Fe concentrations in: As-grown EFG silicon...



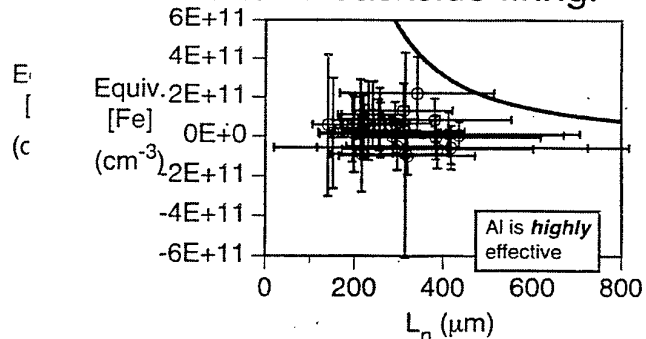
EFG after P-diffusion and H passivation...



EFG silicon after P-diffusion...



EFG after P-diffusion, H-pass., and Al backside firing.



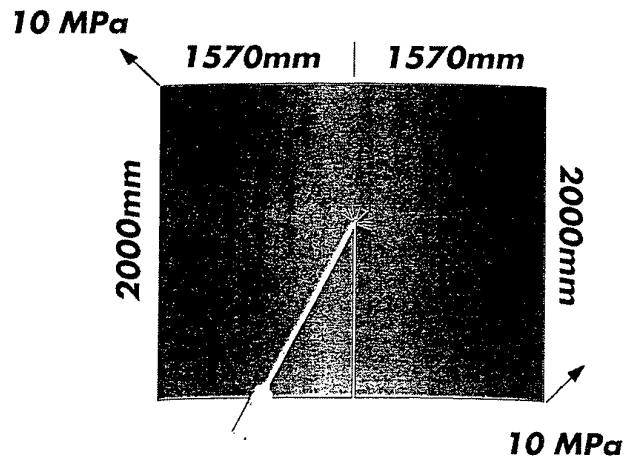
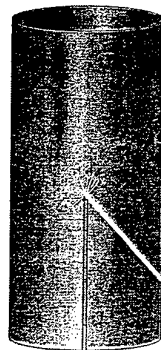
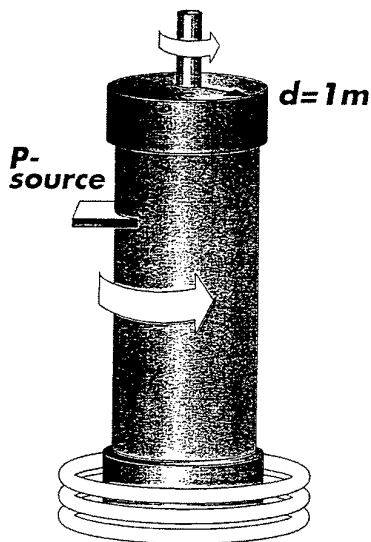
EFG 21st Century Manufacturing Technology

100 μm Thick Cylinder

1. Growth
 $\geq 60\text{rpm}$ rotation
in situ P-doping

2. Laser Cutting
Low damage cut to
"unzip" cylinder

3. Wafers
75 micron thickness
2 per cylinder
One 5'x6.5' wafer/module
10MPa bending stress



A-S-E

Americas, Inc.

EFG Crystalline Silicon Wafer Manufacturing Technology

Process Control Variables

- * Graphite die design and purification
- * Ambient Control
- * Octagon tube wall thickness (weight control)
- * Melt Replenishment
- * Temperature uniformity and stability

Evaluation of bulk GaAs melt growth processes: Links between crystal growth research and crystal production

*H. Wenzl, A. Fattah, E. Kuessel, W.A. Oates, K. Sonnenberg
Institut für Festkörperforschung, Research Centre Juelich, Germany*

Hot-wall Czochralski methods were developed and extensively used by the GaAs pioneers (Welker and Gremmelmaier, Siemens Research Labs, Erlangen) for growing relatively small crystals with low dislocation densities. They allowed active melt stoichiometry control via gas pressure adjustment and low-pressure synthesis. Alternatively, hot-wall horizontal Bridgman methods have been used although mostly restricted to atmospheric pressure due to the use of externally heated quartz tubes as containers. Stoichiometric melts require about 1.8 bar pressure at the congruent point. Kapiza has invented this method for materials which are expanding during crystallisation from the melt due to a fundamental misunderstanding of the atomistics of the triple phase boundary interaction with crucible walls during crystallisation.

Today, these hot-wall methods have essentially been replaced by the much simpler cold-wall liquid encapsulation techniques, especially by the LE-Czochralski method, which dominates the semi-insulating GaAs crystal production and has reached 15 cm crystal diameter. Since it operates close to the congruent point of the liquid-solid co-existence region macrosegregation can be neglected. The main disadvantage of the LEC method is the necessity of large temperature gradients of more than 100 K/cm across the relatively shallow encapsulant to prevent excessive As-loss of crystal regions emerging from the encapsulation. This generates large dislocation densities.

With increasing crystal diameters and volumes there is a feeling now that improved methods with smaller T-gradients are necessary to reduce dislocation densities to optimized levels (extremely small dislocation densities are probably not practical for reaching homogeneous high quality crystals).

The obvious route for improvement, namely the increase of encapsulant thickness up to full encapsulation which would allow a reduction of the temperature gradient, is not being pursued. Instead, there is a trend to revive the hot-wall, As-pressure crystal protection techniques in combination with shallow liquid encapsulation to be able to reduce the temperature gradient across the encapsulation from more than 100 to less than 20 K/cm in combination with the control of the crystal dissociation rate.

This complex and expensive Vapour-pressure controlled Czochralski method is now under fierce competition with the simple, bottom-seeded, efficient and economical Tammann/Vertical Gradient Freeze/Bridgman methods with full encapsulation of the melt. It seems to be a much better alternative for pursuing the aim of dislocation reduction combined with crystal diameter increase above 15 cm.

Thermodynamics reveals the degrees of freedom of the system which is the basis of a rational evaluation and control of the competing crystal growth processes. The parameters to be controlled are: stoichiometry, foreign atoms and dopants content of the melt and the various sublattices of the crystal, cluster formation and precipitation of other phases. Rather complex thermodynamic problems can be

modelled by using the user-friendly computer package ChemSage from GTT, Herzogenrath.

In addition, dislocation and subgrain boundary formation, twinning and various other crystal microstructures have to be handled.

Thermodynamic and kinetic modelling is hampered by uncertainties, complications and discrepancies:

A large number of chemical components have to be taken into account such as Ga, As, B, O, N, H, C, other dopants and foreign atoms, and various mixture phases.

In spite of enormous research efforts the temperature and time dependent defect household of GaAs crystals is controversial. Different schools postulate, for example, stoichiometry ranges from a few ppm to more than 0.1 % deviations from the 1:1 ratio.

The coexistence conditions of the different phases are not known exactly. The total As-pressure at the congruent point is quoted with values between 0.7 and 2 bar, the stoichiometry deviation at this point with a few ppm up to 0.1 %. In view of these uncertainties stoichiometry control by weighing-in sufficient amounts of Ga and As is much more reliable than stoichiometry adjustment via As-pressure in hot-wall systems.

Defect physics of GaAs is quite deficient. Theoretical values of defect formation energies lead to extremely small concentrations even at the congruent temperature which is in disagreement with the schools believing in tenths of percent values for defect concentrations. Temperature dependent values of the standard Gibbs energies of defects and their charge levels in the energy gap are not available.

Oxidic components of the system such as C-containing species are able to migrate through the boric oxide encapsulant. Reliable permeation rates are not available.

The non-isothermal nature of the growth systems, the change of boundary conditions during crystal cooling after growth or annealing runs and the finite reaction rates (freeze-in temperatures) have only rarely taken into account properly.

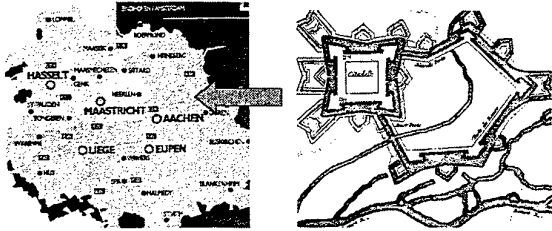
These topics are discussed on the basis of prototype hot-wall and LE-Tammann crystal growth experiments, ChemSage computer analysis of thermodynamic properties and defect studies.

Selected References

- H. Wenzl und W.A. Oates, Verfahren zur aktiven Defektsteuerung bei der Züchtung von GaAs-Kristallen, Offenlegungsschrift DE 196 38 583 A1 vom 2.4.1998; J. Crystal Growth, in print 1998
- W.A. Oates and H. Wenzl, *Calphad* 19(1995)143-152
- H. Wenzl, W.A. Oates, K. Mika, Defect Thermodynamics and Phase Diagrams in Compound Crystal Growth Processes, in: *Handbook of Crystal Growth*, D.T.J. Hurle, ed., Elsevier, Amsterdam, 1993
- W.A. Oates and H. Wenzl, *Calphad* 16(1992)73
- H. Wenzl, A. Dahlen, A. Fattah, S. Petersen, K. Mika, D. Henkel, *J. Cryst. Growth* 109(1991)191
- F. Sajovec, R. Wolf, A. Fattah, K. Bickmann, H. Wenzl, G. Nagel, H. Ruefer, E. Tomzig, P. De Bievre, *phys. stat. sol. (a)* 122(1990)139
- H. Wenzl, A. Dahlen, A. Fattah, K. Mika, D. Henkel, *Semi-insulating III-V Materials*, Toronto 1990, A.G. Milnes and C.J. Miner, eds., Adam Hilger, Bristol, 1990, p. 237
- ChemSage, GTT Herzogenrath, <http://gttserv.lth.RWTH-Aachen.de>

Evaluation of bulk GaAs melt growth processes: Links between crystal growth research and crystal production

H. Wenzl, A. Fattah, E. Küssel, W.A. Oates, K. Sonnenberg
Institut für Festkörperforschung
Research Centre Jülich, Germany



From Liquid-Encapsulated Czochralski (LEC) „back“
to Gremmelmaier's HWC (1955)?

HWC + Boric Oxide = „VCz“ (LE-HWC)
or

From LEC „back“ to Tammann (1903)?

Tammann + Boric Oxide = LE-VGF (LET)

Contributions of the German Ministry of Education and Research
are gratefully acknowledged

ISCGT Beatenberg, 5. - 16. Sept. 1998

22.06.98

1

Survey

- Phase diagrams: graphical representations of thermodynamic equilibrium and driving forces
- l - s - g crystal growth parameters
- Hot-Wall GaAs crystal growth processes
- Dislocations, polygrowth and Ga droplet formation
- Defects and stoichiometry (analysis/range/control)
- Is there an optimum stoichiometry?
- Thermodynamic modelling: control of the degrees of freedom of crystal growth systems
- Problems in non-isothermal environments of real growth systems (melt stoichiometry control in As-pressure controlled open Hot-Wall systems)
- Active chemistry control of crystal growth
- Reaction equilibrium and kinetics

22.06.98

2

Criteria for evaluation of industrial GaAs crystal growth processes

Control of

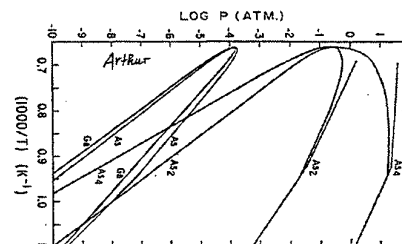
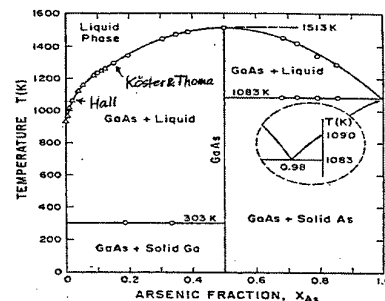
- native defects: As_{Ga} V_{Ga} As_i
- foreign atoms: C_{As} $Si_{Ga/As}$
- dislocations: $10^3 < cm/cm^3 < 10^5$
- microstructure:
defects, def.-agglomerates, As-precipitates,
inhomogeneities (defect diffusion zones
around dislocations)
- mechanical properties (dislocation
distribution \Rightarrow strain)
- time-temperature history, annealing
- polygrowth, twinning
- single crystal & wafer yield
- expenditure

22.06.98

3

Ga-As phase diagrams

As-equil. pressure at congruent operating point of
bulk crystal growth: 1..2 bar!

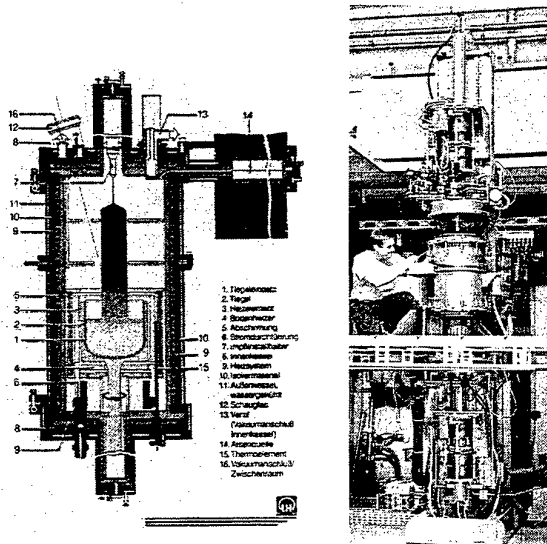


22.06.98

4

Hot-Wall GaAs Czochralski puller

- magnetic levitation seed and crucible holders
- As-source
- active control of s-l-g equil. possible
- rather complex

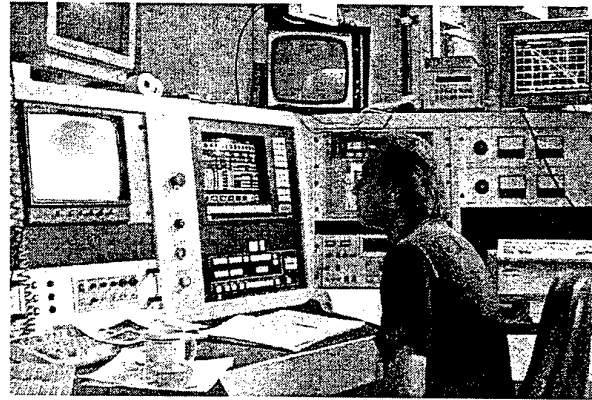


22.06.98

5

Operating the Hot-Wall-Czochralski system

TV camera Crystal and crucible weight monitor



System parameters:
power temperature pressure etc

22.06.98

6

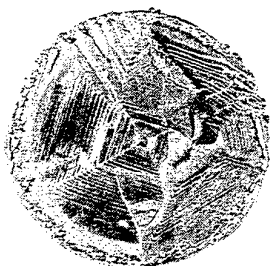
Unencapsulated liquid

surface contamination can interfere with growth process at triple phase boundary

4 mm seed crystal
edge length



<100> crystal 90mm diameter

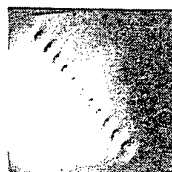


22.06.98

7

From dislocation
multiplication to
subgrain formation.
Twinning at facets

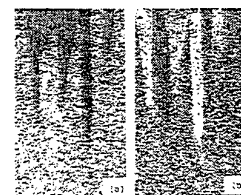
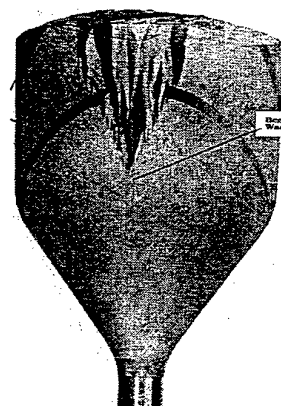
DISLOCATION DENSITY	PROCESS
10^4	COALESCENCE OF SUBBOUNDARIES POLYGRANIZATION (2 STAGE)
10^5	FORMATION OF SUBBOUNDARIES POLYGRANIZATION (1 STAGE)
10^6	
10^7	



Dislocations forming
small angle grain
boundary. IR LM
birefringence contrast

22.06.98

LEVGF 5 cm diam



2° tilt boundaries

8

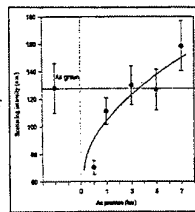
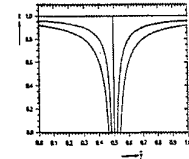
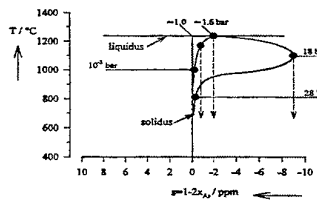
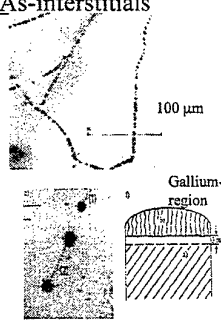
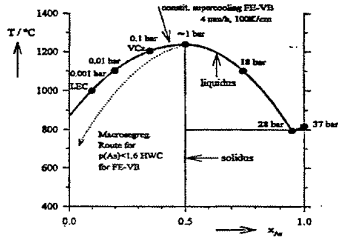
Result of extensive crystal growth research:

Phase range of GaAs-crystals: extremely small

Congruent point: at ppm As surplus

No Ga-rich solid: As-precipitates also in crystals from Ga-rich liquid (macrosegregation!)

Bulk annealing shows: there are mobile As-interstitials



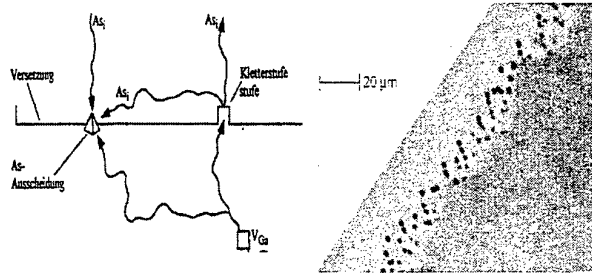
M.Noack, K.W.Kehr, H.Wenzl
JCG 178(1997)438-444

As-precipitate count
in the same sample after
As-pressure annealing

22.06.98

Petroff-Kimerling mechanism during slow cooling to 900°C:

dislocation-defect-precipitate interaction and dislocation climb



Excessive dislocation climb: at
1000 cm disloc. line
length/cm³ only 10¹² disloc.
core sites/ cm³ but more than
10¹⁶ defects/cm³:

Many μm climb distance

22.06.98

10

„Stoichiometry“ information:

density, lattice parameter, titration, precipitates

$$m_{\text{ideal}}^{\text{cell}} = 4(m_{\text{Ga}} + m_{\text{As}})$$

$$m_{\text{cell}} = \rho \cdot a^3$$

m_{Ga} : from titration

m_{As} : from mass balance (?)

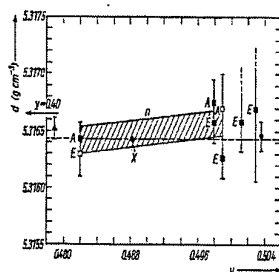
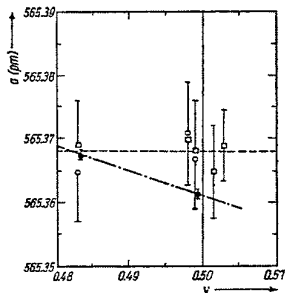
$$s = (N_{\text{Ga}} - N_{\text{As}}) / (N_{\text{Ga}} + N_{\text{As}})$$

α : Ga As V B ..

β : As Ga V C ..

i: V As

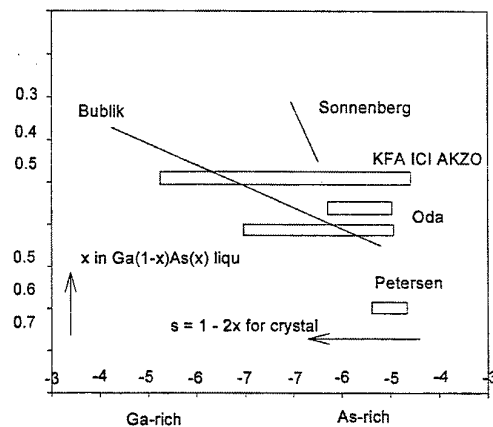
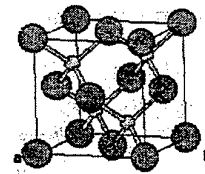
As-precip, voids



22.06.98

11

Melt composition influence on crystal stoichiometry



22.06.98

12

Bragg-Williams-Approximation for

- non-ideal liquid mixture
- Species on GaAs-sublattices

$$\begin{aligned}\mu_{\text{Ga}}^{\text{As}} &= \mu_{\text{Ga}}^{\text{As}} - 4/2 W_{\text{GaAs}} \\ &+ RT \ln [\text{As}_{\text{Ga}}^{\text{As}}]; \\ \mu_{\text{As}}^{\text{As}} &= \mu_{\text{As}}^{\text{As}} + 4/2 W_{\text{GaAs}} + \\ &RT \ln [\text{As}_{\text{As}}^{\text{As}}]; \text{ etc} \\ \mu_{\text{e}^-}^{\text{e}} &= E_{\text{g}}/2 - RT \ln [N_{\text{c}}] \\ \mu_{\text{h}^+}^{\text{h}} &= E_{\text{g}}/2 - RT \ln [N_{\text{v}}]\end{aligned}$$

$$\begin{aligned}\Delta G(l) &= y(1-y)\{L_0 + L_1(1-y)\} \\ &+ RT\{y \ln y + (1-y) \ln(1-y)\} \\ \text{Quasi-chem reactions, e.g.} \\ \text{Aa+Bb} &= \text{Abo} + \text{Bao} \\ \text{MAL with species chem pot} \\ \text{As}_{\text{Ga}}^{\text{As}} &= \text{As}_{\text{Ga}}^+ + \text{e}^- \\ \mu_{\text{As}}^{\text{As}} &= \mu_{\text{As}}^{\text{As}} - E^{+/0}\end{aligned}$$

Standard values of the chemical potentials & excess

parameters of the non-ideal liquid mixture

Energies: high-temperature approx in meV

Ga(l) und As(c) as reference for atomic species

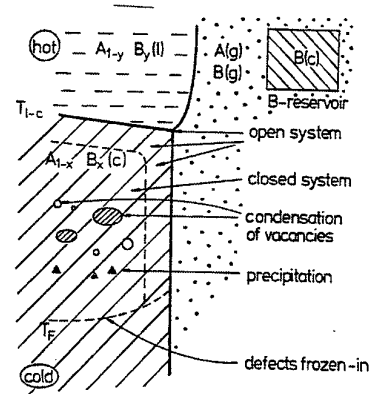
Midgap energy reference for e und h

$\mu_{\text{Ga}}^{\text{Ga}}$	881	$\mu_{\text{e}^-}^{\text{e}}$	927 + 0,383T
$\mu_{\text{As}}^{\text{As}}$	1817	$\mu_{\text{h}^+}^{\text{h}}$	927 + 0,114T
$\mu_{\text{As}}^{\text{Ga}}$	1817	$\mu_{\text{As}}^{\text{Ga}} + W_{\text{GaGa}}$	1854
$\mu_{\text{Ga}}^{\text{As}}$	881	$\mu_{\text{Ga}}^{\text{As}} + W_{\text{AsAs}}$	431 + 0,176T
W_{GaAs}	-917 + 0,088T	Bragg-Williams	Pair-Int En.
$\mu_{\text{As}}^{\text{As(l)}}$	247 - 0,226T	liquid As	
$L_0(l)$	264 - 0,046T	RKMP Param.	non-ideal
$L_1(l)$	53,63	RKMP Param.	asymmetrie

22.06.98

13

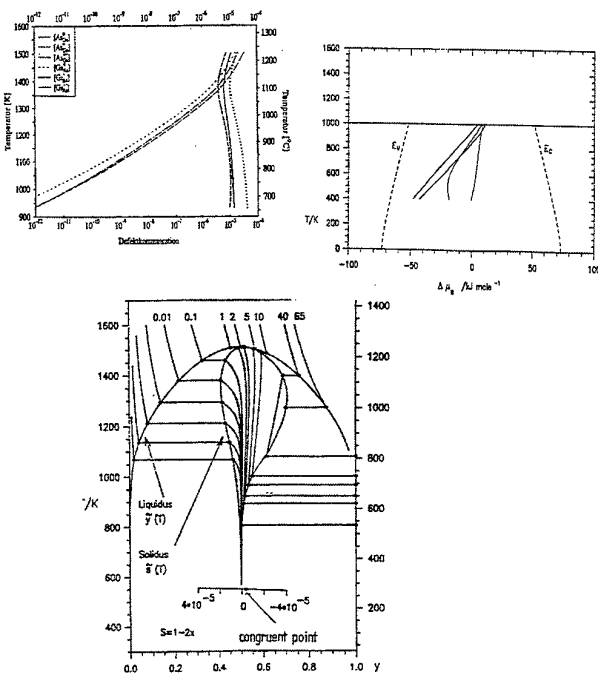
Survey of crystal growth model with open, closed and frozen-in boundary conditions



22.06.98

14

Thermodynamic defect modelling results



22.06.98

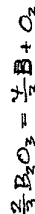
15

Thermodynamic modelling of GaAs melt chemistry

Melt chemistry (1513K)

Solutes

$$C(\text{graphite}) = 0$$



activity coefficients

Crude estimates

$$a_i = \gamma_i x_i$$

segregation coefficient

$$C_s \approx 2$$

$$b \approx 1$$

$$c \approx 0.4$$

Dynamical System Control

Sublative species defect levels etc.
- semi-insulating
- semi-conducting
- regimine

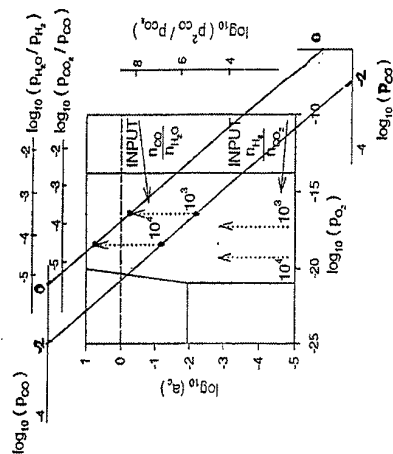
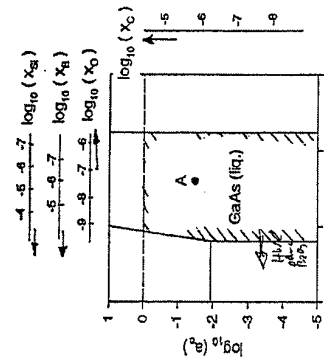


Fig. 3

22.06.98

17

Solidus-Models Hurle (Landolt-Börnstein) Oates and Wenzl (CALPHAD 95)

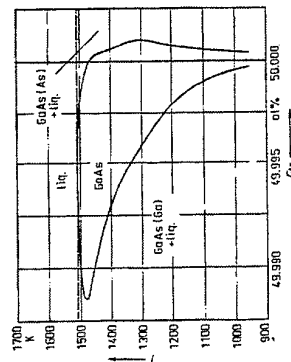


Fig. 23. GaAs. Calculated solidus curve of GaAs [71]. Temperature T vs. c_{As} (As percentage). The area inside the curve is the existence region of GaAs (compare Fig. 22).

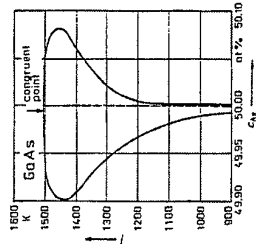
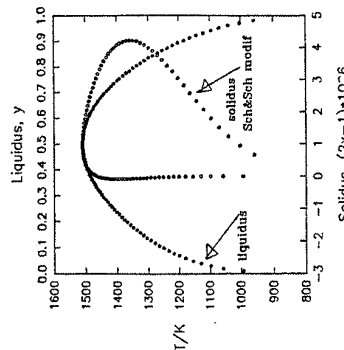
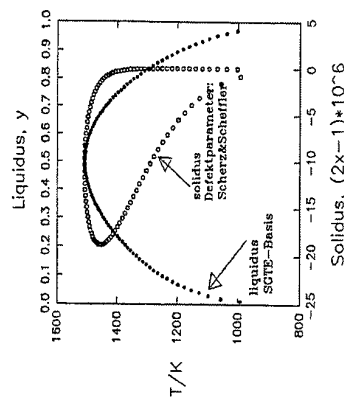


Fig. 22. GaAs. Calculated solidus curve [71]. Temperature T vs. c_{As} (As concentration). The area inside the curve is the existence region of solid GaAs. The congruent melting point of GaAs is 1511 K. The maximum deviation from composition at 1511 K. The maximum deviations from congruency are approximately an order of magnitude greater than those given in Fig. 23 which is discussed in [7011].



W.A.Oates, G.Eriksson, H.Wenzl, J of Alloys and Compounds 220(1995)48-52
W.A.Oates and H.Wenzl, Calphad 19(1995)143-152

22.06.98

16

Future of GaAs melt growth processes

Present: Standard 4" si

Liquid-encapsulation:

Czochralski (LEC, fully LEC)

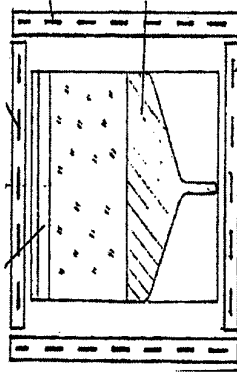
Old and under revival consideration

Hot-Wall:

HW-Czochr (Gremmelmaier)
VCz (LE-HW hybrid)
Horizontal Bridgman (Kapitza..)

Future: LET process

Tammann: 6" LE-Vertical-Gradient-Freeze



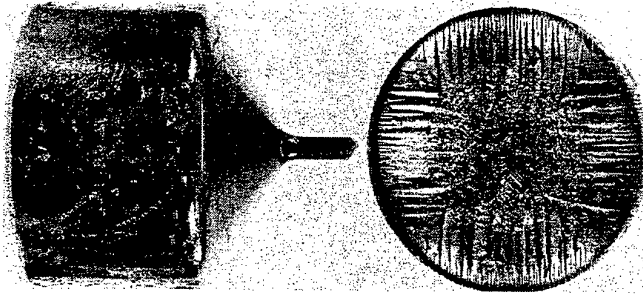
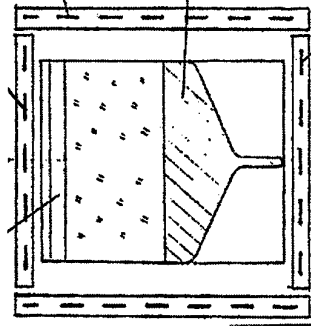
22.06.98

19

LE-Tammann (LET or „VGF“) system

capable of controlling the basic requirements:
geometry quality cost

Schematic cross section
through LET furnace



120 mm LET crystal

Sonnenberg and Küssel
in Jülich with 150 mm
crystal

22.06.98

18

Growth of Low EPD-GaAs by the Vertical Gradient Freeze Method

Georg Müller

Crystal Laboratory, Dpt. Materials Science

University Erlangen-Nürnberg (Germany)

Abstract

GaAs substrate crystals with low dislocation density ($\text{EPD} < 500 \text{ cm}^{-2}$) and Si-doping are required for the epitaxial production of high power diode lasers because dislocations have a deleterious influence on the life-time and performance of laser diodes (LDs) and high brightness light emitting diodes (LEDs). Large size wafers ($\geq 3''$) are needed for reducing the manufacturing costs. These requirements can be fulfilled by the Vertical Bridgman (VB) and Vertical Gradient Freeze (VGF) techniques.

In our laboratory we have developed a newly designed multizone VGF furnace. The thermal growth conditions were optimized by the aid of numerical process modelling. The simulations of the VGF process were carried out by using a new computer code called CrysVUN++, which was recently developed in our crystal laboratory in Erlangen [1,2]. The numerical model of the growth process is based on a so-called "global heat transfer model", which means that the calculations include all details of the growth configuration like crystal, melt, crucible, heaters, insulation and the water cooled steel vessel. Thermal radiation and conduction are considered in this work as the dominating heat transfer mechanisms in the VGF process, whereas the contribution of convection in the GaAs melt and in the gas atmosphere are neglected. Former investigations at our laboratory have shown that these two mechanisms play a minor role in the VGF configuration with bottom seeding [3, 4]. The numerical calculations were performed for different time steps of the growth process on a conventional 200 MHz Pentium Personal Computer. Convergence of a calculation is reached after approximately 2 h of CPU time. Since thermal stress in the crystal is caused by non-linearities of the axial temperature gradient, a constant axial temperature gradient should result in very low thermal stress conditions. From

our experience with the 2" VGF growth of GaAs [4], we decided to use a constant axial temperature gradient of 7 K/cm in the growing crystal and 2K/cm in the melt to keep the overheating of the GaAs melt as small as possible. By the aid of the computer modelling we have calculated the temperatures at the heaters which were then used in the growth experiments.

The 3" GaAs crystals were grown in pBN crucibles having a small diameter seed and a conical part (for more details see Amon et al. [5]). Boric oxide was used for a fully encapsulation of the crystal and the melt. An initial silicon content in the GaAs melt of $c(\text{Si}_{\text{melt}}) = 3 \cdot 10^{19} \text{ cm}^{-3}$ is used in order to achieve a carrier concentration of $n = (0.8 - 2) \cdot 10^{18} \text{ cm}^{-3}$ which is the specification of the laser diode device manufacturers. One special growth experiment was carried out by rotating the crucible (1 rpm) for approximately 10 minutes at different time steps of the growth run. By means of the rotation we intentionally induced striations in the growing crystal. These interface demarcations enabled us to carry out a quantitative comparison between the numerical results and the experiments [5].

In order to demonstrate the usefulness and importance of the numerical process modelling we compare the results before and after the optimization of the thermal boundary conditions by the aid of computer simulation. The EPD could be reduced to values between 500 cm^{-2} and 280 cm^{-2} with a Si-doping level of $8 \cdot 10^{17}$ to $1 \cdot 10^{18} \text{ cm}^{-3}$. The 3" wafers have rather large dislocation-free areas. The lowest EPD's ($< 100 \text{ cm}^{-2}$) are achieved for long seed wells of the crucible. The remaining dislocations are classified according to their Burgers vectors. It seems that these dislocations are not induced by thermal stress but by other mechanisms [6].

A quantitative test of the accuracy of the numerical simulations concerning the positions and shapes of the solid/liquid (s/l) interface is made by evaluating the striations which were induced by rotating the crucible at 9 different time steps during growth. Near infrared transmission topographs of longitudinally cut (110)-oriented wafers of this crystal show that the bending of the striations corresponds very well to the calculated shapes of the s/l interfaces at corresponding axial positions. A nearly flat interface in the crystal center and a slightly concave one at the rim were obtained. This bending is caused by the highly anisotropic thermal conductivity of the pBN crucible. A constant (!) growth rate of 1.8 mm/h is achieved in the experiment, which is a little smaller than the calculated one (2.5 mm/h) [5].

The influence of the shape of the crucible is investigated by using four different angles ϕ (60° , 90° , 120° , 144°) of the conical part of the pBN crucible [7]. We find a decrease of the length of the $\{111\}$ edge facets in the conical region with increasing cone angle. The $\{111\}$ As facets are always larger and show a higher tendency to twinning compared to $\{111\}$ Ga facets. The model of Hurle [8] which correlates the formation of twins with the growth of facets at the three phase boundary (TPB) is confirmed. The maximum angle between the edge facet and the

extension of the crystal surface at which the facet should detach from the TPB is found experimentally to be between 95.3° and 107.3° which corresponds well with the value of 104° calculated by Hurle for encapsulated GaAs.

References

- [1] M. Kurz, A. Pusztai and G. Müller ICCG 12 (accepted)
- [2] M. Kurz and A. Pusztai, Int. J. Numerical Methods for Heat and Fluid Flow 8 (1998) 304 - 320
- [3] J. Amon, D. Zemke, B. Hoffmann and G. Müller, J. Crystal Growth **166** (1996) 646.
- [4] H. Weimann, J. Amon, T. Jung and G. Müller, J. Crystal Growth **180** (1997) 560.
- [5] J. Amon, P. Berwian and G. Müller, ICCG 12 (accepted)
- [6] J. Amon, J. Härtwig, W. Ludwig and G. Müller ICCG 12 (accepted)
- [7] J. Amon, F. Dumke and G. Müller, J. Crystal Growth 187 (1998) 1 - 8
- [8] D.T.J. Hurle, (J. CrystalGrowth 147 (1995) 239)

Author's address:

Prof. Dr. G. Müller
Institut für Werkstoffwissenschaften WW6
Universität Erlangen-Nürnberg
Martensstr. 7

D - 91058 Erlangen
Germany

Tel.: ++49-91 31-85 76 36
Fax.: ++49-91 31-85 84 95
e-mail: georg.mueller@ww.uni-erlangen.de

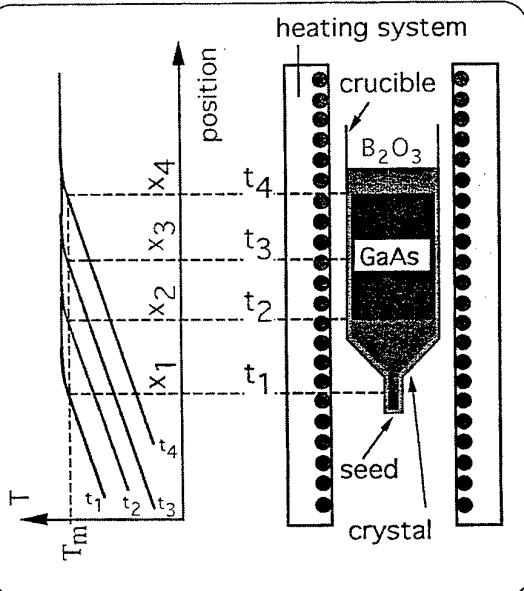
Variant	axis	movement	crucible	B ₂ O ₃ encapsulant	Silicia ampoule	As, P source	heating system	growth direction	remarks
HB	hor	furnace	SiO ₂	no	yes	yes	tube furnace	111	Si-contamination no undoped s.i. GaAs possible
HGF	hor	no	SiO ₂	no	yes	yes	tube furnace	111	
VGF	vert	no	pBN pBN	yes no (1)	yes yes	no yes	tube furnace	100 100	1 = is possible but with low yield
	vert	no	pBN SiO ₂ (2)	yes	no	no	graphite heater	100	
VB	vert	furnace	pBN	yes	yes	no/yes	tube furnace	100	2 = special technique for removal of SiO ₂ crucible
	vert	crucible	pBN	yes	no	no	graphite heater	100	

Table Gradient Freeze and Bridgman variants for growth of GaAs, InP and characteristic features

VGF growth of GaAs

Specification:

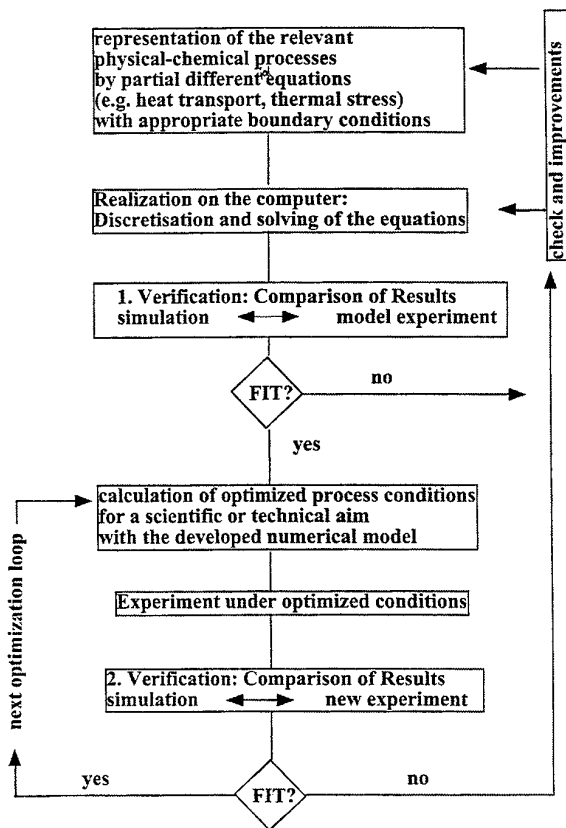
- ☞ EPD < 500 cm²
- ☞ Si-doping: $0.8 < n < 2 \cdot 10^{18} \text{ cm}^{-3}$
- ☞ diameter: 2", 3"



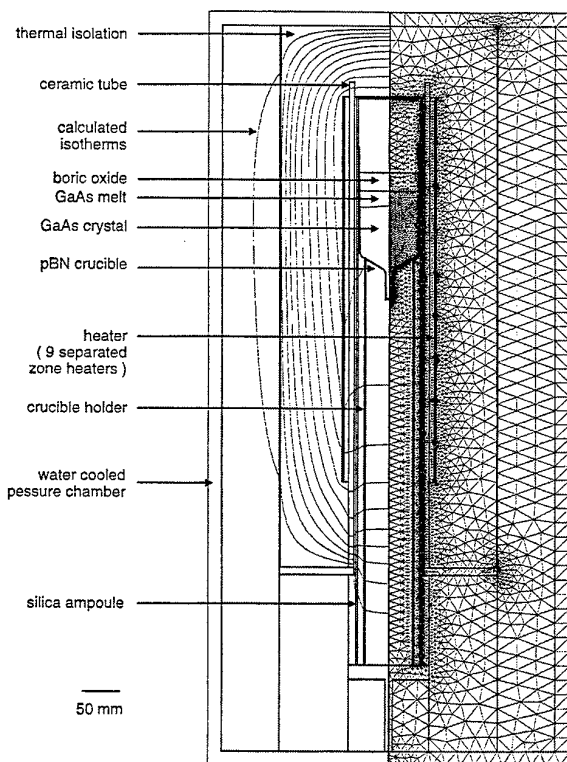
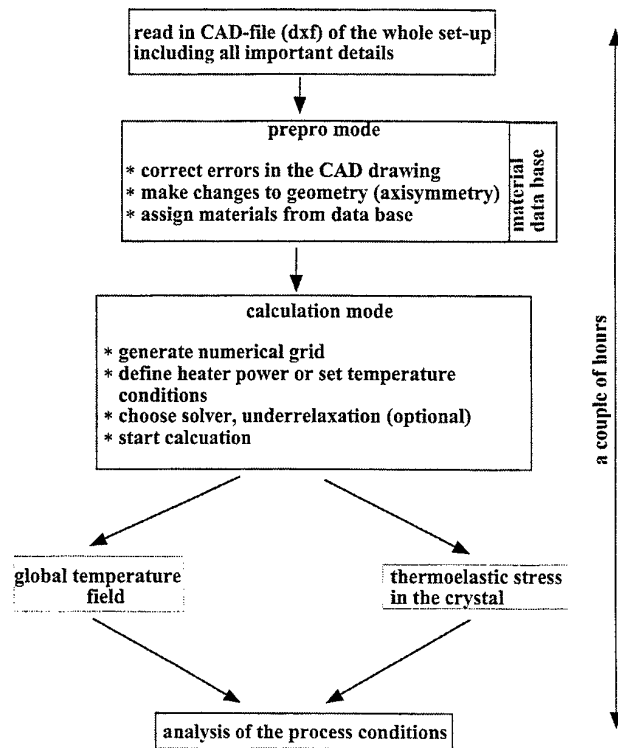
process development:

- ☞ study of VGF variants
- ☞ e.g. crucible preparation
- ☞ use of numerical simulation for furnace and process optimization
- ☞ Si-doping
- ☞ types and distribution of residual dislocations
- ☞ optimization of cone angle for control of facets and avoidance of twinning

Strategy for development of a numerical process model

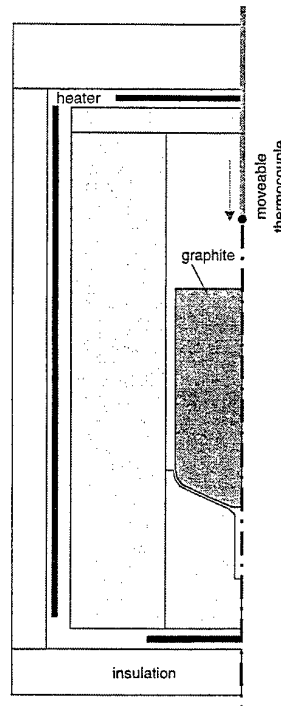


CrysVUN++ a highly efficient, userfriendly computer code for designing equipment and optimizing processes

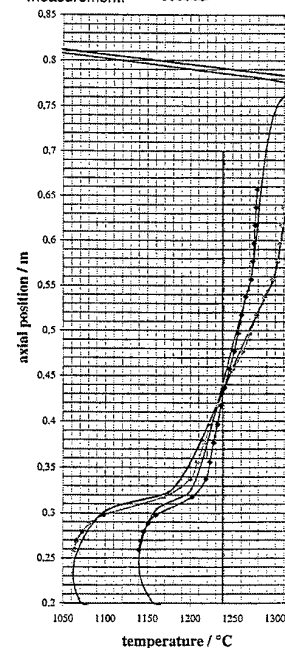


Comparison of simulated (code CrysVUN ++) and measured axaial temperature profiles in a 4" Vertical Gradient Freeze furnace

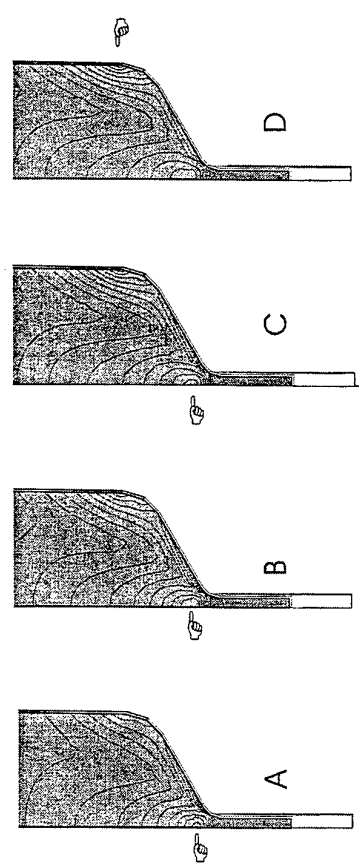
VGF set-up with graphite dummy
and moveable thermocouple



axial temperature profiles
for two different sets of heater powers
simulation: ————
measurement: - - - - -

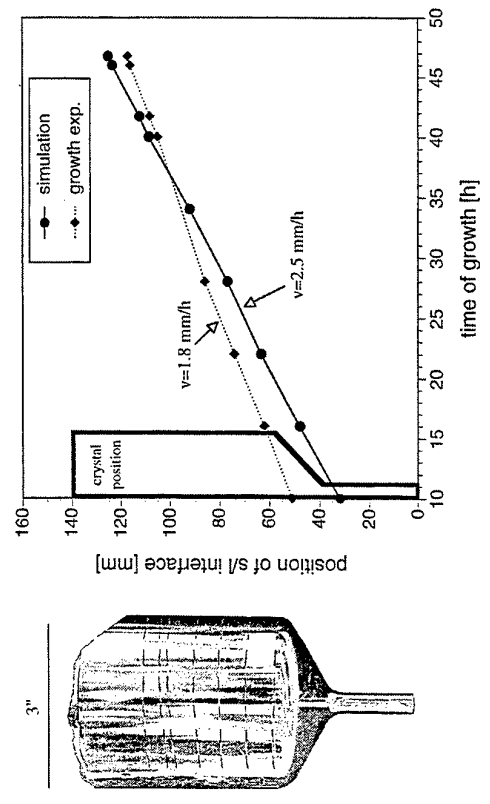


σ_{\max} ,
 max. v. Mises
 stress: 3.57 MPa (A) 2.39 MPa (B) 1.89 MPa (C) 1.72 MPa (D)
 $\Delta\sigma$,
 distance betw.
 lines of eq.
 v. Mises stress: 0.32 MPa (A) 0.22 MPa (B) 0.17 MPa (C) 0.16 MPa (D)



Calculated distribution of thermal stress (lines of equal von Mises stress) in the conical part of the GaAs crystal for a VGF-set-up with different materials A, B, C, D (thermal conductivity) for the crucible support.

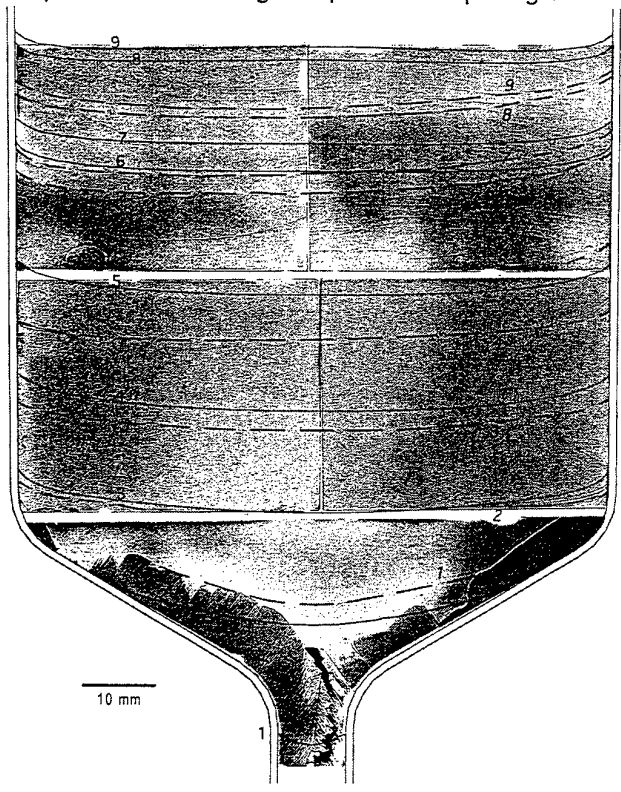
Comparison of simulated and measured axial positions of the s-l interface



3" VGF GaAs crystal grown under crucible rotation

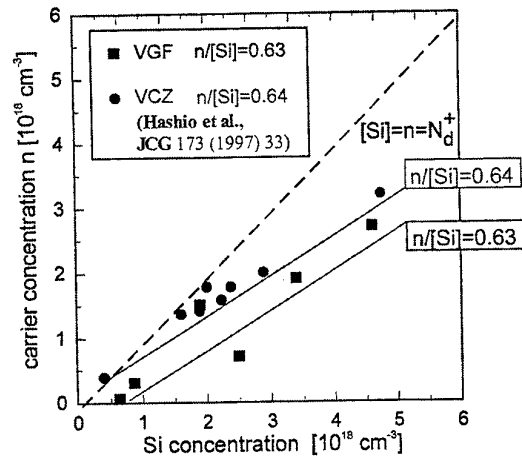
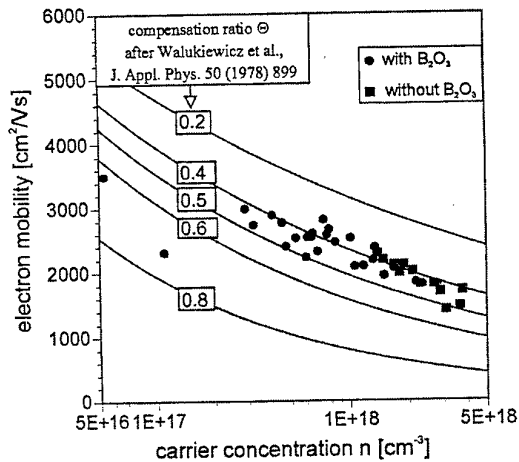
IR-transmission topography
 of (110) axial cut s-l interface :
 experimental (dashed), calculated (solid)

equal numbers belong to equal time steps of growth

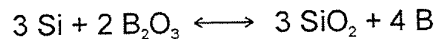


Silicon doping in VGF growth of GaAs

- amphoteric behaviour: shallow donor (Si_{Ga}) + shallow acceptor (Si_{As}) \Rightarrow self compensation $\Theta \approx 0.4 - 0.5$
- compensation ratio $\Theta = N_{\text{a}}^- / N_{\text{d}}^+$ \Rightarrow n-type conductivity
- predominant portion (80% - 90%) as Si_{Ga} \Rightarrow $n/[\text{Si}] = 0.63$
- chemical analysis (GDMS) + Hall-effect and conductivity

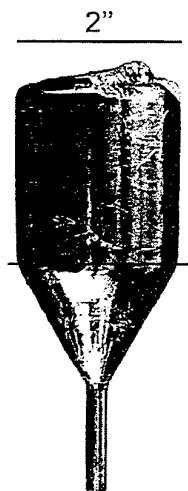


problem: chem. reaction of Si with B_2O_3 leads to a loss of Si as dopant:



\Rightarrow measures for compensating the loss of silicon must be used

Influence of Si-doping on the dislocation density (EPD) in Si-doped GaAs

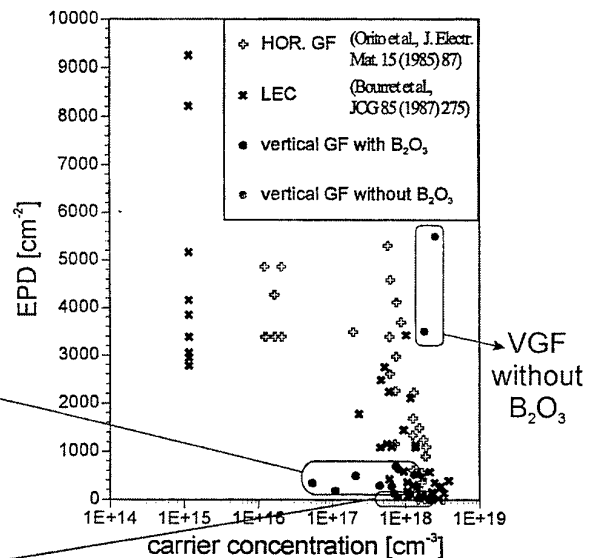


GaAs crystal

VGF with B_2O_3
EPD > 200 cm^{-2}



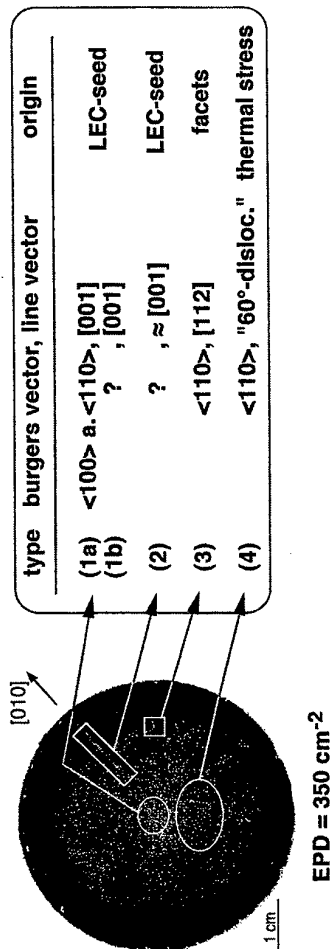
VGF with B_2O_3
EPD > 200 cm^{-2}



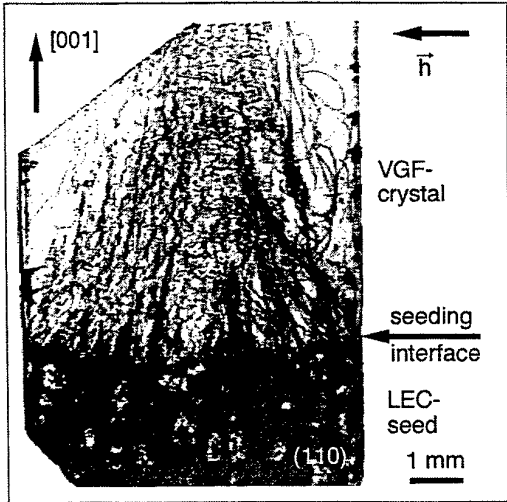
VGF with B_2O_3

- EPD < 1000 cm^{-2} independent of Si-doping, i.e. lattice hardening plays a minor role
- other mechanisms for formation of residual dislocations

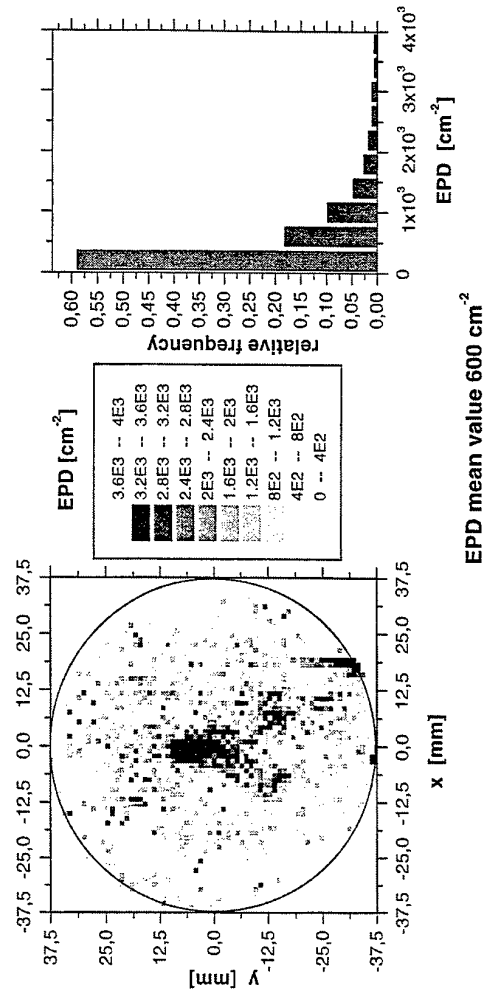
Types of residual dislocations in a 3" VGF-grown (100) wafer



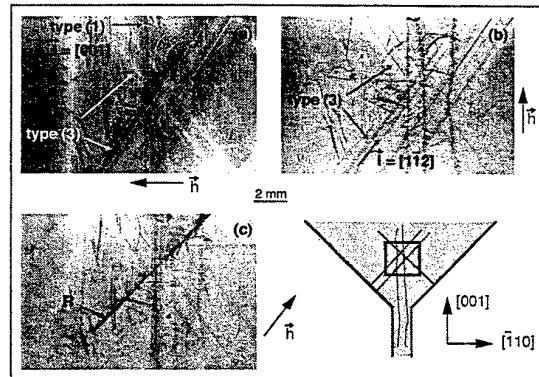
Reduction of dislocation density at the seeding interface
 X-ray topography with synchrotron white beam
 (220) reflection, $\lambda = 0.23 \text{ \AA}$ (55 keV)
 (110) wafer with thickness 0.55 mm



Automized mapping of the EPD of a 3" Si-doped VGF GaAs Wafer



Types of residual dislocations in VGF-GaAs
 X-ray topography with synchrotron white beam
 (10 - 120 keV, ESRF Grenoble)



l = line vector
 h = diffraction vector (004 - reflection)
 b = burgers vector : $\langle 110 \rangle$

Czochralski growth of high-quality GaAs crystals

Peter Rudolph

Institute of Crystal Growth, Rudower Chaussee 6, 12489 Berlin, Germany

1. Introduction

Today, there is an immense interest for the enlargement of the GaAs crystals production due to the two key application branches of *high frequency microelectronics* and *optoelectronics*. The growth technologies for single crystals to meet the needs of these two application fields have diverged. Whereas microwave devices require high-purity quasi-undoped (EL2 and carbon controlled) semi-insulating (SI) wafers optoelectronic devices require n⁺ (usually, Si-doped), i.e. semiconducting (SC) substrates. In the first case the growth from slightly As-rich melt is required, mainly, by using the well established inert gas pressurized liquid encapsulated Czochralski (LEC) method constituting nearly 92 % of all industrial supplied SI GaAs substrates. On the contrary, optoelectronic material is usually grown from uncovered near-stoichiometric melts under ca. 0.1 MPa controlled As pressure by the old-established horizontal Bridgman (HB) technique. Due to the rising need in SI GaAs wafers for important global electronic applications, like cellular phones and telecommunication but also for IR optics, solar cells etc., the present lecture deals priority with the crystal growth issue in this area. Recently, a detailed overview was given by Rudolph and Jurisch [1].

2. Czochralski growth methods

2.1. Liquid encapsulated Czochralski (LEC) growth

Adapted to GaAs by Mullin et al. [2] the LEC growth is nowadays the most widely used growth method for SI GaAs crystals. The method has matured to grow huge single crystals up to 6" in diameter from melts up to about 28 kg. To define the electrical resistivity of the material and to compensate for macrosegregation crystals are grown under carbon- and EL2-control. *Advantages* are (i) free growth without container contact, (ii) use of the gettering ability of boron oxide to influence background impurities, (iii) in-situ carbon control. *Problems* cause (i) stoichiometry control, (ii) selective As evaporation of the crystal surface resulting in Ga droplets which reduce yield, (iii) high temperature non-linearities in the growing crystal resulting in a rather high and inhomogeneously distributed dislocation density in the range of $(0.5-1) \times 10^5 \text{ cm}^{-2}$, and (iv) necessity of a post growth multi-step heat treatment in order to improve the residual stress level and homogeneity of the electrical properties. Nevertheless, the LEC will remain the leading method for mass production of SI GaAs wafers, especially, for ion-implantation based device technologies.

2.2. Vapour pressure controlled Czochralski (VCZ) method

A powerful method to realize more homogeneous temperature fields with low temperature gradients in the range 15 - 35 K/cm in a Czochralski growth system for 4" - 6" diameters is the VCZ method [3,4]. The main constructive feature is the presence of an inner chamber leading to the shielding of the growing crystal and hot gas from the water cooled walls of the outer high pressure recipient and, therefore, to the promising precondition of markedly reduced temperature gradients in axial and radial directions. In order to avoid the decomposition of the very hot crystal surface a temperature controlled As pressure within the inner chamber is maintained during the whole growth. The main *advantages* are: (i) reduced thermal stresses leading to a reduced dislocation density ($\leq 10^4 \text{ cm}^{-2}$), a more homogeneous distribution and a larger substructure cell size across the crystal, (ii) mirror like surface of the crystal indicating a near stoichiometric composition and leading to increased yield, (iii) low level of residual strains. *Disadvantages* are: (i) difficulty of visual process control, (ii) control of carbon content, (iii) relatively high complexity

of the equipment and therefore increased investment costs. However, VCZ is one of the most promising techniques for a constraint-free crystal growth of GaAs with large diameters in a „tailored“ temperature field to ensure minimal thermally induced stresses that is of interest for HBT production, for example.

2.3. Fully encapsulated Czochralski (FEC) growth

Aimed at a reduction of stress level during growth, especially at the contact boundary between crystal and B_2O_3 surfaces, and avoidance of selective As evaporation from the free crystal surface the full encapsulation of the growing crystal by boron oxide was used to grow SI GaAs single crystals by Nakanishi [5] for the first time in 1984. Newer results are described by Elliot et al. [6]. A significant lower dislocation density could be demonstrated. Main problems, however, concern limitations in length and diameter of the crystals as well as the control of the carbon content.

2.4. Hot wall Czochralski (HWC) technique

Early in the history of GaAs crystal growth HWC systems were used by Gremmelmaier [7], Steinemann and Zimmerli [8] since they are capable to a reversible in-situ control of stoichiometry via the total As pressure in the growth chamber. A gas-tight growth chamber with hot walls requiring additional heating above the As source temperature, an arsenic source the temperature of which must be carefully controlled at about 620°C and feed through mechanisms for translation and rotation of seed and crucible are the most important ones of the complex ingredients of a HWC system. Due to the much lower temperature gradients very low-dislocation 2“ crystals have been grown by Tomizawa et al. [9] and Nishizawa [10]. A serious technical problem, however, is the difficulty to control stoichiometry accurately due to temperature gradient across the free GaAs melt surface.

2. R&D tasks to be solved

6“ LEC SI GaAs single crystals exhibit typically an enhanced dislocation density and a reduced cell size as compared to 4“ material. To *optimize the 6“ LEC growth technology* with regard to stress field the *numerical simulation* including the gas convection has to be further developed. The optimization of the *temperature field, interface morphology and cooling program* is of highest importance to control the density and rearrangement of dislocations. At the same time the correlation between *unsteady thermal stress* and *dislocation generation and clustering* has to be studied more carefully. It seems that the use of *VCZ for 6“ growth* can help to solve these problems effectively.

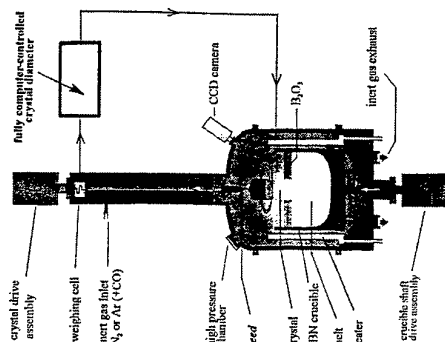
Further, due to the correlation between the dislocation structure and physical properties including their *mesoscopic and macroscopic homogeneity*, a more detailed knowledge about the interaction of dislocations with *ex- and intrinsic defects* and their *relation to the stoichiometry* is required.

- [1] P. Rudolph, M. Jurisch, Proc. Int. Conf. Crystal Growth ICCG-12, Jerusalem 1998 (to be published in JCG).
- [2] J. B. Mullin, B. W. Stauphan, W. S. Brickell, J. Phys. Chem. Solids 26 (1965)782.
- [3] M. Tatsumi, T. Kawase, Y. Iguchi, K. Fujita, M. Yamada, in: Semi-insulating III-V Materials, M. Godlewski (ed.), (World Scientific, Singapore 1994) p. 11.
- [4] P. Rudolph, M. Neubert, S. Arulkumaran, M. Seifert, Cryst. Res. Technol. 32 (1997) 35.
- [5] H. Nakanishi, H. Kohda et al., Ext. Abstr. 16th Conf. on Solid-State Devices and Materials, Kobe 1984, p. 63.
- [6] A. G. Elliot, A. Flat, D. A. Vanderwater, J. Crystal Growth 121 (1992) 349.
- [7] R. Gremmelmaier, Z. Naturforschung 11a (1956) 511.
- [8] A. Steinemann, U. Zimmerli, in: Crystal Growth, Ed. H. S. Peiser (Pegamon, Oxford 1967) p. 81.
- [9] K. Tomizawa, K. Sassa, Y. Shimanuki, J. Nishizawa, J. Electrochem. Soc.: Solid-State and Techn. 131(1984)2294.
- [10] J. Nishizawa, J. Crystal Growth 99 (1990) 1.



Liquid Encapsulated Czochralski (LEC) Growth

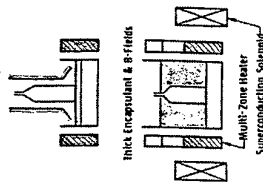
principle



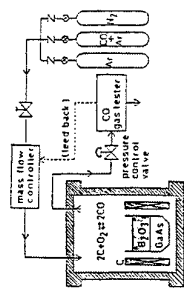
growth parameters

growth rates 5 - 10 mm/h
<100> seed orientation
≤ 20 bar inert gas pressure
up to 28 kg GaAs charges
(6 inch diameter)
EL2 control by Ingot annealing

Heat Shield Configurations

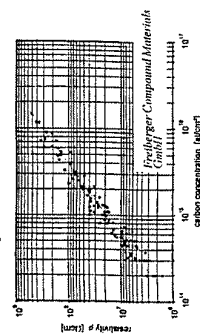


in-situ control of carbon content

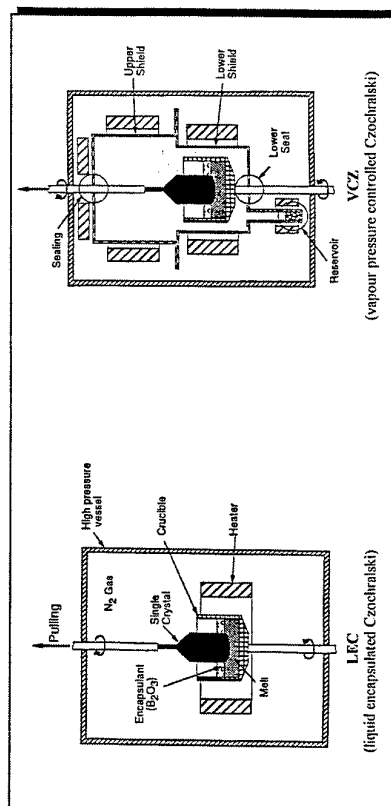


N. Sato, M. Kahane, Y. Kanoda (Tohoku 1999)

resistivity vs. carbon concentration



Schematic drawing of high-pressure Czochralski growth methods of III-V crystals



The challenges of advanced opto-/microelectronics for GaAs crystal growth



- * informations
- * signalizations
- * colour displays
- * laser systems



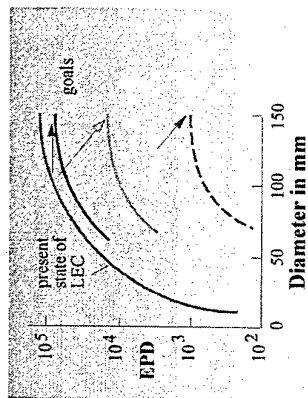
- * telecommunication
- * mobile telephony
- * automotive electronics
- * satellite broadcasting
- * IR optics

production share:
ca. 60 %

- semiconducting
Si(1e)-doped
- very low dislocation density

ca. 40 % (increasing!)

- semi-insulating
C-doped (compensated)
- low/medium dislocation density
(HBTs need very low!)
- high EL2/p uniformity



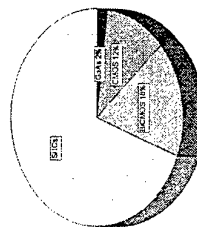
Growth of high-perfect and large GaAs crystals (100 - 150 mm) !



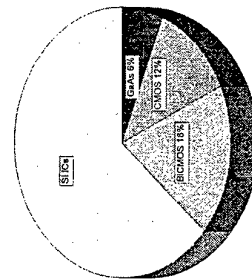
Market Forecast for Si and GaAs Low-Voltage Applications

* after Markt & Technik, April 1997

1996: \$ 17,5 billion



2001: \$ 36,3 billion



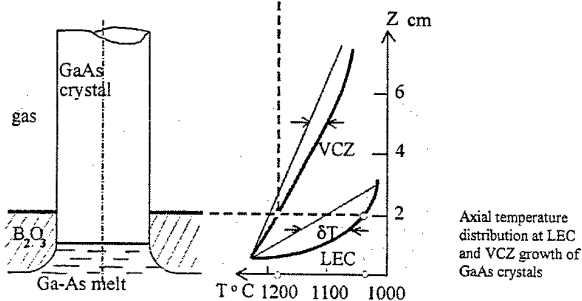
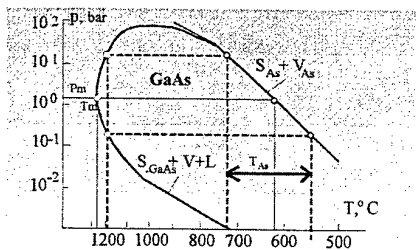
GaAs Market Share: \$ 350 million

GaAs Market Share: \$ >2 billion



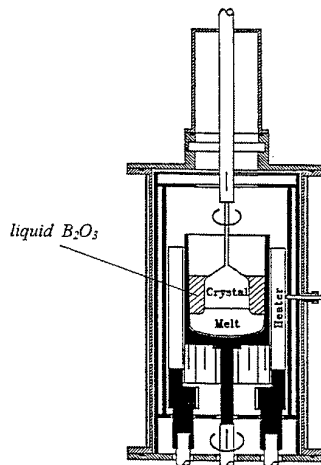
The Principle of VCZ Growth of GaAs

The P-T - projection of the GaAs phase diagram



The thermomechanical stress (i.e. dislocation density) correlates with deviation from $T(z)$ linearity and decreases with decreasing T gradient

$$\sigma = \alpha_T E L^2 (\partial^2 T / \partial z^2) \rightarrow \text{CRSS}_{(\text{GaAs})} \text{ at } T_m \approx 0.7 \text{ MPa}$$



Fully Encapsulated CZ

Elliot et al. (1992)

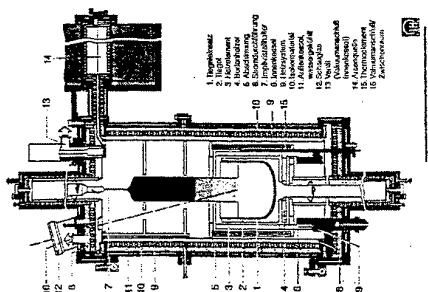
Hewlett Packard Co.

T -Gradient 6 - 60 K cm^{-1}

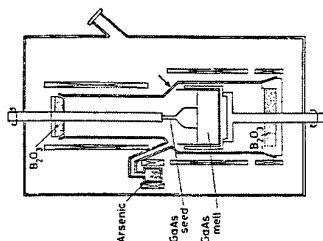
$v = 6 \text{ mm h}^{-1}$

$\text{EPD} < 10^4 \text{ cm}^{-2}$

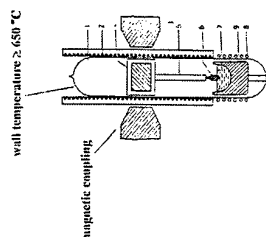
Hot Wall Czocharski (HWC) Technique



H. Wenzel, A. Fatihah (1995)



K. Tomizawa, K. Sasaka, Y. Shimizu, J. Nishizawa (1987)



R. Gremmelhuber (1956)

A. Steinmann and U. Zimmerli (1967)

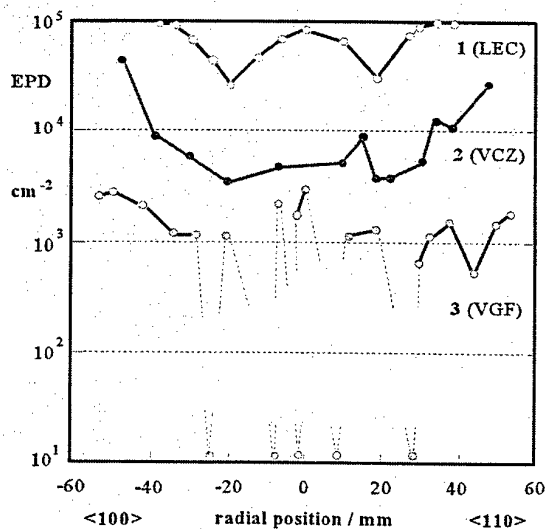


Radial EPD distribution across undoped LEC, VCZ and VGF wafers

1 (LEC) - IKZ Berlin

2 (VCZ) - IKZ Berlin

3 (VGF) - Forschungszentrum Jülich (K. Sonnenberg and E. Küssel)

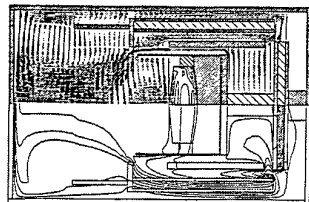




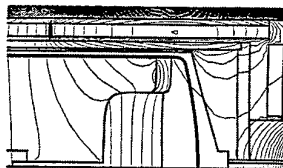
Tailoring of CZ GaAs Growth Arrangements by Global Temperature and Stress Field Computer Simulation

LEC

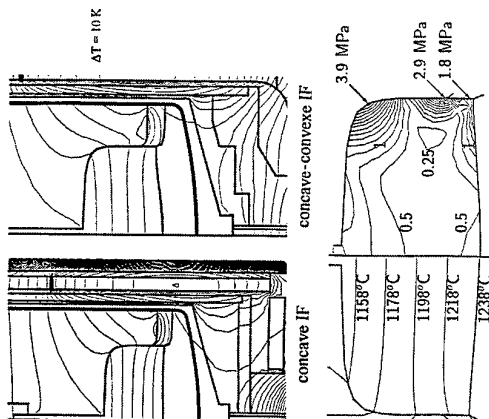
J. Fainberg, H.-J. Leister, G. Müller, JCG 180 (1997) 517
finite-volume computer code STH/AMAS (k - ε model)
isotherms (left), gas flow (right), von Mises stress in the crystal (right)



0.4 bar Ar
laminar convection



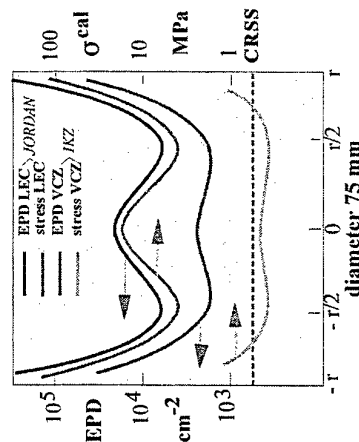
7 bar Ar
turbulent convection



computer optimized VCZ growth arrangement
(with slightly convex IF)



Comparison between radial distribution of calculated thermoelastic stress close to the growth temperature (σ^{th}) and measured EPD in undoped 3" GaAs LEC* and VCZ** crystals



* after A.S. Jordan et al. (1981) and Thomas et al. (1993), ** own results, CRSS - critical resolved shear stress ($G_{As} = 0.7 \text{ MPa}$)



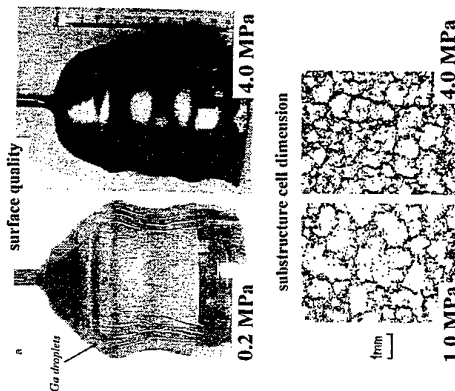
comparison between GaAs CZ growth methods

method	LEC	VCZ	HWC	FEC
crystal diameter	150 mm	150 mm	75 mm	50 mm
T gradient	90 - 120 K/cm	15 - 30 K/cm	10 K/cm	50 K/cm
EPD (cm^{-2})	$(0.5 - 1) \times 10^5$	$(0.3 - 1) \times 10^4$	$(0.2 - 1) \times 10^4$	10^2
uniformity of dislocation distribution	moderate	good	good	moderate
in-situ C control	very good	not solved	not solved	not possible (?)
stoichiometry/EL2 control	good	good	very good	poor
technical realization	good	possible	poor	good
investment cost	high	very high	very high	high
process maturity	very high	medium	low	medium
productivity	high	medium	low	medium



Correlation between 3" GaAs crystal quality and argon inert gas pressure

M. Seifert, M. Neubert, W. Ulrich, B. Wiedemann, J. Knege, E. Wolf, D. Klingner, P. Rudolph, JCG 138 (1996) 409

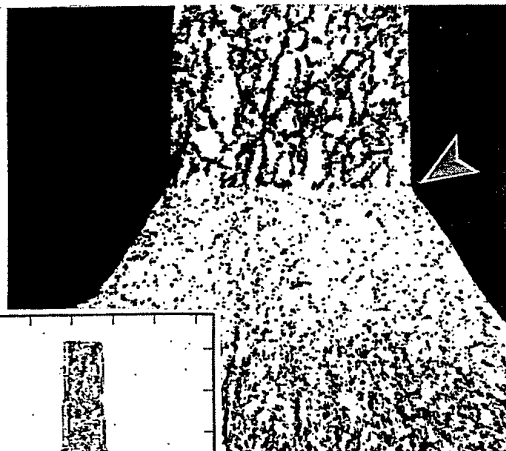


increasing radial temperature gradient (i.e. thermomechanical stress) with increasing pressure due to the increase of convective heat transfer ($h_r \sim p^{1/2}$)

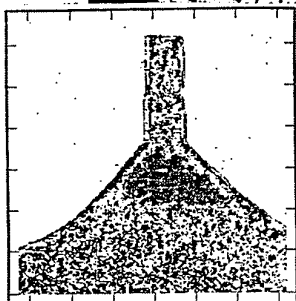


dislocation features in the seeding region

GaAs VCZ (IKZ Berlin)

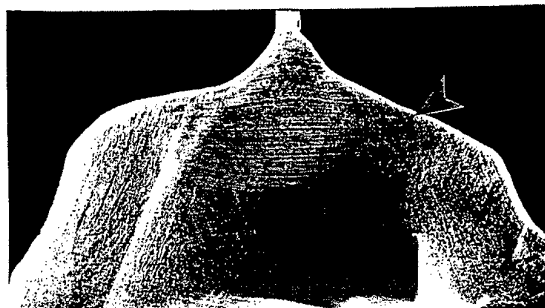


EPD pattern



PL mapping

GaP LEC (IKZ Berlin)



X-ray Lang topography

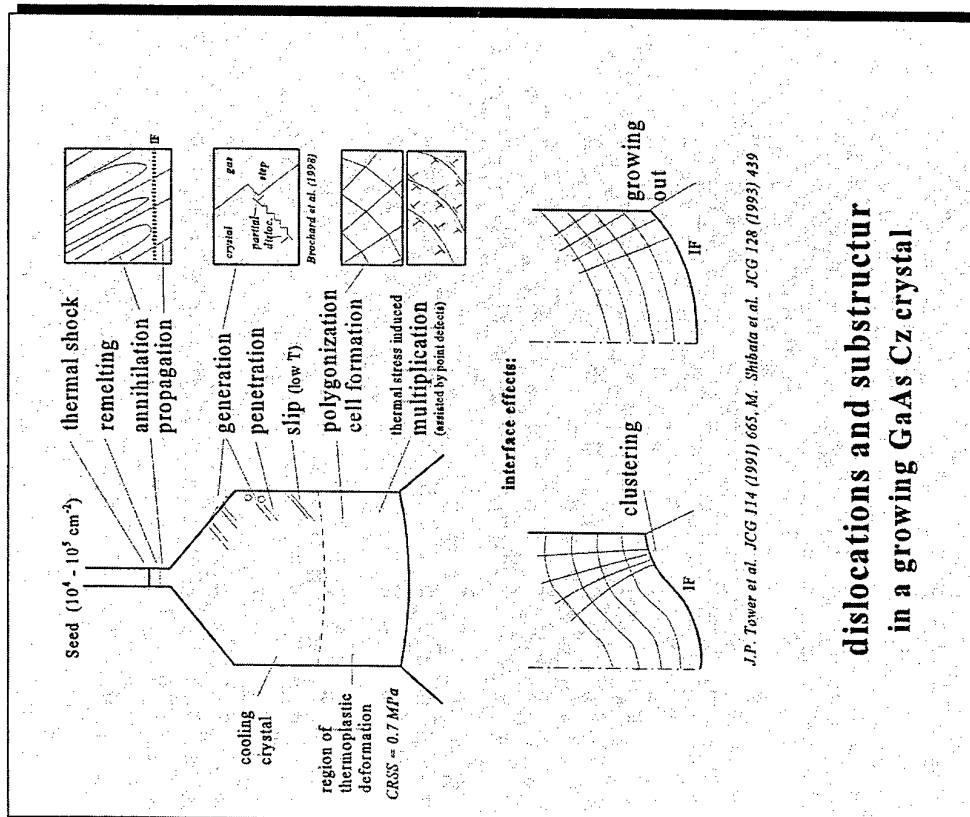
- ✓ reduction of dislocation density at the seed-crystal interface by one or two order of magnitude !

conformity with InP LEC growth by

- S. Tohmo et al. *J. Appl. Phys* 54 (1983) 666

- O. Oda (private communication 1996)

- dislocation annihilation by linking together during the remelting process of the seed
- Lomer sessile-type dislocations
- generation of new dislocations at the crystal surface (facet edges)





- dislocation dynamics -

strain rate (Orowan equation):

$$\partial \epsilon / \partial t = N_m v b$$

N_m - density of mobile dislocations

v - mean dislocation velocity

b - Burgers vector

$$v = K (\tau_{\text{eff}})^m \exp(-E/kT)$$

$\tau_{\text{eff}} = \tau - A\sqrt{N}$ - effective stress at the dislocation
(reduced by strain hardening due to N presented dislocations)

$$A = Gb/2\pi(1-\nu)$$

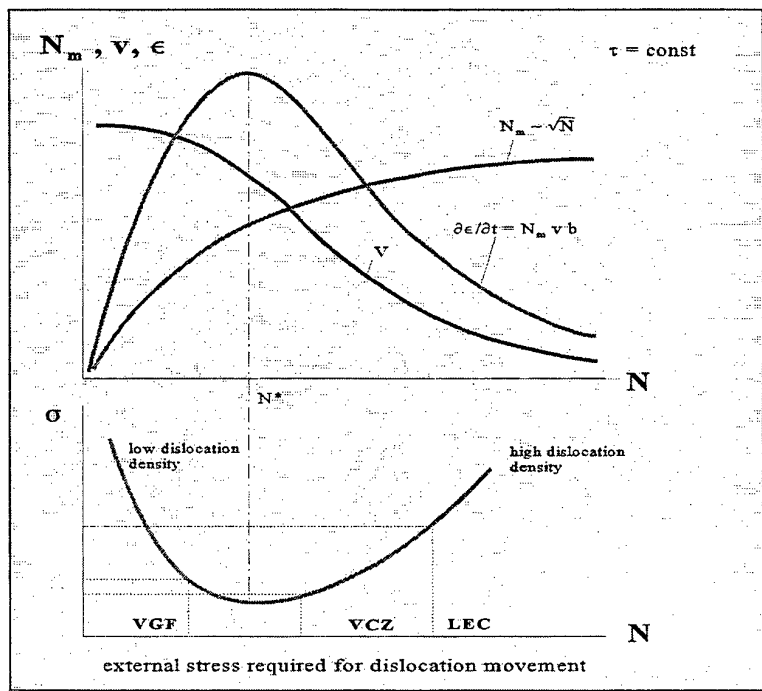
K - constant, G - shear modulus, ν - Poisson number,
 E - activation energy, m - stress exponent

$$\partial \epsilon / \partial t = b N_m K \exp(-E/kT) (\tau - A\sqrt{N})^m$$

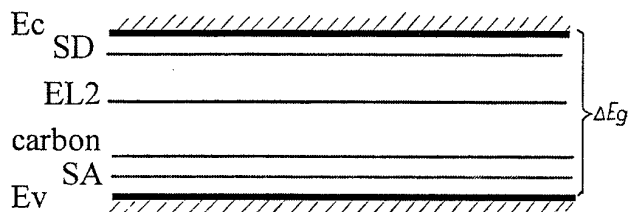
multiplication rate of dislocations:

$$\partial N / \partial t = N_m K \exp(-E/kT) (\tau - A\sqrt{N})^{m+1}$$

more details: H.Alexander, P.Haasen, Solid State Phys. (1968)
J.Völkl, G.Müller, JCG 97 (1989) 136



- control of EL2 concentration -



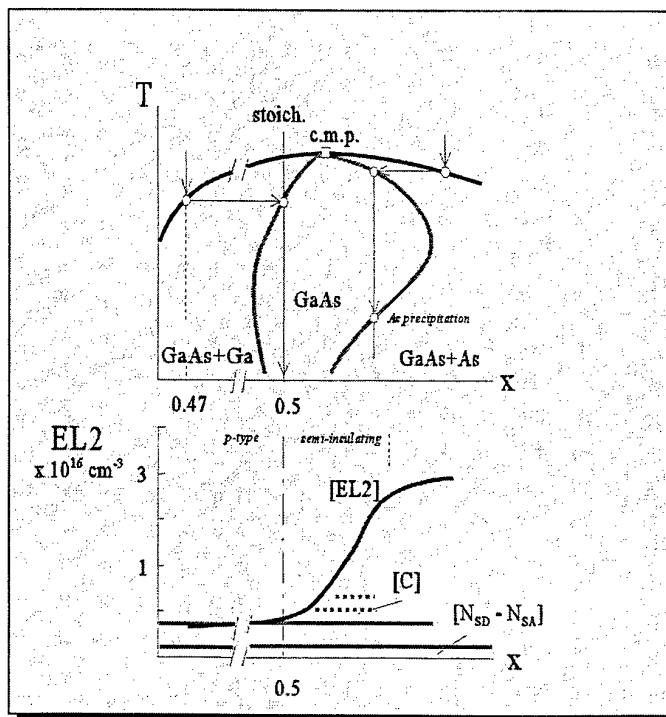
EL2: As_{Ga} or $[\text{As}_{\text{Ga}}-\text{As}_i]$

$$n = 4.7 \times 10^{17} (N_{\text{EL2}} / (N_{\text{SD}} - N_{\text{SA}}) \exp(-E_{\text{EL2}}/kT))$$

condition of semi-insulating n -GaAs:

$$[N_{\text{EL2}}] > [C] - [N_{\text{SD}} - N_{\text{SA}}] > 0$$

✓ growth from slightly As-rich melt



Growth Methods on Large Diameter GaAs Single Crystals with Low Dislocation Density -Possibility of VCZ and VB-

Yasuhiro Nishida
Sumitomo Electric Industries, Ltd.

GaAs substrates are now mainly used for both optical devices and microwave devices. With the recent advance of mobile communication there has been an increasing demand of semi-insulating GaAs. At the same time stringent requirements for lower cost as well as higher quality for the substrates have emerged. Many device manufacturers apt to use larger diameter substrates, since the process cost depends directly on the diameter. To meet today's needs suppliers have sought to develop larger diameter GaAs substrates having both higher quality and lower cost.

In order to reduce crystal cost, it is necessary to grow longer single crystals at a higher yield by using low-cost facilities. The single crystals must have high quality with a high uniformity in the electrical and optical properties. Moreover, both dislocation density and residual strain in a larger diameter crystal must be suppressed to the same extent as that of a smaller diameter crystal, though they generally increase with the crystal diameter. A low residual stress(strain) is indispensable to prevent cracking or the generation of slip defects in the crystal during the processes of the device fabrication. The surface qualities of the substrate are also critical to the device qualities.

Four main growth methods have been considered for production to satisfy the above qualities, namely, the Horizontal Bridgman (HB), Liquid Encapsulated Czochralski (LEC), Vapor Pressure Controlled Czochralski (VCZ) and Vertical Bridgman (VB) methods. (A) HB can give a low dislocation crystal but it is difficult

to grow large diameter crystal due to the asymmetric temperature profile along the growth direction.

(B) LEC is suitable for growing a large diameter and long crystal but the steep temperature gradient generates considerable dislocations. The high price of puller due to the high pressure is another drawback. The electrical properties of the crystals for microwave uses are well controlled by the matured technology.

(C) VCZ is a modified LEC method, which improves the drawbacks in the LEC method, such as high dislocation density, deviation from the stoichiometry and high pressure puller. This method was first achieved by SEI as a production technology of InP single crystals. By applying an arsenic vapor pressure in an inner hot-wall growth chamber, we can reduce the temperature gradient without inducing a dissociation of arsenic from both the melt and crystal. Reducing the thermal stress during growth brings about low dislocation density and low residual strain in a crystal, which is promising for growing a large diameter crystal.

(D) VB (VGF) is also a promising method for growing a low dislocation density and low residual strain crystal having a highly controlled diameter because of growth in a crucible. The most serious problem in this method has been the generation of twinning, lineage and polycrystallization due to wetting of the melt to the crucible near the growth interface, though the majority of the problems have been solved. Another disadvantage is that we are unable to observe the seeding process, especially twinning or polycrystallization, due to the crucible. So the growth conditions must be strictly controlled in order to achieve a stable and reproducible thermal environment.

In the selection of growth methods, an important points to be considered is production cost, which includes productivity (mainly depends on the growth rate of crystals) and price of the growth equipment.

The cost of a crystal directly depends on the yield of crystal which satisfies the demands on crystallinity, electrical and optical qualities and their uniformity. It is said that the control of a growth interface shape is essential to growing a crystal with high reproducibility. A convex interface to the melt especially at the peripheral region of a crystal is necessary to prevent polycrystallization and to reduce dislocation density. The growth interface shape is dependent on the heat flow into/out of the growth interface and the latent heat (growth rate). The growth conditions to realize an optimized growth interface is determined on the basis of numerical simulation as well as experimental results. Under a lower temperature gradient, control of both the growth interface and the crystal diameter becomes difficult since the isothermal line becomes sensitive to the variation of the temperature near the growth interface. Increase of the crystal diameter also makes it more difficult to control it.

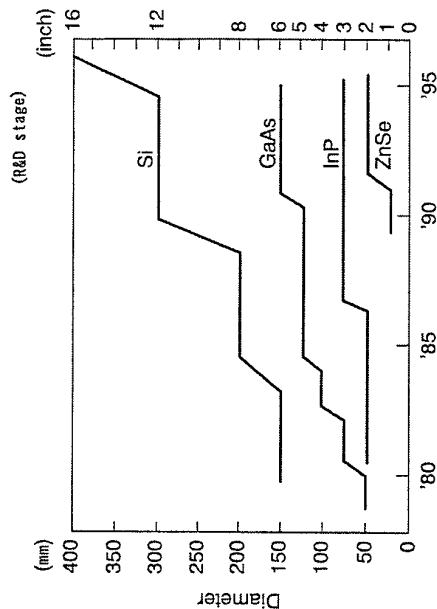
The electrical properties, which are the result of the amount of impurities (intentionally or unintentionally doped) and their distributions, are considered not strongly dependent on the growth methods virtually. Post growth heat treatment can precisely control the properties through controlling deep levels such as EL2 or other defect levels.

Future demands for GaAs substrates presumably will become stronger in regard to larger diameter, lower cost, higher uniformity, lower dislocation density and lower residual stress. In order to satisfy these requirements, we must choose suitable crystal growth methods. For optical uses, VB (VGF) will replace HB. As for electronic uses, LEC will continue to be used as the ion implantation substrates for some time. VCZ or VB will be promising for electronic uses, especially as an epitaxial substrate. Whichever method survives is considered to depend on the advancement of each technology.

Trend of GaAs Crystal Technologies

	'75	'80	'85	'90	'95
Growth Technique	HB/HGF LEC	VB/VGF VCZ			
Wafer Diameter	2" ϕ LEC 2" ϕ HB	3" ϕ LEC 3" ϕ HB 3" ϕ 4" ϕ LEC 5" ϕ LEC	6" ϕ VCZ, LEC		
Ingot Length		2' ϕ 100cm HB 3" ϕ MLEC 40mm ϕ D.F. Si(HB)	3" ϕ 45cm LEC 3" ϕ D.F. In(LEC) 3" ϕ D.F. Si(VGF)	4" ϕ 50cm LEC 6" ϕ 25cm VCZ, LEC	
Dislocation Density		Cr doped S.I.	Undoped S.I.		
Purity		Undoped S.I.	In doped D.F.		
Uniformity			Undoped Ingot Annealing		Multi-step Annealing

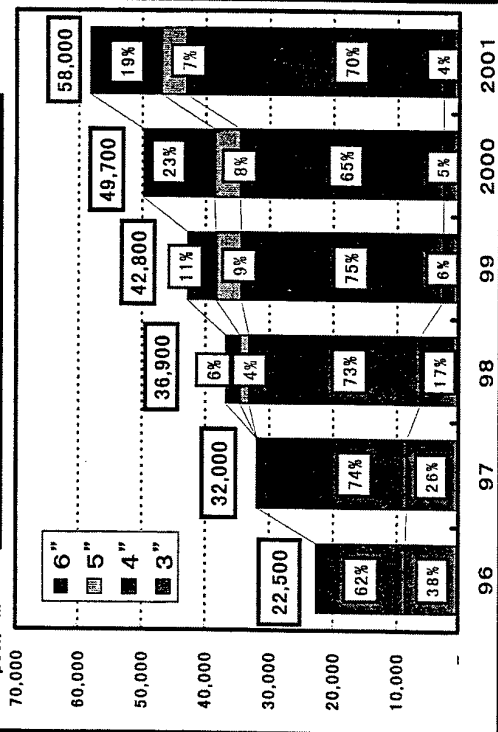
Progress in Wafer Diameter



Microwave Wafer Market by Size

(in terms of 4 inch)

pos./M



Trend of Device Technologies

Devices	Trend of Performances	LED	Laser Diode	Microwave & Digital IC
	Higher Brightness	Higher Power	Higher Frequency	Higher Frequency
	Shorter Wavelength	Shorter Wavelength	Lower Noise	Lower Noise
			Higher Integration	Higher Integration
			Saving Electric Power	Saving Electric Power
Active Layers	Materials	LED	Laser Diode	Microwave & Digital IC
	GaAs (IP)	GaAs (IP)	AlGaAs (Red)	GaAs
	GaAsP (Red~Yellow)	GaAsP (Red~Yellow)	InGaAlP (Red~Green)	AlGaAs/GaAs
	GaP (Red~Green)	GaP (Red~Green)	InGaAsP (IR)	AlGaAs/InGaAs
	AlGaAs (Red)	AlGaAs (Red)		InGaP/GaAs
	InGaAlP (Red~Orange)	InGaAlP (Red~Orange)		AlInAs/InGaAs
Process	LPE	✓	✓	✓
	VPE	✓	✓	✓
	OMVPE	✓	✓	✓
	MBE	✓	✓	✓
	Ion Implantation	✓	✓	✓

Requirement for GaAs Substrates

		Optical use		Electronic use	
		present	near future	present	near future
Crystal diameter (ϕ)	larger	2	3	4	6
Crystal length (cm)	longer	—	—	20	50
Dislocation density (cm^{-2})	lower	$\leq 10^3$	$\leq 10^2$	$(\leq 10^5)$	$(\leq 10^4)$
Residual strain	lower	—	—	$(< 10^{-4})$	$(< 10^{-5})$
Impurity (cm^{-3})	lower	—	—	$\leq 10^{16}$	$\leq 10^{15}$
Uniformity (mV) (σ/Vth)	higher	—	—	≤ 20	≤ 10

Characteristic Parameters of GaAs

	Elemental	III - V Compound		II - VI Compound	
		GaAs	InP	InP	ZnSe
Band Gap Energy (ev)	Si	1.40	1.35	1.35	2.70
Band Structure	indirect	direct	direct	direct	direct
Electron Mobility ($\text{cm}^2/\text{V}\cdot\text{s}$)	1,900	8,800	4,600	500	500
Crystal Structure	diamond	zinc blend	zinc blend	zinc blend	zinc blend
Lattice Constant (nm)	0.543	0.565	0.587	0.568	0.568
Density (g/cm^3)	2.33	5.32	4.79	5.26	5.26
Melting Point ($^{\circ}\text{C}$)	1,410	1,238	1,062	1,520	1,520
Dissociation Pressure (atm)	10^{-7}	0.9 (As)	25 (P)	2 (Zn), 0.6 (Se)	2 (Zn), 0.6 (Se)
Thermal Expansion Coefficient (K^{-1})	2.33×10^{-6}	5.93×10^{-5}	4.5×10^{-5}	7.7×10^{-6}	7.7×10^{-6}
Thermal Conductivity ($\text{W}/\text{cm}\cdot\text{K}$)	1.41	0.46	0.7	0.19	0.19
Critical Shear Stress (dyn/cm^2)	1.850×10^7	0.587×10^7	0.6×10^7	lower*	lower*
Cleavage Face; Cleavagity	{111}; weak	{110}; strong	{110}; strong	{110}; strong	{110}; strong

at 25°C (exception; Dissociation Pressure; at melting Point (M.P.)
Critical Shear Stress; at (M.P. -40°C)

* Speculation

Important Factors Related to Yield of Substrate

(A) Yield of Crystal

- Fraction Solidified
- Fluctuation of Diameter
- Shape of Crystal
- Crack

(B) Crystallinity

- Polycrystallization
- Twinning (micro twins)
- Lineage
- Dislocation Density
- Slip Line
- Residual Stress \rightarrow Crack
- Precipitation
- Void

(C) Electrical Properties

(Absolute Value and its Uniformity)

- Dopants
- Impurities
- Deep Level (EL2)

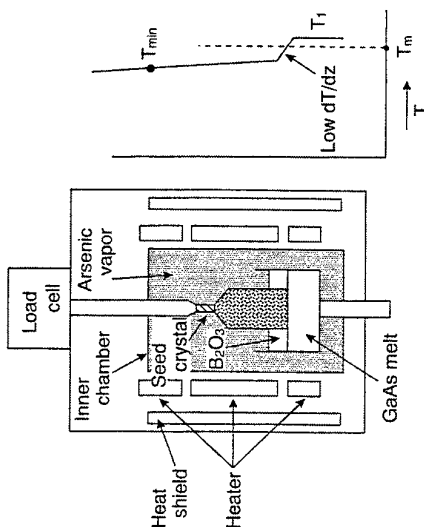
Comparison of Growth Techniques for GaAs Single Crystals

	HB(HGF)	VB(VGF)	LEC	VCZ
Low Temperature Gradient (without Dissociation)	\bigcirc	\bigcirc	$\times \sim \Delta$	\bigcirc
S-L Interface Control	$\times \sim \Delta$	\bigcirc	\bigcirc	\bigcirc
Non-Contact with Crucible	$\times \sim \Delta$	$\times \sim \Delta$	\bigcirc	\bigcirc
Diameter Control	$\Delta \sim \bigcirc$	\bigcirc	$\times \sim \Delta$	$\times \sim \Delta$
"In Situ" Observation	\bigcirc	\times	\bigcirc	\bigcirc
Simplicity of Apparatus	\bigcirc	\bigcirc	Δ	$\times \sim \Delta$
Maturity of Technology	\bigcirc	$\times \rightarrow \Delta$	\bigcirc	$\times \rightarrow \Delta$

\bigcirc : good, Δ : fair, \times : poor

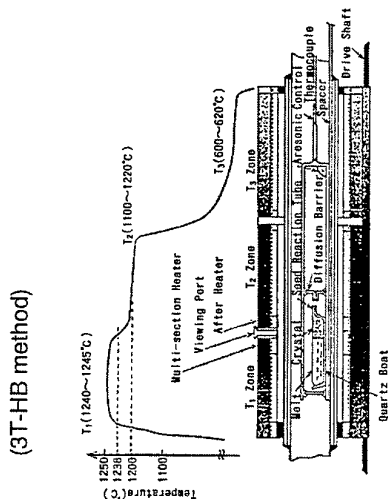
VCZ (Vapor Pressure Controlled Czochralski) Method

- [Advantage]**
- ① Stoichiometry control
 - ② Low temperature gradient
→ Low dislocation density
 - ③ Small temperature fluctuation
→ Stable growth
 - ④ Cylindrical crystal
 - ⑤ Growth from free surface
- [Drawback]**
- ① Low dT/dr
→ Diameter control
 - ② Complicated structure



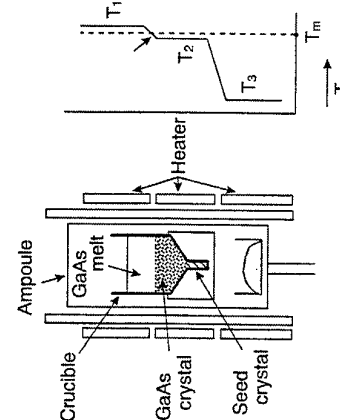
HB (Horizontal Bridgman) Method

- ① Stoichiometry control
 - ② Low temperature gradient
→ Low dislocation density
 - ③ Doping control of Si
 - ④ Growth of long crystal
 - ⑤ Automatic growth
- [Drawback]
- ① Si contamination
 - ② Growth in a boat
→ wetting
 - ③ Asymmetric temperature profile
 - ④ Difficult to grow cylindrical crystals



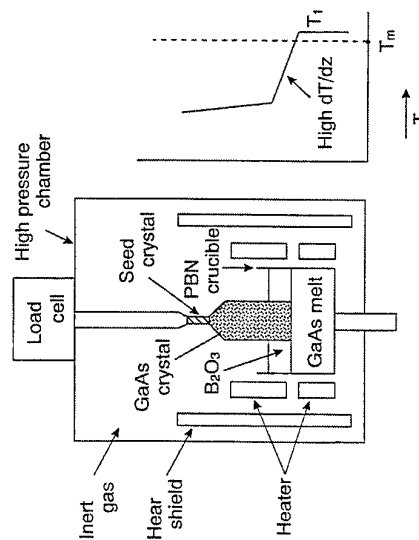
VB (Vertical Bridgman) Method

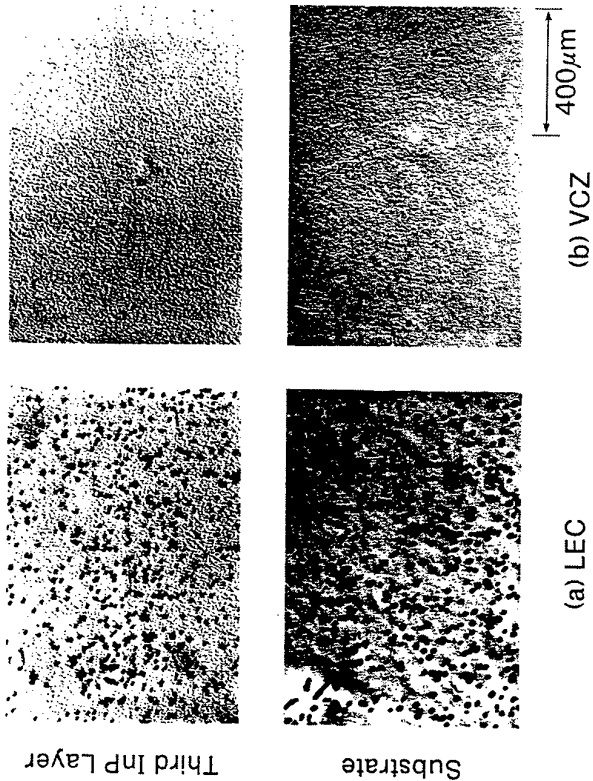
- [Advantage]**
- ① Stoichiometry control
 - ② Low temperature gradient
→ Low dislocation density
 - ③ <100>-round shape
 - ④ Stable growth
(weak melt flow)
- [Drawback]**
- ① Difficult to observe states of growth
 - ② Growth in a crucible
⇒ wetting



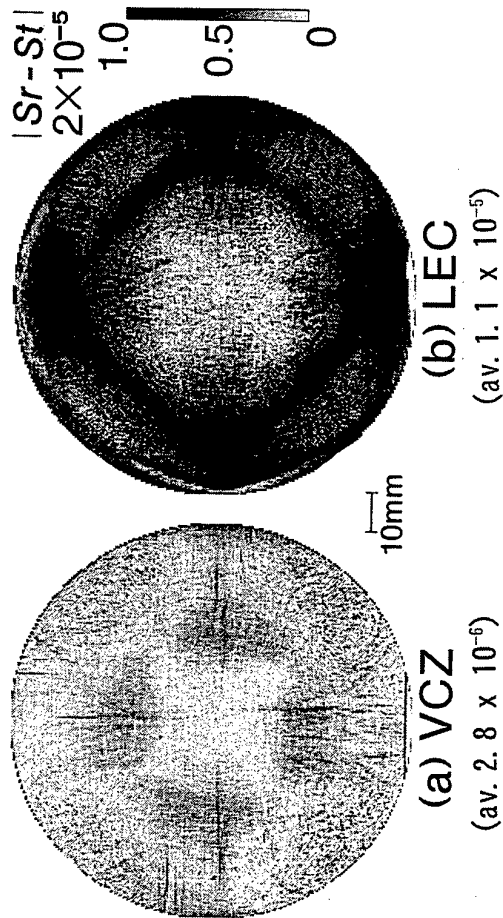
LEC (Liquid Encapsulated Czochralski) Method

- | | |
|---|--|
| <p>[Advantage]</p> <ul style="list-style-type: none"> ① Growth from free surface
→ Large diameter crystal ② Gettering effect of B_2O_3 ③ Cylindrical crystal ④ High dT/dz
→ High growth rate | <p>[Drawback]</p> <ul style="list-style-type: none"> ① High dT/dz
→ High dislocation density ② Stoichiometry control ③ Diameter control |
|---|--|

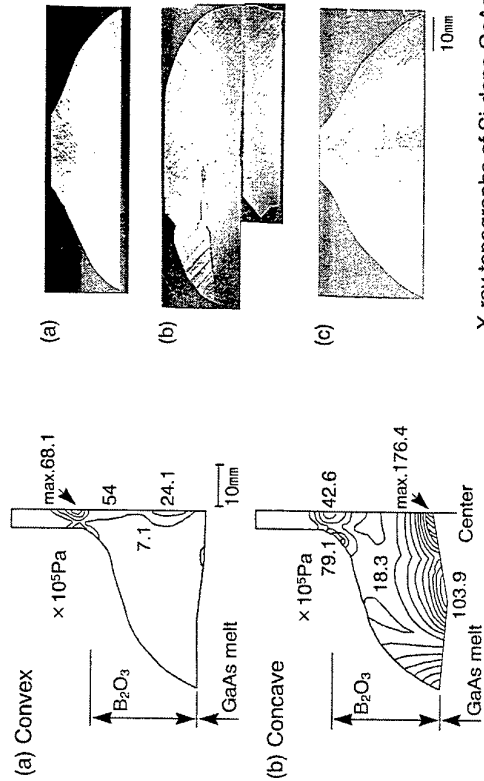




Residual Strain of 4-inch Wafers



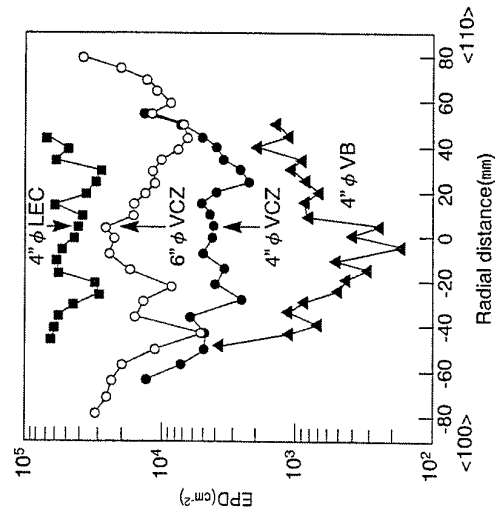
Effect of Solid-Liquid Interface Shape



X-ray topographs of Si-doped GaAs
 B_2O_3 thickness (a) 5mm, (b) 25mm, (c) 37.5mm

Calculated resolved shear stress

Comparison of Etch Pit Density



6" SI GaAs LEC-Crystals

T. Flade, M. Jurisch, A. Kleinwechter, A. Köhler, U. Kretzer, J. Prause, Th. Reinhold, B. Weinert
Freiberger Compound Materials GmbH, D-09599 Freiberg/Germany, Am Junger Löwe Schacht 5

Connected with the necessity of lower specific costs per die in large-scale device manufacturing, 6"- semi-insulating (SI) GaAs wafers will play an increasing role in the next years. At the same time, the requirements of the users concerning device-relevant physical properties of the wafers like electrical homogeneity, control and thermal stability of defect structure and defect density, mechanical strength, local and global flatness and reproducible and stable surface state etc. will increase, too.

The $\langle 100 \rangle$ -oriented 6" SI GaAs crystals have been grown in a standard LEC-process similar to the 4" growth technology using pretreated 9" pBN crucibles and charges of 20 kg at this stage of development. A new generation of high pressure pullers equipped with a fully computerised process and diameter control system and designed for crucibles up to 12" in diameter allow charges up to 50 kg. Synthesis is performed from high purity constituents either in a puller according to the direct-synthesis method or in a separate high-pressure equipment. The development of the growth technology has been supported by model calculations using a finite-volume code which, apart from heat transfer by conduction and radiation, accounts for turbulent convection in the gas phase at pressures typical for LEC growth, too [1]. In order to meet customers' requirements with respect to electrical resistivity of the crystals, carbon content is defined and controlled in the range from 2×10^{14} to $1 \times 10^{16} \text{ cm}^{-3}$ by the CO-partial pressure in the growth atmosphere similar to [2]. Stoichiometric control of the crystals is performed by growth from a melt with predetermined As excess during synthesis. In connection with heat treatment this allows to define EL2-concentration and thus to influence resistivity. The crystals are heat-treated by a two-step ingot annealing procedure in evacuated, pretreated quartz ampouls under As overpressure [3].

The crystals were subjected to an intensive inspection program including for seed- and tail-end test-wafers structural control after KOH-etching, measurement of resistivity, carrier concentration and mobility, determination of the C- and B-content by FTIR-spectroscopy and examination of macroscopic homogeneity by TDCM-mapping [4] and radial EL2⁰-line scans along a $\langle 110 \rangle$ -direction. BB-photoluminescence, high-resolution EL2⁰-and PCT-mappings [5] and LST-topographs of selected areas are made to evaluate the mesoscopic homogeneity of the crystals. The impurity content is followed by GDMS- and AES-analysis. Residual strains are controlled by an IR polariscope similar to [6], and breakage tests are performed according to [7]. Finally, there are measured various geometrical parameters of the wafers and the residual particle density on the surface is classified.

As common for LEC-GaAs, dislocations are arranged in a well-pronounced cellular structure with globular cells in the central and peripheral regions and elongated cells in between corresponding to a rather weak W-shaped local etch pit density. As expected, a slight increase can be seen due to a higher stress level relaxing in a higher dislocation density. Related to the enhanced average dislocation density of 6"-crystals the average cell size is lower as compared to 4"-crystals. The mean variation of epd is lower in comparison to 4" LEC crystals.

The electrical resistivity of high-purity SI GaAs is determined by the concentration of the mid-gap donor EL2 through the compensation of net shallow acceptors, mainly carbon, if the residual concentrations of donor and acceptor impurities are low. At constant EL2⁰-concentrations this results in $\rho \propto [C]$ by which the purity of the crystals can be controlled. There is no significant difference between 6"- and 4"-crystals. Furthermore, it follows that the resistivity of 6"-crystals can be controlled by the carbon content over the whole range required for device manufacturing.

The well known relation between average Hall mobility and resistivity is found for 6"-seed- and tail-end wafers with a shallow maximum around $2 \times 10^7 \Omega \text{cm}$.

For evaluation of the macroscopic homogeneity across a wafer, TDCM mappings were measured with a lateral resolution of 2.3 mm. The standard deviation of radial electrical resistivity has been found for 6"-crystals to be typical $< 20 \%$.

The radial $\text{EL}2^0$ -concentration was analysed by IR-absorption with a lateral resolution of 280 μm . The mean standard deviation of the radial $\text{EL}2^0$ -distribution averaged over all 6"-crystals amounts to 3.0 % as compared to 4.6 % for 4"-crystals. The improved radial homogeneity of 6"-crystals results from the enhanced dislocation density and the corresponding reduction in mean cell size.

The average axial homogeneity of the electrical resistivity of 6"-crystals is better than $\sim 25 \%$. This again compares well with 4"-material.

In order to characterize the mesoscopic homogeneity scaled by the cellular structure a typical point-contact-current (PCT)-mapping measured in the (critical) R/2-region in $\langle 110 \rangle$ -direction of a 6" seed-end test wafer is represented. The lateral resolution of the measurement was 50 μm . The cellular structure can be clearly seen. Deviating from usual results [3], an increased electrical resistivity at the cell walls as compared to the cell interior has been observed in this example. As shown by variations of the annealing procedure, the resistivity behaviour can be influenced by the annealing parameters in the medium temperature step. The standard deviation of the mesoscopic resistivity slightly depends on the position: the largest value has been found in the region of elongated cells. Averaged over measuring fields at center, half-radius and periphery of all 6"-crystals studied until now, the value found is $< 10 \%$. The behaviour of the electrical resistivity around cell walls is directly correlated to the mesoscopic $\text{EL}2^0$ -concentration.

Systematic LST-topography of 6"-crystals revealed that in close agreement with corresponding results on 4"-crystals supersaturated arsenic has been precipitated at dislocations as well as in the cell interior forming a denuded zone between these regions.

FREIBERGER developed a new technology for 6"-wafer manufacturing. It compares the main global and local geometrical parameters of 6" and 4"-wafers. Despite of a 2.25 times larger area and 23 more $20 \times 20 \text{mm}^2$ sites of the 6"-wafers there is no significant difference as compared to 4"-wafers.

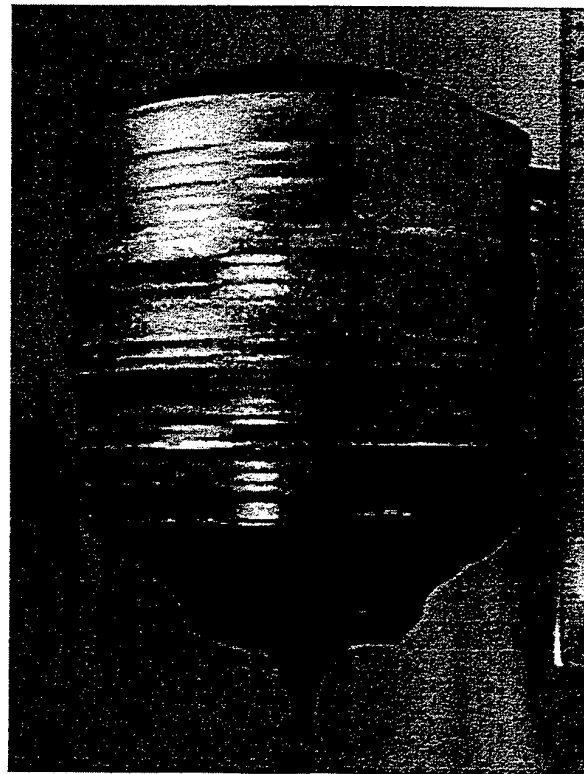
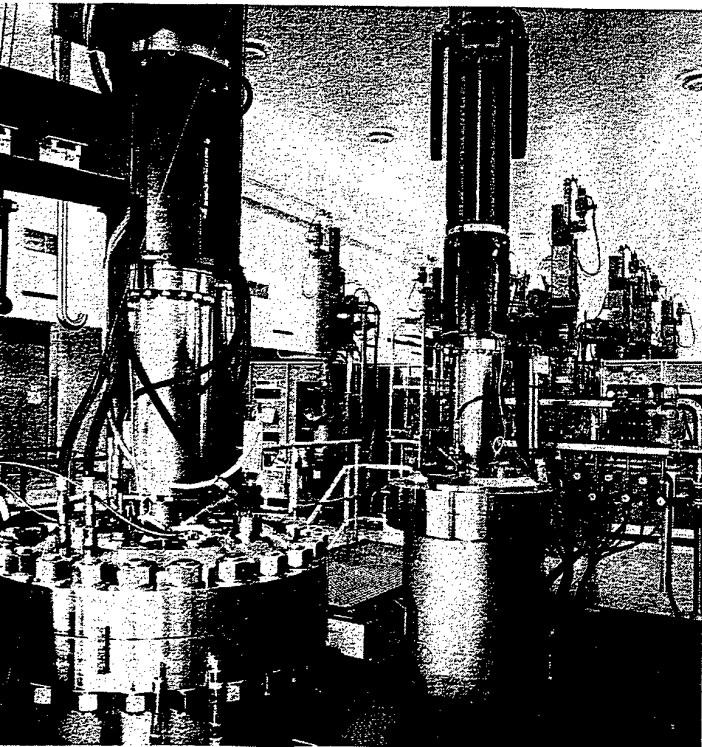
Furthermore, the investigation of the Light-Point-Defect density (LPD) clearly shows that the specific LPD density of 6"-wafers is very similar to that of 4"-wafers.

Acknowledgements

Financial support by the Bundesministerium fuer Forschung und Technologie (01 BM 404/6) is gratefully acknowledged. Thanks are also given to Dr. R. Bindemann for his helpful discussion and the critical reading of the manuscript.

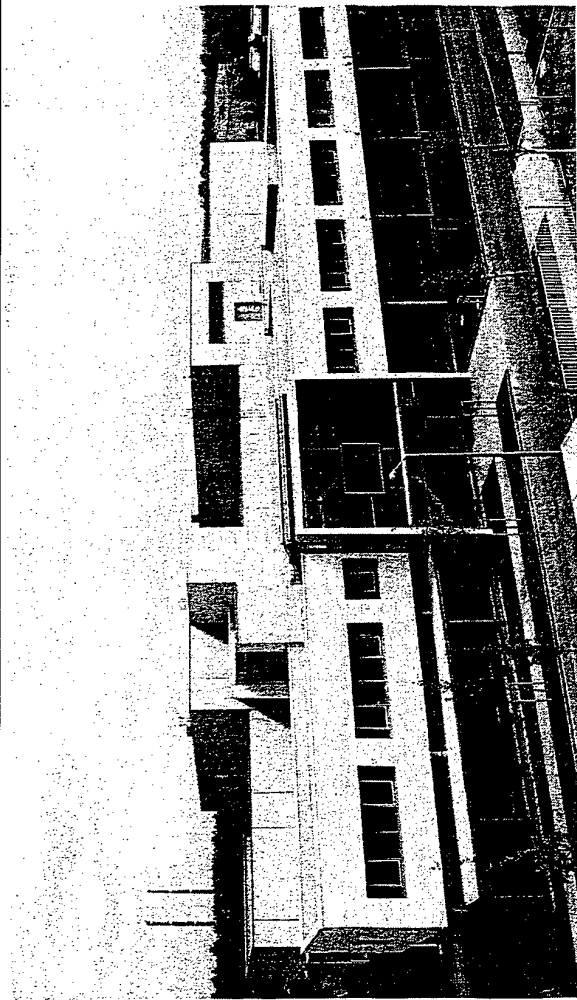
References

- [1] J. Fainberg, H.-J. Leister and G. Müller, *J. Cryst. Growth* 180 (1997) 517.
- [2] R. M. Ware, P. J. Doering, B. Freidenreich, R. T. Koegl and T. Collins, *Semicond. Sci. Technol.* 7 (1992) A224.
- [3] B. Hoffmann, M. Jurisch, G. Kissinger, A. Köhler, G. Kühnle, T. Reinhold, W. Siegel and B. Weinert, in: *Proc. SIMC'9*, Toulouse, France, 1996, p. 63.
- [4] R. Stibal, J. Windscheif and W. Jantz, *Semicond. Sci. Technol.* 6 (1991) 995.
- [5] W. Siegel, G. Kühnel, C. Reichel, M. Jurisch and B. Hoffmann, *Mat. Sci. Eng. B44* (1997) 238.
- [6] M. Yamada, *Rev. Sci. Instrum.* 64 (1993) 1815.
- [7] M. S. Wdowik, *US-Conf. on GaAs Manufacturing*, April 23, 1990, Reno, USA.



6" LEC GaAs single crystal from 20 kg melt

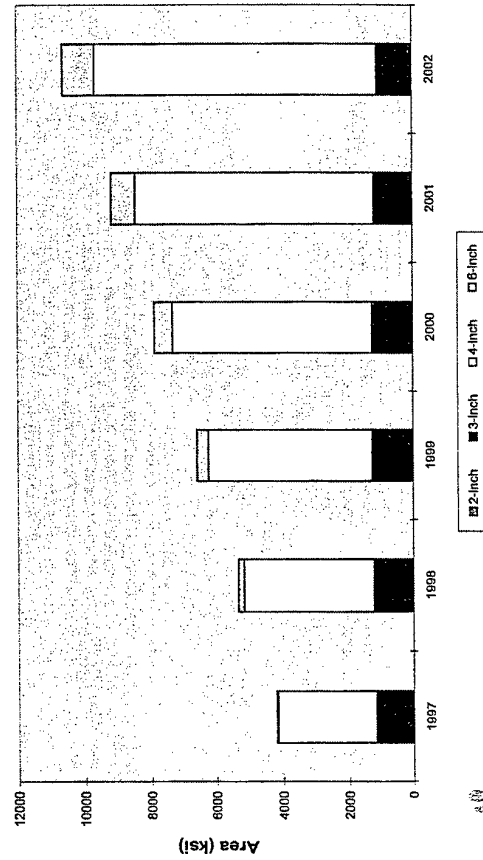
Freiberger



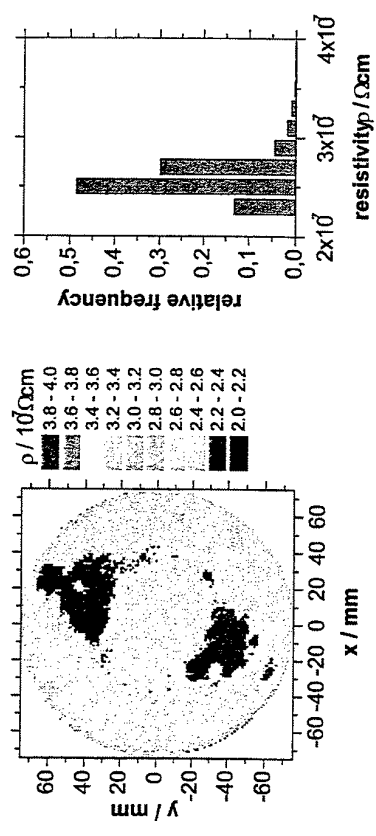
New production facility of FCM

Freiberger

GaAs SI Wafer Merchant Market by Area: 1997 - 2002
by Strategy Analytics, December 1997

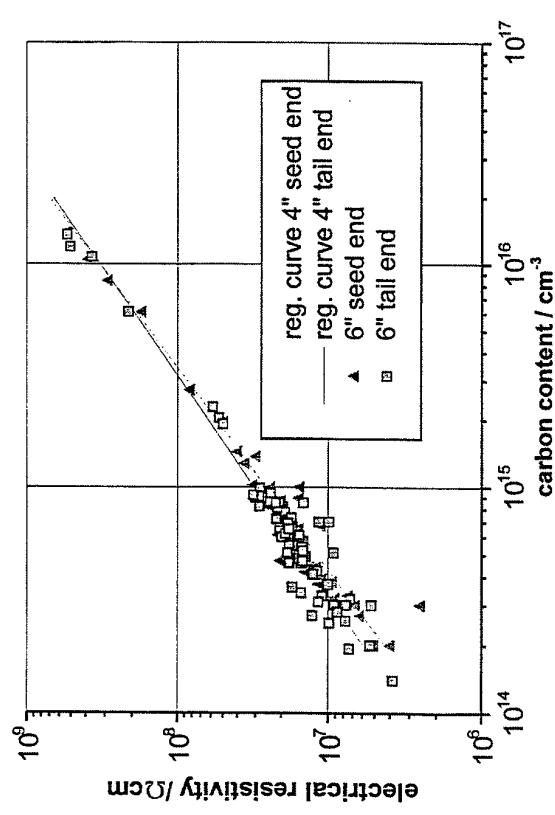


Freiberger

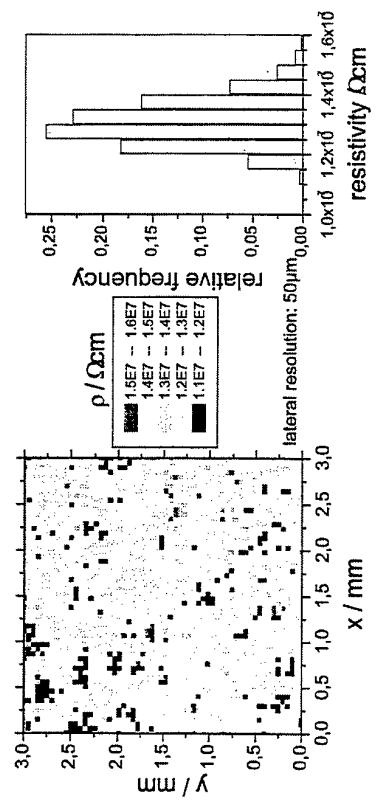


TDCM-topograph of a 6" low carbon wafer

Freiburger

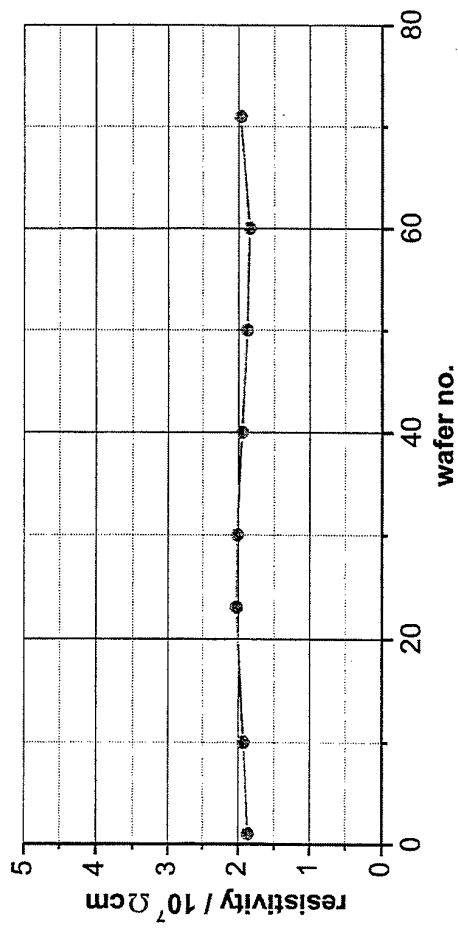


Electrical resistivity of 6" crystals in dependence on the carbon concentration, lines indicate corresponding data of 4"-crystals

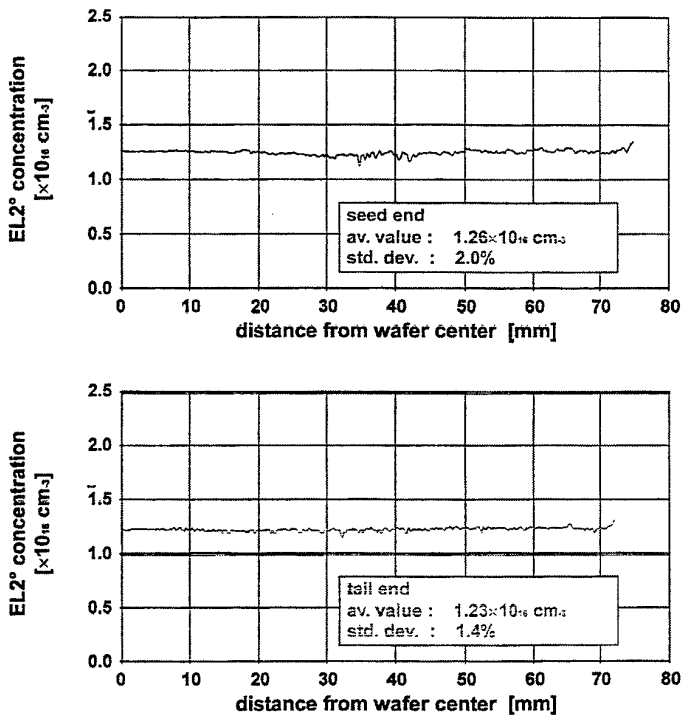


PCT - mapping (tail-end, R/2) of a 6" crystal

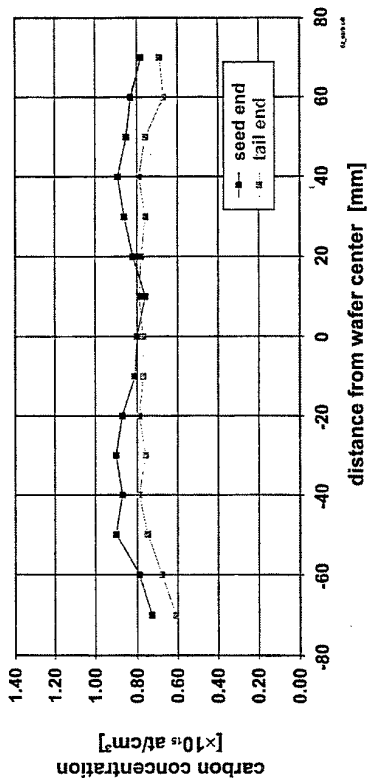
Freiburger



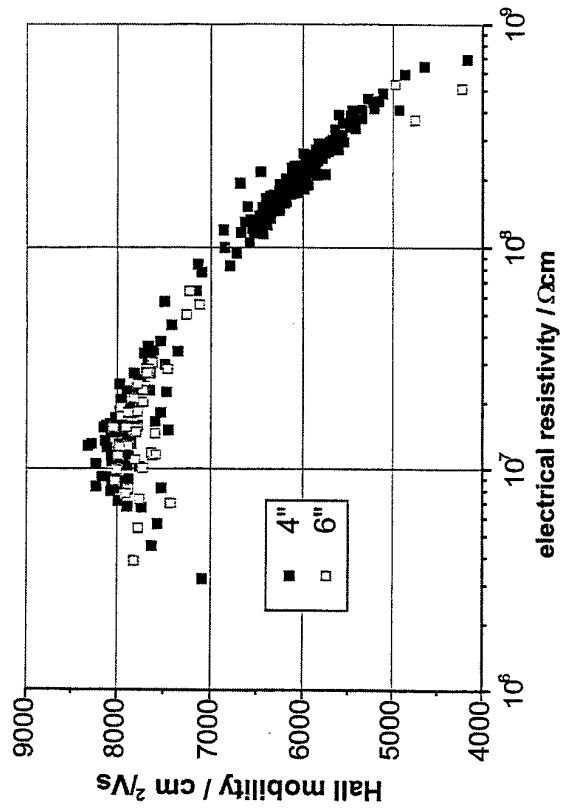
Electrical resistivity along 6" - crystal axis



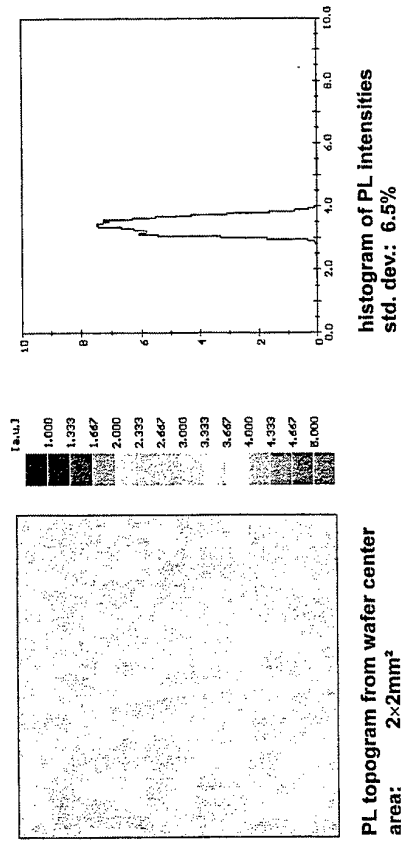
Radial Distribution of EL2⁺
in an undoped 150mm LEC-GaAs crystal



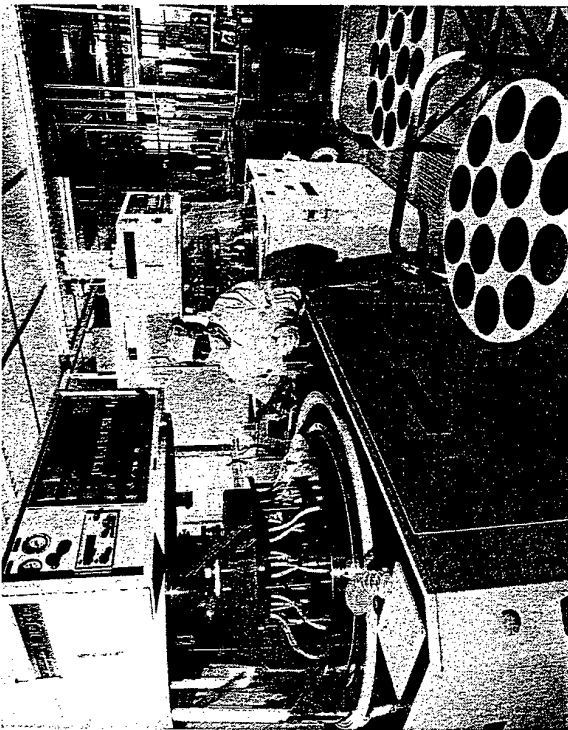
Radial Distribution of Carbon
in an undoped 150mm LEC-GaAs crystal



Hall mobility in relation to electrical resistivity for 6" crystals
in comparison to 4" material



PL topogram of an undoped 150mm LEC-GaAs wafer



GaAs polishing area with single and double side equipment

Freiberger

150mm GaAs Wafer in Superflat Quality

LTV

32 - 20.0 x 20.0 mm sites
5 mm edge exclusion

45	57	28	58						
42	39	32	52	48	38				
47	48	24	44	39	47				
60	54	49	45	40	59				
41	26	36	33	48	54				
52	54	44			34				

LTV_{max} = 0.60 µm

LTV_{avg} = 0.44 µm

LTIR

32 - 20.0 x 20.0 mm sites
5 mm edge exclusion

46	57	29	63						
41	35	32	47	43	36				
42	41	28	47	48	53				
55	46	45	38	38	53				
39	31	40	30	53	52				
52	51	40	36						

LTIR_{max} = 0.63 µm

LTIR_{avg} = 0.43 µm

LFPD

32 - 20.0 x 20.0 mm sites
5 mm edge exclusion

31	34	15	41						
22	22	16	31	22	20				
21	21	13	34	29	32				
28	25	23	19	22	35				
22	16	25	20	27	37				
36	27	23	22						

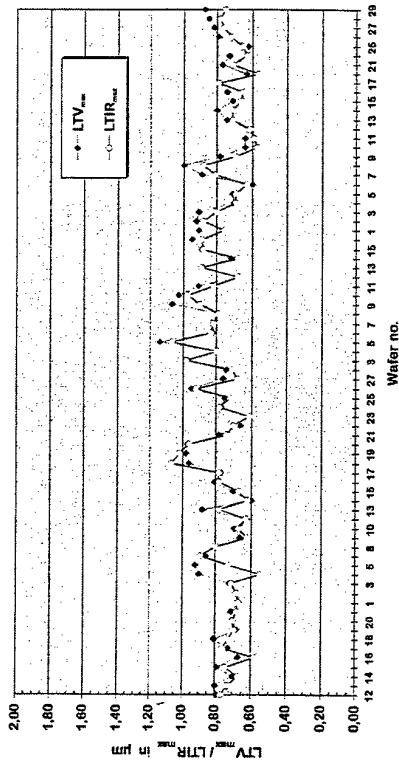
LFPD_{max} = 0.41 µm

LFPD_{avg} = 0.25 µm

Freiberger

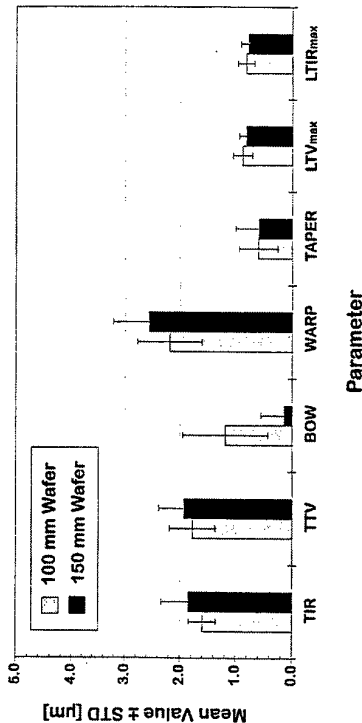
Geometrical Data for Local Flatness of a 6" S.I. GaAs Wafer
(#25889-006); all units in 0.01 µm

Geometrical Data of Local Flatness of 6" GaAs Wafers



Comparison between LTV_{max} and LTIR_{max} values of a batch of 50 6" GaAs wafers (20 x 20mm site size; 32 sites; 5mm edge exclusion)

Freiberger



Geometrical characteristics of a 6"-wafer

Freiberger

High Pressure Liquid Encapsulated Growth of Semi-Insulating GaAs

Rowland Ware
III-V Materials, AMP – M/A-COM

Abstract

The III-V compounds, particularly the commercially important members, GaAs, GaP and InP, possess significantly high partial pressures of the volatile elements at their melting points. This means that an attempt to grow these materials in a standard Czochralski crystal puller, would result in the distillation of the phosphorus or arsenic to the cold walls of the apparatus. Early growth of GaAs by the Czochralski method employed variations on the "hot wall" technique, with the whole of the operating chamber was kept at about 615°C, at which temperature the vapour pressure of arsenic is equal to the dissociation pressure of the melt, and no condensation takes place on the walls. These methods, whilst producing high quality small crystals, were extremely difficult to scale up, due to their employment of high temperature rotating seals, or magnetic levitation. The situation was transformed by the invention of the Liquid Encapsulated Czochralski technique by Metz, Miller and Mazelski¹ who used it to grow lead telluride. The method was soon applied to GaAs and InP by Mullin et al.² and to GaP by Bass & Oliver³

In the LEC technique, the melt is covered by a layer of molten boric oxide. So long as the overpressure of inert gas, usually argon, exceeds the dissociation pressure of the melt, then the loss of arsenic is slight, being confined to that which diffuses through the oxide.

At first, crystals grown by this method, were n-type semiconductors because the starting material was synthesized in silica crucibles. Semi-insulating material was obtained by chromium doping. Direct synthesis^{4,5} in the puller yielded 'undoped' material that was semi-insulating, with resistivities in the range 1.10^7 to 1.10^8 ohm.cm. In this process, arsenic, gallium and boric oxide are loaded into the crucible. The puller is evacuated and pressurised to about 30 atmospheres with an inert gas. Upon heating the boric oxide melts and encapsulates the charge at about 450 – 550°C. An exothermic reaction between gallium and arsenic is initiated at about 800°C (melting point of arsenic is 818° at 29 atm.) This process has been scaled up from 500-600gm to 24kg, with weight losses remaining at a few tens of grams.

Five key technologies enabled HPLEC to become the major method for the production of semi-insulating GaAs. They are

- Liquid encapsulation (Mullin et al²)
- Direct synthesis (Rumsby and Ware⁴, Aucoin⁵)
- PBN crucibles (Swiggard et al.⁶)
- Ingot anneal (Rumsby, Ware et al.⁷)
- Automatic diameter control (Bardsley et al.^{8,9})

The direct synthesized material has a very low level of n-type impurities, so that the dominant shallow impurity is carbon, p-type in GaAs. As a result the material is semi-insulating so long as the concentration of the deep donor EL2 is greater than the net concentration of shallow acceptors i.e.

$$N_{EL2} > N_{sa} > N_{sd}$$

And the carrier concentration is given by

$$n \propto N_{EL2} / (N_{sa} - N_{sd})$$

The first condition is easily met. In well annealed material grown from stoichiometric or slightly arsenic -rich melts, the EL2 concentration falls in the range $1\text{-}2\cdot 10^{16}\text{ cm}^{-3}$. Provided that the background concentration of electrically active impurities is less than about $5\cdot 10^{14}\text{ cm}^{-3}$, the carrier concentration, and hence the resistivity, become a function of the carbon concentration[C].

We have shown that the concentration of carbon in the crystal is a function of the carbon monoxide concentration in the puller atmosphere, and by monitoring and controlling this parameter, have controllably grown crystals with [C] ranging from $< 5\cdot 10^{14}$ to $> 5\cdot 10^{16}\text{ cm}^{-3}$, yielding resistivities from $1\cdot 10^7$ to $5\cdot 10^8\text{ ohm.cm}$. Low CO concentrations are obtained by gettering the puller atmosphere, and high concentrations by adding CO_2 , which is converted to CO by reaction with the hot graphite. The puller atmosphere is monitored throughout the growth run with a Residual Gas Analyzer (Leybold Inficon Transpector CIS - 100). By this means crystals can be grown with tightly controlled resistivity to meet the device manufactures needs, rather than relying on selection of crystals from a loosely controlled process.

In semiconductor materials production, there is a strong economic pressure to increase the size of the crystals. This can be clearly seen in the silicon industry where the crystal diameter has increased from 0.525 inches to 12 inches over about thirty years, and the charge weight from a few grams to several hundred kilograms. The reasons are clear. The device manufacturer's economics improve with larger diameter wafers, since the cost of wafer processing does not increase linearly with area, and larger wafers give better utilization of 'real estate'. However to increase the crystal diameter at constant charge weight actually increases the substrate makers cost per unit area of wafer. Thus for larger diameters lengths must increase, and over the last few years we have demonstrated an increase in charge weight for 100mm diameter ingots from 8 to 24 kg. The critical factor in growing long crystals is control of the melt/crystal interfaceshape. This increase in crystal size has been made possible by the availability of a range of high pressure pullers of increasing size.

It is also important to control the diameter of the long crystals, since otherwise grinding the crystal to exact wafer diameter would cause excessive material wastage. The automatic diameter control system developed by Bardsley et al ⁸ fulfils this function well, provided that the thermal design of the puller yields stable growth conditions. Using this method crystals have been grown with diameters of $110 \pm 1\text{ mm}$ over lengths of 420mm.

Further development of this process in the MR 15/25 puller is expected to lead to crystals of 110 mm diameter weighing 40kg, and 160mm dia. weighing 60 kg. Mechanical handling systems will be necessary to process these crystals into wafers.

References

1. Metz, E.P.A., Miller, R.C. and Mazelsky, R. (1962) J.Appl.Phys., **33**, 2016
2. Mullin J.B., Heritage, R.J., Holliday, C.H., and Straughan, B.W. (1968) J.Cryst.Growth **3 & 4**, 281
3. Bass, S, and Oliver, P.E., (1968) J.Cryst.Growth **3 & 4**, 286
4. Rumsby, D., and Ware R.M., (1979) IEEE Workshop on Compound Semiconductors for Microwave Materials and Devices, Atlanta.
5. Aucoin, T.R., Ross, R.L., Wade, M.J., and Savage, R.O. (1979) Solid State Tech., **22**, 59
6. Swiggard, E.M., Lee, S.H., and von Batchelder F.N., (1977) Inst.Phys.Conf.Series, No. 33b IOP Bristol, 23.
7. Rumsby, D., Smith B., Ware, R.M., Brozel M.R., and Foulkes, E.J., (1983) GaAs IC Symposium, Phoenix, 34.
8. Bardsley, W., Green G.W., Holliday C.H., and Hurle D.T.J., (1972) J.Cryst.Growth., 277
9. Bardsley, W., Cockayne, B., Green, G.W., Hurle, D.T.J., Joyce, G.C., Roslington, J.M., Tufton, P.J., and Webber, H.C., (1974) J.Cryst.Growth **24 & 25**, 369

Key Enabling Technologies

- Liquid Encapsulation
- Direct Synthesis
 - ‘undoped’ semi-insulating GaAs
- PBN Crucibles
- Ingot Anneal
 - stress relief, electrical uniformity
- Automatic diameter control



High Pressure LEC Growth of Semi-Insulating GaAs

Rowland Ware

III-V Materials

M/A-COM



Summary

- The LEC Process
- Undoped Semi-insulating GaAs
- Resistivity Control by Carbon Concentration
- The Thrust to Larger Crystals
 - Economic incentives
 - Maintaining single crystallinity
 - Automatic diameter control
- Future Trends

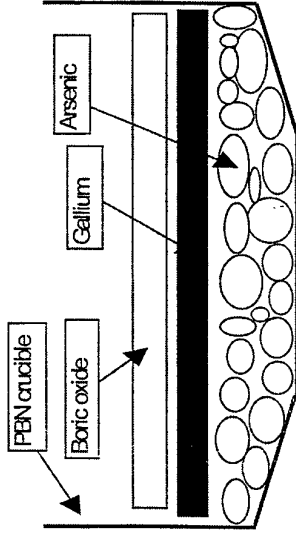


Carbon Controlled GaAs Crystal growth

- Factors Affecting Carbon Incorporation
 - Carbon Partial Pressure
 - Concentration and Absolute Pressure
 - Diffusion Through Boric Oxide
 - Temperature, Temperature Gradient and Concentration Gradient
 - Water in Boric Oxide
 - Reactions at Oxide /Melt Interface
 - Segregation between Melt and Crystal



Direct Synthesis of GaAs



Resistivity Control

- Governing Processes:
 - In the growth chamber:
 - $C + H_2O = CO + H_2$
 - $2C + O_2 = 2CO$
 - $CO_2 + C = 2CO$
 - Interaction with the melt
 - $2C_{melt} + 2[OH]_{borox} = 2CO + H_2$
 - $4Ga_{melt} + 2[OH]_{borox} = 2Ga_2O_{borox} + H_2$
 - $CO + 2Ga = C + Ga_2O$
 - Crystal/melt interface
 - $[C]_{crystal} = k_{eff}[C]_{melt}$



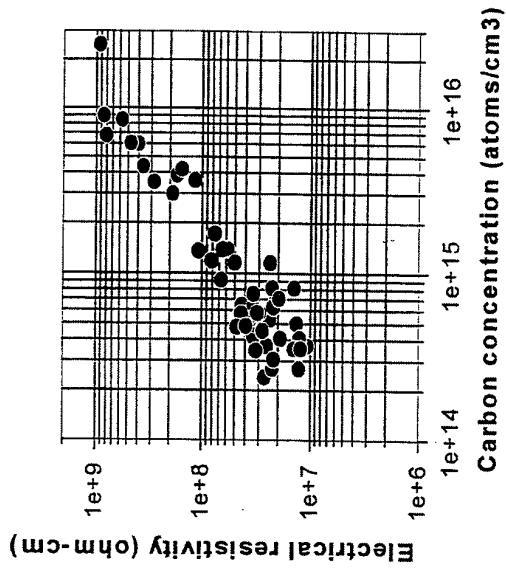
‘Undoped’ semi-insulating GaAs

- 3 Level model
- Semi - insulating condition

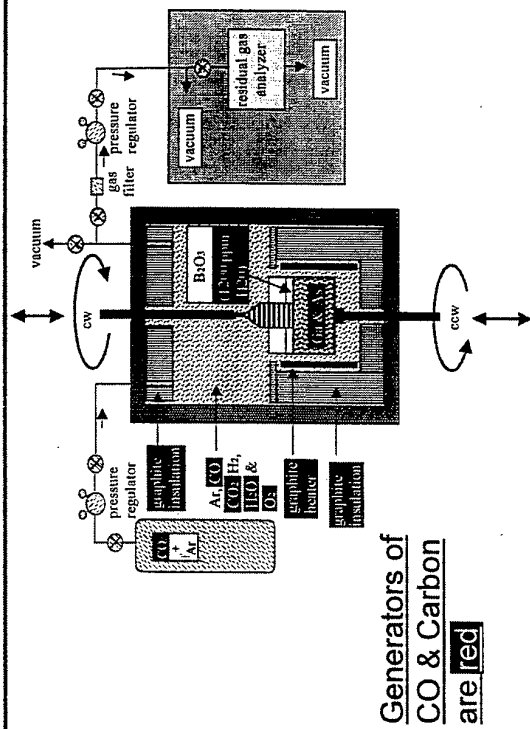
$$N_{E12} > \sum N_{sa} > \sum N_{sd}$$
- $n \propto N_{E12} / (\sum N_{sa} - \sum N_{sd})$
- Carbon - main shallow acceptor & key to resistivity control



[C] vs. electrical resistivity

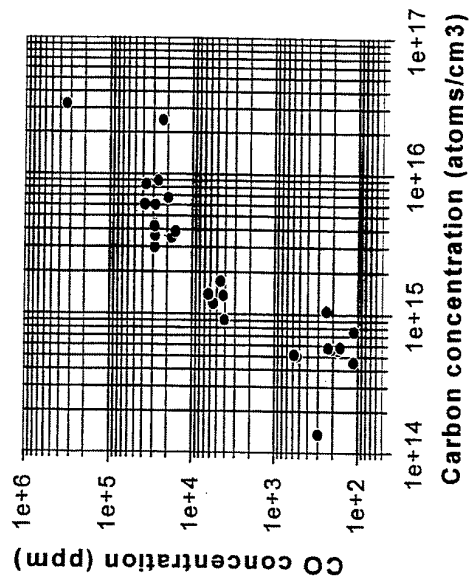


Crystal puller, gas manifold, & RGA

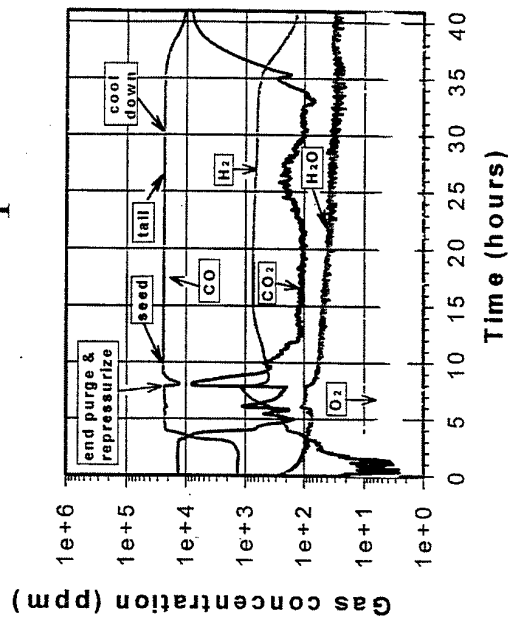


Generators of
CO & Carbon
are red

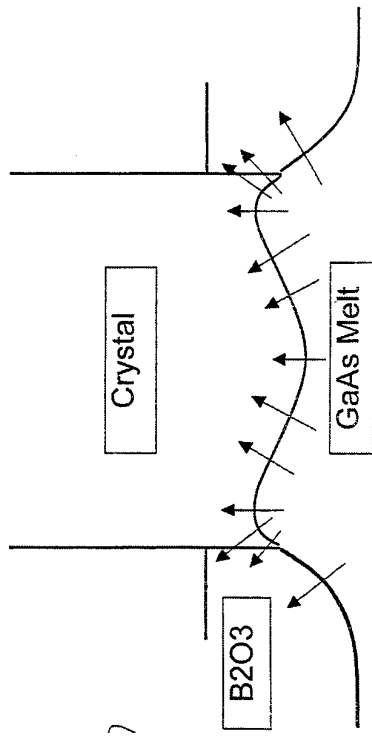
[C] vs. [CO]



Controlled atmosphere run



Heat Flux at Interface causing peripheral turnaround



Why Large Crystals ?

- Increased diameter - improves economics of device manufacture
- Increased length - improves economics of substrate manufacture

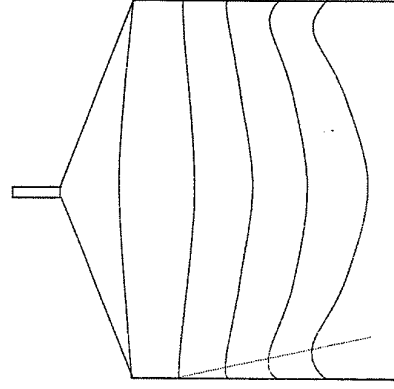


Diameter Control

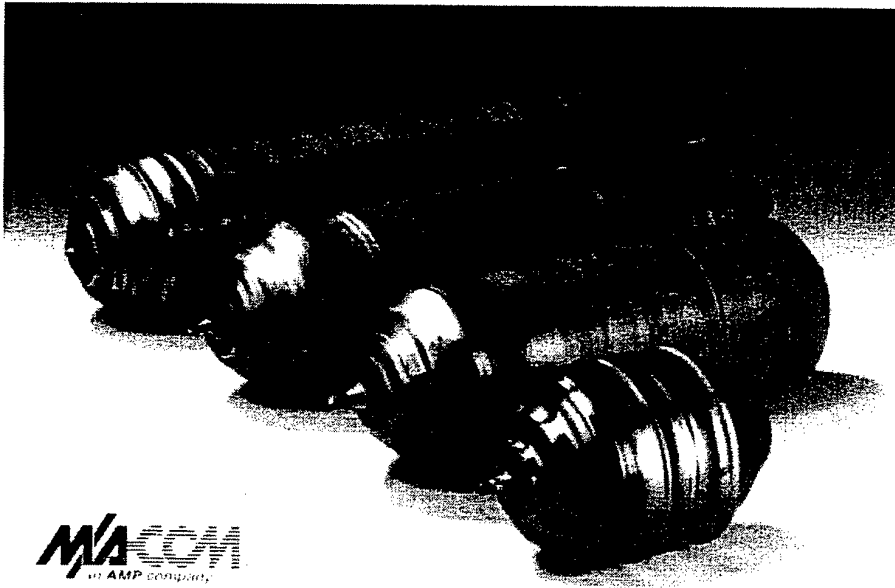
- Passive
 - e.g. floating ring or 'coracle'
- Active
 - Open loop temperature ramps
 - Closed loop optical control
 - Closed loop weight control



Melt /Crystal Interfaces



Increasing crystal length @ 4" diameter (1995 -6)



Future Trends

- Still larger crystals
 - 4" diameter / 40 kg / 775 wafers
 - 6" diameter / 60 kg / 430 wafers
- Mechanical handling of ingots
- Complete process automation
- Stress reduction by improved thermal environment
- Useful process modelling



InP Crystal and Wafer Manufacturing

Ian R. Grant
Wafer Technology Ltd
34 Maryland Rd, Tongwell
Milton Keynes MK15 8HJ, UK

InP is well established as the base material for opto-electronic components in long distance fibre optic telecommunications and is becoming increasingly important in mm wavelength communications devices. Initial technological interest in the material arose because of its favourable electron transport properties for high speed operation and its optimum bandgap for solar cell applications, but the principal uptake has been as a lattice matched substrate for the epitaxial growth of direct gap alloys with band energies between 1.2 and 1.6 eV, suitable for lasers and detectors for low loss, low dispersion, fibre transmission.

The greater difficulty and expense of material processing compared with GaAs has delayed any extensive utilisation for microwave electronic devices. Recent requirements for operation in the 100 GHz range have renewed interest in InP for electronic devices and this is leading to demand for large diameter InP wafers [1].

Preparation of the compound is governed by the high vapour pressure of phosphorus over molten InP. Whereas GaAs production may be simplified by the in-situ direct synthesis of the elements at a uniform temperature in the single crystal growth furnace, the very high P vapour pressure at the reaction temperature renders this impractical for InP. Instead the approach is to thermally isolate the In and P components and supply P vapour at sufficient pressure from a controlled solid source to obtain a stoichiometric melt. This can either be achieved within a sealed ampoule with separate temperature controlled melt and P source zones, or under a liquid (boric oxide) encapsulant by bubbling P vapour through an In / InP melt above the compound melting temperature, all contained within a pressurised vessel.

High purity, undoped polycrystalline ingots prepared by such methods have weights up to 8kg and residual n-type carrier concentration $<5 \times 10^{15} \text{ cm}^{-3}$. The polycrystalline compound is then used to provide the growth charge for

single crystal production employing the Liquid Encapsulated Czochralski (LEC) technique. Optionally, the same method may be used to crystallise an intermediate, large grain polycrystalline ingot for improved or more consistent stoichiometry and purity.

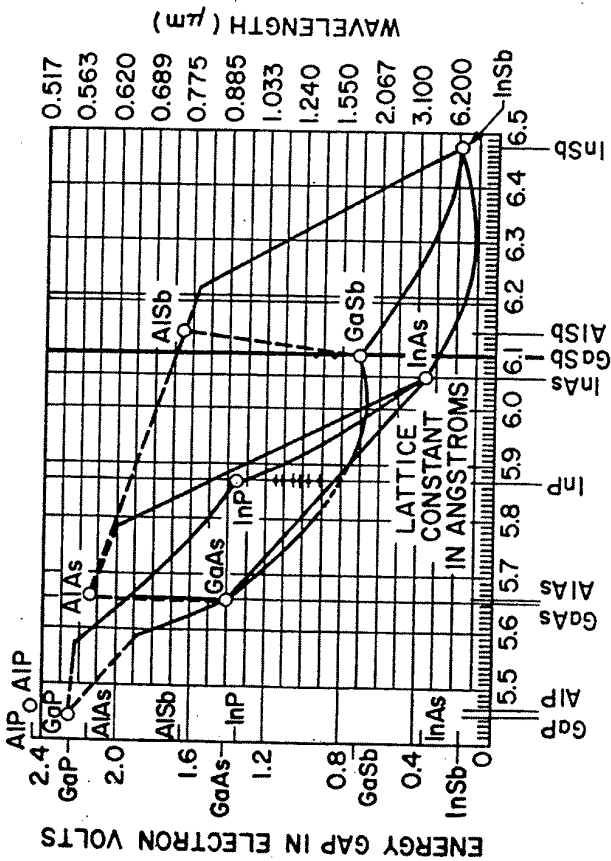
Single crystal growth is carried out in similar high pressure LEC equipment to that used for GaAs. Melt weights from 1 kg to around 8kg are used for growth at diameters from 2 inches to 4 inches. The ambient pressure is typically 40 bar. Direct doping of the melt is applied to achieve n-type (Sn, S); p-type (Zn, Cd) and semi-insulating (Fe) electrical behaviour.

The high ambient gas pressure leads to strong and turbulent convective heat flows in the growth chamber, supporting large and fluctuating temperature gradients. The consequences of this are increased dislocation density and interface instabilities giving rise to problems of diameter control and twinning. Efforts in crystal growth technology have therefore been concentrated on minimising such effects and on improving crystallinity and uniformity. Variants on the LEC method, such as VCZ [2] are used in production and other techniques, principally VGF [3], are being investigated.

Wafers are manufactured and used commercially at diameters of 2 and 3 inches, with dimensional specification parameters similar to those for GaAs. Surface polishing, cleaning and wafer packaging is designed for "epi-ready" behaviour.

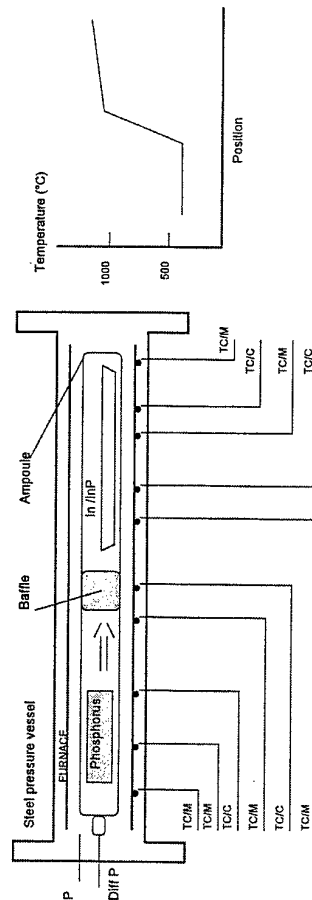
References

- [1] J. Elliott et al., Proc. Int. Conf. on Indium Phosphide & Related Materials, Cape Cod, (1997), IEEE, pp 501–504.
- [2] Y. Yabuhara et al., Proc. Int. Conf on Indium Phosphide & Related Materials, Schwabisch Gmund, (1996), p35
- [3] W.A. Gault et al., J. Cryst. Growth, 74, (1986), p491



Ref: R. A. Laudise J. Crys. Growth 65 1 (1983)

INP POLYCRYSTALLINE SYNTHESIS SYSTEM

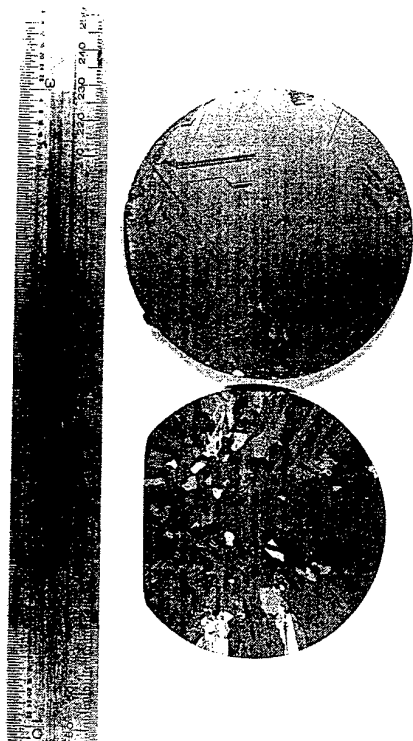


PROPERTIES OF InP

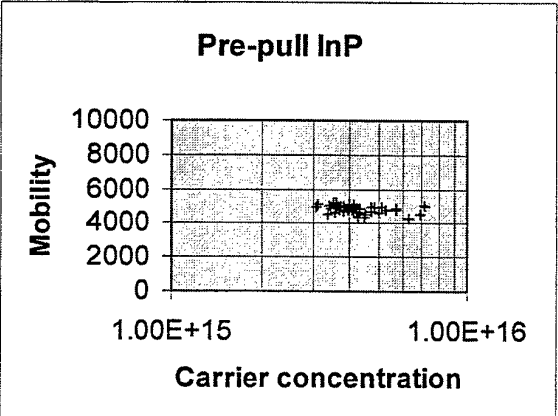
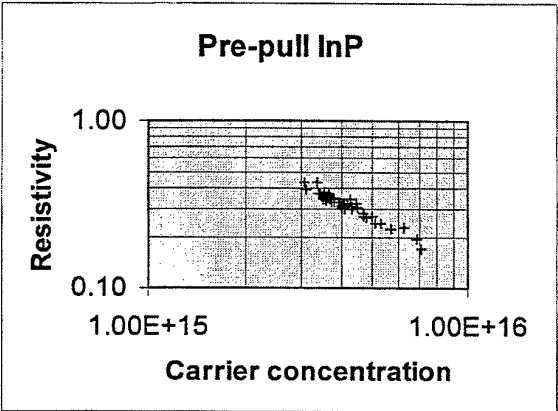
Crystal Structure	Zincblende (FCC)
Lattice parameter (Å)	5.868
Bandgap (eV)	1.35 [Direct]
μ_e (cm ² /Vs) R.T.	4700
μ_h (cm ² /Vs) R.T.	150
Intrinsic Res. (ohm.cm)	8x10 ⁷
Density (g/cm ³)	4.79
Thermal Cond (W/cm.deg)	0.68
Melting Temp (°C)	1062
Dissoc. Press at M.P. (bar)	27

SEMICONDUCTOR WAFER MARKETS

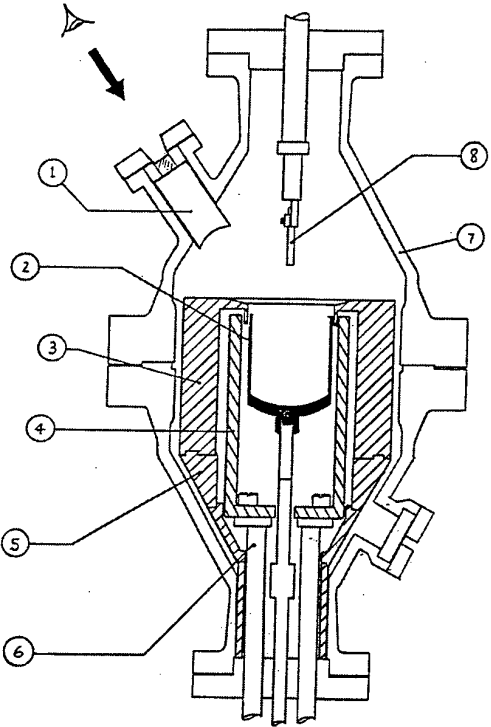
Material	Wafer Forms	Applications	Market Size (\$M)	Price (\$/sq.in)
GaAs doped Si, Zn	D, 2", 3"	Opto (LED, LD) Microwave Discrete	60-80	12 - 25
GaAs SI (Un)	2", 3", 100mm (150mm)	MMIC, Digital IC	80	15 - 20
GaP	2", 2.5"	Visible LED	60	10 - 15
InP	2", 3"	Fibre Opt. Telecom mm wave	20	50 - 80
GaSb, InSb	Irreg, 2", (3")	Long λ (2-5 μ m) emitters & det.	2	80 - 100
Si	Up to 200mm (300mm)	VLSI etc.	>2500	<5



Element	Conc.	Element	Conc.	Element	Conc.
Li	<1	Mn	<0.2	In	Major
Be	<0.7	Fe	<0.3	Sn	<0.8
B	100	Co	<0.3	Sb	<0.4
C	1300	Ni	<0.3	Te	<0.9
N	200	Cu	<2	I	<1
O	1000	Zn	13	Cs	<1
F	<25	Ga	<30	Ba	<0.2
Na	<0.7	Ge	<2	La	<0.06
Mg	<0.5	As	90	Ce	<0.07
Al	<0.3	Se	<5	Hf	<0.1
Si	15	Br	-	Ta	-
P	Major	Rb	<0.2	W	<0.2
S	56	Sr	<0.2	Pt	<0.4
Cl	16	Y	<0.2	Au	<10
K	<50	Zr	<0.1	Hg	<1
Ca	<10	Nb	<500	Tl	<0.2
Sc	<0.4	Mo	<0.5	Pb	<0.4
Ti	<0.3	Pd	-	Bi	<0.2
V	<0.2	Ag	<1	Th	<0.1
Cr	<0.7	Cd	<10	U	<0.06



351 PULLER



KEY

- 1. Viewing rod
- 2. Crucible support (attached to crucible lift rod)
- 3. Graphite heat shield
- 4. Graphite heater element
- 5. Graphite heat shield support cone
- 6. Leadthroughs
- 7. Water cooled chamber
- 8. Seed holder and seed (attached to pull rod)

InP DOPANTS AND APPLICATIONS

DOPANT	APPLICATION	CRYSTAL PROP	MARKET (%)
Un	Source for LPE	n-type $< 1 \times 10^{16} \text{ cm}^{-3}$	1
Fe	OEIC , mm wave	n-type SI $> 10^7 \Omega \cdot \text{cm}$	22
S	LD, LED, detectors	n-type $> 1 \times 10^{18} \text{ cm}^{-3}$ "zero-D" $< 500 / \text{sq.cm}$	47
Sn	LD, LED, detectors	n-type $> 1 \times 10^{18} \text{ cm}^{-3}$	22
Zn	LD, LED, detectors	p-type $1\text{--}10 \times 10^{18} \text{ cm}^{-3}$ low epd	8

Fe:InP R2459 (ICI)

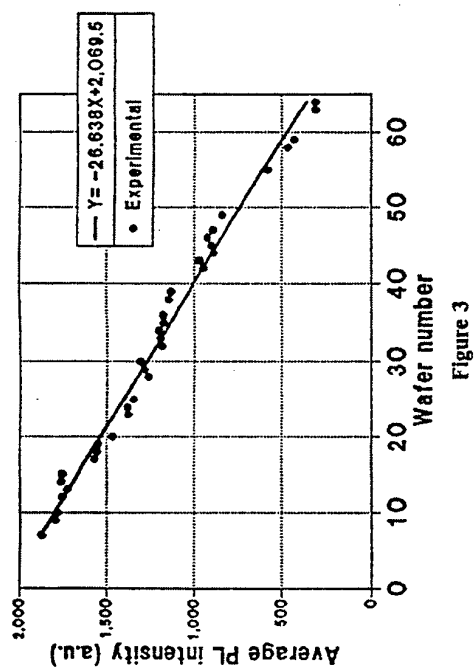


Figure 3

Fe:InP R2459 (ICI)

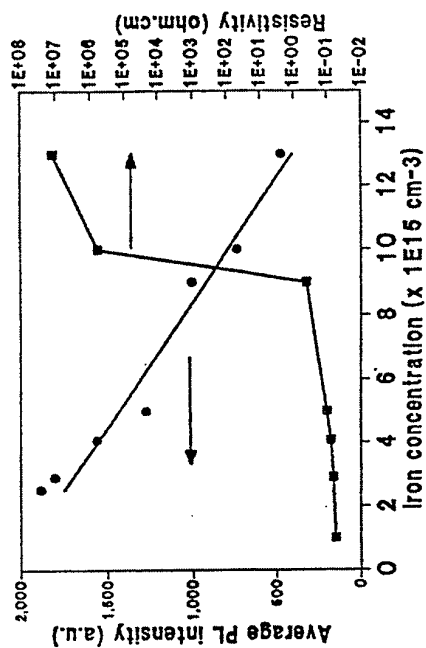
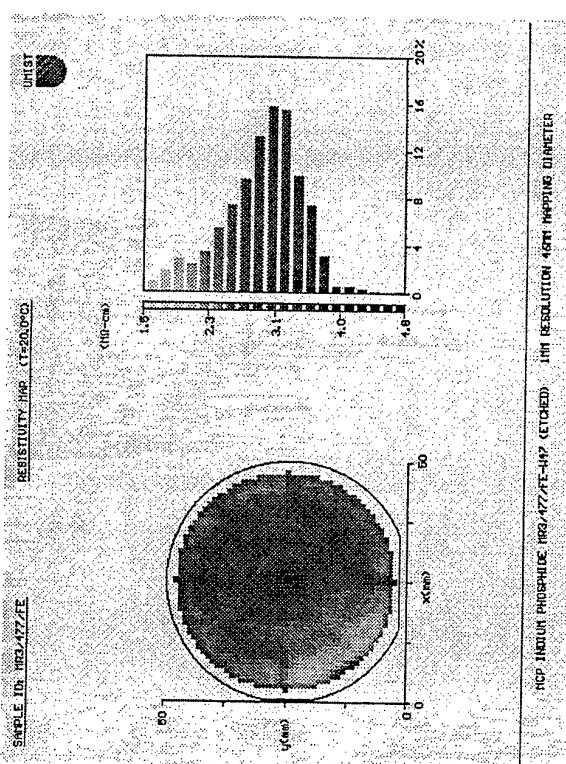
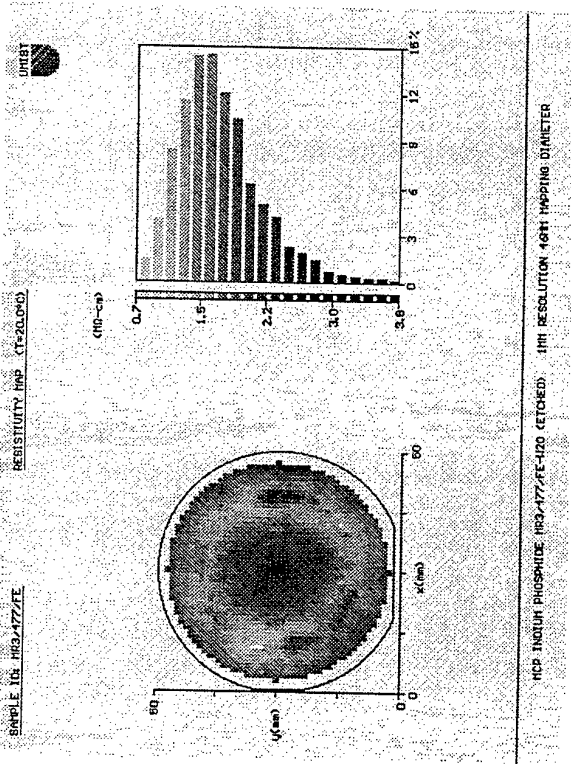


Figure 4



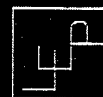
RT PHOTOLUMINESCENCE MAPPINGS

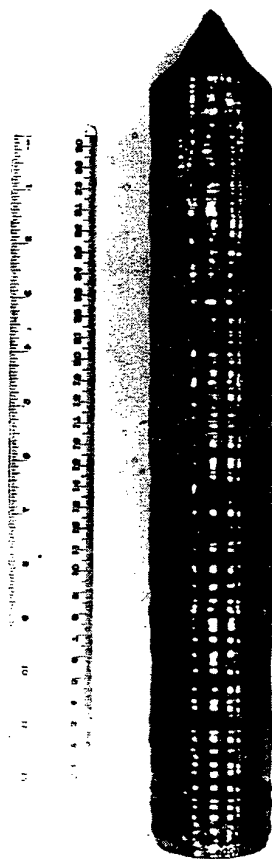
2 inch wafer

2.54*2.54 mm

Fe: InP R2456Fe/31

Laboratoires d'Electronique Philips

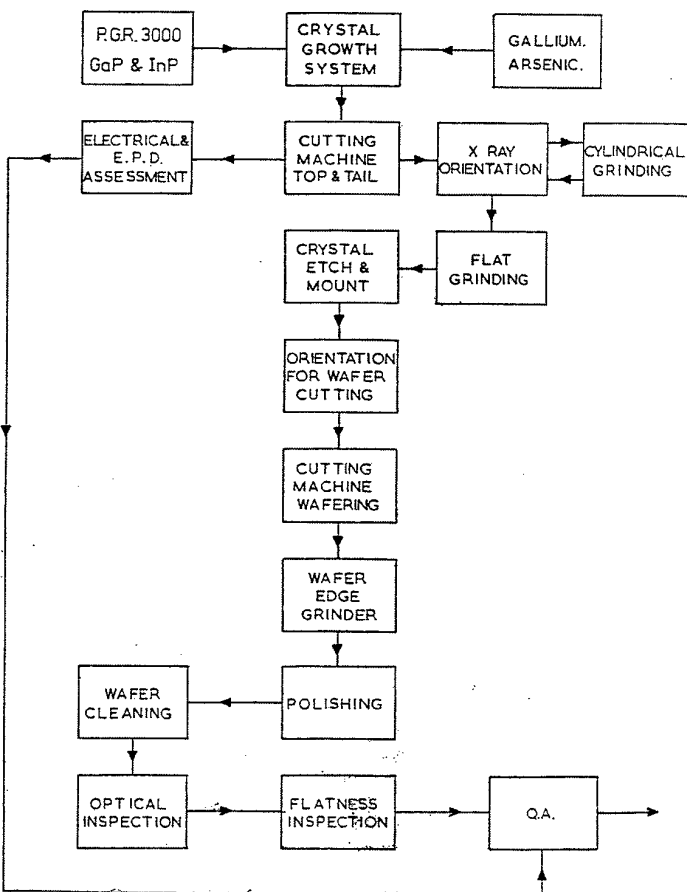




3 INCH GROWTH PARAMETERS

Growth Equipment	CI354 HPLEC
Ambient	Nitrogen @ 600 psi
Crucible	SiO ₂
Crucible Diam	150mm
Boric Oxide Weight	600g
Charge	Pre-pull InP ($<5 \times 10^{15} \text{ cm}^{-3}$)
Charge Weight	3.5 kg
Seed	6x6mm (100)
Dopant	Fe
Pull rate	~10mm/hr
Rotations	Crystal and Crucible

FLOW DIAGRAM OF III-V WAFER PRODUCTION



2-inch InP POLISHED WAFER PROPERTIES

PROPERTY		VALUE / DESCRIPTION	TOLERANCE (±)
Diameter (mm)		50.8 50.0	0.3
Thickness (μm)		300 - 500	25
Surface Plane		(100)	0.1 deg
Surface Misorientation		0 - 2 deg	0.1
Flat position		Clockwise [EJ] Counterclockwise	0.1deg on major 1 deg on minor
Flat length	Major	16	2
	Minor	8	
Finish	Front	"Epi-ready" polish Polish or cut/etched	
	Rear		
Flatness (μm) [TIR, TTV, Bow, Warp]		<12	
Lasermarking		Alpha-numeric Major flat	
Packaging		Individual in N ₂	

Growth Technology of InP and CdTe Single Crystals

T. Asahi, K. Kainosho, K. Kohiro and O. Oda

Central Research Laboratory, Japan Energy Corporation

3-17-35 Niizo-Minami, Toda, Saitama 335-8502, Japan

TEL: +81 48 433 2051, FAX: +81 48 445 5400, e-mail: asahi@j-energy.co.jp

Abstract

II-VI and III-V compound semiconductor materials which have advantages in their physical and optical properties are promising materials for optical and electronic devices. GaAs is applied for high frequency devices such as MESFETs, HEMTs and HBTs. InP is used as substrates for optical devices like LDs and PDs, and it is expected for high frequency devices such as HEMTs and HBTs. CdTe and CdZnTe are applied as substrates for HgCdTe epitaxial films which are used for far-infrared detectors. Semi-insulating CdTe is used for X-ray or Gamma-ray detectors. However the production amount of these compound semiconductors-based devices is much less than that of Si devices. 250mm diameter Si wafers are mainly used in device production, while in the case of GaAs which have the largest market scale among compound semiconductors, only 75 mm and 100 mm wafers are used in device production.

It is therefore very important to produce high quality large diameter compound semiconductor crystals in order to accelerate the advancement of the compound semiconductor based devices. In this context, we have been investigating better growth methods for high quality large diameter InP and CdTe single crystals.

50mm diameter InP single crystals are mainly produced by the LEC method. 75mm diameter crystals can be grown by the PC-LEC / VCZ methods, in which the phosphorous pressure is controlled to prevent the decomposition of grown crystals.[1,2]. Kohiro et al first succeeded in developing the PC-LEC method for growing long length 75mm diameter InP single crystals. Grown crystals showed good qualities compared with the same diameter crystals grown by the conventional LEC method[1]. Recently, the VGF method which has the advantage in growing low dislocation density crystals is attracting many attentions, because in this method crystals can be grown under low axial temperature gradients which can reduce the thermal stress in the crystals.

It is however known that the growth of InP single crystals by the VGF method is very difficult because of the easiness of twin occurrence due to its low stacking fault energy. It seems that the temperature fluctuation causes twinning, because solidification and remelting at the solid-liquid interface are repeated by the temperature fluctuation. In the VGF method, since the axial temperature gradient is low, the solid-liquid interface position is largely influenced by the temperature fluctuation. There were only a few reports in the success of the growth of <100> InP single crystals by the VGF method[3,4]. Recently, we succeeded in the growth of twin-free 100mm

diameter <100> InP single crystals by the VGF method using a high pressure furnace[5]. In our experiment, the temperature fluctuation was reduced to less than $\pm 0.03^{\circ}\text{C}$ by controlling the gas flow. Temperature gradients were lower than $10^{\circ}\text{C}/\text{cm}$ and growth rates were larger than $0.4\text{mm}/\text{h}$. 8mm diameter <100> InP single crystals were used for seed crystals. The average EPD of grown crystals was about $2,000\text{ cm}^2$ which was much less than that of conventional LEC crystals.

CdTe and CdZnTe are also one of the most difficult material to grow single crystals among compound semiconductor materials because of its low thermal conductivity and its low stacking fault energy. We first succeeded in growing 100mm diameter CdZnTe single crystals by the VGF method without seed crystals as shown in Fig.1[6]. Crystals were grown under a low temperature gradient of less than $10^{\circ}\text{C}/\text{cm}$ and a growth rate of larger than $0.1\text{mm}/\text{h}$. The temperature fluctuation near the ampoule is less than $\pm 0.1^{\circ}\text{C}$. Crystals were grown to the spontaneous <111> orientation and the average EPD was $40,000 \sim 60,000\text{cm}^2$.

As mentioned above, InP and CdTe are difficult to obtain single crystals. It is however possible to grow high quality large diameter single crystals by the recent highly developed VGF technology. The VGF method has a short history in industrial production, but it is believed to become an important crystal growth method in production in the near future because of its possibility to be able to achieve high quality crystal growth with low labor cost and low furnace fabrication cost.

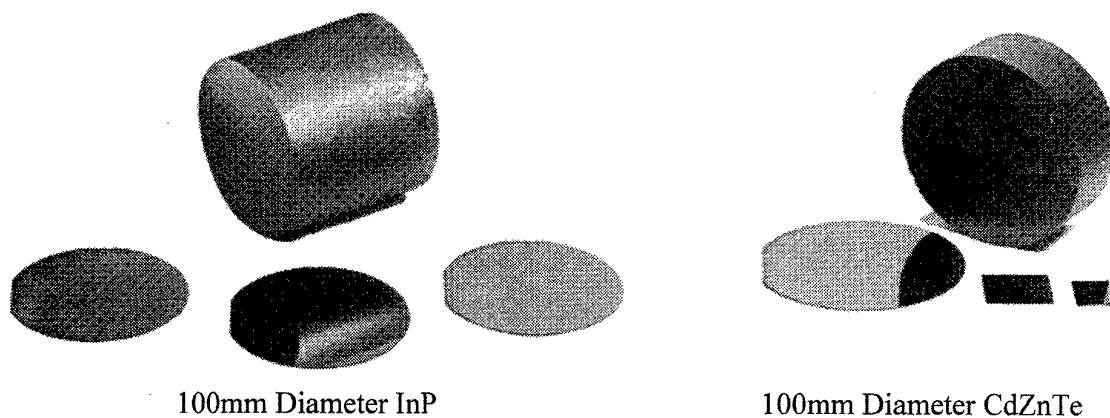


Fig.1 Grown Crystals by the VGF Method

References

- [1] K. Kohiro et al., J. Crystal Growth, 158 (1996) 197
- [2] M. Tatsumi et al., Materials Science and Engineering, B28 (1994) 65
- [3] X. Liu , III-Vs Review, 8 (1995) 1
- [4] M. Young et al., Proc. 10th Int. Conf. on InP and Related Mater., Tsukuba, 1998, p.30
- [5] T. Asahi et al., Proc. 10th Int. Conf. on InP and Related Mater.(Post-Deadline Papers), Tsukuba, 1998, p.1
- [6] T. Asahi, O. Oda, Y. Taniguchi ,A. Koyama, J. Crystal Growth, 149 (1995) 23

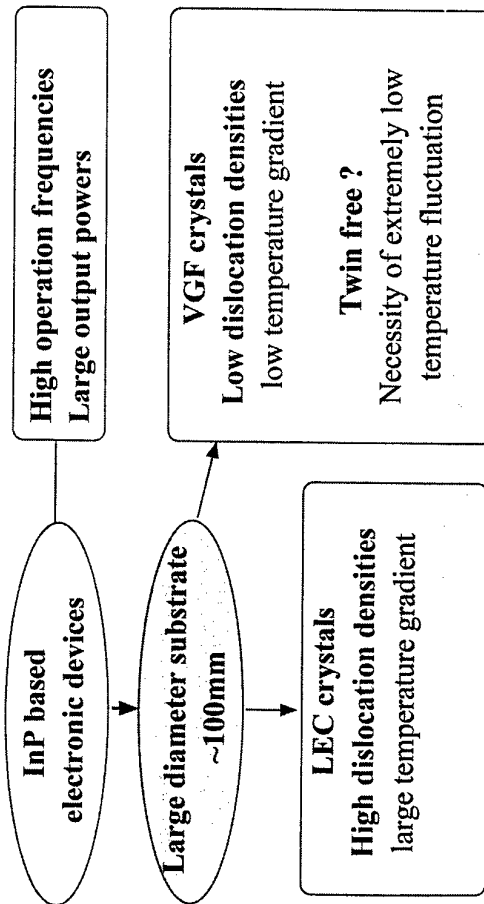
ADVANTAGE OF THE VGF METHOD

1. Low production cost
2. High crystal quality
3. Skilled operators are not necessary

DISADVANTAGE OF THE VGF METHOD

1. Low growth velocity
2. Easiness of twinning

BACKGROUND



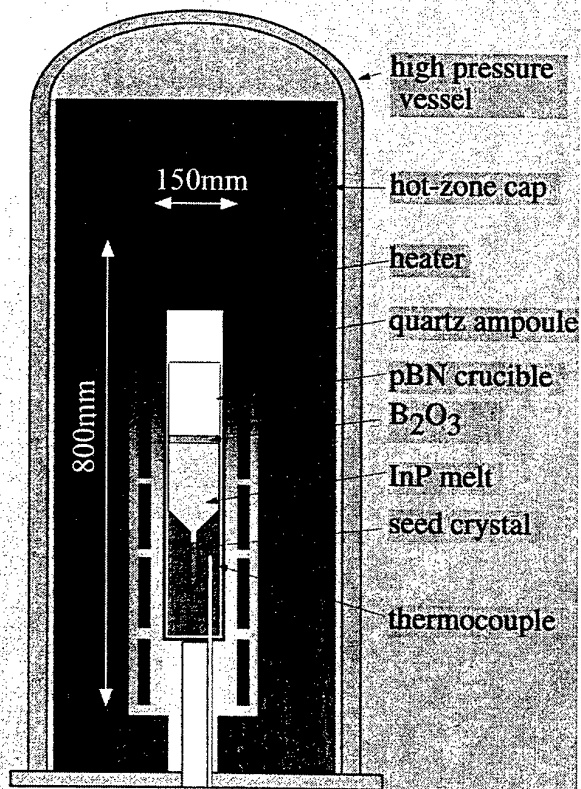
Growth Technology of InP and CdTe Single Crystals

T. Asahi, K. Kainosho, K. Kohiro, O. Oda
Central Research Laboratory
Japan Energy Corporation

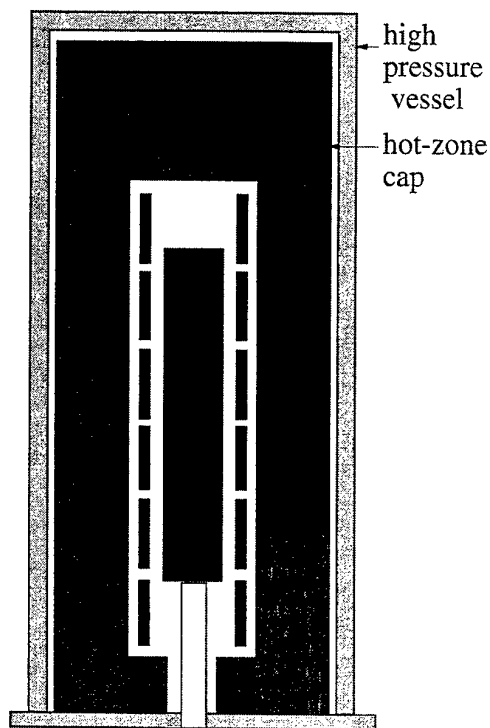
Physical Properties

Material	k (Wcm ⁻¹ °C)	CRSS (MPa)	SFE (erg cm ⁻²)
CdTe	0.01	0.11	10
InP	0.1	0.36	20
GaAs	0.07	0.4	48
Si	0.21	1.85	70

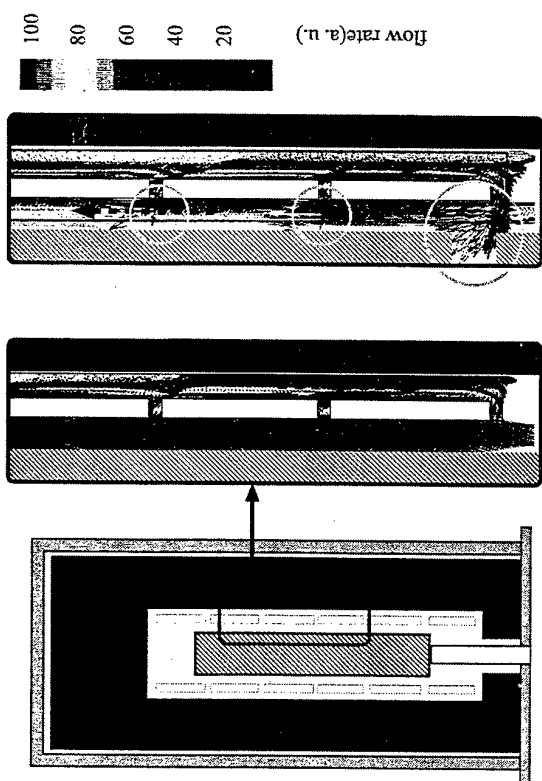
Ref. R.N. Thomas : J. Crystal Growth 99(1990)643
CRSS : critical resolved shear stress
SFE : stacking fault energy



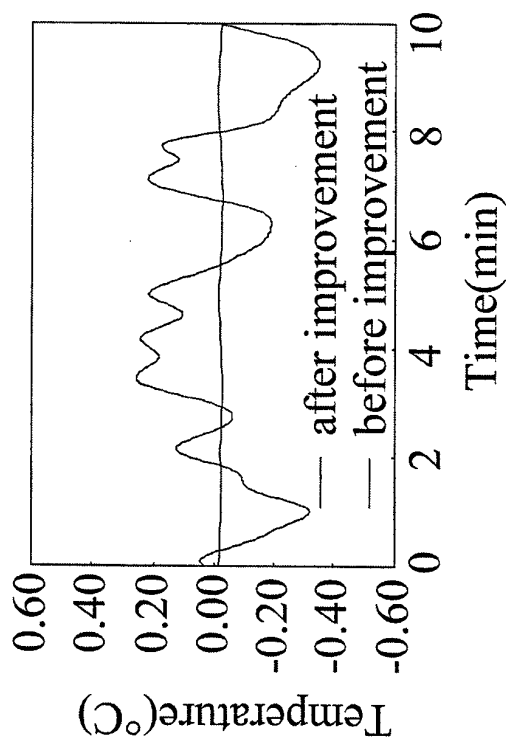
Schematic Diagram of the VGF-Furnace



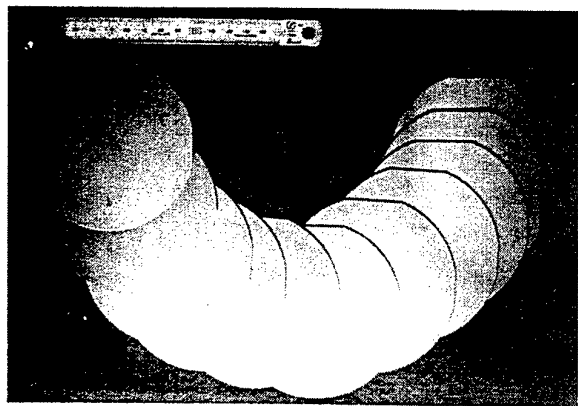
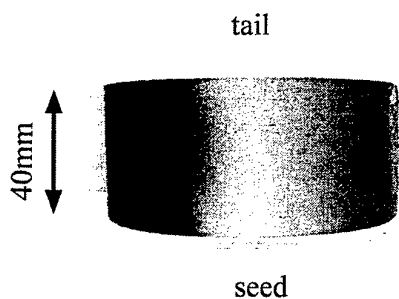
Simulation Model of the VGF-Furnace



Results of Computer Simulation

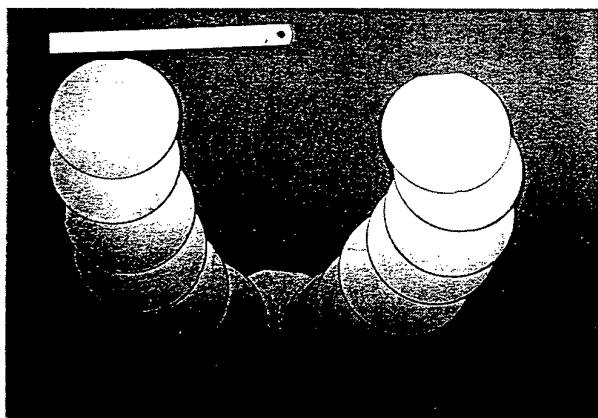
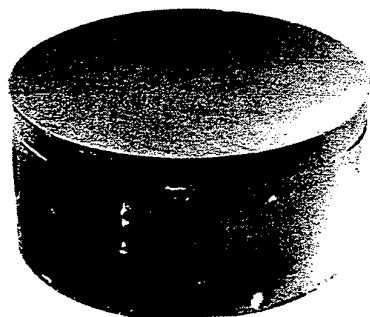


Temperature Fluctuations near the Seed Crystal

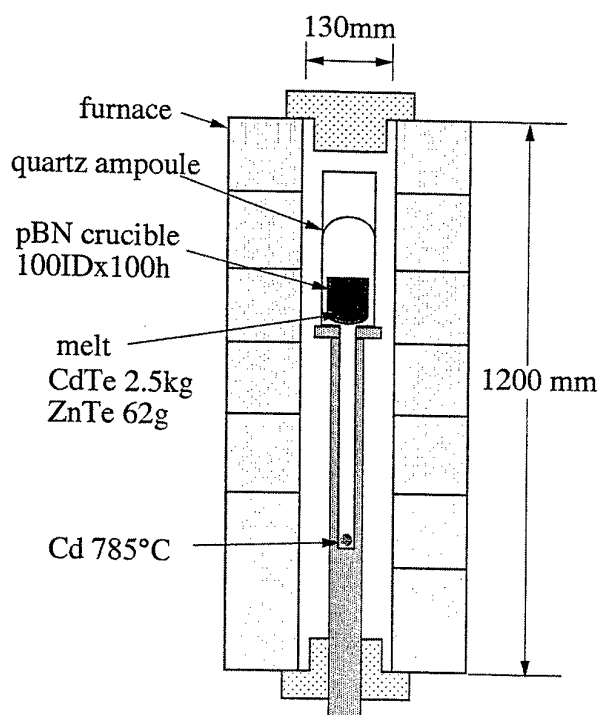


Grown Crystal and Wafers

Grown Crystal and Wafers



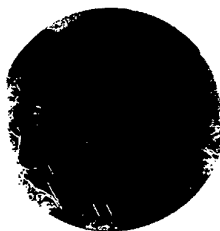
VGF Furnace



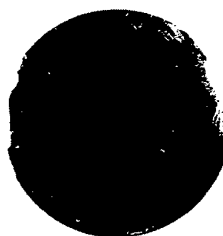
(111) Wafers after
Nakagawa Etching



top



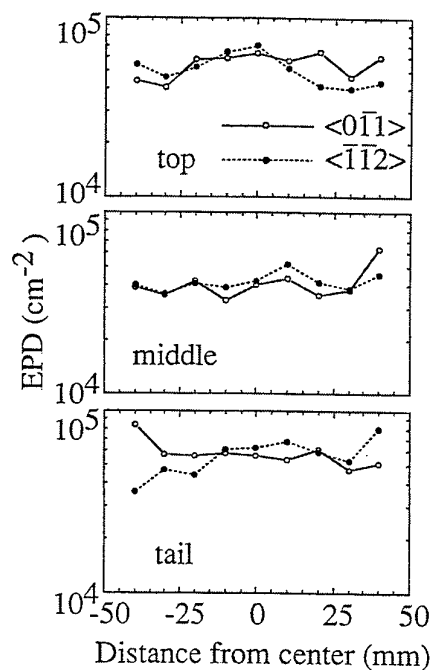
middle



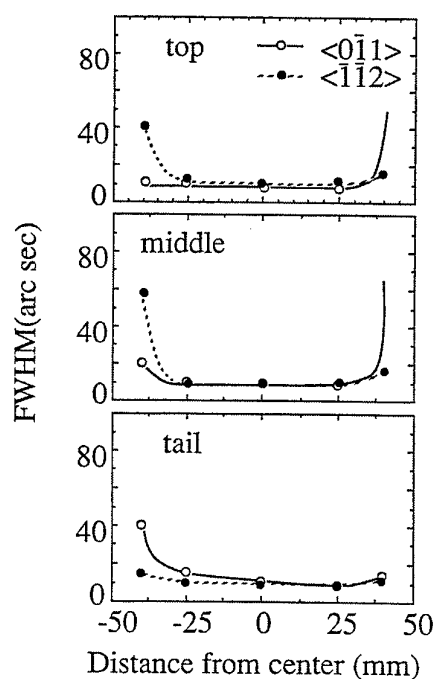
tail

20mm

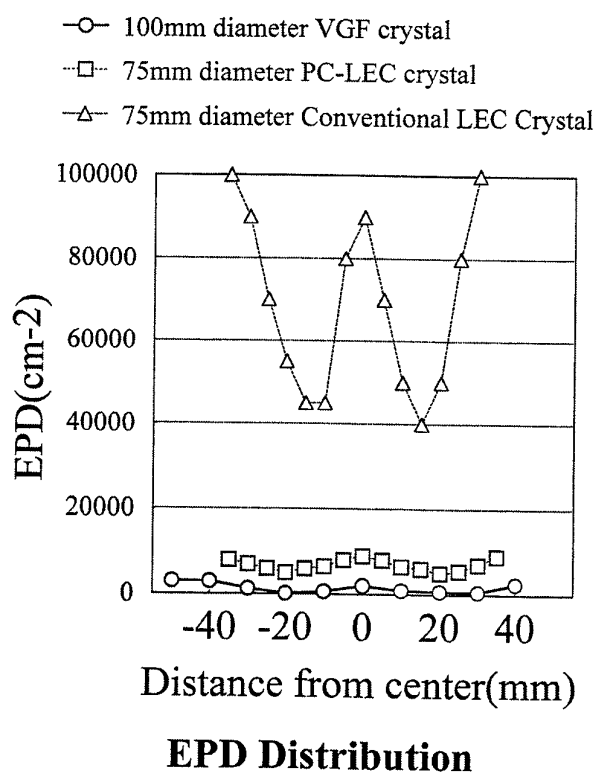
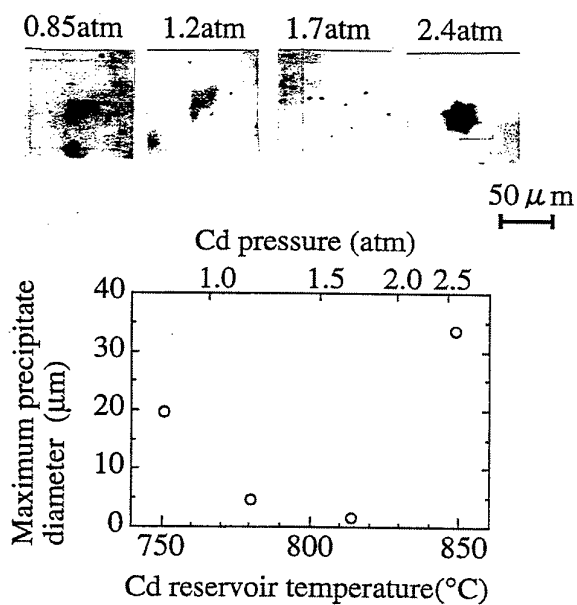
EPD Distributions



FWHM Distributions



Relationship between the Cd Pressure and the Precipitate Diameter



Crystal growth of CdTe requires precise knowledge of the existence regions of the solid, liquid and gas phases with respect to temperature, pressure and composition. The Cd-Te phase diagram has been recently revisited by Greenberg [1] from total vapor scanning experiments to determine the P-T-x equilibrium. His results have been confirmed by Fang and Brebrick [2] from optical density measurements. Several significant conclusions can be drawn from these studies, beside the previous published diagrams :

- CdTe shows a congruent fusion (cf) with a maximum melting point $\sim 1092\text{ }^{\circ}\text{C}$
- at T_{cf} CdTe is Te-saturated
- at T_{cs} (cs : congruent sublimation), crystalline CdTe is also Te-saturated
- $T_{\text{cs}} < T_{\text{max}}$ by 41K
- stoichiometric CdTe is in equilibrium with a Te-rich melt and a virtually pure Cd vapor
- no constant congruent sublimation composition ; the congruent sublimation line lies on the Te-rich side, rather far from the stoichiometry
- the maximum Te-non-stoichiometry $\sim 4.10^{18}\text{ cm}^{-3}$, the maximum Cd non-stoichiometry $\sim 10^{18}\text{ cm}^{-3}$.
- recent results of Brebrick and Fang [3] throw a new light on the stoichiometric line determination : singly ionizable Te antisite model gives a good fit of the high temperature electrical measurements.

The characteristics of Cd and Te atoms, as seen from their position in the periodic chart of the elements, make the Cd-Te chemical bond of ionic-covalent nature, with a pretty high ionicity of 0.55, that conditions most of the properties of CdTe, and even its growth, as will be shown further. The tendency to twinning and to hexagonal structure appears usually in such ionocovalent compounds when ionicity exceeds 0.5.

Several obstacles coming essentially from the ionocovalent nature of the CdTe chemical bond prevent from achieving easily its melt growth. CdTe presents :

- a sharp liquidus compared to III-Vs
- a wide homogeneity range (some 10^{18} cm^{-3})
- a retrograde solidus shape
- a low thermal conductivity
- pre-transition phenomena : highly associated superheated melts and phase transitions in the solid state

All these factors have a strong influence on the melt growth and make it difficult to obtain large crystals of high quality : the wide homogeneity range and the retrograde solidus shape necessitate a careful control of the stoichiometry to adjust the electronic properties of the crystals and avoid the presence of precipitates ; the highly associated melts lead to some duality between superheating and supercooling, making it difficult to use seeds ; the low thermal conductivity makes it difficult to control the growth interface shape and to achieve Czochralski pulling. In order to overcome these difficulties, different mechanisms have been proposed : growth in a reduced temperature range, to avoid the phase transitions in the solid state ; growth under high superheating conditions ; growth under forced convections regimes, as ACRT, micro- or macro-gravity conditions ; growth under vibrational stirring, with the vibrations aimed at breaking the CdTe associates ; growth under electric or magnetic field...

Because of these difficulties, just about all the techniques of growth of semiconductor materials have been applied to CdTe ! They can roughly be divided in several classes : growth from stoichiometric and off-stoichiometric melts, growth from the vapour phase either by

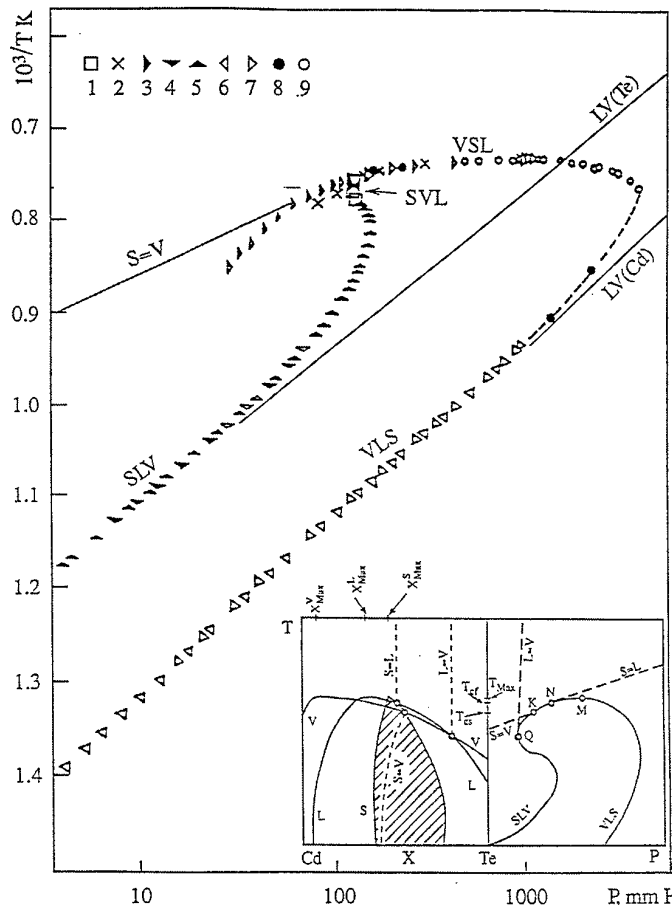
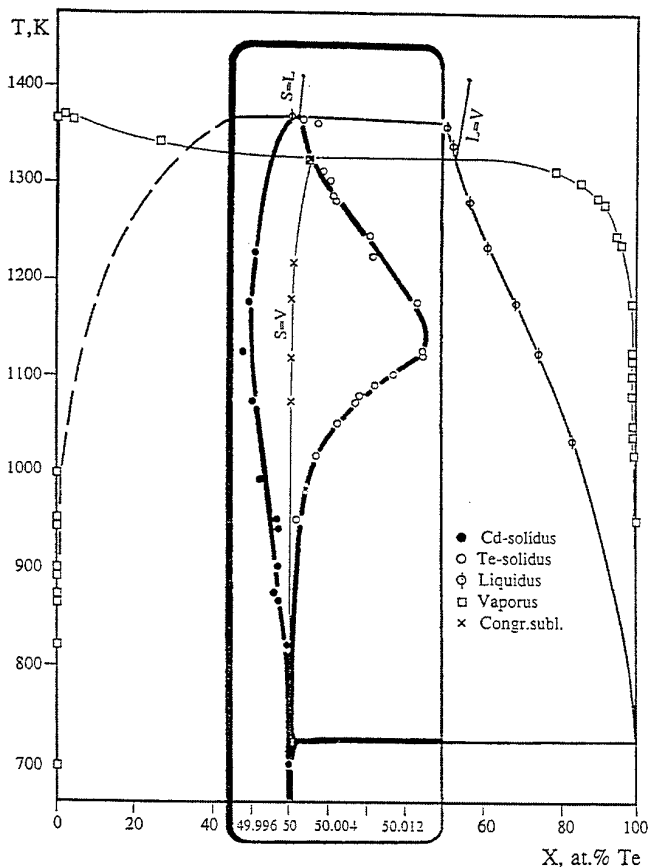
sublimation or by chemical vapour transport. Even now, some communications deal with 'new' methods of CdTe growth ! Concerning the growth from stoichiometric melts, the vertical and the horizontal Bridgman techniques, according to a lot of variants, the vertical zone melting and even the Czochralski pulling have been or are used. For the growth from non-stoichiometric melts, the vertical Bridgman technique using Te-solutions ; the Traveling Heater Method, either according to a classical configuration using Cd or Te as the solvents, or according to several variants, like 'Multipass' THM, 'Cold' THM, THM with ACRT or horizontal THM with rotation ; the Solvent Evaporation Technique and the Convection Assisted Solution Growth have been implemented. The heterosolvent growth has been proposed as well, either by THM using In or CdCl₂ as the solvents, or by flux growth with tin or bismuth as the solvents. The hydrothermal growth in (OH)⁻ solutions of NaOH and KOH has been used too. The growth from gels has been unsuccessful because of the Te ion instability. Even the CdTe synthesis in water at room temperature from metallurgical Cd and Te powders has been successfully achieved ! The vapour growth is practised in numerous laboratories and comes back into vogue periodically, as it does now. It is carried out either by sublimation, in a vertical or in an horizontal configuration, with or without seed, or by chemical vapour transport, with iodine or chlorine as chemical agents.

It is essential to point out that cadmium telluride has been now replaced, for most and perhaps all the applications it gives rise to, by cadmium zinc telluride (CZT) which possesses very specific properties beside CdTe. The main applications of CZT are epitaxial substrates, nuclear detectors and photorefractive devices. At macroscopic scale, the CdTe lattice is strengthened by the incorporation of Zn, as shown by the increase of the shear modulus which is a key signature of a material stability, because the Zn-Te bond length and ionicity are smaller than the Cd-Te ones and the Zn-Te binding energy is higher than the Cd-Te one. The CZT solution hardening has been modelled and experimentally demonstrated. At microscopic scale, the very strong repulsive mixing enthalpy in the solid leads to a miscibility gap for temperatures below 428°C, as theoretically predicted [4] and experimentally verified both in thin films and even bulk crystals [4,5].

The presence of Zn in CdTe has obviously consequences on its growth. The Cd-Zn-Te phase diagram is not well known, and has not been subjected to vapor scanning analysis like the Cd-Te one. The presence of Zn leads to segregation during Bridgman growth of the alloy. Different ways have been used to overcome this segregation : the simultaneous control of both Cd and Zn vapor pressures during the growth process [6], the use of a replenishing melt and crucible [7], the use of THM with particular composite source material geometry [8].

The main industrial growth processes of CZT are vertical and horizontal Bridgman, for substrates, and high pressure Bridgman, for nuclear detectors. Their most recent achievements will be presented and discussed.

- [1] J.H. Greenberg, *J. Crystal Growth* 161 (1996) 1
- [2] Rei Fang and R.F. Brebrick, *J. Phys. Chem. Solids* 57 (1996) 443.
- [3] R.F. Brebrick and Rei Fang, *J. Phys. Chem. Solids* 57 (1996) 451.
- [4] A. Marbeuf, R. Druilhe, R. Triboulet and G. Patriarche, *J. Crystal Growth* 117 (1992) 10.
- [5] M.-O. Ruault, O. Kaitasov, R. Triboulet, J. Crestou, M. Gasgnier, *J. Crystal Growth* 143 (1994) 40.
- [6] M.S. Azoulay, S. Rotter, G. Gafni, R. Tenne, M. Roth, *J. Crystal Growth* 117 (1992) 276.
- [7] Y. Tao, S. Kou, *J. Crystal Growth* 181 (1997) 301.
- [8] A. El Mokri, R. Triboulet, A. Lusson, A. Tromson-Carli, G. Didier, *J. Crystal Growth* 138 (1994) 168.



Cd-Te phase diagramme

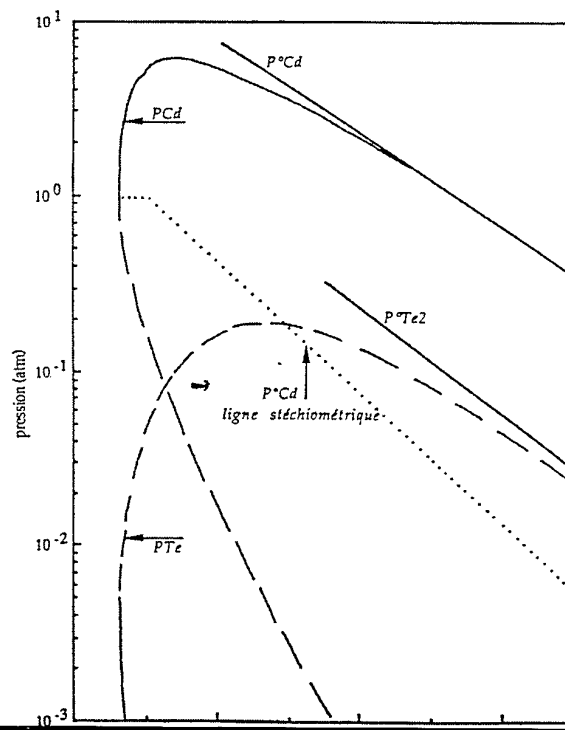
- > At T_{cs} , crystalline CdTe is Te saturated
- > $T_{cs} < T_{max}$ (maximum melting point) by 41 K
- > at T_{cf} CdTe is also Te saturated
- > stoichiometric CdTe is in equilibrium with a Te-rich melt and a virtually pure Cd vapor
- > no constant congruent sublimation composition
- > maximum Te non stoichiometry $\sim 4.10^{18} \text{ cm}^{-3}$
- > maximum Cd non stoichiometry $\sim 10^{18} \text{ cm}^{-3}$

Compound	Ionicity	Structure
ZnS	0.77	Cub./Hex.
CdS	0.74	Hex.
CdSe	0.64	Hex.
ZnSe	0.63	twin.Cub.
CdTe	0.55	twin.Cub.
HgTe	0.50	Cub.
ZnTe	0.49	Cub.

Hex. = hexagonal; cub. = cubic; twin. = twinned

J. Steiniger et al., *J. Electrochem. Soc.* 117 (1970) 1420
 N.R. Kyle et al., *J. Electrochem. Soc.* 118 (1971) 1791
 D. de Nobel, *Philips Res. Rept.* 14 (1959) 361
 S.A. Metvedev et al., *Inorg. Mater.* 8 (1972) 1064
 A.J. Strauss et al., *Proc. Intern. Symp. CdTe*, Strasbourg (1972) (P. Siffert and A. Cornet eds)
 M.R. Lorenz et al., *J. Phys. Chem. Solids* 23 (1962) 1449

$$P_{Cd}(CdTe_{stoichi}) = -7.63 \times \frac{10^3}{T_{CdTe}} + 5.842$$





CdTe pretransition phenomena in the solid

- hexagonal structure reported at high temperature (Appell 1954, Kendall 1964, Höschl 1963)
- tendency to hexagonal structure (and twinning) found from the CdTe-MnTe phase diagram study (Triboulet 1991)
- phase transition in the 893 - 920 °C temperature range found from electromotive forces measurements (Leibov et al. 1976)
- solid phase transformation (?) observed by eddy-current (Clarkson University)
- solid phase transformations below the melting point reported by Ivanov 1996
- pretransition phenomena observed by electrical conductivity and DTA measurements, Shcherbak 1997

440



CdTe accounting for the pretransition phenomena

- growth in a reduced temperature range (Ivanov et al.)
- growth under high superheating conditions
- growth under a forced convection regime (ACRT, micro- or macro-gravity conditions ?)
- growth under a vibration regime (frequency ?)
- growth under electric or magnetic field



CdTe obstacles in the melt-growth

- sharp liquidus compared to III-Vs
- wide homogeneity range
- retrograde solidus shape
- low thermal conductivity
- pre-transition phenomena
 - highly associated superheated melts
 - phase transitions in the solid state
- contamination at the growth temperature



CdTe pretransition phenomena in the liquid

- strong interaction between Cd and Te → theory of associated solution model for liquid CdTe, first proposed by Jordan 1970
- association coefficient of 0.95 determined by Yu and Brebrick
- supercooling effects (Rudolph), postmelting processes (Shcherbak), explained by the presence of clusters
- use of new calorimetric data for CdTe, HgTe and liquid Te (Jianrong)
 - association coefficient of 0.92 for CdTe just above the melting point (0.61 by comparison for HgTe)
- determination of the enthalpy of formation of the liquid phase from calorimetric measurements → very strong departure from ideality, explained by a short range order corresponding to CdTe associates (Amzil et al.)

Growth from stoichiometric melts

- Vertical Bridgman
 - without controlled Cd partial pressure
 - with controlled Cd partial pressure (so-called "modified" Bridgman technique)
 - under inert gas pressure (HPB)
 - under hydrogen pressure
 - with accelerated crucible rotation (ACRT)
 - under low amplitude 60 Hz mechanical vibrations
 - with heat exchanger (HEM, Crystals Systems Inc.)
 - asymmetrical Bridgman
 - "gradient freeze technique"
- Horizontal Bridgman
 - with relative movement of furnace and charge
 - with electronic displacement of the temperature gradient
 - "gradient freeze technique"
 - with or without control of the Cd partial pressure
 -
- Vertical zone melting
- Czochralski pulling under encapsulation (LEC)

- vertical Bridgman in Te-solution
- classical THM
 - with Te as the solvent
 - with Cd as the solvent
- THM variants
 - multipass THM
 - cold THM
 - THM with ACRT
 - horizontal THM with rotation
- Solvent Evaporation Technique (SET)
- Convection assisted solution growth

Heterosolvent growth

- THM
 - with In as the solvent
 - with CdCl₂ as the solvent
- flux growth with tin or bismuth as the solvents
- hydrothermal growth in (OH)⁻ solutions of NaOH and KOH, at 350 °C (Kolb, 1968)
- unsuccessful growth from gels because of the Te ion instability (Blank et al., 1971)
- successful synthesis in water at room temperature from Cd and Te metallurgical powders (Matsushita Electronics, 1983)

Vapor Phase Growth

- SUBLIMATION
 - vertical configuration
 - without seed {
 - Yellin et al., 1982
 - Durham technique, 1985
 - physical vapor transport, Wiedemeier et al. 1
 - THM Sublimation, Triboulet & Marfaing 1981
 - with seed {
 - dynamic vacuum, Kuwamoto 1984
 - physical vapor transport, Grasz et al. 1992, Palosz et al. 1997, Myzcieliski et al. 1997
 - semi-closed system, Markov-Davydov 1971 (Durham, Freiburg)
 - horizontal configuration
 - without seed {
 - Akutagawa and Zanio, 1971
 - evaporation-condensation method, Szczerbakow et al. 1993
 - with seed {
 - automatic selection, Buck and Nitsche 1980
 - semi-closed system, SPVT, Boone et al. 1994
- CHEMICAL VAPOR TRANSPORT, with iodine or chlorine as chemical agents, Paorici 1972

key words : *closed systems or semi-closed systems ; with or without seed ; automatic seed selection ; with or without control of the stoichiometry, before or during growth ; vertical or horizontal configuration ; with or without contact of the crystal with the walls*



CdZnTe

MACROSCOPIC BEHAVIOR OF Zn IN CdTe

- Zn-Te bond length (0.2643 nm) shorter than the Cd-Te one (0.2794 nm)
- ZnTe binding energy (-4.7 eV) higher than the CdTe one (-4.3 eV)
- ZnTe ionicity (0.49) smaller than the CdTe one (0.56)
- inverse relationship between reduced stacking fault energy and ionicity
 - ➔ the less ionic a material, the more stable is its lattice
- interaction energies between dislocations proportional to d^{-5} to d^{-11} (low absolute powers for pure covalent materials)
 - ➔ the shorter the bond length and the less ionic a semiconductor, the more stable is its lattice
- a key structural signature of a material is the shear modulus,
 - energy of creation of dislocations proportional to Cs
 - energy of creation of vacancies proportional to Cs
- Cs proportional to a covalency parameter and inversely proportional to the power five of the interatomic distance ➔ Cs higher for ZnTe than for CdTe



CZT

MICROSCOPIC STRUCTURE

- EXAFS results interpreted using a model of Keating : positive mixing enthalpy leading to the a miscibility gap below 435 K (Motta 1985)
- miscibility gap below 605 K for $x = 0.623$ from calculations (Wei et al. 1990)
- very strong repulsive mixing enthalpy in the solid ➔ immiscibility predicted in CZT below 428 °C (Marbeuf 1991)
- DTA experiments and calculations of isopleths sections based on the optimized coefficients of the free enthalpy of the three binary systems Cd-Te, Zn-Te, Cd-Zn (Halaoui 1996)
-
- verified in thin films grown by MOCVD or MBE
 - moiré fringes visible on TEM images
 - lattice mismatch in good agreement with the phase diagram determinations
- verified as well in bulk CZT crystals

for the First International School on Crystal Growth Technology, ISCGT-1

The Use of High Performance Computing for Modeling Crystal Growth from the Melt and Solution

Jeffrey J. Derby*

Department of Chemical Engineering and Materials Science, Army HPC Research Center,
and Minnesota Supercomputer Institute
University of Minnesota, Minneapolis, MN 55455-0132, U.S.A.

Crystal growth is an art which is evolving into a science, and modeling via the use of high performance computing represents a modern tool for speeding this evolution onward. The use of realistic theoretical models can augment traditional experimental inquiry for obtaining fundamental understanding of crystal growth. Such models have been extremely successful in the analysis of systems which exhibit two-dimensional behavior due to symmetries in design and which are dominated by long time-scale phenomena which allow the effective use of quasi-steady assumptions.

However, many systems contain imperfections in design or operation which disrupt their inherent two-dimensional symmetry and lead to three-dimensional effects. Even more significantly, fully three-dimensional and time-dependent behaviors have long been known to occur in crystal growth systems, in spite of system symmetries and slow process dynamics. The analysis of these effects requires the development of modeling techniques which allow the simulation of fully three-dimensional and time-dependent phenomena. However, these calculations continue to be extremely costly and difficult to perform.

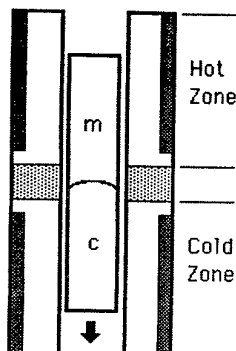
Recent advances in massively parallel supercomputers have dramatically affected the prospect of studying three-dimensional macroscopic transport effects in many systems. To take advantage of these advances, we have developed finite element methodologies for computing three-dimensional, time-dependent, incompressible flows on the Cray T3E, a distributed memory, multiple processor supercomputer. The large memory and high sustained computation rates provided by these platforms allow us to perform extremely large simulations appropriate for the calculation three-dimensional phenomena occurring in crystal growth systems.

In this presentation, the most salient features of these models will be highlighted and examples will be presented from their application to analyze several melt and solution growth systems. Specific results from simulations of Czochralski growth of oxide crystals, melt growth of cadmium telluride, and the solution growth of potassium titanyl phosphate will be discussed.

This work was supported in part by the U.S. National Science Foundation, the U.S. National Aeronautics and Space Administration, Sandia National Laboratories, the Minnesota Supercomputer Institute, and the U.S. Army, Army Research Laboratory, Army HPC Research Center. No official endorsement should be inferred.

Realistic theoretical models can play an important role in understanding the processing of materials

UNIVERSITY OF MINNESOTA



Experimental Challenges

- Phenomena at microscopic length scales are important, yet only macroscopic tools are available to affect process
- Process conditions make in-situ observations and control difficult
 - High temperatures
 - Opaque systems
 - Slow process dynamics
 - Few direct measures available to characterize solid state
- Long process times make rapid experimental turnaround difficult

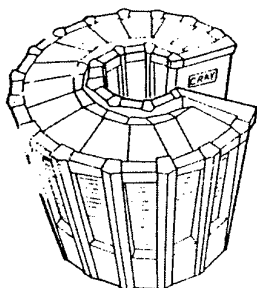
Realistic theoretical models will complement traditional experimental analysis!

Providing:

- explanation of experimental observations
- mechanism for systematic process optimization

Modeling Challenges

- Complicated, multi-dimensional geometries
- Nonlinear, time-dependent effects
- Strongly coupled phenomena, especially fields and interfaces
- Phase transitions



Understanding bulk crystal growth requires analysis at several disparate scales

UNIVERSITY OF MINNESOTA



Flows during KDP solution growth

Length scales: 0.01-1 m



Inclusion formation during KTP growth

0.1-10 μm



Tellurium chaining in molten CdTe (Bridgman growth)

1-100 \AA



Novel approaches are needed to model the coupling between continuum, meso-scale, and atomistic phenomena.

Where is our understanding of bulk crystal growth incomplete?

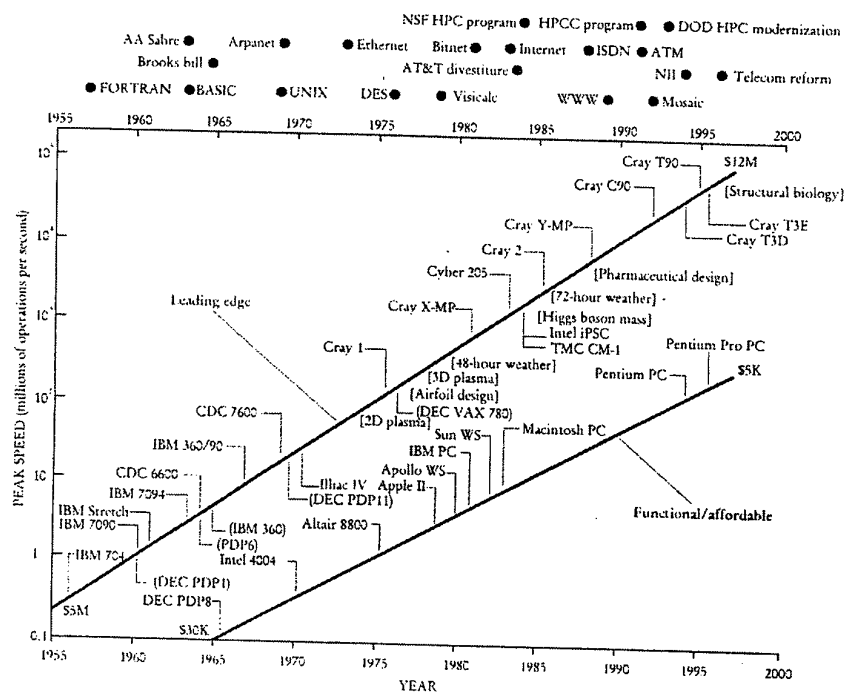
UNIVERSITY OF MINNESOTA

- Detailed knowledge of any given growth system
- Transient phenomena
 - Time-dependent processing strategies (e.g., growth and pause)
 - Striations
 - Kinetic growth effects
- Three-Dimensional Phenomena
 - Complicated or imperfect geometries (e.g., ampoule misalignment)
 - Melt convection
 - Anisotropy of physical properties
- Coupling between atomistic phenomena and continuum effects
 - Dislocations
 - Twinning
 - Inclusions

⇒ *New understanding will require innovative approaches to theory and modeling!*

Computing technology has advanced exponentially

UNIVERSITY OF MINNESOTA

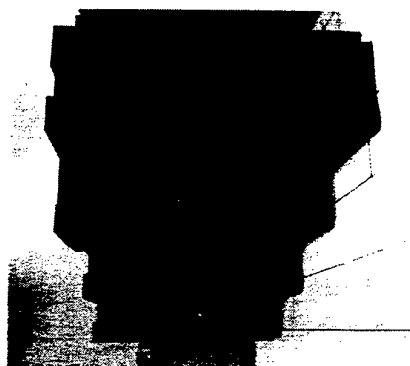


from A.E. Brenner, *Physics Today*, October 1996.

⇒ *Computational modeling has become a powerful research method and an affordable design tool.*

We employ a massively parallel, finite element method (FEM) for 3D, transient flow calculations

UNIVERSITY OF MINNESOTA



CM-5 at the
Army HPC Research Center at the
University of Minnesota

Key Features

- Galerkin FEM with mixed interpolation (hexahedral triquadratic elements, structured mesh) or Galerkin-Least Squares FEM with equal-order interpolation (tetrahedral linear elements, unstructured mesh)
- Fully implicit transient time integration (backward Euler)
- Residuals and Jacobian elements calculated on an elemental basis (achieves effective load balancing and memory utilization)
- GMRES iterative technique for solution of resulting linear algebraic equations
 - Diagonal preconditioning
 - Local matrix-vector multiplications
 - Mesh partitioning (minimizes communications overhead)
- Code implemented on the Connection Machine 5 (CM-5) and Cray T3D

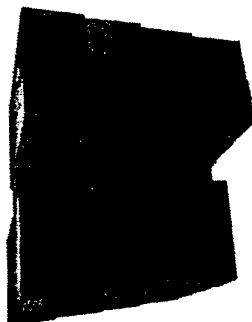
High Performance Computing is defined by the largest, fastest computers available

UNIVERSITY OF MINNESOTA



MANIAC, 1952

- 1.2×10^3 operations/second
- 5 KByte RAM
- 50 KByte magnetic drum



Cray T3E-1200, 1997

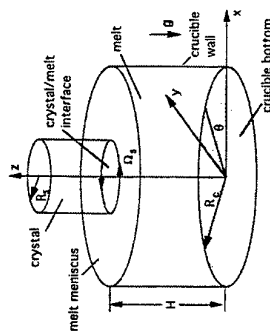
- 1.2×10^8 operations/second/node
- 1 GByte RAM/node
- >100 GByte disk

➡ 45 years of development has resulted in 10^6 - 10^8 increase in power!

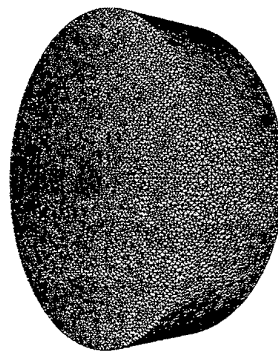
AHPCRC & CEMS / University of Minnesota

Bulk 3D Model for Czochralski Configuration

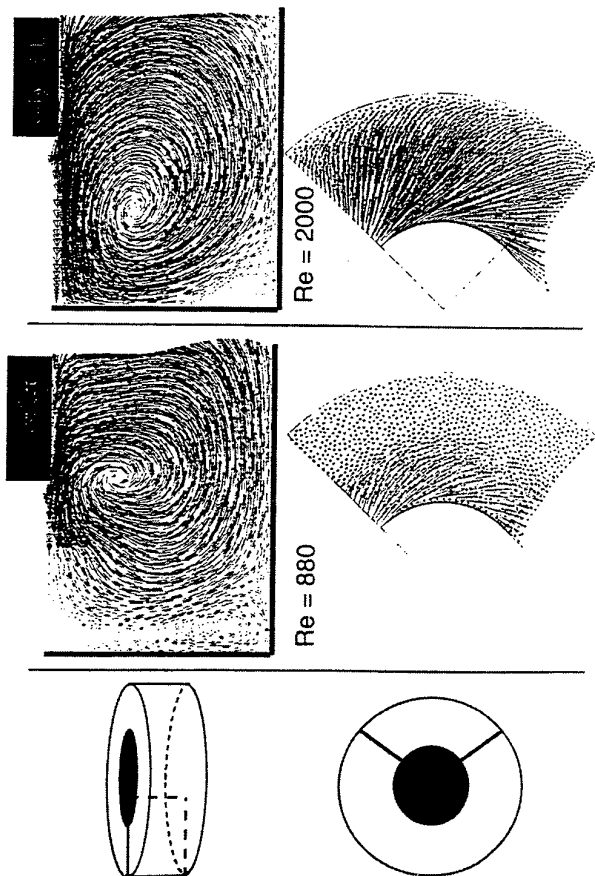
- Idealized Czochralski system (Bulk model) and unstructured mesh



- Numerical methodology
 - Over 870,000 tetrahedral elements comprising more than 720,000 unknowns
 - Equal-order linear approximation for temperature, velocity, and pressure
 - Galerkin Least-Square (GLS) method used to stabilize the numerical approach
 - Solved using a 512-node CM5 Thinking Machine

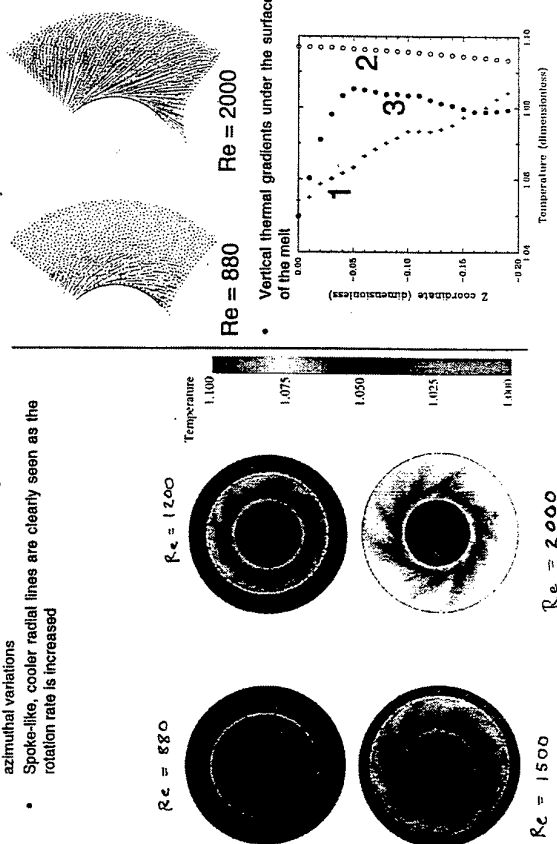


Competition between forced and buoyant flows



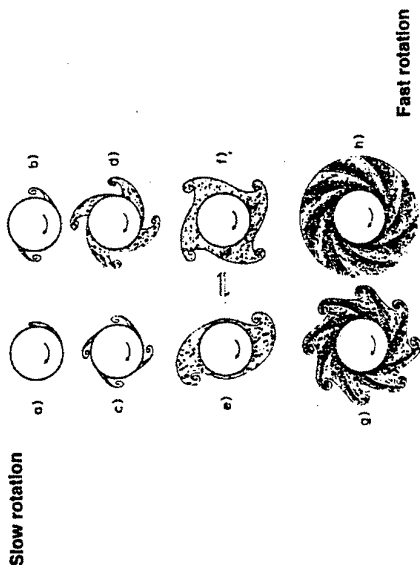
Spokes Patterns on Meniscus Surface of Molten BSO

- Temperature distribution in the cooler region exhibits azimuthal variations
- Spoke-like, cooler radial lines are clearly seen as the rotation rate is increased



Annular vortex patterns and spoke patterns are observed on the surfaces of BSO during crystal growth

Surface flows observed in physical model of BSO growth ($Pr \approx 26$):



from Whiffin, Bruton, and Brice, *J. Crystal Growth* 32 (1976) 205-210.

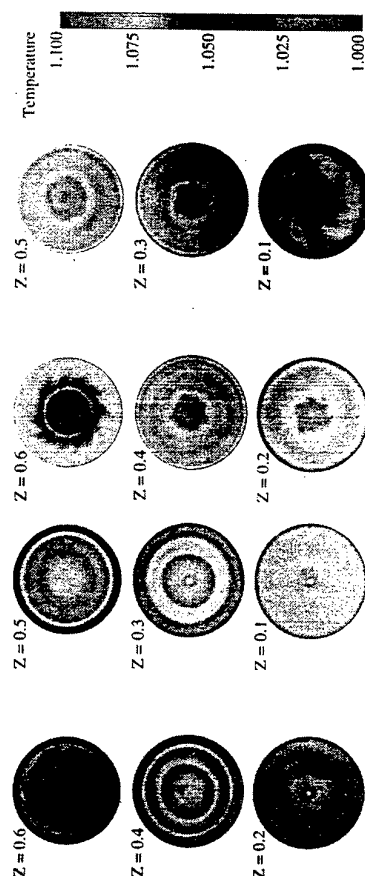
Wave-like Annular Bulk Structure for BSO system

- Three-dimensional analysis of the BSO system shows a destabilization of the axisymmetric flow state for high rotational Reynolds numbers leading to a annular wave structure in the bulk of the melt

$Pr = 26$; $Gr = 1.3 \cdot 10^5$

$Re = 1500$

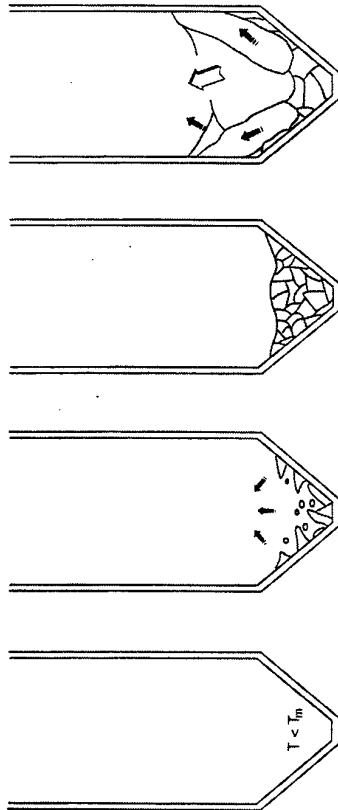
$Re = 2000$





Unseeded growth relies on successful grain selection to produce large, single-crystal regions

UNIVERSITY OF MINNESOTA



Melt is undercooled to initiate nucleation and growth

Burst of Growth
Multiple nuclei form & grow simultaneously

System restored to equilibrium by arresting grain growth

Grain selection is facilitated by fast growth rates

However, growth rate is limited by constitutional supercooling effects!



A number of factors impact CdZnTe substrate quality, cost, and availability

UNIVERSITY OF MINNESOTA

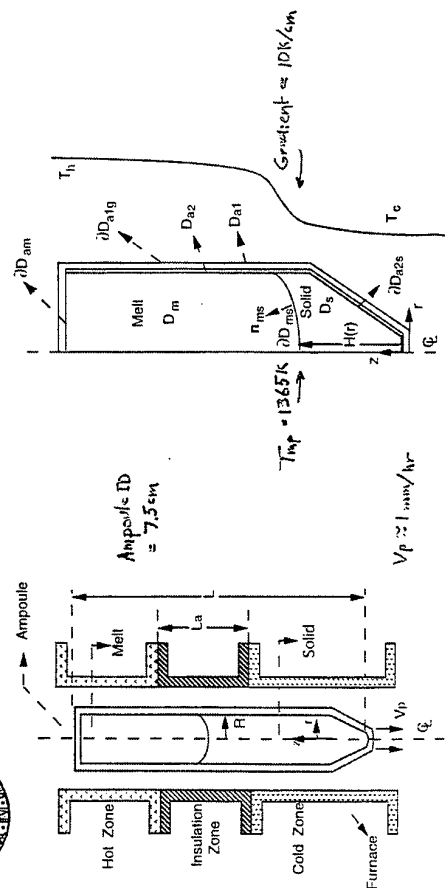
- Crystallinity (Single Crystal)
- Purity
- Zn Uniformity (Lattice Matching)
- Dislocation Density
- Te Precipitate Size and Density

Increased yields will have greatest impact! (Current yield, defined as weight of usable substrate/ total weight of grown material, is 2.5%)
 $\leq 10\%$ for 11B

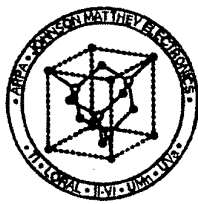


2D finite element model for vertical Bridgman growth of CdZnTe

UNIVERSITY OF MINNESOTA

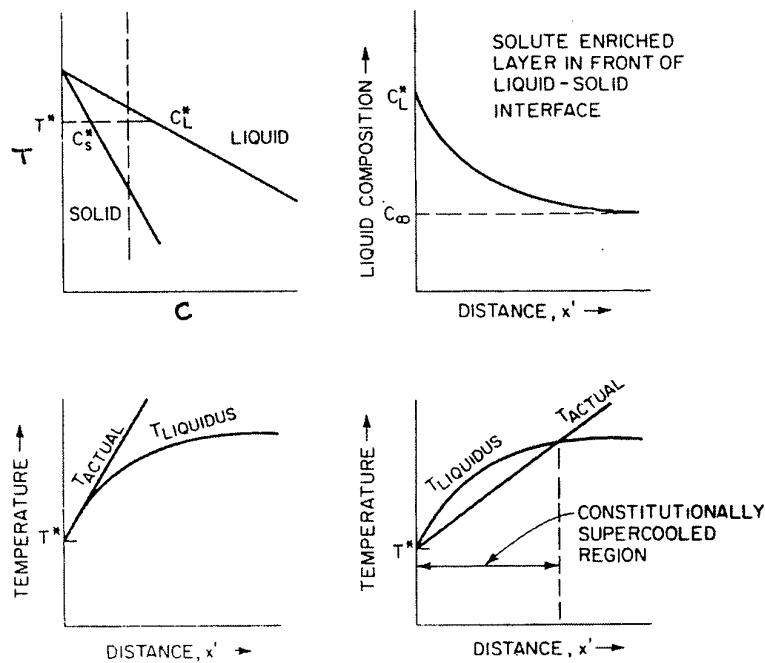


Calculates steady or transient heat & mass transfer, melt convection, and solid/liquid interface shape with complete CdTe phase diagram

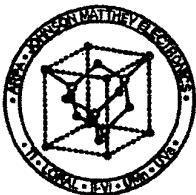


Constitutional supercooling results in morphological instability of plane-front solidification interface

UNIVERSITY OF MINNESOTA



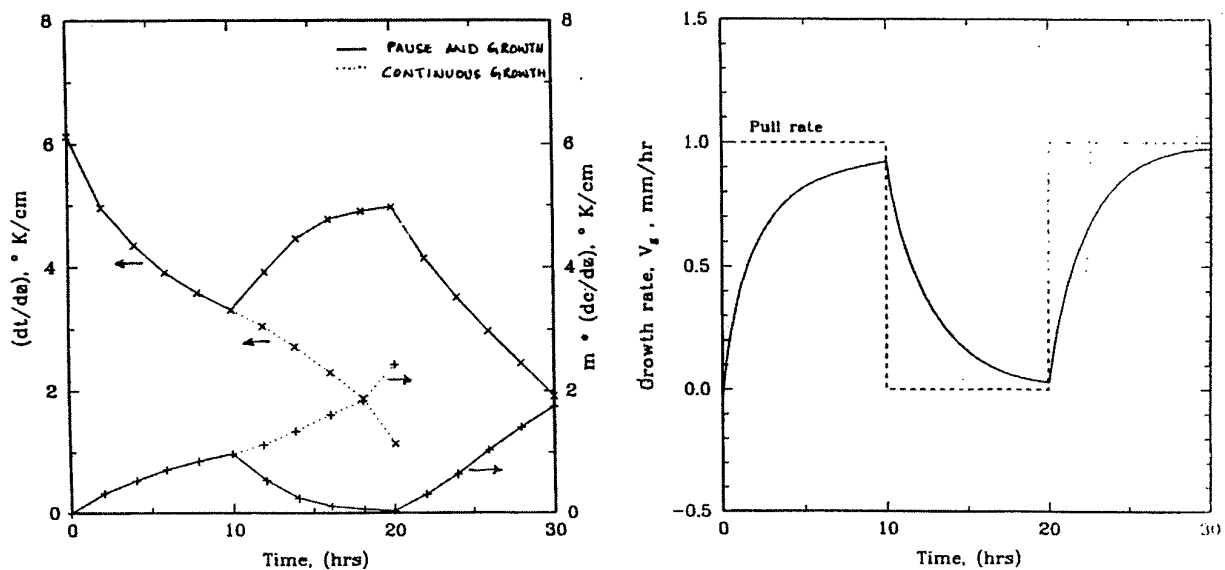
Stability requires $dT/dx \geq m_L(dc/dx)$ (Chalmers et al., 1953)!



Growth and pause strategy delays the onset of morphological instability thus allowing higher growth rates

UNIVERSITY OF MINNESOTA

Constitutional supercooling arises if $dT/dx < m_L(dc/dx)$



Comparison of MOCVD, MBE and LPE for Performance of Optoelectronics Devices

Jun-ichi Nishizawa

Semiconductor Research Institute of Semiconductor Research Foundation, Kawauchi Aoba Sendai 980, Japan

Stoichiometry controlled LPE and bulk crystal growth (TDM-CVP)

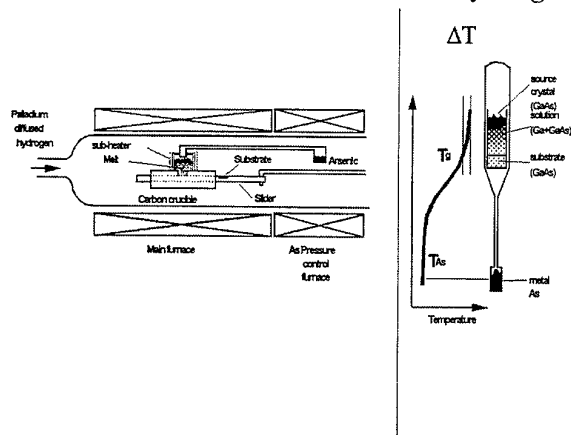


Fig.1 Schematic drawing of the TDM-CVP growth apparatus

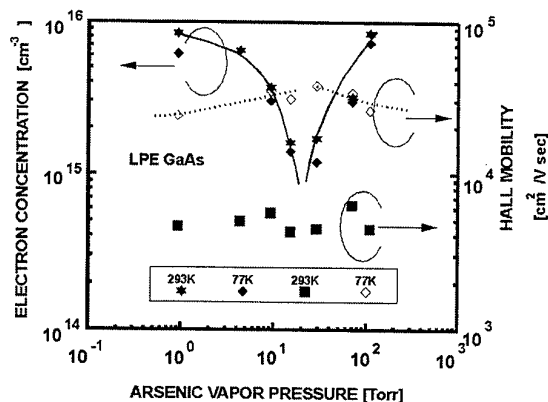


Fig.2 Arsenic vapor pressure dependencies of electron concentration and Hall mobility in TDM-CVP grown LPE GaAs

TDM-CVP (temperature difference method under controlled vapor pressure) liquid phase epitaxy¹, as well as melt growth², enables growth of stoichiometry controlled compound crystals. This technology was first developed for III-V compounds GaAs³ and GaP⁴. The fundamental growth systems are shown in Fig.1. It was found that dislocation density and nonstoichiometric point defect density of grown crystals show minima at optimum applied vapor pressures of volatile element As or P. Figure 2 shows the result on LPE GaAs. The most important evidence is that the optimum vapor pressure of LPE GaAs is in well coincidence with the stoichiometric vapor pressure found by the heat-treatment of GaAs under the As vapor pressure, as shown in Fig.3. The principle was applied not only for LPE but also for bulk single crystal growth such as horizontal Bridgmann growth of GaAs by Akai et. al.⁵ of Sumitomo Company, and also Czochralski growth at Mitsubishi Materials Company. The vapor pressure controlled best quality HB GaAs now share more than 90% of the world demands.

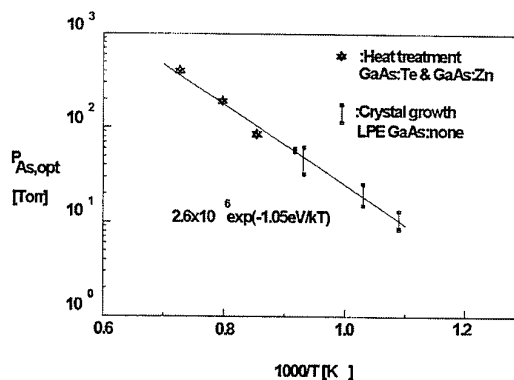


Fig.3 Temperature dependence of the optimum arsenic vapor pressure of GaAs

Applications of TDM-CVP LPE

It had been believed that near gap light emission from GaP needs nitrogen impurities, because of its indirect bandgap nature, but the nitrogen incorporation resulted in yellow-green color with peak wavelength 570nm. TDM-CVP LPE grown GaP LEDs enabled efficient nitrogen-free pure green light emission (550nm)⁶. It was shown that, when nonstoichiometric defects concentration is extremely low, free exciton recombination with accompanying

momentum conserving phonons are dominant emission transition mechanism even at room temperature which cause pure green light emission.

The highest efficiency is obtained from AlGaAs heterostructure red light emitting diodes which are produced by TDM-CVP LPE. It was shown that density of deep levels was minimized in these diodes. In the case of double heterostructure AlGaAs LED, the external efficiency reach higher than 30%.

Extension of TDM-CVP to other compounds

The general advantage of TDM-CVP LPE is that the defect concentration is the lowest among other growth methods. Its other advantage is the low production costs. TDM-CVP ZnSe pn junction blue LED was realized⁷ in 1982. Although MOCVD grown GaN blue LEDs has achieved extreme high efficiency, the above mentioned advantages for LPE grown ZnSe will be still effective if some difficulties such as non ohmic electrode will be overcome. TDM-CVP LPE is also being extended for the growth of InP⁸ and far infrared laser materials like PbTe⁹ and PbSnTe. We will give the recent results for those materials. It will be also effective for the growth of high temperature superconducting materials.

It was shown by H.J.Scheel et. al. that the LPE grown surfaces are atomically much more flat than those of MBE grown and MOCVD grown epitaxial layers¹⁰. LPE technology has been extended to the growth of high temperature superconducting materials.

MBE, MOCVD and molecular layer epitaxy (MLE)

The two major categories in vapor phase growth processes are PVD and CVD. Typical epitaxial growth methods in each category are MBE and MOCVD. Vapor phase growth is convenient for mass production and offers maximum control of material properties such as thickness and composition.

In principle, MBE is one of the vacuum evaporation methods using solid sources. For the growth of single crystalline epitaxial layers, the supply of evaporated species must be well controlled under ultra high vacuum. MBE can be used at relatively low temperature range as 400 – 600°C with slow growth rate by precise control of the supply of constituents, like as atomic accuracy¹¹. Because the MBE growth is proceeded under extremely non-thermodynamic equilibrium condition, this method can be frequently used to grow various combination and composition of the compound semiconductors. On the other hand, it can cause the formation of the defects. In order to grow epitaxial layers with device quality, surface migration for the adsorbed species is very important. Generally, PVD at low temperature and high growth rate results to make more defects, in the worse case polycrystalline or amorphous films. Crystalline defects such as grain boundaries, stacking faults, twins, dislocations or vacancies are known to affect the device properties seriously. They have been shown to act as non-radiative recombination centers, thus to reduce the minority carrier lifetime and quantum efficiency in LEDs or LDs¹².

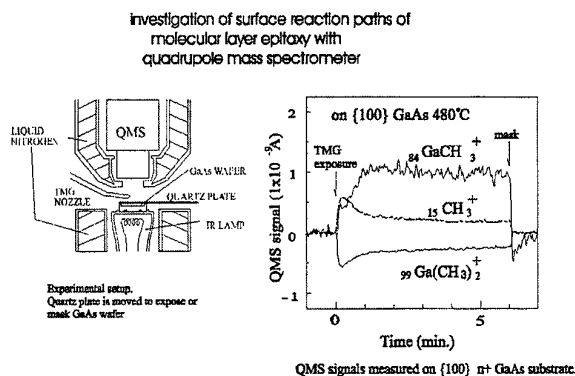


Fig.4 Schematic set-up of QMS and results for the surface reaction mechanism of TMG on {100} oriented GaAs

MOCVD is usually carried out in a cold wall reactor, under 10-760 Torr, using volatile organometallic compounds with hydrides. Since the supply of constituents is done in gas phase, this technique is much suitable for mass-production. One of the disadvantages in MOCVD can be caused when the epitaxial growth is carried out under the viscous flow conditions. GaAs epitaxy using TMG and AsH₃ in ultra high vacuum had been performed to investigate the growth mechanisms¹³. Later, this method is called MOMBE, chemical beam epitaxy (CBE) or gas source MBE (GSMBE). Another approach is MLE^{14,15}, based on the idea of ALE which was applied to grow II-VI polycrystalline films^{16,17}. In the MLE process, the component atomic species are supplied as compounds and the monomolecular epitaxial layer is formed by the chemical reaction on the surface. It is essential to understand the surface reaction mechanisms. Fig.4 shows the schematic drawing of the surface reaction of TMG on (100) GaAs surface using QMS analyses. From QMS measurements, the temporal adsorption of Ga(CH₃)_x will occur at lower temperature, and a Ga desorbed layer will be formed with additional CH₃ adsorption at higher temperature^{18,19}. Fig.5 shows the temperature dependence of AsH₃ IR absorption in H₂. It is noticed that the decomposition of AsH₃ is enhanced by the existence of Ga and GaAs, due to the effect of surface catalysis.

MLE has a big potential not only as the ultimate growth preciseness, so called atomic accuracy, but also the analytical tool for the epitaxial growth mechanism.

References

- ¹ J.Nishizawa, Y.Okuno and H.Tadano, *J. Crystal Growth*, **31**, 215(1975).
- ² K.Tomizawa, K.Sassa, Y.Shimanuki and J.Nishizawa, *J. Electrochem. Soc.*, **131**, 2394. (1984)
- ³ H.Otsuka, K.Ishida and J.Nishizawa, *Jpn.J. Appl. Phys.*, **8**, 632 (1969).
- ⁴ J.Nishizawa and Y.Okuno, *IEEE Trans. Electron Device*, **ED-22**, 716. (1975).
- ⁵ T.Suzuki and S.Akai, *Bussei*, **12**, 144 (1971).
- ⁶ J.Nishizawa, Y.Okuno, M.Koike and F.Sakurai, *Jpn.J.Appl.Phys.*, **19**, 377 (1980).
- ⁷ J.Nishizawa, K.Ito, Y.Okuno, F.Sakurai, M.Koike and T.Teshima, *Proc. IEEE Electron Device Meeting* (Washington D.C. 1983).
- ⁸ J.Nishizawa and Y.Oyama, *Materials Science and Engineering*, **R12**, 276 (1994).
A.Shimizu, J.Nishizawa, Y.Oyama and K.Suto, *IPRM 98* (Tsukuba, 1998).
- ⁹ Nugraha, O.Ito, K.Suto and J.Nishizawa, *J. Crystal Growth*, **163**, 353 (1996).
- ¹⁰ H.J.Scheel, G.Binning and H.Rohrer, *J. Crystal Growth*, **60**, 199 (1982).
- ¹¹ J. J. Harris, B. A. Joyce and P. J. Dobson, *Surf. Science*, **103**, L90, (1981).
- ¹² G. B. Stringfellow, P. F. Lindquist, T. R. Cass and R. A. Burmeister, *J. Electron. Mat.*, **3**, 497, (1974).
- ¹³ E. Veuhoff, W. Pletschen, P. Balk and H. Luth, *J. Crystal Growth*, **55**, 30, (1981).
- ¹⁴ J. Nishizawa and Y. Kokubun, in "Extended Abstracts of 16th Conference on Solid State Devices and Materials", pp.1, Kobe, Japan, (1984).
- ¹⁵ J. Nishizawa, H. Abe and T. Kurabayashi, *J. Electrochem. Soc.*, **132**, 1197, (1985).
- ¹⁶ T. Suntola, U.S. Pat. No. 4058430,(1977).
- ¹⁷ M. Ahonen, M. Pessa and T. Suntola, *Thin Solid Films*, **65**, 301, (1980).
- ¹⁸ J. Nishizawa, H. Sakuraba and Y. Oyama, *Thin Solid Films*, **225**, 1, (1993).
- ¹⁹ J. Nishizawa, H. Sakuraba and T. Kurabayashi, *Appl. Surf. Sci.*, **92**, 89, (1996).

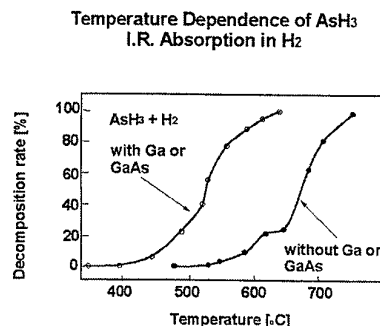
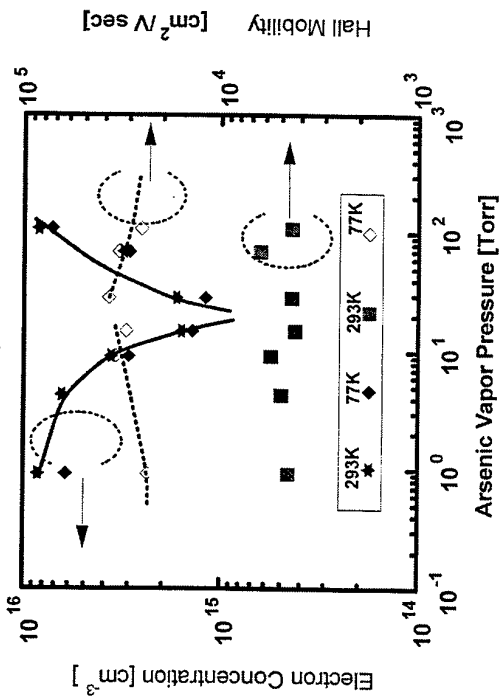


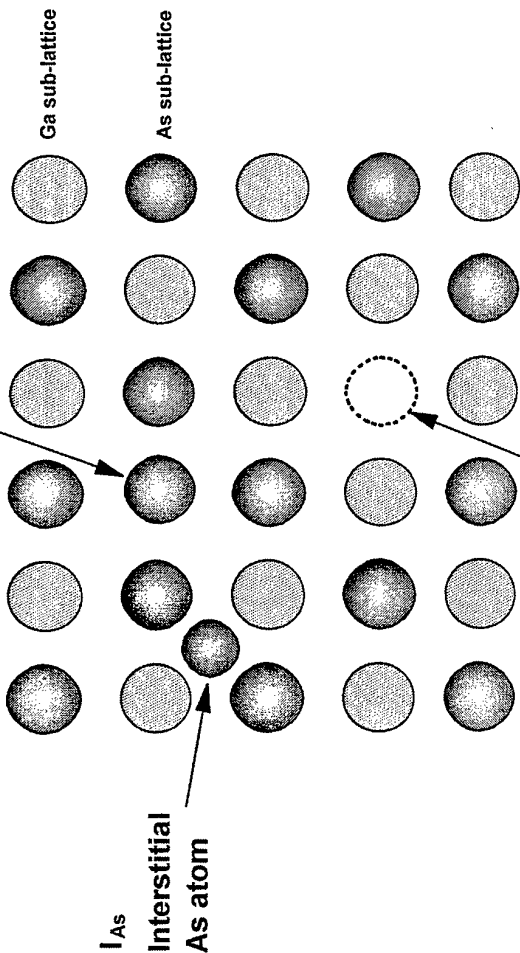
Fig.5 Decomposition of AsH₃ in H₂ with and without Ga or GaAs

LPE GaAs by TDM-CVP



J.Nishizawa

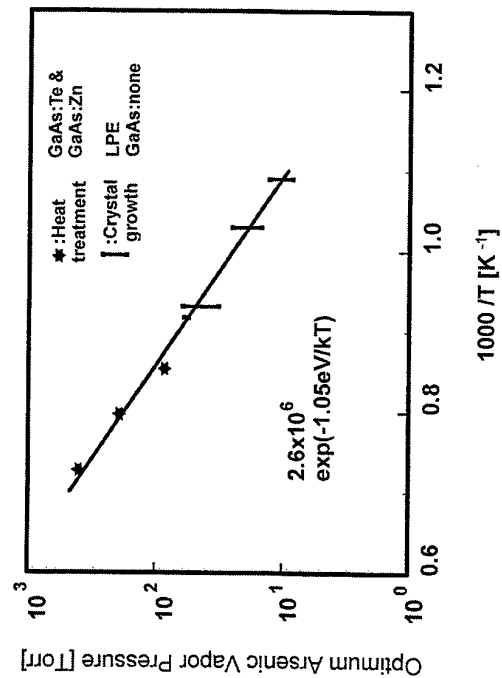
As_{Ga} anti-site defect



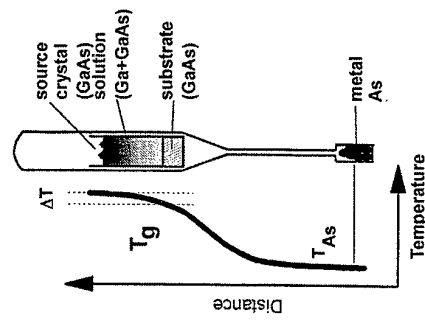
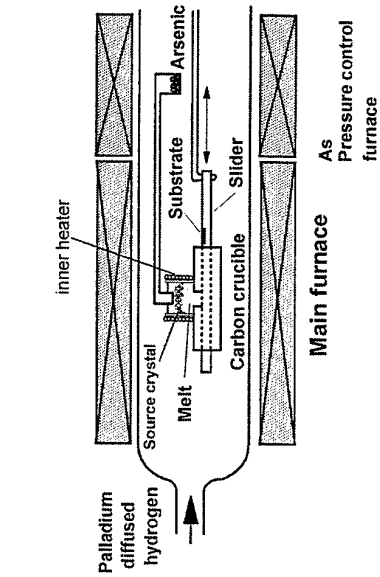
As vacancy

J.Nishizawa

Liquid Phase Epitaxial growth
by
Temperature Difference Method under Controlled Vapor Pressure (TDM-CVP)

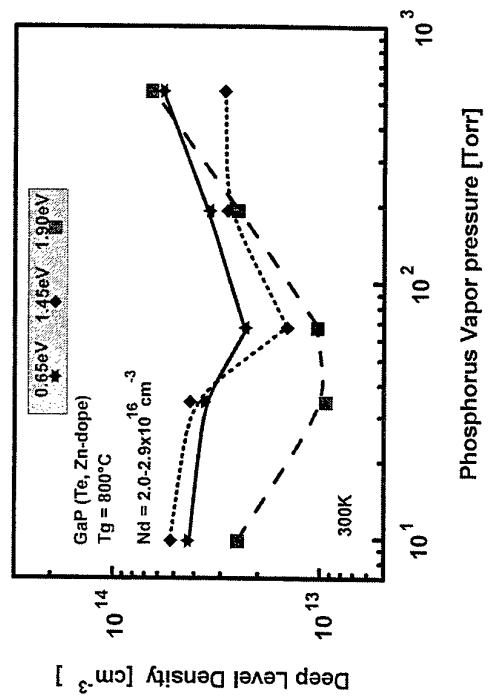


J.Nishizawa



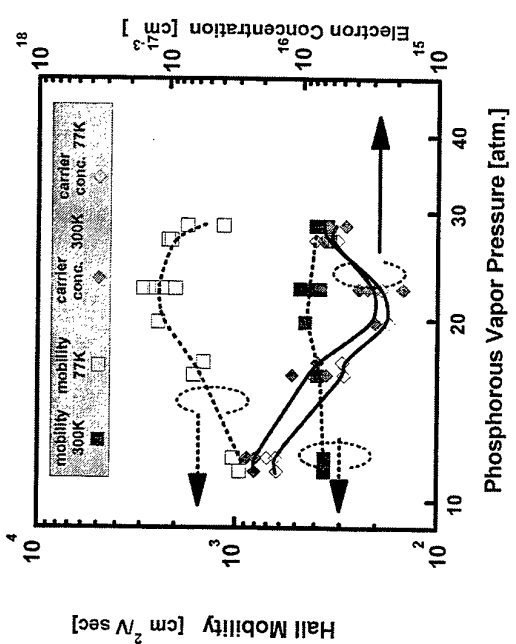
J.Nishizawa

Phosphorous vapor pressure dependence of deep level density in LPE GaP by the TDM-CVP

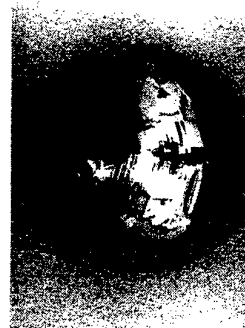


J.Nishizawa

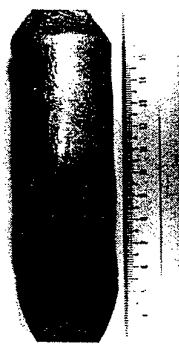
Phosphorous vapor pressure controlled zone melting - grown InP



J.Nishizawa

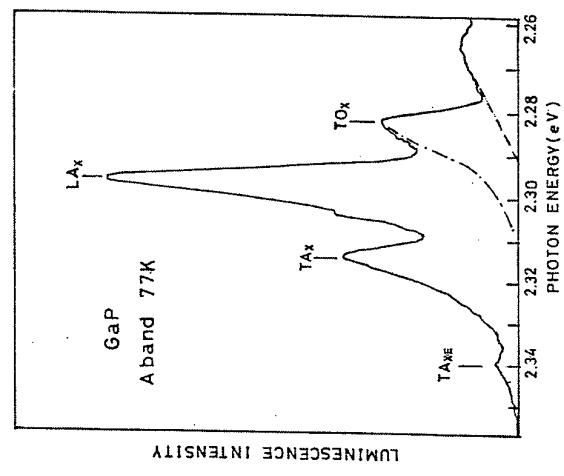


(a) Vapor Pressure Controlled Czochevski (PCZ) grown GaAs

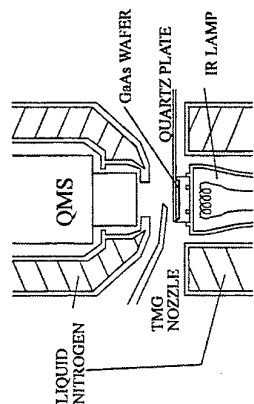


(b) Conventional LEC grown GaAs

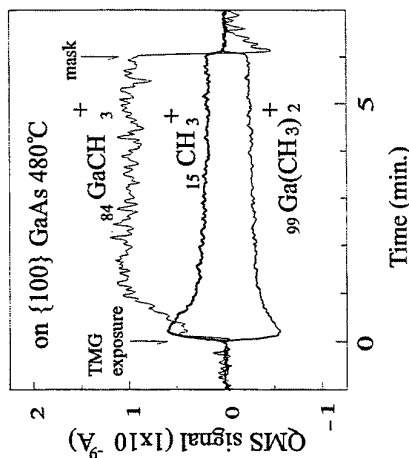
J.Nishizawa



Investigation of surface reaction paths of molecular layer epitaxy with quadrupole mass spectrometer

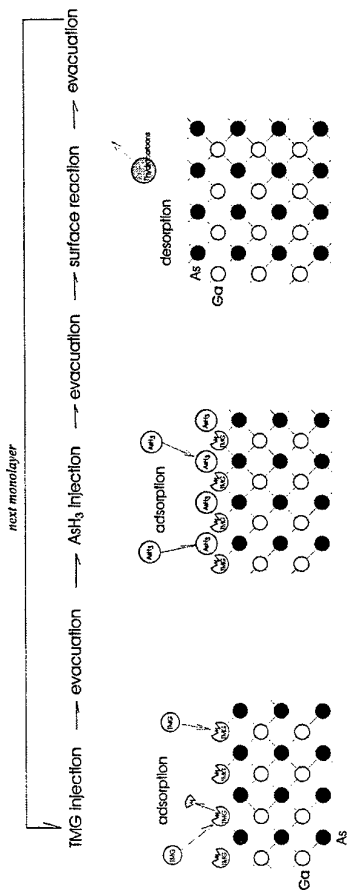
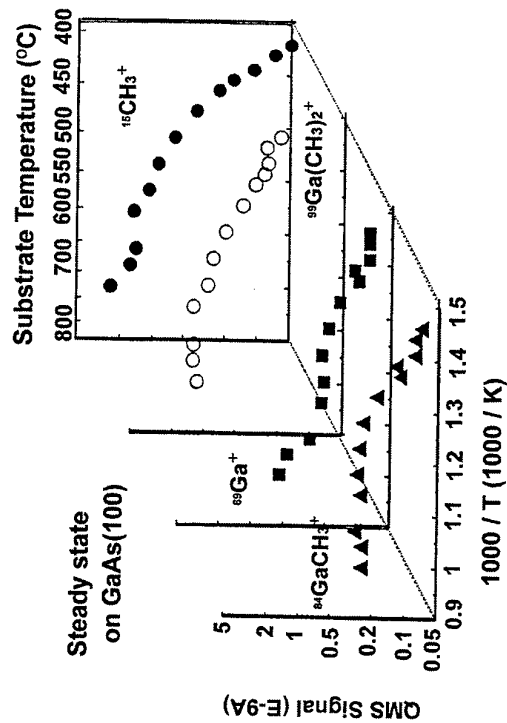


Experimental setup.
Quartz plate is moved to expose or mask GaAs wafer



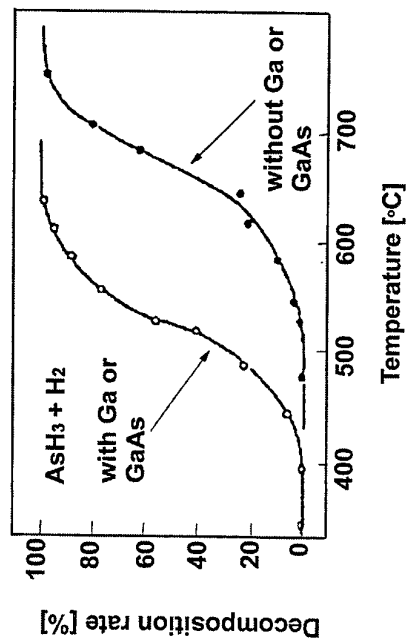
QMS signals measured on {100} n+ GaAs substrate.

Substrate Temperature Dependence of Net QMS Signals in Steady State on GaAs(100), TMG:2.3E-7 Torr



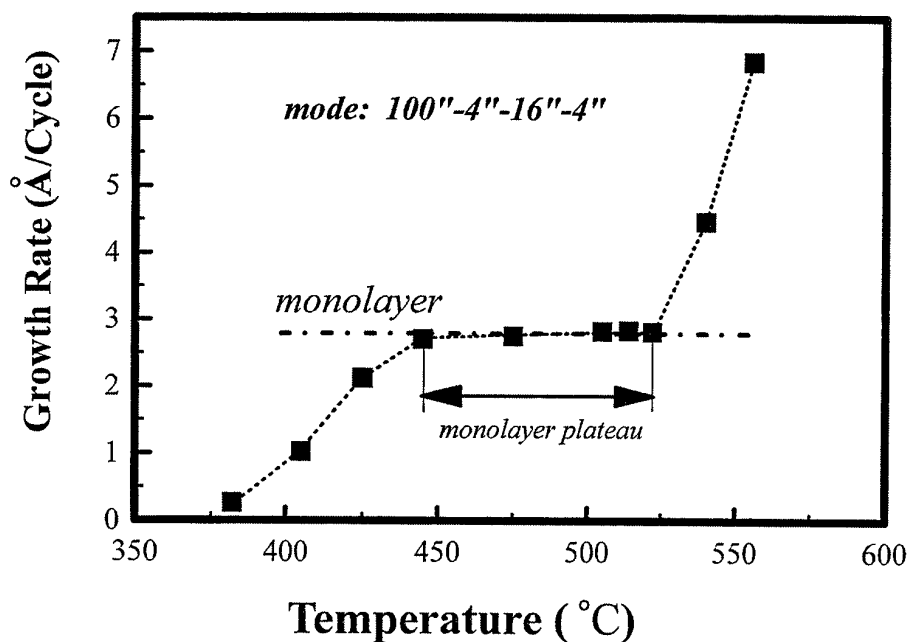
principle of molecular layer epitaxy

Temperature Dependence of AsH_3 I.R. Absorption in H_2

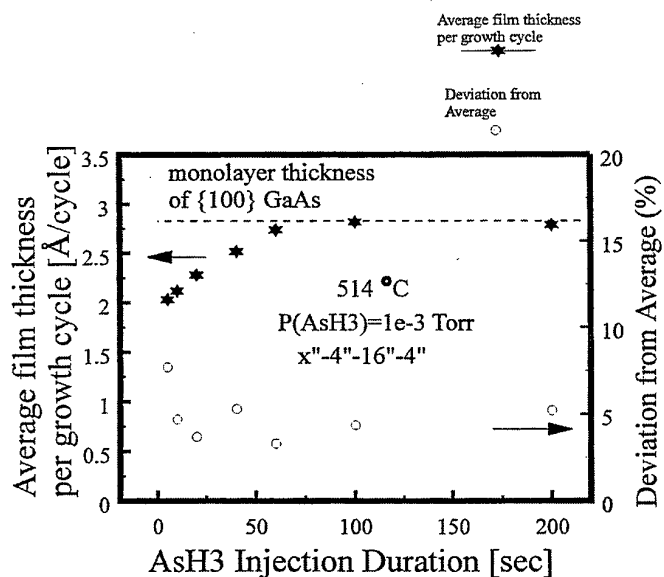


Dependence of Growth Rate on Temperature

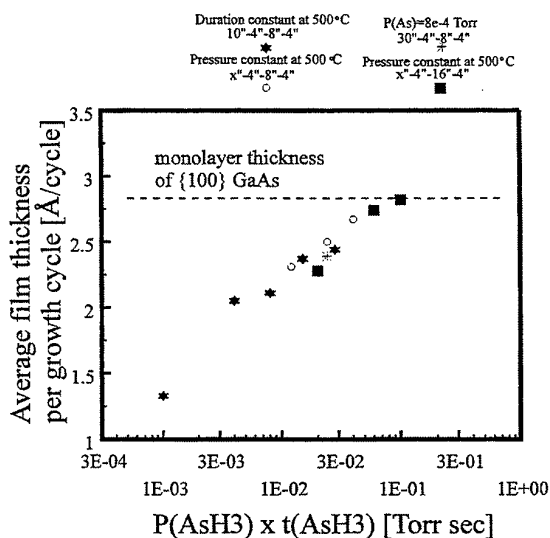
GaAs(100), TMG:5E-5 Torr, AsH₃:1E-3 Torr



AsH₃ in molecular layer epitaxy

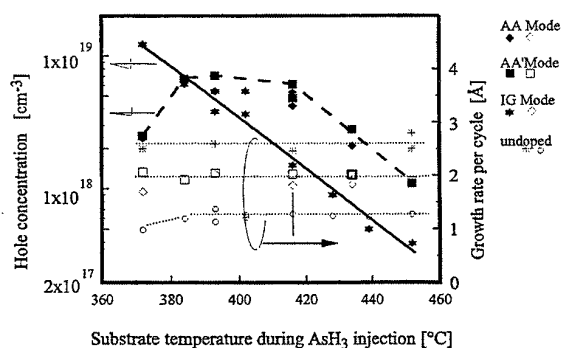
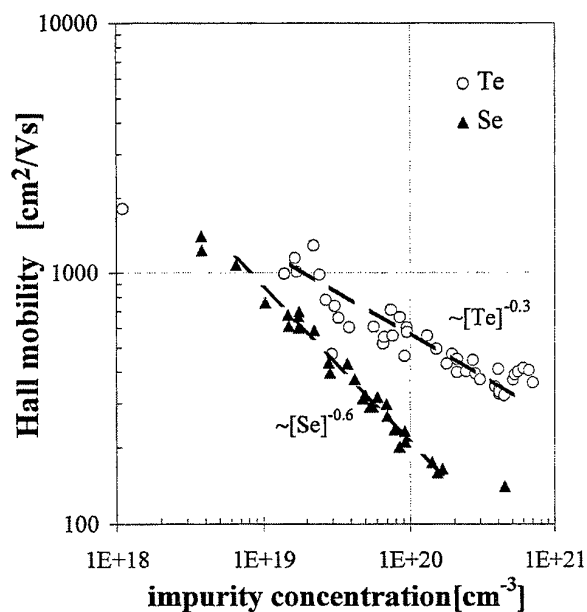
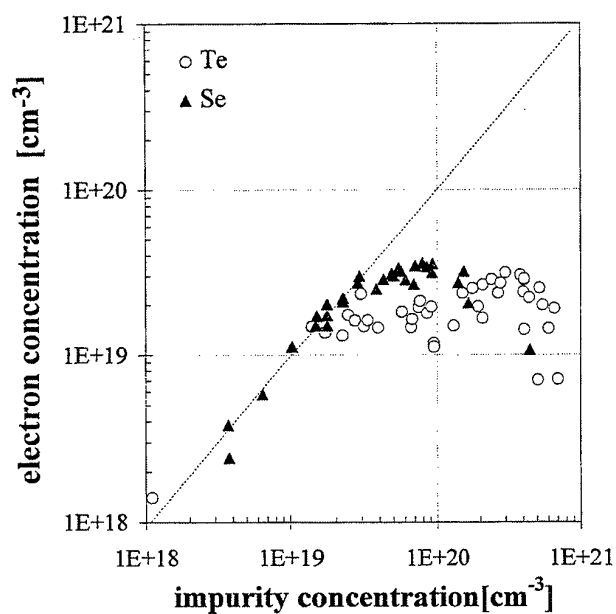


AsH₃ injection duration dependence of film thickness per growth cycle - saturates at monolayer thickness of {100} GaAs for duration longer than 100"

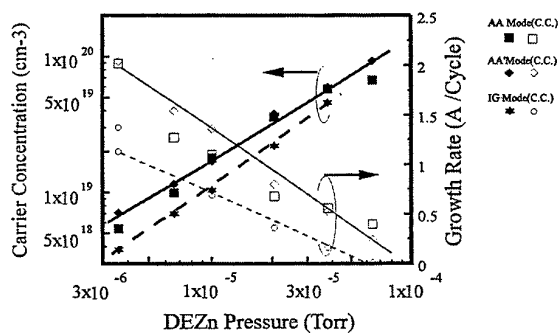
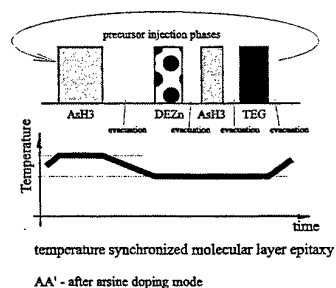


AsH₃ dosage dependence of the average film thickness per growth cycle.

Carrier concentration and Hall mobility in Te and Se doped MLE layer



Growth rate and hole concentration vs. temperature during arsine injection for Zn doped GaAs grown with temperature synchronized MLE.



Hole concentration vs. DEZn pressure for Zn doping for temperature synchronized MLE.

Zinc doping of GaAs grown with
temperature synchronized
molecular layer epitaxy

AsH₃ treatment prior to MLE - low temperature reduction of native oxides

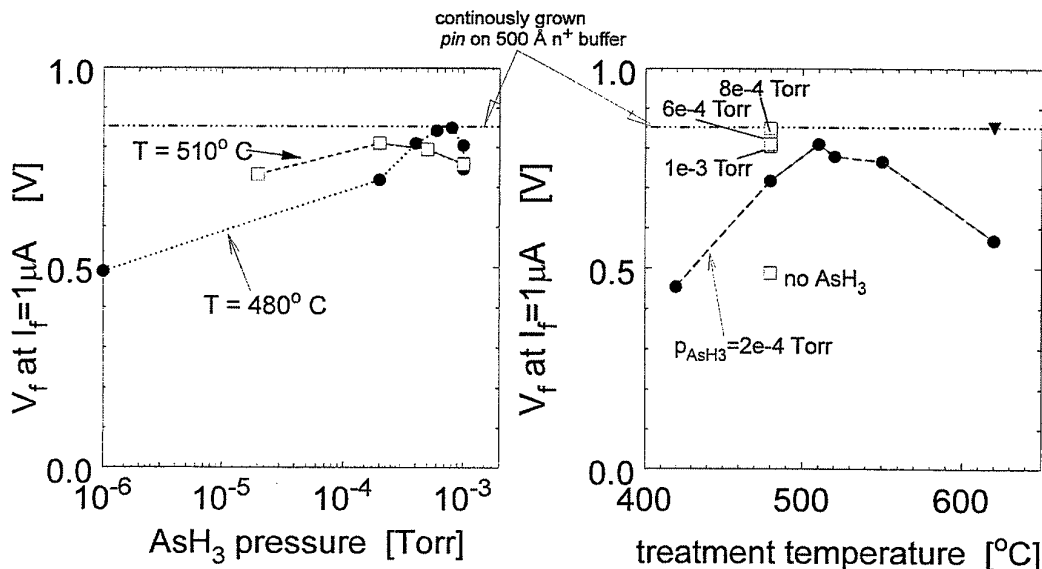
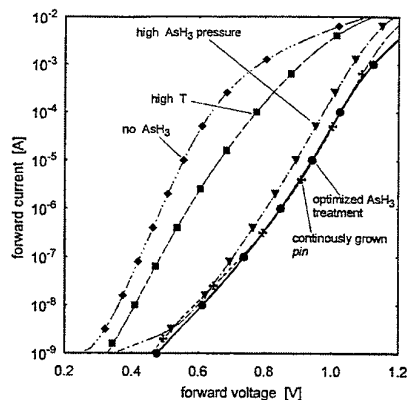
p⁺⁺/p⁺/150_Å_u. regrown on MOCVD n⁻/n⁺

regrown structure:
(100 μm × 120 μm)

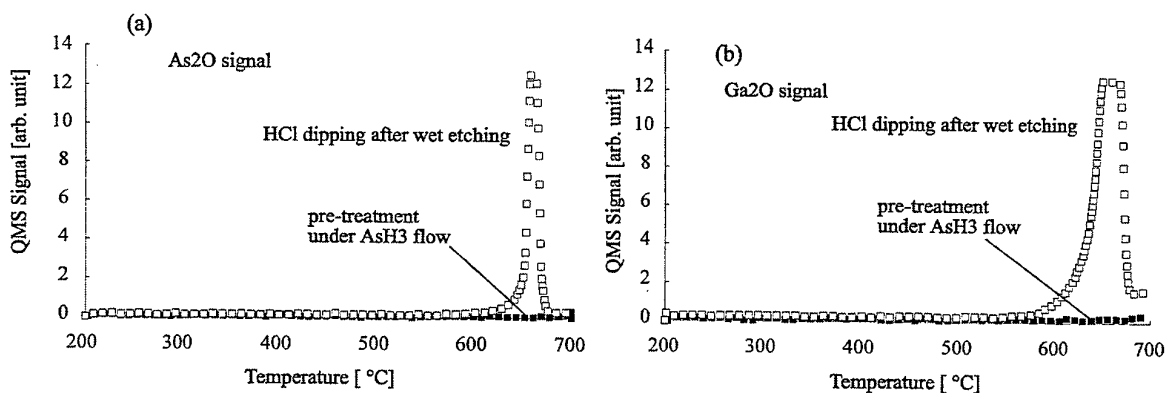
p⁺⁺ 100 Å
Zn doped 6×10¹⁹ cm⁻³
p⁺⁺ 250 Å
Zn doped 5×10¹⁸ cm⁻³
undoped 150 Å

n⁻ 3000 Å MO CVD
layer on n⁺ (100) GaAs
host-regrown interface

treatment time:
30 min. for T < 600° C,
3 min. for T = 620° C,
Hg lamp light



quadrupole mass spectroscope analysis of low temperature native oxide reduction on (100) GaAs with AsH₃

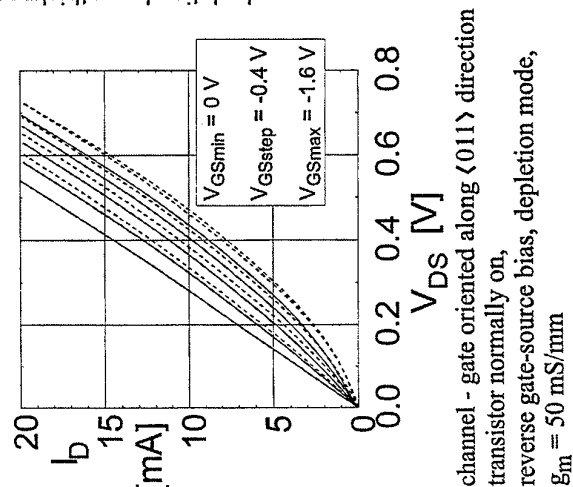
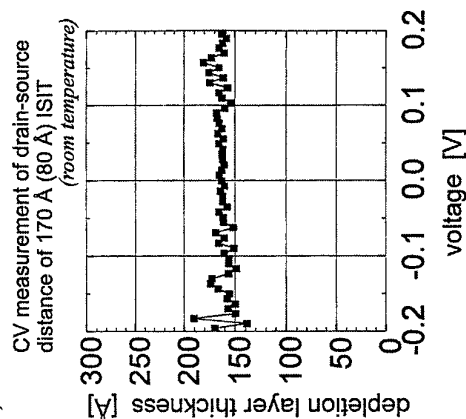
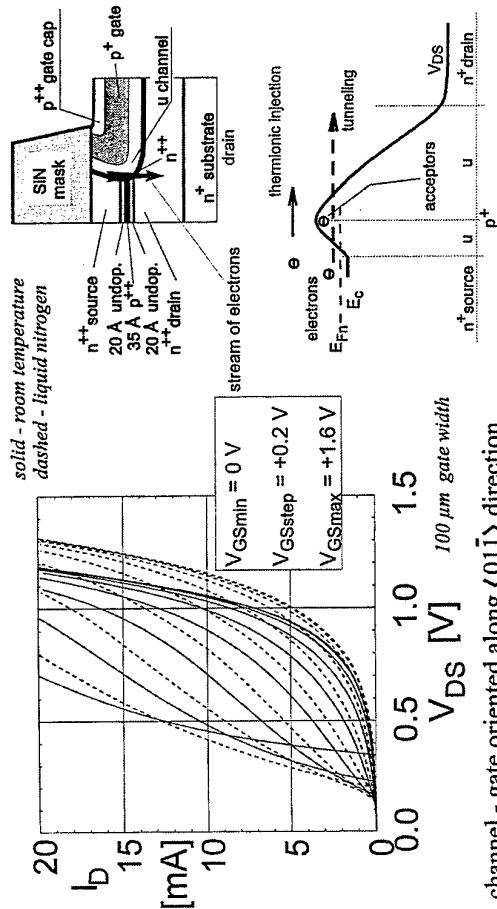


Thermal desorption spectra of arsenic and gallium oxides from (100) n⁺ GaAs
with and without AsH₃ pretreatment.

AsH₃ pretreatment: 2×10⁻⁴ Torr, 510 °C, 30 min.

Output characteristics of 170 Å (80 Å) ISIT

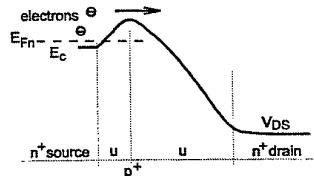
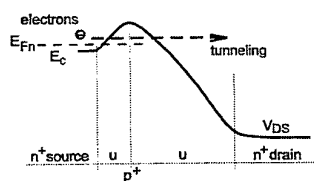
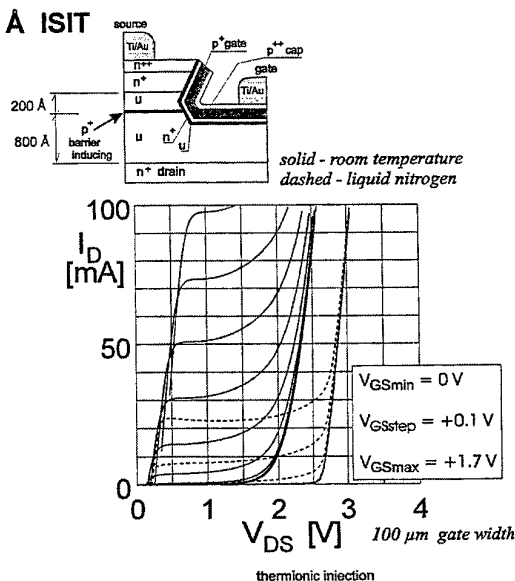
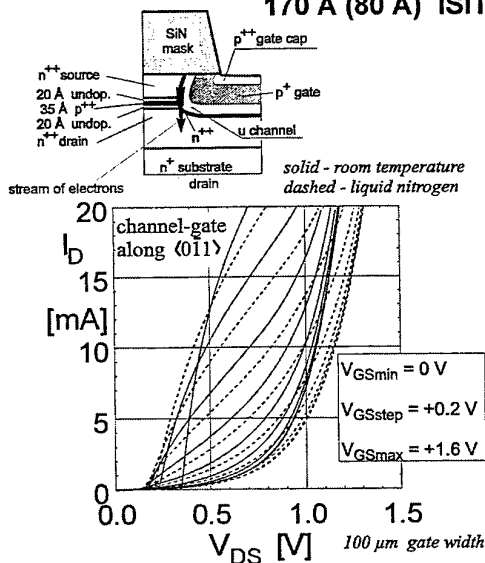
intradrain source-drain electron tunneling mode;



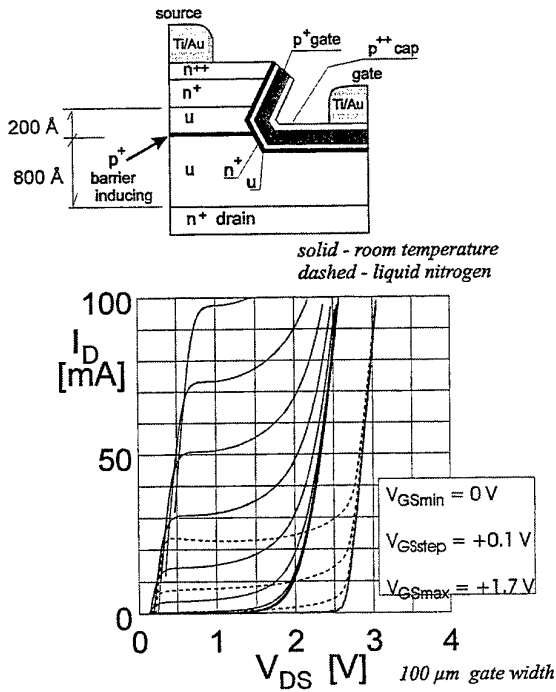
Tunneling and thermionic injection mode GaAs ISITs - temperature dependence

170 Å (80 Å) ISIT

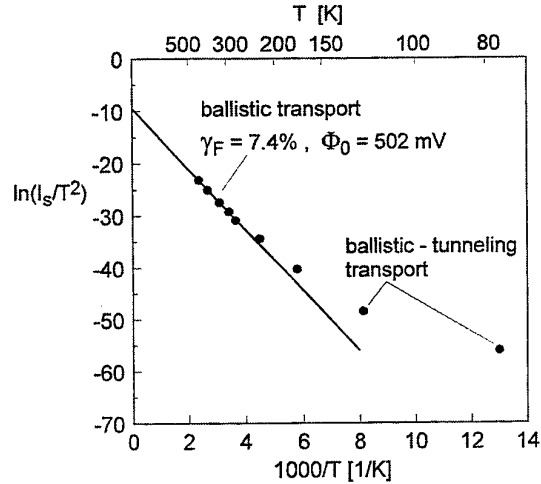
1000 Å ISIT



Ballistic and tunneling transport in 1000 Å ISIT



channel - gate oriented along $\langle 01\bar{1} \rangle$ direction or along $\langle 011 \rangle$ direction; transistor normally off, forward gate-source bias,



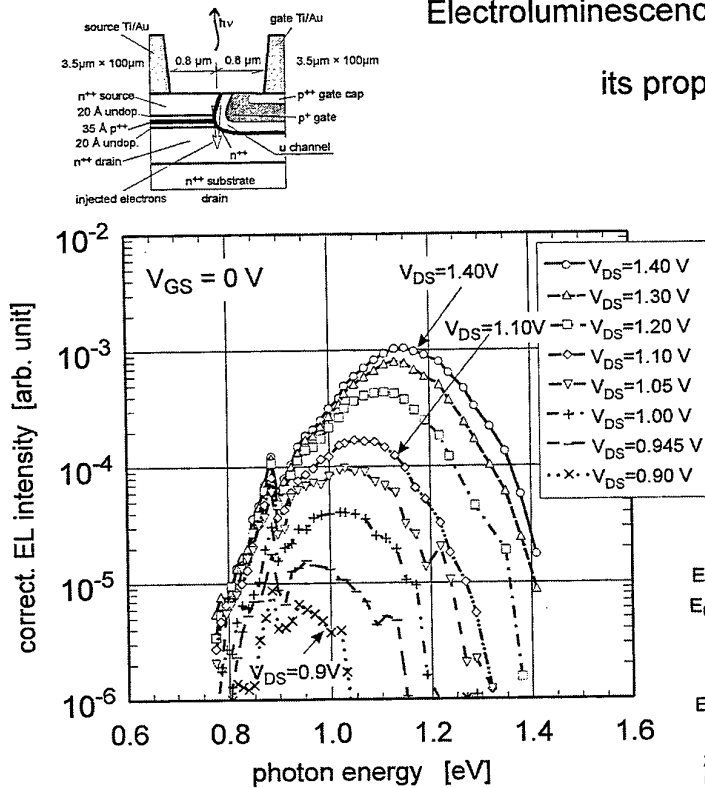
ballistic electron transport in 1000 Å ISIT

electron transit time < 1ps

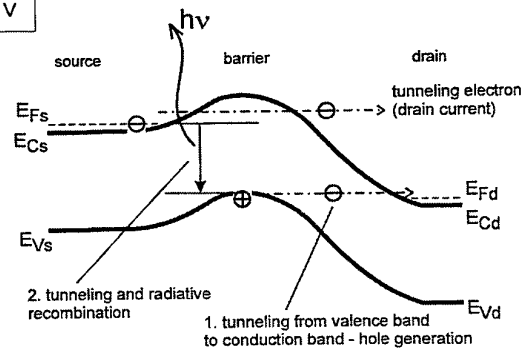
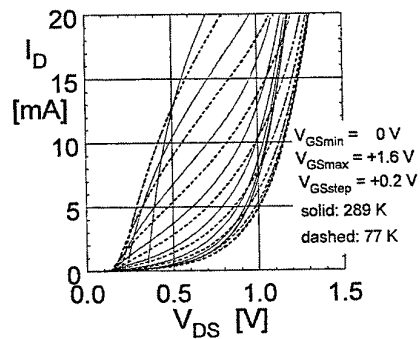
for intrinsic ISIT $f_T \approx 800$ GHz

(J.Nishizawa 1981)

Electroluminescence of 160 Å vertical GaAs ISIT and its proposed mechanism



Room temperature electroluminescence spectra dependence on drain-source voltage. Intensity corrected for detector characteristic.



Control of growth modes in epitaxy from the vapor phase and from the liquid phase

Hans J. Scheel

Cristallogénèse - IMO

Swiss Federal Institute of Technology

Chemin de Bellerive 34, CH-1007 Lausanne, Switzerland

Phone +41-21-693-4452; FAX +41-21-693-4750; e-mail Hans.Scheel@epfl.ch

The three classical epitaxial growth modes are defined (1) by the interfacial energies between substrate and layer:

- 1) The layer-by-layer or Frank-van der Merwe (F-VM) growth mode,
- 2) the Volmer-Weber (V-W) birth-and-spread growth mode, and
- 3) the intermediate Stranski-Krastanov (S-K) growth mode.

Deposition of epitaxial layers is normally performed under non-equilibrium conditions, especially when the layers are grown by physical vapor deposition PVD (MBE, sputtering, pulsed laser deposition) or by chemical or metal-organic chemical vapor deposition (CVD, MOCVD). In these cases the growth modes are controlled by the chemical potential, i.e. by the deviation from thermodynamic equilibrium respectively by the supersaturation. But also other factors play a role in the control of growth modes, such as the misfit between substrate and layer, the misorientation of the substrate, the growth temperature, and mass transport phenomena controlled by aerodynamics or by hydrodynamics (2). In addition to the three growth modes discussed above, the step-flow mode, the spiral-island growth, columnar growth, and step bunching

can be observed as non-equilibrium growth modes.

The effects of the most important growth parameters on the growth modes will be discussed. Especially, it will be shown, that for compounds with thermodynamic stability limits like incongruent melting or incongruent evaporation (examples GaAs, cuprate superconductors) the F-VM growth mode and thus quasi atomically flat surfaces can only be achieved by liquid phase epitaxy (LPE) when misfit and supersaturation are extremely small (3-7).

The control of the growth modes is not only of crucial importance for the surface morphology, but also for the structural perfection of epitaxial layers, and for the performance of microelectronic, optoelectronic, and superconducting devices.

- 1) E. Bauer, Zeitschrift f. Kristallogr. 110 (1958)372.
- 2) H. J. Scheel at 6th Internat. Symp. on Superconductivity (ISS'93), in Advances in Superconductivity VI, editors T. Fujita and Y. Shiohara, Springer, Tokyo 1994, p.29-36.
- 3) H. J. Scheel, Appl. Phys. Lett. 27 (1980) 70.
- 4) H. J. Scheel, G. Binnig, H. Rohrer, J. Crystal Growth 60 (1982) 199-202.
- 5) A. A. Chernov and H. J. Scheel, J. Crystal Growth 149 (1995)187.
- 6) H. J. Scheel et al., Appl. Phys. Lett. 65 (1994) 901.
- 7) C. Klemenz et al., in preparation.

Control of Growth Modes in Epitaxy

Hans J. Scheel
Cristallogénèse - IMO
Swiss Federal Institute of Technology
ch. de Bellerive 34, CH-1007 Lausanne, Switzerland
Tel. +41-21-693-4452 Fax +41-21-693-4750
e-mail : Hans.Scheel@epfl.ch

Introduction

3 → 7 Growth Modes

Effects of Growth Parameters

Concentration

Supersaturation

Misfit between Layer and Substrate

Misorientation of Substrate

Comparison

Physical Vapor Deposition PVD

Chemical Vapor Deposition CVD

Liquid Phase Epitaxy LPE

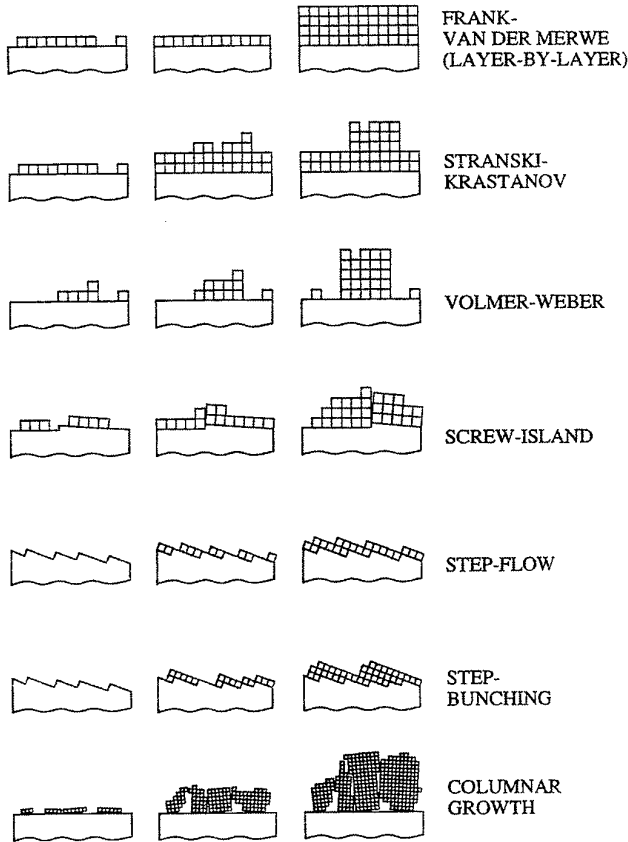
Examples

GaAs

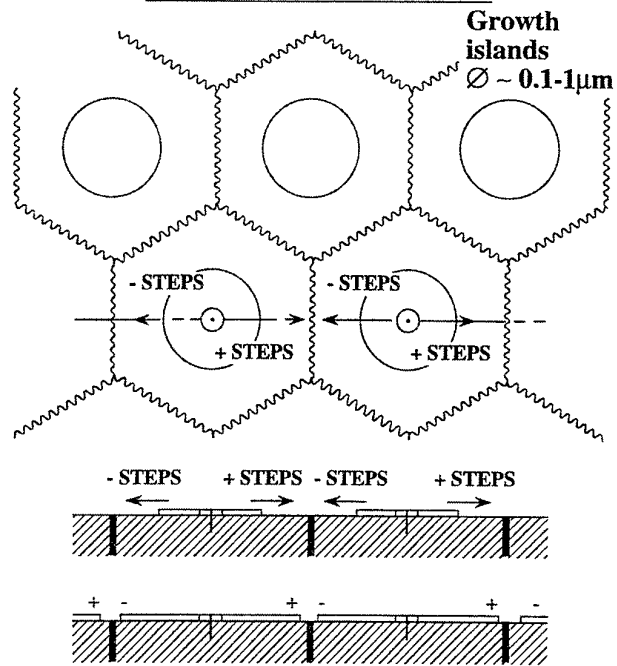
High-Tc Superconductor YBCO

GaN

Conclusions



MBE & MOCVD of GaN



No. of growth islands $\sim 10^8 - 10^{10} / \text{cm}^2$

No. of triple crossings $\times 2$

Length of lines $200 \text{ m} \cdot \text{cm}^{-2}$

Growth centers at defects (screw dislocations, etc.)

Inclination of islands $< 2^\circ$ (substrate surface ; growth rate)

Step distance $y_0 \approx 100 (< 500) \text{ \AA}$

Supersaturation & Step Distance

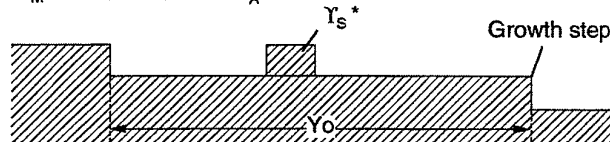
2 D Nucleation

$$\text{Critical radius of surface nucleus } \gamma_s^* = \frac{\gamma_m V_M}{a^2 RT \sigma} = \frac{\gamma_m a}{kT \sigma}$$

$$\sigma = \frac{n - n_e}{n_e} = \frac{\Phi \Delta T}{RT^2}$$

γ_m = energy per growth unit $\approx a \gamma_e$
with γ_e edge energy of nucleus [J/cm]

V_M = molar volume $= N_A a^3$



Step Distance

Archimedian spiral $\Upsilon = 2 \gamma_s^* \theta$

$$Y_0 = 2 \gamma_s^* (\theta + 2 \pi) - \theta = 4 \pi \gamma_s^* \quad (\text{BCF 1951})$$

$$Y_0 = 19 \gamma_s^* = \frac{19 \gamma_m a}{kT \sigma} \quad (\text{Cabrera \& Levine 1956})$$

	PVD, MOCVD	LPE	} $\sigma_{\text{PVD}} \approx 200 \times \sigma_{\text{LPE}}$ MOCVD
Y_0	140 - 300 \AA	6 μm (0.6 - 17)	
γ_s^*	~ 8 - 16 \AA	~ 3000 \AA	

(1) AlN buffer layer



(2) Nucleation of GaN



(3) Geometric selection



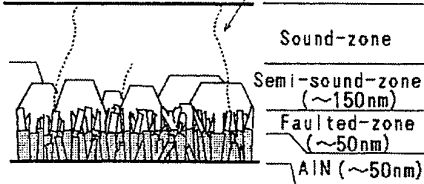
(4) Island growth



(5) Lateral growth Trapezoid crystal



(6) Uniform growth Dislocation



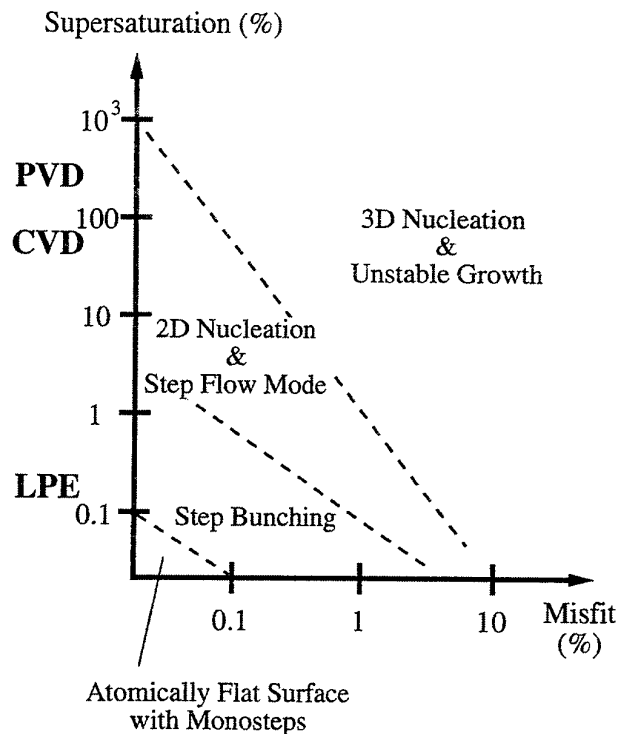
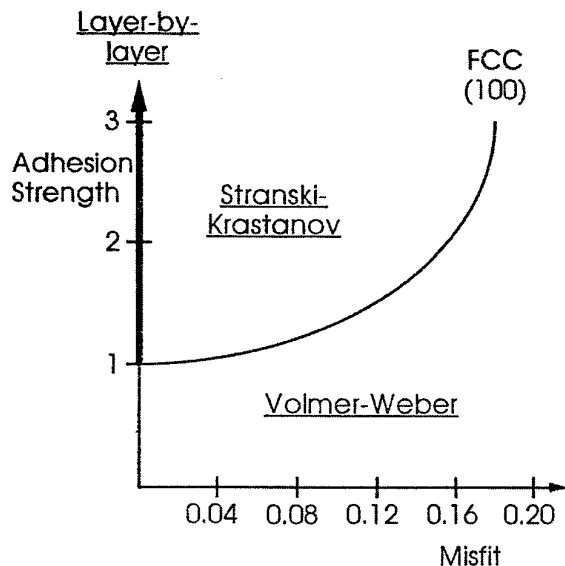
Comparison of Supersaturation in Gas-Phase Epitaxy (PVD, CVD) and in Liquid Phase Epitaxy (LPE)

	Measured step distances y_0 [μm]			Supersaturation ratios from	
				step distances	free-energy estimates
	PVD	CVD	LPE	$\frac{\sigma(\text{PVD,CVD})}{\sigma(\text{LPE})}$	$\frac{\sigma(\text{PVD,MOCVD})}{\sigma(\text{LPE})}$
GaAs	0.05	0.05	6	120	375-390
YBCO	0.03	0.03	1-6	33-200	1500

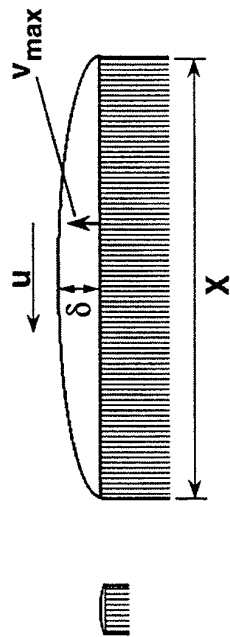
13.8.98 HJS

Growth Modes

(from atomistic simulations using a Lennard-Jones interatomic potential, Grabow and Gilmer 1988)



Conditions for stable growth



$$\delta = \left[\frac{2}{3} \cdot Sc^{1/3} \cdot \left(\frac{\rho_s u}{\eta X} \right)^{1/2} \right]^{-1} \quad (1)$$

$$Sc = \text{Schmidt Number} = \frac{\eta}{\rho_s \cdot D}$$

$$v_{\max} = \left(\frac{0.214 D u \sigma^2 n_E^2}{Sc^{1/3} \rho^2 X} \right)^{1/2} \quad (2)$$

$$\sigma = \text{Relative Supersaturation} = \frac{n_s - n_E}{n_E}$$

δ = thickness of the solute diffusion boundary layer

n_E = equilibrium solute concentration

n_s = concentration in the bulk of the solution

ρ_s = density of the solution

u = solution flow rate ($u \approx 0.1$ cm/s for stirring by natural convection)

(1) after Carlson (1958)

(2) H. J. Scheel, D. Elwell, J. Crystal Growth 12 (1972) 153
ch. 6 of D. Elwell and H. J. Scheel "Crystal Growth from High-Temperature Solutions", Academic Press, London-New York 1975.

EPITAXY PARAMETERS & SURFACE ROUGHNESS

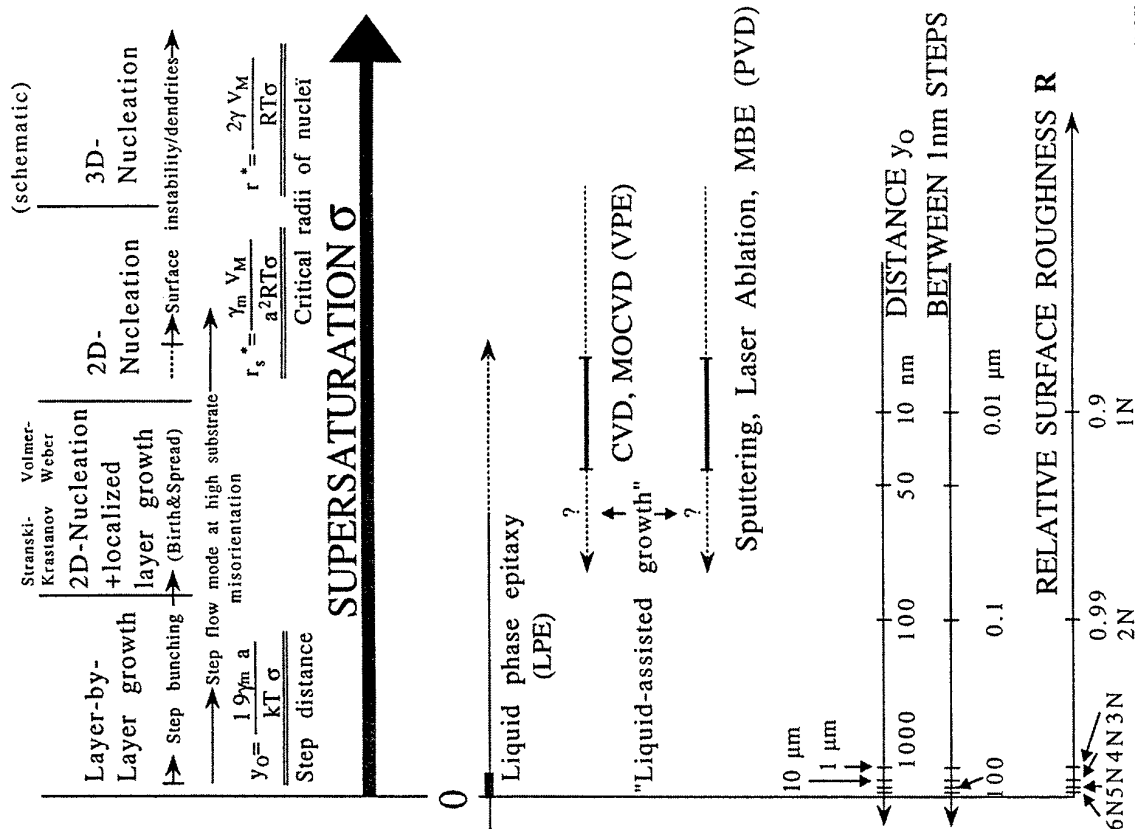
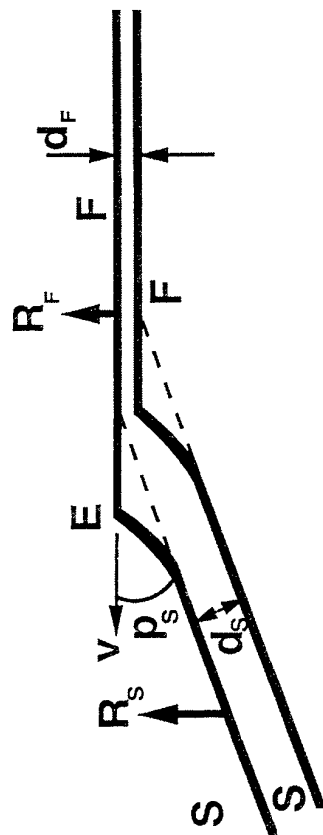


Table 1. Parameters for Control of Growth Modes

Surface energy of substrate	γ_{SV}
Surface energy of film	γ_{FV}
Interface energy substrate - film	γ_{SF}
according to	$\gamma_{SV} = \gamma_{FS} + \gamma_{FV} \cos \Theta$
Supersaturation, relative	$\sigma = \frac{n - n_e}{n_e}$
Supersaturation ratio	$\alpha = \frac{n}{n_e}$
Misfit substrate - film (at growth temperature)	$f = \frac{a_s - a_F}{a_F}$

490



$$d_S = d_{S1} + d_{S2} = 2 \left(\frac{\Delta T}{CS} \frac{\partial Ce}{\partial T} \right) \left(\frac{D}{\pi} \right)^{1/2} t^{1/2} + \frac{3}{2} \left(\frac{\dot{T}}{CS} \frac{\partial Ce}{\partial T} \right) \left(\frac{D}{\pi} \right)^{1/2} t^{3/2}$$

$$v_{S(st)} = (C/C_{S(st)}) \beta_{S(st)} \Delta\mu/kT$$

$$\beta_S = \beta_{St} | p |$$

$$d_0 \equiv \frac{19 \omega^2 C_e \alpha D}{4 \pi \beta_{st} h k T} ; \chi \equiv \frac{4 \beta_{st} h k T}{19 \omega C_e \alpha} \sqrt{\frac{\pi}{D}} \frac{\partial C_e}{\partial T}$$

$$L = 2ps^{-1} d_0 \int_0^t \left[\sqrt{1 + \chi_{\Delta T} + \left(\frac{9}{4}\right) \chi \dot{T} t^{1/2}} - 1 \right] \frac{dt}{t}$$

$$L = 6 d_0 \chi \dot{t}^{3/4} = \frac{2 \omega}{p} \left(\frac{19 \omega_{\text{Ce}} \alpha \dot{t} \partial \text{Ce}}{\beta_{\text{st}} h k T \partial T} \right)^{1/2} \left(\frac{D t}{\pi} \right)^{3/4}$$

A. A. Chernov & H. J. Scheel: Extremely flat surfaces by liquid phase epitaxy

Oxidation stage of surface species and partial pressure of reactive species (oxygen, arsenic etc.) during growth

Surface liquid or surface melting due to impurities (VLS mechanism) or due to partial decomposition

Θ = contact (wetting) angle
 n = effective concentration (or vapor pressure)
 n_e = equilibrium concentration (or vapor pressure)
 a_s = lattice constant of substrate
 a_f = lattice constant of film

12.8.97 HJS

Liquid Phase Epitaxy :

Potential for large-scale multilayer production

- 1) Liquid phase epitaxy for highest-quality semiconductor multilayer devices
(LEDs, lasers, detectors, photovoltaic solar cells)
- 2) Best technology for highest-performance optoelectronic devices

because

- near equilibrium + low temperature } • **minimum inherent defects**
 - **stoichiometry control**
 - quasi-perfect-growth, constantly improving as long as below V_{max} ! Still high growth rates (1-50nm/sec)
 - extremely flat surfaces (facets) and p-n junctions
 - thin layers possible
 - thick layers possible
 - multilayers possible
- } with automatic slider-free technology
- large-area substrates possible (10x10 to 25x25cm²)
 - economic mass production possible (e.g. km²/machine-month)

- 3) Factors to be observed or developed :

Loading / de-loading in quasi-continuous process

Solvent which is not interfering with electronic properties, $k_{eff} \ll 1$

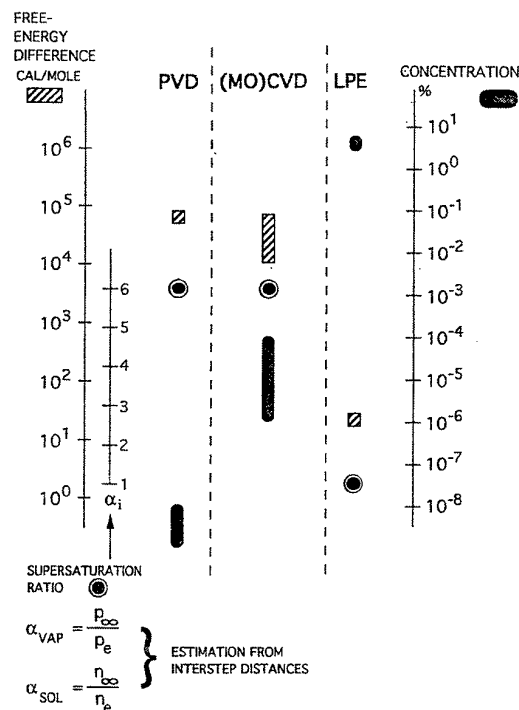
Solubility curve

Corrosion-resistant crucible

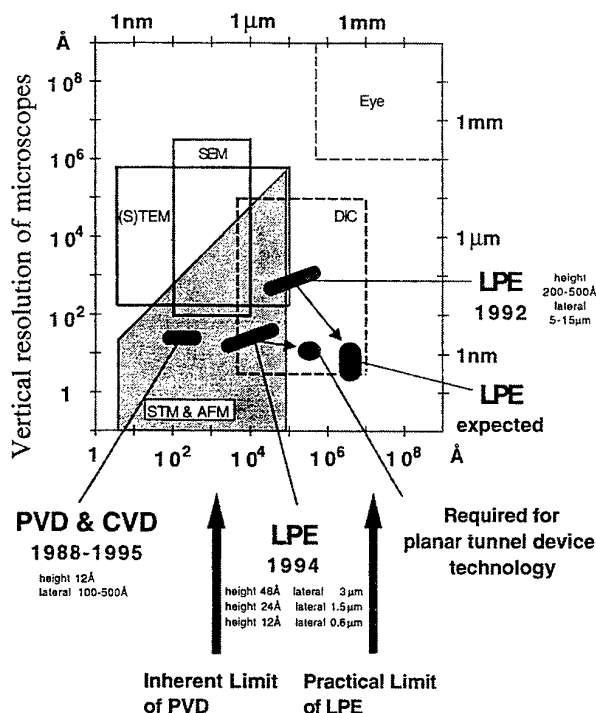
Substrates : low-cost; low misfit; similar thermal expansion coefficients

29.9.95

EPITAXY OF GaAs



Lateral resolution of microscopes



Step heights and interstep distances of YBCO and NdBCO layers.

Growth Modes & Device Performance

Initial Growth Modes in PVD and CVD

Increasing Layer Thickness

Volmer-Weber
Stranski-Krastanov
Spiral-Island

Columnar Growth
and
Grain Coarsening

~ 10⁸-10¹⁰ Grains · cm⁻²
~ 10⁸-10¹¹ Dislocations · cm⁻²
Voids, Pinholes etc.
Mosaic Linewidth 0.1°-2° FWHM

Reduction at
Low Growth Rate
or High T

In PVD & CVD

In LPE

Step-Flow Mode

Frank-Van der Merwe Layer-by-Layer Growth

by Well-Adjusted
Substrate Misorientation

by Low Supersaturation
and Substrates of Low Misfit
and Small Misorientation

High-Quality Devices
Large-Scale Production Possible

Ultimate Device Performance
Large-Scale Production Possible

Investment/Economy of Process/Safety

Conclusions

Choice of epitaxy method

- personal experience or copy others
- salesman of equipment
- physicists : PVD

Future:

Performance & lifetime of device

Economic large-scale fabrication process

Investments & infrastructure

Skills of manpower

Safety

→ Control of growth modes

by choice of epitaxy method

(vapor versus liquid)

by optimized growth parameters

by optimized substrate

Progress of several technologies determined by crystal growth & epitaxy technology:

e.g. photovoltaic cells, optical data storage, lasers, green & blue LEDs for display, high-T_c superconductors.

Microchannel Epitaxy-A combination of selective area epitaxy and epitaxial lateral overgrowth for high quality heteroepitaxy-

T. Nishinaga

Department of Electronic Engineering, Graduate School of Engineering,
The University of Tokyo, 7-3-1, Tokyo, 113 JAPAN
e-mail: tatau@ee.t.u-tokyo.ac.jp

There are large demands to grow a high quality film on a substrate with large lattice mismatch. III-V compounds on Si, III-V Nitrides on sapphire, II-VI compounds on various substrates are the examples for such highly lattice mismatch heteroepitaxy (HM²). Among them GaAs on Si and GaN on sapphire are the most exciting topics towards obtaining respectively opto-electronic integrated circuit (OEIC) and blue laser and light emitting diodes. However, a large lattice mismatch between the film and the substrate brings in a large density of defects in the grown layer such as dislocations, twins and stacking faults. To decrease the density of these defects, two step growth has been employed. In this method, a buffer layer is deposited at relatively low temperature and the epitaxial growth is conducted at normal growth temperature. However, the reduction of the defect densities is not enough and much more effective way for the defect reduction has been required.

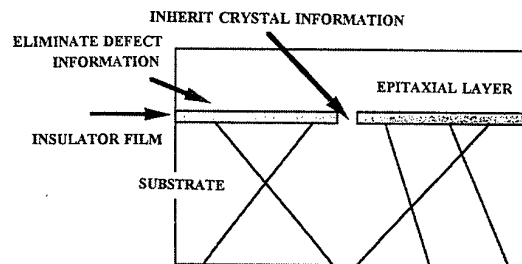
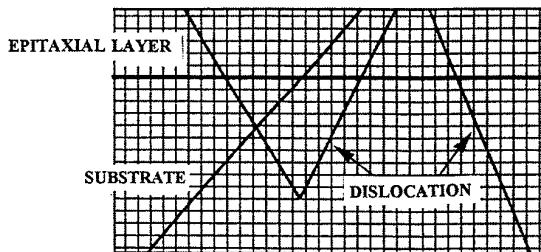


Fig. 1 Inheritance of defects in normal epitaxy Fig. 2 Concept of Microchannel Epitaxy

In normal epitaxy, as shown in Fig. 1, the defect information of the substrate is transferred to the epitaxial layer as well as the crystal information. Hence, it is difficult to obtain epitaxial layer of plane defect and dislocation free, if they are present in the substrate. In this talk, we explain the microchannel epitaxy(MCE) as a very effective technique to eliminate most of the defects. The main idea of MCE is to inherit the crystal information of the substrate through a narrow microchannel and to eliminate the defect information as shown in Fig. 2. Real processes of MCE

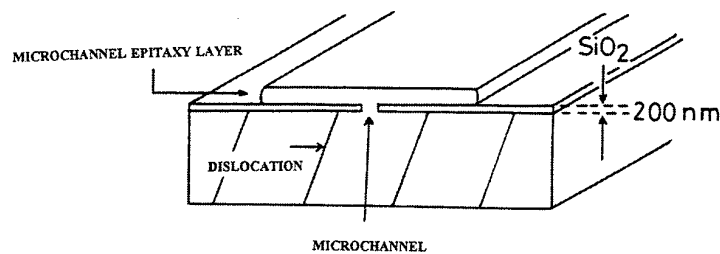


Fig. 3 Structure of typical MCE layer.

are as follows. First, a mask epitaxy is carried out through narrow line seeds opened in an insulating film on the substrate and then a growth is conducted in lateral direction using the grown film in the window as the seed. Since the area containing the defects generated at the interface between the substrate and heteroepitaxial layer is restricted within the region over the line seed, one can get a lateral part between the line seeds almost free of defects. Fig. 3 shows schematically the structure of MCE layer and substrate. So far, defect free regions have been successfully obtained for GaAs on GaAs substrate[1], Si on Si[2], GaP on GaP[3], GaAs, InP on Si[4-7] and very strong reduction of dislocation density have been reported for GaN on sapphire. In Fig. 4 is shown a photograph of the MCE layer of GaAs on Si after KOH etching.

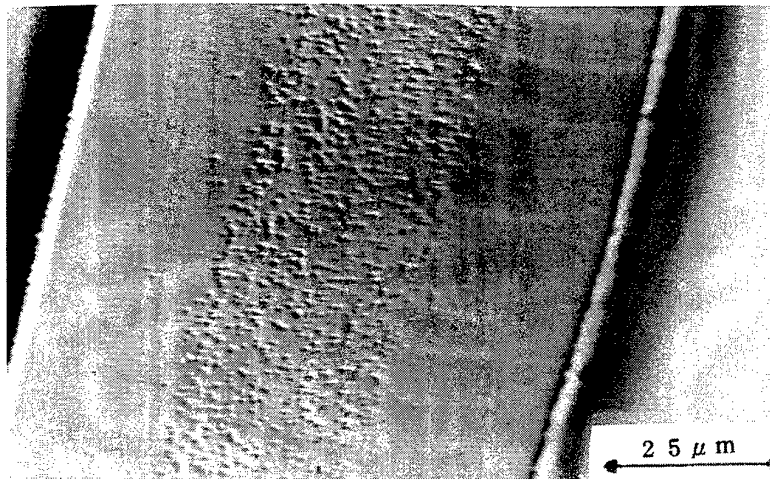


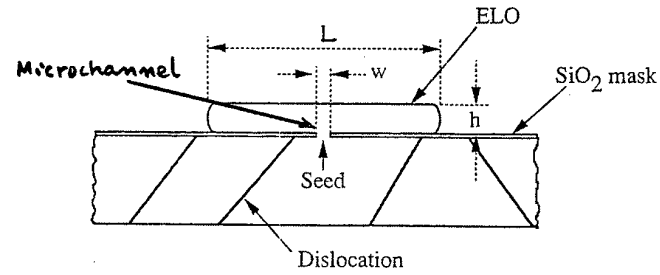
Fig. 4 MCE layer of GaAs on Si after KOH etching.

References

- [1] T.Nishinaga, T.Nakano and S.Zhang : Japan.J.Appl.Phys.27(1988)1964.
- [2] Y.Suzuki and T. Nishinaga : Japan.J.Appl.Phys.28(1989)440.
- [3] S.Zhang and T.Nishinaga : Japan.J.Appl.Phys.,29(1990)545.
- [4] Y.Ujiie and T.Nishinaga : Japan J.Appl.Phys.28(1989)L337.
- [5] S.Sakawa and T. Nishinaga : Japan.J.Appl.Phys. 31(1992)L359.
- [6] S.Naritsuka and T.Nishinaga : J.Crystal Growth 146(1995)314.
- [7] S.Naritsuka, T.Nishinaga, M.Tachikawa and H.Mori : Japan.J.Appl.Phys.,34(1995)L1432.

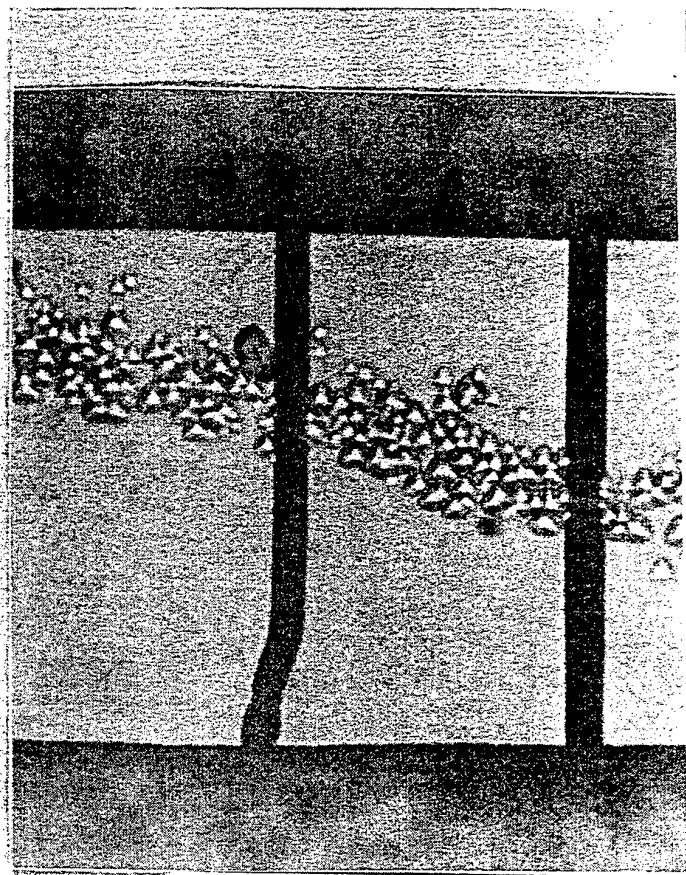
Microchannel Epitaxy (MCE)

I. Horizontal Microchannel Epitaxy



1. Growth from Microchannel
2. Growth in Lateral Direction
Epitaxial Lateral Overgrowth

ELO



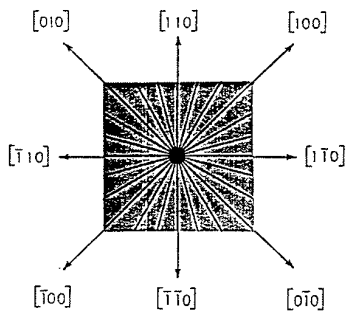
← 50 μm →

GaAs on Si(111)

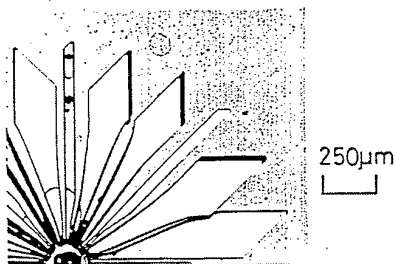
JJAP 1989

GaAs on GaAs
(001)

JCG ('90)



(a)



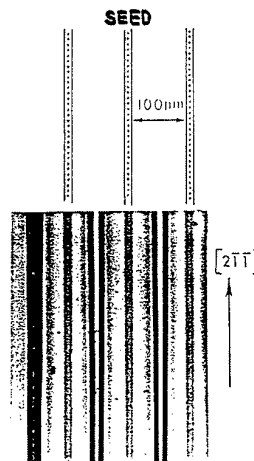
(b)

MCE of GaP on

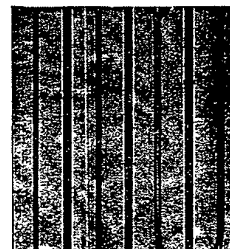
(a) GaP(111)B sub.

JJAP'90

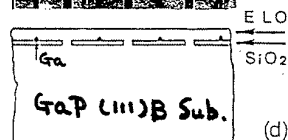
connection of ELO
layers



(b)

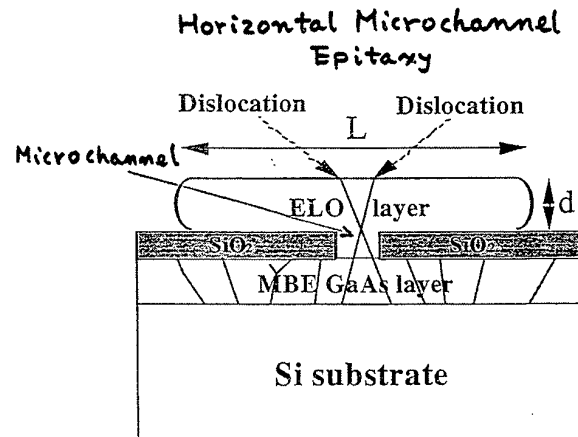
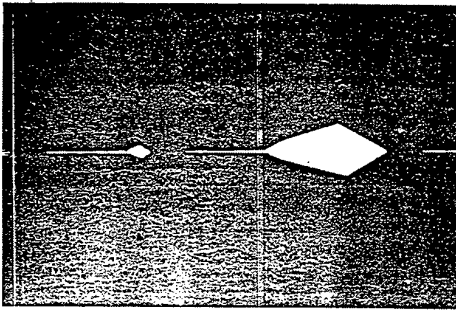


(c)



(d)

GaAs on Si Sub.



$$\text{ELO ratio} = L / d$$

Epitaxial Lateral Overgrowth

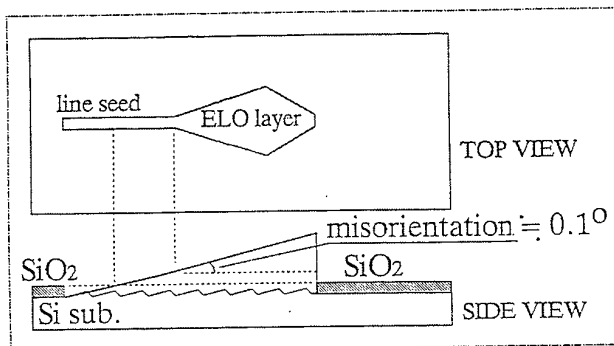
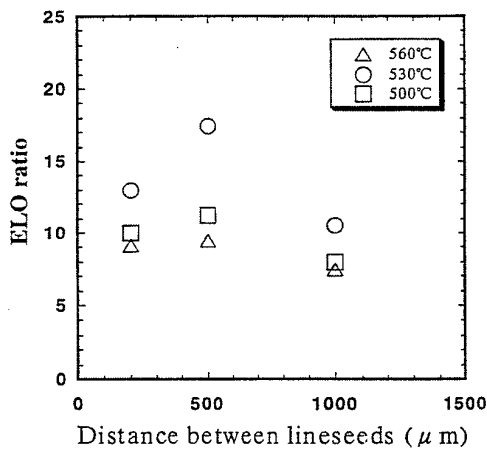


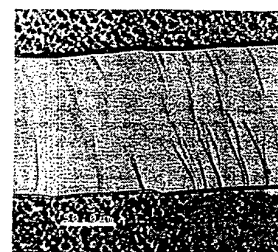
fig.3-19

Dependence of ELO ratio on line seed separation



Maxium ELO ratio is obtained with line seed separation of 500μm.

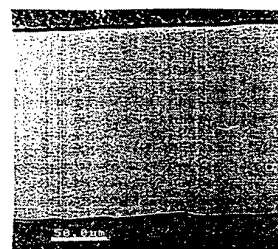
Optical microphotograph of ELO layer with different growth time



3h

$$L = 130\mu\text{m}$$

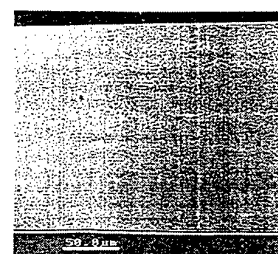
$$d = 7.5\mu\text{m}$$



5h

$$L = 175\mu\text{m}$$

$$d = 10\mu\text{m}$$

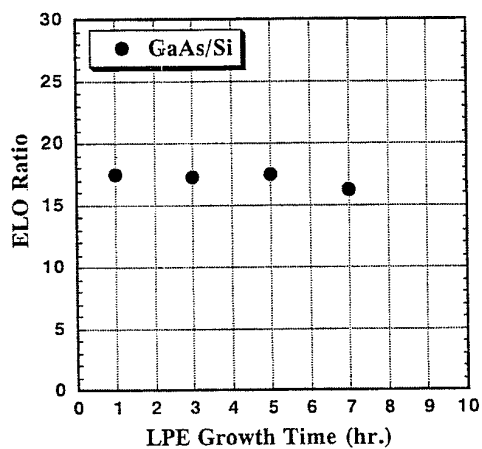


7h

$$L = 195\mu\text{m}$$

$$d = 12\mu\text{m}$$

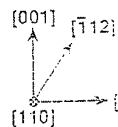
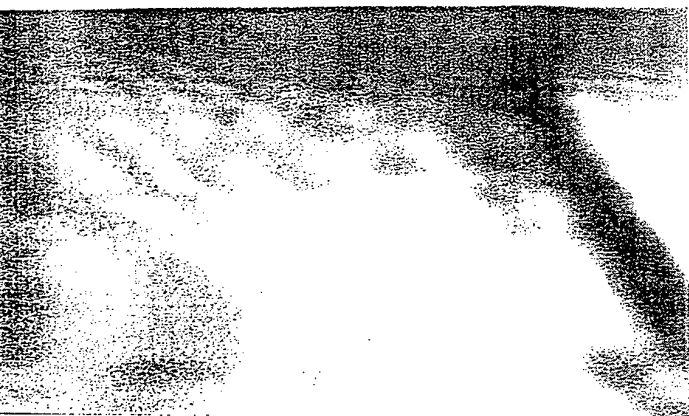
Dependence of ELO ratio on LPE growth time



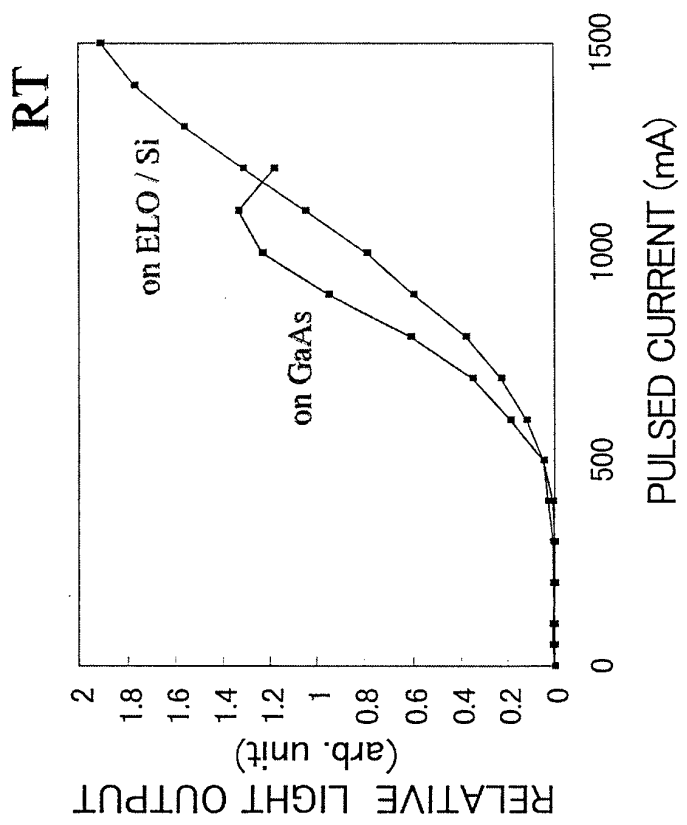
ELO ratio is as high as 16.5 even with a LPE growth time of 7h.



Masao TAMURA (JRCAT-ATP)

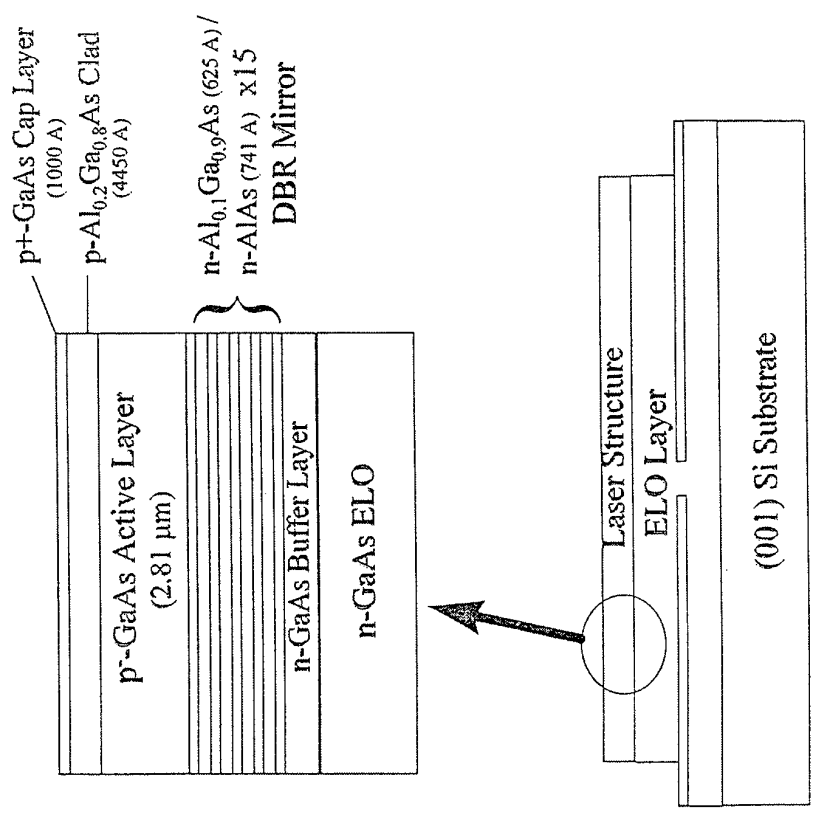


I-L Curve for VCSELs



	I _{th}	J _{th}
on ELO / Si	700 mA	35.7 KA/cm ²
on GaAs	590 mA	30.0 KA/cm ²

FABRICATION of VCSEL for CURRENT INJECTION

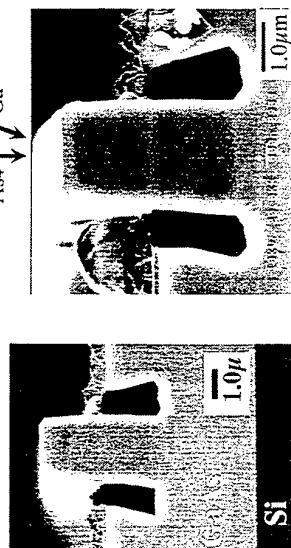


◆ Results

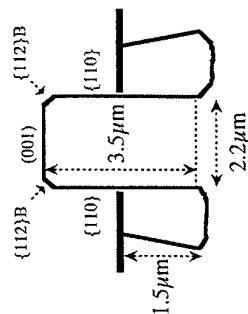
○ Low V/III ratio

Growth condition
 substrate temperature : 655°C
 growth time : 11 hours
 growth rate : $0.3\mu\text{m/h}$
 As₄ pressure : $1.2 \times 10^{-5}\text{Torr}$

Cross sectional SEM images



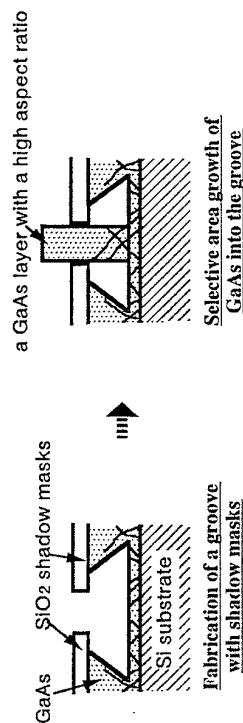
- The ridge structure with a high aspect ratio.
- $\{110\}$ facets on the sidewalls.
- Development of a (001) top surface.



The aspect ratio of the layer : 1.6

II. Vertical Microchannel epitaxy (VMCE) of GaAs on Si(001) substrates using SiO₂ shadow masks

- A new selective area MBE growth aiming to reduce both threading dislocations and residual strain



○ Purposes of this study

- Investigation of growth mechanism in VMCE of GaAs on Si(001) substrates using SiO₂ shadow masks.
- Characterization of the grown layer by the molten KOH etching.
- Photoluminescence measurements for the grown layer.

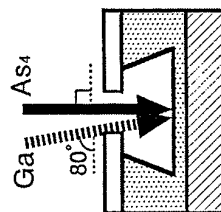
○ VMCE growth condition

- * High growth temperature ($640 \sim 655^{\circ}\text{C}$) & low growth rate ($0.3\mu\text{m/h}$)

- Selective growth is desirable.
- To prevent change of aperture shape due to polycrystal deposition.

* Molecular beam directions

- As₄ beam is normal to the surface.
- Ga beam is inclined with an incident angle of $\sim 80^{\circ}$.



* Insertion of markers

- To investigate growth mechanism, markers were inserted in some samples.
- The markers were made by doping Si and Be alternatively.

MBE for the Production of III-V Devices

G. Weimann, Fh-IAF, Freiburg

The inherent advantages of molecular beam epitaxy (MBE) for the growth of III-V compound semiconductors have been obvious from the very beginning of this technology, for more than two decades now.

The two-dimensional atomic layer-by-atomic layer growth at rather low substrate temperatures allows the reproducible growth of heterostructures and quantum wells (QW) with interfaces and δ -dopings in atomic scales, arbitrary compositional gradings and strained layers, prerequisites for a variety of novel devices, e. g. modulation doped field effect transistors (HEMTs), MQW lasers, tunneling structures and surface emitting lasers (VCSELs). Recent advances in MBE systems include hot-lipped Ga effusion cells, reducing the density of oval defects to $10 - 20 \text{ cm}^{-2}$ and valved crackers for phosphorus, yielding stable and well controlled P_2 -fluxes from white phosphorus, generated in-situ within the cell, so making elemental source MBE a viable growth technique for mixed group V compounds.

Of the three generally used epitaxial growth techniques for the production of III-V devices, liquid phase epitaxy (LPE) is usually applied for structures not requiring layer thicknesses in the nanometer range, e. g. the volume production of LEDs. Metalorganic vapour phase epitaxy (MOVPE) and MBE have, for obvious reasons, replaced LPE for all devices based on extremely thin layers with stringent thickness control, sharp interfaces and doping profiles, especially if strained layers are necessary, as both growth processes are further away from thermodynamic equilibrium. MOVPE seems, at present, to be favoured for optoelectronic devices, due to its higher growth temperature in comparison to MBE and the capability to grow phosphorus containing compounds. A further major advantage of MOVPE over MBE stems from not having to open the growth chamber for replenishing the sources.

MBE, on the other hand, has distinct advantages over MOVPE in using solid elemental sources, thus reducing toxic hazard. The purity of these sources is generally much higher than that of metalorganic compounds, giving lower background doping levels. MBE, being a UHV process with direct molecular beams impinging on the growth surface, avoids complex boundary layers and pre-reactions in the gas phase. The absence of downstreaming gas flows makes uniformity of substrate temperature and epitaxial layers easier to achieve, with temperature variations of less than 5 K and thickness, composition, and doping level variations below 1 % across 4" wafers

in commercial multiwafer MBE systems. Interfaces in heterostructures and δ -doping sheets can be kept within ± 1 monolayer, much sharper than in MOVPE growth.

With the use of large effusion cells, production type multiwafer MBE reactors now have to be opened far less frequently. These MBE systems allow the growth of more than 1000 μm total epilayer thickness, yielding 5000 4"-HEMT-epiwafers in a 4-wafer reactor between vacuum breaks or 4 months' growth in two shifts.

The advent of valved cracker cells for stable and highly reproducible As_2 - and P_2 -fluxes alleviates recalibration of the group V beams, whereas group III-fluxes can be predictably adjusted by control of source temperatures. MBE provides in-situ control of growth and layer parameters by RHEED, ellipsometry and pyrometry, ensuring high reproducibility from run to run. The MBE growth process can be totally automated, giving high throughput. MBE can thus be viewed as a cost effective production technology for volume markets and dominates the market for HEMTs, MMICs and related devices.

Today's existing volume markets, e. g. for HEMTs and MMICs for mobile communication, MQW lasers for CD players, and 0.98 μm pump lasers for fiber amplifiers rely on conventional solid source MBE of group III-arsenides. High yield and excellent reproducibility result in low epitaxial costs, with the substrate already making the major contribution to the epiwafer manufacturing costs. Device manufacturers in volume markets are shifting unanimously to large wafers, the present move to 4" diameter will inevitably be followed by the rapid introduction of 6" wafers. The first multiwafer 6" MBE systems are currently under construction.

Although solid state MBE has been shown to be capable of growing mixed group V structures, e. g. for 1.3 μm and 1.55 μm laser diodes for fiber communications, MOCVD is the generally favoured production technique for phosphorus containing optoelectronic devices and e. g. HBTs with high carbon doping. Future applications in dense wavelength division multiplexing using many closely spaced wavelengths may, however, make use of the superior compositional and dimensional control in MBE epilayers.

Chemical beam epitaxy (CBE) using MO-group III sources and hydrides combines the advantages (and disadvantages) of MBE and MOCVD. The outstanding feature of CBE is area selective growth allowing the monolithic integration of different optical devices, such as lasers and waveguides. This growth method has led to convincing modules in integrated optics, however, failed to mature as a production technique so far.

MBE for the Production of III-V Devices

1. Introduction

- A brief comparison of epitaxial technologies

2. MBE and its derivatives

3. MBE as a production technology

4. A few examples

- HEMTs, QW-Lasers

5. Essentials: markets, costs and manufacturability

Epitaxial Techniques for III-V Materials and Devices: LPE, VPE, MBE

Liquid Phase Epitaxy: LPE

growth from supersaturated group III-melt
close to thermodynamic equilibrium
no group III point defects: low non-radiative
recombination
excellent lattice matching by crystal pulling,
no strained layers
pure material $N_D + N_A = 10^{13} \text{ cm}^{-3}$
highest growth temperature ($\sim 1100 \text{ K}$ for GaAs)
high growth rates, upscaleable: cost effective
poor thickness control $\pm 50 \text{ nm}$
"soft" heterojunctions $\pm 20 \text{ ML}$, no QW structures
no δ -doping, no compositional gradients
GaAs, GaP, InP and alloys, also As/P alloys
LEDs, photovoltaics, DH-lasers

Vapour Phase Epitaxy: VPE, MOVPE

growth from laminar gas flow (halides,
MO-compounds and hydrides
with - w/o carrier gas)

diffusion through stagnant layer and surface
reaction

pressure in reactor 10^5 - 1 Pascal: gas phase
reactions possible

high growth temperature ($\sim 1000 \text{ K}$ for GaAs)

growth temperature and precursor supply control
critical to achieve uniformity across (large)
wafer and in multiwafer reactor, upscaleable
wide range of growth rates (1 - several $10 \mu\text{m}$)

heterojunctions $\pm 3 \text{ ML}$, QWs possible

selective area growth, lateral mass transport makes
composition and thickness aperture dependent

high V/III ratios

As/P compounds, (InGa)(AsP), (GaAl)N: lasers, HBTs

Molecular Beam Epitaxy: MBE, MOMBE, CBE

growth from molecular beams, no gas phase
reaction

lowest growth temperature (800 - 900 K for
GaAs/AlGaAs)

extremely sharp interfaces $\pm 1 \text{ ML}$, sharp δ -dopings

excellent control of thickness, composition and
uniformity

reduced lateral mass transport, excellent selective
area growth with CBE

phosphorus containing compounds only with
cracker cells

(AlGa)As, InP, QW-Lasers, HEMTs

MBE and its Derivatives

There is no "best epitaxial growth technique"

MBE is suited for the following devices (a selection):

- HEMTs, lattice relaxed (metamorphic) HEMTs
- QW-Lasers (lattice matched and strained)
- QW structures with atomic precision (RTDs, QWIPs)

There are no "general growth parameters for MBE"

Optoelectronic devices e. g. lasers, require high growth temperatures and low V/III ratios to reduce density of Ga-vacancies and non-radiative recombination.

MODFETs require lower growth temperature and/or higher V/III ratios to suppress dopant segregation.

General characteristics:

- molecular flow, UHV process with growth pressures of 10^{-4} Pascal in MBE and 10^{-2} Pascal in CBE
- no gas phase pre-reaction
- no complex boundary layer as in MOVPE
- low growth temperature allows highly strained layers
($\frac{\Delta a}{a_0} \cdot d_c \approx 30 \text{ nm } \%, 2 \times \text{critical MB thickness}$)
- two-dimensional layer by layer growth
- practical growth rates of $1 \mu\text{m/h}$
- good substrate temperature control and reproducibility
(independent of growth parameters, only substrate and layer dependent)
- excellent substrate temperature uniformity across large wafer and in multiwafer reactor
- in situ monitoring possible:
 - flux control
 - residual gas control
 - RHEED, pyrometry and ellipsometry

FolienF-060795b-k

FolienF-060795b-k

MBE = conventional solid elemental III-and V-sources

(AlGaIn)As

(AlGaIn)(AsP) with valved crackers to produce P_2

Antimonides

II-VI compounds

high purity sources: $(N_D + N_A) \sim 10^{14} \text{ cm}^{-3}$

e. g. intentionally undoped GaAs

$p \leq 5 \cdot 10^{13} \text{ cm}^{-3}$ with As_4

$n \leq 2 \cdot 10^{14} \text{ cm}^{-3}$ with As_2

uniformity across 4" wafer: $\text{Al}_x\text{Ga}_{1-x}\text{As:Si}$

$\Delta d/d \sim 1 \%$

$\Delta n/n \sim 1,5 \%$

$\Delta x = 0.005$

abrupt interfaces $\pm 1 \text{ ML}$

wide process windows for T_s , V/III

low defect density $< 20 \text{ cm}^{-2}$

no area selective growth: polycrystalline on

dielectric mask

mature technology, upscaleable

production technology

4 x 4" MBE systems available

4 x 6" MBE systems under construction

MOMBE = metalorganic MBE with III-MO-compounds and elemental As and P-sources

+ no III-flux-transients (3 % in MBE)

+ no crucibles (Al source problematic in MBE)

+ no nucleation on dielectric masks, as in CBE

GSMBE = gas source MBE with elemental Ga, In, Al and gas phase V-sources (hydrides, MO)

+ high source purity

+ good control of As/P-ratio in solid phase

CBE = chemical beam epitaxy with gas phase
III-MO-compounds and hydrides (AsH_3 , PH_3) or
V- MO-sources

- + no nucleation on dielectric masks (e. g. Si_3N_4)
area selective epitaxial growth
in-filling epitaxy for integration of opt. devices
- + low growth temperature (InGaAsP: 520° C
with MOVPE: 620° C)
increased strain in epitaxial layers
- + reduced lateral mass transport (in comparison to
MOVPE)
layer thickness and composition independent
of mask aperture
- + reduced V/III ratios (1/10 of MOVPE ratio)
- + no carrier gas
- + accurate compositional control for mixed V-alloys
- narrow process windows e. g. $\Delta T \pm 10$ K
(control in multiwafer reactors ?)
- immature technology, no production reactors
available

CBE combines advantages and disadvantages of MBE and MOVPE

⇒ cost effectivity lower than in
existing MBE, MOVPE and LPE

⇒ for sophisticated devices only

FolienF-060739/NK

FolienF-060739/NK

MBE as a Production Tool for III-V Devices

Necessities: large wafers = 4" or 6"

- high throughput = multiwafer epitaxy
- high yield = control of specifications
- uniformity of layer thickness, doping
level and composition ~ 1 % over
full wafer
- uniformity over all wafers in run
- reproducibility from run to run
- low defect density

manufacturability, e. g. easy calibration
and volume markets

MBE of 4" PHEMT Epilayers

Thickness 1 μm - Growth Rate 1 $\mu\text{m}/\text{h}$ - Growth Time 1 hr

Daily operation (2 shifts) = 15 hrs : 12 growth runs

Multiwafer MBE Machine 4 x 4" wafers

Daily output 48 4" wafers

Annual output (250 up days) 12 000 wafers in 3 000 runs

Annual costs:	MBE Machine Invest	\$ 2 Mio	
	annual depreciation (20 %)	= \$	400 000
	maintenance (7 %)	= \$	140 000
	clean room 30m ² x US\$ 3 000	= \$	90 000
	salaries 2 x US\$ 150 000	= \$	300 000

Costs per run:	wafers 4 x US\$ 200	= \$	800
	materials, Ga, Al, etc.	= \$	15
	electricity, LN ₂ etc.	= \$	45
	per run	= \$	860
	3 000 runs/year	= \$	2 580 000

Total manufacturing costs:	\$ 3 510 000
	= \$ 292.50 / wafer

Inspection, characterization 1 wafer/day
 annual costs 250 wafers = \$ 72 000
 salary = \$ 150 000
 total = \$ 222 000
 : 12 000 = \$ 18.50

Total manufacturing cost per 4" wafer = \$ 311
 usable area = 0.8 · wafer area = 6 300 mm²

"Real estate" price of PHEMT structure by MBE
 = \$ 311/6 300 mm² = 0.049 \$/mm²

1 mm² epitaxial structure for PHEMT costs 5 ¢

1 mm² s. i. substrate costs 3.2 ¢
 (ionimplanted MESFET)

BeichteF-080795/x

Manufacturing costs for epitaxial structures by MBE
 on 4" substrates in 4 wafer MBE system:
 (yield ~ 80 %)

1 mm² semiinsulating GaAs substrate (MESFET) = 3 ¢
 1 mm² P-HEMT for MMICs (thickness 1 µm) = 5 ¢
 1 mm² MQW laser epistruktur (thickness 5 µm) = 11 ¢

*epitaxy costs are not the limiting factor
 if a volume market is available*

e. g. automotive radar with GaAs MMICs:

system price \$ 200,-
 MMIC chip set (≈ 20 mm²) \$ 20,-
 epitaxy for 20 mm² \$ 1,-

MQW laser for CD player: packaged device \$ 2,-
 epitaxial structure ~ 0.2 mm² 2 ¢

Quantum well lasers for CD player ~ \$ 2/device
 High power laser diodes for material processing ~ \$ 20/Watt
 for bars and stacks

Epitaxial layer total thickness 5 µm = 5 hrs growth time
 with 3 growth runs per day = 12 wafers/day
 or 750 growth runs per year = 3000 wafers/year

MBE machine, depreciation, salaries etc. per year \$ 930,000.-
 Running costs/run: substrates 4 x \$ 200 = \$ 800
 materials etc. \$ 75
 supplies \$ 225
 Total per run = \$ 1100
 Annual total for 750 runs \$ 825,000.-
 Total manufacturing costs for 3000 wafers \$ 1,755,000.-
 Manufacturing costs for one 4" laser wafer \$ 585.-

Inspection, characterization 1 wafer/day (1 out of 12)
 annual costs for 250 wafers \$ 146,250.-
 salaries \$ 150,000.-
 Total \$ 296,250.-
 Characterization, testing per wafer \$ 98,75

Manufacturing incl. characterization = \$ 685,-
 1 mm² epitaxial MQW laser structure incl. substrate
 costs 11 ¢

FolienF-080795/x

Are there Volume Markets ?

Automotive Radar:

annual German car production = 10 million
 every car is equipped with ICC (intelligent cruise control)
 annual MMIC real estate = 10 · 10⁶ · 20 mm² = 2 · 10⁸ mm²
 = 32000 4" wafers with 80 % yield

1 4 x 4" MBE machine supplies 12000 wafers/year
 (two shifts assumed)

3 machines can produce all MMICs required

Laser diodes:

1 MBE machine yields 3000 4" wafers/year
 or 10⁸ laser diodes (0.5 x 0.4 mm²)/year

in 1997: audio CD players ~ 100 million
 CD ROM game players ~ 12 million
 video CD players ~ 12 million

Sophisticated Devices:

(InGa)(AsP) based 1.55 μm single mode laser diodes
with defined wavelength for optical communication
systems
(dense WDM $\Delta\nu = 50 \text{ GHz}$ or $\Delta\lambda = 0.4 \text{ nm}$)

total annual InP-wafer sales: 70000 2" wafers

for 1.3 and 1.55 μm lasers around 40 % are used
= 28000 wafers/year

total annual laser production in 1997 = $1.5 \cdot 10^6$ lasers
one 2" wafer gives > 10000 lasers (yield 0.8)

total real estate required = 150 wafers

$$\text{overall yield} = \frac{150}{28000} \approx 0.5 \% !$$

Essential Technologies:

epitaxy (usually MOCVD)
lateral structure (e. g. ridge)
dfb/dbr gratings (e-beam, etching)
epitaxial overgrowth (generally MOCVD)
clearing
mounting, packaging

FolienVf-060798nk

FolienVf-060798nk

MBE on 4" wafers

Defect density (0.8 - 10 μm): 10 - 20 cm^{-2}
(hot lipped Ga-cell, large source substrate distance)

Uniformity: thickness $\pm 1 \%$ (GaAs)
 composition $\pm 1 \%$ (AlGaAs)
 doping $\pm 1.5 \%$ (GaAs)
 for 4 x 4" wafers

Reproducibility: from run to run (platen to platen) $\pm 2 \%$

Growth time between vacuum breaks: $\sim 1200 \text{ hrs}$
 \Rightarrow 1200 μm epilayers
 \Rightarrow 5000 4" PAEMT-epiwafers

Cell stability: $\pm 1 \text{ K/day}$

flux stability: $\Delta T = 1 \text{ K} \Rightarrow \Delta j_{\text{III}} = 2,5 \%$
- linear, predictable variation
 $\Delta T = 0.1 \text{ K/run}$

FolienVf-060798nk

Molecular Beam Epitaxy is a cost-effective
production technology for III-V devices and MMICs

The epitaxial costs are not the limiting factor
if we make useful devices in large volumes.

Manufacturing Science is necessary with respect to
manufacturability,
reproducibility
and yield.

MBE is well prepared for the emerging volume markets
and does not fear the competition in many (not all) fields.

MOCVD for Production of III-V Devices

Michael Heuken

14.09.1998

AIXTRON AG, Kackertstraße 15-17, D - 52072 Aachen, Germany

Tel. +49 (241) 8909 -54, Fax +49 (241) 8909 - 40, e-mail: heu@aixtron.com

Electronic consumer products (Cellular Phones, data storage units, LED and LASER-printers and LED full-colored displays) require state of the art compound semiconductor devices. Large quantities are needed and the fabrication process has to provide high wafer throughput and yield. To meet the targets of this market, a well proven production tool, the Planetary Reactor[®], has been improved to meet the production focus and flexibility required. The wafer capacity of the advanced reactors is between 15 x 2" and 35 x 2" or 9 x 4". Main features are: an inductive heating system with extremely low thermal mass for precise and fast heating, high flexibility in the reactor size and the option to use a fully automated cassette-to-cassette wafer loading system. The benefits of this new design are very short cycle times, hot wafer loading/unloading, extreme run-to-run stability and even further reduced cost of ownership.

To demonstrate the possibilities of this reactor concept we will report the development of a production like process of GaInP, AlGaAs and AlGaInP layer systems on 4" GaAs wafer. Thickness uniformity of GaInP on 4" wafer is demonstrated to be 0.24 % whereas the uniformity of PL intensity at room temperature can be as low as 12%. GaAs/GaInP heterostructure field effect transistor structures with a uniformity of the sheet resistance of 1.47 % were obtained.

To obtain these data in a production like process in a multiwafer reactor, a detailed knowledge of the growth process is required. We will discuss our growth

experiments together with our theoretical modeling efforts to understand the impact of temperature distribution in the reactor, the gas flow dynamics, reactor designs and the basic growth conditions (V/III ratio, gas flow velocity, growth temperature) on layer and device properties. Special focus will be put on production aspects such as efficiency (which is up to 40% for group III elements), turn around time and cost of ownership.

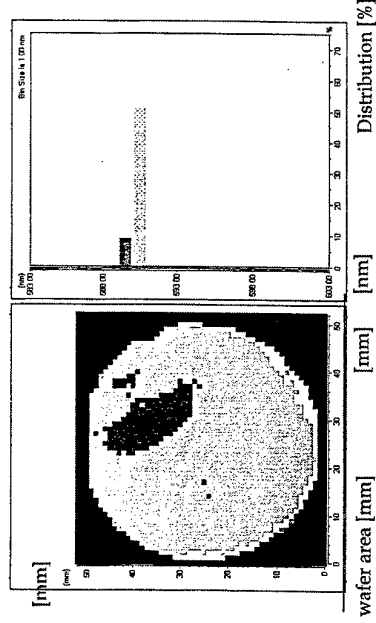
In addition, results from the employment of a multiwafer Planetary Reactor[®] with 7x2" wafer capacity for the growth of InGaN/GaN device structures will be presented. Single layers of GaN have been deposited at a growth rate of 2 μ m/h on 2" sapphire wafers having a thickness uniformity of < 2%. Undoped films exhibited a carrier concentration of < 5x10¹⁶cm⁻³. Sheet resistance mapping of Si- and Mg doped layers revealed a uniformity of < 2% and < 20%, respectively. We achieved reproducible resistivities in p-type material as low as 1 Ω cm (p = 10¹⁸cm⁻³). Low temperature (12K) PL revealed a full width at half maximum (FWHM) of 3meV. Growth of high quality ternary GaN-based films has also been achieved in our multiwafer Planetary Reactor[®]. Single layers of InGaN (x ~0.3) as well as InGaN/GaN structures having strong bandedge related PL have been achieved on 2" sapphire wafers. Low temperature (14K) PL of InGaN (x~0.1) revealed a FWHM of < 135 meV. Additionally, mappings of the room temperature photoluminescence show a standard deviation in peak wavelength of < 2 nm on these wafers. Concurrently, wafer-to-wafer deviation of < 2 nm was obtained. Room temperature PL mappings of AlGaIn (x~0.1) demonstrate a standard deviation of <1nm across 2" wafers. Low temperature (14K) PL of these films revealed a FWHM of <20meV. For the fabrication of high brightness light emitting diodes, growth of InGaIn/GaN double heterostructures and multiquantum structures with GaN and AlGaIn confinement layers was undertaken. The details of electroluminescence at 435nm (FWHM ~30meV) and other device characterization will be reported .

References:

- G. Lengeling, R. Beccard, E. Woelk, B. Wachtendorf and H. Jürgensen
„MOCVD Systems for Industrial Scale Production of High Efficiency Tandem Solar Cells“,
Proceedings of the 14th European Photovoltaic Solar Conference, Volume II, Barcelona, Spain,
30 June-4 July, 1997, 1709-1711
- R. Beccard, H. Protzmann, D. Schmitz, G. Strauch, M. Heuken and H. Juergensen
„Growth of AlInGaP in Multiwafer Planetary Reactors“, paper submitted to the IPRM 1998,
University of Tsukuba, University Hall, Ibaraki, Japan, May 11-15, 1998
- F. Steinhagen, H. Hillmer, R. Lösch, W. Schlapp, H. Walter, R. Göbel, E. Kuphal, H. L. Hartnagel,
H. Burkhard
„AlGaInAs/InP 1.5µm MQW DFB Laser diodes exceeding 20 GHz bandwidth“, ELECTRONICS
LETTERS, 16th February 1995, Vol. 31, No. 4., 274-275
- R. Beccard, D. Schmitz, M. Deufel, H. Protzmann and H. Juergensen
„InP Based Materials for Long Wavelength Optoelectronics Grown in Multiwafer Planetary
Reactors“, 9th International Conference on Indium Phosphide and Related Materials, Hyannis,
11.-15 May, 1997,
- R. Niebuhr, K.H. Bachem, U. Kaufmann, M. Maier, C. Merz, B. Santic, P. Schlotter
„Electrical and Optical properties of Oxygen doped GaN grown by MOCVD using N₂O“,
Special Issue, Jour. of Elec. Mats, Vol. 26, No. 10., 1997, p. 1123-1126
- R. Beccard, O. Schoen, B. Wachtendorf, D. Schmitz, H. Juergensen and E. Woelk
„Al-Ga-In-Nitride Heterostructures: MOVPE Growth in Production Reactors and Characterization“
Special Issue of Jour. of Elec. Mats, , Vol. 26, No. 10, 1997, p. 1123-1126
- R. Beccard, R. Niebuhr, B. Wachtendorf, D. Schmitz and H. Jürgensen
„Multiwafer MOVPE Technology for low Dimensional Ga-Al-In-N Structures“, Materials Science
and Engineering B51 (1998), 39-43
- M. Deschler, R. Beccard, B. Wachtendorf, D. Schmitz and H. Juergensen
„Efficient and Uniform Production of III-Nitride Films by Multiwafer MOVPE“, Materials Science
and Engineering B50 (1997) 1-7

Uniformity of Wavelength on 2" GaAs

AlGaInP/GaAs AIX2400 (15x2")



12.08.1997

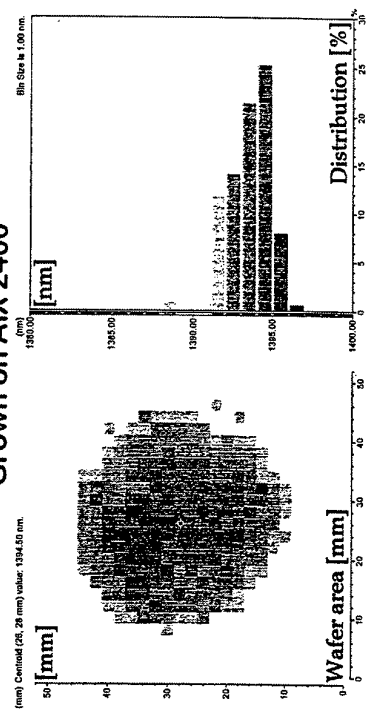
helec97.rpt

Kor

AIXTRON

Peak Wavelength of GaInAsP/GaInAsP MQW

Grown on AIX 2400



08.03.98

h:\market\olent\1899

O-3

AIXTRON

Planetary Reactor® Series

Concept:

- ◆ Radial Gasflow with central Injection
- ◆ Double Gas Foil Rotation®
- ◆ Controlled Boundary Conditions (no reactor walls)
- ◆ Common Reactor Design

Capacity:

- 7 x 2" up to 95 x 2"
- 5 x 3" up to 40 x 3"
- 5 x 4" up to 25 x 4"
- 9 x 6"
- 5 x 10"

12.08.1997

helec97.rpt

Kor

AIXTRON

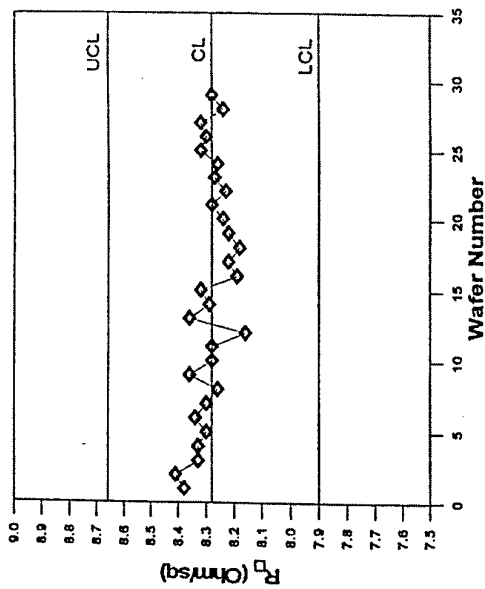
AIX 2400/2600G3 Planetary Reactor®



AIX 2400/2600G3 Planetary Reactor® with Automated Cassette-to-Cassette Wafer Loading

AIXTRON

4" HBT Sheet Resistance



AIXTRON

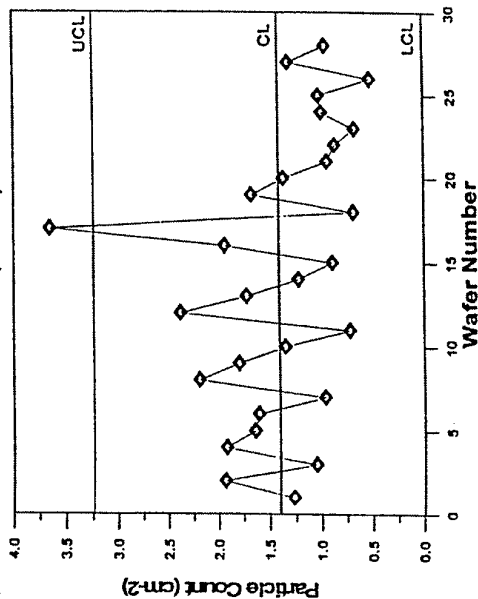
No File Name

QCS

04.03.98

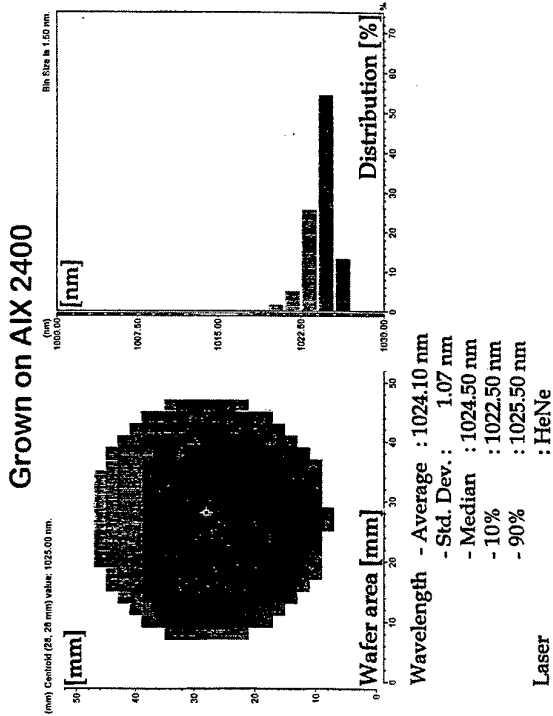
4" HBT Particle (>0.28 μm^2) Count

\bar{X} Chart
4" HBT Particle (>0.28 μm^2) Count



AIXTRON

Peak Wavelength of GaInAsP ($\lambda = 1.025 \mu\text{m}$)



AIXTRON

08.03.88

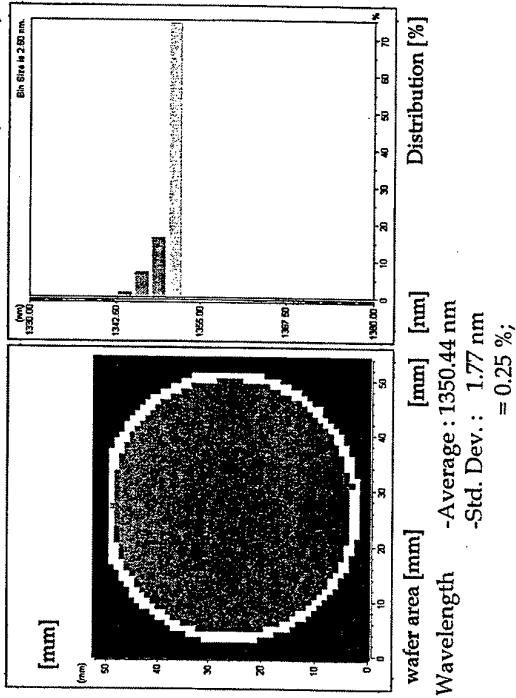
2

QCS

Ichimarkelkoden1886

Uniformity of Wavelength on 2" InP

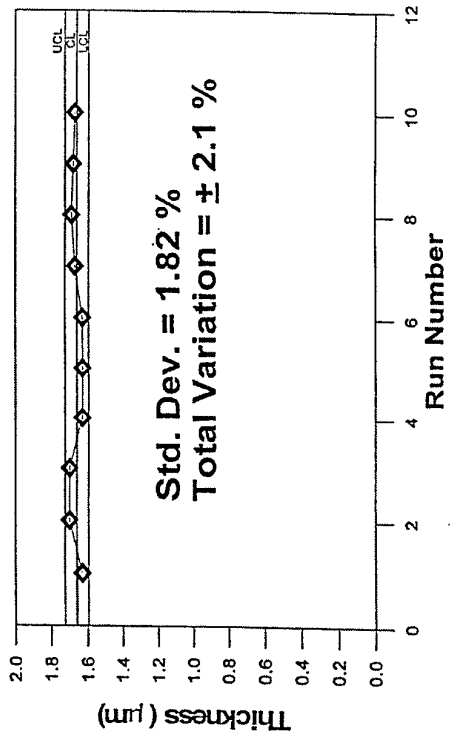
GaInAsP, 1.3 μm AIX2400 (15x2")



AIXTRON



HBT Thickness Uniformity among Ten Runs



AIXTRON

04.03.98 No File Name Ocs

4" AlGaAs/GaAs-HFET Structure

Material	Composition	Thickness (µm)	Carrier Density	Dopant
GaAs	-	0.050	$>2.4 \cdot 10^{18}$	n (Si)
AlGaAs	0.25	0.040	$2.0 \cdot 10^{18}$	n (Si)
AlGaAs	0.25	0.007	-	undoped
GaAs	-	0.600	-	undoped
GaAs	-	0.004	-	undoped
AlGaAs } x 20	0.25	0.005	-	undoped
GaAs	-	0.050	-	undoped

contact layer
dopant layer
spacer
channel
buffer

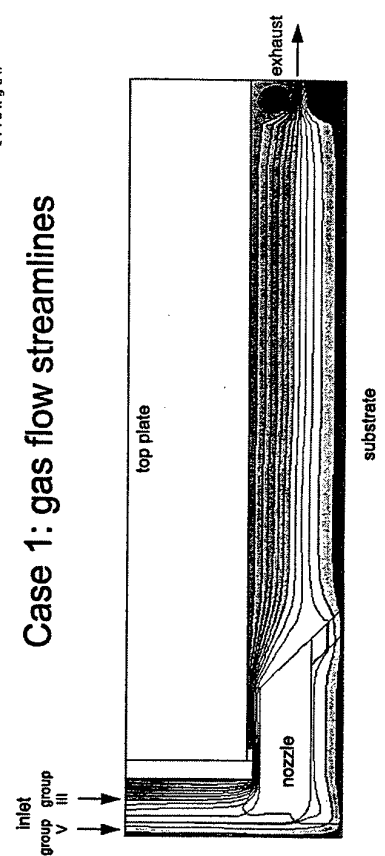
Hall Data
 μ (300 K) = $2730 \text{ cm}^2/\text{Vs}$
 n_a (300 K) = $1.0 \cdot 10^{13} \text{ cm}^{-2}$
Defect density $< 10 \text{ cm}^{-2}$
 μ (77 K) = $41660 \text{ cm}^2/\text{Vs}$
 n_a (77 K) = $2.5 \cdot 10^{12} \text{ cm}^{-2}$

Sheet Resistance
 $R_s = 284 \Omega/\square$
Uniformity 5%

AIXTRON

02/08/98 k:\labord\laser\corv\simul\3.ppt Egonv

Case 1: gas flow streamlines

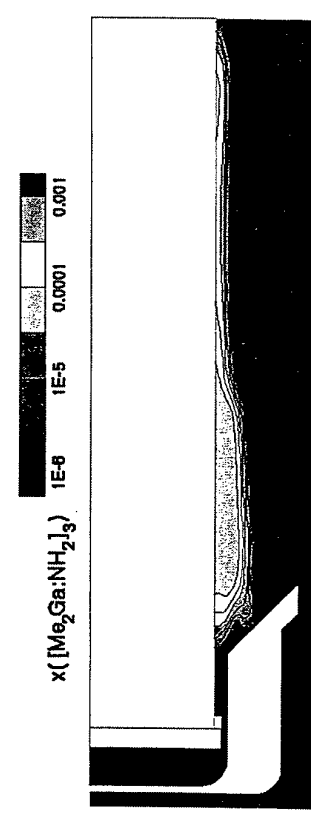


Colour indicates the streamfunction value shape of the streamlines → laminar flow

AIXTRON

02/08/98 k:\labord\laser\corv\simul\3.ppt Egonv

Case 1: molar fraction of GaN-containing cyclic adduct



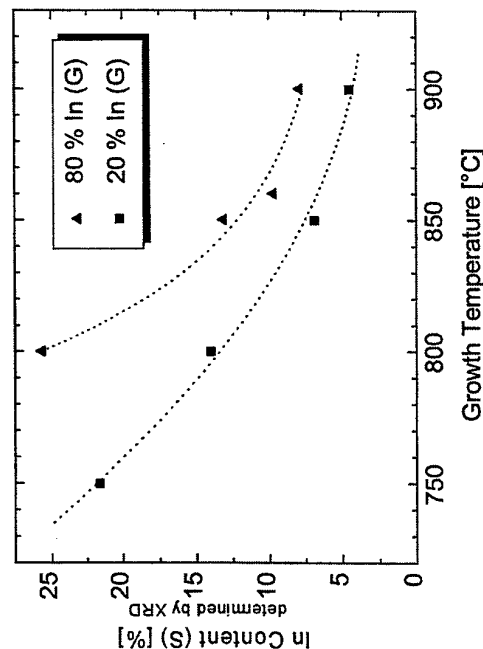
Line of decomposition correlates with temperature contour line of 500°C

AIXTRON

02/08/98 k:\labord\laser\corv\simul\3.ppt Egonv

In content vs growth temperature

GaInN (200 nm)/GaN (1.8 μm)



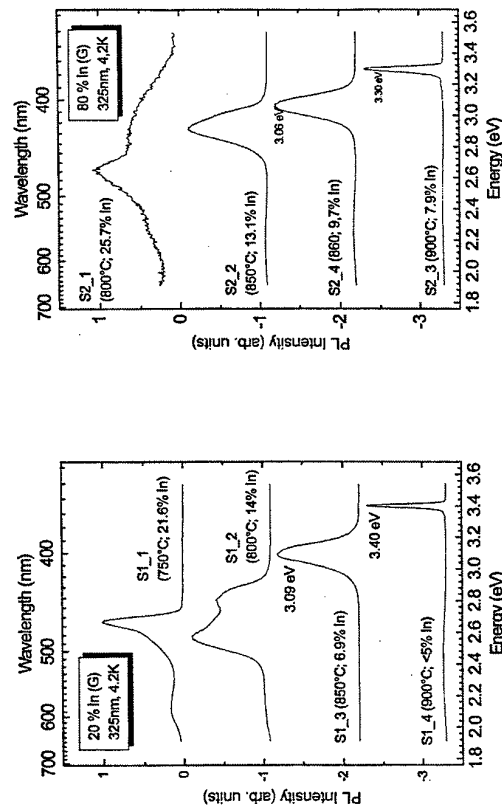
AIXTRON

h:\labor\folien\gan\mov\pagitt.ppt

28.01.98

7

Comparison of LT PL of InGaN films

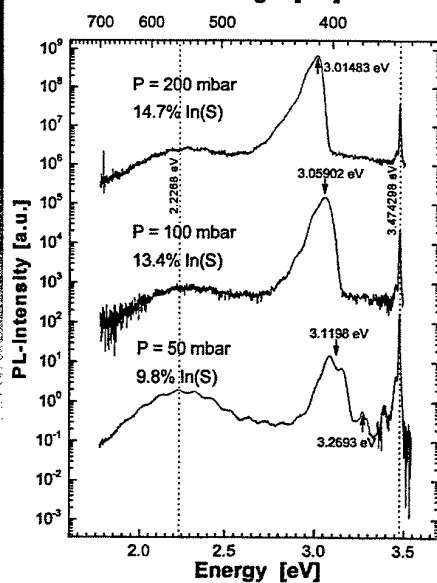


Ga_{0.9}In_{0.1}N (200nm)/GaN (1.8 μm)

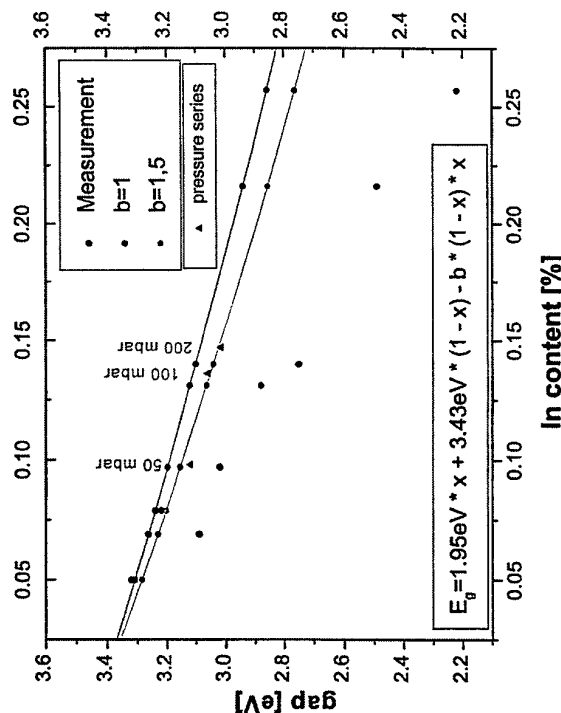
AIXTRON

LT PL of InGaN/GaN

PL @ 20 K: InGaN (50 nm) / GaN (1.6 μm)



Inconsistency of PL & XRD measurements



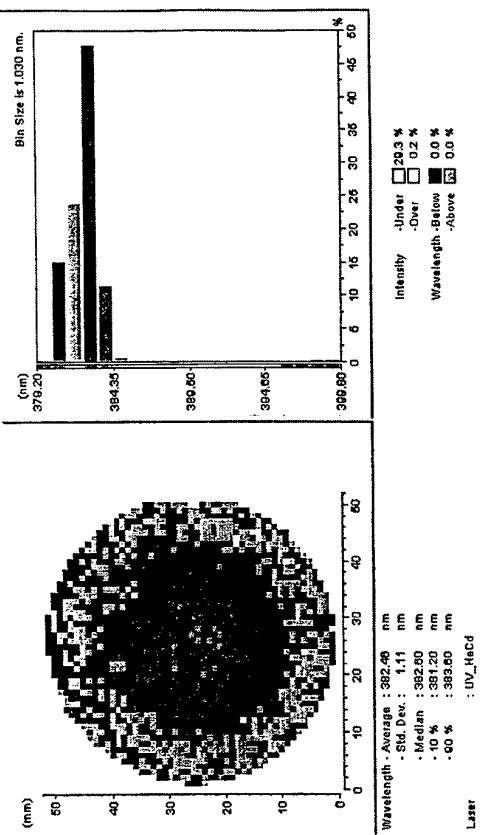
In content [%]

AIXTRON

AIXTRON

Composition homogeneity of InGaN

PL mapping of $\text{Ga}_{0.9}\text{In}_{0.1}\text{N}$ (200nm)/GaN (1.8 μm) grown at 860°C



AIXTRON

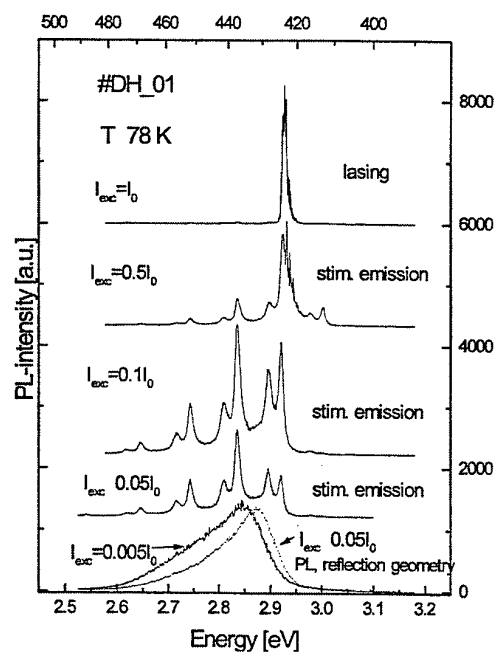
MS

h:\lab\ref\InGaIn\mox\gagan.ppt

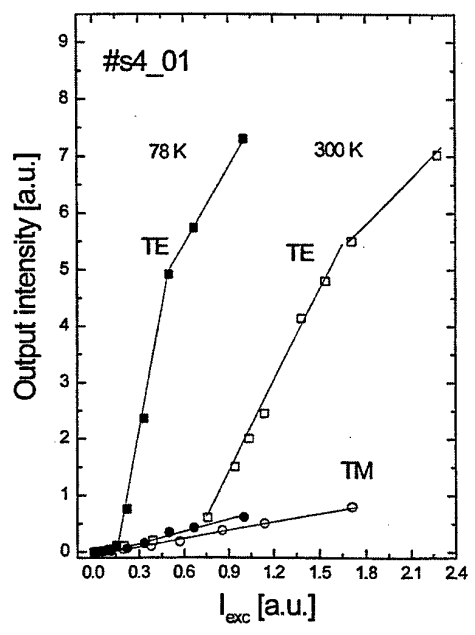
28.01.98

4

PL, stimulated emission and lasing of a InGaN/GaN DH at T=78 K under different excitation intensities



Emission intensity from "cavity" end as a function of excitation intensity for TE and TM modes at T 78 K and T 300 K



LPE in Production

K. Gillessen

Extended abstract

Starting with a typical phase diagram, the principle of liquid phase epitaxy is explained. LPE is a deposition method working close to thermal equilibrium and usually applying metal-rich melts.

If LPE is applied as a production method some specific demands have to be met. For example the epitaxial material should be deposited on many slices simultaneously and from a sequence of different solutions. These and further demands can be summarized as low cost of production.

Numerous arrangements for LPE in production are described in the literature. Some important examples are presented.

The specific features of LPE define certain domains where LPE is advantageously applied. These are binary compounds, ternary compounds with small lattice mismatch, thick layers, and radiation emitting devices. On the other hand, there are also weak points of LPE which limit its applicability.

The most important application of LPE is the production of III-V material layer sequences for infrared and light emitting devices. 10 examples of IRED, LED, and Laser structures are explained.

After these general aspects some specific items of LPE are treated:

The solute can be transported in the melt by diffusion and/or convection.

These mechanisms are compared and assessed with respect to their use in LPE.

The different roles of various doping elements in III-V compounds are described. Doping during LPE can be accomplished from solid, liquid, and gaseous sources. Two examples of doping methods are explained.

A short survey is given of characterization methods applied for assessment of LPE grown layers.

Some items used in the periphery of LPE are also treated, including boat materials, ambient gases, cleaning of wafers, melt removal, and surface corrections.

Finally, the flow of material in conjunction with LPE is considered, using gallium as an example. It is shown that LPE is quite advantageous from an environmental point of view.

References

Nelson, RCA Review Dec. 1963, 603 (1963)

Blum, Shih, J. Appl. Phys. 43, 1394 (1972)

Bergh, Saul, Paola, J. Electrochem. Soc. 120, 1558 (1973)

Saul, Roccasecca, J. Electrochem. Soc. 120, 1128 (1973)

Saul, Lorimor, J. Crystal Growth 27, 183 (1974)

Dawson, J. Appl. Phys. 48, 2485, (1977)

Niina, J. Electrochem. Soc. 124, 1285 (1977)

Niina, Yamaguchi, IEEE Trans. El. Dev. ED-24, 946 (1977)

Nishizawa et al., Jap. J. Appl. Phys. 17, 87 (1978)

Iwamoto et al., Jap. J. Appl. Phys. 19, 2157 (1980)

Heinen, J. Crystal Growth 58, 596 (1982)

Niina et al., IEEE Trans. El. Dev. ED-30, 264 (1983)

Index:

1. General aspects of Liquid Phase Epitaxy

1.1 Principle of LPE

1.2 Demands of production

1.3 Arrangements for LPE

1.4 Domains of LPE

1.5 Applications of LPE

2. Specific items of Liquid Phase Epitaxy

2.1 Transport of solute in melt

2.2 Doping with LPE

2.3 Characterization of LPE layers

2.4 Periphery of LPE

2.5 Material flow

Demands of production:

- # Simple process and equipment
- # Stable and reproducible process
- # Flexible LPE system
- # Large area wafers
- # Many wafers at the same time
- # Homogeneous properties of epitaxial layers
- # Little consumption of materials and energy
- # High yield

can be summarized as LOW COST

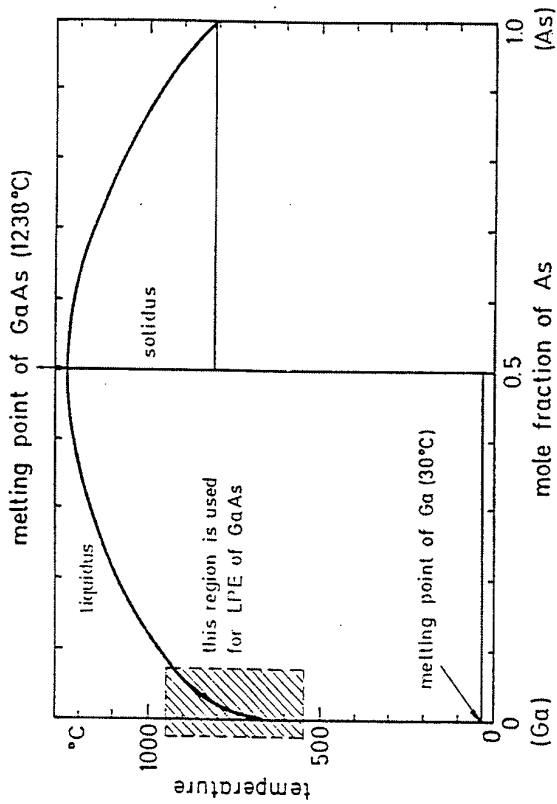
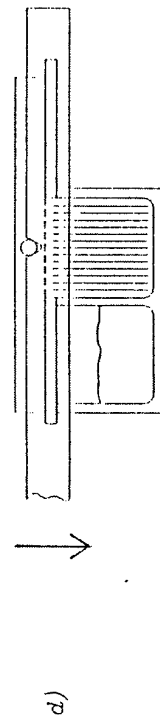
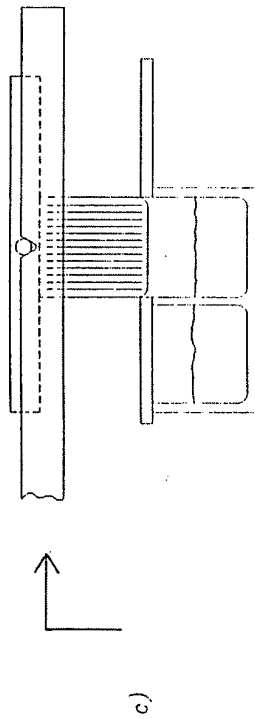
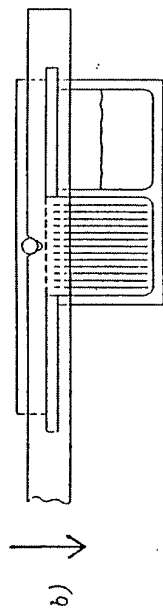
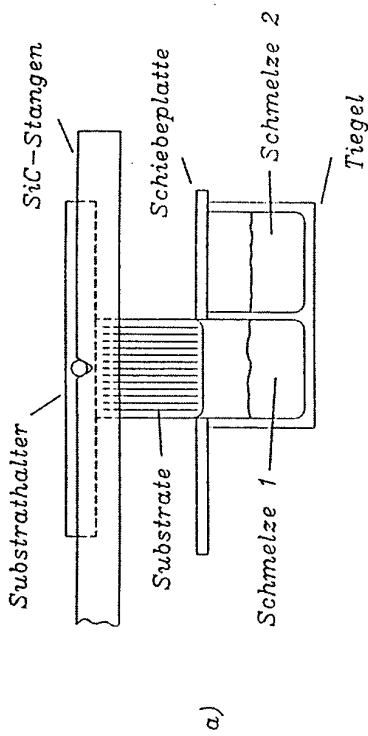


Fig. 3-4 Phase diagram of the Ga-As system

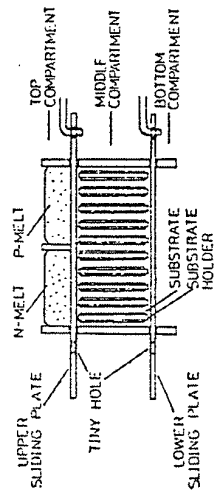


Fig. 1. Schematic structure of LPE boat. The figure shows the state when Ga melts and GaP substrates are set in two compartments prior to LPE growth.

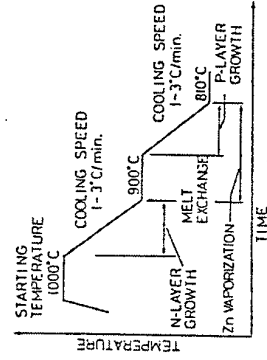


Fig. 2. Temperature program and related operations for LPE growth procedure by the two melt type.

LPE in Production

Domains of LPE:

- 1) Binary compounds: GaAs, GaP
- 2) Ternary compounds with small lattice mismatch:
 $\text{Ga}_{1-x}\text{Al}_x\text{As}$
- 3) Thick layers: 50 to 200 μm
- 4) Materials with low concentrations
of metal vacancies or related defects,
e. g. $[\text{V}_{\text{Ga}}]$ or $[\text{V}_{\text{Ga}}\text{P}^{+2}_{\text{Ga}}\text{V}_{\text{Ga}}]$

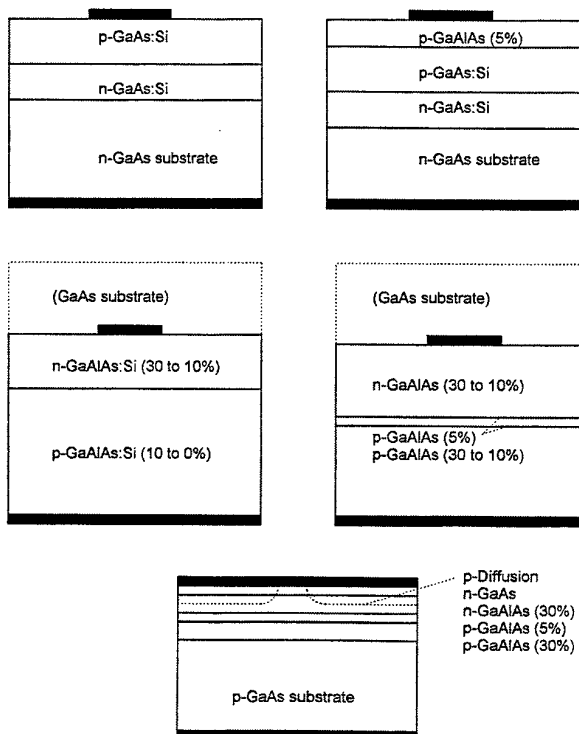
LPE in Production

Applications of LPE:

Material	Devices
GaAs:Si	IR emitting diodes 950 nm 15 %, 500 ns
GaAs:Si/GaAlAs	IR emitting diodes 950 nm 20 %, 500 ns
$\text{Ga}_{0.92}\text{Al}_{0.08}\text{As:Si}$	IR emitting diodes 870 nm 20 %, 500 ns
$\text{Ga}_{0.98}\text{Al}_{0.02}\text{As DH}$	IR emitting diodes 870 nm 30 %, 15 - 50 ns
$\text{Ga}_{1-x}\text{Al}_x\text{As DH}$	IR laser diodes 850 - 780 nm
$\text{Ga}_{0.6}\text{Al}_{0.4}\text{As SH}$	Light emitting diodes 650 nm (red), 3 %
$\text{Ga}_{0.6}\text{Al}_{0.4}\text{As DH}$	Light emitting diodes 650 nm (red), 6 %
$\text{Ga}_{0.6}\text{Al}_{0.4}\text{As DH, TS}$	Light emitting diodes 650 nm (red), 12 %
GaP:N	Light emitting diodes 565 nm (yellow-green), 0.3 %
GaP	Light emitting diodes 555 nm (pure green), 0.1 %

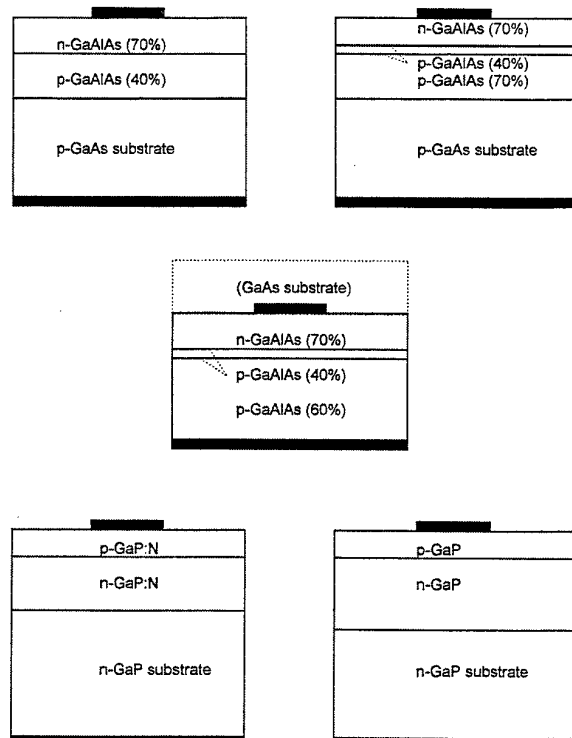
LPE in Production

Cross sections of chips made by LPE (1)



LPE in Production

Cross sections of chips made by LPE (2)



LPE in Production

Transport of solute in melt:

Mechanism	Diffusion	Convection
driven by difference in	concentration	temperature
	temperature	density
		surface tension (Marangoni effect)
transport speed	low	high
control of transport	good	bad
useful for	epitaxial growth	mixing of melts
predominates in	thin melts, boundary layers	bulky melts

LPE in Production

Doping:

Type of doping	Group	Element(s)
n	VI IV	S, Se, Te Sn
amphoteric	IV	Si in GaAs/GaAlAs
p	IV II	Ge Be, Mg, Zn
isoelectronic	V	N in GaP
unintentional	III, IV, VI	B, C, O

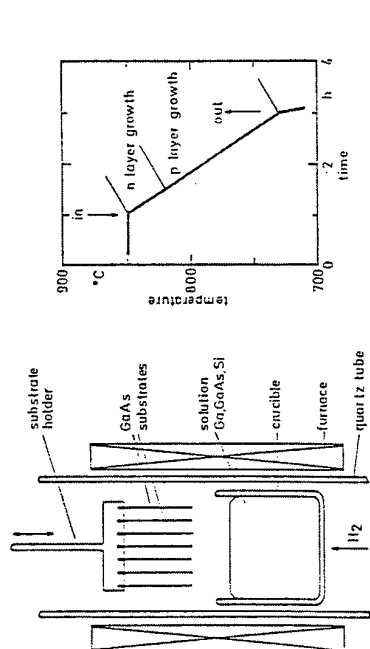


Fig. 3-6 Vertical dipping process for LPE of GaAs:Si, left: apparatus, right: temperature program

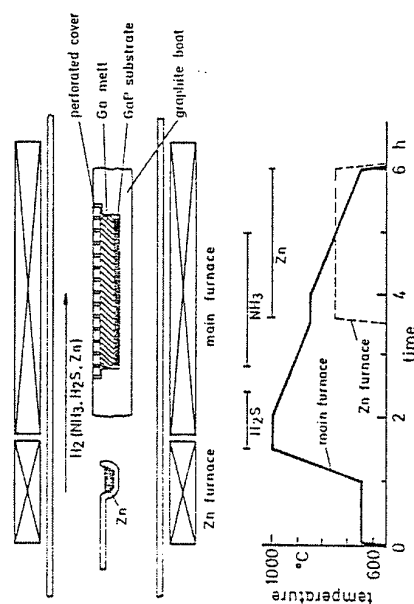


Fig. 3-8 Melt-back LPE of GaP with doping from the vapor phase, top: apparatus, bottom: temperature program

LPE in Production

Characterization of LPE layers:

Surface quality

- visual inspection
- phase contrast microscopy
- scanning tunnel/atomic force microscopy

Layer thickness

- vertical cleavage, etching, microscopy
- bevel (groove) grinding
- scanning electron microscopy

Crystal composition

- photo-/electroluminescence
- microprobe, cathodoluminescence
- x-ray methods

Doping

- sheet resistance
- SIMS

Dislocations

- etching, microscopy
- transmission electron microscopy

LPE in Production

Material flow:

Deposition efficiency of LPE is high: > 90 %

- small amount of waste, non-hazardous waste
- LPE is a "green" process

Gallium flow:

Annual world production of Ga: around 50 tons
Annual world production of LEDs: 500 billions (5×10^{11})
Weight of an LED: 1×10^{-4} g
Total weight of LEDs per year: 5×10^7 g = 50 tons

Recycling/re-use of Gallium is rewarding and practised:

- Gallium melts are re-used
- Ga residues are recycled
- GaAs waste is recycled (broken wafers, crusts, powder from cutting and grinding)

LPE in Production

Periphery of LPE:

Boat materials

- Most frequently used material: graphite
- For melts without aluminum: quartz

Process ambient

- Cleaning with vacuum
- Generally used process gas: hydrogen
- Less frequently used process gas: nitrogen

Cleaning of wafers

- Degreasing with organic solvents
- Etching with a non-preferential etch
- Rinsing with deionized water
- Drying in nitrogen
- Dissolution of surface layer in melt

Melt removal

- centrifugeing, ultrasonic agitation in glycerine
- boiling in sodium hydroxide solution
- etching in acids (HCl, organic acids)

Surface corrections

- Grinding (rim of wafer, protrusions)
- Polishing

Melt Growth of Oxide Crystals for SAW, Piezoelectric, and Non-Linear Optical Applications

Tsuguo FUKUDA

*Institute for Materials Research, Tohoku University,
2-1-1 Katahira, Aoba-ku, Sendai, 980-8577, Japan
E-mail: fukuda@lexus.imr.tohoku.ac.jp*

1. Introduction

Oxide crystals has been shown to be important materials for broad range of device applications. Selection of suitable growth method mainly depend on phase diagram of corresponding mixture (congruency, volatility, etc.). Czochralski (CZ) method is considered in present report to be a basic technique which allow mass production of large and perfect crystals. However two- and one-dimensional [1] crystals are often necessary for device applications. In such cases liquid phase epitaxy (LPE) and fiber growth methods (micro-pulling-down, μ -PD) are used also.

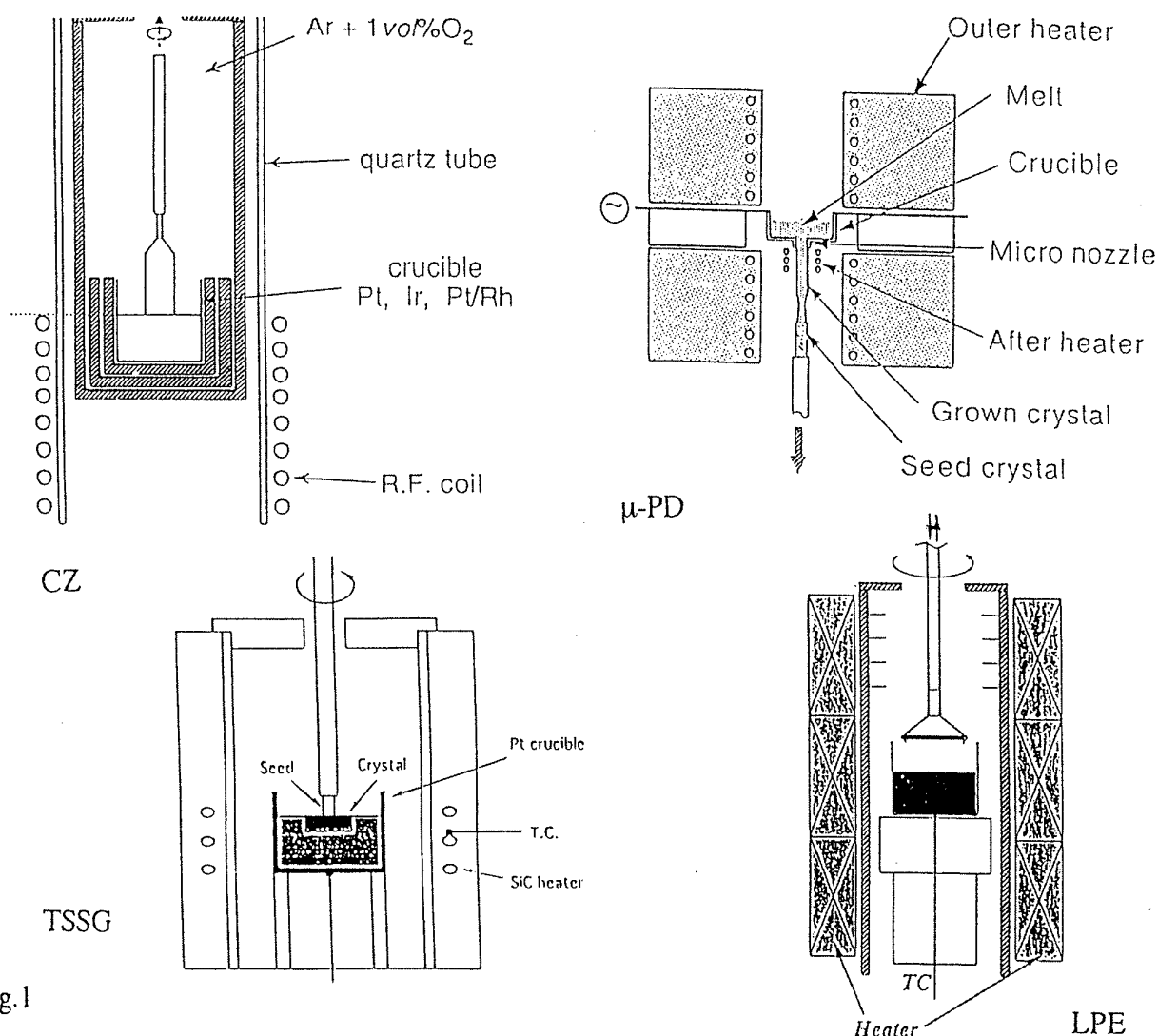


Fig.1

2. Growth of LiTaO₃ for SAW devices

CZ technique is widely used in mass production of both 3- and 4-inch diameter LiTaO₃ (LT) crystals for surface acoustic wave (SAW) device application. The crystal growth technology of 5-inch level is also developed in laboratory conditions. The requirements for production growth of LT are given in Table 1.

Table 1

Quality Factors	1. Compositional Variation → Tc Distribution
	2. Surface Quality (flatness, rear roughness, polishing defects, etc.)
	3. Impurity Concentration
	4. Durableness against Cracking
	5. Cut Orientation Accuracy
	6. Perfectness of Poling

3. Growth of langasite family crystals for piezoelectric applications

There is also considerable interest in the development of new materials for acoustic wave devices. One of the crystals that has been studied extensively over the last three years is langasite, $\text{La}_3\text{Ga}_5\text{SiO}_{14}$. Today it serves as a model for a family of isomorphic crystals which have zero temperature coefficient and large electromechanical coupling factor. These crystals is known to melt congruently and can be produced by conventional CZ technique from the melts slightly shifted from stoichiometric composition.

4. Non-linear optical crystals for SHG in blue wavelength range

Various niobate crystals are known to be excellent non-linear optical materials for second harmonic generation (SHG) of YAG:Nd and near-infrared GaAlAs lasers.

KNbO_3 (KN) with perovskite structure has large optical nonlinearity. It melts incongruently and can be grown by TSSG μ -PD techniques. However mechanical shocks and heating above 40 °C result depolling of the crystals by the creation of multidomain ferroelectric structure [2]. $\text{K}_3\text{Li}_2\text{Nb}_5\text{O}_{15}$ (KLN) and $\text{K}_3\text{Li}_2(\text{Ta,Nb})_5\text{O}_{15}$ (KLTN) crystals with tungsten bronze structure have higher mechanical and chemical stability and can be grown by TSSG, μ -PD and LPE technique using μ -PD crystals as substrates. The results shows that the KLN and KLTN μ -PD crystals and LPE films have high optical quality [3].

LiNbO_3 thin films were also grown on LiNbO_3 substrates by LPE method from solid-liquid-coexisting flux with thickness of 10-30 μm with small composition gradient and the crystallinity better than that of substrates.

References

- [1] R.S.Feigelson, J.Cryst. Growth 79 (1986) 669.
- [2] J.J.E.Reid, Appl.Phys.Lett. 62 (1993) 19.
- [3] V.I.Chani, K.Nagata, M.Imaeda, T.Fukuda, Ferroelectrics, 1998 (in press).

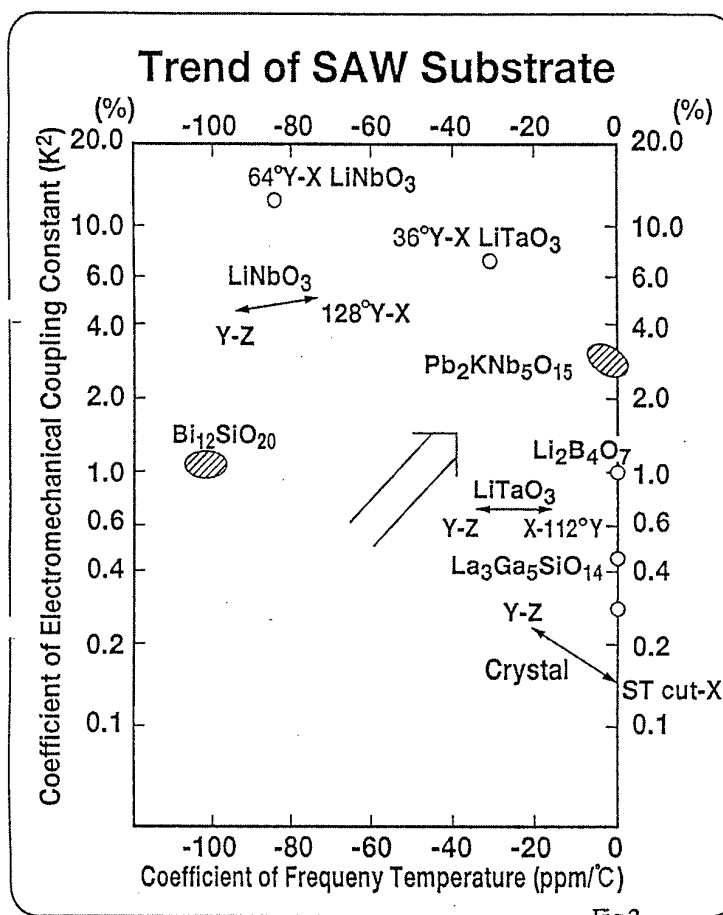
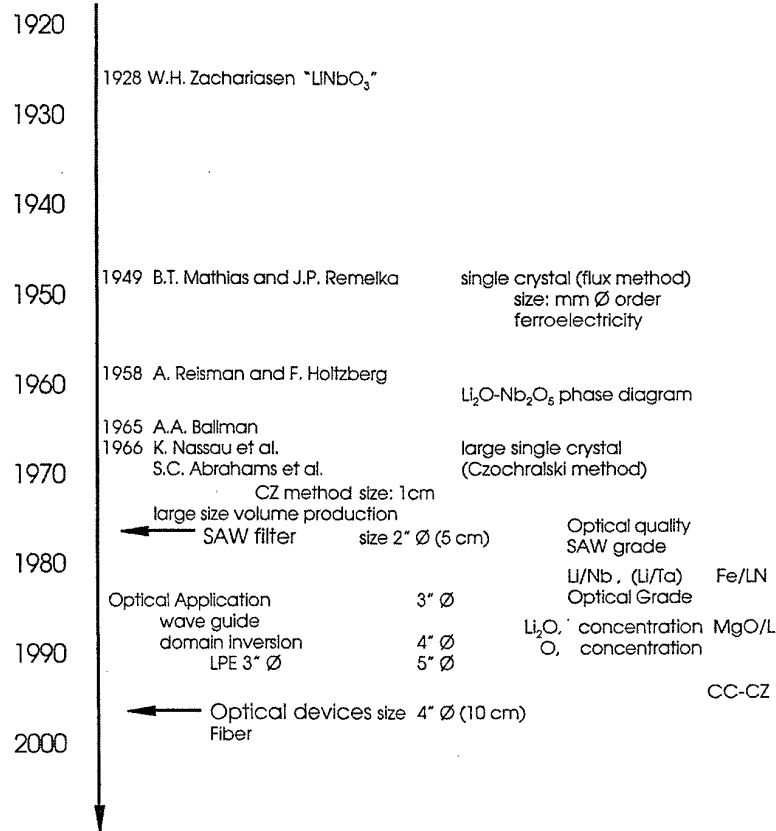


Fig.2

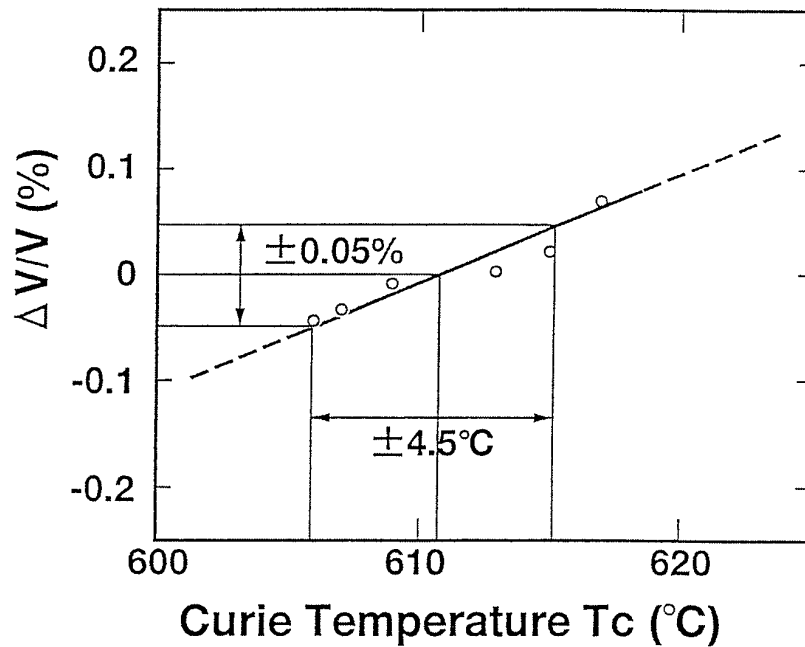
History of LiNbO_3 , LiTaO_3 crystal development



Variation of SAW Velocity

	X-112°Y LiTaO_3 SAW Wafer	128°Y-X LiNbO_3 SAW Wafer
Variation Rate by Composition	~8 m/s/ Li_2O mol%	~43 m/s/ Li_2O mol%
Variation Rate by Curie Temp. (T_c)	~0.4 m/s/°C	~0.85m/s/°C
Condition for Controlling within ± 1 m/s SAW Velocity Change	<ul style="list-style-type: none"> $\Delta T_c < 2.5^\circ\text{C}$ $\Delta \text{Li}_2\text{O}$ mol% $< \pm 0.12$ mol% 	<ul style="list-style-type: none"> $\Delta T_c < 1.2^\circ\text{C}$ $\Delta \text{Li}_2\text{O}$ mol% $< \pm 0.02$ mol%

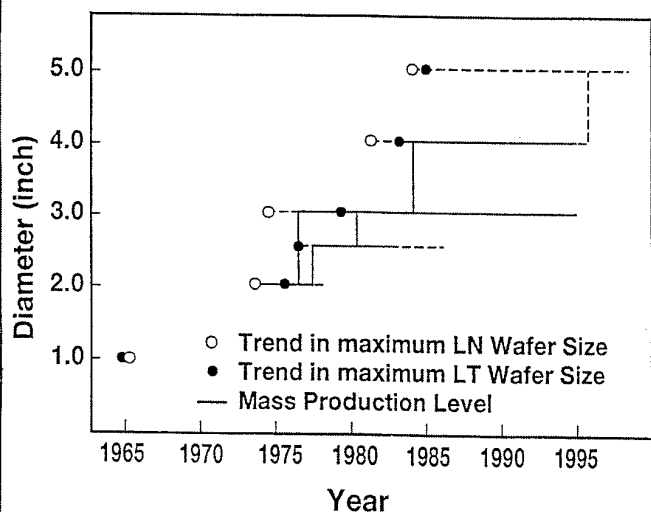
Relation between the SAW Velocity and Tc (LiTaO₃)



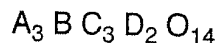
Comparison of Main Single Crystal SAW Substrates

Crystal Substrate	X cut LiTaO ₃	36°rotated Y cut LiTaO ₃	128°rotated Y cut LiNbO ₃	ST cut Quartz	45°rotated X cut Li ₂ B ₄ O ₇	64°rotated Y cut LiNbO ₃
SAW Propagation Direction	112°rotated Y axis	X axis	X axis	X axis	Z axis	X axis
SAW Velocity(m/s)	3296	4178	3960	3158	3401	4475
Electric Mechanical Coupling Coefficient(%)	0.75 (○)		5.5 (⊙)	0.16 (×)	1.0 (○)	11.3 (⊙)
Frequency Temperature Coefficient(ppm/°C)	-18 (○)	-36 (Δ)	-74 (×)	0 (⊙)	0 (⊙)	-81 (×)
Effective Dielectric Constant (ε)	44	44	39	4.5	8	39
Main Feature	<ul style="list-style-type: none"> • most SAW Properties are Middle • Bulk Spurious Level is Superior 	<ul style="list-style-type: none"> • Temperature Property is Good with very Large Coupling Coefficient 	<ul style="list-style-type: none"> • Coupling is Large, but Temperature Property is Worse 	<ul style="list-style-type: none"> • Temperature Property is the Best but Coupling is the Worst 	<ul style="list-style-type: none"> • Coupling and Temperature Property are Good • Weak for Acids 	<ul style="list-style-type: none"> • Coupling is very Large, but Temperature Property is Worst
Application Frequency Area	High and Middle	High	Middle and Low	High and Middle	High and Middle	High
Relative Bandwidth	Wide and Middle	Wide and Middle	Wide	Narrow	Middle and Narrow	Wide

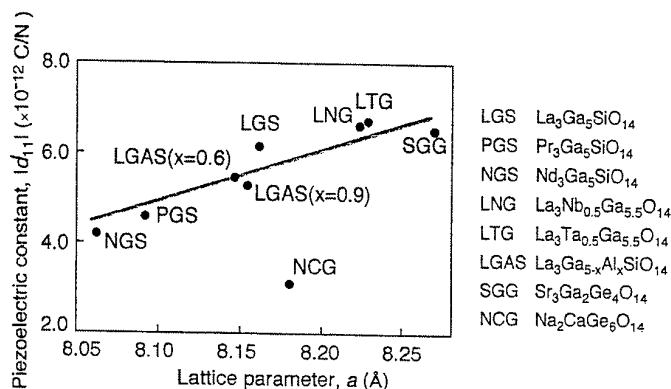
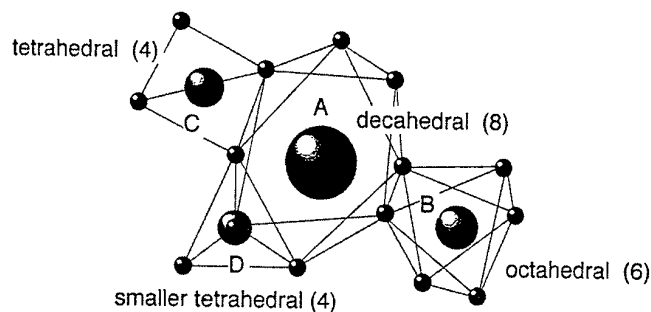
Diameter Trend of SAW Wafer



Langasite-type crystal

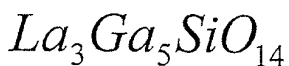


Crystal system : Trigonal Space group : P321

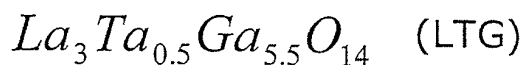
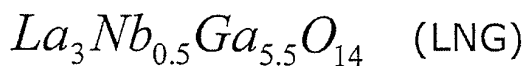
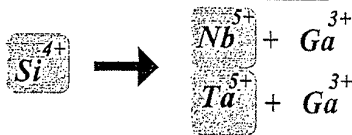


Dependence of piezoelectric constant on lattice parameter

Search for new materials



Aliovalent substitution



Comparison of properties

	LiTaO ₃	LGS	LNG	LTG	quartz
phase transition	exist	none	none	none	exist
melting point (°C)	1650	1490	1470	1500	—
hardness	5.5	6~7	6~7	6~7	7
electromechanical coupling factor k (%)	43	15~25	~30	~30	7
Q - factor	5000	30,000~40,000	40,000~60,000	40,000~60,000	60,000~80,000
equivalent series resistance (Ω)	—	5~10	2~5	2~5	10~20
thermal stability (ppm) (20~70°C)	200~400	~150	~150	~150	10~20

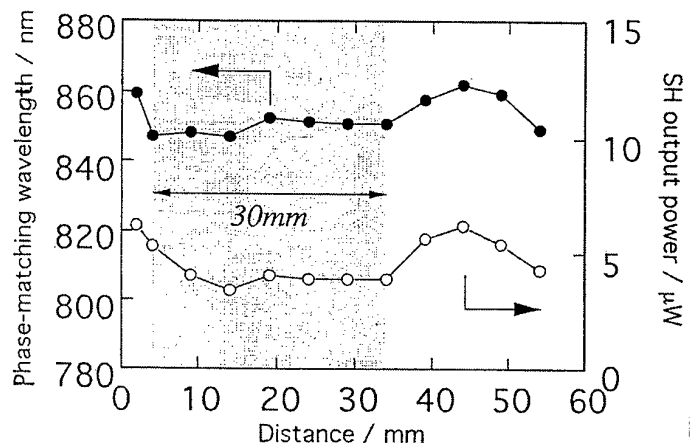
Blue SHG crystal

$\text{KNbO}_3(\text{KN})$: Small temperature allowance, Twin

$\text{K}_3\text{Li}_{2-x}\text{Nb}_{5+x}\text{O}_{15+2x}(\text{KLN})$:

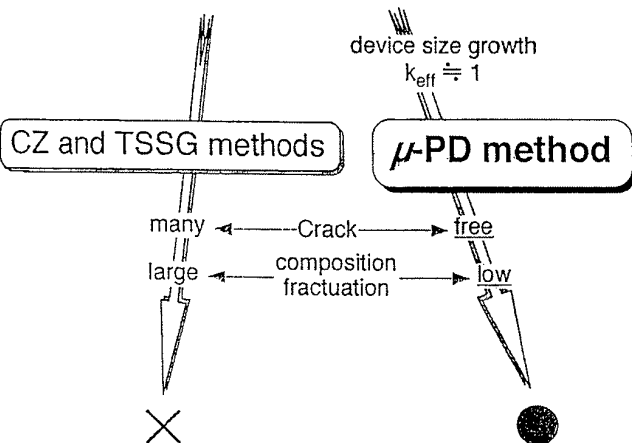
- Large nonlinear coefficient
- No optical damage
- Mechanical and chemical stability

SHG properties along the growth axis



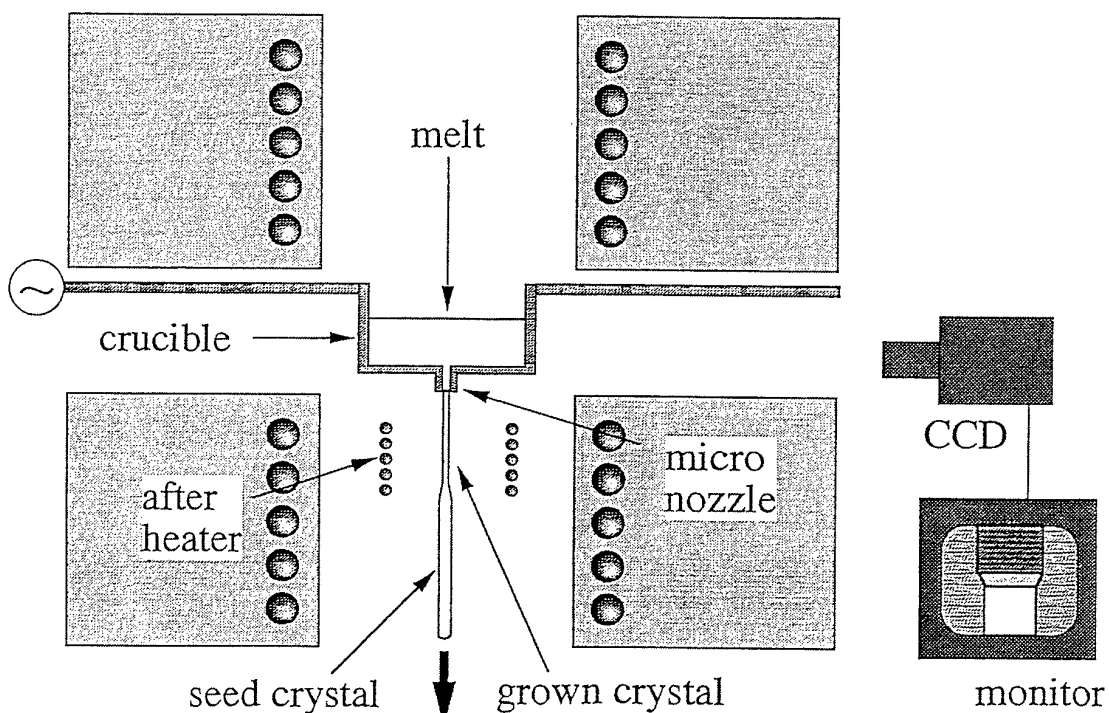
◇ Deviations

Phase-matched wavelength : $\pm 2.6 \text{ nm} / 30 \text{ mm}$
SH output power : $\pm 18\% / 30 \text{ mm}$

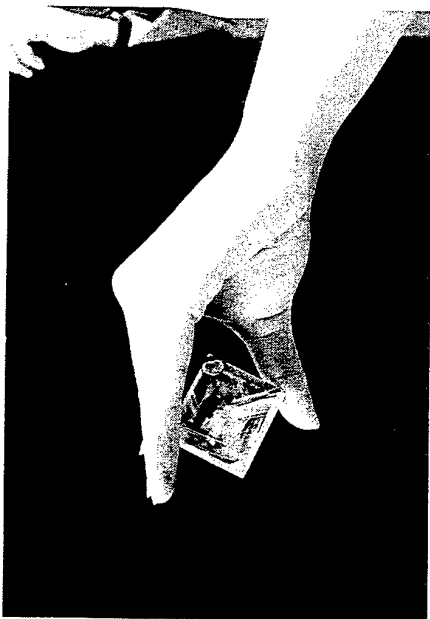


Experimental

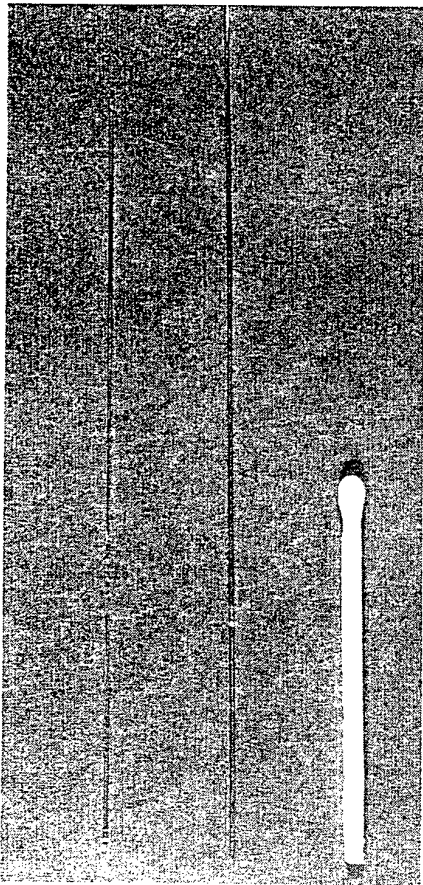
μ -PD apparatus



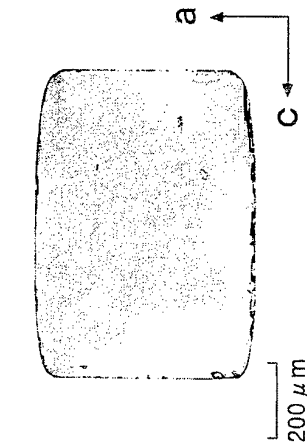
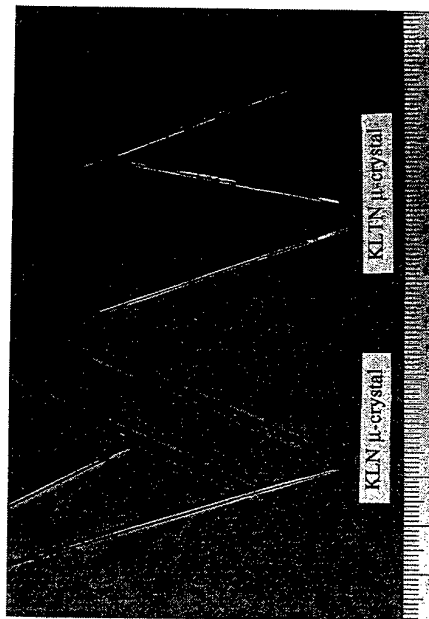
3. Characterization



KLN single crystal fiber



$K_3Li_2Nb_5O_{15}$ (KLN) and $KNbO_3$

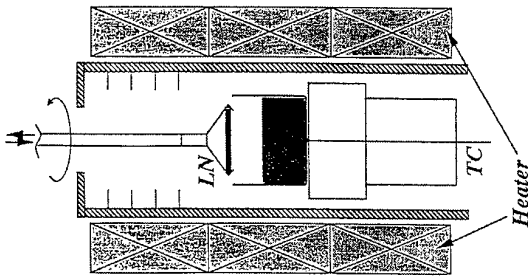
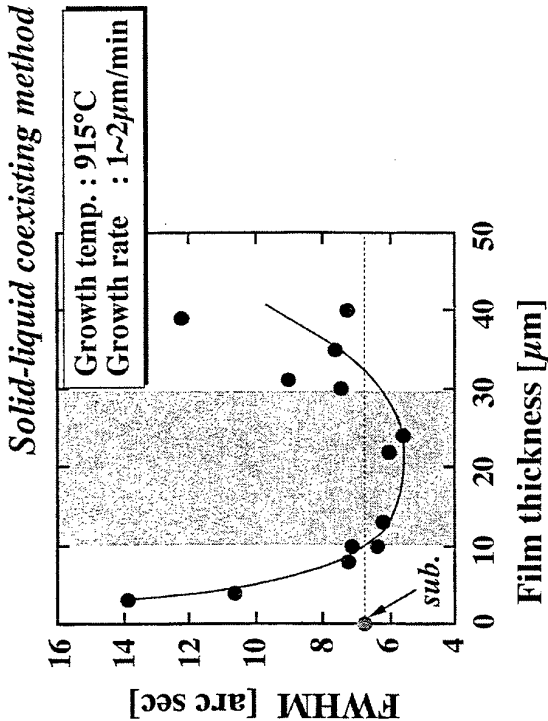


cross-section

side

microscopic image

- Rectangular cross-section, $\square 0.5-0.8\text{mm}$
- Uniform diameter
- Maximum length $\sim 300\text{mm}$
- No macro defects (crack, inclusion, bubble)



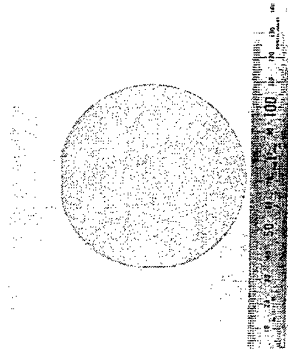
Film growth

- 3-zone vertical LPE furnace
- Substrate : Optical-grade Z-plate LN
- Horizontal dipping
- V₂O₅-Li₂O flux system

Characterization

- X-ray rocking curve (XRC) analysis
- SHG measurement
- Electron probe microanalysis (EPMA)

3-inch wafer size LN epitaxial film



- Perfect mirror-smooth surface morphology.
- Available in the conventional device fabrication processes.

Phase Diagram Studies Necessary for Cz-Growth of Practical Electro-Optic Single Crystals

Shintaro MIYAZAWA

USHIO Research Institute of Technology (URIT)

USHIO Inc.

Electro-optic (EO) crystals are very attractive in applications to light modulators, photorefractive memories and electro-optic sensors. For practical applications of EO single crystals, the reproducibility of optical quality is quite important so as to rely device performances. Therefore, the study of phase diagram or phase relation is strictly needed for reproducing crystals, and also the understanding of a phase relation is a basic science of crystal growth technology and able to clarify the causal relationship between crystal properties and growth history. In fact, semi-insulating properties of undoped GaAs single crystals have been argued by considering the solid solution of GaAs¹⁾.

In this talk, how to establish experimentally a minute phase relation around a compound to be grown will be presented for LiTaO₃ and Bi₁₂TiO₂₀ as representatives of electro-optic crystals. LiTaO₃ is now practically used for electro-optic light modulators as well as SAW (surface acoustic wave) devices, and Bi₁₂TiO₂₀ crystal has become attractive for developing high sensitive probe of ultrahigh speed signals in LSIs through its electro-optic effect²⁾. So, the reproducibility of crystal quality is strongly required from the crystal growth technology point of view.

In the case of LiTaO₃, the stoichiometry dependence of para/ferro-electric phase transition temperature, Curie temperature (T_c), is powerful for determining a phase relation. Figure 1 summarizes the measured T_c of single crystals grown from different Li₂O/Ta₂O₅ melts and of crystalline grains in solidified melts. The figure gives us a conclusion that a compound of Li₂O/Ta₂O₅=48.75/51.25 in molar ratio is congruently melting³⁾, which is Ta-rich from the stoichiometric composition of Li₂O/Ta₂O₅=50.0/50.0, similar to LiNbO₃⁴⁾. Based on this figure,

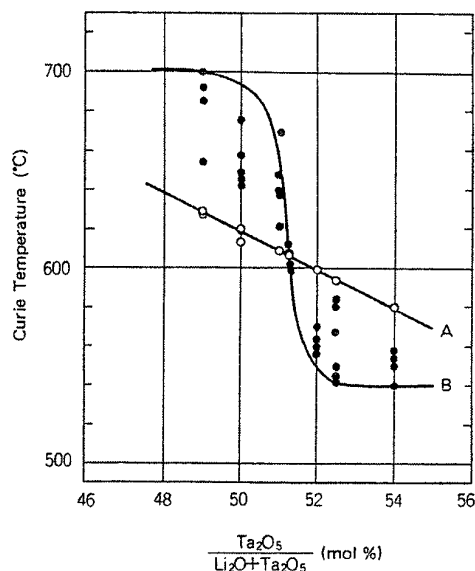


Fig.1 Curie temperature as a function of the melt composition

a minute phase relation was established and its certainty was recognized by measuring optical inhomogeneity induced during the crystal pulling of a single crystal from the stoichiometric melt. This will be discussed in detail.

$\text{Bi}_{12}\text{TiO}_{20}$ (BTO) is isostructural to sillenite $\text{Bi}_{12}\text{SiO}_{20}$ (BSO) family but melts incongruently. BTO decomposes at about 875°C to a liquid and $\text{Bi}_4\text{Ti}_3\text{O}_{12}$ ^{5). Therefore BTO single crystals must be grown from solutions of 3 to 12 mol% TiO_2 by means of TSSG-pulling. However, the best starting solution for reproducible growth of the crystals with high homogeneity has not been established. Figure 2 illustrates a renewed phase relation established by precise lattice constant measurements^{6). The retrograde solidus line was verified by growing a relatively long single crystal from a 10.1 mol% TiO_2 solution. The existence of this retrograde solid solution is the first report in incongruently melting compounds so far. The detailed process for the determination will be presented.}}

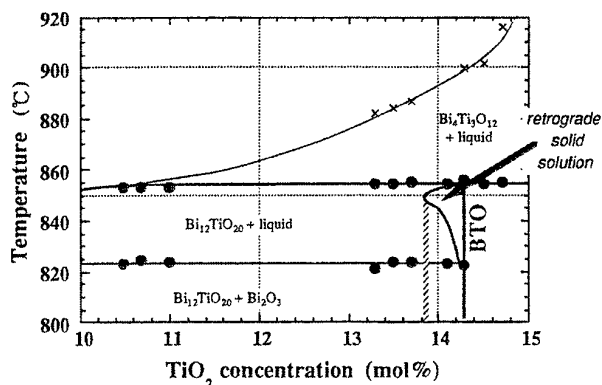


Fig.2 Renewed phase relation of Bi_2O_3 - TiO_2 binary

The re-examination of a phase relation close to the single phase compound to be grown is quite indispensable for practical applications of single crystals. To establish a phase relation precisely, we take stoichiometry dependences of electrical and/or physical properties such as Curie temperature in ferroelectrics, lattice constants, composition analysis and optical homogeneity jointly with DTA (differential thermal analysis) measurements.

References

- 1) S.Miyazawa, in "Progress in Crystal Growth and Characterization of Materials (Edt. by N.Niizeki, Pergamon Press), Vol.23 (1992) p.23
- 2) M.Shinagawa, T.Nagatsuma and S.Miyazawa, IEEE J.Quant.Electr., (1998 in press)
- 3) S.Miyazawa and H.Iwasaki, J.Cryst.Growth, 10 (1971) 276
- 4) R.J.Esdaille, J.Appl.Phys., 58 (1985) 1070
- 5) T.M.Bruton, J.Sol.Sta.Phys., 9 (1974) 173
- 6) S.Miyazawa and T.Tabata, J.Cryst.Growth, (1998, in press), S.Miyazawa, M.Shinagawa and T.Nagatsuma, to be published in Jpn.J.Appl.Phys.,(1998)

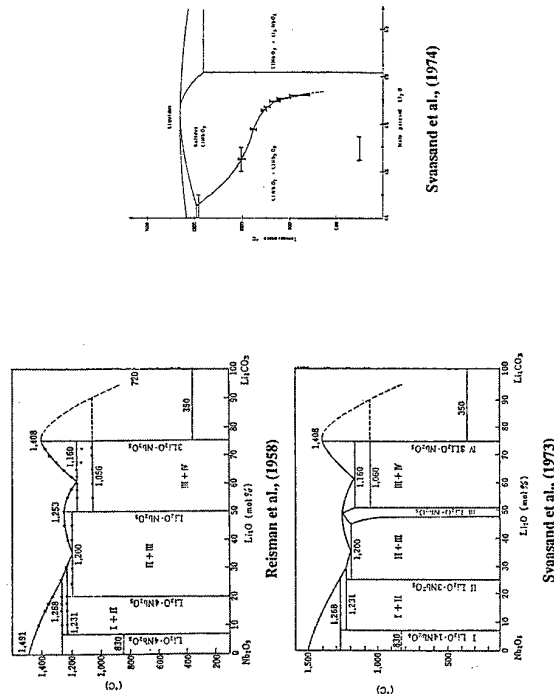
How to Determine Phase Diagram

In general,

1. Differential thermal analysis (DTA)
2. Lattice constant measurement
3. Chemical analysis of composition
4. Optical property measurement
5. Measurement of characteristic temperatures proper to compounds ; phase transition
6. Crystal growth experiment

The combination of 1, 2, 3 and 6 is widely used. 5 is very practical, when its stoichiometry dependence is obtainable.

Phase Diagram of Ferroelectric LiNbO₃



Phase Diagram Studies Necessary for Cz-Growth of Practical Electro-Optic Single Crystals

Shintaro MIYAZAWA

USHIO Research Institute of Technology (URIT)
USHIO Inc.

E-mail : miyazasn@mail.ushio.co.jp

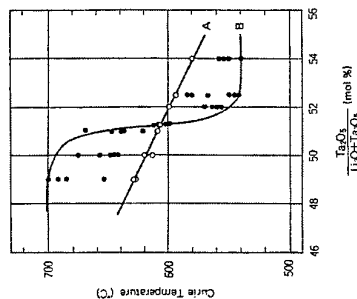
Necessity of Minute Phase Diagram

Device peoples do not doubt that supplied single crystals have the same characteristics. Therefore, crystal growth peoples must guarantee crystal quality, even if crystal lots vary.

- Reproducibility of optical quality is strictly required ;
for device applications, fluctuation/change of optical properties such as refractive index from crystal to crystal must be avoided from the viewpoint of device/system reliability.
- Crystal growth technology includes a guarantee of crystal quality ;

by not only crystal growth techniques but also insights of origins affecting optical quality.

The first step of crystal growth is the understanding of phase diagrams of the compound to be grown.

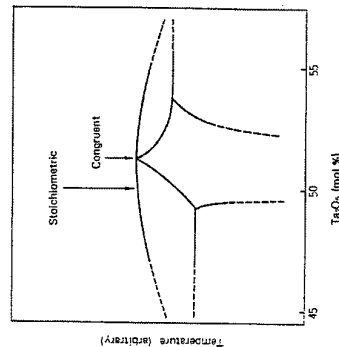


A ; the primarily crystallized part of single crystals
B ; crystalline grains in solidified melts after crystal pulling

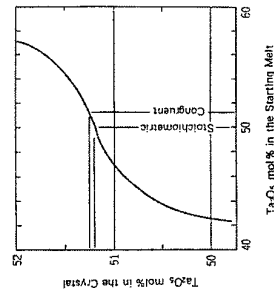
Scattering of solidified melts can be explained by considering a solidification process on a simple binary phase diagram.

Phase Relation of Li_2O - Ta_2O_5 Binary System

Phase diagram

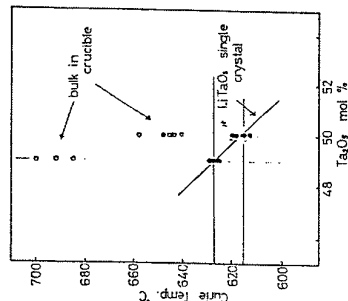


Variation of crystal composition deduced from the phase relation



Clues of Studying Phase Diagram of LiTaO_3 : I

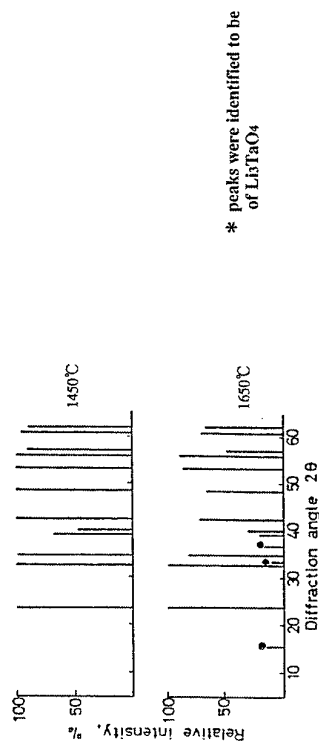
1. Large scattering of Curie temperatures of solidified melts



Curie temperatures of LiTaO_3 appeared in literatures varied from paper to paper ;
665°C ; Z.I. Shapiro et al., Fiz.Tverd.Tela., 6 (1964) 316
660±10°C ; H.L. Levinstein et al., J. Appl. Phys., 7 (1966) 4585
630°C ; Z.I. Shapiro et al., Sov. Phys. Crystallo., 10 (1969) 618
618°C ; A.M. Glass, Phys. Rev., 172 (1968) 172
620-660°C ; A.A. Ballman et al., J. Am. Ceram. Soc., 30 (1967) 657

Clues of Studying Phase Diagram of LiTaO_3 : II

2. Difference in X-ray diffraction patterns of calcined powder



3. Observation of solidified melt in a crucible

Part of the Phase Diagram of the System Bi2O3-SiO2

(after Brice et.al.)

J.F.C. Brice et al., Philips Techn. Rev., 37 (1977) 250

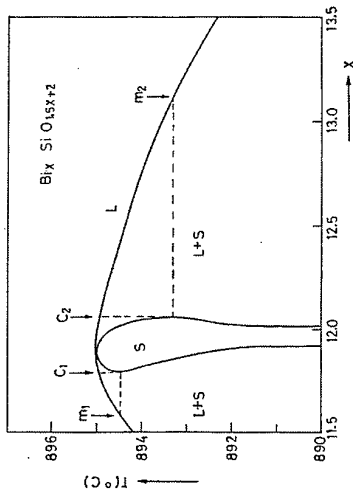
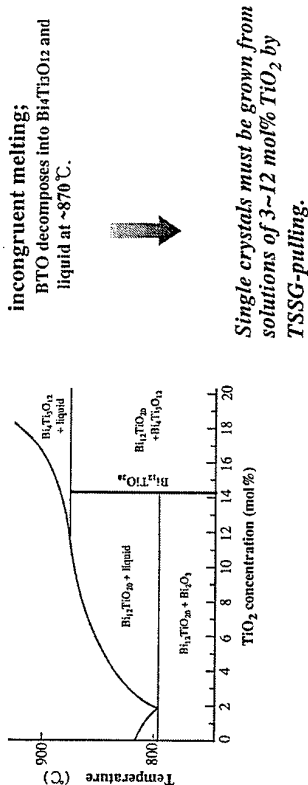


Photo-current and crystal composition are strongly dependent on the starting melt composition, reported by Tada et al. and Hill et al., respectively.

Bi2O3-TiO2 Binary Phase Diagram (by Bruton)

T.M. Bruton, J. Sol. Sta. Chem., 9 (1974) 173



incongruent melting;
Bi4Ti5O20 decomposes into Bi2TiO5 and liquid at ~870 °C.

Single crystals must be grown from solutions of 3-12 mol% TiO₂ by TSSG-pulling.

Analysis of Birefringence Change in a LiTaO3 Crystal Grown from Stoichiometric Melt

Validity of the established phase relation was analyzed by measuring a birefringence change induced by intentional change of a melt temperature during the crystal pulling.

$$\frac{d(\Delta n)}{dT} = \frac{d(\Delta n)}{dCs} \cdot \frac{dCs}{dk_{eff}} \cdot \frac{dk_{eff}}{dT}$$

$$k_{eff} = \frac{k^*}{k^* + (1-k^*) \exp(-\frac{\delta}{D} R)}$$

$$\frac{d(\Delta n)}{dCs} = 1.6 \times 10^{-2} / \text{mol\%}$$

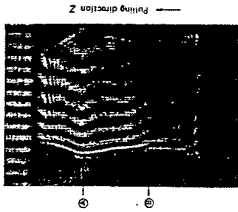
$$\frac{dCs}{dk_{eff}} = C_L = 1.25 \text{ mol\%}$$

$$\frac{dk_{eff}}{dT} = -4.8 \text{ sec/cm}$$

$$\frac{dR}{dT} = \frac{K_L}{\delta T L} = \sim 2 \text{ cm/sec}^\circ\text{C}$$

Measured : $\sim 2.0 \times 10^{-5} / ^\circ\text{C}$
Calculated : $\sim 5.0 \times 10^{-5} / ^\circ\text{C}$

Δn : birefringence, T : temperature, C_s : concentration in crystal, k_{eff} : effective distribution coefficient, R : growth rate, δ : diffusion boundary layer thickness, D : diffusion coefficient,



Mach-Zehnder interference pattern

Evaluation of Optical Quality of Congruent LiTaO3 Single Crystal

Macro-conoscopic interference pattern

Extinction ratio measurement

Theoretically, Extinction ratio is proportional to an inverse root of beam diameter.

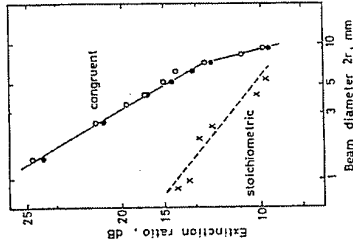
(a) grown from the stoichiometric melt



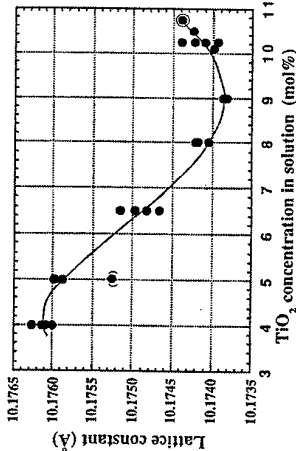
(b) grown from the congruent melt



(c) grown from 52.5 mol% Ta2O5 melt



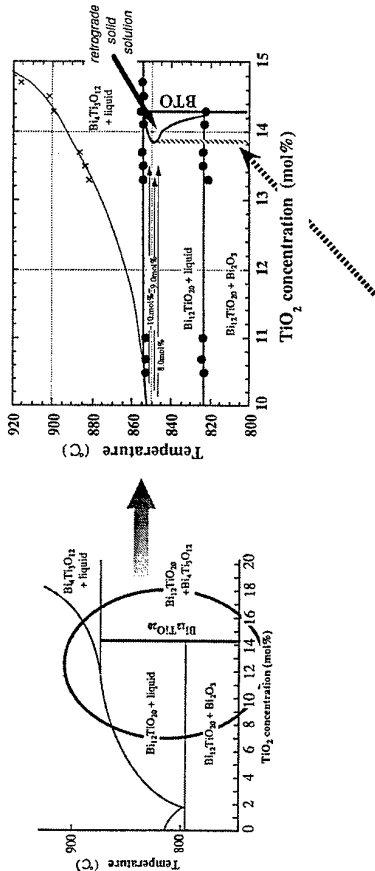
Successively grown BTO single crystals
grown from different solutions



© The crystal was grown from a solution very close to the peritectic composition.

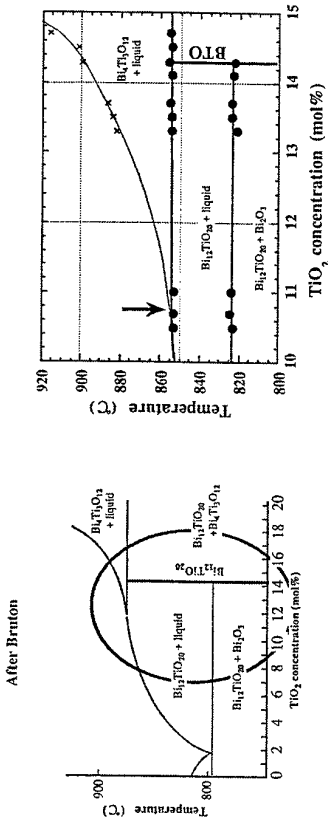
The figure strongly suggests the retrograde solidus curve of solid solution.

Renewed Phase Relation of $\text{Bi}_{12}\text{TiO}_{20}$



From the starting solutions of 8.0~10.1 mol % TiO_2 , reproducibility of BTO crystals is within $\pm 2.5 \times 10^{-5} \text{ \AA}$ of lattice constant.

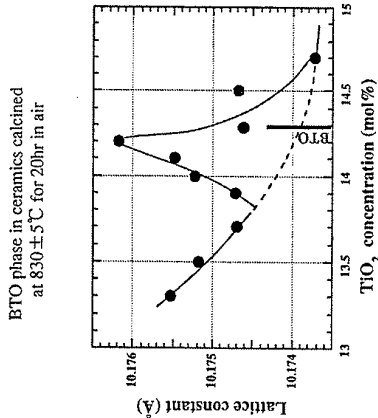
Renewed Phase Relation obtained by DTA and crystal growth



Differences from Bruton's diagram

- @ The eutectic temperature ; $\sim 823^\circ\text{C}$
- @ The peritectic temperature ; $\sim 855^\circ\text{C}$
- @ The peritectic composition ; $\sim 10.75 \text{ mol\% TiO}_2$

Stoichiometry Dependence on Lattice Constant of $\text{Bi}_{12}\text{TiO}_{20}$: I



The figure indicates the existence of solid solution region.

Growth Technology of LiNbO_3 and LiTaO_3

D. Cochet-Muchy

CRISMATEC SA

2, rue des Essarts

F-38610 Gières, France

1. Introduction

Lithium niobate LiNbO_3 and lithium tantalate LiTaO_3 , namely LN and LT, are two ferroelectric oxides which were first synthesized in 1949 [1]. Since this early work, LN and LT have been widely investigated due to an unusual range of interesting properties: piezoelectricity, pyroelectricity, electro-optic and acousto-optic properties, non-linear optical properties, photorefractive properties, etc ... The development of cost-effective growth processes by Czochralski pulling, started in the late 1960s, led to the use of large quantities of LN and LT in piezoelectric devices, such as SAW filters. Later on, the growth of optical grade LN crystals was achieved. This was a significant contribution to the development and manufacturing of integrated optics devices. Today, there is a renewed interest in non-linear optical properties of LN, due to the very efficient frequency conversion obtained using quasi-phase matching in periodically-poled crystals. It opens the wide field of the blue or green micro-lasers systems to this mature material.

2. Materials considerations

When speaking about the structure, properties and growth of LN and LT, one has to emphasize that these are uniaxial crystals. They have rhombohedral structure, belonging to the space-group $R3c$ below the Curie temperature (T_C). They are built on a succession of oxygen octahedra along the three-fold axis, containing the cations in the following sequence : Li, Nb or Ta, an empty octahedron. The origin of the ferroelectricity lies in the displacement of the cations from the center of the octahedra. Above the Curie point, in the paraelectric state, the cations move to the center of the octahedra, and the structure becomes centrosymmetric ($R3c$).

This description of the atomic arrangements corresponds to the stoichiometric compounds, LiNbO_3 or LiTaO_3 , but a large solid solution range exists for both phases. The maximum range for the Li_2O content is 45-51% near 1200°C for LN ($T_m = 1253^\circ\text{C}$) and near 1600°C for LT ($T_m = 1650^\circ\text{C}$). Many different congruent compositions have been reported in the literature for both compounds [2-5], but all are deficient in Li compared to the stoichiometry. The possible origin of the discrepancies among the reported congruent compositions will be discussed during the lecture.

A consequence of the strongly anisotropic crystal structure of LN and LT is a very different behavior upon crystallisation when different growth axes are used. Therefore, one should consider the crystal growth operations for different growth axes as separate processes. More specifically, one can say that the anisotropy of the thermal expansion coefficients creates high thermal stresses within the crystals during growth and cooling. This can lead to fractures, more or less easily, depending on the orientation and the size of the growing crystal. For a given size, the yield associated to fractures decreases in the following growth axis sequence : [00.1] or Z, [01.0] or Y, [21.0] or X , for LN, Y, X, Z, for LT. Low thermal gradients and growth parameters optimized for each case should be used to prevent the crystals from cracking.

At the beginning of the 1990s, we worked under governmental contracts at Crismatec to develop growth processes for Z- and Y-LN (3 inches diameter), and Y and X-LT (4 inches diameter).

3. Growth technology

Due to the favorable congruent melting and low vapor pressure of LN and LT, the Czochralski pulling technique has been recognized as the sole industrial growth process. The main technological problem faced with this technique is finding a convenient set of the following elements : crucible, insulators, heating source and diameter control system.

Platinum (LN), platinum-based alloys or iridium (LT) are the materials of choice for the crucibles.

Insulators are generally made of refractory ceramics including alumina and silica for LN, and mostly pure alumina or zirconia for LT.

The choice of a heating source has the biggest impact on the general growth station characteristics (size, versatility, reliability, purchase cost and operation cost). Resistance heating is commonly used for LN, owing to good thermal homogeneity and control of gradients. Induction heating can also be used. In this case, the heat generation into a « skin depth » at the outer surface of the crucible makes the thermal field control more difficult. In order to get the desired gradients, one must pay more attention to the design of the ceramics and, sometimes, extra-heaters must be introduced, such as secondary metallic susceptors (or reflectors) over the crucible, or a resistance heated zone. The position of the crucible with respect to the coil also plays a significant role. Due to the high melting point of LT, induction heating is used.

Diameter control is generally achieved by weighing the growing crystal, rather than by temperature control or by weighing of the crucible. Specific software is used to program the desired shape of crystal, process the weight signal and make the necessary corrections of heating power.

4. Growth operations

For SAW-grade crystals, 99.95% pure raw materials are largely sufficient, whereas a lot more attention should be paid to this purity when growing optical grade crystals. Li_2CO_3 and Nb_2O_5 (or Ta_2O_5) are mixed together in the selected composition and prereacted during several hours at high temperature for solid state formation of LiNbO_3 (or LiTaO_3). The prereacted powder is used to fill the crucible and pull the crystal.

Practically, the size of the crystal is limited by the size of the crucible and by the thermal gradients in the crystallization area. A good ratio between the crucible diameter and the crystal diameter is 2. However, for cost reasons, there is a tendency to lower this ratio as much as possible. The convenient vertical thermal gradient just above the melt is close to or below $15^\circ\text{C}/\text{cm}$. When induction heating is used, the length of the crystal is limited by the drop of the melt level as far as the crystallization runs. This changes the thermal gradients in such a way that spiral growth may occur. In this case, the use of a crucible lift has proven to be very useful. The position of the melt surface can remain constant and this helps to keep the necessary gradients. Another limitation of the crystal length comes from the composition used. Any difference with the congruent composition leads to a melt enrichment in one of the components which finally results in crystal defects.

Once good growth conditions have been met, the next requisite for succeeding the growth of LN and, to a lesser extent, LT, is to avoid the formation of extended structure defects, like twins, at the beginning of the growth process. Much attention should be paid to the quality of the seed and to the temperature of the melt when dipping the seed into the melt. When twinning occurs, it is easily visible on the shoulder of the crystal going from the seed diameter to the final diameter. When this happens, the shoulder is remelted and a new dipping is made.

The ordinary growth rates are generally close to 5 mm/hr, whereas for optical grade crystals it should be decreased to between 1 and 3 mm/hr. Rotation rates generally vary between 10 and 40 rpm.

After growth, cooling the crystal down to room temperature is completed in about 30 hours, in a region of the furnace with the least temperature gradients.

5. Quality control

The compositional homogeneity is checked by either electrical or optical methods. The method consists of measuring significant variations of some physical parameters, like Curie temperature or refractive indexes [6], with composition, to detect any differences from one part of the crystal to another, that is to say any deviation of the melt composition from the congruent composition. The measurement of the E_{33} dielectric constant over a convenient temperature range allows one to determine the Curie points with good accuracy as it passes through a sharp maximum at this phase transition.

X-ray topography is used to control the structural perfection. Subgrain-free crystals are considered to be top quality.

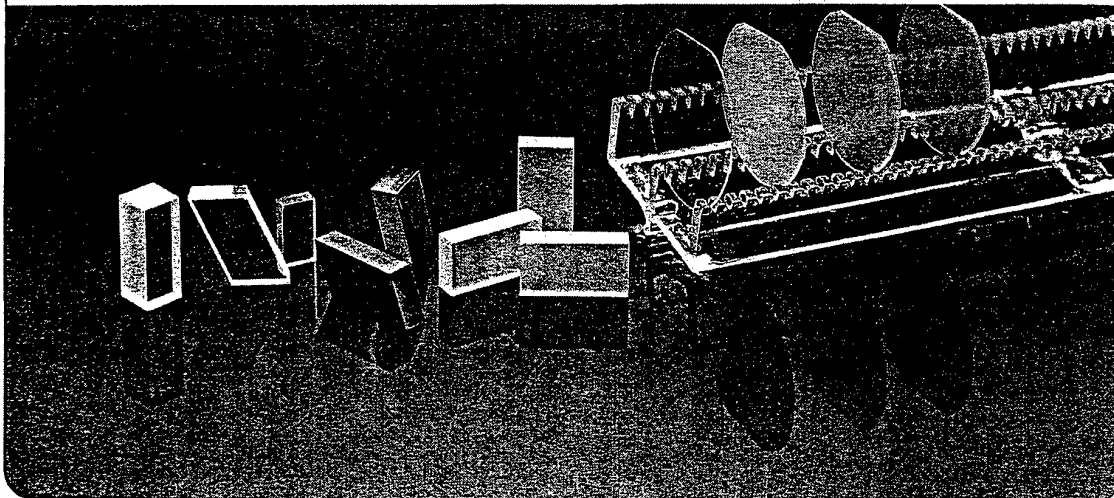
Finally, the purity of the crystals is controlled by using spark-source mass spectrometry or glow discharge mass spectrometry. These analytical techniques can also be used to measure purity of the raw materials.

References

- [1] Matthias B.T., Remeika J.P., Phys. Rev. **76** (1949) 1886
- [2] Lerner P., Legras C., Dumas J.P., J. Cryst. Growth **3/4** (1968) 231
- [3] Carruthers J.R., Peterson G.E., Grasso M., Bridenbaugh P.M., J. Appl. Phys. **42** (1971) 1846
- [4] O'Bryan H.M., Gallagher P.K., Brandle C.D., J. Am. Ceram. Soc. **68** (1985) 493
- [5] Bordui P.F., Norwood R.G., Bird C.D., Calvert G.D., J. Cryst. Growth **113** (1991) 61
- [6] Properties of Lithium Niobate, EMIS Datareviews Series N°5, INSPEC, The Institution of Electrical Engineers, London and New-York (1989)

STANDARD ACOUSTIC GRADE SPECIFICATIONS

Polished wafers or plates	LITHIUM NIOBATE	LITHIUM TANTALATE
Diameter	up to 76.2 mm (± 0.1 mm)	up to 100 mm (± 0.1 mm)
Length along polar axis (z)	up to 220 mm (± 0.100)	up to 80 mm (± 0.100)
Thickness	from 0.300 mm (± 0.050)	from 0.300 mm (± 0.050)
Surface orientation	Y or Z or Y + 128° cuts (± 0.5 deg)	X or Y cut (± 0.5 deg)



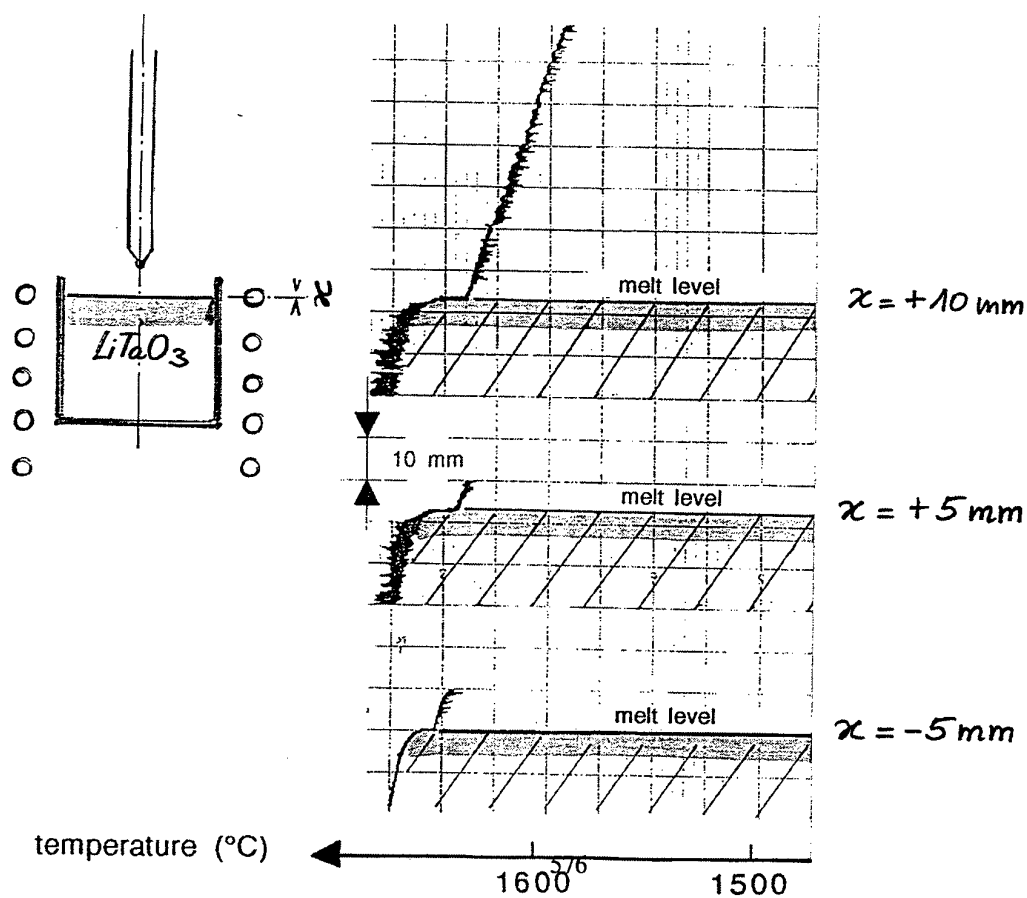
Physicochemical features of LiNbO_3 , LiTaO_3

		LiNbO_3	LiTaO_3
Crystal structure		Rhombohedral	Rhombohedral
Lattice parameters (nm) at RT (hexagonal)	a c	0.5147 1.3856	0.5154 1.3782
thermal expansion coefficients at RT	a-axis c-axis	14.1×10^{-6} 6.0×10^{-6}	16.1×10^{-6} 4.1×10^{-6}
melting point	(°C)	1253	1650
congruent composition		48.5 % Li_2O	48.75 % Li_2O
Curie point for the congruent composition	(°C)	1143	610

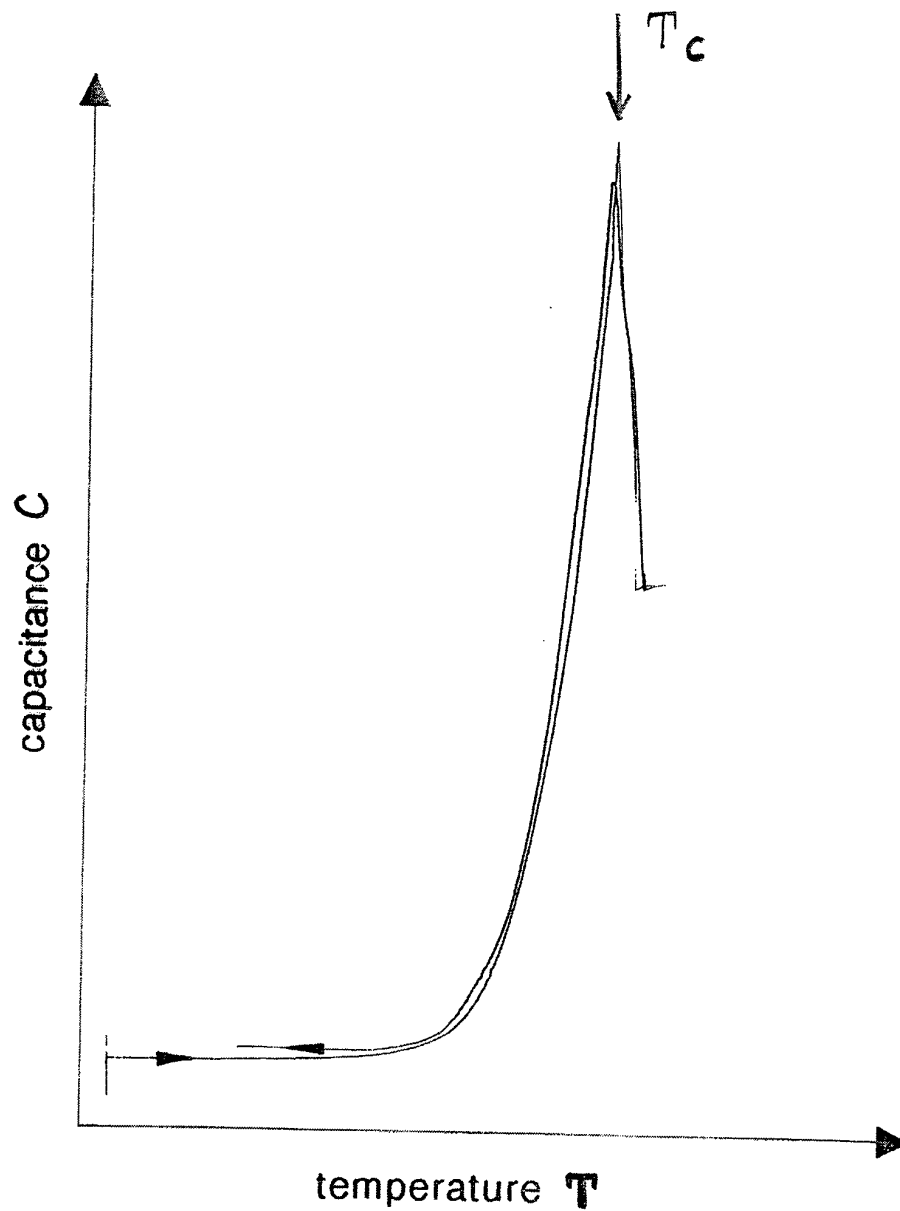
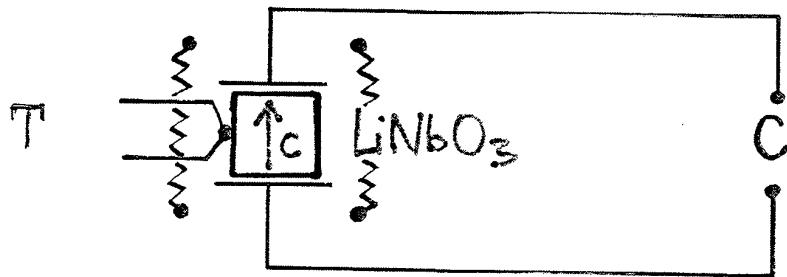
Crucibles used for some piezoelectric oxides

Oxide	T_m (°)	Crucible	T_m (°C)	Atmosphere
LiNbO ₃	1253	Platinum	1769	preferably oxidizing
LiTaO ₃	1650	Iridium Platinum-Rhodium (~ 30 %)	2454 1930	neutral preferably neutr

Axial thermal gradient



Curie temperature measurements



Growth of Stabilized Zirconia Crystals by Skull Melting
V.V.Osiko
Laser Materials and Technology Research Center of CPI, RAS
Moscow, Russia

J.F.Wenckus
Zirmat Corporation. Westford, M.A.
USA

Abstract

Pure zirconium dioxide (ZrO_2) exists in three polymorphic modifications. The ZrO_2 melt crystallizes at 2680°C in cubic modification, ($\text{Fm}3\text{m}$, fluorite). At 2370°C cubic modification transforms into tetragonal one ($\text{P}4_2/\text{nmc}$), and at 1160°C it transforms again into monoclinic ($\text{P}2_1/\text{C}$) modification (baddeleyite). This means that it is impossible to grow single crystals of pure zirconia by melt crystallization. Fortunately cubic modification can be stabilized by incorporation of special dopants, such as MgO , CaO , Y_2O_3 . The addition of these stabilizers form numerous vacancies in the oxygen sub-lattice of ZrO_2 and thus prevents transformation of cubic phase on cooling: cubic zirconia (CZ) then remains the stable form down to room temperature.

High melting point and extreme chemical reactivity of the melt make it impossible to melt and crystallize CZ in conventional metallic or graphite crucibles.

In the end of 60th the new technique of melting and solidification of refractory dielectrics was proposed. That was so called direct RF melting in a cold container or skull melting. The physical ground for this technique is specific temperature dependence of electroconductivity of dielectrics: electroconductivity rises with temperature up to the melting point, and then sharply by jump increases in the melt. Typically the jump of electroconductivity reaches two orders of magnitude. The skull-melting process may be thought of as a very high temperature analog of microwave cooking where the microwave energy heats the contents in the dish-but not the dish itself. Skull-melting utilizes a water-cooled, copper crucible-like structure to surround the RF-heated molten zirconia which is contained by a thin shell or «skull» of its own composition. Thus the contained melt is not in contact with, or contaminated by, the cold crucible. The melt is then slowly cooled by lowering container towards the RF coil until complete solidification. By this way molten charge is converted to a mass of elongated CZ crystals. The crystallized ingot consists of the columnar shaped single crystals, the weight of the separate single crystals reaches 3-5 kg. The CZ single crystals are characterized with the unique set of physical and chemical properties. They are water clear and transparent in the range of 0.26 - 7.5 μm , with the refractive index $n_0 = 2.17 - 2.21$, and dispersion of the refractive index 0.06. It is relatively hard, (the Mohs hardness 8,5) and extremely chemically inert. Besides CZ possess significant electro-conductivity of ion type at

elevated temperatures. Due to such combination of properties the CZ crystals are very attractive as diamond simulants, substrates, selective electrodes and different technical components, utilizing its mechanical and optical properties.

The additional advantage of CZ is that many dopants of different chemical nature can be incorporated in these crystals significantly varying, spectroscopic, electrical and mechanical properties.

Over 98% of the CZ crystals produced today are fabricated into gemstones.

The current market for CZ crystals is in the range of 50 to 100 tons per month. There are several commercial plants in the world producing CZ crystals. For instance Ceres Corporation in the USA produces approximately 20 tons of CZ per month using 45" diameter skull furnaces holding 2.5 to 3.5 ton charges.

Some data on the defects in CZ crystals will be also given in the lecture.

References

1. V.I.Aleksandrov, V.V.Osiko, V.M.Tatarintsev. Synthesis of Laser Materials from the Melt by Direct Radio Frequency in a Cold Container. Otchet FIAN, Moscow, 1968.
2. Y.Roulin, G.Vitter, C.C.Deportes. New device for melting without a crucible. Fusion of high melting oxides in a multitubular furnace. *Revue Internationale des Hautes Temperatures et des Refractaires*, vol.6 p.p. 153-157, 1969
3. J.F.Wenckus, W.P.Menashi, A.Castonguay. Cold crucible system. United States Patent, 4,049,384. Issued September 20, 1977.
4. V.I.Aleksandrov, V.V.Osiko, A.M.Prokhorov and V.M.Tatarintsev. Synthesis and crystal growth of refractory materials by melting in a cold container, in *Current Topics in Materials Science*, Volume 1, edited by E.Kaldis, North-Holland Publishing Company, 1978.
5. K.Nassau. Cubic Zirconia. An Update. *The Lapidary Journal*, Inc. Vol 35 № 6, PP 1194-1200, 1210-12M. September, 1981.

Growth of Stabilized Zirconia Crystals by Skull Melting

V.V.Osiko

Laser Materials and Technology
Research Center of GPI,RAS

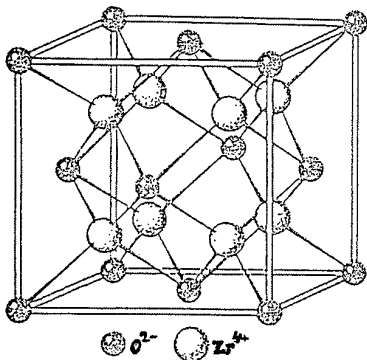
Moscow. Russia

J.F.Wenckus

Zirmat Corporation. Westford M.A.
USA

Contents

- 1.Introduction. What is Stabilized Zirconia.
- 2.Physical Aspects of the Direct Radio Frequency Melting in a Cold Container (Scul Melting).
- 3.Growth Processes of Stabilized Zirconia (CZ) and Partially Stabilized Zirconia(PSZ).
- 4.Defects in Melt Grown CZ Single Crystals.
- 5.Large Industrial- Scale Skull Melting Furnaces.
- 6.Characterization of Large CZ Crystals.
- 7.Application of CZ Crystals.
- 8.Economic and Market Aspects.



The structure of
cubic zirconia

Co - ordination: Zr - 8, O - 4

Tetragonal: P4₂/nmc

Lattice parameters: a=b=5.085,
c=5.166, a/c=1.016
(slightly distorted fluorite)

1. Introduction. What is Stabilized Zirconia.



Polymorphic transitions:

m.p.

cubic (2680 - 2370) → tetragonal

(2370 - 1160) →

monoclinic (below 1160° C)

modifications

Cubic: Fm3m (fluorite)

Monoclinic: P2₁/C (baddeleyite).

Lattice parameters:

a= 5.169, b=5.232, c=5,341Å

Stabilization of cubic modification

Stability criterion for fluorite cubic lattice (after Goldschmidt, Magnus, and Pauling) :

$$R_C/R_A \geq 0.736$$

For ZrO₂ $R_C/R_A = 0,66$

Stabilization with additional dopants:
alkaline-earth oxides:

Ca, Sr, Y₂O₃, rare- earths.

Some properties of CZ crystals

Melting point 2680°C
(ZrO_2 : Y_2O_3 10mole %)

Density 5910 kg m^{-3}
 Y_2O_3 10.3 mole. %

Refractive index (D_{Na}) 2.173
(Y_2O_3 10 mole %)

Dispersion of refractive index 0.06

Optical transparency 0.26-7.5
mcm

Thermal expansion $(7.5-13) \cdot 10^{-6}$
 $^{\circ}\text{C}^{-1}(0-1000^{\circ}\text{C})$
coefficient

Heat capacity (20°C)
 $0.015 \text{ kcal mole}^{-1} \text{ grad}^{-1}$

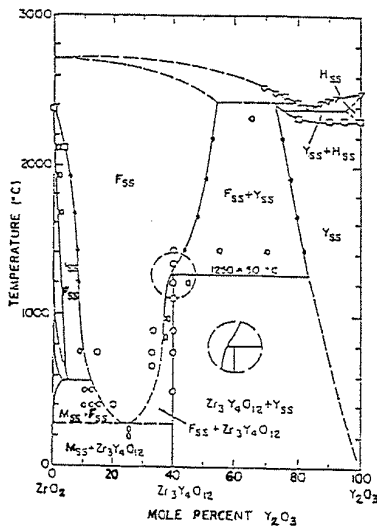
Heat conductivity 2.2 kcal m^{-1}
 $\text{h}^{-1} \text{ grad}^{-1}$

Hardness 8.5(Mohs),
15.29. Gpa

Shock resistance, K_{1c} $2-3 \text{ MPa} \cdot$
 $\text{m}^{1/2} (\text{Y}_2\text{O}_3 \text{ 10 mole \%})$
 $8-14 \text{ MPa} \cdot$
 $\text{m}^{1/2} (\text{Y}_2\text{O}_3 \text{ 2.6 mole \%})$

Electroconductivity $10^{13} \text{ ohm m}^{-1}$
 (20°C)

10^4 ohm m^{-1}
 (1000°C)

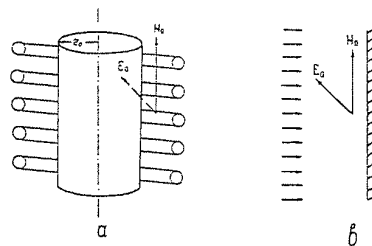


Phase diagram of the
 ZrO_2 - Y_2O_3 system

Crystal-chemical structure

Structure elements (after
F.A.Kröger): Zr_{Zr} , O_{O} , Y_{Zr} , (Ca_{Zr}) , V_{O} ;
 $n \text{ V}_{\text{O}} = n \text{ Ca}_{\text{Zr}}$; $n \text{ V}_{\text{O}} = 0.5 n \text{ Y}_{\text{Zr}}$

2.Physical Aspects of the Direct
Radio Frequency Melting in a Cold
Container (Skull Melting)



$$H_{\text{ampl}} = H_0 \exp(-Z/\Delta) \text{ and } E_{\text{ampl}} = H_0 \sqrt{2} \exp(-Z/\Delta) \gamma \Delta$$

H_0 - The amplitude of the magnetic field on the surface of the body;
 Z - depth;
 γ - specific electrical conductivity;
 Δ - penetration depth
 $\Delta = 5.03 \cdot 10^3 (\rho/\mu f)^{1/2} [\text{cm}]$, where
 ρ - the specific resistivity,
 μ - magnetic permeability;
 f - the frequency of the electromagnetic oscillations.

The active energy flow: $S_a = H_0^2 \exp(-2Z/\Delta)/2\gamma\Delta$.

Substituting 'Z for $Z = 0$ and $Z = \Delta$ in this formula, we have

$$S_0 - S\Delta = 0.864 H_0^2 / 2\gamma\Delta = 0.864 S_0$$

V - the volume of the initial drop,
 P - the power absorbed per unit volume,
 K - the coefficient of heat transfer from the melt to the cooling water,
 T_m - the temperature of the melt,
 T_0 - the temperature of cooling water,
 D - the diameter of the drop,

$$D > (6K/P)(T_m - T_0)$$

Zr, Hf, Y metals as a seed loading for RF melting of the charge.

The condition of phase equilibrium (stationary regime)

$$\lambda/\sigma\alpha = (T_m - T)/(T - T_0)$$

$T_m - T = \Delta T$ - overheating of the melt

δ - the Thickness of solid layer,

α - the heat emission conductivity,

λ - the thermal conductivity of solid layer.

If $\Delta T \rightarrow 0$, then $\delta \rightarrow \infty$

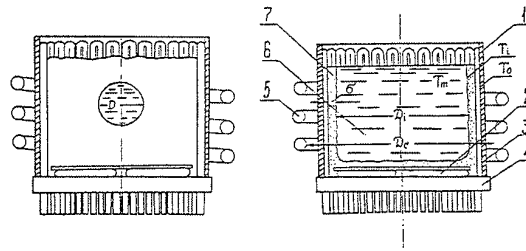


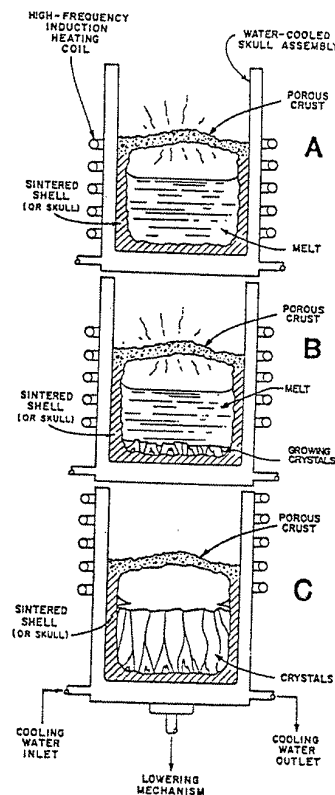
Illustration of the initial melting (a) and melt-solid equilibrium (b) in the cold container.

(1) Water-cooled tubing, (2) water-cooled bottom, (3) insulating screen, (4) insulating bottom, (5) RF-coil, (6) melt, (7) solid shell.

The condition of the initial melt drop vitality

$$VP > K (T_m - T_0) \pi D^2$$

3. Growth Processes of CZ and PCZ Crystals

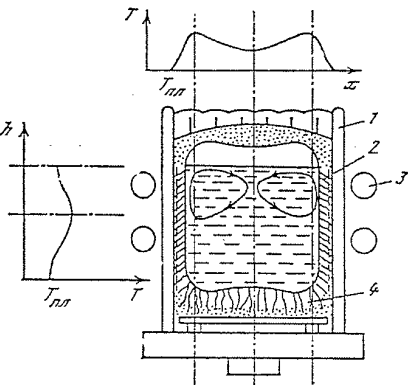


Commercially Available Installation
for Skull Melting

Parameter	Crystal 401	Crystal 403	Crystal- 405
Total power,kw	100	200	280
Power of oscillati- ons, kw	60	160	160
Frequency ,MHz	5.28	1.76	1.76
Crucible diameter, cm	20	40	50
Crucible height,cm	30	70	100
Productivi ty, kg/h	0.1	3.0	3.0

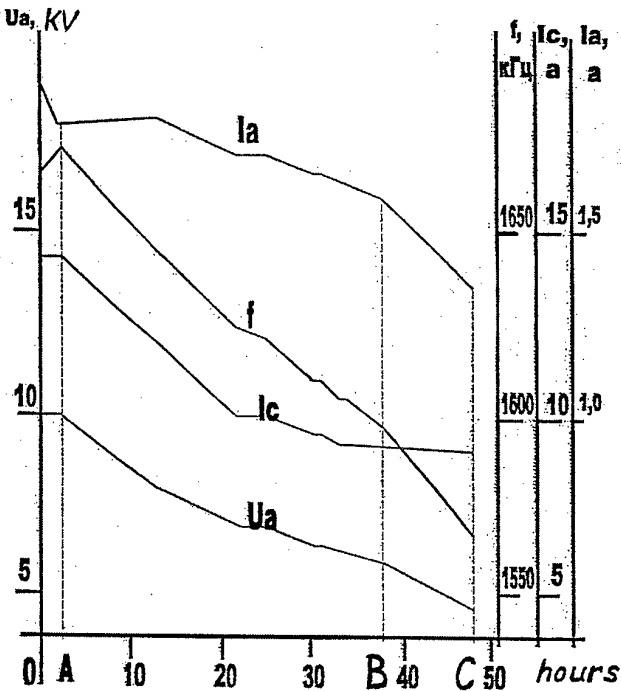
Initial Materials

Admixtures,wt %	ZrO ₂	Y ₂ O ₃
Silicon	< 5 10 ⁻³	5 10 ⁻⁴
Aluminium	< 1 10 ⁻³	-
Iron	< 5 10 ⁻⁴	1 10 ⁻³
Chromium	< 1 10 ⁻⁴	5 10 ⁻⁴
Titanium	5 10 ⁻³	-
Manganese	1 10 ⁻⁴	1 10 ⁻³
Vanadium	1 10 ⁻⁴	-
Cobalt	1 10 ⁻⁴	5 10 ⁻⁴
Praseodimium+ + Neodymium	-	4 10 ⁻³
Terbium + Holmium	-	2 10 ⁻³
Dysprosium	-	2 10 ⁻³
Sulfate ion	1 10 ⁻²	-
Chlorides	2 10 ⁻²	-



The scheme of the temperature
distribution in a cold container.

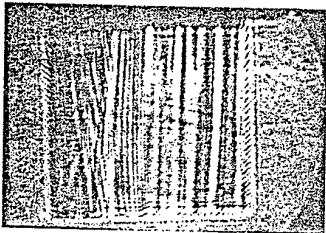
- (1) copper elements of the cold
container;
- (2) solid shell of polycrystalline CZ
- (3)RF- coil; (4) growing crystals.



The drift of the RF-generator
parameters during homogenization
(O - A), growth (A - B), and
annealing (B -C) stages of the
process.

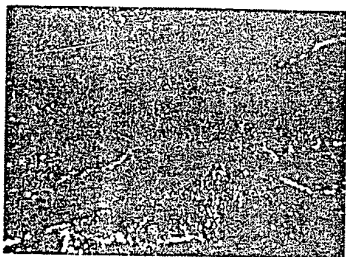
4.Defects in Melt Grown CZ Single Crystals

- a - striations; non -uniform distribution of the solid solution components;
 $K_{Y_2O_3} = 1.088$ for ZrO_2 ;
 Y_2O_3 10 mole%
 $\Delta n_{max} = 3 \cdot 10^{-3}$



Shade-projection picture of CZ single crystal grown in inappropriate conditions.

- c - microscopic and submicroscopic solid-phase inclusions; the concentration of the particles reaches 10^6 mm^{-3} and depends mainly on the chemical purity of the materials and the growth conditions; typical size $\sim 0,1 \text{ mcm}$; the most «dangerous» impurities: silicon and aluminium



Solid-phase inclusions in $ZrO_2:Y_2O_3$ (10 mole %): Nd_2O_3 (0,5 mole %) single crystal.

b - thermal stresses;

$\Delta n_{max} = 7,7 \cdot 10^{-4}$;

annealing at 2100^0C in vacuum



CZ plate under polarized light; before annealing (left) after annealing at 2100^0C (6 hours) in vacuum (right).

PROPERTIES OF SIMULATED DIAMONDS					
MATERIAL	DENSITY	REF INDEX	DISPERSION	HARDNESS	STRUCTURE
DIAMOND	3.51	2.417	.044	10.0	CUBIC
CUBIC ZIRCONIA	5.6	2.15	.060	8.5	CUBIC
GGG	7.07	2.03	.038	7.5	CUBIC
STRONTIUM TITANATE	5.13	2.409	.190	6.0	CUBIC
YAG	4.55	1.8	.028	8.25	CUBIC
CORUNDUM	3.99	1.77	.018	9.0	HEXAGONAL
RUTILE	4.24	2.7	.280	6.0	TETRAGONAL

THERMAL CONDUCTIVITY OF SIMULATED DIAMONDS	
MATERIAL	THERMAL CONDUCTIVITY (W/CM* ⁰ K)
DIAMOND	10-26 *
CORUNDUM	0.35
YAG	0.11
GGG	< 0.1
STRONTIUM TITANATE	< 0.1
RUTILE	0.08
CUBIC ZIRCONIA	0.02

* DEPENDANT UPON IMPURITY LEVEL

Sapphire Crystal Growth Technology Using Heat Exchanger Method (HEM)TM

Frederick Schmid and Chandra P. Khattak
Crystal Systems, Inc.
Salem, MA 01970
USA

Phone : 978-745-0088; Fax : 978-744-5059

The Heat Exchanger Method (HEMTM) is a solidification technique that has been utilized for growth of sapphire crystals from the melt. Large crystals can be grown by HEM since it has the unique feature for independently controlling the heat input and heat extraction, as shown in Figure 1. A crucible with a single crystal seed centered at the bottom is loaded with sapphire crackle (meltstock) and placed on a high-temperature, helium-cooled heat exchanger. After evacuation of the heat zone, heat is applied and the charge is melted. The seed is prevented from melting by flowing helium gas through the heat exchanger. After melting into seed, growth is initiated and progressed by increasing the helium flow through the heat exchanger and/or decreasing the furnace temperature. After complete solidification of the charge is achieved, the furnace temperature is reduced below the melting point of sapphire, and the helium flow through the heat exchanger is reduced to achieve *in situ* annealing of the boule. Thereafter, the furnace temperature is reduced in a controlled manner for cooldown of the boule.

The above-mentioned crystal growth procedure was developed for sapphire consistent with the properties of sapphire and problems involved in growing high-quality crystals. Some of the features developed in HEM furnaces specifically related to sapphire crystal growth include helium cooled refractory metal heat exchanger, molybdenum crucibles, a graphite or carbonaceous heat zone with resistance heating and a furnace design that allows operation up to 2200°C with optimum control. It is essential to prevent spurious nucleation during crystal growth as it can cause cracking of the boules after growth. In this context, growth during HEM is achieved

under stabilizing temperature gradients as the hot melt is near the top of the crucible and the colder solid is at the bottom of the crucible, thereby minimizing convection. The crystal growth parameters have been optimized to ensure that the solid-liquid interface is submerged below the liquid during most of the growth cycle. Under these conditions, the thermal and mechanical properties are damped out by the surrounding liquid before reaching the interface. The submerged interface also produces low temperature gradients at the growth site. This minimizes the propensity for spurious nucleation and growth under low temperature gradients and produces higher quality crystals. In HEM sapphire growth, the last material to solidify is along the crucible wall. Most impurities have a low segregation coefficient and are segregated near the crucible wall in the last material to solidify. The material near the surface of the boule containing a higher level of impurities can be removed easily, and the remainder of the boule is significantly purer than the starting meltstock.

HEM furnaces are typically operated under vacuum using a mechanical pump so that the reaction products are removed from the heat zone. Under these conditions, the vapor species and the reaction products are removed from the heat zone, reducing the probability that these impurities will be incorporated in the growing crystal.

During melting, ambient gas can be trapped in the liquid and incorporated in the growing crystal. This typically shows up as voids or scattering sites when the crystals are examined under intense light illumination. Near the melting point of sapphire, the melt has high viscosity and it is difficult to remove the trapped gas. Typically, the melt is superheated above the melting point to remove this trapped gas prior to crystal growth. Operation of the heat zone under vacuum also aids removal of trapped gas. The ability of HEM to control heat input and heat extraction during crystal growth allows the melt to be superheated to remove the trapped gas and still grow sapphire crystals under low temperature gradients to achieve high crystal perfection. These features have allowed production of light-scatter-free sapphire by HEM.

The low thermal conductivity of sapphire, combined with large shrinkage upon solidification, demands that low growth rates are used. The simple directional solidification system of HEM and absence of temperature gradients built into the heat zone allow controlled crystal growth at low growth rates. For sapphire crystal growth, low linear growth rates of the

solid-liquid interface result in high volume growth rates for large boules because of the large size of the interface. After crystal growth is completed, the crystal is still under a temperature gradient and susceptible to cracking. In HEM growth, the boule is still in the heat zone. After growth, the furnace temperature can be reduced below the melting point of sapphire along with reducing the temperature gradient on the boule by reducing the helium flow through the heat exchanger. Therefore, the unique feature of *in situ* annealing of HEM can be utilized to reduce temperature gradients on the crystal and relieve stresses due to solidification. The reduced stresses also aid in higher crystal perfection. After annealing, the crystal can be cooled at a rate conducive to preventing cracking of the boule. Typically, the low thermal conductivity of sapphire and the thermal gradient in large boules require a prolonged cooldown cycle. In boules of 34-cm diameter, 65 kg, the cooldown cycle can be a week or longer.

The HEM has been used to produce 340-mm sapphire boules in production. A larger HEM furnace has been designed to grow 500-mm diameter sapphire boules. The furnace, heat zone and instrumentation have been assembled and tested. Initial growth of 340-mm diameter sapphire crystals in this furnace has provided satisfactory results. The first attempt at 500-mm diameter crystal growth is in progress. Satisfactory results of 500-mm diameter crystal growth will allow future scale up to 750-mm diameter sapphire boules.

Fixed Abrasive Slicing Technique (FAST)TM

Crystal Systems has transferred the concept of wafering with fixed diamond abrasive as used in inner diameter (I.D.) slicing by using thin wire blades. Round wire is rolled to a teardrop shaped blade to reduce the kerf and improve guidance. Multiple layers of diamond can be plated only on the cutting edge with this approach.

High forces are required for fixed diamond abrasive to cut efficiently. With outer diameter (O.D.) or I.D. blades it is possible to achieve high cutting forces. To achieve high cutting forces with wire blades, the contact length must be reduced by rocking the workpiece to achieve a radial cut profile. A multiwire machine in which a workpiece is rocked was developed to efficiently cut with minimum kerf loss using fixed diamond on wire.

Sapphire Crystal Growth Technology

Using

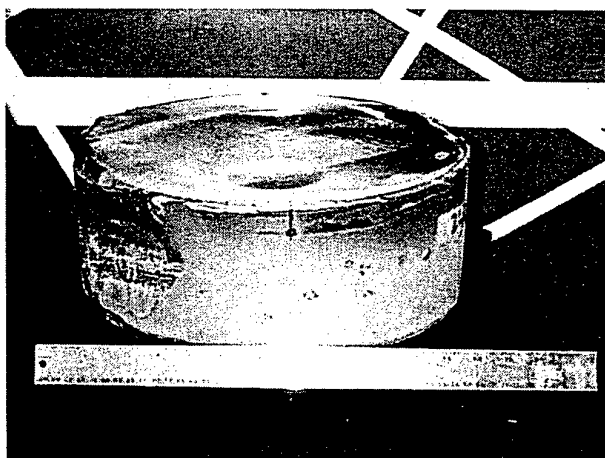
Heat Exchanger Method (HEM)

F. Schmid and C. P. Khattak
Crystal Systems, Inc.
27 Congress St., Salem, MA 01970
USA
Telephone 978-745-0088
Facsimile 978-744-5059

ISCGT-1

5-17 September 1998

Beatenberg, Switzerland



13" Diameter HEM Sapphire Boule

Advantages of HEM

- Control of a single crystal growth process
- Stabilizing temperature gradients
- Minimize convection
- No stirring of melt
- No rotation of the crucible
- Ability to control shape of solid-liquid interface during growth
- Last material to solidify is along crucible wall
- Good rejection of impurities
- Simple

Unique Features of HEM

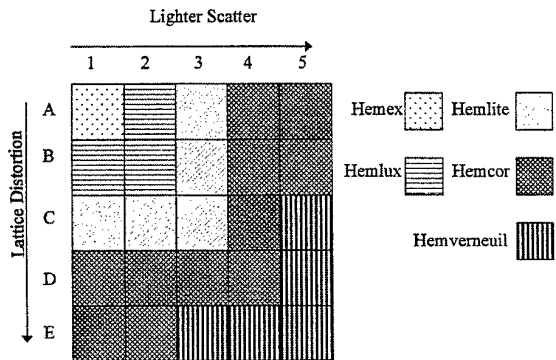
- Ability to control heat input and heat extraction
- In situ* annealing of the ingot before cooldown

Anisotropic Properties

Crystal Orientations

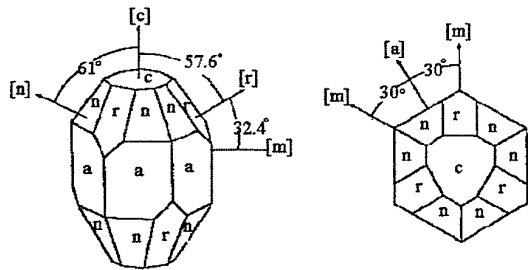
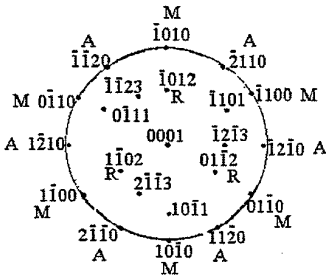
- [0001] - *c*-axis - 0°
- [11̄20] - *a*-axis - 90°
- [101̄0] - *m*-axis - 90°
- [11̄02] - *r*-axis - 60°

Non-Uniform Thermal Expansion

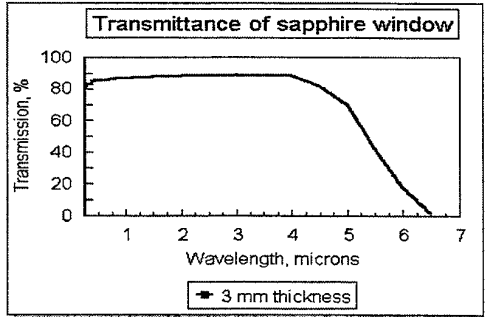
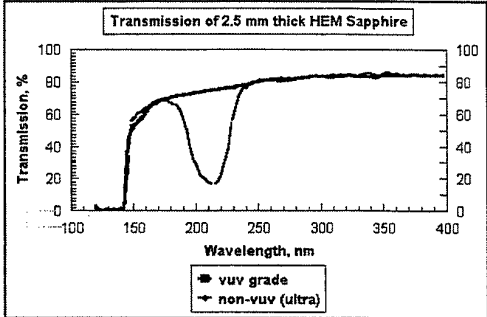


Representation of lattice distortion and light scatter in various grades of sapphire

Structural Indices	Mineralogical Symbol
11̄02	r
011̄2	r
1012	r
0001	c
1010	m
1120	a
1011	s
211̄3	n



Sapphire Crystallographic Diagrams



Sapphire Windows

- High Strength
- Broad Band-Pass
- Minimal Optical Scatter
- Excellent Index of Refraction Homogeneity
- Very High Abrasion Resistance

Table I. Typical Window Requirements

Aperture:	200-450 mm diameter
Thickness:	5 mm to 25 mm+
Wedge:	10 arc-sec
Surface Quality:	Scratch/Dig: 60/40 Within CA 80/50 Outside CA
Figure:	$\leq \lambda/8$ rms (10 cm ϕ) @ 0.63 μ M @ RT
Surface Finish:	15 – 30 Å rms
Transmittance @ RT: (Thickness Dependent)	Window Assembly 0.4 - 0.7 μ m 73% 1.4 - 1.7 μ m 80% 3.0 - 4.3 μ m 80% 4.3 - 5.0 μ m 73%

Crystal Systems, Inc.

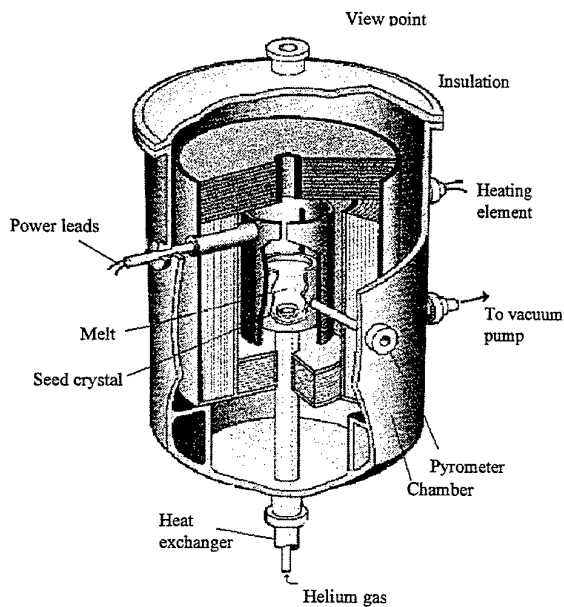
Transmitted wavefront distortion data for various grades and orientations of sapphire samples

Sample		Grade	Homogeneity	Homogeneity, rms	pV (Wave)
Orientation	ID				
[1120]	10	Henex	2.78349E-06	3.340857E-07	0.041
[1120]	9	Hemlux	3.41919E-06	4.347430E-07	0.051
[1120]	7	Hemlite	3.05817E-06	3.660218E-07	0.045
[1120]	8	Hemcor	5.11889E-06	5.744561E-07	0.076
[1120]	6	Hemverneuil	4.21734E-06	6.179205E-07	0.063
[0001]	5	Henex	1.47575E-06	1.867685E-07	0.022
[0001]	3	Hemlux	1.68367E-06	2.175566E-07	0.025
[0001]	1	Hemlite	3.05309E-06	4.535550E-07	0.046
[0001]	4	Hemcor	3.83489E-06	6.469233E-07	0.058
[0001]	2	Hemverneuil*	9.40220E-06	7.169225E-07	0.141

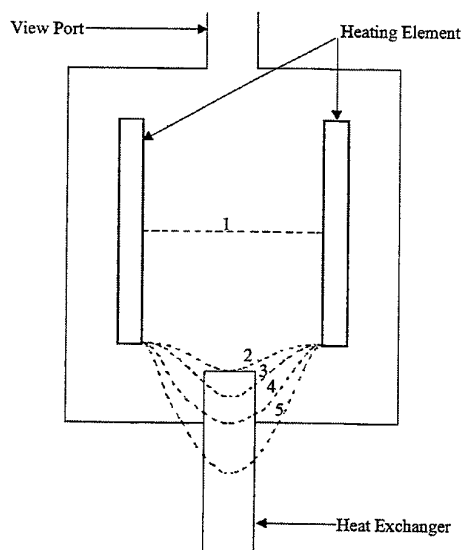
*This sample had a severe localized lattice distortion, and it was included in the analysis.

Growth of 20-Inch Diameter Sapphire

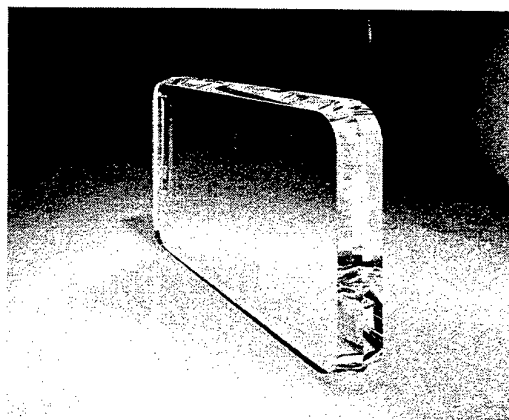
- Selected a HEM Furnace Chamber
- Designed and Fabricated a Heat Zone
- Automated Control System
- Crucible Fabrication
- Crystal Growth



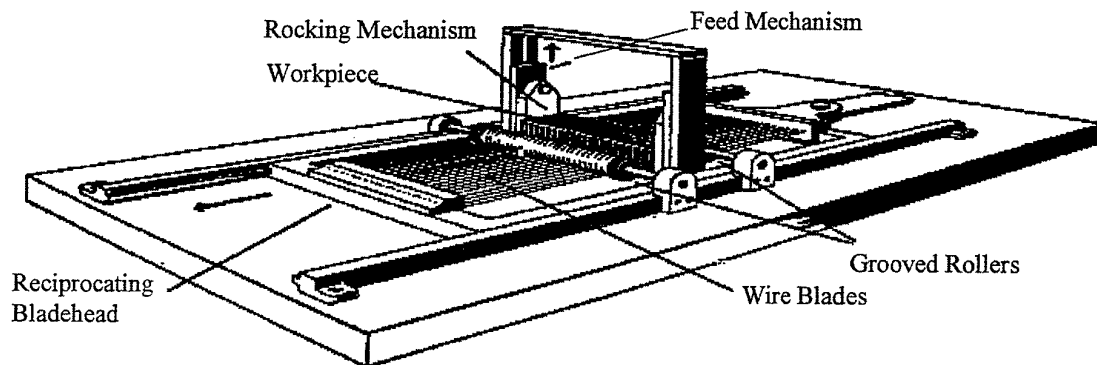
A schematic of an HEM furnace.



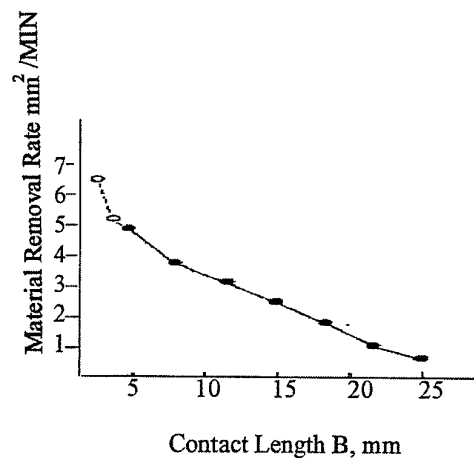
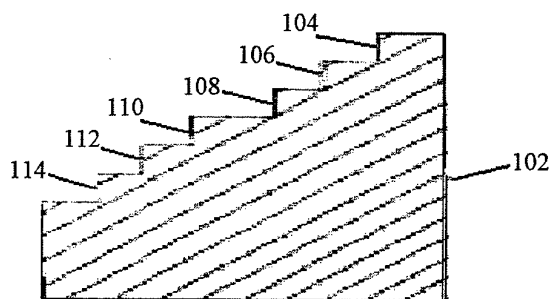
Isotherms in an HEM furnace showing affect of increasing helium flow through the heat exchanger



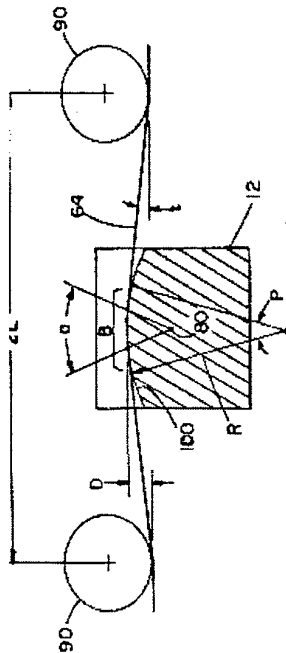
A large rectangular window produced from HEM sapphire



Schematic of the Fixed Abrasive Slicing Technique (FAST) Machine.



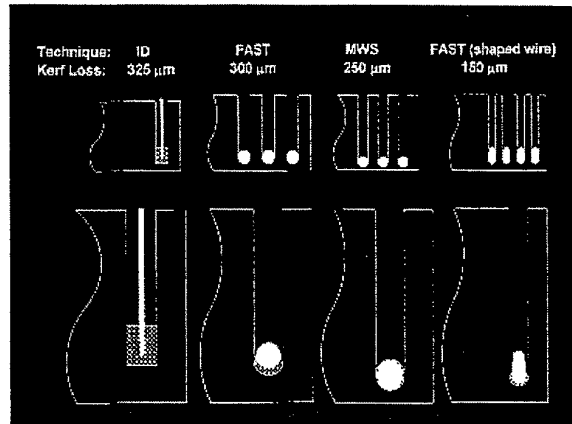
Step block cut at a constant feed force. Graph shows significantly increasing material removal rate with decreasing in contact length of steps.



Schematic showing rocking of workpiece between guide rollers to reduce contact length to increase force between fixed diamond abrasive and work.



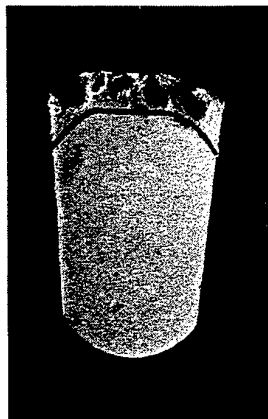
Crystal Systems, Inc.



Comparison of Slicing Techniques



Crystal Systems, Inc.



A 200X magnification of shaped wire with diamond plating on cutting edge.

Shaped wire delineating wire nickel plating interface.

Growth of sapphire by horizontal directional crystallization.

Kh.S.Bagdasarov

Institute of Crystallography of Russian Acad. Sci.
Leninsky prosp. 59, Moscow 117333, Russia
phone/fax: (095) 135-6350

E.V.Zharikov

General Physics Institute of Russian Acad. Sci.
Vavilov Street 38, Moscow 117942, Russia
phone (095) 132-8352, fax: (095) 135-0270
e-mail: zharikov@llcg.mail.gpi.ru

Abstract.

Sapphire remains the most widely using dielectric crystalline material, and needs in these crystals are continuously rising. It is because sapphire is superior to ordinary materials in many respects: melting point, heat conductivity, hardness, mechanical strength, optical transparency, chemical and radiation stability. In addition sapphire crystals have extraordinary low losses in microwave range; the couple made from sapphire has extremely low friction coefficient.

Due to these unique properties sapphire is using in many fields, in particular, in optical instruments making, microelectronics, holography, computer facilities, microwave technique, clock industry, jewellery etc. Sapphire crystals doped by Cr^{3+} and Ti^{3+} are excellent laser materials.

However, all remarkable properties of sapphire and its wide use would not be realized in practice without development of efficient growth technologies of high quality and large size crystals. Today the main techniques of sapphire production are the following methods: Verneuil, Czochralski, Stepanov, GOI (Musatov method), HEM (heat exchanger method) and HDC (horizontal directional crystallization or Bagdasarov method).

HDC method for sapphire growth was offered by Kh.S.Bagdasarov in the middle of sixties [1]. The concept of HDC-process is well known [2]. The boat filled with charge is moving through temperature gradient. The initial charge melts and then crystallizes. This method has a number of advantages in comparison with other melt methods. First, HDC is rather simple and inexpensive in realization (this is especially important when we mean industrial technology level). Typical lack of HDC-process — absence of opportunity to see crystallization front — had been eliminated in Bagdasarov method.

Low temperature gradients and weak convection in a melt because of its small height characterize this technique. This gives an opportunity to grow unstressed crystals of

large size. It has to be noted that open boat minimizes tensions occurring in crystal during cooling process.

Dislocation density in HDC-sapphire is about $5 \cdot 10^2 \div 1 \cdot 10^3 \text{ cm}^{-2}$. This is by 3 orders of magnitude less than in sapphire crystals grown by Verneuil or Stepanov technique [3]. Melt height is constant during whole process that promotes crystallization process stability. In addition, large melt surface, which characterizes HDC method, provides effective impurities evaporation during crystallization process (self-purification).

Grown crystals have plate-type shape, suitable for subsequent treatment. Bagdasarov technique has high yield and, in this connection its wide expansion allow to overcome chronical deficit of sapphire crystals.

Developed technique has been transferred to a number of plants in former Soviet Union, as well as conveyed to Japan, South Korea, France and Bulgaria.

A series of industrial installations for this technique: Sapphire-2M, Sapphire-2U and Sapphire-3 — has been developed. These installations have high operational reliability what ensure their work at 2000°C without major repairs for 3-5 months.

A heater with screens system is the main assembly of the installation. Heater is made from tungsten bar and has a shape creating temperature field with rectangular section. Heat insulation is provided by set of plate-type screens fastened to each other. First level of screen is made from tungsten, others — from molybdenum. There is an opportunity to change separate part of heat insulation system.

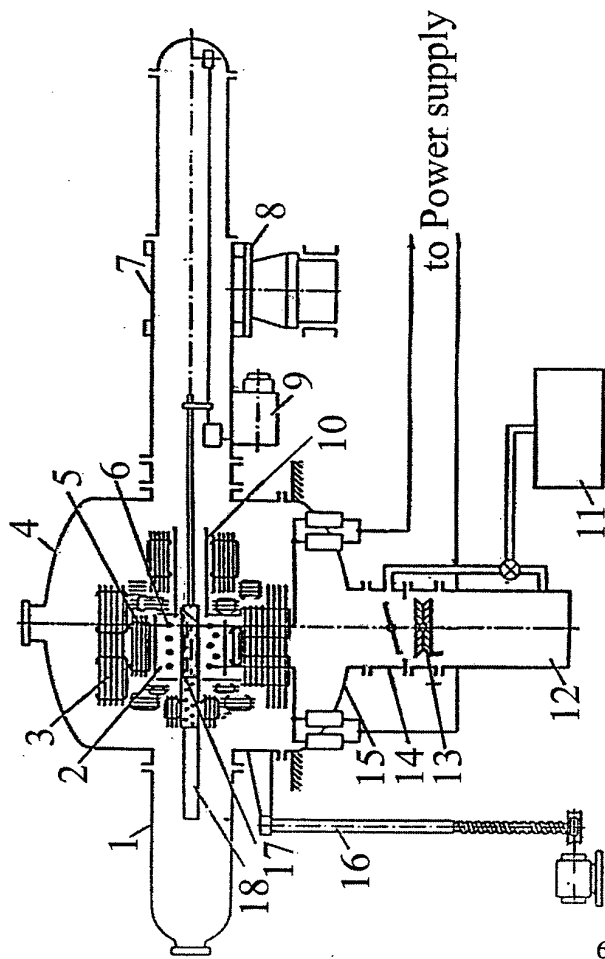
Growing of sapphire is carried out in molybdenum boat in vacuum $5 \cdot 10^{-5}$ millimeter of mercury column. A charge, preliminarily, is pressed and burned at temperature close to melting point. In this case container space ratio reaches value about 0.8. Melting of initial charge takes 4 hours. This process ends with partial melting of a seed crystal (for 10-15 mm of its length), situated on the apex of the boat. Control of seeding and crystallization front position during growth is carried out visually through top window of crystallization chamber. The growth rate for pure sapphire is 8 mm per hour. The total process duration, including installation heating up, the growth itself and crystal cooling, is 37 hours. For residual tensions release the additional annealing at temperature about 0.95 of melting point is used. The following annealing regime is used: heating for 3-5 hours, exposure under working temperature for 5 hours and temperature decrease for 6 hours.

Thermal dissociation of initial substance, its dissociative evaporation during growth run as well as possible chemical reactions under interaction of the melt with ambient atmosphere and container material is discussed in lecture. All this processes essentially influence on crystallization kinetic and on real structure of crystals.

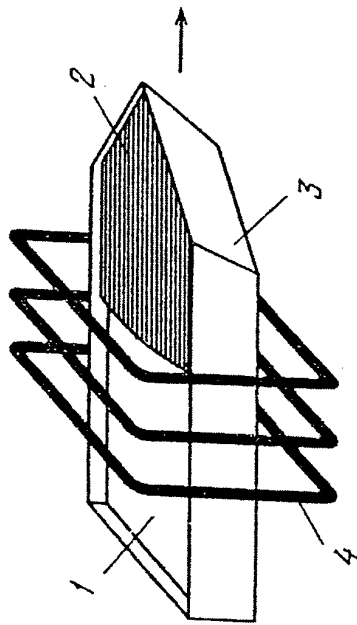
The problems of crystal growth of doped sapphire (ruby $\text{Cr}^{3+}:\text{Al}_2\text{O}_3$ and $\text{Ti}^{3+}:\text{Al}_2\text{O}_3$) and of other oxide crystals fabrication, in particular, garnets, Nd:YAG, Er:YAG, Nd:GSAG etc will be considered. The regimes of growth and annealing of crystals as well as problems related to scaling of technology are discussed.

References

1. Kh.S.Bagdasarov et al. Avt. svid. SSSR (Soviet patent) № 276921 (19 Aug. 1968); Swiss Patent № 566170 (11 Oct. 1972); UK Patent № 1383400 (7 Nov. 1972); US Patent № 4303465 (1 Dec. 1981).
2. Kh.S.Bagdasarov. Physico-chemical principles of high-temperature crystallization and crystal growth methods. Moscow, VINITI, 1987, 140p. (in Russian).
3. E.R.Dobrovinskaya and V.V.Pishchik. Corundum single crystals: problems of fabrication and quality. Moscow, NIITECHIM, 1988, 76p. (in Russian).



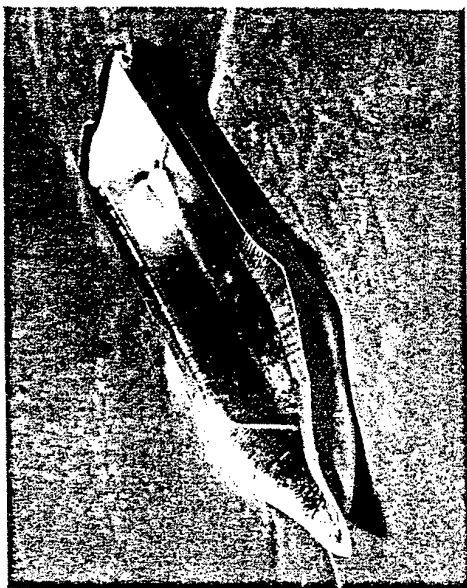
1. - Initial chamber;
2. - Furnace zone;
3. - External screens;
4. - Crystallization chamber;
5. - Internal screens;
6. - Heater;
7. - Receiving chamber;
8. - Rotary carriage;
9. - Translation mechanism;
10. - Rod screens;
11. - Forvacuum pump;
12. - Diffusion pump;
13. - Water trap;
14. - Vacuum lock;
15. - Bottom part of chamber;
16. - Lifting mechanism;
17. - Container (boat);
18. - Moving facility.



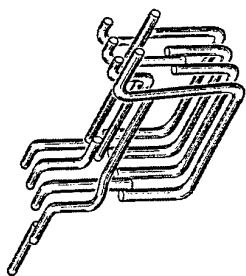
Scheme of horizontal directional crystallization method or Bagdasarov method
1 - melt; 2 - crystal; 3 - container (boat); 4 - heater



Three possible crystallization front positions relative to container bottom

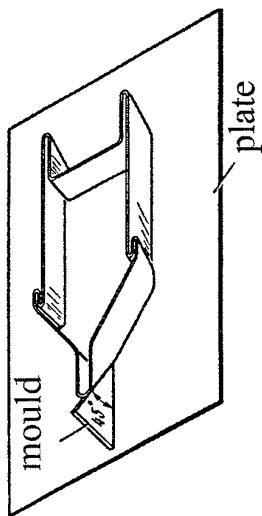
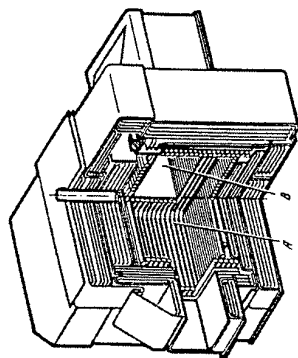


Pressed molybdenum container.

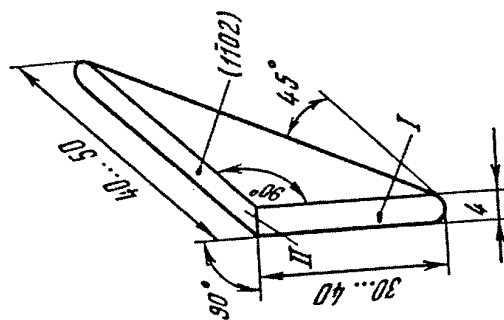


Heating element of the
"Sapphire-2M" growth station

Thermal insulation screen system
A — melting zone
B — annealing zone



Seed crystal (all sizes in mm) →



Molybdenum container (boat)

THERMAL DISSOCIATION IN ALUMINUM OXIDE MELT

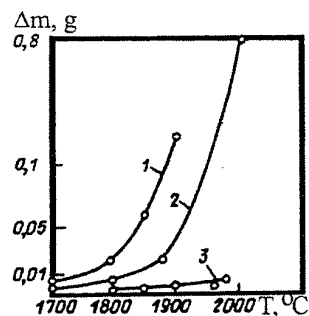
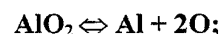
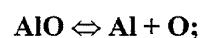
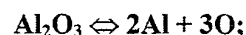
The composition of aluminum oxide melt strongly depends upon the temperature (extent of superheating). At low superheating the following dissociation reactions preferably run:



At more significant superheating the following reactions become possible:

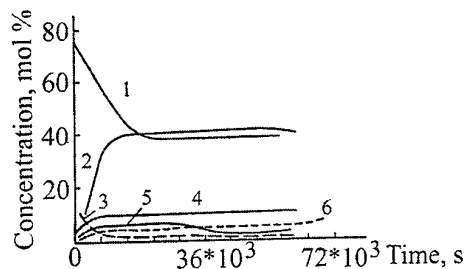


At very great superheating the reactions of the following types are running:



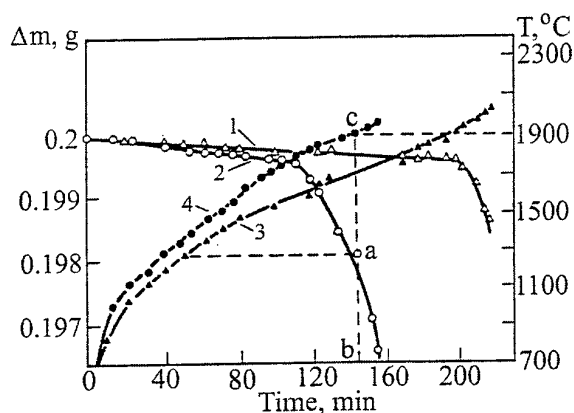
Temperature dependence of Al_2O_3 evaporation intensity from temperature in different ambient atmospheres

1 – Hydrogen; 2 – Vacuum; 3 – Nitrogen.



Kinetic of change of gas mixture composition during vacuum crystallization of sapphire.

1 – CO; 2 – H_2O ; 3 – C;
4 – H_2 ; 5 – CO_2 ; 6 – O_2 .

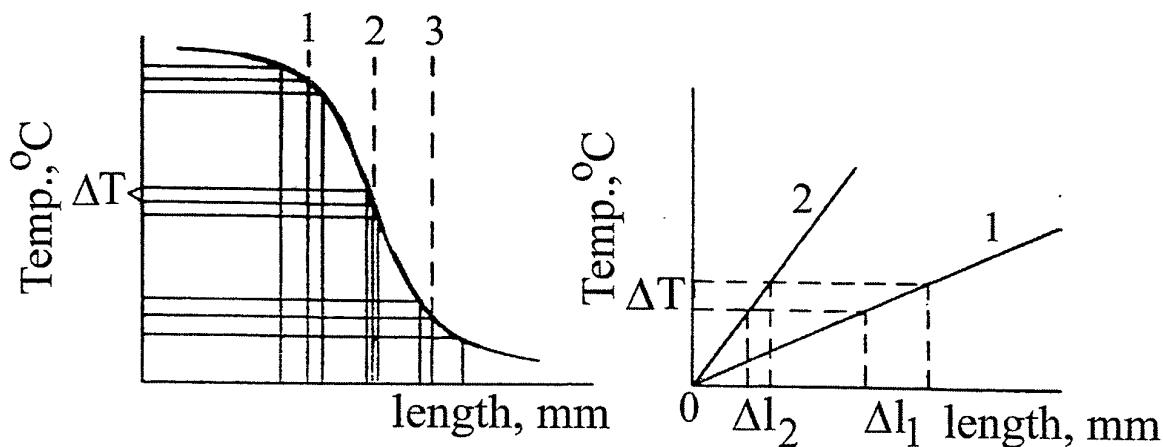


The character of changes of corundum specimen mass:

1,2 — temperature variation of sapphire and ruby samples correspondingly;

3,4 — mass changes in the same samples.

The dotted lines point to correlation of temperature (point c), exposure time of the sample (point b), and mass change of the sample (point a).

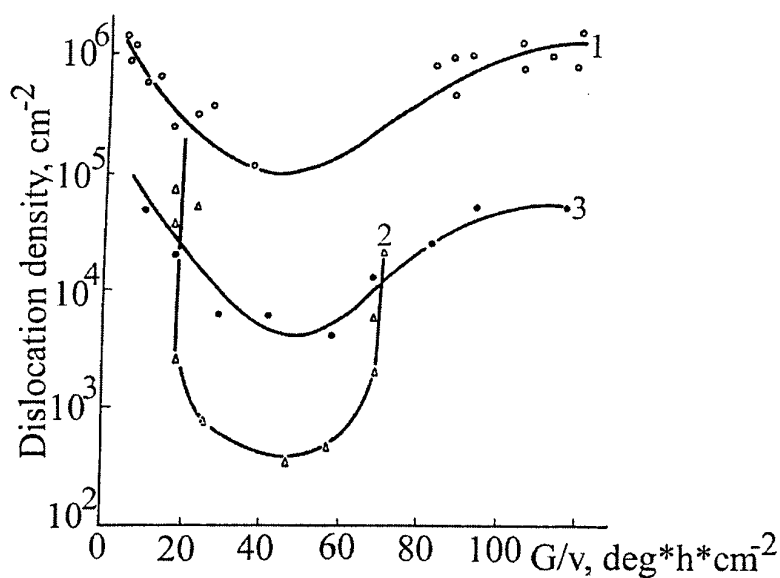


Correlation between temperature gradient nonlinearity and scale of temperature oscillations:

- 1 – $(-\Delta l) > (+\Delta l)$; 2 – $(-\Delta l) = (+\Delta l)$;
- 3 – $(-\Delta l) < (+\Delta l)$

Translations of crystallization front under different axial temperature gradients:

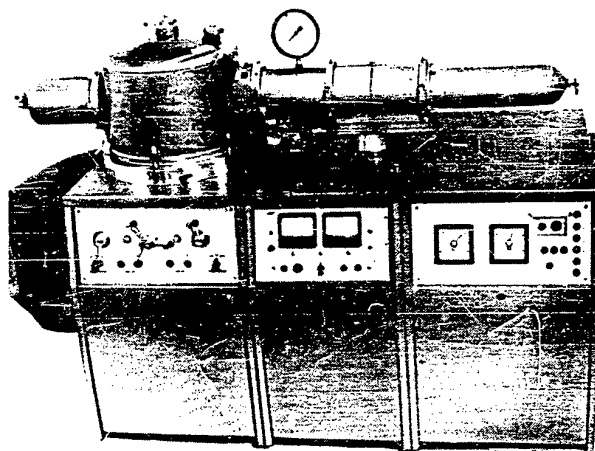
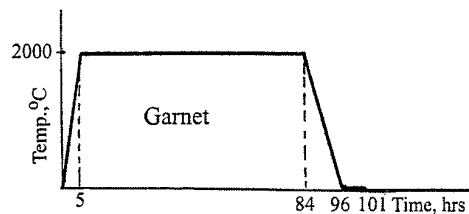
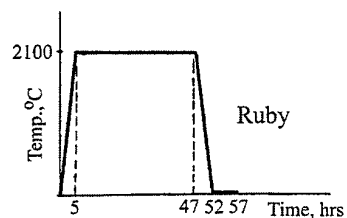
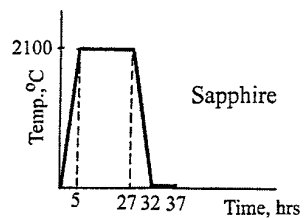
- 1 – small; 2 – large.



Dependence of dislocation density upon ratio of axial temperature gradient to growth rate:

- 1. crystals grown by Verneuil and Stepanov technique;
- 2. crystals grown by horizontal directional crystallization and Czochralski technique;
- 3. model experiments. ⁶¹⁸

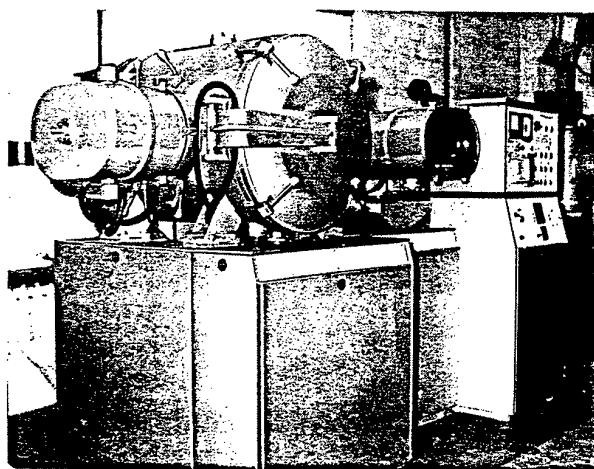
Regimes of crystal growth.



Sapphire-2M" growth station.

Size: 2.2×1.4×1.6m.

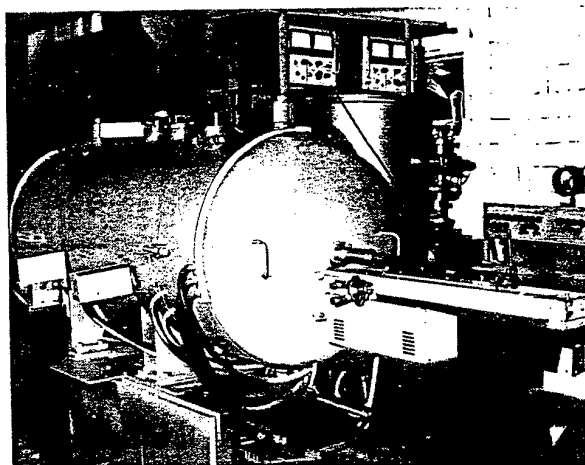
Power consumption: 60 kW.



"Sapphire-2U" growth station.

Size: 3×1.7×1.7m.

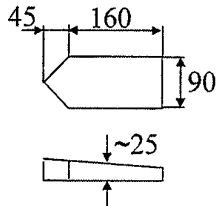
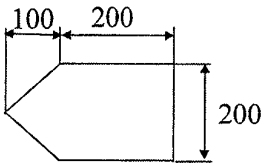
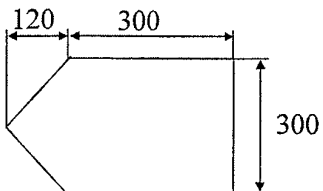
Power consumption: 40 kW.

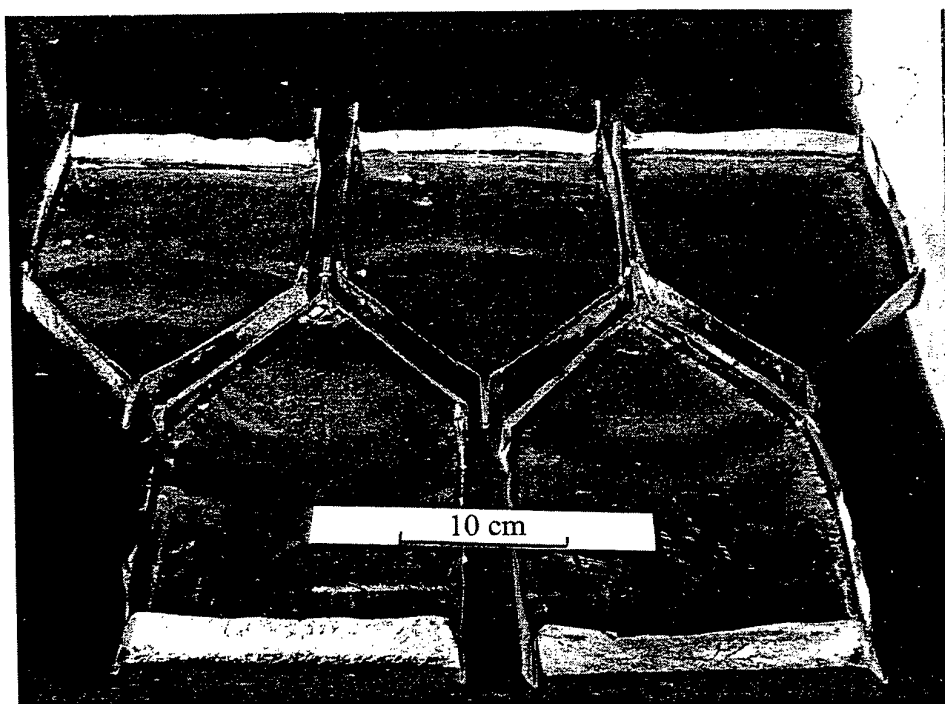


"Sapphire-3" growth station.

Size: 3×2×1.7m.

Power consumption: 60 kW.

INSTALLATION	POWER, kW·h	DIMENSIONS OF CRYSTAL, mm	WEIGHT, g	TIME, h	YIELD, g/h
"Sapphire-2M"	25		1700	26	65
"Sapphire-2U"	40		5000	37,5	133,3
"Sapphire-3"	60		10800	52,5	205,7



Sapphire crystals in boats

"GOI" Growth of Large Perfect Sapphire Crystals"

Prof. Dr. Mikhail I. Moussatov

Scientific Center "S.I.Vavilov GOI", Saint-Petersburg, Russia.

In GOI's metod (fig.1) the growth of crystals occurs by decrease of temperature in each point of a thermal field of the special form. A melt as against a Czochralski's method, is used on 100% in each process. The form and size of crystals are close to the form and internal sizes crucible (fig. 2), but the growing and cooled crystal hangs on seed and does not concern crucible. It enables considerably to increase speed of decrease of consumed power by a stage of cooling of a crystal in comparison with a HEM'S method, where the crystal concerns crucible. A crystal cools down much slower, than crucible, because specific heat capacity of sapphire almost in 10 times more. than at crucible, and heat conductivity on the contrary almost in 15 times it is less. Large different of temperature between a crystal and crucible results in formation residual stresses in places of their contact. Very large speed of temperature decrease results in formation of polycrystal (fig. 3). The crystals GOI'S grow and are cooled inside crucible, where the gradients of temperature do not exceed 0,5 - 1,0 K/mm, that considerably reduces the charge of the electric power (working volume is minimal) and does not result in formation of residual stress in crystals as against a Czochralsky method.

We have compared our crystals and crystals grown by the most used methods in table I:

Table I

No	Growing method	Temperature gradient, K/mm	Residual stress, MPa	Dislocation density, cm^{-2}
1.	Verneuil	30	100 — 150	$10^5 — 10^8$
2.	HDC	3	30	$10^4 — 10^5$
3.	Czochralsky .	1 — 10	30	$10^2 — 10^4$
4.	HEM	0.4 — 12	—	$10^3 — 10^5$
5.	GOI	0.05 — 1.0	1.0	$10 — 10^2$

As it seen from table quality of our crystal is better then others. In GOI's metod crystals grow without rotation, and the insignificant rise is made only at a final stage of growth to reduce probability of a contact between crucible and crystal. It relieves crystals of defects

connected to rotation and rise, and also allows considerably to increase a diameter and weight of crystals at the same duration of process and thus a diameter crucible in comparison with a Czochralsky method. The crystals in the GOI's method have the sharp-convex form of crystallisation front (fig. 4), that increases growth rate in some times at the same speed of movement of crystallization front and denies the statements, that at such form in crystals there are residual stresses. On fig.5,6 and 7 are submitted to a photo of the sapphire crystals, the ruby and IAG (diameter-200 mm, weight-20 kg.) grow up on a GOI's method. The distributions of residual stresses along GOI's sapphire, thickness 12 mm. is shown on a fig.8. It do not exceed 10 kg/cm^2 on the average and it is increased only at seed. The interferograms of GOI's sapphire, diameter 120 mm, thickness of 12 mm is shown in a fig.9 : a) shadow graph; b) with horizontal optical wedge; c) with vertical optical wedge (C-crystal optic axis; E-direction of polarization vector). The dislocations on periphery of GOI's sapphire it does not exceed $100/\text{cm}^2$, and at the centre there are sites without dislocation (fig. 10). Thus, the optical uniformity of GOI crystals is close to the best optical glasses. The UV transparency border of GOI sapphire is shown in the fig. 11: curve I - growth up with use W crucible concentration Cr - 0,0001 mass.%; curve 2 - Ir-crucible, Cr- 0,0003% ; curve 3 - Ir-crucible, Cr- 0,0014%; curve 4- W crucible, concentration Va -0,00075%. The concentration Cr in sapphire melt in vacuum at temperature 2400 K dependences from endurance time in the various crucible is shown on fig. 12: Ir -1; W-2; Mo-3; Nb - 4. From a fig. II and 12, in particular follows, that the growth of the sapphire is more favourable the application of the tungsten crucible, instead of Ir. In W crucible the part of impurity (for example, Cr) evaporates at the expense of interaction with material of crucible. The inclusion of bubbles in Sapphire crystals (fig. 13) arise at definite speed of crystallization front movement. This speed is depended on material of crucible and it is increased in direction from Mo to W and to Ir.

In a fig. 14- transparency of GOI sapphire - 1; Verneuil- 2; HDC - 3 and Hidrothermal -4. Fig. 15 - diagrams of change of concentration Cr on length of a GOI ruby. In large manufacture (there are more 100 machines, fig. 16) on a GOI's method of sapphire crystals growth by a diameter up to 150 mm and weight up to 16 kg. Laboratory samples have a diameter 300 and 500 mm. On a combination of such parameters, as the large sizes, high optical quality and low cost, the GOI's sapphire - outside of a competition.

Fig. 1

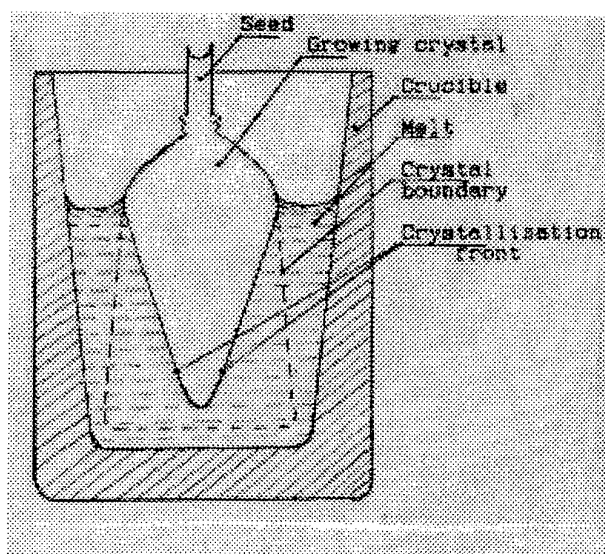
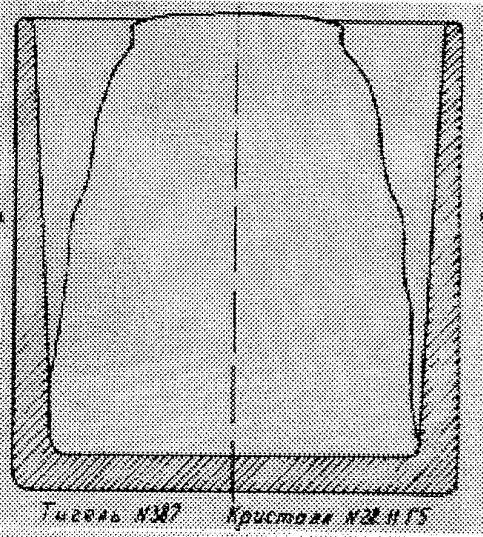
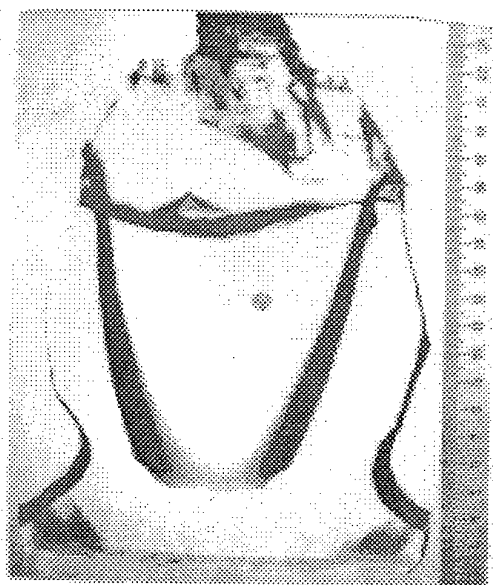
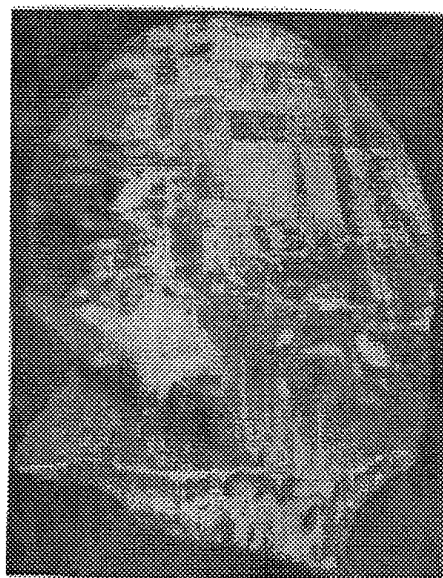


Fig. 2



Real crystal in crucible



Real crystallisation front

Fig. 3

Fig.4

Fig. 8

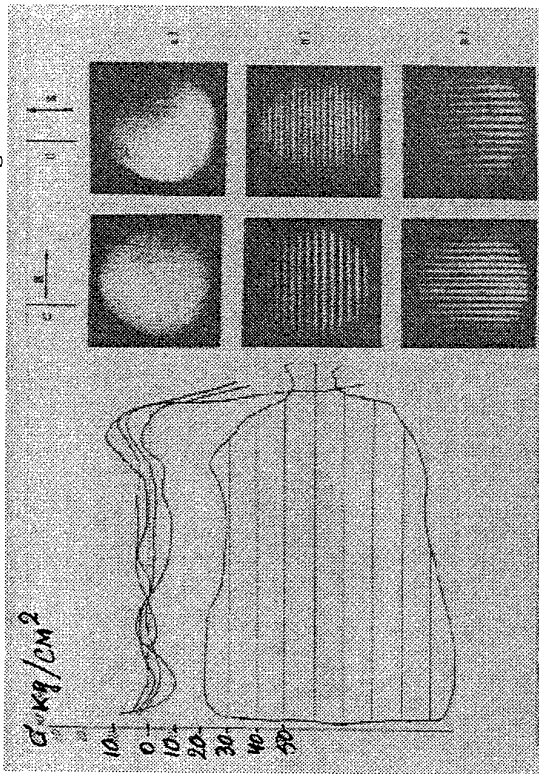


Fig. 9

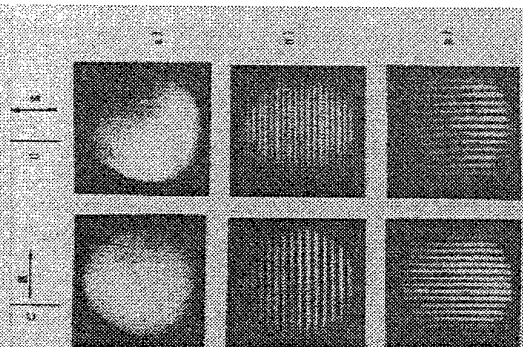


Fig. 10

Dislocations
in GOI-sapphire

Fig. 11

UV - Transparency
of Sapphire
1 - W, Cr - 0.0001%
2 - Ir, Cr - 0.0003%
3 - Ir, Cr - 0.0014%
4 - W, V - 0.00075%

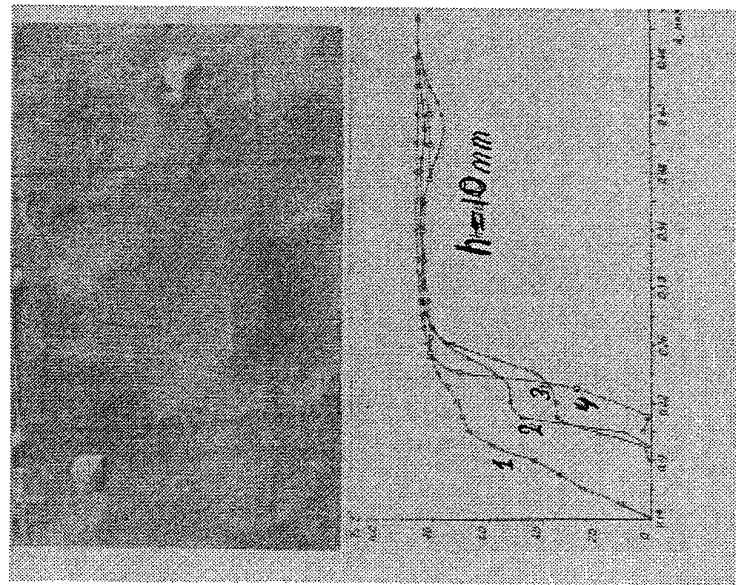


Fig. 5 Sapphire

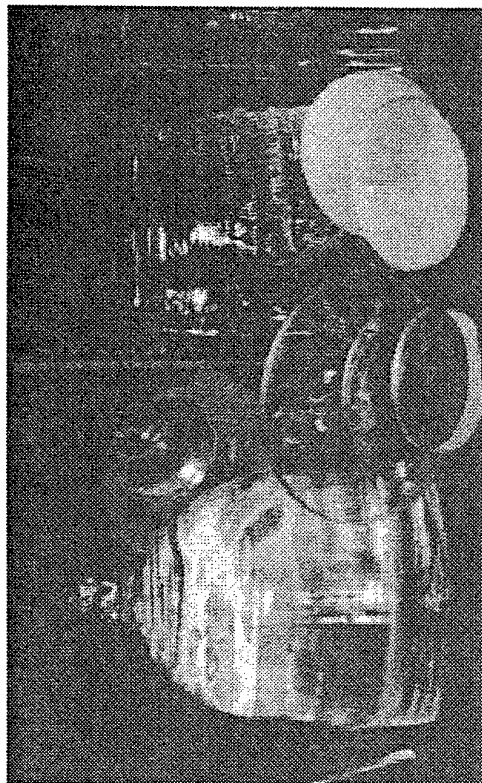


Fig. 6 IAG

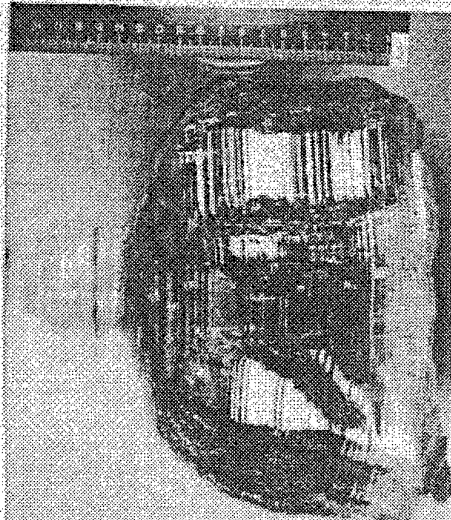
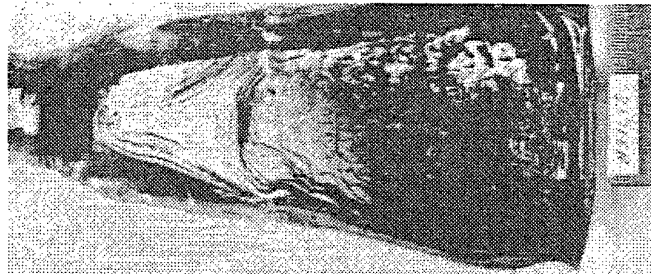


Fig. 7 Ruby



The chromium distribution on length of the ruby crystals

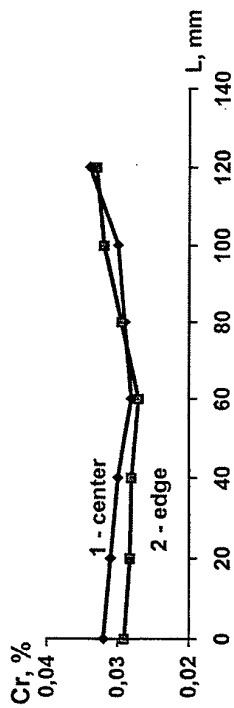


Fig. 15

Cr-concentration dependence on endurance time and crucible material

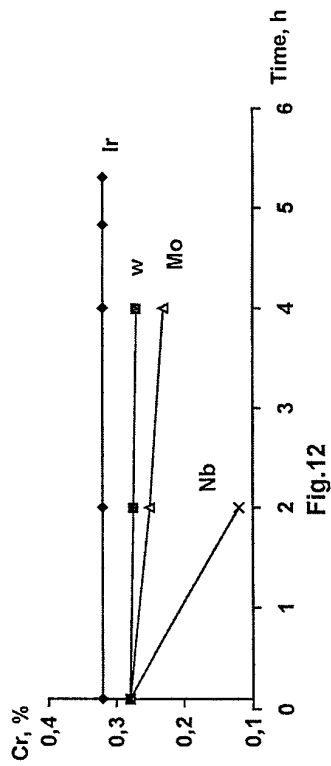


Fig. 12

Fig. 13
Bubbles

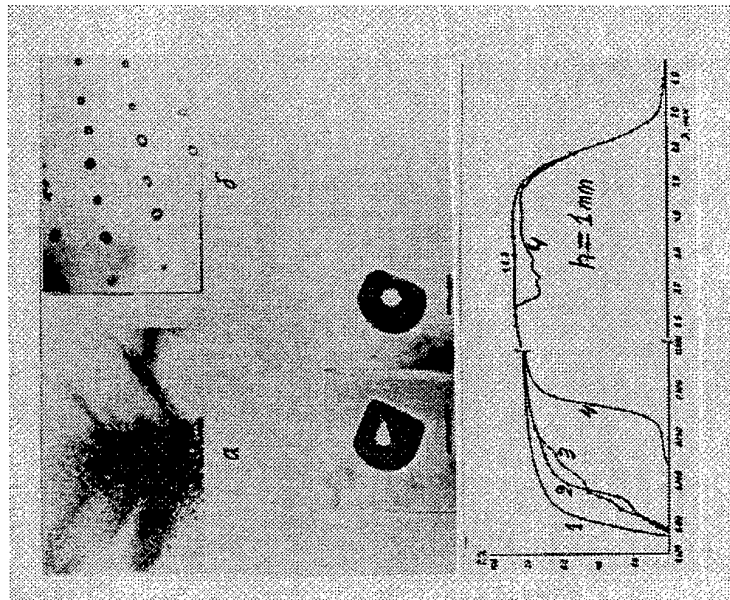


Fig. 14
Transparency,
h - 1 mm
1 - GOI
2 - Verneuil
3 - HDC
4 - Hydrothermal

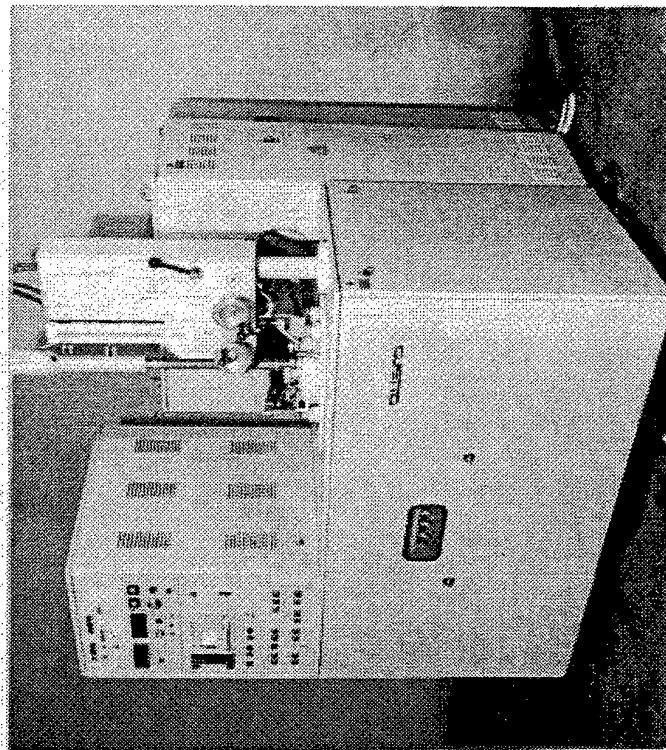


Fig. 16

Growth of nonlinear optical crystals for laser frequency conversion

Takatomo Sasaki

Department of Electrical Engineering, Faculty of Engineering, Osaka University

1. Introduction

Nonlinear optical (NLO) crystals are very important for laser frequency conversion. So far various kinds of crystals have been developed. Here I will introduce the growth examples of NLO crystals to obtain large size crystals over few centimeters as practical use by solution method; KDP and organic NLO crystals such as LAP, DAST ect. for low temperature and KTP, CBO and CLBO as high temperature method.

2. Crystals by low temperature solution method

2.1 KDP(Potassium Dihydrogen Phosphate)

KDP is a suitable crystal for higher harmonic generator of big laser system for fusion experiments because of easiness of huge crystals and high laser damage threshold. Ten years ago we grew crystals with $40 \times 40 \times 70 \text{ cm}^3$ size by temperature falling method. The growth rate in C-axis was at most 1 - 2 mm/day and it took about one year to grow. The most important point was how to prevent spontaneous nucleation and prevent spurious crystals to attach to the growing KDP surfaces, which sometimes brings the crystal fatal cracks. Another important point is to prevent microbes generate in the mother solution, which will be incorporated in growing crystals and make laser damage threshold lower. Recently the very fast growth rate, 20 mm/day, was reported to grow such huge crystals by paying attention for preparing the mother solution. It seems that the important point is to prevent clusters generate in the mother solution before crystal growth starts.

2.2 Organic NLO crystals

Various kinds of organic NLO crystals have been developed in these twenty years because of the possibility of extreme high optical nonlinearity. But almost crystals had van der Waals chemical bonding and had fragility. Almost of them could not be used for practical devices. According to our experience, crystals with

the Vickers hardness of over 40 can only be used. In this sense, the organic crystals with ionic bonding or organo-metalic crystals are preferable. Besides the ionic crystals are easy to grow to large size. We tried ionic crystals, LAP (L- Arginine Phosphate) and DAST(4-dimethylamino-N-methyl-4-stilbazolium Tosylate). These crystals could be grown in large size easily. The Vickers hardness were 55 and 49, respectively.

3. Crystals by high temperature solution method

The high temperature solution method is essentially same as the low temperature method. The crystals with better crystallinity can be obtained by setting seed crystals inside the mother solution, compared with the top seeded solution growth (TSSG) method. But when the growing temperature is over 900 °C, it becomes difficult to observe a crystal growing inside the mother solution, therefore TSSG method is unavoidable.

3.1 KTP (Potassium Titanyl Phosphate)

KTP is a useful crystal to get efficiently green light by frequency doubling of Nd:YAG laser. It has high optical nonlinearity, large temperature and angular allowance and it is not water-soluble and mechanically hard. It can be grown by TSSG method at about 950 °C in P_2O_5 - K_2O - TiO_2 ternary system. This crystal is solid solution, therefore the crystal composition changes with solution composition, that is the refractive index changes as the crystal grows.

3.2 CBO and CLBO

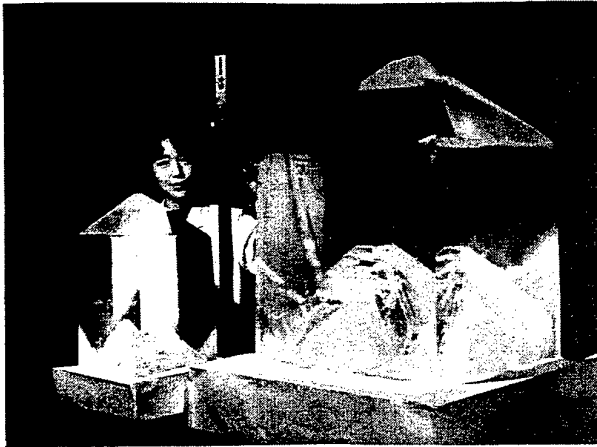
Borate crystals are promising for UV generation because of its wide band gap and adequate optical nonlinearity. BBO(Barium borate), LBO(Lithium borate), KBBF(Potassium beryllium borofluoride) and SBBO(Strontium beryllium borate) have been developed by C.Chen's group in China. We have developed CBO(Cesium borate) and CLBO(Cesium lithium borate). CLBO($CsLiB_6O_{10}$) is more suitable for 4HG and 5HG of Nd:YAG laser than BBO. CLBO has congruent composition and has melting point of 848 °C. The crystal of good quality with 14 x 11 x 11 cm³ size could be grown only in three weeks by TSSG method.

KDP's for GEKKO XII 3rd Harmonic Generation



ILE Osaka

45 cm x 45 cm x 70 cm, GROWTH PERIOD > 1 YEAR



- For laser fusion experiments.
- Blue, UV is more effective than Infrared light.
- Need to have high laser damage threshold.
- Takes a very long time to grow.
- Growth temperature is between 60°C - R.T.
- Sometimes bacteria will breed in the solution.
- Main reason of L.D. is impurity from bacteria.
- $\text{TOC} \approx 1 \text{ ppm}$ is desirable to have a good crystal.

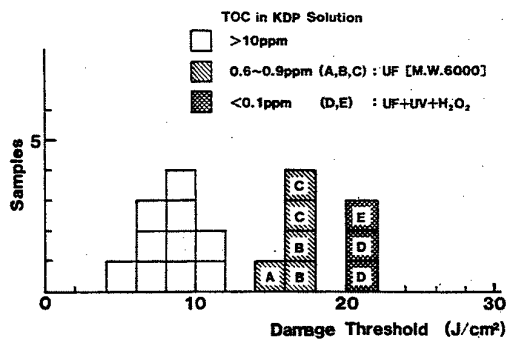
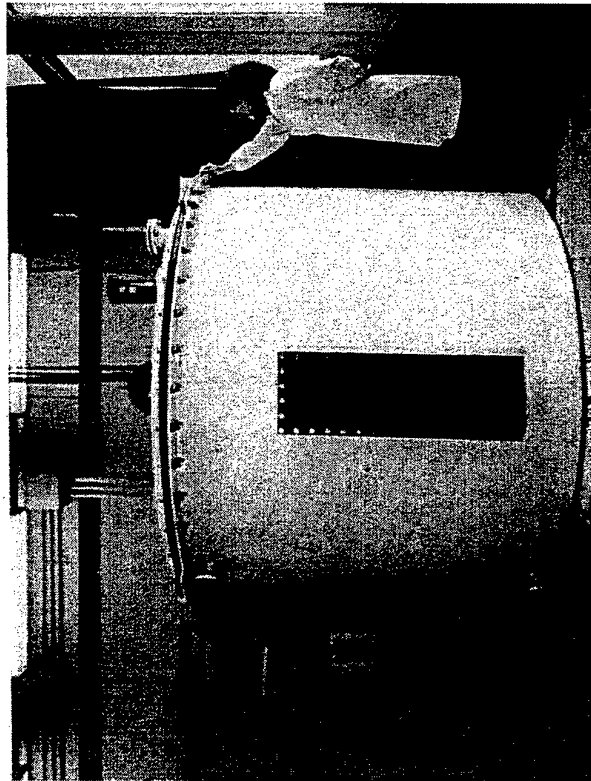


FIG. 2. Histogram of the bulk laser damage threshold measured for KDP crystals grown in the solution reduced the organic impurities (laser: 1 ns, 1.053 μm).

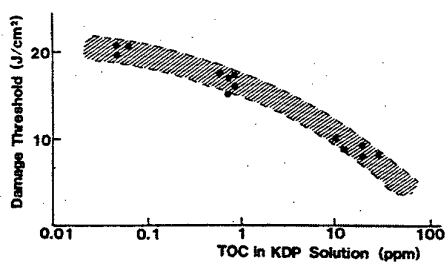


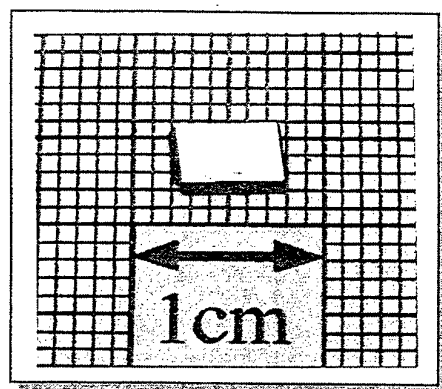
FIG. 3. Relation between the damage threshold of KDP crystals and TOC in the solution.



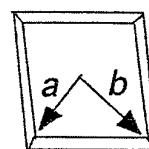
LAP

$a=6\text{cm}$ $b=9\text{cm}$ $c=16\text{cm}$

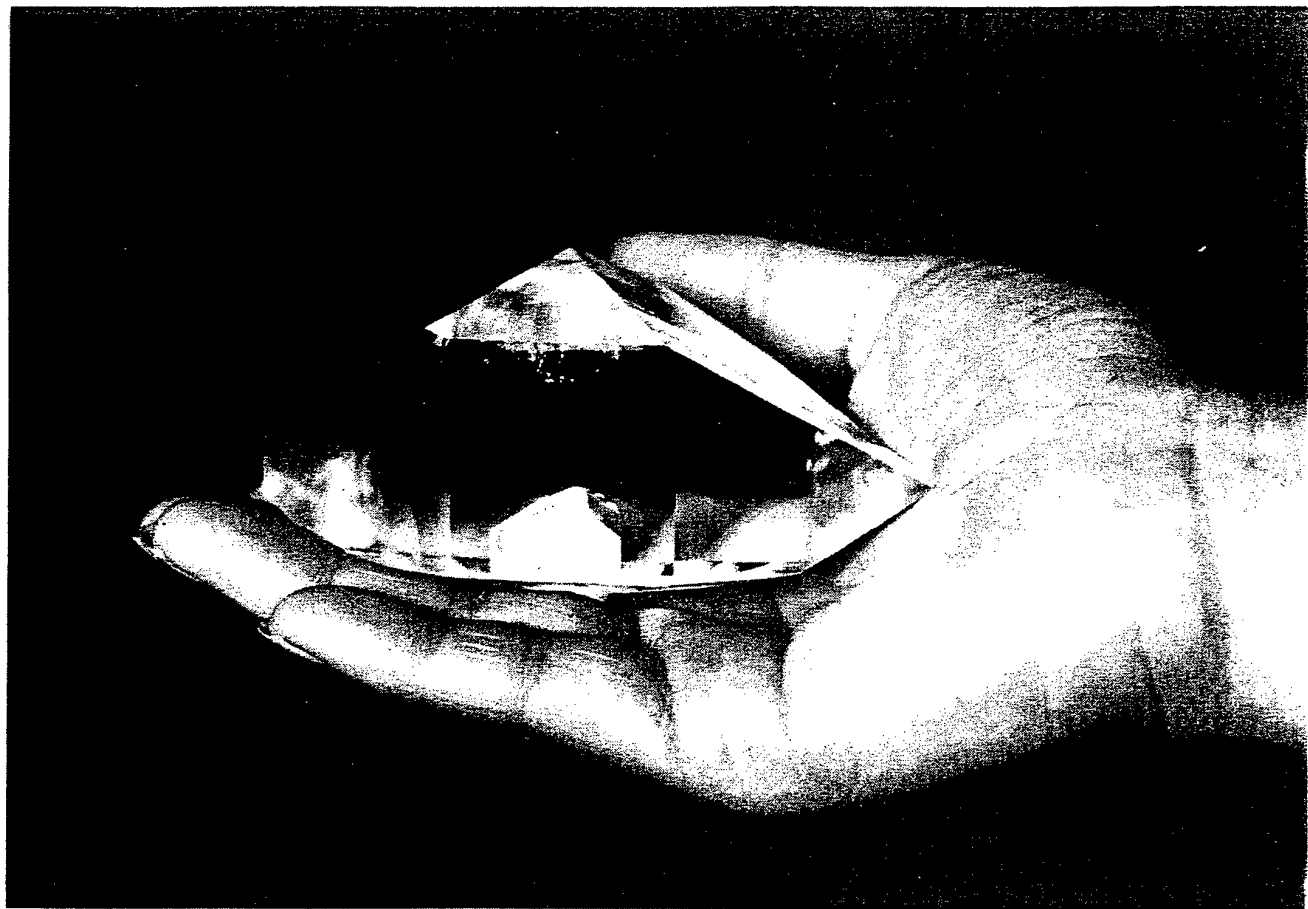
種結晶から育成したDAST結晶



育成条件	
◦ 育成期間	11日
◦ 結晶サイズ	$5.8 \times 3.4 \times 1.0 \text{ mm}^3$
◦ 成長速度	0.14 mm/ day



測定方向



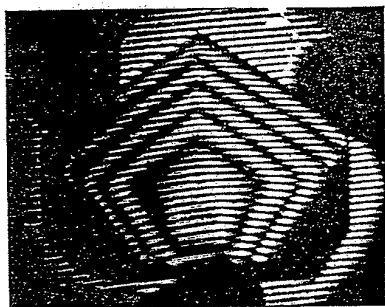
KTP (KT:OP0₄)

32 × 42 × 87 [mm³] (173 g)

40 days

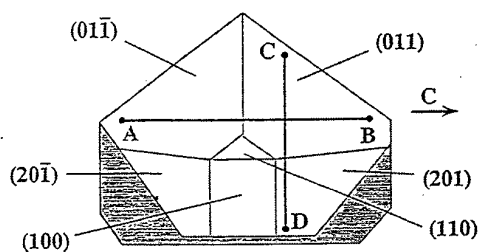
~ 3 °C / day

Birefringence Interferometric Pattern of a KTP
Slice Cut for Second Harmonic Generation



10 mm

Polarization of He - Ne Laser : Circular

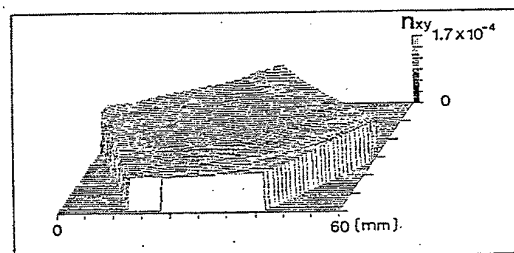


Sample size : 55 x 45 x 7^t [mm³]

SHG Type II cut for 1.06 μm

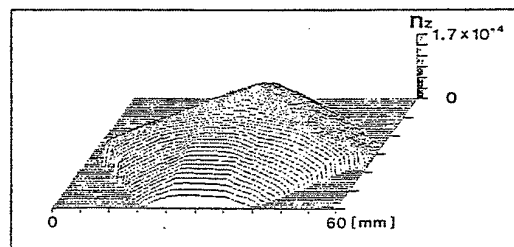
(θ = 90°, φ = 24°)

Confour Lines of Refractive Indices in SHG Sample
Measured by an Interferometry (Zigo Mark IV)



(n_{xy})

Difference of Max. and Min. Indecies : Δ n_{xy} = 7.1x10⁻⁴



(n_z)

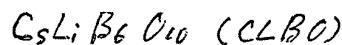
Difference of Max. and Min. Indecies : Δ n_z = 1.6x10⁻⁴

Polarization of He - Ne Laser : Linear

Properties of Borate Crystals

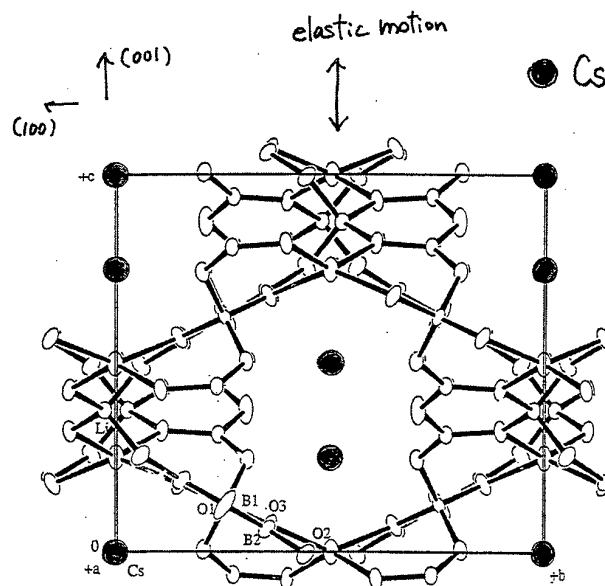
1. Composed of anionic borate groups and alkali metal or alkali earth metal.
2. Wide optical bandgap. Cutoff wavelength is below 200 nm.
3. High laser damage threshold.
4. Large $\chi(2)$.
5. Chemically stable.
6. Cheap.

Borate crystals are very promising for UV generation.

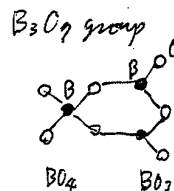


• Tetragonal (正交晶)

• 晶系 $\bar{4}2m$

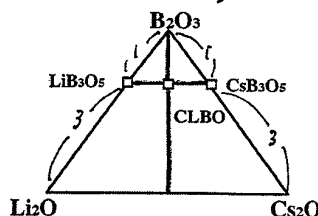


Cs atoms → weak covalent bonding

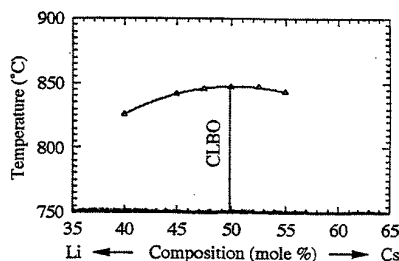


Phase diagram for CLBO by DTA & XRD

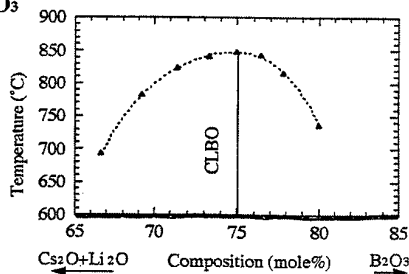
• Cs₂O - Li₂O - B₂O₃
ternary



• Li₂O - Cs₂O
binary



• (Li₂O + Cs₂O) - B₂O₃
binary

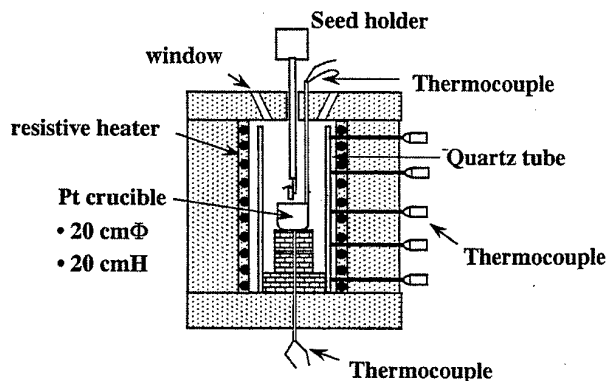


- CLBO can melt congruently at 848 °C.
- PDs show stoichiometric congruent point.

Growth of large CLBO crystal

• Top Seeded Solution Growth method
(Kyropoulos)

Furnace equipped with 5-zone resistance heater
to get spatial T. uniformity.

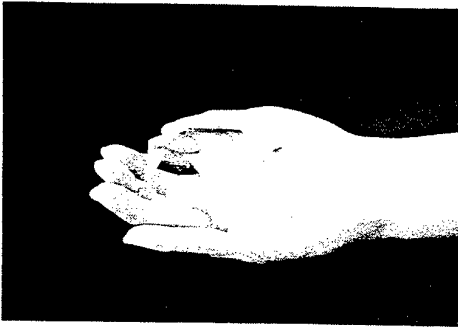


• Starting material
mixture of Cs₂CO₃, Li₂CO₃ and B₂O₃
ratio = 1 : 1 : 5.5

• Growth temperature
from 844.3 °C

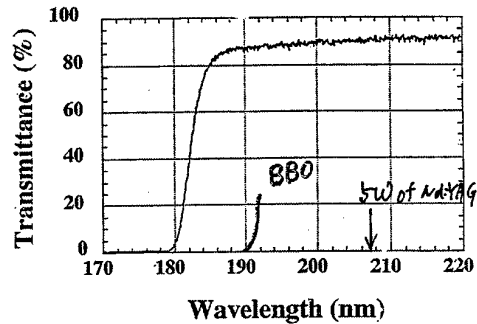
• Rotation ratio
15 rpm

CLBO Crystal



- Grown from flux method
- 14 x 11 x 11 (axcxa) cm³
- 3 weeks growth
- 1.8 kg

Transmission Spectrum of CLBO



- Transparent region : 180~2750 nm
- Absorption edge : 180 nm

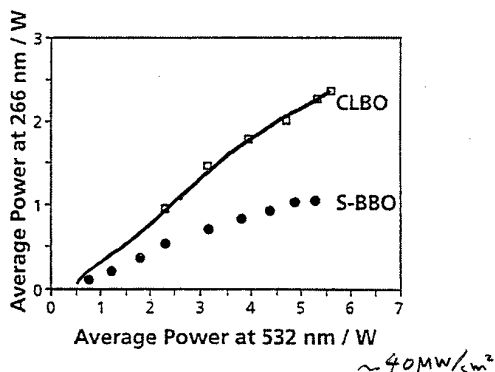
High repetition rate all-solid-state UV laser

(1000 Hz)

Landa Physik

i) 2.5 W of 4 ω Nd:YAG laser at 266 nm
Conversion efficiency from 1064 nm = 28 %

ii) 1 W of 5 ω Nd:YAG laser at 213 nm
Conversion efficiency from 1064 nm = 11 %



example of Rare-Earth Calcium Oxyborate Crystal

(Photo: Gd_{0.23}Y_{0.77}COB Crystal)



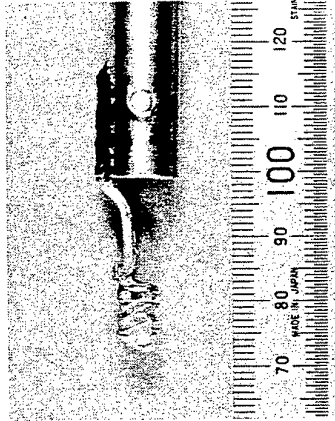
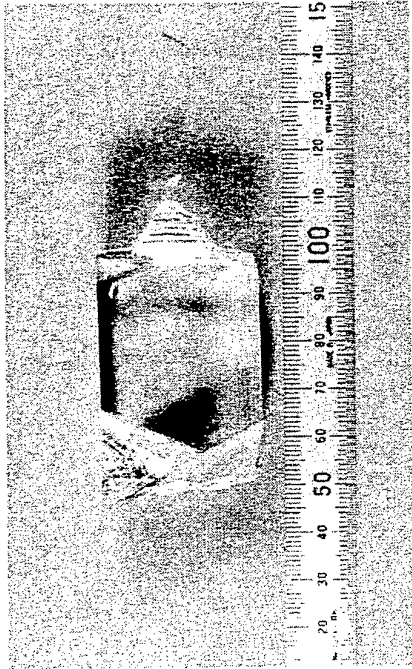
Grown by Cz method
Growth Temp. 1500°C
Pulling rate 3mm/h
Rotation rate 20rpm
Crystal length 61mm
Diameter 23mm

Comparison of nonlinear optical characteristics

		d _{eff} [pm/V]	Angular acceptance [mrad·cm]	Temperature acceptance [°C·cm]	Walk-off angle [mrad]
YCOB	THG I (XY)	0.52	3.5	10	8.5
KDP	THG II	0.35	1.6	5.2	26.5
LBO	THG II (YZ)	0.50	5.0	3.7	9.30
Gd _{0.24} Y _{0.76} COB	NCPM	0.54	9.0	10	0

各温度降下速度で育成した結晶

引き上げたCBO結晶



Growth of oxide crystals for solid-state lasers

A. V. Shestakov

State R&D Institute "Polyus",
Vvedensky Street 3, Moscow, 117342, Russia,
phone/fax (095) 334-8640, e-mail: avshest@ipolus.msk.su

E. V. Zharikov

General Physics Institute of Russian Acad. Sci.,
Vavilov Street 38, Moscow, 117942, Russia,
phone (095) 138-8352, fax (095) 135-0270, e-mail: zharikov@llcg.mail.gpi.ru

Abstract

In the lecture we discuss the growth technology of single crystals production of several important oxide compounds using in solid-state lasers.

R&D Institute "Polyus" is the central institution in Russia where are both laboratories for solid-state laser components and laser systems design as well as facilities for crystal growth. There are 20 crystal growth stations and more 55 engineers/technicians are working at crystal growth/treatment facilities now.

Working closely together with GPI and some other academician institutes "Polyus" developed growth technologies of a number oxide crystals including YAG/YAP/GSGG/YSGG etc. which were transferred to several plants in the country.

In 1984-85 "Polyus" and GPI has introduced in production an important laser crystal Nd,Cr:GSGG. High power/energy systems have been elaborated for different applications, including range finding material processing. In 1985-87 very significant results on the high efficient tunable laser based on crystal of $\text{Ti}^{3+}:\text{Al}_2\text{O}_3$ were reported. The latter event and discovery useful properties Cr^{4+} in garnets have served to catalyze more interest in laser hosts for both tunable and high efficiency laser systems. Results of the investigations were elaboration of technologies heavily doped bulk $\text{Ti}^{3+}:\text{Al}_2\text{O}_3$ with FOM more then 300 and high quality $\text{Cr}^{4+}:\text{YAG}$ for both tunable near IR lasers and Q-switch applications.

The garnet Nd: YAG and perovskite Nd:YAlO₃ remain as the most useful for 1.06 μm operation for lamp and laser diode pump as well as the LiNbO₃/LiTaO₃ remain more applicable nonlinear/electrooptical crystals for Q-switches, spectral conversion and OPO.

Technological procedures

Although laser crystals can be grown by many various method we use the Czochralski technique of pulling from a melt, because the method is very productive and adaptable to most host laser crystals at low activator contents and the technologies are applicable to production level.

The issues following below are of main concern in the growth of above-mentioned crystals for a laser application. Each issue may contribute to the success or failure of the final product, uniformity of properties, and final cost of the component.

Chemical purity and starting material preparation.

Chemical compounds, which are used in "Polyus", namely Al_2O_3 , Ga_2O_3 , RE_2O_3 and other oxides are produced in Russia. These compounds are available in 4N and 5N purity mostly at cost \$50-100/kg. Chemicals are purchased only from recognized suppliers and we are able to characterize and analyze their products with reliability.

Chemicals are mixed thoroughly in needed proportions for a long time (24 h) in pure $\text{C}_2\text{H}_5\text{OH}$ to get homogeneous mixture. Then follow the raw material tablet forming and hot pressing. The last procedure in tablet preparation is annealing (20 h, 1400-1450C) in air atmosphere. The final product is the sintered material with high density. Usually the tablet consists of more the 90% of required crystalline phase and has more then 80% of single crystal density. To make shorter crucible filling, the tablet has special form – disk with central hole.

Ceramics

$\text{ZrO}_2/\text{Y}_2\text{O}_3$ sectorial ceramics are used to assemble crystallizer. The design of single ceramics sector is convenient for assembling and any modification of crystallizer. The chemical purity of ceramics is 99,9%, regular cost is about \$20/kg. The ceramics parts can be used for many times after post-growth cleaning.

Crucibles

The most common crucibles for laser crystal growth made from Ir or Pt. However, for LiTaO_3 growth Pt–Rh crucibles are used. Although the material gives some crystal coloration in visible, because of Rh–doping, our experience shows that the coloration is not really important for electrooptical application. Crucibles are available in Russia in large sizes and high purity. Typically 100x100x2 mm and 120x120x2 mm crucibles are used in production of YAG/YAP/LN/LT crystals. As an example it can be mentioned that the typical crucible lifetime (YAG-growth) is about 3000-3500 hours and weight losses are 7-8% per year.

Growth facilities

In former Soviet Union it was produced the family of oxide crystal growth stations called "Crystal". Nowadays last members of the family "Crystal-2" and "Crystal-3M" are used in crystal production. Both stations have the same chamber, vacuum system but the former one is provided with motor generator and the latter one with solid-state inverter as a power supply operating at 8kHz with 60 and 100 kW.

Great emphasis is placed on short and long term stability and maintenance. The low frequency units have good skin depth of currents penetration into the crucible. The solid state units have good short term (1-7 days) stability and they are acceptable for LiNbO_3 and LiTaO_3 growing but for longer time periods as for YAG/YAP growth (2-3 weeks) motor generator looks more reliable.

Ambient atmospheres

Ideally the oxide crystals are grown under some fixed partial pressure of oxygen. In fact we use pure Ar atmosphere in YAG/YAP growth to prevent Ir oxidation. Unfortunately Ar can be easily ionized in RF systems and it dictates some special demands to use growth installations. $\text{N}_2 + 2\text{vol}\% \text{O}_2$ atmosphere is used for gallium

garnets growing. Usually Czochralski method has some difficulties to grow crystals under vacuum but for $\text{Ti}^{3+}:\text{Al}_2\text{O}_3$ growth we need in vacuum to get good quality crystals. The elaborated Ti-sapphire technology is based on domestic equipment, which can successfully operate under high vacuum conditions.

Annealing

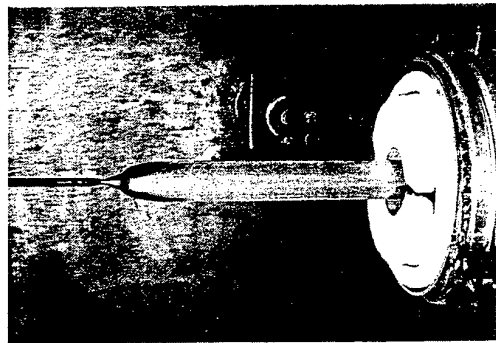
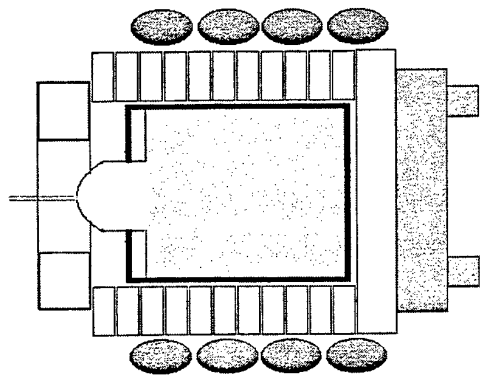
To improve operating characteristics of laser crystals and total production yield the special thermal treatment is necessary. Normally we use multistage high temperature treatment in air or under reducing atmosphere to prevent crystal cracking, increase solarization stability and improve optical properties.

Results and products

In R&D Institute "Polyus" during last 10 years about 2000 crystalline boules of different laser crystals have been successfully grown. Average total yield of current crystal growth technologies is 55-60%.

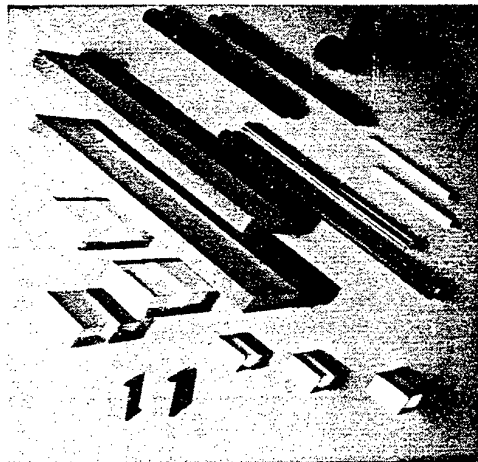
"Polyus" crystal product line consist of more than 50 different products and includes laser rods made of Nd:YAG, Nd:YAP, CTH:YAG, Er:YAG, $\text{Cr}^{+4}:\text{YAG}$, Nd,Cr:GSGG, Nd,Cr:YSGG, $\text{Ti}^{3+}:\text{Al}_2\text{O}_3$ crystals, passive and EO Q-switches based on $\text{Cr}^{+4}:\text{YAG}$ or $\text{LiNbO}_3/\text{LiTaO}_3$. Nd:YAG/Nd:YAP laser rods with 10 mm clear aperture and length more 150 mm are available now as well as high aperture $\text{LiNbO}_3/\text{LiTaO}_3$ EO Q-switches. Whole set of other special components has been designed to satisfy various technical requirements of modern laser systems.

TYPICAL CRYSTALLIZER DESIGN (YAG:Cr⁺⁴, 120x120x2 mm crucible)



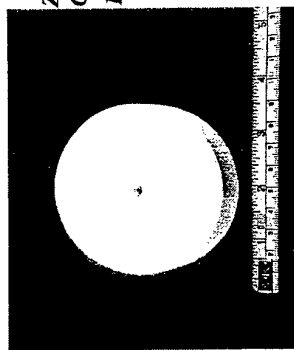
CRYSTAL PRODUCT LINE

YAG: Nd
YAG: Er
YAG: Cr, Tm, Ho
YAG: Yb
YAG: Cr+4
YAP: Nd
YAP: Er
Al₂O₃: Ti
LiNbO₃/LiTaO₃
GSGG/YSGG: Nd, Cr

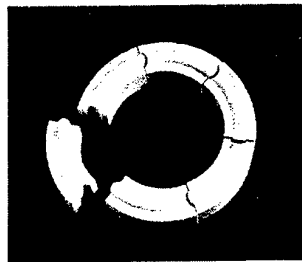


Process preparation:

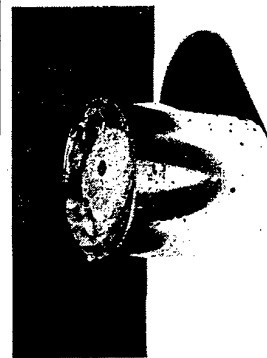
- Making of starting material tablet
- ZrO₂-Y₂O₃ ceramics annealing/cleaning
- crucible filling up



STARTING MATERIAL :
UNDOPED YAG,
DENSITY >3,5 g/cm³
pressed/annealed/holed disk



ZIRCONIA SECTORIAL
CERAMICS - ZrO₂-Y₂O₃
150/120/100/80 mm SETS



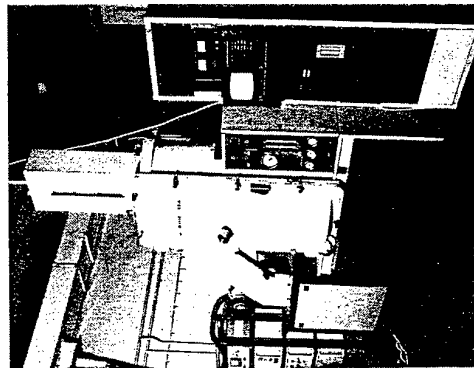
FILLED CRUCIBLE

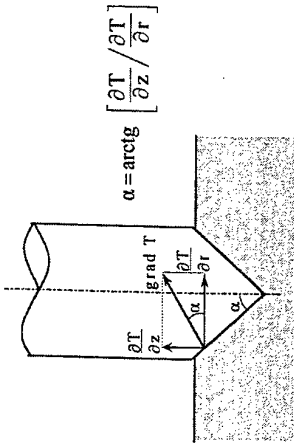
TECHNOLOGICAL EQUIPMENT

«CRYSTAL - 3M/496» INSTALLATION

CZOCHELSKI METHOD

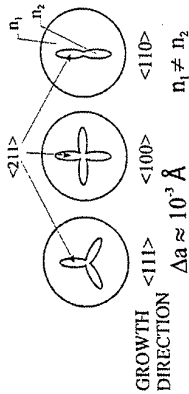
- inductive heating furnace
- 6,65*10⁻³ ... 10 kPa working pressure
- oil free vacuum system
- real time fine crystal weight measurements
- IBM PC computer control
- max. crucible diam. 150 mm
- tyristor power supply
- 100kW @ 8 kHz
- total weight - 5400 kg
- Min. space - 20 m²



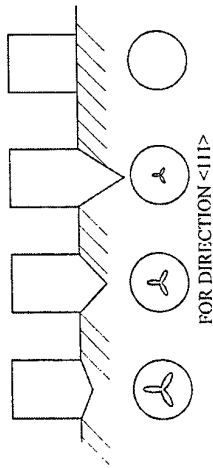


Insulation bottom/top	Temperature gradient (axial/radial), deg/cm	α (deg)	
		without crystal	with crystal
-/-	200/40	79	64
-/+	70/65	47	51
+/-	220/30	82	86
+/+	170/45	75	71

CORE IN GARNETS



INFLUENCE OF SUPERCOOLING TO FACETTING



Stages of growing process YAG:Cr+4 from 100 mm crucible as an example

- Raw material preparation (3.5 g/cm3, >95% single phase)
- oxide mixing and tablet forming (C2H5OH, 48h shaking/rotating/drying)
- final drying after tablet formation (800C, air, 2 h)
- thermal annealing/pressing/synthesis (1300-1400C, 5 ton press, air)
- Crystallizer assembling/Seed adjustment
- Crucible filling up (Ar - 1 atm)
- Growth
- Manual narrowing of crystal seed
- Automatic conic part growth (~30 mm, 1...2 mm/h, 10-20 rpm)
- Automatic cylinder part growth (diameter 35mm, length 250 mm, 4 mm/h, 12-15 rpm)
- Automatic conic part growth (30mm) and manual narrowing crystal up to 1-2 mm
- Freezing of melt and cutting crystal boule from crucible

CONCENTRATION DEPENDENCE OF CR+4 LEVEL after whole set of technological procedures

C [Ca] at. %	C [Cr] at. %	α [cm-1] at 1064 nm
0,5	0,5	4,96
0,5	1,5	6,1
0,5	0,5	2,88
0,5	1	4,81
0,2	0,01	0,72
0,15	0,05	0,86
0,5	0,1	3,2
0,5	0,15	3,4
0,5	0,5	4,9
0,5	1	4,8
0,5	1,5	6
0,5	2	4,3

C [Mg] at %	C [Cr] at. %	α [cm-1] at 1064 nm
0,3	0,1	3,1
0,3	0,03	1,9
0,2	0,5	2
0,25	0,5	2,5
0,1	0,5	1,5
0,35	0,1	2,5
0,35	0,35	3,1
0,35	0,5	5,1
0,4	0,25	3,55
0,5	0,025	1,4
0,5	0,35	3,55
0,5	0,5	3,5
1	0,025	1,6
1	0,35	5,5
1	0,5	4,8

GS GG:Cr,Nd and YAG:Nd Comparison of technology parameters

PARAMETER	YAG:Nd	GS GG:Cr,Nd	Comments
K_{Nd}	0.18	0.7	
K_{Cr}	2.4	1	
Pulling rate (mm/h)	0.75 – 1.2	2 – 4	Nd ³⁺ concentration quenching in GS GG is weaker than in YAG
C_{Nd} [10^{20}cm^{-3}]	1.5	2 – 5	
C_{Cr} [10^{20}cm^{-3}]	–	1 – 3	
Crucible diameter for growth of crystal with Ø 20-22 mm	80 – 100	50 – 60	From crucible with Ø 100 mm it is possible to grow GS GG:Cr,Nd crystal with Ø 50-60
Coefficient of melt use	0.2	0.6 – 0.7	
Melting point [°C]	1940	1850	Longer life of crucible in case of GS GG
Duration of growth of crystal with length 100 mm [days]	6	2	It is possible to get quantity of GS GG crystals 2-3 time more than YAG from the same park of growth facilities

Congruently melting compositions (CMC) and distribution coefficients of Cr³⁺ and Nd³⁺ ions in garnets.

Garnet	CMC	[Sc _{oct}], %	K _{Cr}	K _{Nd}
GS GG	{Gd _{2.95} Sc _{0.05} } [Sc _{1.85} Ga _{0.15}](Ga ₃)O ₁₂	93	1.0	0.7
GS AG	{Gd _{2.88} Sc _{0.12} } [Sc _{1.77} Al _{0.23}](Al ₃)O ₁₂	88	1.1	0.6
YSGG	{Y _{2.93} Sc _{0.07} } [Sc _{1.36} Ga _{0.64}](Ga ₃)O ₁₂	68	1.4	0.6
YSAG	not found	var	1.6-2.1 ^{*)}	0.2-0.3 ^{*)}
YAG	{Y ₃ } [Y _{0.02} Al _{1.98}](Al ₃)O ₁₂	–	2.4	0.18
GGG	{Gd ₃ } [Gd _{0.05} Ga _{1.95}](Ga ₃)O ₁₂	–	3.3	0.63

^{*)} depending on the composition

After growing treatment (for YAG:RE/Cr+4)

- annealing
- cutting
- preform making
- preform annealing
- cutting/slicing
- polishing/AR deposition

-After growth vacuum annealing

24 h, 1700-1750C, Ar

- Conic parts cutting@ ends polishing

- Defect area determination@ boule cutting on sectors

- Preforming (cylinder/ slabs/ plates)

- Main annealing process

1700-1750C, 36 h, air

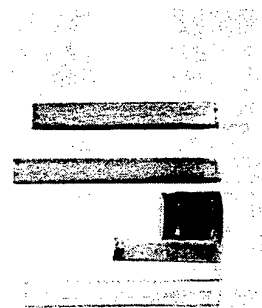
- rod forming @ polishing

- After forming annealing

1200-1250 C, 72 h, air

- Final polishing@control

- AR deposition



Conic parts cutted
and annealed garnet boules

DISTRIBUTION COEFFICIENTS OF COMPONENTS AND DOPANTS (Cr, Nd) IN CRYSTALS OF GS GG_xGS AG_{1-x} AND YSGG_xGS AG_{1-x} SOLID SOLUTIONS

Crystal	K _{Gd}	K _Y	K _{Sc}	K _{Al}	K _{Ga}	K _{Cr}	K _{Nd}
GS GG _{0.17} GS AG _{0.83}	–	–	–	–	–	1.06	0.65
GS GG _{0.33} GS AG _{0.67}	1.03	–	0.99	0.99	0.99	1.04	0.69
GS GG _{0.50} GS AG _{0.50}	–	–	–	–	–	1.04	0.70
YS GG _{0.33} GS AG _{0.67}	0.98	1.13	1.01	1.02	0.99	1.24	0.51
YS GG _{0.67} GS AG _{0.33}	0.98	1.12	0.96	1.04	0.94	1.28	0.52
YS GG _{0.83} GS AG _{0.17}	0.86	1.11	0.93	0.99	1.09	1.46	0.53

YAG:Cr⁺⁴ laser rods @ passive Q-switches

TECHNICAL SPECIFICATIONS:

Absorption range..... 950 - 1100 nm

Initial transmittance* 15...95 %

Initial absorption coefficient..... 0.1...5 cm(-1)

Aperture..... 3...10 mm

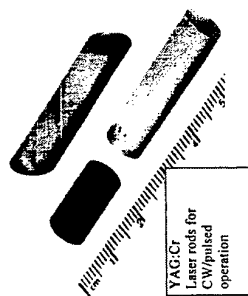
Contrast* > 20

Optical length..... 0,5...50 mm

Damage threshold..... > 4 J/cm²

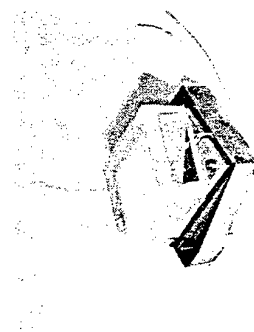
Optimized threshold CW power – less then 200 mW
1064 um, TEM₀₀, 2W₀=80um

* - for Q-switch only



LiNbO₃ EO Q-SWITCHES

High clear aperture - 5;7;8;10mm
low control voltages - $U\lambda/2 = 3,2 \text{ kV}$
damage threshold - 500 MW/cm²
high transmission > 97%
high extinction ratio > 30
temperature range -60...60C
«Brewster» or «plane» geometry
wide spectral range - 900...1600 nm
energy density for pulse >5 J/cm²
duration 1-30 ns



10 mm aperture
LiNbO3 Brewster
angled EO-Q-switch

Typical thermal treatment procedures

Crystal	Post growing annealing	After growing annealing	Post mechanical thermal treatment
YAG:RE	1750-1800C,10 h 1atm,Ar	1350 C, 36 h, O2	700-800c, 24h, air
YAP: RE	1750-1800C,10h, 1atm,Ar	1500,Vacuum (H2), 36 h	700-800c, 24h,air
YAG:Cr+4	1750-1800C,10 h 1atm,Ar	1400-1450C,72 h, air	700-800,24h, air
LiTaO3/LiNbO3	1200C,10h, air	1000C,24 h,air	700C,10 h, air

Procedure	Production		yield		for different		Crystals
	YAG:Nd (1%)	YAP:Nd (1.3%)	YAG:Cr+4	LiNbO3	YAG:Nd (1%)	YAP:Nd (1.3%)	
Raw material preparation	100%	100%	100%	100%	100%	100%	100%
Crucible filling	90%	95%	85%	95%	85%	95%	95%
Growth/annealing (cylindrical part SPECS/ regimes)	90%/ (diam.38mm, 250 mm length 1.0 mm/h,14 days)	70% (diam.36mm, 250mm length, 1.5mm/h, 10 days)	90% (diam.40mm, 200mm length, 4 mm/h, 6 days)	85%	90%	85%	85%
Cutting	85%	90%	90%	85%	90%	85%	85%
Annealing	100%	100%	100%	100%	100%	100%	100%
Optical treatment/AR deposition	95%	95%	95%	80%	95%	80%	80%
Testing	80%	90%	80%	75%	80%	75%	75%
Total yield	54%	50%	50%	45%	50%	45%	45%

CRYSTAL GROWTH TECHNOLOGY OF HIGH-QUALITY QUARTZ

BY VLADIMIR S. BALITSKY
INSTITUTE OF EXPERIMENTAL MINERALOGY RUSSIAN ACADEMY OF SCIENCES,
142432 CHERNOGOLOVKA, MOSCOW DISTRICT, RUSSIA
TEL/FAX: (7-095) 913- 2112
E-MAIL: BALVLAD@IEM.AC.RU

ABSTRACT

Quartz crystals, due to the piezoelectric effect, ability to rotate a plane of polarization and high transparency in a wide range of wave lengths into UV, visible and IR-regions of the spectrum, can be widely applied in radioelectronic technique and optics. Moreover, quartz forms numerous coloured varieties, which have been long used in jewelry and cut-stone industry. High cost and restriction of store of perfect and quite large crystals of natural quartz stimulated investigations on their artificial growing. Especially intensively these investigations were performed before the World War II, within this period and after-war period due to the development of the military and later civil purpose. In the 50-s this problem was in principle solved in the USA and USSR. Similar result was reached by some other countries later (1)*.

By the present time the industrial production of synthetic quartz has been performed in almost 20 countries and may be estimated as it attains (approximately) 2500 tons per year. The approximate level of prices for different types of crystals is (in USD per kilo): optical quartz - 180-630; piezoquartz of different purpose - 20-100; amethyst - 100-160; other kinds of coloured quartz - 60-80.

A hydrothermal method of temperature gradient is in the basis of all the existing technologies of growing crystals of quartz. Its choice is caused by the fact that * only low temperature α -quartz has a piezoelectric effect (symmetry group C_{3i2} and C_{322}). At temperature 573°C (pressure 1 kg/cm^2) α -quartz transforms into high temperature β -quartz (symmetry group C_{622} and C_{642}) with the loss of the piezoelectric effect.

* - copies of transparencies

The reverse transition of β -quartz into α -quartz is accompanied by twinning and cracking. It excludes the possibility of growing of piezoquartz from the own melt (temperature $\sim 1670^{\circ}\text{C}$) and high temperature hydrothermal solutions and flux. At the same time, quartz at temperature $250\text{-}500^{\circ}\text{C}$ and pressure $50\text{-}200\text{ MPa}$ is characterized by a rather high solubility, especially in alkaline (NaOH , Na_2CO_3 , KOH , K_2CO_3) and fluoride (NH_4F) solutions (2). Temperature coefficients of solubility in these solutions have positive values, but a change of density characteristics of solutions under the conditions of direct temperature gradient provides a continuous convective transpose of the dissolved silica from the lower (hotter) chamber into the upper (less hotter) chamber of crystal growth. The process is performed in vertically established vessels of high pressure (3) with good systems of heating and heat isolation (4) and control by thermobaric parameters (5). One of the versions of the basic operations at performing of cycles of industrial growing of quartz is shown on scheme (6). The real industrial vessels, their assembling and placing are demonstrated in pictures (7). Specific conditions of industrial growing of quartz crystals and their coloured varieties are reported in the most general form (8,9,10). However, using them one can practically always reproduce the process of crystal growth. Numerous data on study of crystal-forming systems with the determination of the structural-morphological characteristics (including different defects) and properties of grown crystals contribute to this fact (11,12). To find optimal conditions of process of growing it was important to determine in aqueous silicate-alkaline systems phenomena of layering of the solutions into "light" and "heavy" phases (13,14). It has become clear that to grow high-quality quartz it is necessary to choose such relationships of thermobaric parameters and concentrations of mineralizes which would exclude layering of solutions or reduce the appearance of "heavy" phase to minimum. It was defined that quartz crystals grown from such solutions at the growth velocities $0.5\text{-}1\text{ mm/day}$ on seeds of orientation (0001) elongated along the axis Y (ZY - crystal and \bar{Y}) or along the axis X (ZX - crystal) as well as on plates of orientation (1120) elongated along the axis Y have the best

relationship of qualitative and economic characteristics. The improvement of technological ways and a transition to average and large-scale vessels made it possible to develop new technologies of growing crystals of the block low dislocation, optical, radiationally stable quartz and new varieties of coloured quartz (15,16). On the whole the problem of creation of their industrial technologies can be considered completely solved. Further perspectives of their development relate to finding the ways of cheapening of the process and improvement of qualitative characteristics of grown crystals.

References

- ◆ Kerr P.F. and Armstrong E. Recorded experiments in the production of quartz. Bull. Geol. Soc. Amer., 54, Sup. 1, 1943, p. 1-34.
- ◆ Laudise R.A. The growth of single crystal. Bell Telephone Laboratories, Morray Hill, New Jersey, 1970
- ◆ Balitsky V.S. Experimental Study of the Processes of Rock Quartz Formation. Moscow, Nedra, 1978, p. 148 (in Russian)
- ◆ Nassau K. Gems Made by Man. Published in Randor, Pensilvania, by Chilton Book Company, 1980, p. 364
- ◆ Khadzi V.E., Tsinober L.I., Shterenliht L.M., et al. Synthesis of minerals, Moscow, Nedra, 1987, p. 488 (in Russian)

Acknowledgments

Besides personal results in the lecture there have been used the data of numerous investigations of a large body of researchers and engineer-technical staff of workers of The Russian Research Institute for the synthesis of Materials (VNIISIMS). The author is very much obliged to them, as well as the Company Kinseki and Dr's H. and F. Iwasaki.

(1)

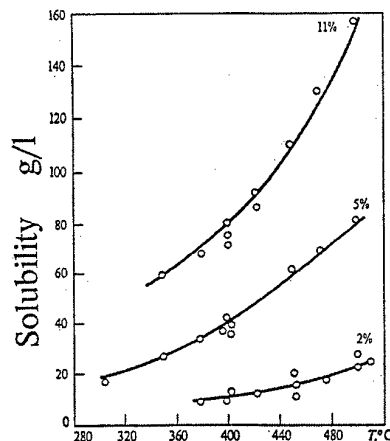
Basic events related to the development of methods and technologies of growing quartz crystals

EVENT	YEAR	REFERENCE
The first synthesis of microscopic quartz crystals	1845	G.Schafhautel, 1845
The first growing of quartz crystals on seeds in the conditions of temperature gradient	1906-1908	G.Spezia, 1909
The first growing of quartz crystals on seeds under isothermal-isobaric conditions.	1930	R.Nacken, 1943, 1944
The first making of quartz resonators from synthetic quartz	1948	L.Thomas, N. and W. Wooster, 1949
Development of hydrothermal methods of temperature gradient for growing quartz crystals	1949-1953	E.Buehler and R.Walker, 1949 R.Walker, 1953
Creation of the first industrial production of crystals of synthetic quartz	1956	Sawyer Research Products, Inc. K.Nassau, 1980
Creation of large,	from	Different

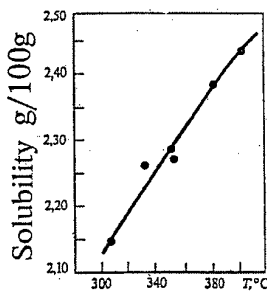
Continue (1)

middle and small plants on growing quartz crystals in USA, Russia, England, Japan, Germany, France, Brasil, Singapore, Hon-Kong, Tiwan, etc	1958 to present time	sources
Getting of the first crystals synthetic quartz from ammonium fluoride solution	1967	Balitsky, 1967
Start of industrial production of synthetic coloured quartz:		
Amethyst (from alkaline solution)	1970	Khadzi et.al, 1970
Amethyst (from ammonium fluoride solution)	1970	Balitsky et.al, 1970
Citrine	1970	Khadzi and Reshetov, 1974
Blue quartz	1959	Khadzi and Lushnikov, 1959
Green quartz	60-s	Nassau, 1980
Brown quartz	60-s	Nassau, 1980
Pink quartz	1992	Balitsky et.al, 1998
Ametrine	1994	Balitsky et.al, 1995

(2)



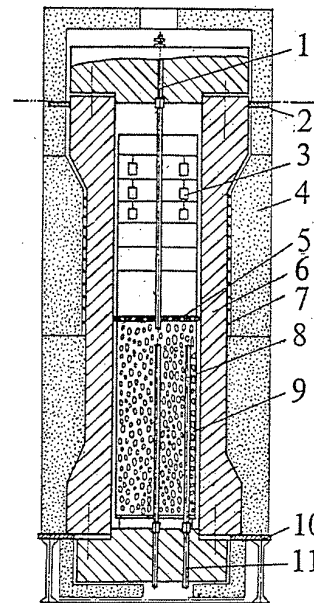
Polibars of solubility of quartz in solutions of sodium carbonate. Coefficient of filling in all the cases is equal to 70%. AFTER L.V.BRYATOV, 1953



AFTER LAUDISE R.A. 1960

Depends of quartz solubility in solution of 0.5n NaOH on temperature at the degree of filling 80%. 662

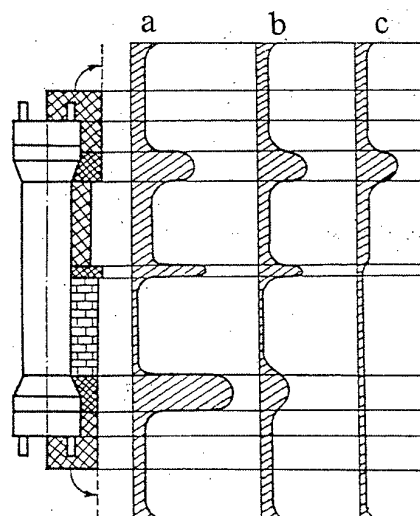
(3)



Schematic drawing of apparatus of hydrothermal synthesis: 1,10 - technological inputs; 2,11 - fixing elements; 3 - container with seeds; 4 - thermoinsulation; 5 - diaphragm; 6 - vessel; 7,8 - heaters; 9 - container with charge. AFTER KHADZI et al., 1987

INDUSTRIAL VESSELS FOR GROWING OF QUARTZ CRYSTALS

TYPE	LOW SCALE	AVERAGE SCALE	LARGE SCALE
FORM	CYLINDRIC		
INTERNAL DIAMETER, MM	UP TO 300	300 - 600	> 600
LENTH, MM	2000 - 6000	6000 - 8000	8000 - 12000
COMMON WEIGHT, TON	UP TO SEVERAL	DAZENS	UP TO 100
WORKING TEMPERATURE, °C	UP TO 500	UP TO 400	UP TO 400
WORKING PRESSURE, MPa	200	80 - 150	40 - 80
RELATIONSHIP OF HIGHT OF WORKING CHAMBER TO THE INTERNAL DIAMETER	8 - 15 SOMETIMES 20 - 30	8 - 15 SOMETIMES 20 - 30	40 - 80
DURATION OF THE CYCLE, MONTH	1 - 2	2 - 4	3 - 12
WEIGHT OF CRYSTALS, kg	0,5 - 1 SOMETIES UP TO 2 - 4	2 - 4 SOMETIMES UP TO 10 - 15	2 - 4 SOMETIMES UP TO 15 - 18
GENERAL WEIGHT OF CRYSTALS FROM THE ONE CYCLE, kg	100 - 200	300 - 1500	1500 - 4500



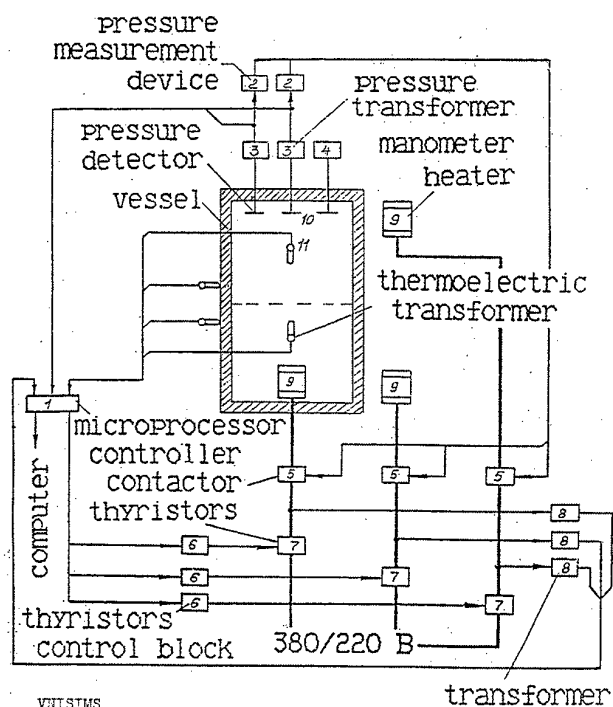
Diagrams of distribution of densities of thermal flows on the external surface of thermoinsulation of the industrial vessel.

Schemes of fixing:

a-low without additional thermoinsulation of fixing elements and external heater;
b-low with additional thermoinsulation of fixing elements and external heater;
c-upper.

(5)

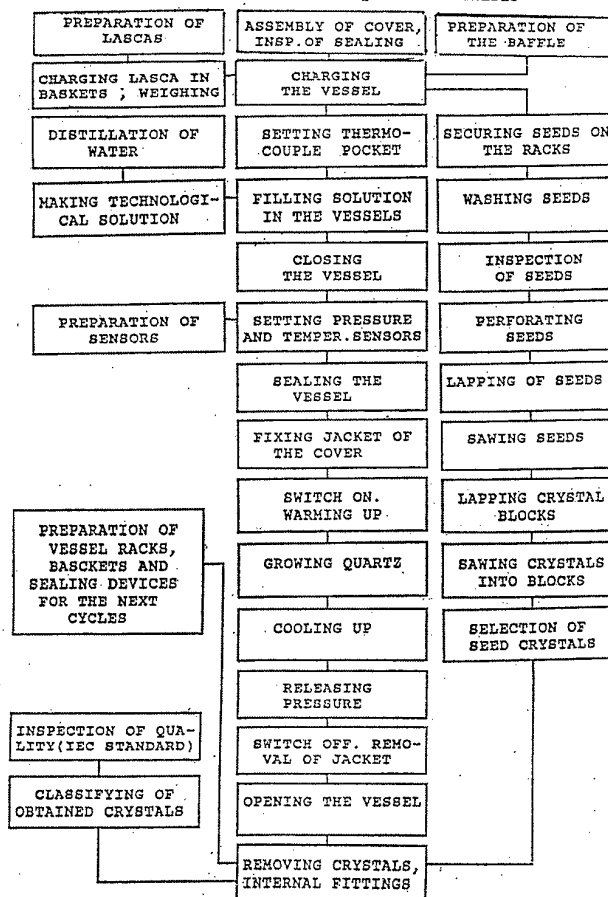
AUTOMATIC CONTROL SYSTEM OF CRYSTAL SYNTHESIS TECHNOLOGICAL PROCESSES



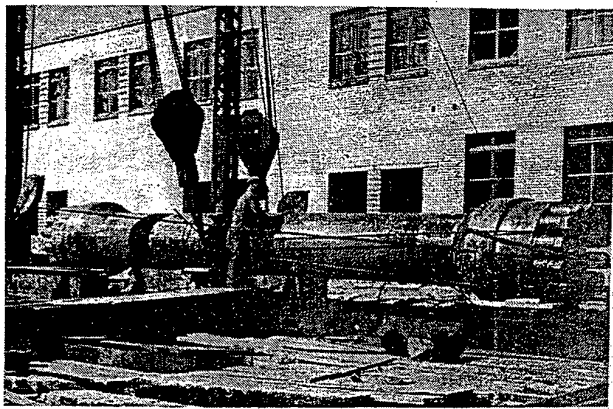
VNIISIM

(6)

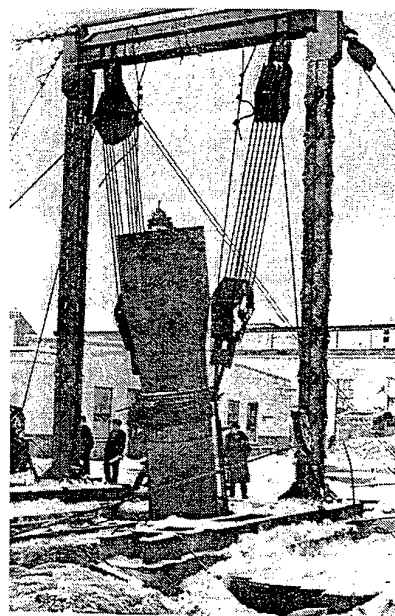
OPERATION CHART OF QUARTZ SYNTHESIS



Assembling of industrial vessel for growing quartz crystals



Industrial vessel for growing quartz crystals



(8)

(9)

TYPICAL COLOURLESS QUARTZ GROWTH CONDITIONS

CONDITIONS	COLOURLESS QUARTZ			
SOLUTION	Na ₂ CO ₃ 0,5-0,8 M	Na ₂ CO ₃ 5-7 wt.% + NaOH 0,4-0,5 wt. %	NaOH 1 M + Li ₂ CO ₃ 0,025 N	NaOH 0,5 M + LiNO ₃ or LiNO ₂ 0,1-0,01 M
GROWTH TEMPERATURE, °C	335 - 350			
BOTTON FEED TEMPERATURE, °C	350 - 395			
PRESSURE, MPa	70 -100		130 -190	
TYPE OF SEED	ZX - plate, ZY - plate, Y -bar			
GROWTH RATE, MM/DAY	0,2 - 1.0			
VOLUME OF VESSEL, l	from 200 to 12000		from 200 to 1500	
WEIGHT OF CRYSTAL, kg	from 0,5 to 18			
REFERENCE	K. Wilke (1963); K. Nassau (1980); K. Suzuki et al (1986); V. Khadzi et al (1987)			

TYPICAL COLORED QUARTZ GROWTH CONDITIONS

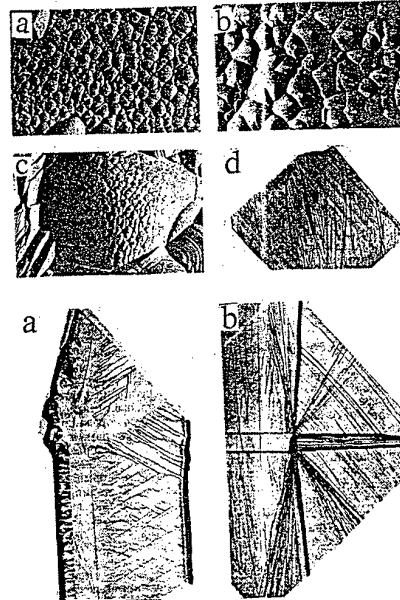
CONDITIONS	COLOURED QUARTZ		
	AMETHYST-1	AMETHYST-2	AMETRINE
SOLUTION	K ₂ CO ₃ 0,3-1 N + LiNO ₂ or Mn(NO ₃) ₂ 2-5 g/l	NH ₄ F 5-15 wt.% LiF 0.5 g/l	K ₂ CO ₃ LiNO ₃ or Mn(NO ₃) ₂ 2-5 g/l
ADDITIONAL COMPONENT	Fe ₂ O ₃ 15-20 gm/l	Fe ₂ O ₃ 15-20 gm/l	Fe ₂ O ₃ 15-20 gm/l
GROWTH TEMPERATURE, °C	300-370	250-400	300-370
TEMPERATURE GRADIENT, °C	20-25	10-20	20-25
PRESSURE, MPa	120-170	2-30	120-170
TYPE OF SEED	R-plate r-plate	Z-plate S-plate	Z-plate
GROWTH RATE, MM/DAY	0,1-0,4	0,2-0,5	0,1-0,4
VOLUME OF VESSEL, l	1500	300, 500	1500
WEIGHT OF CRYSTAL, kg	1 - 2	0,5 - 2	0,5 - 4
REFERENCE	Khadzi et al. (1975)	Balitsky et al. (1975)	Balitsky and Balitskaya (1986)

TYPICAL COLORED QUARTZ GROWTH CONDITIONS

CONDITIONS	COLOURED QUARTZ		
	GREEN	BROWN	PINK
SOLUTION	K ₂ CO ₃ 0.5 N	K ₂ CO ₃ 0.5 N	NH ₄ F 5-15 WT. %
ADDITIONAL COMPONENTS	Fe	Fe	H ₃ PO ₄
GROWTH TEMPERATURE, °C	270-320	325-350	240-310
TEMPERATURE GRADIENT, °C	30-40	20-30	15-30
PRESSURE, MPa	80-100	80-100	7-30
TYPE OF SEED	Z-PLATE	Z-PLATE	Z-PLATE
GROWTH RATE, MM/DAY	0,6-0,9	0,3-0,5	0,2-0,4
VOLUME OF VESSEL, l	1500 - 4000		1,5-3
WEIGHT OF CRYSTAL, kg	1 - 3		0,15-0,2
REFERENCE	TSINOBER et al. (1959)		BALITSKY et al. (1998)

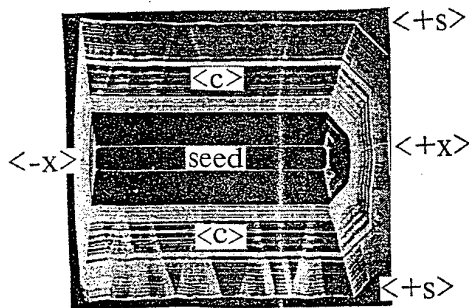
Reliefs of pinacoid

a - "cobbles" type; b - with active accessories of growth; c - of an intermediate type; d - X-ray topogram of the sample, described in figure. Reflex 1011.



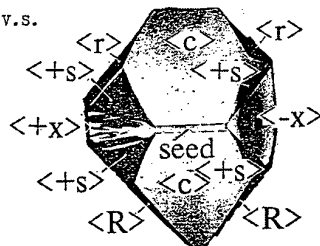
X-ray topohrams. Reflex 1011.

a-piramide of <+x> crystal, grown in fluoride solution; b-pseudozoning in sectors <+x> and <+s>. AFTER KHADZI et al., 1987

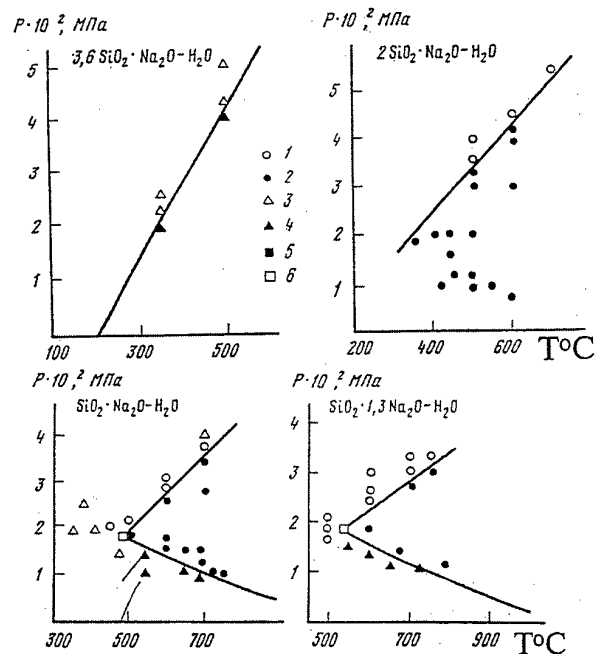


Distribution of the nonstructural impurity in synthetic quartz revealed after heating at temperature 700 °C during one hour: plates with the thickness 2 mm from c-crystal oriented parallel to the plane ZX. AFTER KHADZI et al., 1987

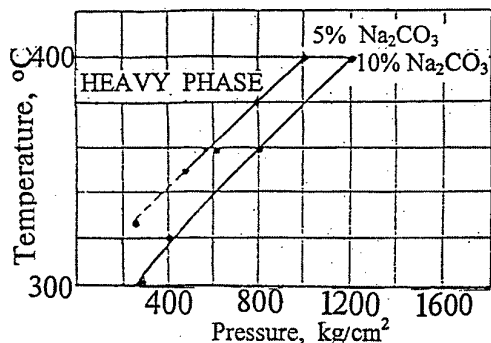
AFTER BALITSKY V.S.
1981



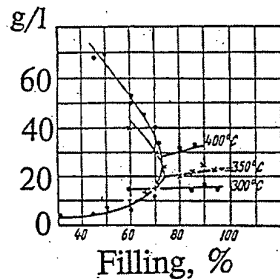
Character of distribution of smoky colouring in crystals of synthetic quartz. Sectors of growth of negative <r> and positive <r> rhombohedrons, pinacoid <c>, positive trigonal prisma <+x>, dipiramid <+s> and negative trigonal prisma



Phase associations obtained as a result of quenching runs of the system SiO₂-Na₂O-H₂O and boundaries of fields of heterogeneous equilibria. 1-liquid; 2-liquid+glass; 3-liquid+crystals; 4- liquid+glass+crystals; 5-liquid+glass+crystals; 6-critical equilibrium l₁=l₂-s (nonvariant point). AFTER VALYASHKO V.M., 1990



P-T-DIAGRAM FOR EXISTING FIELDS OF HEAVY AND LIGHT SILICATE PHASES AFTER BUTUSOV, BRYATOV 1957



ISOTHERMS OF SOLUBILITY OF QUARTZ IN 5% SOLUTION OF SODIUM CARBONATE.—SOLUBILITY CURVES; — LOSS IN WEIGHT DUE TO FORMATION OF THE HEAVY PHASE IN THE AUTOCLAVE

BRYATOV, 1953



Optic quartz is obtained as single crystal blocks of Z and X-orientation thick - up to 40 mm, of right and left rotation. Only one growth pyramid and absence of solid or fluid inclusions are special qualities of piezoquartz in blocks.

The crystals are grown on the seeds of ZY, XY-cuts (thickness - 15-30mm, length - 150-250mm). Q-factor, determined by IR-absorption method is $\geq 2.5 \cdot 10^6$ for the first grade and $\geq 1.8 \cdot 10^6$ for the second one.

Crystals contain neither electrical nor optical twins and no cracks and chippings. The orientation of Z-surface in respect to X-axis is $0^\circ 00' \pm 30'$. Roughness of the cut surfaces is no more than 40 mkm. Flatness of the cut surfaces is less than 0.1mm.

VNIISIMS

Low dislocation piezoquartz is obtained in forms of block ZY, XY and crystals ZY grown on rectangular seeds of right-hand enantiomorphic modification.

Crystals have dimensions:

by Y-axis up to 200 mm

X-axis up to 70 mm

Z-axis up to 60 mm

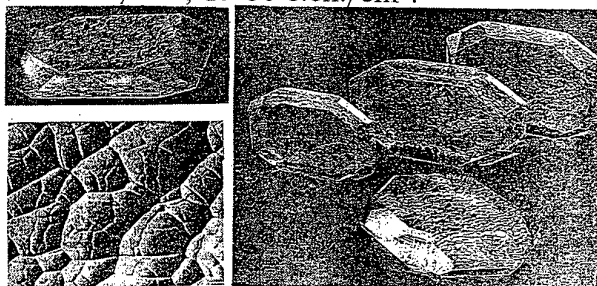
Blocks have dimensions:

by Y-axis up to 170 mm

X-axis up to 70 mm

Z-axis up to 35 mm

The quality of etch channels depends on quartz grade. It may be the following: 2-5 e.ch./cm², 5-15 e.ch./cm², 13-30 e.ch./cm².



Relief of surface of basal pinacoid of nondislocation synthetic quartz.

VNIISIMS

SCINTILLATORS ON THE BASE OF OXIDE CRYSTALS

M.Korzhik

Institute for Nuclear Problems, 220050, 11 Bobryiskaya, Minsk, Belarus

Inorganic scintillation materials fascinate us, both from the point of view of application for ionizing radiation detectors and as instrumental of the material science development. Although its fraction in crystal's industrial and experimental production does not exceed of twelve percents, they have a stable growing demand in industry, medical radiology and scientific research. Detectors made on a base of scintillation crystals still are the most frequently used for this applications and some of them have a perspective to be used in new generation of medical radiology equipment and particle physics experiments if their properties will satisfy to the new requirements. These requirements to the scintillator include Large Photo-absorption Fraction, High Light Yield, Fast Scintillation Decay, Fast Scintillation Rise Time, and Affordable price [1]. Unfortunately, among a wide used commercially available scintillators from such classes as alkali holides, cross luminescence materials, Bi and W complex oxides, and fluorides there is no one which satisfies simultaneously to the noted above requirements. Nevertheless oxide crystals have a great potential to construct new advanced scintillation materials. Among recently proposed materials lead tungstate PbWO_4 scintillator is a good compromise to be applied in high energy physics experiments, however low light yield makes it useless for medical radiology [2]. Other scintillators which have good correspondence to main requirements of medical radiology application are recently proposed. They are rear-earth oxioresilicate (RE_2SiO_5) and perovskite (REAlO_3) crystals doped with Ce ions. The crystals are dense, fast, high light yield scintillators and are produced by the well developed crystal growth methods [3-5].

Approach at the scintillators development, peculiarities of the oxide crystal's growth technology as well as new challenges are discussed. In this paper we will accent mainly on the physical aspect of the scintillator research, development and

production. Ce- doped and lead tungstate scintillators will be discussed. Both are subjects of our study during last decade.

CRYSTAL GROWTH

Czochralski and some modifications of the Bridgman methods are most frequently used to grow oxide scintillation materials. Peculiarities of the crystal growth of Ce-doped crystals in vacuum and gas atmosphere are discussed. Crystal growth of lead tungstate crystals in atmosphere close to air in composition also is considered.

POINT STRUCTURE DEFECTS IN OXIDE CRYSTALS

Parameters of scintillation materials are very sensitive to the purity of raw material. Specification of the oxides and prepared raw materials for different scintillation materials production is discussed. Most of the investigated color centers in oxide scintillation crystals are proven to be electron centers created under irradiation or light excitation with participation of anion and cation vacancies. Such centers affect the scintillation properties of the crystals and strongly influence the distribution of the emitted light among scintillation and afterglow as well as the recovery of the crystal transmission after irradiation. Creation of the cation and anion vacancies and their compensation or suppression in different oxide crystals at crystal growth or by additional annealing are reviewed.

MACHINING OF OXIDE SCINTILLATION CRYSTALS

Crystal surface damage to be appeared at machining of relatively soft scintillation materials is reported. The thickness of the perturbed crystal layer is usually less than 20 mikrones, however it influences on reflecting properties of the crystal surface, concentration of luminescence absorbing color centers and long time unstability of light yield. The methods of the crystal machining are debated.

SCINTILATIONS IN OXIDE CRYSTALS

An understanding of the scintillation origin in crystals comes through the study of its radiating centers. Spectroscopic properties of some trivalent rare-earth ions in crystals of garnet, oxorthosilicate and perovskite structure and tendencies of their change from crystal to crystal are reviewed. An important role of regular and irregular radiating centers in tungstate crystals is described.

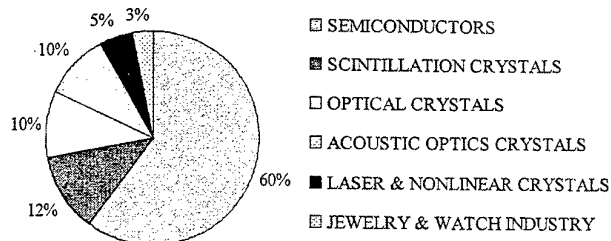
SCINTILLATORS IN RADIATION ENVIRONMENT

One of the important modern requirement to scintillation material especially to be applied in high energy physics experiments is stability of the parameters in radiation environment. The effect of irradiation on lead tungstate scintillator properties has been studied. Lead tungstate crystals, grown with the oxides content in the melt tuned to the stoichiometry or pure scheelite or scheelite-like crystal types and doped with heterovalent, trivalent and pentavalent impurities, have been studied in order to optimize their resistance to irradiation. Some methods of the crystal radiation hardness improvement are considered.

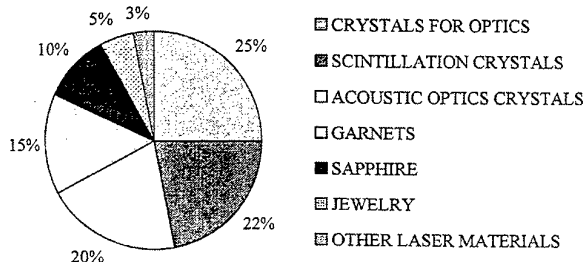
REFERENCES

1. C.W.E.van Eijk, New Scintillators, **New Light Sensors, New Light Sensors**, In the Proceeding of International Conference on Inorganic Scintillators and Their Applications, September 22-25, 1997 Shanghai, China, P48
2. A.A.Annenkov, V.L.Kostilev, V.D.Ligun, M.V.Korzhik, P.Lecoq, **Progress on RAD of the PbWO₄ crystals for CMS ECAL**, In the Proceeding of International Conference on Inorganic Scintillators and Their Applications, September 22-25, 1997 Shanghai, China, P19
3. C.L. Melcher and J.S. Schweitzer, IEEE Trans.Nucl.Sci., **39**, 502 (1992).
4. W.W.Moses, S.E.Derenzo, A.A.Fyodorov, M.V.Korzhik, B.I.Minkov, V.Aslanov, and A.V.Gektin, in IEEE Nucl. Sci. Conf. Abs. NSS09-04 (1994).
5. V.A. Aslanov, S.A. Smirnova W.P. Trower, M.V. Korzhik, A.A. Fyodorov, **Cerium doped lutetium - based single crystal scintillator**, Presented at SCINT'95 27-30 September, Delft, The Netherlands

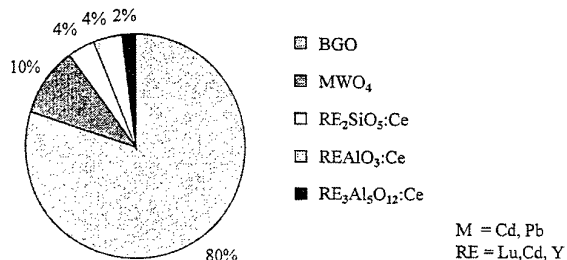
CRYSTAL PRODUCTION



OXIDE CRYSTAL PRODUCTION



OXIDE SCINTILLATION CRYSTAL PRODUCTION



KORZHIK/INP/MINSK/Sept'98

ADVANTAGES OF OXIDE SCINTILLATORS

- LONG TERM STABILITY IN OXYGEN WORLD
- MAJORITY OF THE CRYSTAL GROWTH TECHNOLOGIES ARE ACCEPTABLE TO PRODUCE OXIDE CRYSTALS

MAIN FIELDS OF APPLICATION

- HIGH ENERGY PHYSICS AND ASTROPHYSICS
- MEDICAL RADIOLOGY
- INDUSTRY
- RESEARCH

BGO	• most wide used oxide scintillator
PbWO ₄ (PWO)	• most attractive candidate for high energy physics applications in coming decade
Gd ₂ SiO ₅ :Ce	• good candidate for some applications in astrophysics and high energy physics
Lu ₂ SiO ₅ :Ce (Lu-Y)AlO ₃ :Ce YAlO ₃ :Ce	• good candidates to be applied in medical radiology and industry

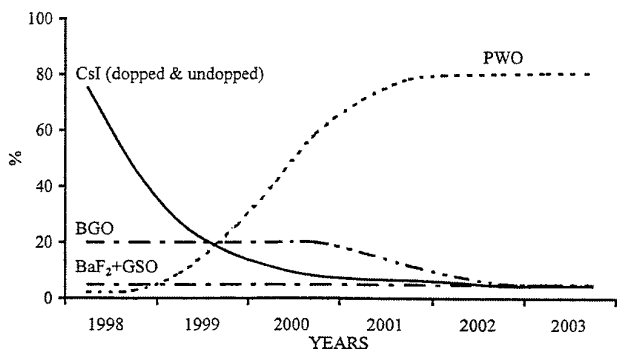
MODERN REQUIREMENTS TO THE SCINTILLATORS

REQUIREMENTS	HIGH ENERGY PHYSICS	MEDICAL RADIOLOGY	INDUSTRIAL APPLICATIONS
High density	✓	✓	✓
Fast scintillation	✓	✓	more or less
High light yield	more or less	✓	✓
Small afterglow	✓	✓	more or less
Chemical stability	✓	✓	✓

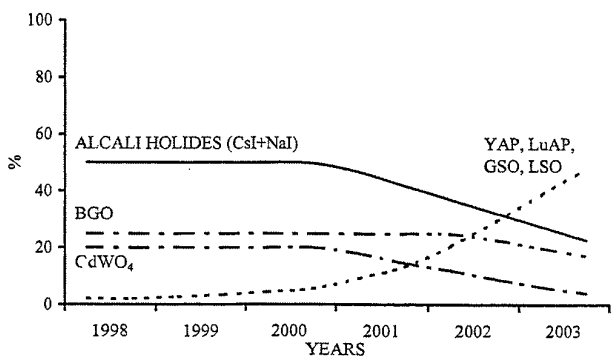
KORZHIK/INP/MINSK/Sept'98

PROSPECTS OF OXIDE SCINTILLATORS MARKET

HIGH ENERGY PHYSICS



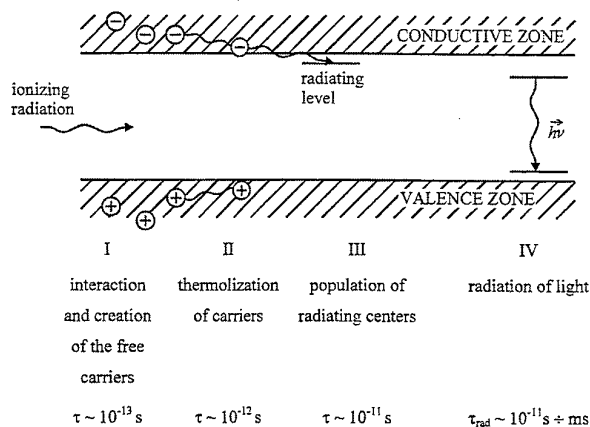
MEDICAL RADIOLOGY



KORZHIK/INP/MINSK/Sept'98

WHAT IS SCINTILLATOR?

STAGES OF THE SCINTILLATION CREATION



SCINTILLATOR • TRANSFORMATOR OF THE IONIZING RADIATION ENERGY TO THE LIGHT

YIELD OF SCINTILLATIONS

$$Y = \eta S Q$$

- η • conversion efficiency
- S • efficiency of the excitation transfer from matrix to emitting center
- Q • quantum yield of light

APPROACHES AT THE SCINTILLATION MATERIALS RESEARCH AND DEVELOPMENT

- CASUAL SEARCH OR STUDY OF THE CRYSTALS GROWN FOR ANOTHER APPLICATIONS

Majority of oxide scintillators were developed at search of new solid state media.

- SYSTEMATIC STUDY OF BRIGHTNESS AND SCINTILLATION KINETICS OF POWDERED SAMPLES OBTAINED AT SOLID STATE SYNTHESIS (Moses&Derenzo&Weber, LBL, USA)

The most completed data base for the compounds scintillating under irradiation.

Relatively cheap method of search.

- ASSOCIATION AND CONCENTRATION OF THE EFFORTS OF USERS, SOLID STATE SCIENTISTS AND CRYSTAL GROWERS

Carel W.E.van Eijk Group, Delft University, The Netherlands

Lead tungstate scintillator R&D carried out by CERN&INP&BTCP is a good example of such association.

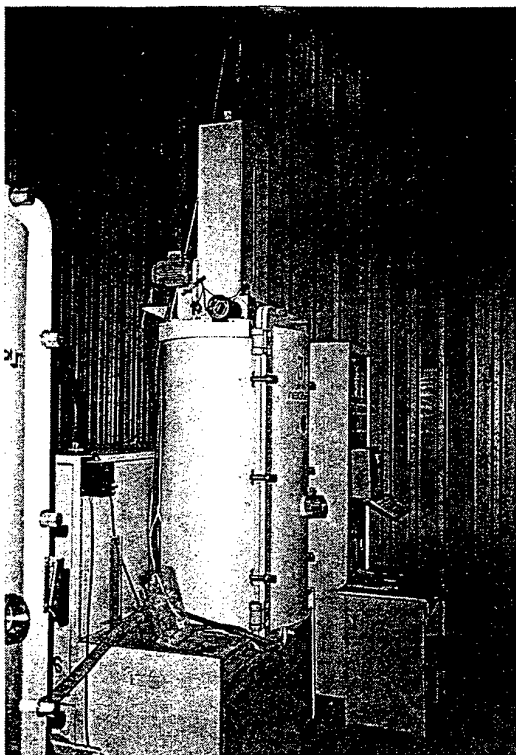
KORZHIK/INP/MINSK/Sept'98

MOST ATTRACTIVE OXIDE SCINTILLATION CRYSTALS AND THEIR PROPERTIES

SCINTILLATOR	Density, g/cm ³	Light Yield, Photon/Mev	Decay time, ns	Emission, nm	Method of the crystal growth
BGO (Bi ₄ Ge ₃ O ₁₂)	7,13	8000	300	480	Czochralski Brigeman
CdWO ₄	7,9	10000	20000	470/540	Czochralski
GSO (Gd ₂ SiO ₅ : Ce)	6,71	12500	60 (fast)	430	Czochralski
YAP (YAlO ₃ : Ce)	5,55	14000	28 ±0,2	350	Czochralski Bagdasarov (horizontal oriented crystallization)
LSO (Lu ₂ SiO ₅ : Ce)	7,41	25000	40 ±2	420	Czochralski
LuAP (LuAlO ₃ : Ce)	8.13	14000	~10	350	Czochralski
(Lu-Y)AP (Lu _{0.5} Y _{0.5} AlO ₃ : Ce)	≈7	15000	30 ±2	350	Bagdasarov (horizontal oriented crystallization)
PWO (PbWO ₄)	8,28	10	10 (eff)	420	Czochralski Modified Brigeman

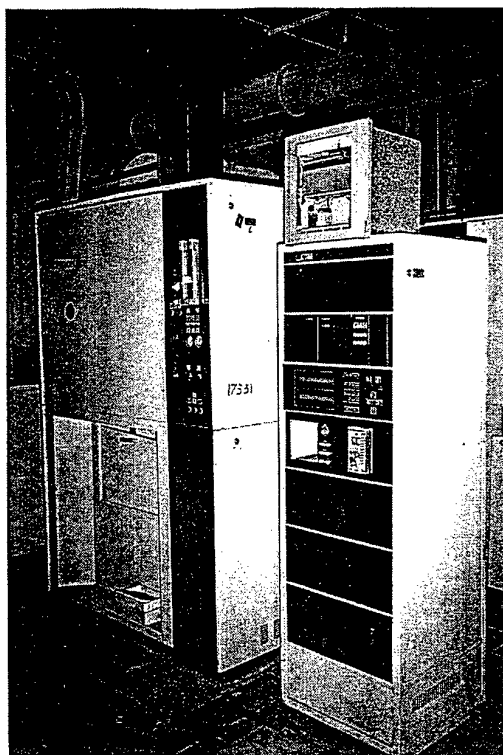
JUST STUDIED: LiLuSiO₄: Ce (high light yield); K₃Lu(PO₄):Ce (extra high light yield)

KORZHIK/INP/MINSK/Sept'98



CZOCHELSKI CRYSTAL GROWTH FURNACE

KORZHIK/INP/MINSK/Sept'98



OVEN FOR CRYSTAL ANNEALING

KORZHIK/INP/MINSK/Sept'98

SCINTILLATION MATERIALS FOR APPLICATION IN HIGH ENERGY PHYSICS EXPERIMENTS

What is essential in high energy physics experiments in coming decade?

EXPERIMENTS:

• LARGE HADRON COLLIDER (CERN)

CMS	85 thousands of PWO crystals
ALICE	30 thousands of PWO crystals

• SPS(CERN)

COMPASS	3 thousands of PWO crystals
---------	-----------------------------

• ASTROPHYSICS

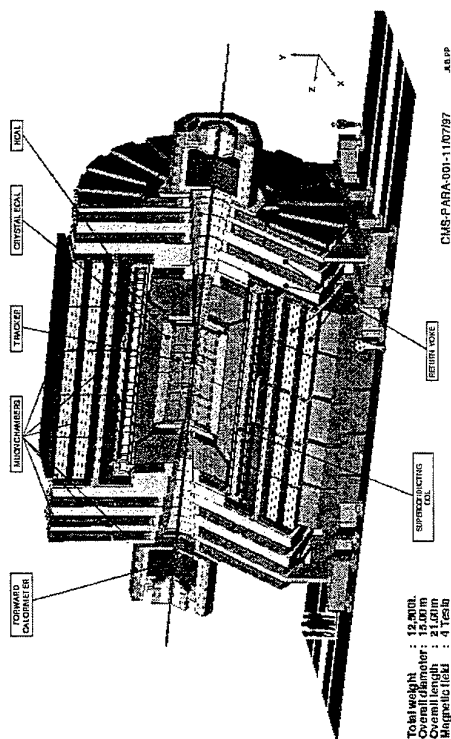
Space ALPHA Spectrometer	some thousands of BGO crystals
--------------------------	--------------------------------

• UNK(Russia)

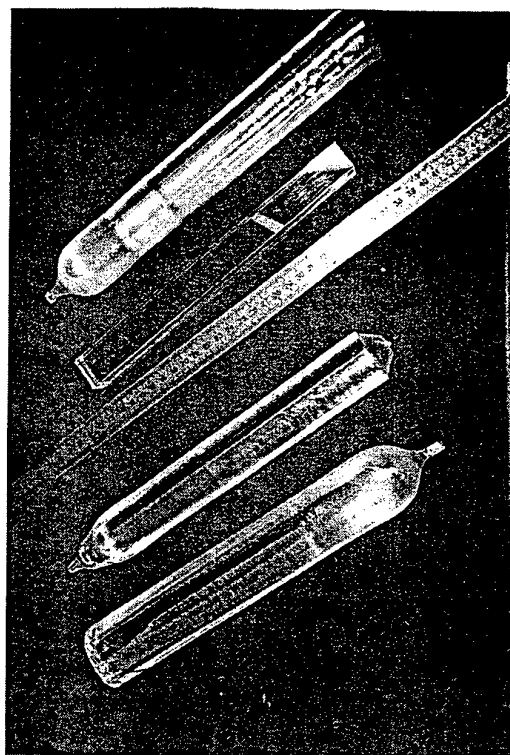
NEPTUN(?)	some thousands of PWO crystals
-----------	--------------------------------

KORZHIK/INP/MINSK/Sept'98

CMS A Compact Solenoidal Detector for LHC

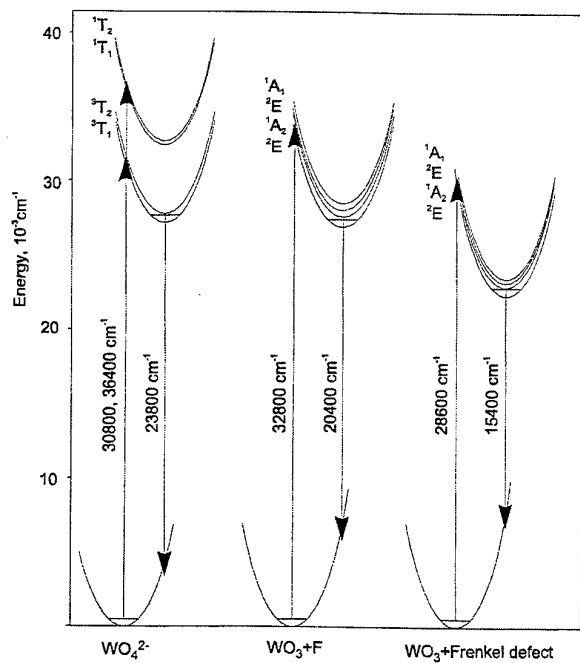


KORZHIK/CMS/Sept'98



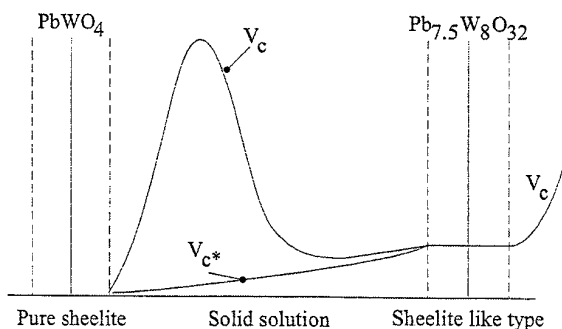
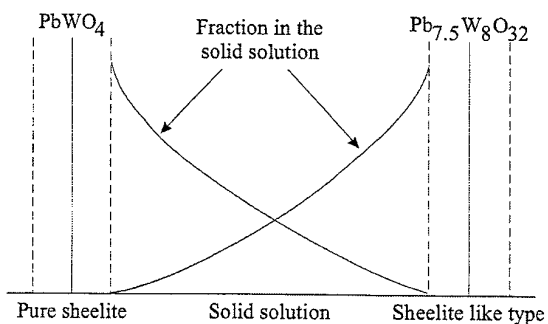
PWO INGOTS AND SCINTILLATION ELEMENTS TO BE APPLIED IN CMS ELECTROMAGNETIC CALORIMETER AT LHC

KORZHIK/INP/MNSK/Sept'98



ENERGY-LEVEL DIAGRAM OF THE OPTICAL TRANSITIONS IN PWO CRYSTALS. THE SPLITTING OF THE FIRSTS EXCITED STATES IN WO_3 GROUPS IS SHOWN.

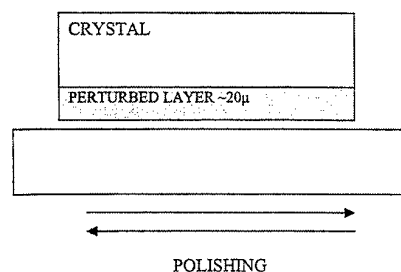
KORZHIK/INP/MNSK/Sept'98



DEFECTS IN PWO CRYSTALS WITH CRYSTAL STRUCTURE.

KORZHIK/INP/MINSK/Sept'98

SURFACE DAMAGE PHENOMENON IN PWO SCINTILLATOR



SURFACE DAMAGE APPEARS AT THE MACHINING OF THE RELATIVELY SOFT MATERIALS

IT CAUSES IN PWO CRYSTALS:

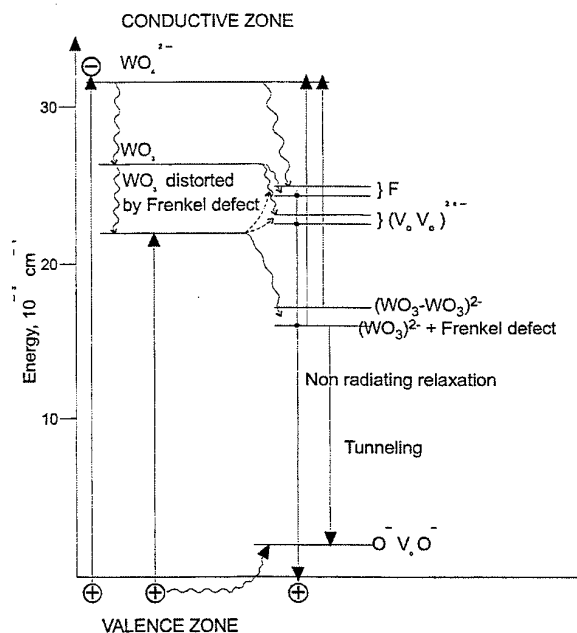
- CHANGE OF THE REFLECTING PROPERTIES OF SURFACE,
- CREATION OF THE LUMINESCENCE ABSORBING CENTERS,
- LONG TIME UNSTABILITY OF THE LIGHT YIELD.

DECREASE OF THE SURFACE DAMAGE IS VERY IMPORTANT FOR SCINTILLATORS WITH LOW LIGHT YIELD

MEANS OF THE SURFACE DAMAGE DECREASE:

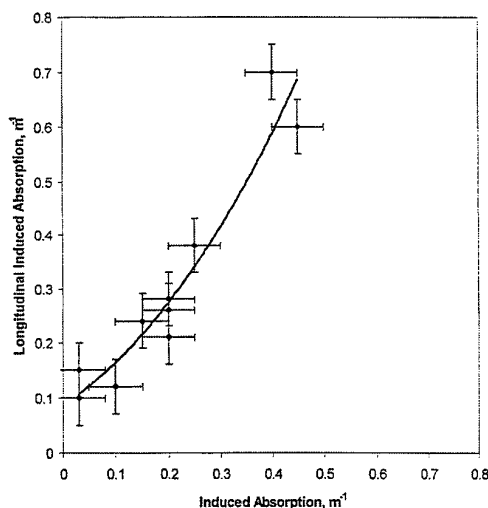
- ANNEALING,
- SLOW FINISHING POLISHING,
- CHEMICAL POLISHING

KORZHIK/INP/MINSK/Sept'98



SCHEME OF THE PROCESSES AT THE DAMAGE AND RECOVERY OF PWO OPTICAL TRANSMISSION.

KORZHIK/INP/MINSK/Sept'98



CORRELATION BETWEEN LONGITUDINAL INDUCED ABSORPTION AT 500 NM MEASURED WITH ELEMENTS OF 23 CM LENGTH (^{60}Co source, 30 krad accumulated dose) AND INDUCED ABSORPTION MEASURED WITH SAMPLES EXTRACTED FROM THE TOP PARTS OF THE SAME CRYSTALS (^{60}Co source, 100 krad accumulated dose), $T = 300\text{K}$

KORZHIK/INP/MINSK/Sept'98

Some aspects of growth technology for scintillation crystals

P.J.Li Z.W.Yin D.S.Yan

Shanghai Institute of Ceramics, Chinese Academy of Sciences

Abstract

Since the emergence of NaI:Tl in 1948, the scintillation crystals have found wide applications in radiation detection. To meet with the increasing demands of radiation detection, the growth of scintillation crystals has become an interesting branch in crystal growth studies.

On the basis of our practice, some aspects of growth technology for scintillation crystals are discussed in the second part of this presentation. It is important for crystal growers to have a good knowledge of the phase conditions of the crystals. Lead tungstate PbWO_4 (PWO) is used as an example in this respect ^[1]. The raw materials for growing scintillation crystals are in demand for high purity. However, it does not imply that it should have high purity blindly for all the elements. The request is only to lower the concentration below the specific limits of those elements which have been proven to be harmful to the performances of the crystals. BGO and PWO scintillation crystals are examples to be discussed in this front ^[2-3]. The growth conditions play a vital role in the process of crystal growth. If the growth parameters are not appropriate, it would certainly lead to the creation of all sorts of defects in the crystal giving a detrimental influence to the crystal quality. The defects which are closely associated with the inappropriate growth conditions and the measures for eliminating these defects are discussed ^[4-5]. In addition to the elimination of thermal stress, annealing would play another role in improving the scintillating performance of the crystals. As an example, the improvement of scintillating properties of PWO crystal through annealing in oxygen atmosphere is reported ^[6].

In the third part of the presentation, examples of scintillation crystal growth are described. We have developed a modified Bridgman technology for mass production of large size high quality BGO crystals. Technical difficulties in the

growth of BGO crystals from melt at high temperatures for long period of time were discussed^[7-8]. By using Bridgman technology in vacuum with a scavenger to remove the oxygen contamination and optimizing the growth conditions during the whole growth process, we have succeeded in growing large size high radiation resistant BaF₂ crystals^[9]. The non-vacuum Bridgman technology was newly developed successfully to grow large size CsI:Tl and PbF₂ crystals with good quality on the basis of the method that had been used to grow oxide scintillation crystals in air^[10-11].

Acknowledgements

We would like to thank our colleagues from the SICCAS working on scintillation crystal growth for their fruitful results that have been summarized in this presentation. This work was partly supported by the National Natural Science Foundation of China, Project No.59732040.

Reference

- [1] J.Y.Liao et al., J. Inorganic Materials 12 (1997) 286
- [2] T.Q.Zhou et al., Nucl. Instr. Meth. A258 (1987) 58
- [3] R.Y.Zhu et al., ibid A376 (1996) 319
- [4] Z.W.Yin et al., J. Inorganic Materials 6 (1991) 391
- [5] J.Y.Liao et al., J. Inorganic Materials 12 (1997) 228
- [6] Z.W.Yin et al., Proceedings of the International Conference on Inorganic Scintillators and Their Applications, Shanghai, China Sept. 22-25, 1997 p.191
- [7] C.F.He et al., Prog. Crystal Growth and Charact. 11(1985) 253
- [8] S.J.Fan et al., Crystal Properties and Preparation 36-38 (1991)42
- [9] P.J.Li et al., Proceedings of the Fourth Annual International Symposium in Super Collider, March 4-6, 1992 New Orleans, USA, in Supercollider 4 ed J.Nonte, Plenum Press (1992) 801
- [10] D.Z.Shen et al., Chinese Patent No. CN1113970A
- [11] D.Z.Shen et al., Chinese Patent No. CN1093419A

In the years ensuing, we have been working on R & D of several kinds of scintillation crystals, both oxides and halides such as PWO , BaF_2 , CeF_3 , CsI:TI , PbF_2 etc.

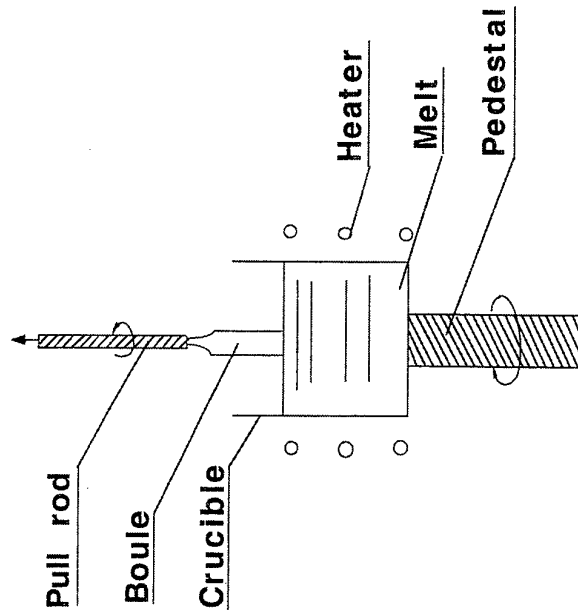
1. Introduction

2. Some aspects of growth technology for scintillation crystals

- Phase conditions
- Raw materials
- Growth conditions and related defects
- Annealing

3. Examples of scintillation crystal growth

BGO , BaF_2 , CsI:TI , PbF_2



Czochralski method

Since the beginning of 1980s
SIC had started R&D on BGO crystal

Modified Bridgman technology
for mass production of large size
high quality BGO crystals

Delivered 11,000 pcs, 12 tons
large size BGO crystals for L3
experiment of Large Electron-
Positron Collider at CERN

Raw materials

High purity 5-6 N

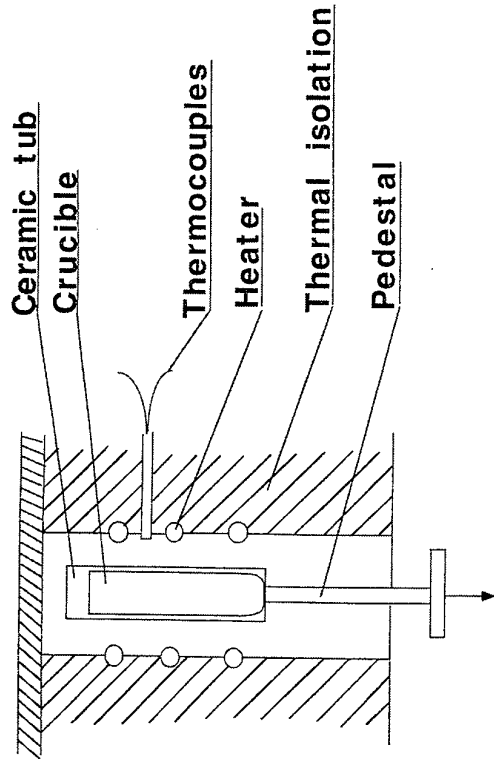
**High purity not for all elements
To lower the concentration
of harmful elements**

Grow doped crystals

Growth conditions

**Segregation coefficient
of dopant**

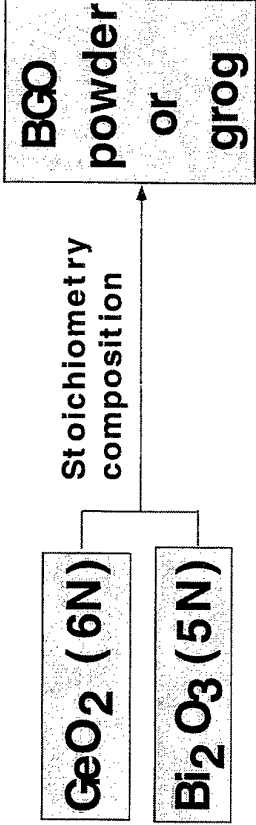
Bridgman method



**It is important for crystal growers
to have a good knowledge
of phase conditions of the crystals,
especially in the initial stage of
growing a new crystal.**

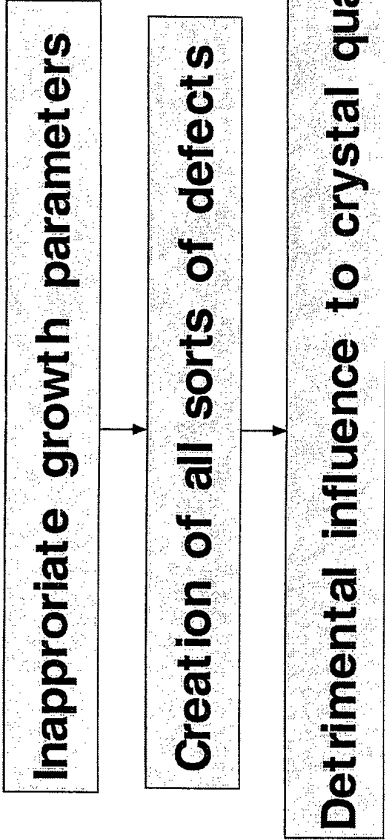
BGO crystal

Bridgman furnaces were designed and manufactured by ourselves

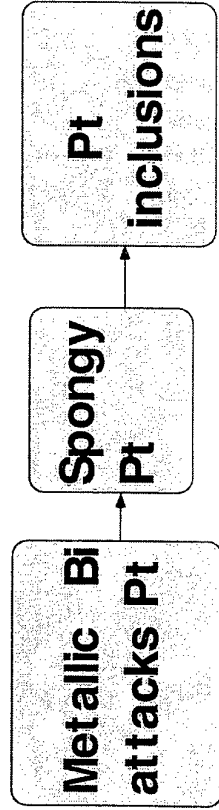


Temperature oscillation < ± 0.5 °C

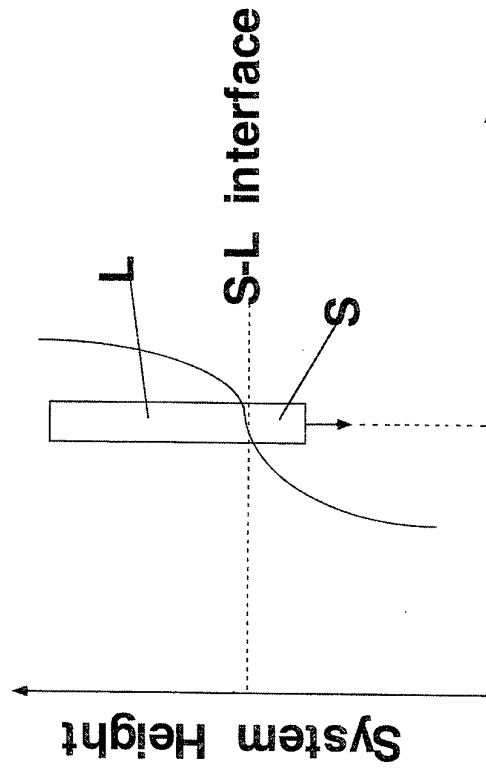
Growth conditions play a vital role in crystal growth



Bi poison



Pt can be recycled



Thermal profile in Bridgman furnace

Growth conditions for PbF₂

Max. temperature 950 °C
Soaking time 6-8 hrs
Thermal gradient 20-30 °C / cm
near S-L interface
Crystal growth speed 0.8-2.0 mm/ hr
Cooling rate ~20 °C / hr

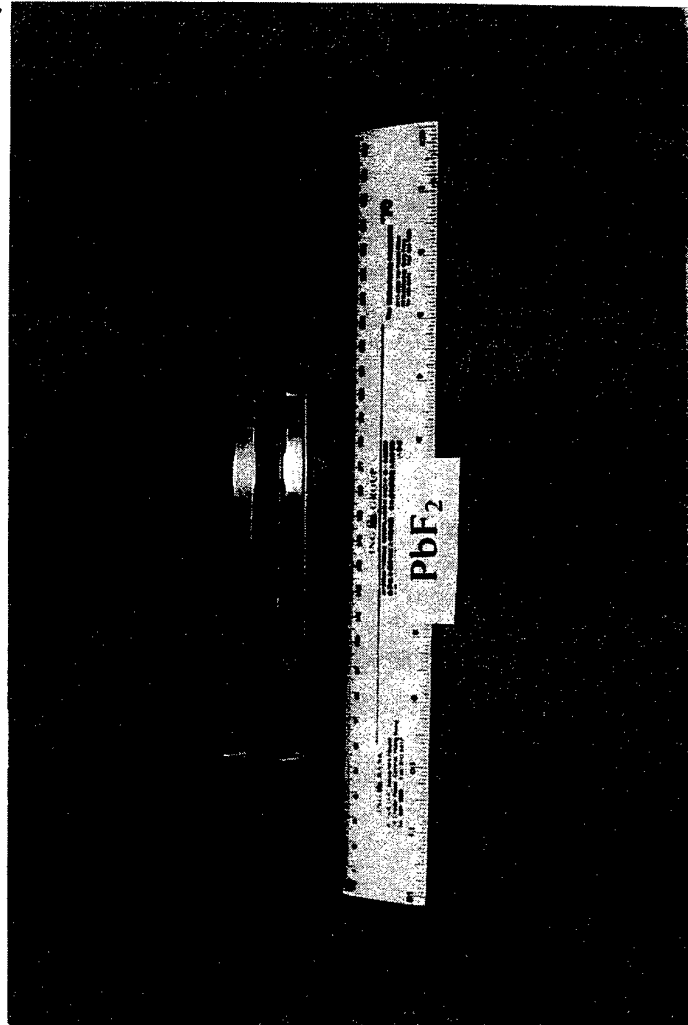
Bridgman method

Grow oxide scintillation
crystals in air

Grow halide scintillation crystals
under non-vacuum conditions

Growth conditions for CsI:Tl

Max. Temperature ~720 °C
Soaking time 6-8 hrs
Thermal gradient ~35 °C / cm
near S-L interface
Growth speed 1 ~2.5 mm/ hr
Cooling rate 20 °C / hr



HALOGENIDE SCINTILLATORS. CRYSTAL GROWTH & PERFORMANCE

A.Gektin

Institute for Single Crystals, 60, Lenin Ave., Kharkov, Ukraine

Introduction

The history of investigation and application of alkali halide single crystals counts doses of years. Recently, such type crystals (Fig.1) are applied for the registration of ionizing radiations. With this, the halogenide scintillators are among the most widespread type of scintillation materials. As a matter of fact they represent two classes of crystals. Firstly, it is alkali halide scintillators (Fig.2) and secondly, it is fluoroperovskites (Fig.3).

The main fields of application of such scintillators – high energy physics, nuclear medicine, geophysics, environmental, security systems (Fig.4). Each kind of application requires special properties of the material. As a result, an ideal scintillator must possess a combination of unique properties (Fig.4).

It should be noted that the modern applications require large size detectors. Thus, detectors for medical diagnostics have the size, comparable with that of the human body. Colorimeters for high energy physics consume thousands of scintillators tens tons in the total weight. The main requirements to the scintillation crystals follow directly from the principles of scintillation origination and registration (Fig. 5).

Apparatus and methods of halogenide scintillators growth

The history of elaboration of methods for growing halogenide crystals lasts for more than 50 years. The 70-s became a turning-point in the development of industrial growth technologies (Fig.6). That time two approaches were separated. The first was based on the creation of big installations for conventional Bridgeman-Stockbarger method. Disadvantages of this method (weak convective mixing of the melt near crystallization front, contact of crystal with crucible, nonuniformity of activator distribution along the crystal) create difficulties for the growth of large crystals. The second was based on the elaboration of automated crystal growth technologies eliminating the contact of the crystal with the crucible.

The main ideas and technical solutions were feeding of the melt in the process of crystal pulling and growth parameter regulation by means of the melt level control. Feeding procedure was realized both with a powder (Fig.7) and with melt (Fig.8). Automation of the pulling process specified for a stabilization of the mass growth rate or crystal diameter is implanted with a help of the melt level sensor. In the both cases the maintenance of levelling the balance owing to the feeding with raw material allows to control both the shape and size of the crystal and its structure perfection.

The procedure of crystal growth is schematically shown in Fig.9. The equations of the mass balance allow to describe all the stages of the process (Fig.10). It should be noted that the

feeding can proceed by both pure and doped raw material. This gives a possibility to vary the residual amount of impurity in the melt. As a result, crystals to 750 mm in length can be grown. The dopant content in them is uniform (the error does not exceed 2-3%).

Uniformity of the material properties is defined by a continuity of the process. The abrupt changes in the pulling rate lead to the nonuniformity of distribution of scattering and activator centers (Fig.11).

Physico-chemical aspects of growing halogenide crystals.

A specific character of scintillation application of halogenide crystals requires crystals with a controlled content of the intrinsic defects and composition of foreign impurities. Otherwise, the relaxation of electronic excitations on foreign defects results in the advent of the outside luminescence and decrease of scintillation efficiency (Fig.12). Most typical is the appearance of emission of different oxygen-containing impurities which can be separated into the main groups. All of them are connected with the interaction of the initial raw material and the melt with the components of air atmosphere.

Possibilities of modern apparatus for the growth of halogenide crystals, for additional purification of raw material with the purpose to obtain super pure crystals were analyzed.

ABX₃ perovskites.

ABX₃ perovskites can be used for scintillation application both in the form of pure crystals and after their doping (Fig.13). Such crystals are grown by the high pressure vertical Bridgman method at the inert gas. This procedure is necessary for preserving stoichiometry of crystals during all the process of their growth.

Introduction of RE ions into crystals (first of all Ce) allows: to shift emission to a longer wave-length region of the spectrum (which is convenient for registering devices), to regulate the decay times (Fig.14, 15).

Oxygen-containing impurities in halogenide perovskites are the most harmful ones. Their presence leads not only to the appearance of a parasite afterglow but also enhances significantly the effect of energy storage (Fig.16). Moreover, it turned out that a complex doping of crystals KMgF₃(Eu,O) converts the scintillator to the storage phosphore on the whole. Such crystals are efficient dosimetric materials.

Conclusion.

In spite of the simplicity of the basic methods of crystal growth there is a big number of special technical solution and technologies directed at growth of crystals with prespecified parameters. Special requirements to halogenide scintillators force to carry out additional R&D. The main trends in scintillation material science are: increase of crystal size, increase of radiation resistance of the material, decrease of the afterglow level, etc. Therefore, the problem of elaboration of "ideal" method for growing such crystals remains open.

Alkali Halide Single Crystals Applications

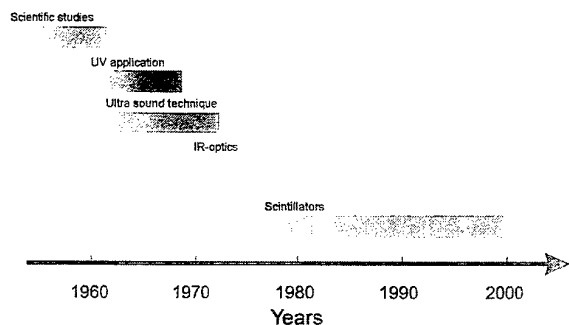


Fig. 1.
A. V. Gektin, "Halogenide Scintillation"

Physical Properties of Alkali Halide Scintillators

	NaI(Tl)	CsI(Na)	CsI(Tl)	CsI (undoped)	CsI(CO ₂)	LiF(W)	LiF(Eu)
Density [g/cm ³]	3.67	4.51	4.51	4.51	4.51	2.64	4.08
Melting point [K]	924	894	894	894	894	1133	719
Thermal expansion coefficient [K ⁻¹]	47.4·10 ⁻⁶	49.10 ⁻⁶	54.10 ⁻⁶	49.10 ⁻⁶	49.10 ⁻⁶	37.10 ⁻⁶	40.10 ⁻⁶
Cleavage plane	<100>	none	none	none	none	<100>	<100>
Hardness (Moh)	2	2	2	2	2	3	2
Hygroscopic	yes	yes	slightly	slightly	yes	no	very
Wavelength of emission maximum [nm]	415	420	550	315	405	430	470
Refractive index at emission maximum	1.85	1.84	1.79	1.95	1.84	1.4	1.96
Light output [% of NaI(Tl)] (for γ-rays)	100	85	45	5-6	60	3.5	30-35
Primary decay time [μs]	0.23	0.63	1	0.01	2	40	1.4
Afterglow (after 6 ms) [%]	0.3-5	0.5-5	0.1		0.06		
Lower wavelength cutoff [nm]	300	300	320	260	300		425

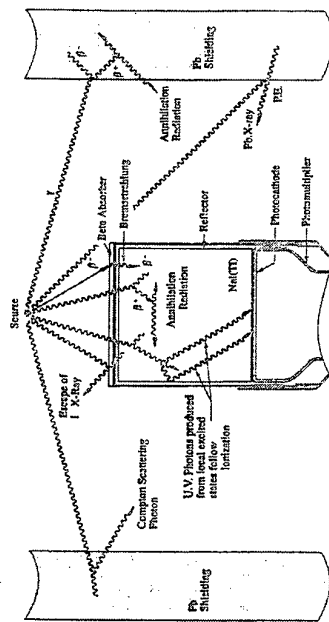
Fig. 2.
A. V. Gektin, "Halogenide Scintillation"

Perovskite Scintillators Core-Valence Transitions

Crystal	Emission, eV	Excitation, eV	τ, ns	Light yield, %
LiBaF ₃	5.0-7.6	18	0.8	0.4
KMgF ₃	5.3-9.1	22	0.9	0.6
KCaF ₃	6.0-8.9		< 2	0.6
RbMgF ₃	2.8-6.2		2.0	0.1
RbCaF ₃	3.0-5.8	16.8	2.8	≥ 1.0
CsMgCl ₃	2.6-5.6	14.1	2.1	1.0
CsCaCl ₃	3.1-5.5	14.0	1.7	≥ 1.0
CsSrCl ₃	3.2-5.4	13.7	2	1.0
CsCaBr ₃	3.2-6.0	14.0	2.3	0.01
CsSrBr ₃	3.1-6.0	14.0	2.6	0.01

Fig. 3.
A. V. Gektin, "Halogenide Scintillation"

Scintillations Registration



Scintillator efficiency (χ)

$$\chi = \alpha \beta S Q$$

where

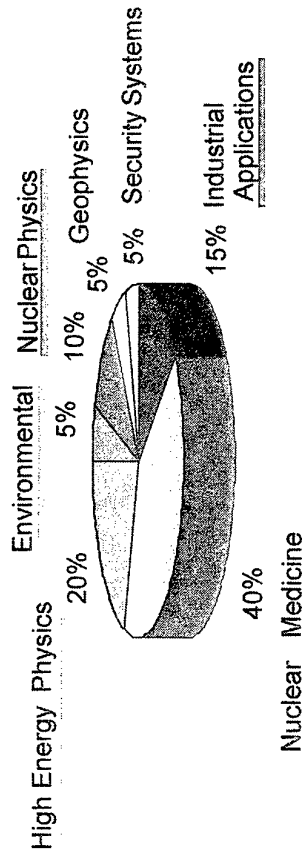
α - eight collection coefficient *

β - conversion efficiency

S - transfer efficiency *

Q - luminescence quantum yield

(*) depends on structure perfection



Ideal Scintillation Material

1. High density and atomic number
2. High light yield
3. Fast response
4. High transparency
5. Convenient emission range
6. Radiation stability
7. Large size of single crystal
8. Low cost

Fig. 5.

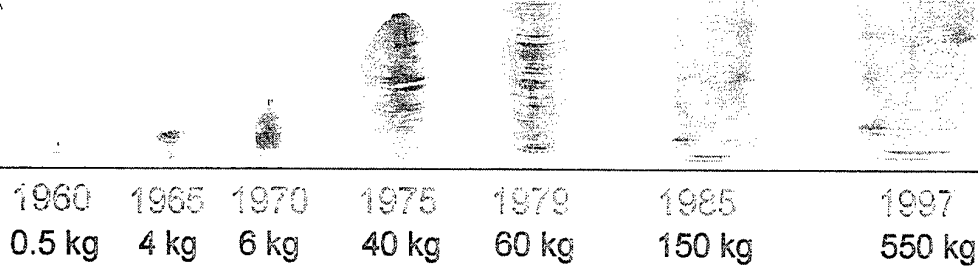
A. V. Gektin, "Halogenide Scintillation"

Fig. 4.

A. V. Gektin, "Halogenide Scintillation"

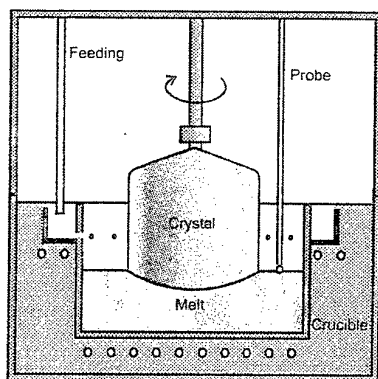
Halogenides Growth Technology Milestones

Fig. 6.
A.V. Gekin, "Halogenide Scintillation"



Crystal Growth Technology "ROST"

Fig. 7.
A.V. Gekin, "Halogenide Scintillation"



$$\frac{\pi d^2}{4} (v_{yp} - v_k) \rho_s = \frac{\pi D^2}{4} v_{yp} \rho_l - v_n$$

where v_n - feeding rate

$$\bar{d} = \frac{D^2 v_{yp} \rho_l - \frac{4}{\pi} v_n}{\rho_s (v_{yp} - v_k)}$$

at $v_{yp} = 0$

$$\bar{d} = \sqrt{\frac{4v_n}{\pi \rho_s v_k}}$$

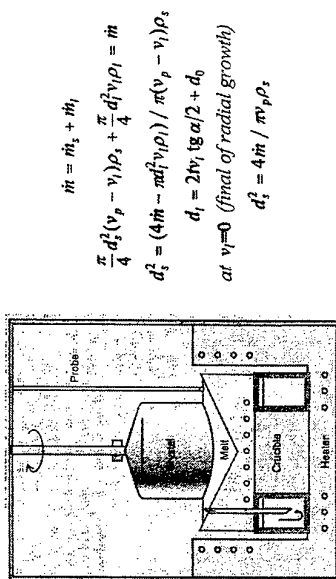


Fig. 8.
A. V. Gektin, "Halogenide Scintillation"

Material balance at automated growing

$$\dot{m} = \dot{m}_s + \dot{m}_L \quad (1)$$

\dot{m} — feed rate, \dot{m}_s — growth rate, \dot{m}_L — melt mass rate

Total mass balance is

$$\pi [d_s(t)]^2 (v_p - v_L) \rho_s + \pi [d_L(t)]^2 \cdot v_L \cdot \rho_L = 4 \dot{m}, \quad (2)$$

where v_p and v_L , $d_s(t)$ and $d_L(t)$; ρ_s and ρ_L — growth rate, diameter of crystal and melt surface, density of the crystal and melt.

For conic (α) crucible

$$d_L(t) = 2t \cdot v_L \cdot \operatorname{tg} \alpha / 2 + d_0, \quad (3)$$

At $v_L = 0$ (radial growth finish)

$$d_s(t) = (4 \dot{m} / \pi \cdot v_p \cdot \rho_s)^{1/2}, \quad (4)$$

Feeding mass rate is

$$\dot{m} = \Delta m_0 / \Delta \tau = \pi \{ [d_L(t)]^2 - [d_s(t)]^2 \} \cdot \Delta h \cdot \rho_L / 4 \Delta \tau \quad (5)$$

where Δh — meniscus height, $\Delta \tau$ — feeding period

Feeding frequency is

$$1/\Delta \tau = [d_s(t)]^2 \cdot v_p \cdot \rho_s / \{ [d_L(t)]^2 - [d_s(t)]^2 \} \cdot \Delta h \cdot \rho_L. \quad (6)$$

Fig. 10.
A. V. Gektin, "Halogenide Scintillation"

Crystal Growth Stages ("Crystal" Technology)

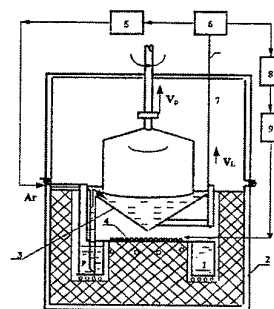
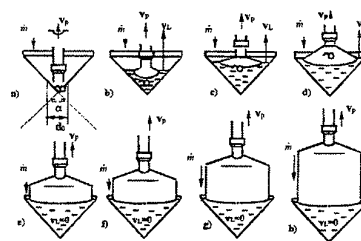
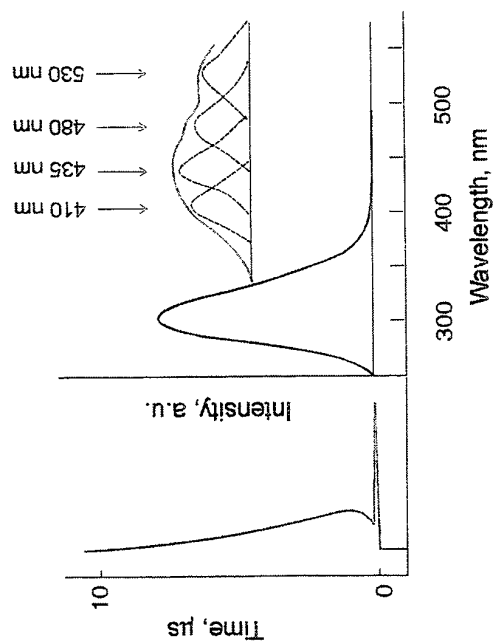


Fig. 9.
A. V. Gektin, "Halogenide Scintillation"

Scintillation Pulse and Emission Spectra of CsI

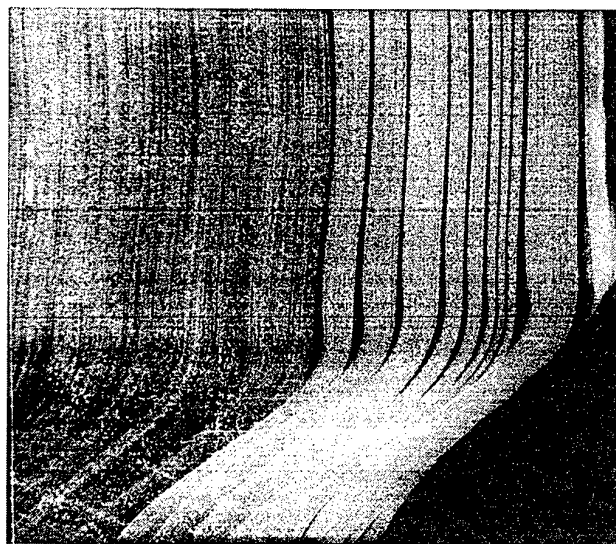


Afterglow Centers in CsI Crystals

1. O_2^- - center; $\lambda_m \approx 480-700$ nm
 $\tau \approx 6-25$ μ s
2. CO_3^{2-} - center; $\lambda_m \approx 410$ nm
 $\tau \approx 1.4-2$ μ s
3. $O^{2-}v_c^-$ - center; $\lambda_m \approx 435$ nm
 $\tau \approx 2-8$ μ s
4. Vacancy type $\lambda_m \approx 460-480$ nm
centers; $\tau \approx 2-8$ μ s

Fig.13.
A.V.Gektin, "Halogenide Scintillation"

Structure Nonuniformity After Growth Rate Variation



(Scattered light)

Fig.11.
A.V.Gektin, "Halogenide Scintillation"

Decay time spectra of pure and Ce doped LiBaF₃

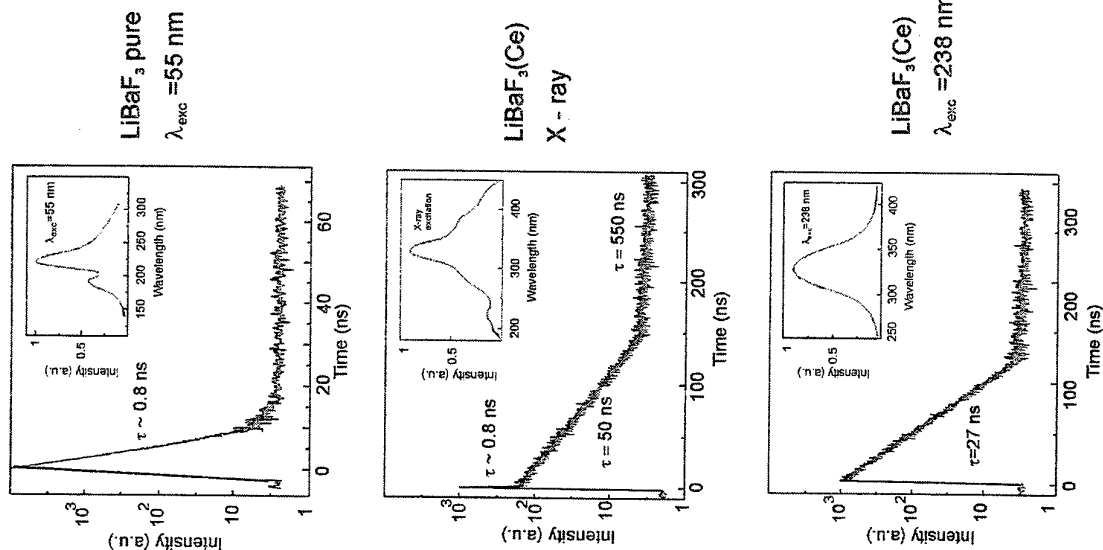


Fig.15.
A.V.Gektin, "Halogenide Scintillation"

KMgF₃(Ce) - Scintillators

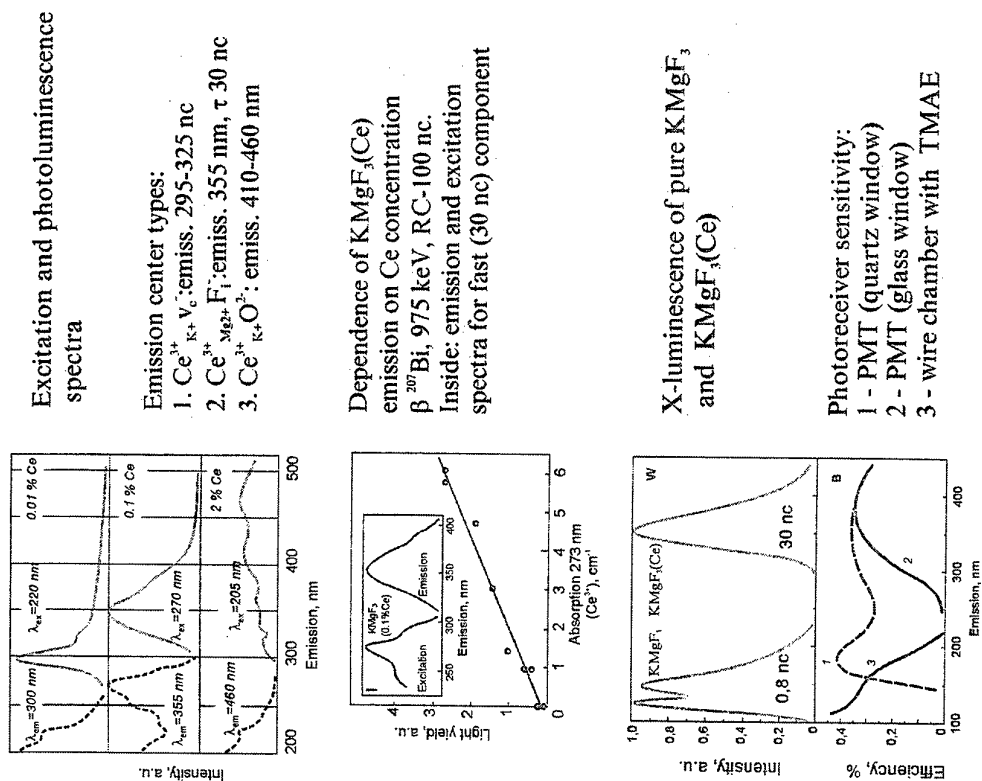


Fig.14.
A.V.Gektin, "Halogenide Scintillation"

Energy store and release in $\text{KMgF}_3(1)$, $\text{KMgF}_3(\text{O}^-)(2)$

Physical Properties of KMgF_3 and LiBaF_3 -based Crystals

	KMgF_3	$\text{KMgF}_3(\text{Ce})$	LiBaF_3	$\text{LiBaF}_3(\text{Ce})$
Density $[\text{g/cm}^3]$	3.2	3.2	5.24	5.24
Atomic number	12.9	12.9	55	55
Hygroscopic	no	no	no	no
Melting point $[\text{K}]$	1070	1070	857	857
Wavelength of emission maximum $[\text{nm}]$	130-160	355	195-220	325
Primary decay time $[\text{ns}]$	1.3	27	0.8	27
Light output $[\% \text{ of NaI(Tl)}]$	~ 5	10	~ 1	10
Light output, photons/MeV	1800	3800	~ 1800	3800

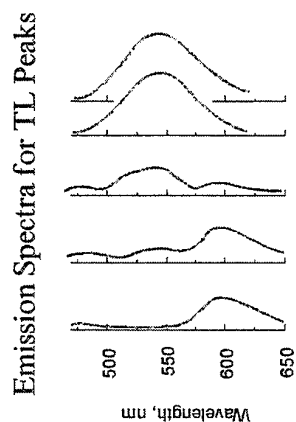
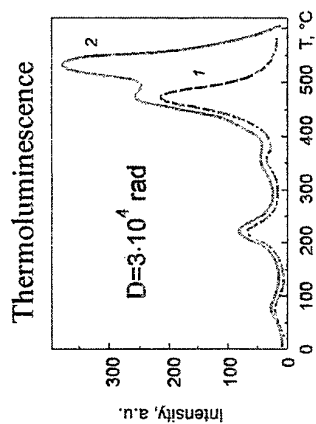


Fig.17.
A.V.Gektin, "Halogenide Scintillation"

Fig.16.
A.V.Gektin, "Halogenide Scintillation"

Growth of shaped high temperature oxides

L.Lytvynov. Institute for single crystals, Ukraine

Due to the ever-increasing demand for shaped high temperature oxide crystals (sapphire and others) new, more efficient methods for their growth have been recently elaborated. They allow to grow sapphire crucibles, vessels with diaphragms and ribs, vessels with a varying over the length cross-section etc. Such profile are grown using special modifications of the Stepanov (EFG) method. The modifications are as follows:

- Making small crucibles by growing «bamboo-like» crystal and cutting it into multiple crucibles.

- Obtaining big crucibles by seeding the crystal on a seed in the form of a thin plate (the bottom of the future crucible), hanging on hooks or by the intergrowth of the latter with crystal rod. A special dice has been designed for prevention of shape distortion near the bottom due to the loss of stability. The latter is a result the difference in pressure inside and outside of the close cavity, which is formed during the growth process.

- Simultaneous coaxial growth of different size or hollow type profiles which are formed one in another.

- The coaxial growth also allows to grow several kinds of crystals simultaneously including crystals of decomposing compounds which can be grown in a closed space from the inner crucible.

- Obtaining complex products by «welding» under thermal and force impact, crystallography and structural perfection of a «welded» sapphire fragments being taken into account. There are already several directions of this method: creation of chemical apparatus of sapphire or ruby, their compositions, hardening of functionally important load-bearing elements [1].

Methods control of crystal structure control (besides described before ones [2]):

- Growth of the profiles group with buffer heating profile of the same composition.
- Growth of crystals with simultaneous coating with reflection layer which allows to decrease the residual tensions, to increase crack resistance.

The aim of the methods of structure perfection control is to improve the crystal structure or to form of the required density of defects in the assigned zones. It is necessary for many profiles which are used in medicine. In these items structural defects can improve the functional properties.

The Stepanov method allows to localize the high density of the structural defects (pores, dislocations, vacancies, vacancies' complexes) in the specified zones better than any other method. It is achieved by using a special shape of the die. The die defines the locations of the collisions of melt streams near the butt-end of the die or with its meniscus. Practically these collisions may be formed at any point of the profile cross-section. The density of structure defects increases of several tens of times.

Structural defects on the surfaces of sapphire medical implants promote the growth of dense joint tissue on the implant surface. This phenomenon provides a more quick adaptation of sapphire implant in the organism.

The sapphire product for technical application with assigned density of defects are designed for metallurgy, laser equipment, etc. The local structural defects located in these products intensify the functional properties of a series of devices.

Seemingly we deal with a principally new approach to structural defects.

REFERENCE:

- 1.H.R.Dobrovinskaya, L.A.Lytvynov, V.V.Pischik. Single crystals of corundum. Kiev. 1994.255 (on Russian).
- 2.Shaped crystal growth. Edited by G.W.Cullen, T.Surek. Amsterdam. 1980.

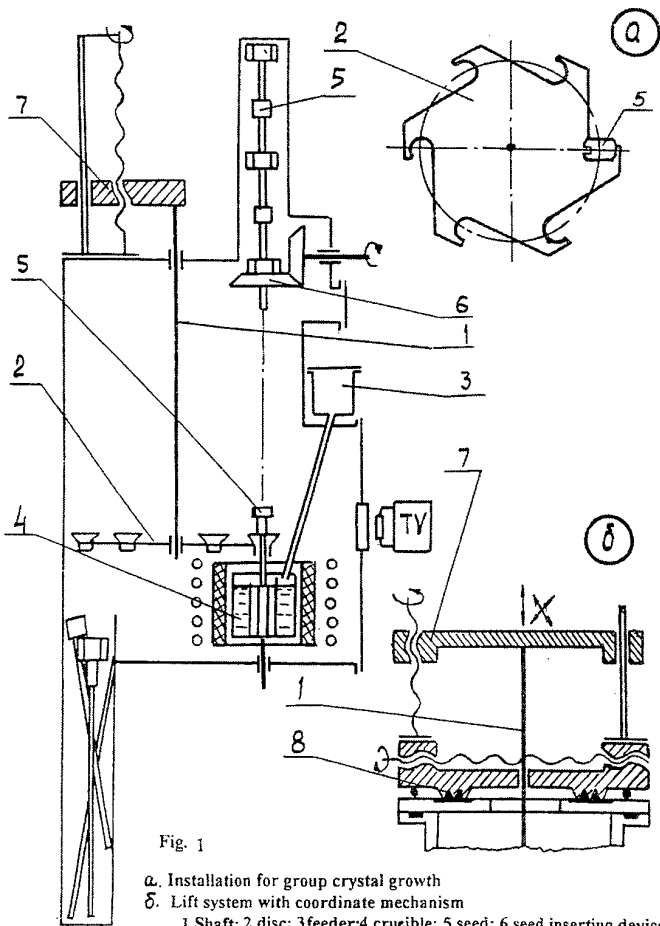


Fig. 1

a. Installation for group crystal growth

б. Lift system with coordinate mechanism

1. shaft; 2. disc; 3. feeder; 4. crucible; 5. seed; 6. seed inserting device; 7. screw pair; 8. magnetic lock.

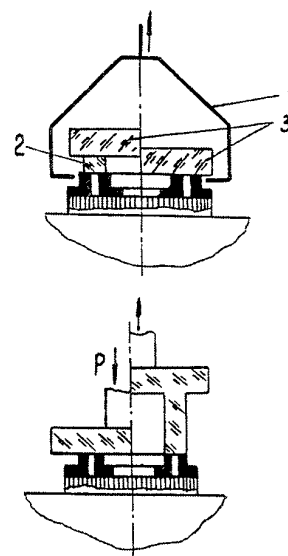


Fig. 2 Device for seeding by disc

1. support; 2. distance ring; 3. seed disc; 4. crystal rod.

Item	Crystal holder type	Seed plate		T, K	dT/dr K/cm	P, Kg/mm ²	Time of endurance test under loading	$\sigma_{comp} / \sigma_{Al_2O_3}$
		Thickness mm	Diameter mm					
Sapphire crucible D=5mm, wall thickness - 1mm	Sapphire rod D=1.5mm	1	8	1770	50	5.0	5	0.05
				1820	50	5.0	5	0.16
				2070	150	3.5	3	0.30
				2220	300	2.0	1	0.40
Sapphire crucible D=28 mm, wall thickness - 2mm	Sapphire pipe D=6 mm, wall thickness - 2mm	2.5	30	1770	50	5.0	10	0.01
				1820	50	5.0	5	0.02
				2070	150	3.0	3	0.30
				2220	300	2.0	2	0.45
				2270	300	2.0	2	0.60

σ_{comp} , $\sigma_{Al_2O_3}$ - values of tensile strength for compound and sapphire correspondingly

Fig. 3 Parameters of the process of two stage seeding and seed compound strength with crystal holder.

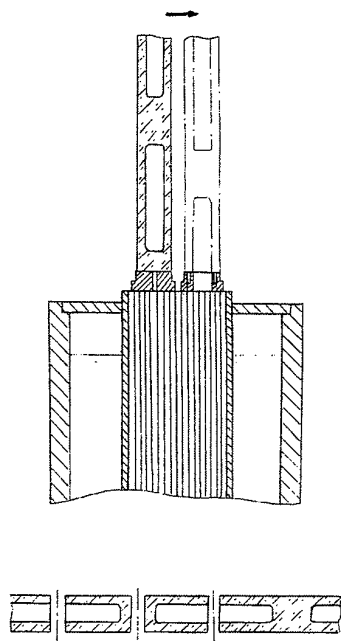


Fig. 4 Obtaining of «bamboo-like» crystals for crucibles.

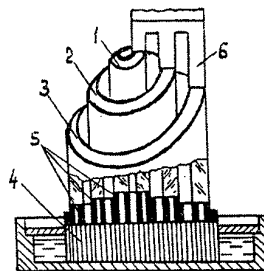


Fig. 5 Coaxial growth of tubes
1,2,3-tubes; 4.capillary; 5.dice; 6.seed.

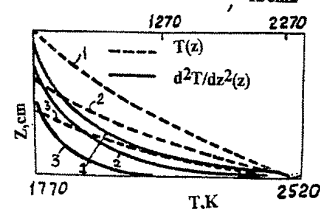


Fig. 6 Heat distribution in 3-coaxial tubes system

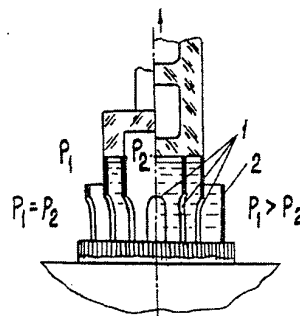


Fig. 7 Device for changing pressure in the growing closed vessel
1.Arch; 2.ring.

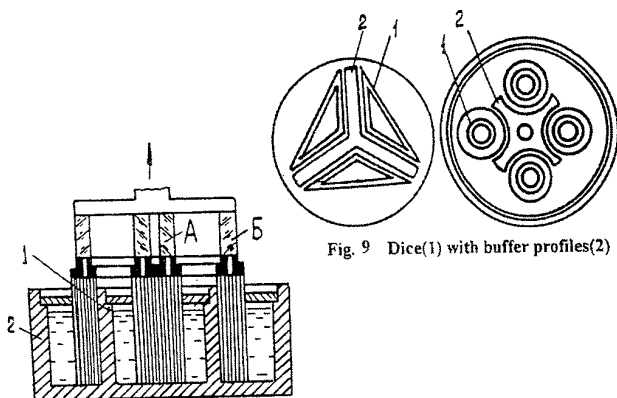


Fig. 8 Coaxial growth of different kinds of crystals
1.Inner crucible; 2.outer crucible

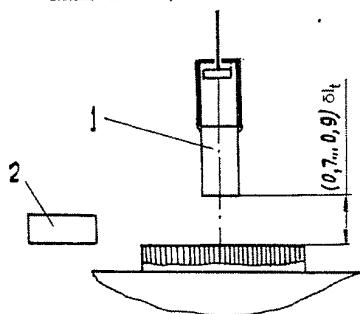


Fig. 10 Seeding by δI_t
1.«Swimming» seed; 2.videcon.

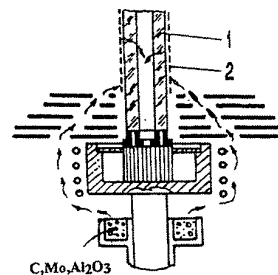


Fig. 11 Growth and coating process
1.Crystal; 2.coating layer

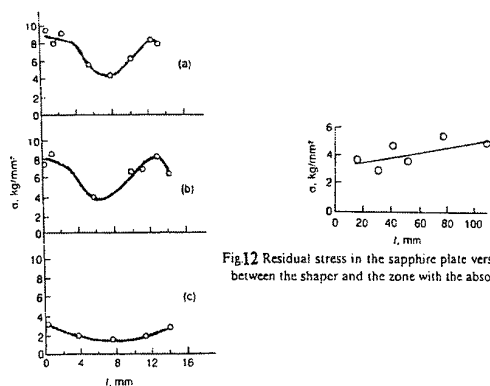


Fig.12 Residual stress in the sapphire plate versus the distance between the shaper and the zone with the absorbing coating.

Fig.13 Distribution of residual stresses in the width dimension of the sapphire plate crystal: (a) without absorbing coating on the crystal surface; (b) with a coating of optical density 1; (c) with a coating of optical density 2.

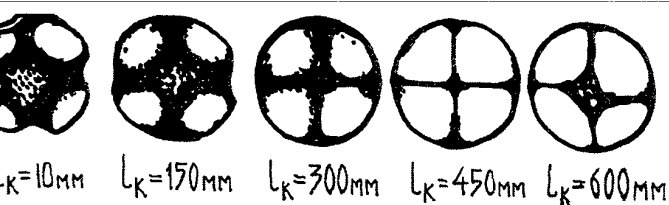


Fig. 14 Bubbles distribution in cross sections of sapphire profile. Multi-capillary replenishment

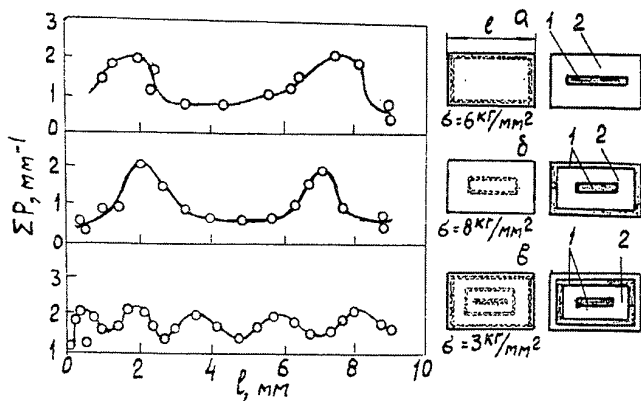


Fig. 15. The scheme of distribution of pores (a, δ, ϵ) and variation of grain boundary length in the thickness cross section of sapphire plate crystals. 1-Capillary, 2-die.

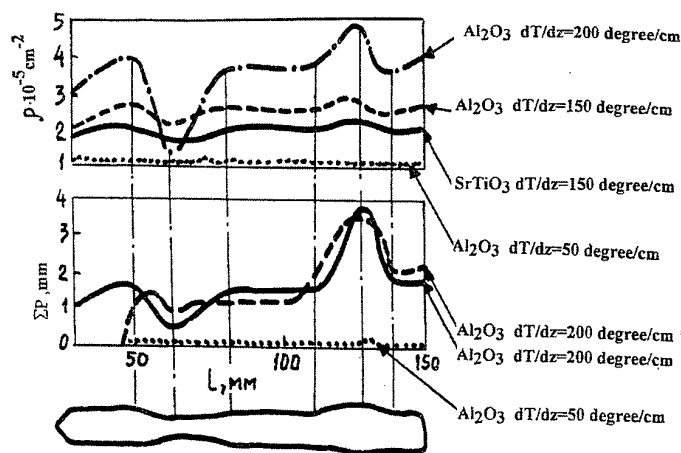


Fig. 16 Sensitivity of ρ and ΣP to the shape changing

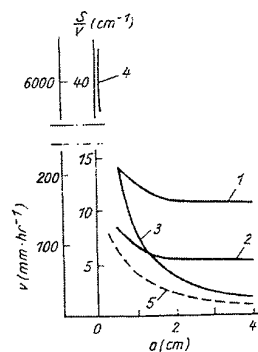


Fig. 17 Dependence of the ratio S/V and the growing rate on the characteristic cross dimension a of the profile crystals: 1 - bud, 2 - tube, 3 - prism, 4 - filaments, 5 - monocrytals grown by Czochralski

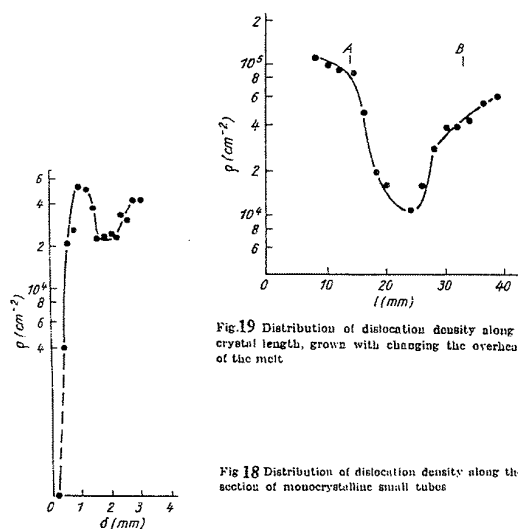


Fig. 19 Distribution of dislocation density along the crystal length, grown with changing the overheating of the melt

Fig. 18 Distribution of dislocation density along the cross section of monocrytalline multi tubes

Thickness of wall

Fig. 20 Critical density of dislocations

Method	$\rho_{kp}^{(0001)}, \text{cm}^{-2}$	$\rho_{kp}^{(11\bar{2}0)}, \text{cm}^{-2}$
Verneuil	$(3...6) \cdot 10^3$	$(5...8) \cdot 10^3$
Stepanov	$(1...4) \cdot 10^5$	$(3...6) \cdot 10^5$
Czochralski	$(5...7) \cdot 10^4$	$(6...8) \cdot 10^4$
Dir. Cr.	$(2...3) \cdot 10^4$	$(4...5) \cdot 10^4$
Kyropulos	$(7...9) \cdot 10^3$	$(1...2) \cdot 10^4$

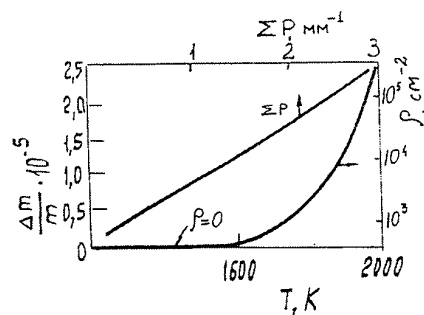


Fig. 21. Corrosion resistance and structure perfection of sapphire items

$$\Delta = 2(a_{A1} - a_{B1})(a_{A1} + a_{B1}) + 2(a_{A2} - a_{B2})(a_{A2} + a_{B2}) + 2(\Phi_A - \Phi_B)/(\Phi_A + \Phi_B)$$

where a_{A1} and a_{A2} , a_{B1} and a_{B2} are periodicity of the location of metal atoms along the first and second chains in the substances A and B. Φ_A , Φ_B are the angles between these chains

Flat index		Chain direction index		Periodicity of chains, Å		Angles between chains, degree		Δ
A	B	A	B	A	B	A	B	
(1100)	(1210)	[0001][1123]	[0001][2021]	6.88 3.89	6.50 3.50	53.9	51.8	0.202
(2111)	(1012)	[1123][2201]	[2201][0221]	3.89 3.89	3.50 3.50	88.8	85.7	0.246

Fig. 22 Correspondence Δ between closely packed chains of Ca and Al atoms in $\text{Ca}_5(\text{PO}_4)_3\text{OH}$, (A) and Al_2O_3 , (B)

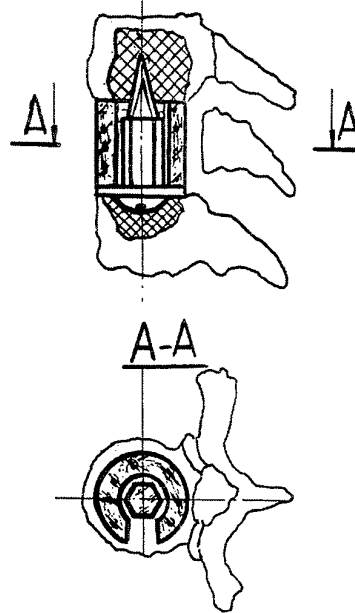


Fig. 23 Sapphire medical implant

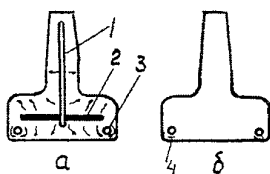


Fig.27 Items with assigned location of pores.
a-light guide, δ -implant, b-laser illuminator

How to Start Your Crystal Growth

SEMI Japan Shin. Takasu
4-7-15, Kudan-minami, Chiyoda-ku, Tokyo, 102-0071, JAPAN
e-mail stakasu@semi.org, KFG 00275@nifty.net

Agenda

- 1) Introduction, Target of this lecture
- 2) Why do you start crystal growth?
- 3) Let make check list of crystal growth.
- 4) With the check list
 - Step 1 : Do you have your Target of Crystal growth?
 - Step 2 : Check the database
 - Step 3 : Term
 - Step 4 : How to find the growing method?
 - Step 5 : Do you have enough resources?
 - Step 6 : Starting check
 - Step 7 : Crystal Growth
 - Step 8 : Characterization Procedure and check of agreement to target
 - Step 9 : For Next Step
- 5) Resume

1) Introduction, Target of this lecture

The target of this lecture is prepared for the person on the starting line of crystal growth.

2) Why do you start crystal growth?

There are many targets of to start t crystal growth.

- Case A : Getting New Materials.
- Case B : Research of Crystal Growing Mechanism.
- Case C : Research Target Materials for yourself, challenge to some one.
- Case D : Research Target Materials for other Researcher.
- Case E : Commercial Production of small quantity.
- Case F : Commercial Mass Production.

Their size and quality takes variety depending on purpose. The size aimed is changes from less than 0.1mm to over few hundred mm depending on usage. The qualities are also very widely scattered, dislocation free crystal, dislocated crystal, very high purity crystal, high transparency crystal in specified wave length, etc.

X-ray structure analysis	(high Tc. super conductor)	$\leq 0.5\text{mm } \phi$	Case A, D
Can we grow the crystal?	(V_2O_5)	few mm ϕ X few mm l	Case B, C
Magentic Study	(YIG, $\gamma\text{-Fe}_2\text{O}_3$)	$\leq 10\text{mm } \phi$	Case A, C,
X-ray monochromator	(Si, GaAs)	10 x 50 x 3 mm	Case E
Infrared detector	(TGS, InSb, YAG)	8mm ϕ x 0.1 mm	Case E
Laser Materials	(Al_2O_3 , $\text{Y}_3\text{Al}_5\text{O}_{12}$)	$\geq 10\text{mm } \phi$ x 50 mm l	Case E, C, D
Semiconductor Device	(Si, GaAs)	450mm ϕ x 1000mm l	Case F
Food	(NaCl, sugar, medicine, ...)	controlled Size	Case F

These differences require different crystal growth method, techniques, starting materials and others.

3) Let make check list of crystal growth Why flow chart is important?

We are not perfect. It is not so easy to check all conditions for crystal growth. A check list assists us eliminating simple mistake and forget something.

Fig. 1 is my check list for crystal growth. Of course, this is an example. Following discussion is after this check list.

4) With the check list

Step 1 : Do you have your Target of Crystal growth?

In section 2, I show that there are many targets of crystal growth. These differences require different growing method, techniques and starting materials and others. First step is understanding your purpose and target. If you have not make clean it yet, you should check your target.

Step 2 : Check the database

Material properties, especially phase diagram

The phase diagram is not equilibrium phase diagram but working phase diagram. I met with incorrect phase diagram two times, Ag-Te, NaCl-CaCl₂. Former was not equilibrium phase diagram. Then, it was not applicable to natural mineral occurrence.

I show several simple Instruments and technique making phase diagram.

Growth method

Following books are very good database.

A.N.Winchel & H.Winchel; The Microscopical Characters of Artificial Inorganic Solid Substances (1964) Academic Press

C.Palache, H.Berman,, and C.Frondel; Dana's A system of Mineralogy I, II, III (1944, 1951, 1962) John Wiley & Sons

Instrument

Check Catalogs. It is not so easy.

Characterization technique, chemical and phase analysis for growing crystals

Simple method is best. Density, melting point, X-ray powder data, optical character

under the microscope.

Check CRC handbook, Merck Index etc.

Starting materials

Check chemicals maker's catalogs. I had several experiences that I was tricked the description in them.

Safety, health, and environmental issue.

Merck Index is good reference.

Step 3 : Term

You should check the term for growing crystals. In some case, you should graduate the school. Another case, you should deliver a certain crystal in limited term. The term may give influences to the selection of method, instrument and starting material.

Step 4 : How to select your growing method

Case 1 Can you find the growing method for your target?

A approach method is selected based on the characters of your target materials from a selection table.

You cannot find the method, you should return to Step 2.

Case 2 What method is best fit your target?

Selection rule. Cost, resources, demand (quality and quantity), term, etc.

If you feel a fear the selection, you should return to Step 1 or make assessment .for the selection from several points of view.

Step 5 : Do you have enough resources?

In Step 4, you may select several candidates. But, you may not use all candidate from the limitation of your term and your resources.

If you have a lot of money, you can buy any thing. And, if you have good machine shop and chemical shop, you can make any thing. But, many case you have not so much money and you

have not so good machine and chemical shop. In this case how do you do?

a) Making low cost instruments

- | | |
|--|--|
| Ex.1 : Using drilling machine for puller | Application of another field instruments |
| Ex.2 : Double thermal insulation | Application of new idea instruments |
| Ex.3 : Application of strip heater | Application of new idea instruments |

b) Synthesis and purification for starting materials

- | | |
|---------------------------------|--|
| Ex.1 : Tri glycine sulfate | Synthesis from starting row materials |
| Ex.2 : Purification of Y_2O_3 | Elimination of SiO_2 (It was cristobalite) |

Step 6 : Starting check

Growth Instrument

Is your instrument enough for your purpose?

Growing Temperature, atmosphere, time, stability, and others.

If no, you must take replace choice of the instruments or reworks or attached something.

Is crucible, furnace materials quite enough for your purpose?

Is your crucible no chemical reaction with target materials or flux including surrounding furnace materials?

PbO and PbF_2 flux and surrounding thermal insulating materials

Pt crucible and surrounding bricks

Your crucible purity is quite enough?

Influence of impurities in quartz glass crucible for growing Si crystals
(It may be discussed in Si crystal growth.)

Starting materials

Do you have good starting materials for your purpose? If no, you rework the starting materials.

Case study 1) Starting materials phase

TeO_2 , two starting materials phase

Carbon source for high pressure diamond transition

Carbon source for CVD diamond film growth

Simple rule 1 :

Starting material phase influences to growing crystals phase.

Case study 2) Increasing charge volume

$Y_3Fe_5O_{12}$ (YIG) flux growth

Pressing of starting materials

$Y_3Al_5O_{12}$ (YAG) melt growth

Sintering of starting materials

GaP melt growth case

Hydrostatic pressing of starting materials

Simple rule 2 :

Large charge volume conduct large crystals and lot of crystals.

Case Study 3) Check the starting material form and content

There are many materials forms, powder, nugget, ribbon, rod, etc. The material form influences to purity and reaction.

Si, Cu, Al, etc

Fine powder surface is oxidized.

La_2O_3

Normally, it changes to amorphous hydroxide contain CO_2 .

Simple rule 3

All starting material should be checked their real contents.

Step 7 : Crystal Growth

Do you rely on former description?

Review the crystal growth theory, and know how

Case study 1 Crystal growth from melt for V_2O_5

Case study 2 Growing speed for MCZ Si crystal growth

Case study 3 Crystal growth of K-alum dimension dependency of growing

- vessel volume
- Case study 4 Crystal growth of tri glycine sulphate (TGS) under Curie point (49°C)
- Case study 5 Crystal growth of NiO, NiFe₂O₄ on MgO by CVD
- Case study 6 Crystal growth of γ -Fe₂O₃ on MgO by CVD

Step 8 : Characterization Procedure and check of agreement to target

Characterization of grown crystals should be start from nondestructive measurement.

Simple rule : From outside to inside.

Taking photograph or sketch is first step. Growing position and distribution are important information.

Dimension and weight is second step. They should be measured before destruction.

Observation of inside structure and texture of growing crystal requires correct direction slicing.

Case study 1 Zoning (striation) pattern is observed from perpendicular direction to growing direction. Example : YIG and natural garnet, Si

Case study 2 GaAs on spherical substrate by CVD epitaxial growth.

Step 9 : For next step

- 1) Recording all data
 - Date, weather, temperature, humidity
 - Case study Cdl spiral growth
- 2) Preservation of starting sample, growing crystal samples
- 3) Starting and after run instrument photographs or description
 - Success and failure
- 4) Recording of laps
- 5) Don't lent your all data to friend without copies.

5) Resume and acknowledgement

Crystal growth is not simple process but it is a system knowledge and technology. I think failure date is

also our important properties. This ISSCG meeting is very important for all attendee in the view point of knowledge exchanges. I propose a cooperation work to make up a crystal growth data base on Internet including failure data.

In this lecture, I show many examples. These examples supported following many person.

Dr. S.Miyazawa, Prof. T.Fukuda, Prof. F.Takei, Prof. M.Wakatsuki, Dr. H.Hirano, Dr. S.Matsumura, Mr. M.Tanaka, Mr. J. Ushizawa, Dr. M.Watanabe, Mr. Y.Matsushita, Mr. T.Sugawara, Mr. M.Ohwa, Mr. K.Homma, Dr. S.Takahashi.

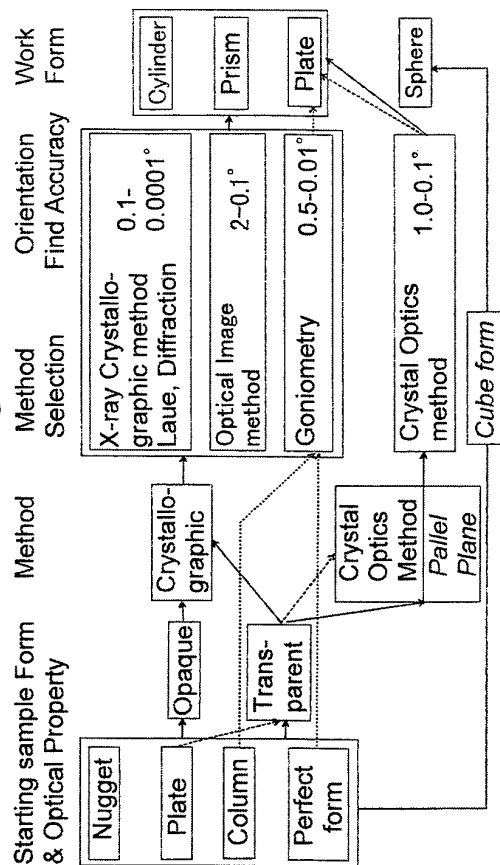
Appendix :A Correct Direction Sample Making

- A-1 Orientation Finding and work
- A-2 For Correct Slicer Setting
- A-3 Optical Image System for Correct Direction Slicing
- A-4 Laue Method System for Correct Direction Slicing
- A-5 Orientated Cylinder Making

Appendix B Making Sphere Crystal

- B-1 Large Sphere Making
- B-2 Bond's Sphere Grinding & Polisher
- B-3 Barrel Polish
- B-4 Two Sphere Polishing Methods

Orientation Finding and Work



For Correct Slicer Setting

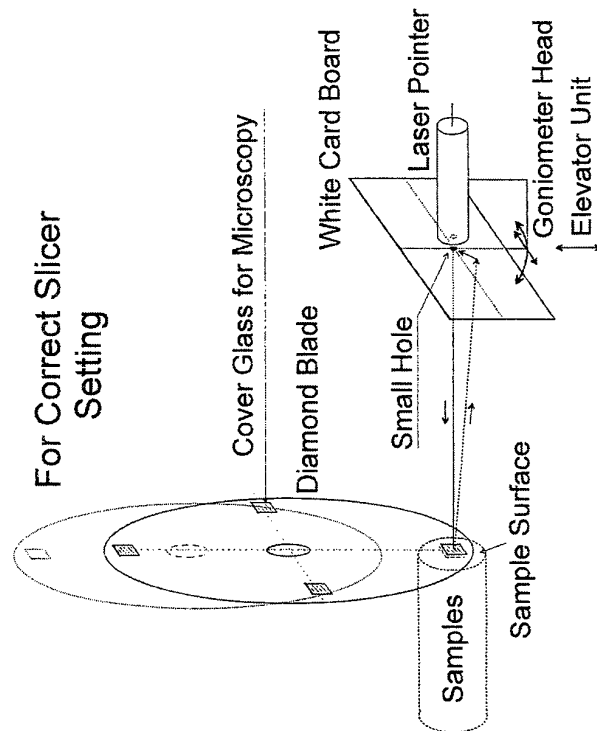


Fig. 1 Check List of Crystal Growth

- 1) Do you have target?
- 2) Do you finish check data base?
- 3) Do you have sufficient growing instrument?
- 4) Do you have safety measure?
- 5) Can you get starting materials?
- 6) Does starting material fit to your target?
- 7) Growth start
- 8) Characterization of Growing Crystals
- 9) Mechanical Working for test
- 10) Test/shipping with packaging

Appendix A Correct Direction Sample Making

A-1 : Orientation Finding Table

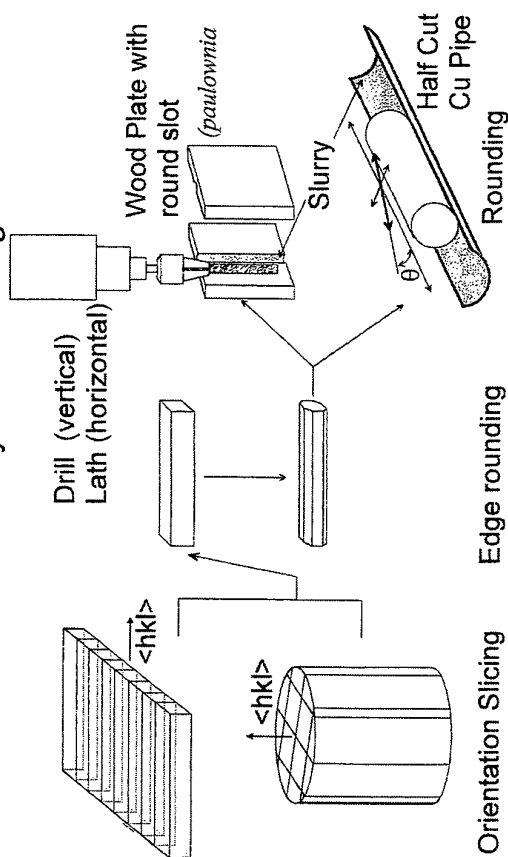
A-2 : For Correct Slicer Setting

A-3 : Optical Image System for Correct Direction Slicing

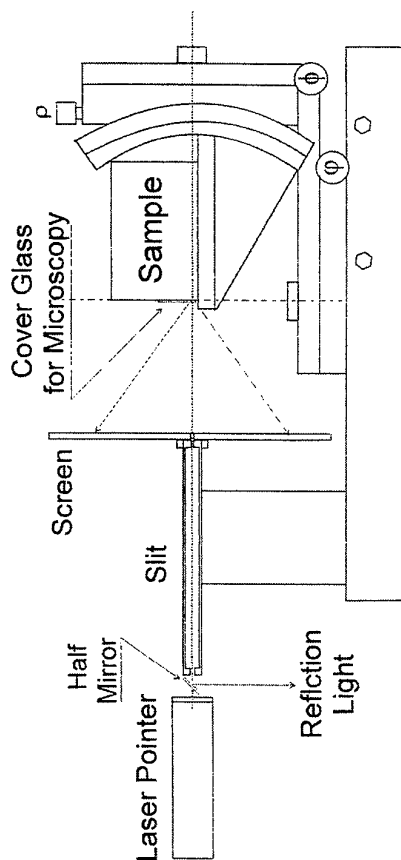
A-4 : Laue Method System for Correct Direction Slicing

A-5 : Orientation Cylinder Making

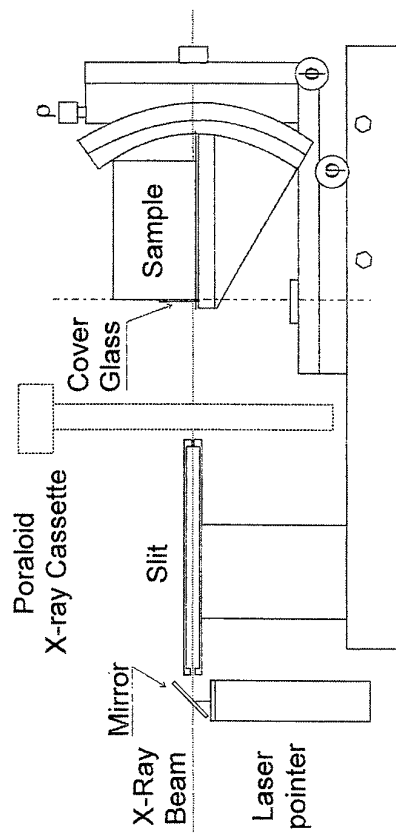
Orientated Cylinder Making



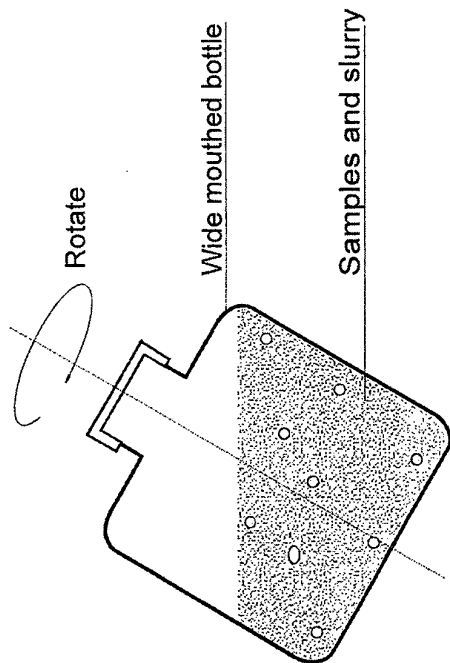
Optical Image System for Correct Direction Slicing



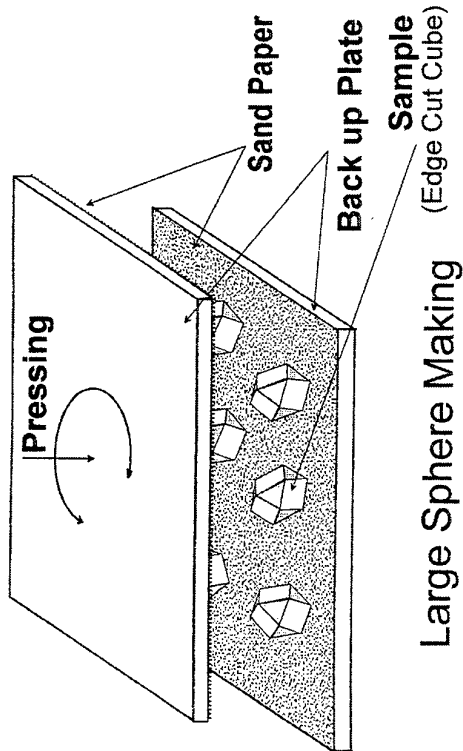
Laue Method System for Correct Direction Slicing



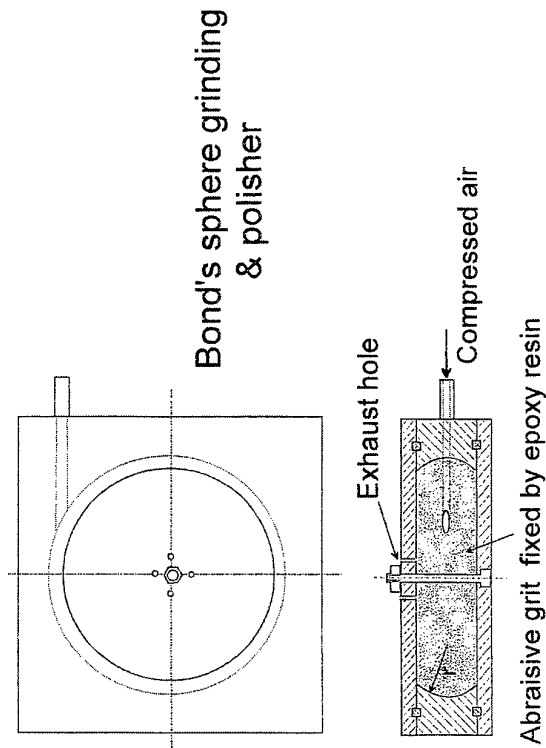
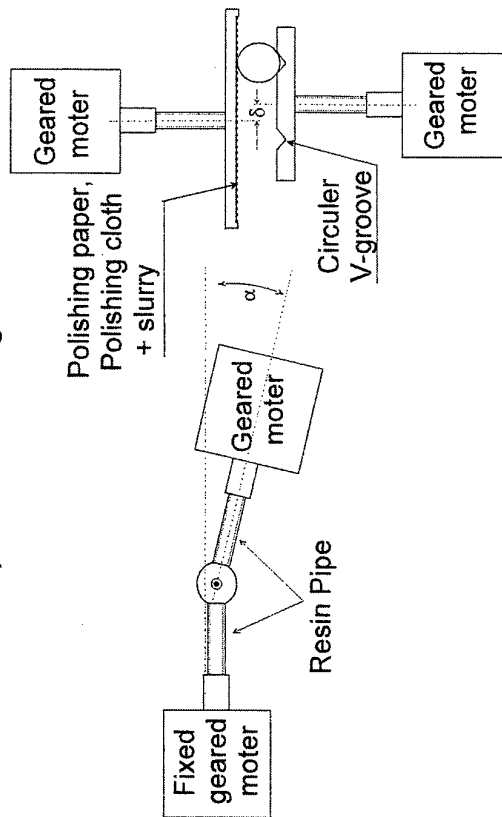
Barrel Polish



- B-1 : Large Sphere Making
- B-2 : Bond's Sphere Grinding & Polisher
- B-3 : Barrel Polish
- B-4 : Two Sphere Polishing Method



Two Sphere Polishing Methods



Silicon Crystal Growth

SEMI Japan Shin. Takasu
4-7-15, Kudan-minami, Chiyoda-ku, Tokyo, 102-0071, JAPAN

e-mail : stakasu@semi.org or KFG 00275@nifty.ne.jp

Agenda

- 1) Introduction
 - Position of Semiconductor and Si Devices Trend
 - Requirement for Si
- 2) History of Si Crystal Growth and Concept Change
 - Growth Method, Pulling Machine, and Heat dissipation
- 3) Temperature Gradient and Pulling Speed
- 4) Crystal Pulling process
- 5) Starting Materials and Crucible
 - Poly Si
 - SiO₂ Glass Crucible
- 6) Impurities in Si
 - Oxygen and Carbon and others
 - Impurities Doping
 - Contamination from poly Si and crucible
- 7) MCZ, Continuous and Recharge Pulling
- 8) Cost of Si Crystal Growth

1) Introduction

Si Position in Semiconductor and Si Devices Trend

Si has the 2nd position in our Earth crust elements and it has not poisonous character. From this character, Si may keep the 1st position in the materials used in the 21st century electronics industry. The 2nd position shows that many impurities should be eliminated from the crude Si materials including Si crystal growth.

Requirement for Si

Fig. 1a,b
Si was 2nd runner in the semiconductor device invention race. But in this stage, Si is the 1st runner in electronic devices material race. All chip performances, speed, memory capacity, is increase. All chip prices, Logic, DSP, and DRAM, are required to make lower for unit performances, for example bit cost and clock frequency cost, and others. These requirements bring that chip sizes are increasing and element devices are shrinking. It is required low cost but high performances Si wafer. Fig. 1a,b are DRAM bit-cost vs capacity trend and wafer diameter change from 1970. The increasing rate is about 6mm/year. Recently, NTRS showed more high rate for growth of Si devices. 300mm era started just now and they required 450mm Si wafer in 2007.

2) History of Si Crystal Growth

Growth Method and Pulling Machine

Fig. 2
Si bulk crystal growth methods are Czochralski (CZ) method and Floating Zone (FZ) method mainly. Pedestal method, EFG method and others are not main method. The largest volume Si crystals are made by CZ method and their volume reached over 5000t per year.
Starting puller heating type was radio frequency heating by carbon crucible using quartz glass crucible with very small capacity, about hundred grs. Now, the largest capacity reached over hundred Kgs and the heating method is used direct current or commercial frequency resistance heating using carbon heater.
Shaft type puller is used yet but many cable puller is used. Cable type puller was used by Czochralski originally. Historically, ball chain puller was used. The pulling rupture strength of 6mm ϕ ball chain is 70Kg order, then modern large puller cannot use it. In this change, thermal dissipation concepts were conducted from heat conduction by shaft to radiation cooling from pulling crystal surface. Atmosphere was changed from normal pressure to low pressure Ar.
Recently, small ball type single crystal (1mm ϕ) is grown by Ar plasma flame fusion method.

Crucible

Crucible was changed from transparent to translucent type with transparent inner layer. Carbon crucible is used holding the SiO₂ crucible

3) Temperature Gradient and Growing Speed

Fig. 3
Pulling speed is proportional to the difference between liquid side and growing side temperature gradient and their thermal conductivity not only the temperature gradient in crystal side. These phenomena are very important for large diameter and good quality crystal growth.

4) Crystal Pulling process

Fig. 4
Fig. 4 shows the Si pulling schedule. This diagram has many meaning on Si crystal growth technique, growth theory, and economy. This schedule is used for economical calculation of Si crystal production.

5) Starting Materials and Crucible

Poly Si

Table 1
Starting material of CZ method is purified poly Si nugget and/or granular form. In very rare case, CZ crystal growth used a center core poly Si for large volume charge. Ingot form poly Si is used in FZ method crystal growth. The first issue of poly Si is purity including contamination at dividing, cleaning, and packaging.

SiO₂ Glass Crucible

Fig. 5, Table 2a, b
Crucible used in CZ method has been selected following reason, 1) no reaction and/or no making harmful compound at pulling condition, 2) the purity, 3) origin of Oxygen and its controllability, 4) others. Modern method requires adding the condition of thermal circumstance and long life at pulling state.
Fig 5 shows the dimension and Table 2a shows their values. The chemical impurity trend inner wall is shown in Table 2b.

6) Impurities in Si

Impurities Doping

Impurity is doped to Si adding initial melt mainly. Phosphorus is doped by neutron irradiation transmutation method for non doped high resistivity FZ and magnetic Czochralski grown (MCZ) crystals.

Oxygen, Carbon and heavy metals

Fig. 6
Oxygen is contaminated a part of resolved oxygen into Si melt from crucible wall made by SiO₂ glass. The concentration is controlled by natural and forced convection in Si melt and acceleration of evaporation from melt surface.
Carbon contamination brings from carbon materials in the furnace mainly. The contamination from poly Si is not main now. Then, the decreasing method is evacuate structure of furnace and its operation manner.
Heavy metal contamination brings from SiO₂ glass crucible wall and used poly Si mainly, too. Analytical results of growing crystals including the distribution and used poly Si and crucibles show good coincidence.

7) Continuous and Recharge Pulling and MCZ Method

Continuous Feeding and Recharge Pulling

Fig. 7a, b, c
Both methods are proposed for high yield for n-type crystal pulling. The dopants of n-type crystal show small partition function, k_{eff} , than p-type dopant, B. Then, the n-type crystal (P, As, and Sb doped crystal) yield gives small value than p-type crystal (B doped crystal).

MCZ Method

Fig. 8
MCZ method was developed suppressing natural and forced convection by means of electrodynamic effect for InSb. Fig. 7 shows the history of magnetic field applied crystal growth. MCZ method is used for very high resistivity crystal and large diameter, ≥ 200 mm, crystal growth. The magnet is normal electro- and superconductive-magnet. And, magnetic field applying manners are horizontal and cusp types.

8) Cost Issues of Si Crystal Growth

Fig. 9, Table 3
Si devices are used wide industrial area and their productions are reached to 5,000 t per year. From this situation, they require many Si crystals in low price and high qualities. The production number and the qualities are required from high yields of devices production and the ultra high integration of devices. In this last section of this lecture, I discussed cost issues of Si crystal growth. Cost issues have relations of theoretical, technical, and strategic side. It is started from Fig. 3.
Table 3 shows an example of Si crystal growth cost calculation format on EXCEL. This format may be applied to other crystal growth cost estimation.

Fig. 2 Si Crystal Growth Methods

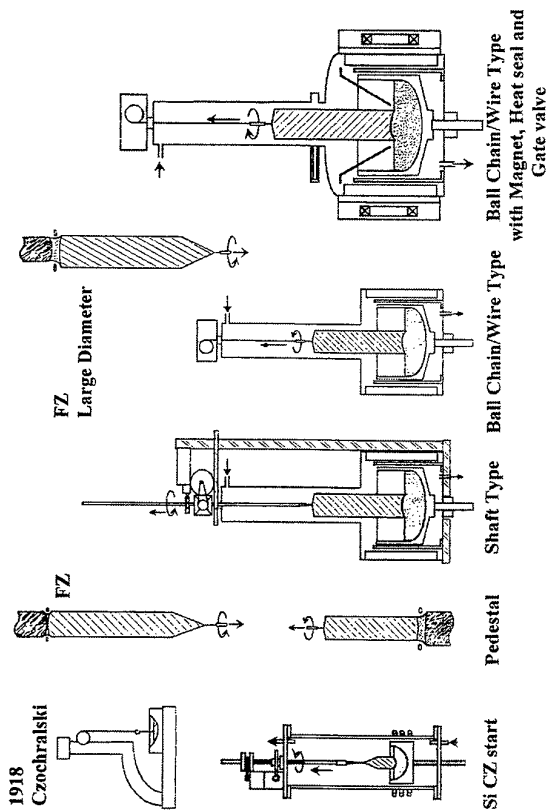


Fig. 1a Bit Cost vs DRAM Capacity (July 22, '99)

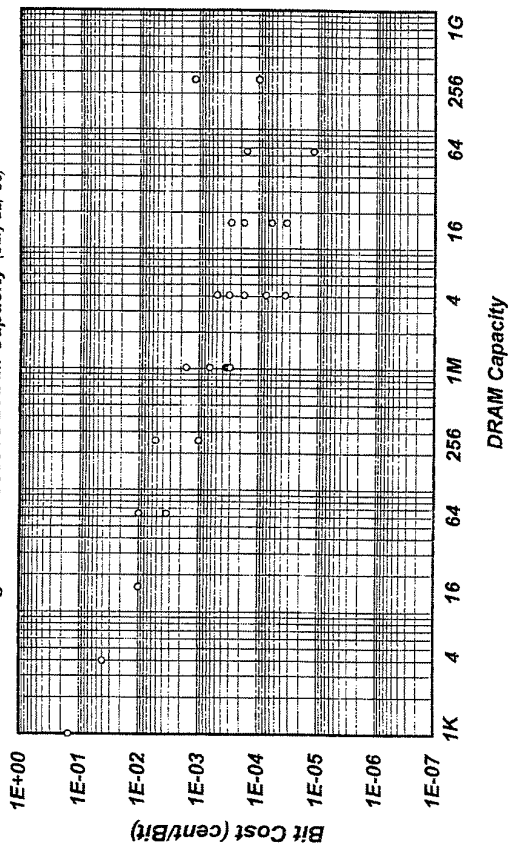


Fig. 3 Si Crystal Pulling Time Scedule

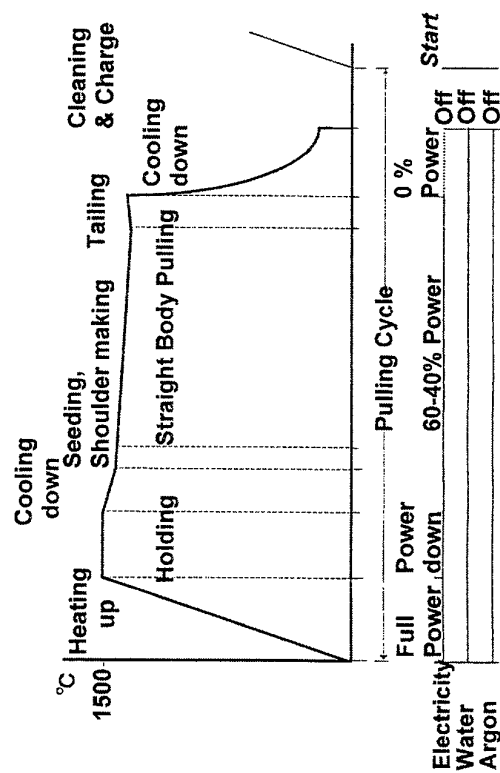


Fig. 1b Si Wafer Diameter Trend

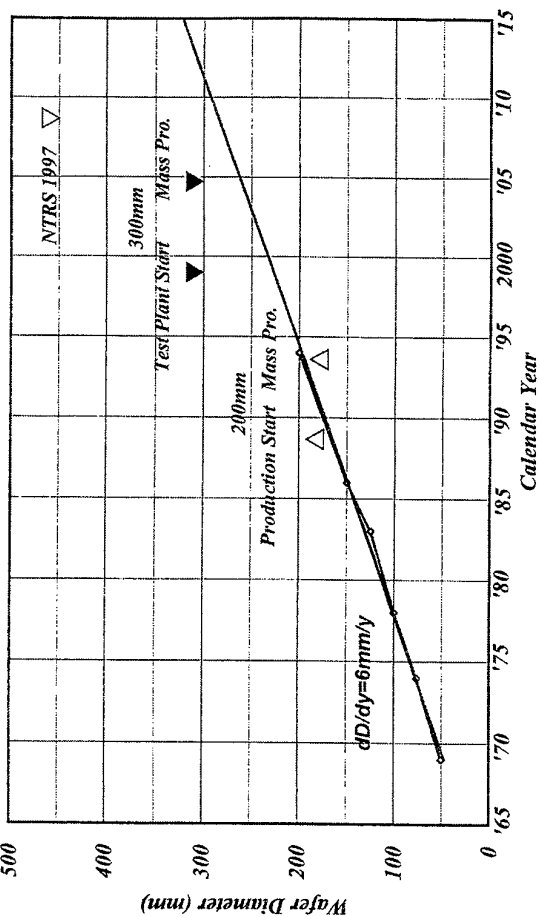
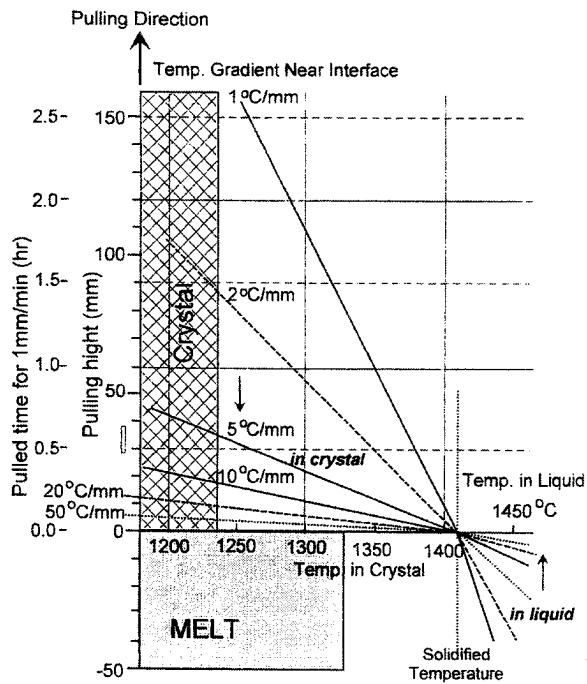


Fig. 4 Thermal Condition of Si Crystal Pulling



$$\frac{dT_s}{dZ} K_s = \frac{dT_L}{dZ} K_L + \rho \Delta L V$$

$$V = \frac{G_s K_s - G_L K_L}{\rho \Delta L} = C (G_s K_s - G_L K_L) \quad C = 1/(\rho \Delta L)$$

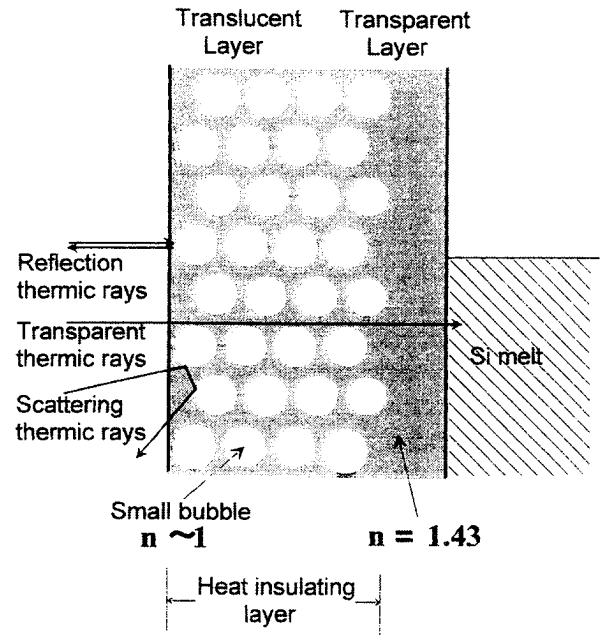


Fig. 5a Silica Glass Crucible Structure and Thermal Character

Fig. 5b Qz. Glass Crucible Dimension

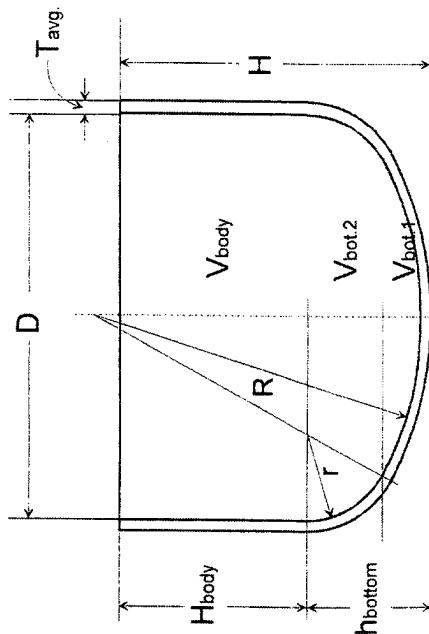


Fig. 7b 3 Crystal Growth Steps

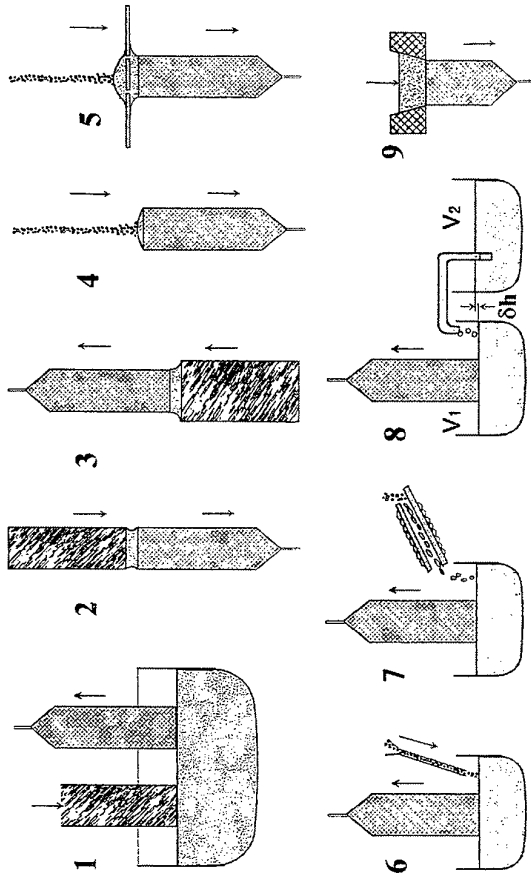
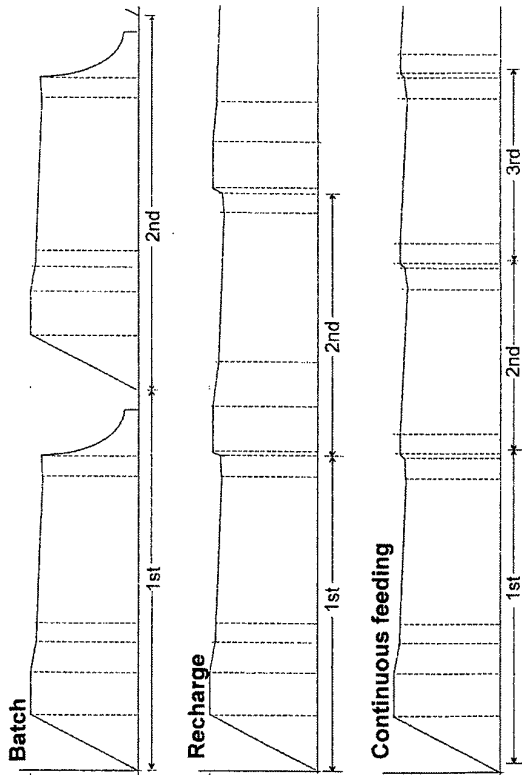


Fig. 7a Continuous Feeding Crystal Growth

Fig. 6 Pulling Crystal Impurities Level (atoms/cm³)

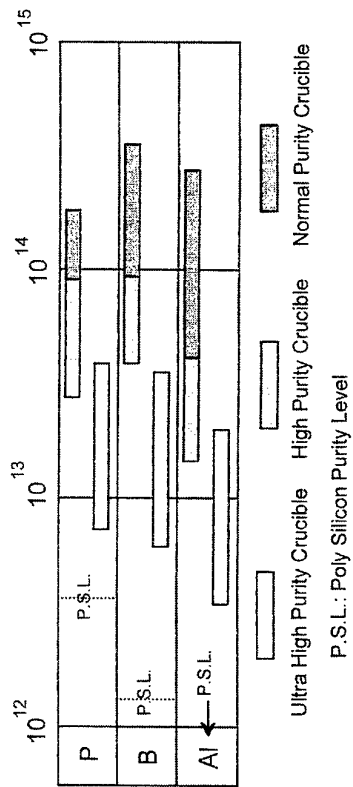


Fig. 7c Continuous Charge Condition

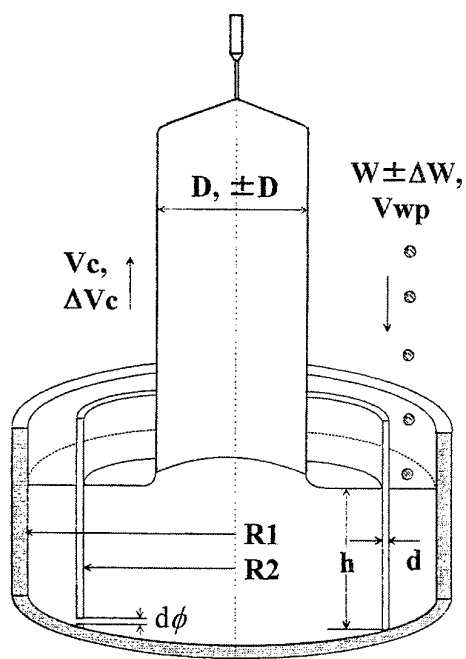


Fig. 8 History of Crystal Growth under Magnetic Field

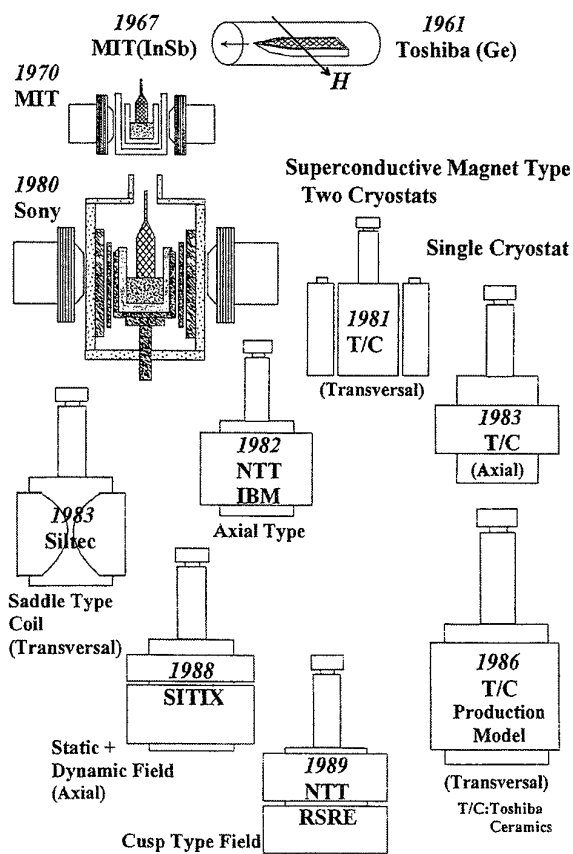


Fig. 9 Loss Parts of CZ Grown Si Crystal

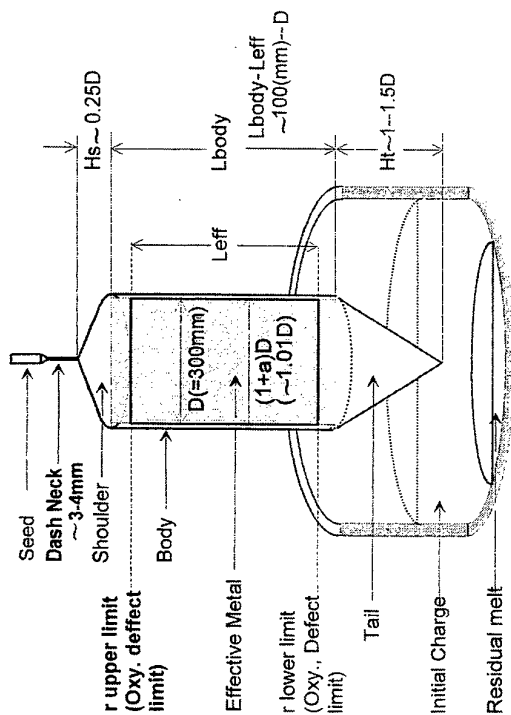


Table 1 Poly Si Surface Contamination

Source	1	2	3	4	5
Na	<3	<3	<3	<3	<3
K	<2	<2	<2	<2	<2
Fe	<1	<1	5	4	<1
Cr	<1	<1	<1	<1	<1
Ni	<5	<5	<5	<5	9
Cu	<1	<1	<1	<1	<1
Al	<5	<5	<5	<5	<5

Unit : $\times 10^{12}$ atoms/cm³

Table 2a Large Crucible Dimension

Dnominal	"	10	11	12	13	14	15	16	18	20	22	24	25	26	27	28	29	30	31	32	33	34	35	36	40	45	48	50	Dnominal
D	cm	25.4	27	30.5	33	35.5	38.1	40.4	48.7	50.8	55.8	61	63.5	66	68.6	71.1	73.7	76.2	78.7	81.3	83.8	86.4	88.9	91.4	101.6	114.3	121.9	127.0	D
H	cm	17.8	21.4	22.8	26	25.4	27.2	30.5	35.5	38.1	38.1	39.4	40.6	41.9	43.2	44.4	45.7	46.2	46.7	47.3	47.8	48.3	49.0	50.8	54.5	56	57	H	
R	cm	30.5	30.5	30.5	30.0	40.0	40.0	40.0	50.0	50.0	60.0	61.0	64.0	67.0	70.0	73.0	77.0	80.0	82.0	84.0	86.0	88.0	90.0	90.0	100.0	112.9	119.6	124	R
r	cm	7.0	7.0	8.0	8.0	9.0	9.0	9.0	12.0	12.0	15.0	18.0	18.0	18.0	18.0	20.0	20.0	20.0	20.0	20.0	22.5	22.5	22.5	22.5	25.0	25.6	26.5	27.1	r
hbottom	cm	7.7	7.9	9.2	9.7	10.3	10.7	11.1	14.1	14.4	16.9	19.9	20.1	20.4	20.6	20.9	22.5	22.8	23.1	23.4	25.5	25.9	26.2	26.6	29.6	31.5	33.1	34.2	hbottom
Hbody	cm	10.1	13.5	13.6	16.3	15.1	16.5	19.4	21.4	23.7	21.2	18.2	19.3	20.2	21.3	22.3	21.9	22.9	23.1	23.3	21.8	21.9	22.1	22.4	21.2	23.0	22.9	22.8	Hbody
Vbody	l	5.1	7.7	9.9	13.9	15.0	18.8	24.9	39.9	48.0	51.9	53.3	61.1	69.3	78.6	88.6	93.2	104.5	112.4	120.8	120.0	128.7	137.4	146.9	172.1	236.0	267.2	288.9	Vbody
Wbody	kg	12	19	24	33	36	45	59	94	113	122	125	144	163	185	208	219	245	263	283	281	302	322	344	403	553	626	676	Wbody
Abody	cm ²	403	572	652	845	845	990	1,232	1,640	1,888	1,860	1,749	1,925	2,100	2,293	2,494	2,530	2,742	2,857	2,973	2,865	2,979	3,091	3,215	3,387	4,130	4,384	4,550	Abody
Vbot.1	l	0.1	0.1	0.2	0.5	0.3	0.6	0.9	1.1	1.6	1.2	1.3	1.7	2.1	2.7	3.3	2.8	3.4	4.3	5.2	4.5	5.5	6.6	8.3	11.5	20.187	26.44	31.34	Vbot.1
Vbot.2	l	2.8	3.2	4.6	5.4	7.1	8.2	9.2	17.7	19.3	28.7	40.4	44.1	48.0	52.1	56.3	66.6	71.6	76.7	82.2	97.0	103.5	110.0	116.4	159.8	209.45	247.18	274.72	Vbot.2
Vbot.tot	l	6.7	7.7	11.3	13.7	17.3	20.5	23.6	44.0	48.8	70.0	97.6	107.2	117.3	128.3	139.5	162.5	175.6	189.5	204.6	237.4	255.1	272.9	291.8	400.7	229.64	273.62	306.06	Vbot.tot
Vtotal	l	8.0	11.0	14.8	19.8	22.4	27.6	35.0	58.8	68.8	81.8	95.0	106.9	119.4	133.5	148.3	162.7	179.5	193.4	208.3	221.5	237.7	254.0	271.6	343.3	465.6	540.8	594.9	Vtotal
Wtotal	kg	18.7	25.7	34.5	46.3	52.4	64.6	81.9	137.5	161.0	191.4	222.4	250.2	279.4	312.4	346.9	380.7	420.1	452.5	487.4	518.3	556.2	594.3	635.5	803.3	1089.6	1265.5	1392.1	Wtotal
0.5Wtot	kg	9.3	12.9	17.3	23.1	26.2	32.3	40.9	68.7	80.5	95.7	111.2	125.1	139.7	156.2	173.5	190.3	210.0	226.2	243.7	259.2	278.1	297.2	317.8	401.7	544.8	632.8	696.1	0.5Wtot
0.6Wtot	kg	11.2	15.4	20.7	27.8	31.4	38.7	49.1	82.5	96.6	114.8	133.4	150.1	167.6	187.4	208.1	228.4	252.0	271.5	292.4	311.0	333.7	356.6	381.3	482.0	653.7	759.3	835.3	0.6Wtot
0.7Wtot	kg	13.1	18.4	24.7	32.8	37.4	46.9	59.1	97.6	113.8	135.8	155.8	175.8	197.4	220.8	245.9	272.8	301.6	331.4	361.2	391.0	420.8	450.6	480.4	602.6	823.9	960.6	1060.6	0.7Wtot
Respect		0.398	0.499	0.446	0.494	0.426	0.434	0.480	0.440	0.466	0.380	0.299	0.304	0.307	0.310	0.314	0.297	0.301	0.294	0.286	0.260	0.254	0.249	0.245	0.209	0.201	0.188	0.180	Respect
A _{bot.1}	cm ²	175	228	312	439	409	543	679	853	1010	949	1010	1177	1354	1552	1750	1664	1873	2110	2371	2222	2493	2766	3100	3835	5413	6379	7075	A _{bot.1}
A _{bot.2}	cm ²	631	665	834	873	1124	1187	1235	2010	2069	2911	3752	3913	4075	4241	4403	5092	5272	5436	5602	6485	6673	6855	6988	8630	9934	10935	11626	A _{bot.2}
A _{bot.tot}	cm ²	806	893	1146	1312	1533	1730	1914	2863	3079	3860	4762	5090	5429	5793	6153	6756	7145	7546	7973	8707	9166	9621	10088	12465	15347	17314	18701	A _{bot.tot}
A _{total}	cm ²	1209	1465	1798	2157	2378	2720	3146	4503	4967	5720	6511	7015	7529	8086	8647	9286	9887	10403	10946	11572	12145	12712	13303	15852	19477	21698	23251	A _{total}
A/W		9.3E-02	9.5E-02	8.7E-02	7.8E-02	7.6E-02	7.0E-02	6.4E-02	5.5E-02	5.1E-02	5.0E-02	4.9E-02	4.7E-02	4.5E-02	4.3E-02	4.2E-02	4.1E-02	3.9E-02	3.8E-02	3.7E-02	3.7E-02	3.6E-02	3.6E-02	3.5E-02	3.3E-02	3.0E-02	2.9E-02	2.8E-02	A/W
T _{avg.1}	mm	6	6	6.5	7.5	7.5	8.5	8.5	11	12	12	12	12.8	13.3	13.8	14.3	14.7	15.2	15.7	16.1	16.6	17.1	17.6	18.0	19.9	22.3	23.7	24.6	T _{avg.1}
T _{avg.2}	mm												12.2	12.5	12.8	13.1	13.3	13.6	13.8	14.1	14.3	14.5	14.7	15.0	15.7	16.6	17.1	17.4	T _{avg.2}
W _{env.1}	kg	2	2	3	4	4	5	6	8	12	15	17	20	22	25	27	30	33	36	39	42	46	49	53	69	95	113	126	W _{env.1}
W _{env.2}	kg												19	21	23	25	27	30	32	34	36	39	41	44	55	71	82	89	W _{env.2}

Table 2b Silica Glass Crucible Purity Trend

		Al	As	B	Ca	Cd	Co	Cr	Cu	Fe	K	Li	Mg	Mn	Mo	Na	Ni	P	Sb	Ti	Zr	OH
'69	Transparent	74		4	16			0.1	1	7	6	7	4	1		9		0.01	0.3	3	3	60
'86	Translucent	7	4E-4	0.03	0.5		0.01	0.03	0.01	0.5	0.05	0.1	0.1	0.01	<0.01	0.05	0.01	0.02	2E-04		<0.01	<1
'86	Translucent	20.3	0.002	<1	1.8		0.01	0.07	0.02	1.9	<3	1	0.5	0.1	<0.01	1.3	0.04	0.23	0.001		2.4	<1
'86	Translucent	17	<0.01	0.22	1			<0.09	0.16	1	1.7	1	0.1	<0.09	-	1.5	0.4	<0.05	<0.06		1.52	<1
'90	Translucent	8.7		<0.03	0.5					0.5	0.4	0.2	0.07			0.7						<1
'92	Translucent	14	<0.01	<0.2	0.4	<0.01		0.05	<0.05	0.2	0.6	0.1	<0.05			0.7	<0.1	<0.2	<0.003	1.1	0.8	<1
'94	Translucent	0.1		<0.01				<0.01	0.05	0.05						0.05						
'94	Translucent	0.1	0.03	0-0.01	0.1	2E-4		nd		0.2	0-0.001	0-0.05	0-0.1	0-0.01		0.04		0.01-0.1	0.002	0-0.1	0-0.001	1200/5

Unit:ppm *:Synthetic silica inside layer

Table 3 Growth Operation Condition and Cost

Ver.1.1E July. 20, '98

Fix	Unit	Value	Variable	Unit	Value	Unit Operation	Unit	Value	Operation Value	Electricity Value	Growth Target		
Puller Value	Yen/gr	200,000,000	Electricity	VKWhr	15	Melt	hr	12.00	%	90	Item	Unit	Value
Merit	%	2	Cooling Water	t/hr	200	Soak	hr	6.00	%	90	Target Dia	mm	300
Depreciation	Y	7	Ar	m ³ /hr	300	Down	hr	4.00	%	85	Pulling Dia	mm	303
Depreciation/hr	Vhr	3,372	Compressed Air	m ³ /hr	10	Leveling	hr	2.00	%	80	Shoulder H	Pull Dia	0.5
Clean Room Cost	Vhr/m ²	3,000	Liquid He	VL	1,200	Seeding	hr	1.00	%	65	Tail H	Pull Dia	1.5
Foot Print	m ² /Puller	3	Labor	Vhr	3,000	Shouldering	hr	4.21	%	55	Test Plate	set	6
			Operator	man/puller	1	Body	hr	19.08	%	60	Test Plate t	mm	3
Administration Fee	%	20	Poly	Vgr	7.00	Tailing	hr	12.63	%	65			
Sales Cost	%	2	Silica Glass Crucible	Yen	350,000	Cool down & take out	hr	4.00	%	0			
R & D Cost	%	6	Carbon Crucible Cos	Yen	800,000	Cleaning	hr	1.00	%	0			
Total Operation Day	day/Y	250	Operation time	times	25	Setting	hr	1.00	%	0			
			Unit Cost	Yen	32,000	Poly Charge	Kg	200					
			Exchange Hr	Hr	36	Average Pulling Speed	mm/min	0.6					
L _{eff}	cm	68.4	Average adding hr	Hr	1.44	Remained Melt	%	25					
Production Cost	Yen/gr	26.51	Carbon Heater	Yen	1,200,000	Max. Power	KWhr	300					
With Admin. Fee	Yen/gr	31.82	Operation time	times	36	Cooling Water	t/hr	1.5					
With R & D Fee	Yen/gr	34.40	Unit Cost	Yen	33,333	Ar	m ³ /hr	1					
Av. Pulling Speed	mm/min	0.60	Exchange Hr	Hr	36	He Consumption	L/hr	0.1					
			Average adding hr	Hr	1.00	Average Heat Treat for Exchange	hr	2.44	%	60	180		

Operation Result	Unit	Operation Value	Production Fee	Production Fee %
Operation Hr	hr	69,357		
Av. Maintenance hr	hr/meint.	2,440		
Total operation hr	hr	71,797		
Electricity	KWhr	1920,000	28,800	0.96
Cooling Water	t	107,695	21,539	0.72
Ar	m ³	64,917	19,475	0.65
He	L	7,180	8,616	0.29
Operator Cost	Yen		215,390	7.19
Puller Fee	Yen		242,089	8.08
CR Cost	Yen		646,169	21.56
Poly Si Cost	Yen		1,400,000	46.71
Crucible Cost	Yen		350,000	11.68
Carbon Crucible Cos	Yen		32,000	1.07
Heater Cost	Yen		33,333	1.11
Total operation hr	Yen		2,997,411	100.00
Effective Grown Crystal Cost	Yen/gr	26.51		
Ideal Pulling Time	Time/month	8		
Ideal Pulling				
Effective Crystal	Kg/month	904		

Ingot Value	Unit	Value
Si Density	gr/cc	2.34
Body Dia	cm	30.3
Total Weight	Kg	150.0
Shoulder Height	cm	15.2
Shoulder Weight	Kg	8.5
Tail Height	cm	45.5
Tail Weight	Kg	25.6
Body Weight	Kg	115.9
Body Length	cm	68.7
Test Pieces Length	cm	1.8
Work Loss	cm	0.84
Total Loss Length	cm	2.64
Total Weight Loss	Kg	0.6
Effective Pulling Body Weight	Kg	115.3
Effective Length	cm	68.4
Effective Crystal Weight	Kg	113.06

Bold italic cells are put your Operating Data.

Bold italic cells are put your Operating Data.

see abstract of lecture for the following 3 posters:

Heat and mass transfer in silicon melt under magnetic fields

K. Kakimoto

Institute of Advanced Material Study, Kyushu University,
6-1, Kasuga-Koen, Kasuga, 816-8580 Fukuoka, JAPAN

**Simulation of bulk crystal growth and evolution of point defects
and dislocations in the crystal**

N. Van den Bogaert, F. Dupret, R. Assaker, V. Regnier,
B. Hoevenaars, S. Kruk

CESAME, Université catholique de Louvain, 4 avenue G. Lemaître,
B-1348 Louvain-la-Neuve, BELGIUM

**Role of structural characterization in development of
large-diameter silicon**

K. Lal

National Physical Laboratory, New Delhi - 110012, India

for the First International School on Crystal Growth Technology, ISCGT-1

The Use of High Performance Computing for Modeling Crystal Growth from the Melt and Solution

Jeffrey J. Derby*

Department of Chemical Engineering and Materials Science, Army HPC Research Center,
and Minnesota Supercomputer Institute
University of Minnesota, Minneapolis, MN 55455-0132, U.S.A.

Crystal growth is an art which is evolving into a science, and modeling via the use of high performance computing represents a modern tool for speeding this evolution onward. The use of realistic theoretical models can augment traditional experimental inquiry for obtaining fundamental understanding of crystal growth. Such models have been extremely successful in the analysis of systems which exhibit two-dimensional behavior due to symmetries in design and which are dominated by long time-scale phenomena which allow the effective use of quasi-steady assumptions.

However, many systems contain imperfections in design or operation which disrupt their inherent two-dimensional symmetry and lead to three-dimensional effects. Even more significantly, fully three-dimensional and time-dependent behaviors have long been known to occur in crystal growth systems, in spite of system symmetries and slow process dynamics. The analysis of these effects requires the development of modeling techniques which allow the simulation of fully three-dimensional and time-dependent phenomena. However, these calculations continue to be extremely costly and difficult to perform.

Recent advances in massively parallel supercomputers have dramatically affected the prospect of studying three-dimensional macroscopic transport effects in many systems. To take advantage of these advances, we have developed finite element methodologies for computing three-dimensional, time-dependent, incompressible flows on the Cray T3E, a distributed memory, multiple processor supercomputer. The large memory and high sustained computation rates provided by these platforms allow us to perform extremely large simulations appropriate for the calculation three-dimensional phenomena occurring in crystal growth systems.

In this presentation, the most salient features of these models will be highlighted and examples will be presented from their application to analyze several melt and solution growth systems. Specific results from simulations of Czochralski growth of oxide crystals and the solution growth of potassium titanyl phosphate will be discussed.

This work was supported in part by the U.S. National Science Foundation, the U.S. National Aeronautics and Space Administration, the Minnesota Supercomputer Institute, and the U.S. Army, Army Research Laboratory, Army HPC Research Center. No official endorsement should be inferred.

SIMULATION OF TEMPERATURE AND THERMOELASTIC FIELDS IN THE AL_2O_3 CRYSTAL FOR THE SET-UP WAVE METHOD CGT.

© Artoush Harutunovich Abgarian

Company: ABGARIAN GROUP
Address: Novatorov St. 34/3 -20,
Moscow, 117421, Russia.
Tel./Fax : +7(095) 935 48 66

1. Introduction

The work deals with the closed statement of the thermoelastic problem for the displacement vector in monocrystals during small deformations. The method developed in papers [1,3] is used. The problem is solved using variable curvilinear 3-dimensional geometry at arbitrary boundary conditions with regard to nonstationary processes. AL_2O_3 and W (the heat source) constitute a multilayer medium. The mathematical model ensures the multilayer structure when AL_2O_3 changes from liquid to solid state. The results of simulation are presented as plots of deformation, strain, temperature pulse multilayer materials [2] and temperature fields and provide a basis for new wave methods of modeling crystal growth technology (CGT).

2. The statement of the problem

Let us consider the problem of the symmetric heating of the crystal like YAG which is put in the vacuum crystallization chamber. One can write the basic equations of thermoelasticity and thermoconductivity in the dimensionless form;

$$\rho \cdot C(\theta) \cdot \dot{\theta} = [K(\theta) \cdot \theta_{,\ell}]_{,\ell}, \quad (1)$$

$$RR1 \cdot \ddot{U}_e - U_{e,rr} - RR2 \cdot U_{r,rc} + RR3 \cdot \theta_{,c} - RR4 \cdot F_e = 0, \quad (2)$$

$$\varepsilon_{eg} = 0,5(U_{e,g} + U_{g,e}) \quad (3)$$

$$\sigma_{eg} = \frac{1}{1+\nu} \cdot \varepsilon_{eg} + \frac{1}{1-\nu} \cdot \left(\frac{\nu}{1+\nu} \cdot \varepsilon_{rr} - \alpha_T \cdot DTHAR \cdot \theta \right) \cdot \delta_{eg}, \quad (4)$$

where $\ell, g, r = 1, 2, 3$. Other designations and solutions of equations (1-4) are presented in Ref.[1]. The size of crystal under consideration is : 8 x 4 x 3 (cm).

3. The solution of the problem

The combined computational method involving the finite difference and finite element methods. The two-step construction of difference mesh is used. Making use of the Cook method [3] the interpolation curvilinear mesh, describing the object under investigation, is constructed in three dimensional curvilinear coordinates. Then the finite element is constructed around every point and the finite difference scheme is applied.

4. Conclusions

The mathematical method and computer programs have been developed to compute the temperature fields and thermoelastic characteristics of AL_2O_3 . They allow the computer simulation of crystallization chamber operation and new methods of CGT. The results are given in Fig. (1-6) as plots of temperature, deformation and strain fields.

A new wave method CGT involving stationary crystallization is investigated. The wave method allows the reduction of crystallization time, the increase of efficiency and quality of crystallization for arbitrary sizes of crystals (lenses 1 m and above in diameter). Note that now

large-diameter lenses are not manufactured anywhere, though they can find wide application in optics, space technology, etc.

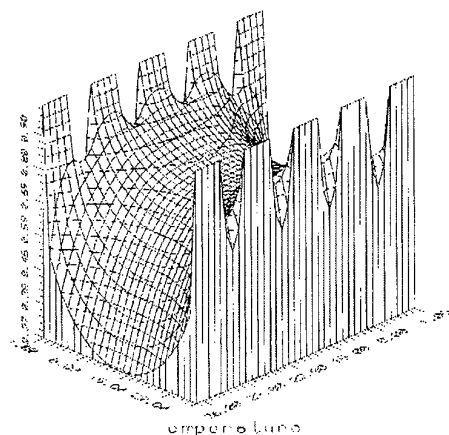


Fig. 1. Temperature fields.

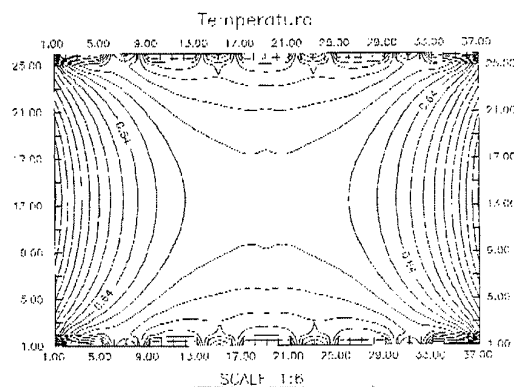


Fig. 2. Temperature fields isolines

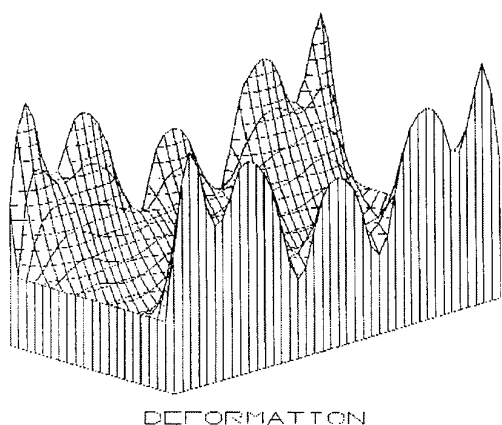


Fig. 3. Deformation fields.

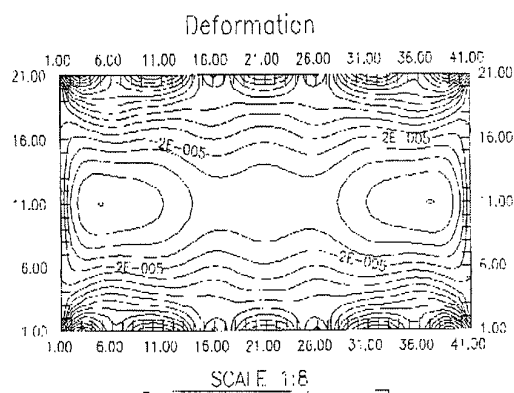


Fig. 4. Deformation fields isolines.

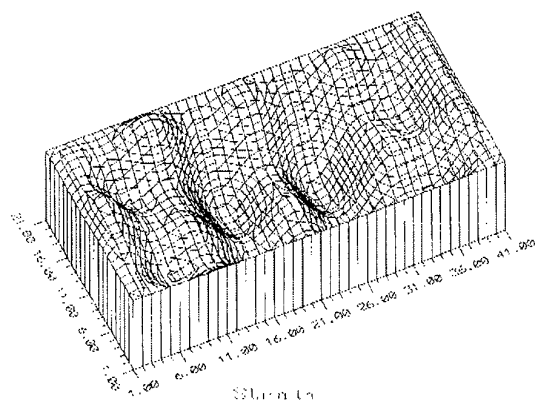


Fig. 5. Strain fields.

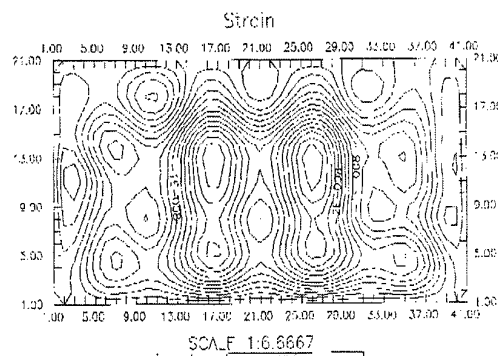


Fig. 6. Strain fields isolines.

5. References

1. Abgarian A.A. Simulation Of Thermoelastic Strain In The Al_2O_3 Crystal Using 3-Dimensional Curvilinear Coordinates. Optical Engineering Bulletin SPIE/Russia, SPIE/Ukraine,.. Quarterly. 1995, № 3(7),pp. 30-33.
2. Abgarian A.A. Temperature Pulse Multilayer Materials Of Anodes Of Electron-Emitting Systems. MATEMATICHESKOE MODELIROVANIE 1998, v.10, № 4, pp. 23-29.(In Russian).
3. Cook W. A. Body oriented (natural) CO-ordinates for generating three-dimensional meshes.- Int. Journal for Number. meth. in engin., 1974, vol. 8, p.27-43.

see abstract of lecture for the following 3 posters:

**Development of new ultra precision machining methods - plasma
CVM and EEM**

Y. Mori, K. Yamauchi, K. Yamamura, Y. Sano, H. Kakiuchi

Department of Precision Science & Technology
Graduate School of Engineering
Osaka University, 2-1 Yamada-oka, Suita, Osaka 565-0871, JAPAN

Striations, an intrinsic problem ?

H.J. Scheel

Cristallogénèse - IMO
Swiss Federal Institute of Technology
Chemin de Bellerive 34, 1007 Lausanne, SWITZERLAND

**Control of growth modes in epitaxy
from the vapor phase and from the liquid phase**

H.J. Scheel

Cristallogénèse - IMO
Swiss Federal Institute of Technology
Chemin de Bellerive 34, 1007 Lausanne, SWITZERLAND

Michel Lebeau

CERN 1211 Geneva 23 Switzerland

tel. 00 41 22 767 2044

fax 00 41 22 767 8930

First International School on Crystal Growth Technology ISCGT-1
Beatenberg, Interlaken, Switzerland September 5-16, 1998

Abstract of Poster

Title: Mechanical Processing of Anisotropic Scintillating Crystals

The Electromagnetic Calorimeter of the CMS experiment at CERN-LHC poses design and construction challenges. 82 000 PbWO_4 scintillating crystals will be assembled in a cylindrical array completed by two endcaps, the hermeticity of which is mandatory for the claimed detector performance.

A safe, accurate and economical solution has been developed at CERN for the mechanical processing of the crystals which will be mass-produced in China and in Russia from now until 2004. For each of the 17 different shapes in the barrel part 3600 pieces will be produced. Each of the two endcaps will consist of about 10 000 identical pieces.

As a result of the claimed dimensional accuracy, the crystal shape error will not contribute to more than 20% of the dead space within the crystal array, the rest being structural material and assembly clearance.

We will describe the basic concepts of the proposed method, which takes the physical and mechanical properties of PbWO_4 on account. First the crystal ingot is oriented to its identified crystal lattice orientation, cut to the required shape and dimension accuracy in one single operation per face, trying to keep the same cutting orientation to identified cleavage planes. The designed surface finish is then reached in only two quick steps, first by lapping and second by polishing. This surface finish

progression minimises the number of operations -and machines-, reduces stock removal, time, and subsurface damage.

The polishing grade of the four side faces is matched to produce the required light collection uniformity.

Standard machine tools have been optimised to the mentioned cutting, lapping and polishing operations by simple accessories or modifications. A quick, accurate and reproducible positioning of the crystals at every operation is performed by a rugged tooling fit for industrial conditions, using a following reference and magnetic fixations. Machining parameters have been optimised to reduce processing time -and therefore capital investment on machines- while maintaining dimensional and shape accuracy and maintaining cutting forces low, thus minimising subsurface damage, chipping or breaking risks. The wheel thickness, the ratio of feed speed vs. revolution speed, the abrasive grain density and size have been carefully selected. The problems of swarf ejection and lubrication have found simple and efficient solutions. Quality control is achieved by simple inspection jigs used at every processing step.

Results recently obtained on the prototype machines at CERN and in Russia will be described. In conclusion the crystal mass production schedule and the corresponding equipment investment for the processing lines will be presented.

Light Scattering Tomography for Characterization of Crystals

Tomoya OGAWA

Dept. of Phys. Gakushuin Univ., Mejiro, Tokyo, 171-8588, Japan
FAX +81-3-3590-2602, E-mail tomoya.ogawa@gakushuin.ac.jp

ABSTRACT

Since light scattering tomography (LST) is one of standard methods for detection of defects, especially, oxygen related precipitates in Cz silicon wafers and non-linear optical crystals including heavy atoms as their composite elements. LST for characterization of crystals is comprehensively discussed here.

From a view point of detection of defects in crystals, high detectability with excellent signal to noise ratio is the most important function. Therefore, LST has been innovated from ultramicroscopy, because this microscopy was, historically, developed for studies on metal colloidal particles in stained glasses and used for observation of Brownian motion of fine particles.

Since quality of lasers is most suitable for illumination as a light source for LST, a focused laser beam is scanned in a crystal to detect defects and thus LST is, sometimes, understood as the acronym of "Laser Scanning Tomography" which is practically same as the original LST because its illuminator is usually a laser.

IR LST was developed for detection of defects in semiconductor crystals, such as EL2 centers in GaAs crystals and, recently, oxygen precipitates in CZ silicon wafers, which is one of the most important methods to characterize CZ silicon wafers [9].

Light amplitude in a transparent material is determined by total sum of the radiations from dipoles that are induced by electric field of an incident optical beam and the beam itself. The total amplitude due to the dipoles generated by an incident laser beam is proportional to the factor f given by

$$(1) \quad f = \int_V \rho(r) e^{ikr} dv$$

where $\rho(r)$ is the density of electrons polarized by the beam within a volume element dv whose mid-point is defined by the vector r , k is the scattering vector and V is the volume illuminated by the beam.

If spatial distribution of the polarizable electrons is uniform or $\rho(r) = \rho_0$, where ρ_0 is the averaged value of the electron density within V , eq. (1) will have a finite value only when the scattered beam is parallel to the incident beam direction. This means that the incident light will pass through an optically uniform specimen without scattering.

When $\rho(r)$ is not uniform and then given by $\rho(r) = \rho_0 + \Delta \rho(r)$, the contribution due to $\Delta \rho(r)$ will be detected as

$$(2) \quad f = \int_V \Delta \rho(r) e^{ikr} dv,$$

this is the light scattering. Therefore, every spatial inhomogeneity acts as a light scatterer, which will be caused by lattice defects, radiation damages due to ion implantation [1], doping inhomogeneity and small particles such as voids and impurity segregation in semiconductors [2,9,10,12,13] and artificial quartz crystals [3]. Inhomogeneously distributed

electrons trapped by electronically deep level centers are also hopeful candidates for IR light scattering[5].

The optical arrangement of an LST instrument is based on the principles of ultramicroscopy[4], which is typical darkfield microscopy with extremely high contrast and detectability. A tomographic picture is obtained by scanning an IR laser beam focused into a few micrometers in diameter on a plane to be studied within a crystal. Layer-by-layer LST [5] is used to obtain a few to several tomographs which are several parallel sections and are obtained by successive scanning with a given interval [10]. Using this method, the structure and distribution of defects and inclusions are studied three-dimensionally [13]. Spectrum of the scattered light obtained by LST was measured by an optical frequency analyzer, by which inelastic components were clearly observed and thus, the tomographic images are separately but simultaneously taken by both the elastic and inelastic components.

Total internal reflection is developed to detect very fine defects just under a mirror-polished surface of a Si wafer [7], because only the light scattered by the defects will be observed through the mirror surface, while the majority of the incident laser beam is totally reflected by the surface.

Fourier transformed imaging LST was developed to observe shape of a scatterer which was usually imaged as a dot, because its size was smaller than resolving power of a microscope used here. Today, most objective lenses of microscopes can make the image to be studied at infinity. Using these microscopes, the Fraunhofer diffraction pattern of an object to be studied can be obtained by slight shift of the objective lens from the focused position along the optical axis. This can be reconstructed into a shape of the scatterer by Fourier transformation of the diffraction pattern. Many shapes constructed by this method are very similar to the shapes observed by transmission electron microscopy (TEM) [8].

Brewster angle illumination [11] is used to observe the defects without cleaving the sample because the p-component of an incident laser beam completely penetrates into a semiconductive wafer, even if its refractive index n is more than 2.5 due to the sp^3 hybrid orbitals. Here, the Brewster angle is equal to $\tan^{-1} n$.

References

- 1) T. Ogawa, K. Sakai & Y. Yamada, Jpn. J. Appl. Phys. 27 (1988) pp.L1327-L1330
- 2) T. Ogawa, DRIP-I, ed. by Fillard, Materials Sci. Monographs, 31 (Elsevier, 1985) pp.1-14.
- 3) K. Moriya & T. Ogawa, Jpn. J. Appl. Phys. 22 (1983) pp.L207-L209.
- 4) T. Ogawa & N. Nango, Rev. Sci. Instrum. 57 (1986) pp.1135-1139.
- 5) S. Kuma, Y. Otoki & K. Kurata, DRIP-I, ed. by Fillard, Materials Sci. Monographs, 31 (Elsevier, 1985) pp.19-25.
- 6) K. Sakai & T. Ogawa, Jpn J. Appl. Phys. 29 (1990) pp.1765-1768, ibid, 31 (1992) pp.2945-2948.
- 7) N. Nango, H. Furuya, J. Furukawa & T. Ogawa, J. Appl. Phys. 78 (1995) pp.2892-2893.
- 8) K. Sakai & T. Ogawa, Proc. 2nd International Symposium on Advanced Sci. & Tech. of Si Materials, ed. by Umeno, (JSPS, 1996), pp.195-200 & Proc. the 2nd Symposium on Atomic scale Surface and Interface Dynamics, 1998, 303-306
- 9) T. Lu, K. Toyoda, N. Nango & T. Ogawa, J. Crystal Growth, 114 (1991) pp.64-70.
- 10) K. Sakai, K. Sawahata & T. Ogawa, J. Crystal Growth, 103 (1990)

pp.61-64.

- 11) T. Ogawa, J. Crystal Growth 88 (1988) pp.332-340 & p.552, ibid., 96 (1989) pp.777-784.
- 12) G. Kissinger, et al., J. Crystal Growth 158 (1996) pp.191-196, PRIP 1995, ed. by A.R. Mickelson, Inst. Phys. Conf. Series No. 149, pp.19-29.
- 13) M. Ma and T. Ogawa, Phil. Mag. A 72 (1995) pp.113-120, and ibid, A 74

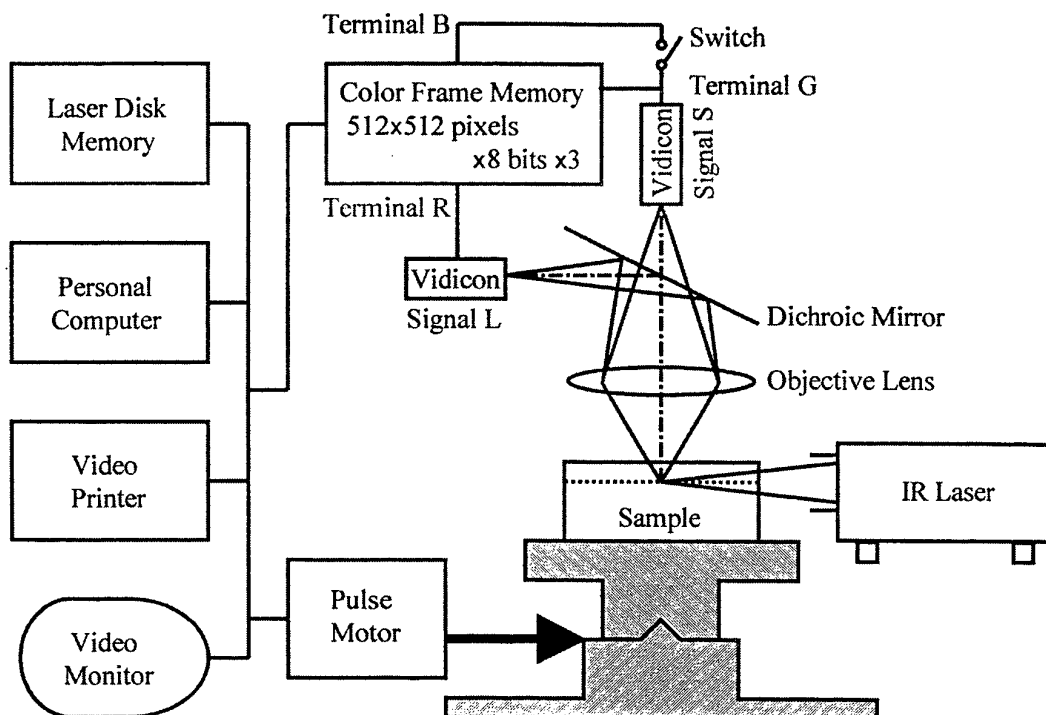


Fig.1 Schematic drawing of Light Scattering Tomography

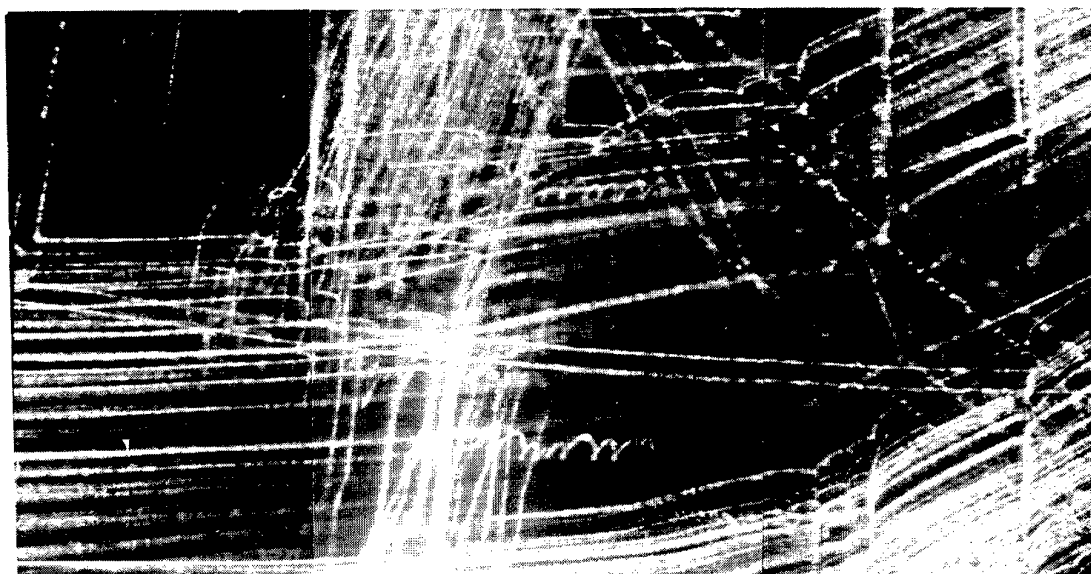


Fig.2 Dislocation forest in An In doped LEC GaAs crystal

AN EXAMPLE OF TEACHING CRYSTAL GROWTH TECHNOLOGY FOR THE U.D. AND M.Sc. STUDENTS-CRYSTALLOGRAPHERS

Nikolai I. Leonyuk (*Moscow State University, Moscow 119899, Russian Federation*)

Crystal growth is taught in many universities, but its scope traditionally is mostly a fragmentary and applied tool of interest to materials scientists, solid-state physicists and chemists, inorganic and physical chemists, electrical engineers, gemologists and mineralogists. This paper is focused on teaching crystal growth technology as part of a new multi-year crystal growth course containing lectures, seminars, laboratory practices and research work. The course has evolved for nearly two decades, and it has combined the educational and research experience of the author of this course in this field of crystal growth at Moscow State University (MSU) and in collaboration with other universities, research institutions and the industry.

The Crystal Growth Technology course is offered for students at the beginning of the 8th semester. By that time, students intending to major in Materials Science and surrounding disciplines are aware of the most general physical laws and phenomena, and chemical processes, and they may already have taken some mathematics courses. Also, they have taken the General Crystal Growth course covered the topics as follows: (1) Nucleation, structurally attributed shape and equilibrium shape of ideal crystals; (2) Growth mechanisms of perfect crystals; (3) Growth of real crystals; (4) Transport processes and morphological stability; (5) Crystal growth methods.

The lectures, seminars and laboratory work of this Crystal Growth Technology course covered the following topics: (1) Experimental equipment; (2) Classification of growing crystals and criteria for choice of growth method; (3) Crystal growth of most important technological oxide materials; (4) Diamond; (5) High T_c superconductors; (6) Jewellery-cut materials; (7) Organic materials; (8) Other novel and unconventional materials; (9) Current problems and future trends.

The students-crystallographers who intend to major in the field of crystal growth and characterization of materials spend on this course 60%, 70% and 90% of the typical student's time in the 8th Spring semester and in the 5th and 6th academic years respectively. Also, research training is planned in industrial laboratories on the

topics: (a) Hydrothermal growth of piezo-quartz, optical calcite, zincite, berlinite; (b) High-temperature flux growth of mica crystals; (c) Czochralski growth of bismuth orthogermanate crystals; (d) Growth of rare earth aluminate crystals by float zone melting; (e) Synthesis of diamond.

Each year, all these students must perform and defend publicly their research projects. Examples of current research project topics are: (a) high-temperature crystallization of new materials with device potential in borosilicate systems; (b) controlled flux growth, composition and morphology of corundum crystals doped with trivalent metals; (c) Growth and morphology of the 123 high- T_c family's single crystals; (d) Epitaxial intergrowth of isostructural phases in Bi-2212 high- T_c single crystals; (e) Czochralski and flux growth, chemical analysis and X-ray study of rare earth oxioorthosilicates; (f) Hydrothermal growth and characterization of zincite single crystals doped with di- and trivalent metals; (g) Low-temperature synthesis and flux growth of rare earth pyro- and metaphosphate laser crystals; (h) Growth and morphology of paraffin crystals grown under various conditions.

For carrying out the U.D. (University Degree) projects, all students may take the opportunity of nine-week internships and/or visiting assignments in university research laboratories, academic institutions or industry during summer periods after 8th semester, and the 10th Spring semester is additionally reserved for completing this research project that should be defended at the end of May. The 6th academic year (the 11th and 12th semesters) is reserved to perform and define the research project directed towards obtaining the M.Sc. degree. Graduates from this program may be invited to work in the field of crystal growth and characterization of materials at universities, at academic institutions or in industry. The most outstanding students encouraged to pass entrance examinations and to begin their work towards the Ph.D. degree.

Strong interaction and integration between the University Education Program, the Academy of Sciences' Institutions, and Industry seems to be one of the keys to developing effective researchers for the future.

CRYSTAL GROWTH OF BORATE MATERIALS WITH DEVICE POTENTIAL: REALITIES AND PERSPECTIVES

Nikolai I. Leonyuk (*Moscow State University, Moscow 119899, Russian Federation*)

To date, more than 600 inorganic borates and various structural derivatives have been synthesized as part of studies of their phase diagrams [1]. A few dozens of them, especially, anhydrous compounds can consider as promising polyfunctional materials with non-linear optical, piezoelectrical, acousto-electrical properties, and also as new laser media with double function and tunability, etc. (for instance, see ref. [2, 3]). However, only a few borate crystals like well known BBO (β - BaB_2O_4) or LBO (LiB_3O_5) has found widespread use in science and modern technology. Most of the borate materials are incongruently melting, and the borate melts have a high viscosity due to their tendency to form numerous polyanions of different composition and configuration. In this paper, an attempt was made to examine the crystallization processes of the most important anhydrous ortho-, pyro, meta- and polyborates with device potential to develop advantageous crystal growth technologies for these new materials.

Orthoborates: $\text{RM}_3(\text{BO}_3)_4$ ($R = \text{Y, La - Lu, In or Bi, and } M = \text{Al, Sc, Cr, Fe, Ga}$), InBO_3 , BaCaBO_3F , $\text{Ba}_7(\text{BO}_3)_3\text{F}_5$, $\text{KBe}_2\text{BO}_3\text{F}_2$. The growth of orthoborate crystals is restricted mostly by the transfer of BO_3 triangles from an associated state of strain, due to linked B-O bonds (about 520 kJ/mole), to separated isolated state at the solid/liquid interface. The change in the coordination number of boron atoms from 4 (in complex borate melts) to 3 (in orthoborate crystals) cannot be excluded, and it is also associated with a high energy consumption. A wide range of complex melts, first of all, based on the alkali molybdates and tungstates will be proposed to destroy boron-oxygen polymers and intensify mass transfer in the orthoborate crystallization process. The fluorides will also destroy the polymers, and they would be preferable for the crystal growth of fluorine-containing orthoborates.

Pyro- and metaborates: $\text{Mg}_2\text{B}_2\text{O}_5$, $\text{Cd}_2\text{B}_2\text{O}_5$, KNbOB_2O_5 , BaB_2O_4 . Isolated B_2O_5 pyroborate dimers and B_3O_6 metaborate rings most likely occur in the borate melts,

in particular, if the complex melts contain a rather large cations like Na^+ , K^+ , Mg^{2+} , Cd^{2+} , and even Ba^{2+} . There is a correlation between the fluxed melt composition and the temperature ranges, in which metaborate chains transform into metaborate rings, and the BBO crystallizes in the low temperature modification. To optimize the crystal growth of pyro- and metaborates, the complex melt compositions and temperature ranges for formation of isolated B_2O_5 pyroborate dimers, B_3O_6 metaborate rings and B_nO_{2n} metaborate chains will be discussed.

Polyborates: $\text{Li}_2\text{B}_4\text{O}_7$, LiB_3O_5 , CsB_3O_5 , SrB_4O_7 , $\text{Sr}_2\text{Be}_2\text{B}_2\text{O}_7$, $\text{SrLiB}_9\text{O}_{15}$. In this case, there are substantial restrictions to transport very large B_nO_m polymers from the melts into the crystal structure that practically has the same polyanion configurations with covalent boron-oxygen bonds. A major problem which awaits clarification concerns the detailed mechanism of polyanion reconstruction along the specific liquid polymer/solid polymer interface. In this connection, a role of various cations as a catalysts will be considered to promote these polyborate to crystallize. This assumption is based on the growth of $\text{LiB}_3\text{O}_5/\text{CsB}_3\text{O}_5$ crystals from non-stoichiometric melts with some excesses of Na_2O , K_2O , MoO_3 , WO_3 and B_2O_3 .

In conclusion, as a consequence of earlier results [4], the crystallochemical approach will be taken as an initial stage to forecast borate systems with desirable structures and to overcome, in part, problems concerned with polymer reconstruction in crystallization processes of these new materials. It can be easily applied to other inorganic polymers like silicates, phosphates, germanates and other many interesting materials which have still not been crystallized and many more of which crystals are not available in good size or quality.

References

1. N.I.Leonyuk and L.I.Leonyuk, Crystallochemistry of Anhydrous Borates. Monograph. Moscow: MSU Press, 1983 (in Russian).
2. N.I.Leonyuk and L.I.Leonyuk, "Growth and Characterization of $\text{RM}_3(\text{BO}_3)_4$ Crystals", Prog. Crystal Growth and Charact. 31 (1995) 179-278.
3. N.I.Leonyuk, "Recent Development in the Growth of $\text{RM}_3(\text{BO}_3)_4$ Crystals for Modern Applications", Prog. Crystal Growth and Charact. 31 (1995) 279-312.
4. N.I.Leonyuk, "Structural Aspects in Crystal Growth of Anhydrous Borates", J. Crystal Growth 174 (1997) 301-307.

Development of CLBO and GdYCOB Crystals for UV Generation

Y. Mori and T. Sasaki

Department of Electrical Engineering, Faculty of Engineering, Osaka University

2-1 Yamadaoka, Suita, Osaka 565-0871, Japan

TEL +81-6-879-7707, FAX +81-6-879-7708

email: mori@pwr.eng.osaka-u.ac.jp

The interest in the use of borate crystals in ultraviolet (UV) nonlinear optics (NLO) has increased because all solid-state UV lasers obtained with NLO are in highly demand. Much effort has been spent on developing borates series, such as β -BaB₂O₄ (BBO) and LiB₃O₅ (LBO), in this decade. Recently another new borate crystals, CsLiB₆O₁₀ (CLBO), YCa₄O(BO₃)₃ (YCOB) and Gd_xY_{1-x}Ca₄O(BO₃)₃ (Gd_xY_{1-x}COB) have been developed by the present author. Here, the growth, NLO and frequency conversion properties of CLBO, YCOB and Gd_xY_{1-x}COB crystals are reviewed and their properties are discussed in relation to those of other nonlinear optical crystals, such as BBO and LBO.

CLBO showed the ease in growth and excellent NLO properties for 4th and 5th harmonics generation of Nd:YAG laser radiation. CLBO crystal with dimensions of 14 x 11 x 11 cm³ could be grown by flux method for three weeks. Moderate birefringence makes CLBO possess a smaller walk off angle to achieve better spatial overlapping of the mixing beams compared to BBO. Thus, higher conversion efficiency and better beam pattern of harmonics generation can be achieved. Its relatively large angular, spectral and temperature acceptance bandwidths have favored CLBO for stable 266 and 213 nm generation of high power Nd:YAG laser.

YCOB and Gd_xY_{1-x}COB crystals are suitable NLO crystals for 2nd and 3rd harmonics generation of Nd:TAG laser radiation. These crystals also showed the ease in growth without cracks and bubbles by the Czochralski method. Gd_xY_{1-x}COB crystals had an uniformity of crystal composition along with growth direction so these crystals confirmed a substitutional solid solution of Gd_xY_{1-x}COB. For frequency conversion applications, it is important to use NCPM along the principal axes due to the large angular acceptance and elimination of walk-off between fundamental and harmonics lights, leading to the higher efficiency. We have succeeded to generate noncritical phase-matched THG of Nd:YAG laser (1064 nm) light in Gd_{0.24}Y_{0.76}COB. Gd_{0.24}Y_{0.76}COB possesses zero walk-off angle, and larger angular and temperature bandwidths compared to LBO. This means that Gd_{0.24}Y_{0.76}COB exhibits the better NLO properties compared to LBO.

Crystal Growth of LBO($\text{Li}_2\text{B}_4\text{O}_7$) by Modified Bridgman Method

Mitsuru ISHII¹⁾, Koji IMAI²⁾, Noriaki TSUTSUI²⁾ and Isao YAMAGA³⁾

1) SIT, Shonan Institute of Technology, Fujisawa 251-0046 Japan

2) Chichibu Fuji Co., Ltd., Ogano Chichibu-Gun, Saitama, Japan

3) Futeck Furnace Co., Ltd., Kanazawa, Yokohama, Japan

We grew a high quality large and long LBO single crystal for surface acoustic wave devices by the modified Bridgman method. Using a Pt crucible, we grew it at growth rate of 0.5mm/h and found that grown crystal was free from cracks and residual strain and EPD is less than $10^3/\text{cm}^3$.

1. Introduction

LBO($\text{Li}_2\text{B}_4\text{O}_7$) is a piezo-electric and non ferroelectric crystal, which has advantage of a large coupling coefficient for surface acoustic wave propagation and a low temperature coefficient of frequency. Much hope is placed thereon as filter material for potable telephone. LBO crystal has so far been grown by CZ method. However, voids and cracks tend to be caused in the crystal and no report of growth of crystals larger than 3 inches has so far been made¹⁾. Fan et al. reported on the growth of larger than 3 inches crystals by Bridgman method²⁾. The purpose of this paper lies in development of a growth technology of long LBO crystals with 3 inches in diameter and offering board material of SAW devices.

2. Crystal growth

Fig. 1 is a macroscopic photograph of an ingot when growing a LBO crystal of 2 inches in diameter by the conventional vertical Bridgman method.³⁾ In the center of the ingot, white bubbles voids are seen in the beginning part of body from shoulder. But, no voids are grown in the latter half part in grown crystals. While crystals are under growth, if the temperature gradient of the furnace and heat flow of crystal are steady state, no bubble will be generated in crystal. Taking notice of this point, we grew crystals using a seed crystal having the same diameter and a grown crystal which basically same as processing of BGO($\text{Bi}_4\text{Ge}_3\text{O}_{12}$) crystals⁴⁾.

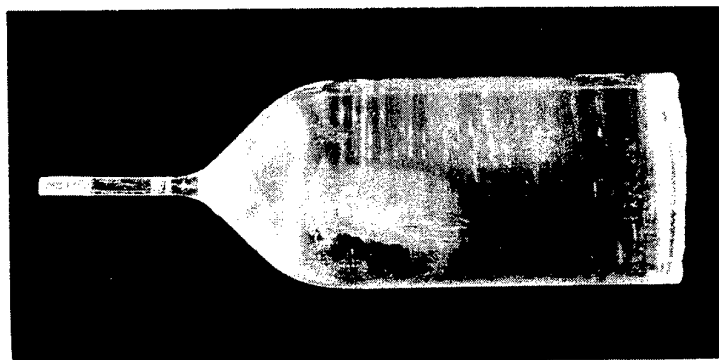


Fig. 1 A LBO crystal grown by conventional Bridgman method.

We used a Pt foil crucible with carbon for crucible holder. The vertical type furnace has a 3-zone heater and welded two thermocouple to a crucible for monitoring the start and finishing of crystal growth. The crucible was down at 0.5 mm/h in nitrogen atmosphere and growth orientation was $\langle 110 \rangle$ direction.

3. Experimental results

The external appearance of grown LBO crystal is shown in Fig. 2. The bubbles of $\sim 1.5\text{mm}$ in diameter were formed on the surface of ingot, resulting in being rough. There was a tendency that the lower in ingot, the many bubbles. However, no voids were formed in the inside of an ingot. The more bubbles at surface of ingot was caused when poly-crystal starting raw materials was used, while the less bubbles caused when recrystallized raw material was used. The more was caused in nitrogen than oxygen atmosphere. When the down speed of crucible exceeds 0.7 mm/h, void in crystal were caused intermittently along the solid liquid interface. But, no voids were caused in 0.5mm/h at all.

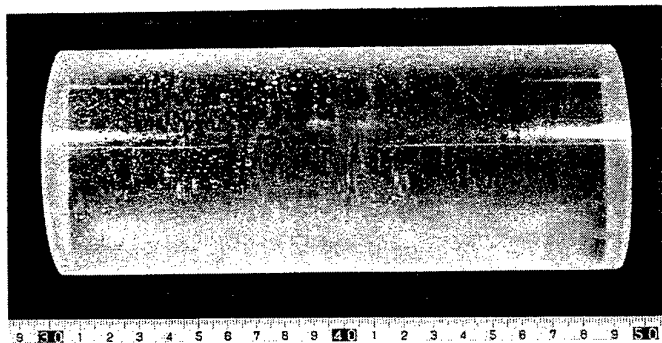


Fig. 2 A large LBO crystal grown by modified Bridgman method.

As for strain in an ingot, when the wall thickness of crucible is thick, it will be caused 4 time symmetry. When the thickness is thin, nothing is observed. Cracks were caused in the ingot when the cooling rate is large and the temperature gradient of the furnace is large at below 700°C . Micro defects such as sub-boundary and dislocation can be decreased using good seed crystals. We found it very high quality which the no sub-boundary in grown crystal and its dislocation etch pits density observed as $10^2 \sim 10^3/\text{cm}^2$.

In conclusion of the above experiments, we can supply such long LBO crystals as 8 inches having 3 inches in diameter for SAW devices for potable telephone.

- 1) R. Komatsu, et al., Appl. Phys. Letters. 70(26)3492.
- 2) S-J. Fan et al., Crystal Properties and Preparation, Vol.36-38,46-51(1991)
- 3) M. Ishii, et al., Symp. on Synthetic Crystals Science and Technology, Fujisawa, Nov. 28, 1991, p.93. (Japanese)
- 4) F. Allegretti et al., J. Crystal growth., 94(1989)373.

Growth of YAG/Sapphire eutectic and YAG single crystal fibers by the micro-pulling-down (μ -PD) method

IMR, Tohoku Univ. [○]Akira Yoshikawa, Kenji Hasegawa, Tsuguo Fukuda

INTRODUCTION Crystal grown as thin fibers are not only useful in miniaturization, but also offer a great improvement of physical properties due to the reduced number of defects. Moreover, the fibers have a flexibility that we can hardly obtain from bulk size crystals.

In this work, we describe the growth of YAG/Sapphire eutectic fibers and report on their strength properties under extremely high temperature, comparing them with bulk crystals. We also report growth of Nd:YAG single crystal fibers.

YAG/SAPPHIRE EUTECTIC FIBERS Recently, it has been found that ceramic matrix composites reinforced with sapphire phase have excellent high-temperature properties. Such high-performance materials are of interest for use in advanced aerospace structures, automobile engines, high efficiency gas generators, and other high-temperature applications.

EXPERIMENTS The starting materials were 4N purity Al_2O_3 and Y_2O_3 in the molar ratio of 81.3 mol% Al_2O_3 / 18.7 mol% Y_2O_3 . YAG/Sapphire eutectic fibers were grown by the micro-pulling-down (μ -PD) method using an Ir crucible and Ir after heater. Induction heating at a frequency of 5 kHz was employed. The growth atmosphere was Ar gas. Tensile strength measurements were performed at room temperature and 1700°C.

RESULTS The length of the crystals exceeded 500mm and the diameter was 0.2-1.0mm. View of the YAG/Sapphire eutectic fibers is given in Fig.1. Microstructures were investigated using a scanning electron microscope (SEM) (Fig.2).

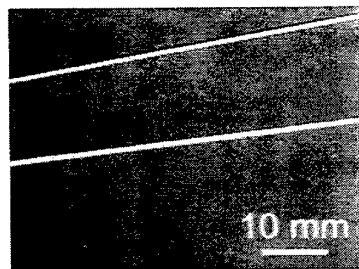


Fig. 1 YAG/Sapphire fibers

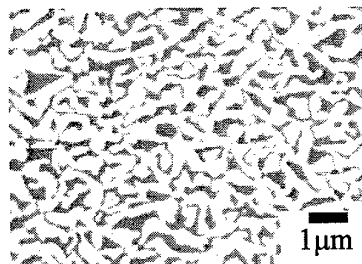


Fig. 2 Back Scattered Electron Image of YAG/Sapphire fibers

From electron-probe microanalysis (EPMA), the bright region was identified as YAG and the dark region as sapphire. The YAG and sapphire phases form a three-dimensional network. Tensile stress-displacement curves of YAG/Sapphire

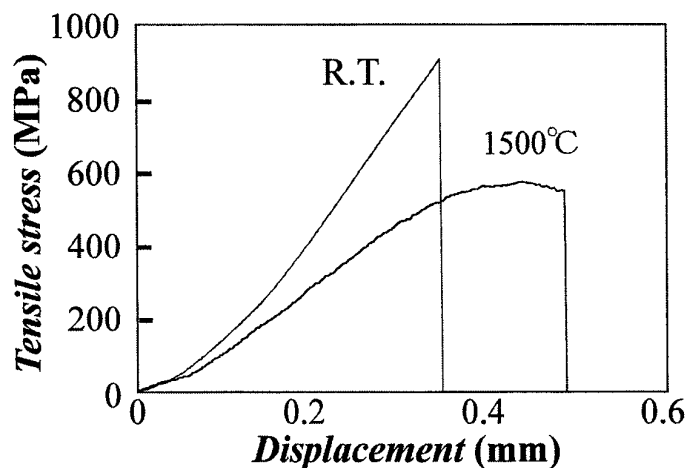


Fig. 3 Tensile stress-displacement curves of YAG/Sapphire eutectic fibers. (in Ar gas atmosphere)

YAG SINGLE CRYSTAL FIBERS There are certain problems in the usual Rod-type Nd:YAG laser. For example, because of limitations of the cooling system, the power and the quality of the mode are also limited. Besides, it is too difficult to produce a flexible laser system. To overcome these problems, we tried to grow YAG single crystal fibers.

EXPERIMENTS The starting materials were YAG single crystals grown by the Cz method or Y_2O_3 (99.999%), Al_2O_3 (99.9999%) and Nd_2O_3 (99.99%) powders. The crystals were grown by the micro-pulling-down (μ -PD) method using an Ir crucible and Ir after-heater. Induction heating at a frequency of 5 kHz was applied. The growth atmosphere was Ar gas.

RESULTS $\langle 111 \rangle$ orientation of the YAG single crystal fibers grown was confirmed by X-ray measurements. The crystal composition was studied by electron-probe microanalysis (EPMA). About 0.5 atm% of Y^{3+} host cations was substituted with Nd^{3+} . The crystals exceeded 500mm in length and were 0.7-2.0mm in diameter. A view of the Nd:YAG crystal fibers is given in Fig.4.

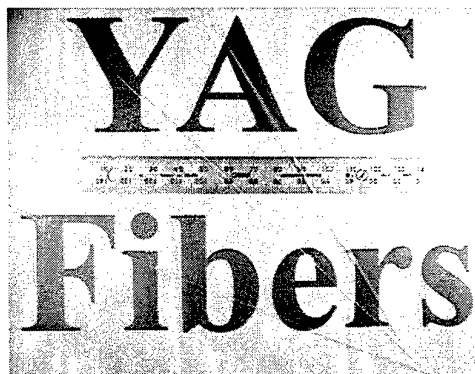


Fig. 4 Nd:YAG single crystal fibers

CZ technology and some properties of scandium-gallium garnets and gadolinium ortovanadate crystals as laser media.

P.A. Studenikin, Yu.D. Zavartsev and A.I. Zagumennyi

Laser Materials and Technology Research Center of GPI RAS,
Vavilov str. 38, build. " D", 117942 Moscow, Russia , Tel/Fax: (095) 135-02-11

Complex investigation on growth and properties of the gallium garnets and gadolinium ortovanadate crystals as well as their melts are presented. Experimental determination of the physical properties of these crystals can provide data for a better understanding of some aspects of theoretical solid-state physics. Their precise values are essential both in physical modeling and in the solution of a number of practical tasks relating to development of new solid-state physics.

For CZ growing gallium garnets investigated influence on the morphological stability such technology parameters as the thermal gradient at the crystal periphery; valence and content of doped impurity in the melt; constant current passed through the crystal/melt interface during crystal growth [1÷3]. The dependencies of morphological stability on the thermal gradient at the crystal periphery and on a valence and content of doped impurity were obtained for yttrium scandium gallium garnet EEGs. In the range of small concentrations (C) of impurities, relative to melt mass of crystal (g_0) has linear dependence from C . A slope of $g_0(C)$ depends on the charge state of the doped impurity. During the crystal growth, the electric current flowing through the crystal/melt interface suppresses the morphological instability of the growth process. Model of morphological stability of gallium garnet growth will be discussed. The present model of morphological stability made it possible to explain the existing methods of suppressing a spiral growth of gallium garnets. The effective method of the suppression the spiral growth is the elimination of the reason of its development the precession of "down flow".

Refractive indices n of a number of gallium garnets were measured with accuracy within 2×10^{-4} in a range 400-1100 nm and a temperature interval 300÷650 K. The thermal coefficient of refractive indices were estimated to an accuracy 5%

[4]. Distribution coefficients of Cr^{3+} , Nd^{3+} , Yb^{3+} , Ho^{3+} , Tm^{3+} , Er^{3+} ions in YSGG and Cr^{3+} , Nd^{3+} ions in GSGG were obtained by X-ray microprobe analysis and absorption spectra. Congruently melting composition of YSGG was determined as

$\text{Y}_{2.95}\text{Sc}_{1.56}\text{Ga}_{3.49}\text{O}_{12}$ [5]. The surface tension δ of the YSGG garnet melt (the melting point is 2150 K) was measured by the method of tearing off the iridium probe from the melt surface [6]. The results are given of an investigation of a Cr:Yb:Ho:YSGG crystal laser in a cavity with a disperse component. Continuous tuning of the output radiation wavelength in the range $2.84\div 3.05\mu\text{m}$ is represented [7].

Different vanadate crystals such as the Nd:GdVO₄, Ho:Tm:GdVO₄, Tm:GdVO₄, Er:GdVO₄, Yb:GdVO₄ were grown by Czochralski technique [8]. Distribution coefficients of Yb^{3+} , Tm^{3+} , Er^{3+} , Nd^{3+} ions depend linearly on average radius of a dodecahedral ion. Refractive indices are measured with accuracy within 5×10^{-5} in a range 400-1100 nm. Constants of the Sellmeier's formulas are received. Refractive indices depend on the size of the average dodecahedral radius. The thermal conductivity of the doped crystals in the temperature range of 50-300K is measured. As a result of analysis it is shown that vanadate crystals have essential advantages for diode pump lasers in comparison with conventional host YAG and YLF: large stimulated emission cross section at lasing wavelength; wide absorption band at pump wavelength; low dependency on pump wavelength and temperature control of a diode laser; low lasing threshold.

REFERENCES:

- [1] P.A.Studenikin, 8All-Union CCG, Kharkov, 1992, Theses, v.3, part 2, 341÷342
- [2] P.A. Studenikin at al., 3rd ECCG, Budapest, 1991, Abstracts, 338÷339
- [3] A.A.Yakovlev, Yu.D.Zavartsev and P.A. Studenikin, The same, 72÷73
- [4] E.V.Zsharikov at al., Kristallografiya, Vol.34, 5 (1989) 1181÷1184
- [5] S.V.Lavrishchev, P.A. Studenikin, 3rd ECCG, Budapest (1991)Abstracts,107÷108
- [6] Yu.D.Zavartsev and A.A.Yakovlev, Crystal Growth 142 (1994) 129÷132
- [7] A.F.Umyskov at al., Quantum Electronics 26 (7) (1996) 563-564
- [8] A.I.Zagumennyi at al., SPIE Vol. 2698 (1996) 182-192.

GROWTH PECULIARITIES OF YAG CRYSTALS AS REVEALED BY USING A SCANNING ELECTRON MICROSCOPE

Valentin IOV

*National Institute of Laser, Plasma and Radiation Physics
PO BOX MG-36, Bucharest-Magurele, RO-76900, ROMANIA*

Solid state lasers requires large crystals of very high quality. Garnets doped with trivalent rare-earth (RE^{3+}) ions are well known solid state laser systems. Cathodoluminescence (CL) imaging in a scanning electron microscope (SEM) offers unique opportunities for mapping the defect areas in laser crystals. The electron beam of an SEM produce luminescence emission which may be connected with high lying RE^{3+} metastable levels [2]. CL emission can be very sensitive to local variation of dopants. In the regions of defects the local variation of dopant concentration changes, leading to variations in emission intensity that can be used for imaging the defects.

Experimental: Both $\text{Nd}^{3+}:\text{YAG}$ and $\text{Cr}^{3+}:\text{Tm}^{3+}:\text{YAG}$ of various concentrations were grown from the melt contained in Ir crucibles using the Czochralski technique. Pulling and rotation rates were (0.9-1.1) mm/h and (30-50) rpm, respectively. The growth atmosphere was N_2 and the seed was oriented along $\langle 111 \rangle$ direction. The samples were sliced transversally on growth direction from regions of good quality crystals and from regions or boules presenting technological defects. Samples were polished, coated with aluminum and then were examined in a SEM operating at accelerating voltages among 10 and 40 KV using the standard CL accessory.

Results and discussion: The defect most clearly observed in $\text{YAG}:\text{Nd}^{3+}$ crystals by CL is the core. A whole transverse section of a $\text{YAG}:\text{Nd}$ (1 at.% Nd) sample (of 16 mm diam.) reveals two distinct areas: the central part (of about 2 mm diam.) and the outer part. A small magnification (x 100) shows (see Fig. 1) a core of approximately 2 mm diameter in the central area, due to $\{211\}$ facetting. In the central part, dark and light bands parallel to each other reflect the trigonal symmetry of $\{211\}$ facets. By

increasing the rotation rate, the faceted growth was stopped (the smaller dark circle)

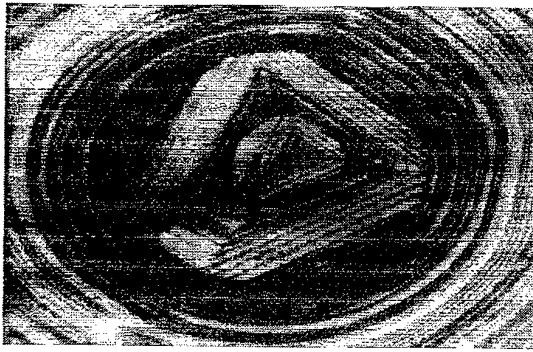


Fig. 1. The core of a Nd:YAG crystal (x 100 magn.) Fig. 2. Growth striations in a Tm:Cr:YAG crystal (out of core)

Clear differences in light intensity emitted from the core area can be seen. It is assumed that the dark and light bands reflect the concentration variations of dopant, because in regions of good quality crystals the light bands do not exist and the CL image shows a full dark pattern over the entire slice. Cockayne [2] stated that in YAG:Nd crystals the concentration of Nd^{3+} ions is about 20% higher in the facet region than in the bulk of the crystal. Further increase of rotation rate stopped the facet formation and the outer part of the core shows a more or less regular dark and light rings. The CL image of the outer part of the core (Fig. 2) reveals alternating dark and light bands due to growth rate fluctuations. The most likely cause of differences in light emission is the strain present in the growth striations produced by variations of the growth conditions by either a non-symmetric temperature distribution around the crystal pulling direction or temperature or pull-rate fluctuations. This compositional variations are present in all samples examined and provide an effective means of studying the history of interface shape of a crystal after it has been grown.

Conclusion: The investigation of Nd:YAG and Cr:Tm:YAG crystals by using the standard CL part of an SEM has shown that this method could prove useful for correcting crystal growth technology and for selecting regions of crystal for processing laser rods of uniform quality.

References

- [1] V. Lupei, 7-th ECDIM, Lyon, 5-8 July 1994, Paper Abstract, p. 362
- [2] B. Cockayne, J. Crystal Growth **3-4** (1968) 60

" Formation of block structure in sapphire crystals. "

Prof. Dr. Mikhail I. Moussatov, Russia.

The stress in crystals we consider as a condition of a crystal lattice, in which its parameters do not correspond equilibrium state for given temperature. There are the next basic sources of stress in crystals resulting in plastic deformation at high temperature: a) change of temperature of a crystal with such speed, at which the structure of a crystal has no time to accept the equilibrium form., b) presence of the large gradients of temperature in a crystal, c) presence in a crystal of impurity and inclusions, d) external mechanical influence (for example, contact with a crucible, injection by indenter, etc.).

The thermal stress in crystals arise during their cultivation or subsequent cooling and, in particular, as a result of its moving to a zone with the large gradients of temperature. The basic defects arising in crystals under action of stress at presence of sufficient plasticity are the dislocations and their wall, the blocks. The mechanical properties of sapphire have appreciable anisotropy, therefore formation of dislocations and blocks should depend and on orientation of an optical axis concerning a direction a basic heat transfer, which determines a direction of action of the thermal stress. When the direction of action of stress coincides with a direction of less power-intensive sliding in crystals, then the formation of block structure and a dislocation walls (fig. 1) is most probable .

So for example, in all methods of growing of sapphire crystals from melt the action of thermal stress is directed so, that the formed blocks miss by a fan from the central axis in a direction of a hotter part of crystals (fig. 2). From a fig. 2 it is visible, that the sliding was realized on planes $(10\bar{1}0)$ and $(01\bar{1}0)$, but it is absent on physically equivalent directions $(\bar{1}010)$ and $(0\bar{1}10)$. It is known, that the growing of zero orientation sapphire crystals (direction basic heat transfer from a crystal coincides with a direction of an optical axis) is complicated or it is impossible. We have found out, that the quality of crystals of sapphire in a GOI method does not

depend on an optical axis orientation a stage of growth. Orientations of an axis influences quality of crystals only on a stage of their subsequent cooling. So, for example, the structural perfection of zero orientation sapphire crystals is identical to crystals 90° - orientation only in the event that the speed of their cooling makes no more than 0,30-0,35 from speed of cooling 90° - crystals. However, the sizes of residual stress in them are higher at 10-15 time, than in 90° - crystals. If this speed to increase up to 0,5-0,6, in crystals of zero orientation occurs blocks (fig. 3). If to cool crystals of zero orientation with the same speed, as well as 90° , in crystals there can be cracks (fig. 4), but blocks in them is not present. It means, that for formation of blocks the influence of stress is necessary during long time in conditions of sufficient plasticity of crystals. We explain the received results by presence in sapphire significant anisotropy of diffusion speeds of vacancies. In this case parameters of a crystal lattice differ from equilibrium for given temperature meanings, , in particular, because of discrepancy of amount of vacancies to given temperature, as they have no time to migrate to a surface, and their concentration becomes higher, than that is required by conditions of thermodynamic balance.

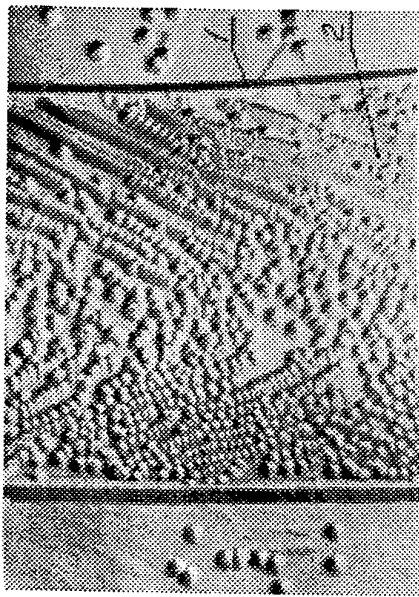


Fig.1

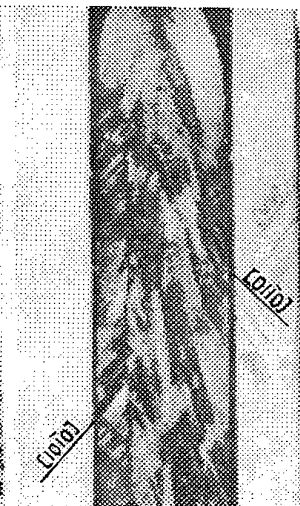


Fig.2

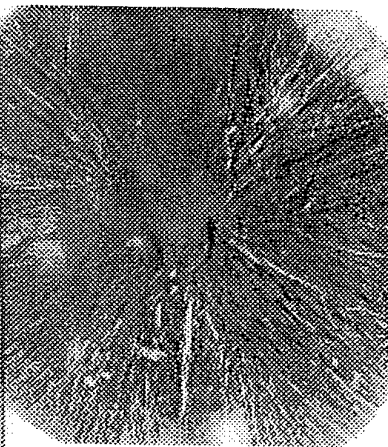


Fig.3

SOME NEW APPROACHES TO OBTAIN THE ORGANIC CRYSTALS WITH HIGH QUALITY

S.V.Budakovsky, N.Z.Galunov, V.P.Seminozhenko

Institute for Single Crystals, Lenin av., 60, Kharkov, 310001, Ukraine

Due to low effective atomic number organic materials characterize by negligible back scattering effect for the process of charged particles absorbtion. In other words inorganic materials are most effective for gamma- and X-ray scintillation detectors and organic ones are the most effective for short range ionizing radiation detection, i.e. for detection the most hazar for man organism radiations (medical and radioecology problem), which are used in many technical applications (e.i. electronic microscopes), etc. Due to high concentration of hydrogen atoms they used in fast neutron spectroscopy. The most effective organic scintillation systems are the organic single crystals. In 80-ies the progress in the characteristics of organic single crystals obtained on the base of classical approach (Bridgemen technique) became hopeless. In the present time new technologies for scintillation plastics design gives the possibility to achieve the light output of the best samples about output of stilbene or *p*-terphenyl single crystals. In addition, the highest dimensions of the organic single crystals usually sold in Western market were diameter about 60 mm and 60 mm height. That is why in 80-ies - 90-ies the organic single crystals disappeared from catalogues of leading companies.

The report consists of two parts which are devoted to new technique of crystal growth with controlled structural perfection and production of new type of organic crystals by hot pressing. Traditionally, crystals were grown for scintillation technique in Institute for Single Crystals. Therefore mentioned techniques were aimed to obtain the system with high quality for scintillation applications. It is well known that the light yield of an stilbene single crystal is lower by factor 1.4...1.5 than for an anthracene one. The highest diameter of organic single crystals produced by traditional Bridgman technique is about 40 mm and highest light yield of anthracene single crystals is about $1.5 \cdot 10^4$ photons/MeV. Using the former technique we can obtain the crystals with highest diameter up to 120 mm and light yield for stilbene single crystals about $1.4 \cdot 10^4$ photons/MeV. Using latter one we obtained polycrystals with diameter about 250 mm and the light yield about its value for single crystals obtained for traditional technology. It should be noted that these techniques can be useful not only for scintillation crystals but to crystals for nonlinear optics application, etc.

The main differences of the former technique from traditional ones are following. When organic single crystal is growing from the melt the interaction forces between molecules (Van der Waals ones) are about 10^{-3} eV. Doping the melt with electron-seeking addition agents (ESAA) allows us to produce the charge-transfer complex-like structures melt molecule-molecule of ESAA. The interaction force becomes too high (about 10^{-1} eV) and the electrostatic field of such a complex forms an orientated parts of the melt because. These orientated melt parts promote the formation of crystallization centres in growing crystal layer, which predeterminates the crystal growth process. Such a "volume" and "surface" (the growth on the cleavages of inorganic crystals) effects are discussed.

The special processes of purification of the raw materials was used before growing the crystal. Doping the melt with ESAA allows to control the structure perfection of the grown single crystals (SC). It results in the change of root-mean-square random orientation σ_c of SC mosaic structure, and therefore the concentration of charge carriers and exciton deep traps, the presence of which in organic SC may usually be explained by accumulation of aggregations and ensembles of dislocation at mosaic block boundaries. The SC with the least σ_c is considered as the most structure perfect one. Annealing increased the intensity of radioluminescence only by 10 %, and for structure perfect SC it was by 40-50 % higher. The initial cause of all effects as a result of doping the melt with ESAA is the formation of the charge-transfer complexes (melt molecule-molecule of ESAA). For ESAA concentrations $C < C_R \sim 0.1$ mol.% the formation of such a single complexes is the process of the primary importance. For $C > C_R$ the supercomplexes in the shape of stacks containing more than one single complex are formed. The formation of «partial melt ordering» causes the aftermath of two types: increase of a growth rate, structure perfection (and therefore the maxima dimensions of growing crystal) due to decrease of the withdrawing heat with the increase of the melt «ordering», as well as increase of probability of generation of crystallization centre due to enter into growing crystal layer groups of mutually orientated melt molecules. For $C < C_R$ with C increase more perfect SC are grown. For $C > C_R$ with C increase the perfection of SC decreases.

To make the scintillation polycrystals we having grown the perfect single crystal grind it. Then having chosen the fractions of needed dimensions we press this grinding. The recrystallization process is the last stage of this technique. Using such a technology now we can obtain the scintillation detectors up to 250 mm in diameter and 5 mm in height. Their light yield is about light yield of the single crystals of the same materials and height.

GROWTH OF SCINTILLATION AND PHOTOREFRACTIVE SINGLE CRYSTALS OF BGO AND BSO AND THEIR CHARACTERIZATION

R.Gopalakrishnan* and P.Ramasamy**

* Department of Physics, Anna University, Chennai-600 025, India.

**Crystal Growth Centre, Anna University, Chennai-600 025, India.

Bismuth Germanium Oxide (BGO) and Bismuth Silicon Oxide (BSO) crystals have found applications in optical light modulators and in particular they are used for transient holographic applications and in scintillation detectors. The common problems in oxide crystal growth are, gas bubble incorporation, colouration, striations and cracking during and after growth. Gas bubble along with voids or inclusions, scatter light and hence very purpose of the material is lost. The various parameters such as crystal rotation rate, pulling rate and growth temperature have been considered to optimise for bubble free growth.

Single crystals of $\text{Bi}_{12}(\text{Ge},\text{Si})\text{O}_{20}$ and $\text{Bi}_4(\text{Ge},\text{Si})_3\text{O}_{12}$ were grown from melt by Czochralski technique using a resistive heating furnace in a platinum crucible (45 mm diameter and 50 mm height). Starting materials were of high purity bismuth trioxide, silicon dioxide and germanium dioxide. BGO and BSO crystals of 15 mm diameter and 40 mm length were grown. Crystal growth was performed at different rotation rate and the effect of rotation rate on the quality of the crystal has been studied.

Crystals grown with rotation rate of 5-15 rpm were found to have gas bubbles. These crystals were cut perpendicular to the growth axis and observed with scanning electron microscope. These bubbles will lead to optical inhomogeneity in the crystals. For the rotation rate 15-35 rpm growth became very difficult and no single crystals were obtained. Good quality single crystals with no bubbles were obtained in the region 35-45 rpm.

A strip heater configuration was designed using platinum strip for better thermal stability during the growth of BGO and BSO crystals, under different growth conditions, for Floating Zone technique. A number of good quality single crystals of BGO and BSO have been grown by Floating Zone technique. The X-ray photoelectron spectroscopic (XPS) studies have been carried out on BGO and BSO crystals to characterize the surface quality and bulk nature of the crystals. The surface contamination on both types of crystals is identified. In addition to the contamination, some amount of Bi atoms are observed with Bi ions on Sellinite $[\text{Bi}_{12}(\text{Ge},\text{Si})\text{O}_{20}]$. It is demonstrated that the eulytite $[\text{Bi}_4(\text{Ge},\text{Si})_3\text{O}_{12}]$ crystals are chemically more robust to degradation than the sellinite crystals. Besides, impurities present over the surface are identified from their characteristic binding energy (BE). The predominant covalent and ionic character of $\text{Bi}_4\text{Ge}_3\text{O}_{12}$ and $\text{Bi}_4\text{Si}_3\text{O}_{12}$ respectively is explained from their oxygen 1s core level spectra.

Thermoluminescence studies have been made on $\text{Bi}_4\text{Ge}_3\text{O}_{12}$, $\text{Bi}_4\text{Si}_3\text{O}_{12}$, $\text{Bi}_{12}\text{GeO}_{20}$ and $\text{Bi}_{12}\text{SiO}_{20}$ crystals. The glow curves of $\text{Bi}_4\text{Ge}_3\text{O}_{12}$ and $\text{Bi}_4\text{Si}_3\text{O}_{12}$ indicate only one peak, each around 133°C and 131°C after 1.36 Mrad gamma irradiation. But the TL glow curves of $\text{Bi}_{12}\text{GeO}_{20}$ and $\text{Bi}_{12}\text{SiO}_{20}$ show two peaks each. In $\text{Bi}_{12}\text{SiO}_{20}$, the peaks observed are at 137°C and 252°C whereas in $\text{Bi}_{12}\text{GeO}_{20}$, the peaks are at 138°C and 255°C . The TL emission spectrum is not observed since the TL glow is very weak. The formation of multiple glow peaks can be attributed to the characteristics of the system. Photoluminescence studies have been carried out on the above crystals before and after gamma irradiation. From the photoluminescence studies, it is found that $\text{Bi}_{12}(\text{Ge},\text{Si})\text{O}_{20}$ crystals are more insensitive to gamma irradiation compared to $\text{Bi}_4(\text{Ge},\text{Si})_3\text{O}_{12}$ crystals.

The dislocation density of the grown crystals has been determined by chemical etching technique and it is found to be 10^4 - $10^5/\text{cm}^2$. An etchant has been established by mixing 37.5 mol% of HCl, 12.5 mol% of HNO_3 and 50 mol% of Acetic acid.

Elimination of Growth on (111)B Side Faces by Rotating Substrate in Fabrication of GaAs Mesa-structure by MBE

D. Kishimoto, T. Noda, Y. Nakamura*, H. Sakaki and T. Nishinaga**

Institute of Industrial Science, University of Tokyo, 7-22-1 Roppongi, Minato-ku, Tokyo 106-8558, Japan

*Quantum Transition Project, JRDC, 4-7-6 Komaba, Meguro-ku, Tokyo 153-0041, Japan

**Department of Electronic Engineering, The Graduate School of Engineering,
The University of Tokyo, 7-3-1 Hongo, Bunkyo-ku, Tokyo 113-8656, Japan

Recently, the surface diffusion phenomena during epitaxial growth on non-planar substrates have been gathering a great deal of interests, because of the importance both in the study of the growth mechanism and in the fabrication of low dimensional microstructures and devices [1-3]. In this article, we report that the elimination of growth on (111)B side facets in MBE is possible by rotation of substrate.

Line-and-space patterns were initially prepared on a (001) GaAs substrate by photolithography and wet chemical etching. The stripes were set along $\langle 110 \rangle$ direction. Growth by MBE on such patterned substrates provides facet structures with two (111)B side faces and a (001) top plane. In our MBE machine, the directions of incident Ga and As fluxes were respectively chosen as 11° and 30° off from vertical line to the substrate. During the growth, (111)B surface was exposed to the fluxes the intensities of which varied sinusoidally with substrate rotation. Growth temperature and substrate rotation speed were changed to see the influence on the growth rate of (111)B surface.

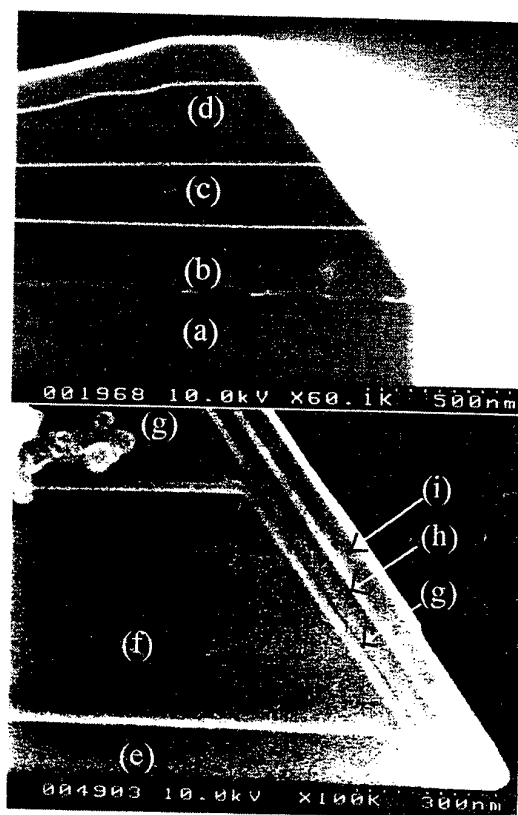
When substrate rotation was as fast as 12 - 20 rpm, (111)B surface did not grow and almost all Ga adatoms on (111)B surface flowed to (001) surface at the growth temperature between 600°C to 640°C (layer (b) (c) (d) in Fig.1 and layer (h) in Fig.2). The ratio of (111)B growth thickness to that of (001), $d_{(111)B}/d_{(001)}$ was found out less than 0.05. On the other hand, under slower rotation speed such as 6 rpm, growth occurred both on (111)B and (001) surfaces and

$d_{(111)B}/d_{(001)}$ was about 0.1 (layer (h) in Fig.2). When the substrate rotation was stopped and (111)B surface was continuously exposed to Ga flux, $d_{(111)B}/d_{(001)}$ was increased to the value about 0.37 (layer (i) in Fig.2).

These phenomena can be understood as follows. When rotation speed is high, Ga adatoms cannot be accumulated to form 2d-nucleation on (111)B surface and all adatoms flow away to (001) surface by surface diffusion. However, under lower rotation speed, Ga adatoms are sufficiently accumulated and growth occurs on (111)B surface. We suppose the critical rotation speed to see the start of the growth may have relation to the relaxation time of Ga adatoms to diffuse from (111)B side to (001) top surfaces.

Fig.1. SEM cross section photograph of the sample. Dark region and white lines indicate respectively GaAs layers and AlAs markers. (a) substrate. (b) - (d) MBE growth layers. Arsenic pressure and GaAs growth rate were kept constant throughout this experiment as 1.0×10^{-5} Torr and $0.21 \mu\text{ m/h}$ respectively and substrate rotation speed was 12rpm. Growth temperature was varied as (b) 600° C , (c) 620° C , (d) 640° C .

Fig.2. Effect of substrate rotation speed. (e) substrate. (f) - (i) grown layers. The rotation speed was 20rpm for (f) and (g), 6rpm for (h) and no rotation for (i). Arsenic pressure, GaAs growth rate and substrate temperature were kept constant as 1.0×10^{-5} Torr and $0.23 \mu\text{ m/h}$ and 600° C respectively.



- [1] T. Isu, A. Watanabe, M. Hata and Y. Katayama, Jpn. J. Appl. Phys. **27** (1988) L2259.
- [2] X. Q. Shen and T. Nishinaga, Jpn. J. Appl. Phys. **32** (1993) L1117.
- [3] S. Koshiba, Y. Nakamura, M. Tsuchiya, H. Noge, H. Kano, Y. Nagamune, T. Noda and H. Sakaki, J. Appl. Phys. **76** (1994) 4138.

New Surface Cleaning Method of GaAs or AlGaAs without Arsenic Flux
for Molecular Beam Epitaxy

Kanji Iizuka, Toshimasa Suzuki and Hiroshi Okamoto*

Nippon Institute of Technology

4-1 Gakuendai, Miyashiro, Minami-Saitama, Saitama 345-8501, Japan

* Chiba University, Faculty of Engineering

1-33 Yayoi-cho, Inage-ku, Chiba 263-0022, Japan

Surface cleaning prior to GaAs/AlGaAs molecular beam epitaxy (MBE) growth is one of the most important processes to obtain high quality quantum well (QW) structure or very flat hetero-interface. The conventional GaAs surface cleaning method includes a flash annealing at 600-650°C in the growth chamber under arsenic vapor pressure. During this process, however, a large amount of oxygen-related impurity gasses such as CO, CO₂ and H₂O are generated inside the growth chamber.

In this study, a new surface cleaning method which can be carried out in the preparation chamber without arsenic flux and its effectiveness for GaAs or AlGaAs have been investigated.

GaAs (100) wafers were first treated with standard chemical etching and then introduced into the preparation chamber. Surface cleaning was carried out by thermal treatment at a temperature as high as 650°C for 30min without arsenic flux. By this procedure a clean and flat surface was obtained, which was confirmed by several methods including RHEED, AES and AFM. Then, a GaAs (23MLs)/Al_{0.3}Ga_{0.7}As (35MLs) multiple QW (MQW) structure was directly grown on this clean surface [1]. Figure 1 shows photoluminescence (PL) spectra at 50K from the MQWs with or without 500nm thick GaAs buffer layer. Both peak intensity and FWHM of the PL of the directly grown MQW were almost the same as those of the MQW with 500nm thick GaAs buffer layer.

Conventionally, surface cleaning of AlGaAs is very difficult because of high reactivity of aluminum. Our new cleaning method was also applied to an epitaxial

AlGaAs wafer with surface oxide formed in deionized water [2]. Stacked GaAs QWs 3, 4.5, 7 and 15nm thick separated by 50nm thick $\text{Al}_{0.4}\text{Ga}_{0.6}\text{As}$ barriers were grown on the cleaned AlGaAs surface. Well-resolved PL peaks were obtained even at 300K for the QWs grown on an AlGaAs wafer cleaned by this new method, which was in marked contrast to the PL spectrum from the MQW grown on an AlGaAs cleaned by the conventional method as shown in Fig.2. To obtain more clean surface, introduction of a passivation layer on the AlGaAs surface was suggested, which was a thin GaAs layer or a thin GaAs/AlGaAs/GaAs double-hetero (DH) layer [3] grown at the final stage of the AlGaAs MBE growth. Passivation layer was very effective to realize HEMT structure on AlGaAs surfaces. These results describe that the new surface cleaning method without arsenic flux is applied successfully not only to GaAs surfaces but also to AlGaAs ones.

References

- [1] K.Iizuka, K.Matsumaru, T.Suzuki, H.Hirose, K.Suzuki and H.Okamoto, J.Crystal Growth 150 (1995) 13.
- [2] K.Iizuka, K.Matsumaru, T.Suzuki, Y.Takahira, T.Nishioka and H.Okamoto, J.Crystal Growth 175/176 (1997) 447.
- [3] K.Iizuka, H.Watanabe, T.Suzuki and H.Okamoto, to be presented in 10th international conference on Molecular Beam Epitaxy (MBE-X) (Aug 31- Sep 4, 1998, Cannes, France).

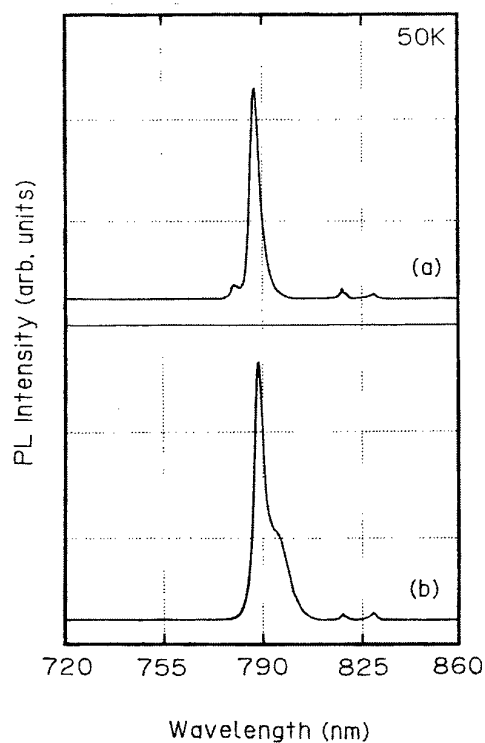


Fig.1 PL spectra at 50K from the MQW on the GaAs substrate which was prepared without As flux: (a) with 500nm thick GaAs buffer; (b) without buffer (directly grown).

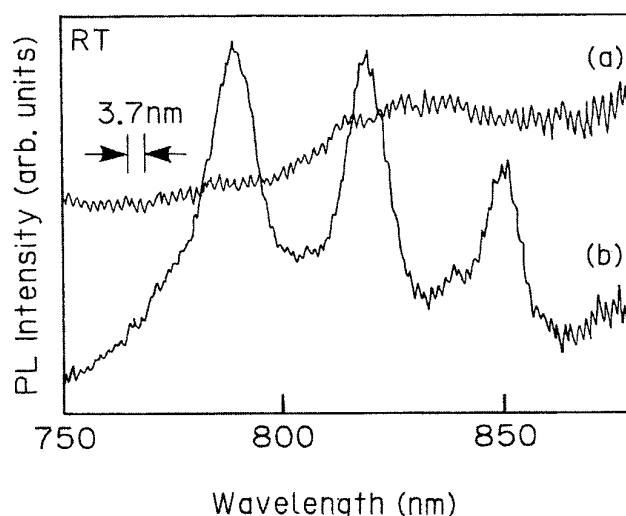


Fig.2 PL spectra from the stacked GaAs QWs regrown on cleaned AlGaAs with 500nm thick AlGaAs buffer layer: (a) cleaned by conventional cleaning method; (b) cleaned by new surface cleaning method without As flux.

LOCALIZED EPITAXY OF GaN BY HVPE ON PATTERNED SUBSTRATES

O. Parillaud, V. Wagner, H. J. Bühlmann and M. Illegems. Institut de Micro- et Optoélectronique, Ecole Polytechnique Fédérale de Lausanne, CH-1015 Lausanne, Switzerland .

High growth rates, large growth anisotropy and good selectivity which are typical features of the Hydride Vapor Phase Epitaxy [1,2] make this technique highly suitable for epitaxial lateral overgrowth (ELO) [3-5] as recently used for the blue lasers realization [6].

We report ongoing experiments on the growth of GaN by HVPE, using a newly designed Aixtron horizontal reactor and special patterned substrates which allow to obtain information on the growth rate and morphology along different directions. These substrates consist of (0001) Al_2O_3 on which a thin GaN layer has been deposited by MOCVD and recovered with a dielectric mask. Then stripes with different widths and orientations are opened. Finally regrowth is carried out by HVPE at atmospheric pressure. Typical experimental conditions are 12 ml/min. HCl on metallic gallium, 0.075 to 1.2 l/min. ammonia, while the total flow rate is completed by nitrogen up to about 6 l/min. Substrate and source temperatures are 1050 °C and around 900 °C respectively.

Cross sectional shape and lateral growth rate of GaN layers grown epitaxially starting from the stripe seeds depend critically on orientation with respect to crystal axes and experimental flow conditions (Fig. 1, Fig. 2).

- [1] D. Pribat, V. Provendier, M. Dupuy, P. Legagneux, C. Collet, Jpn. J. Appl. Phys. 30, L431 (1991) .
- [2] O. Parillaud, E. Gil-Lafon, B. Gérard, P. Etienne, D. Pribat, Appl. Phys. Lett. 68, 2654 (1996).
- [3] A. Usui, H. Sunakawa, A. Sakai, A. A. Yamaguchi, Jpn. J. Appl. Phys. 36, L899 (1997).
- [4] Y. Kato, S. Kitamura, K. Hiramatsu, N. Sawaki, J. Cryst. Growth 144, 133 (1994).
- [5] S. Nakamura, M. Senoh, S. Nagahama, N. Iwasa, T. Yamada, T. Matsushita, H. Kiyoku, Y. Sugimoto, T. Kozaki, H. Umemoto, M. Sano, K. Chocho, Appl. Phys. Lett. 72, 211 (1998).

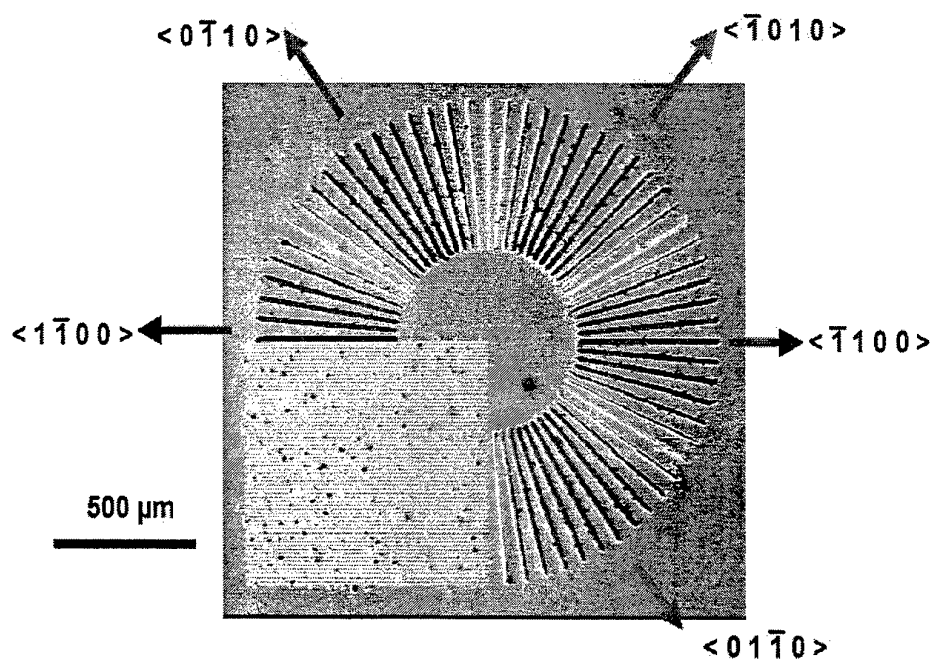


Figure 1. Growth on star shaped pattern (SEM, top view). The lateral growth depends critically on the orientation with respect to the crystal directions of GaN.

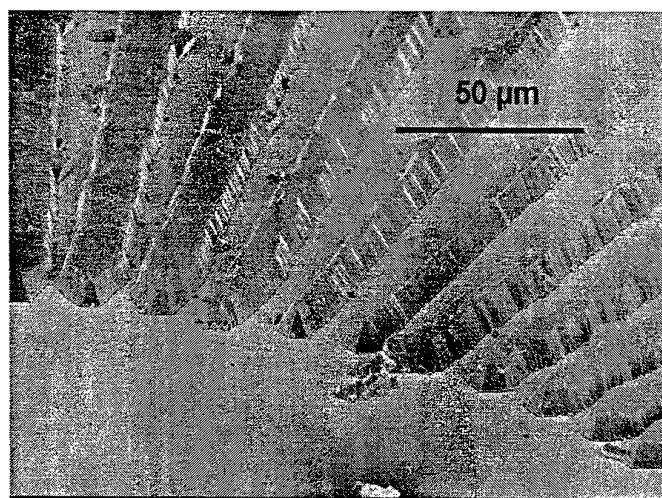


Figure 2: Growth on star shape pattern (SEM, tilted view), change of stripe cross-sections from triangular in $\langle 1\bar{2}10 \rangle$ direction to trapezoidal in $\langle 1\bar{1}00 \rangle$ direction shape reflects differences of lateral growth rates.

CRYSTAL GROWTH OF GaAs & InP AND THEIR DEFECT INVESTIGATION

P.SanthanaRaghavan and P.Ramasamy

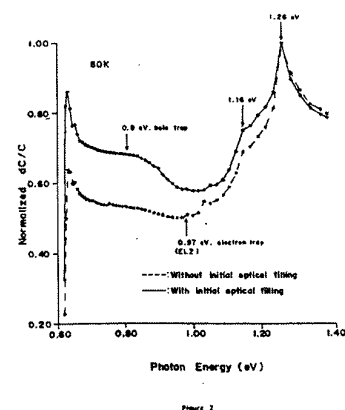
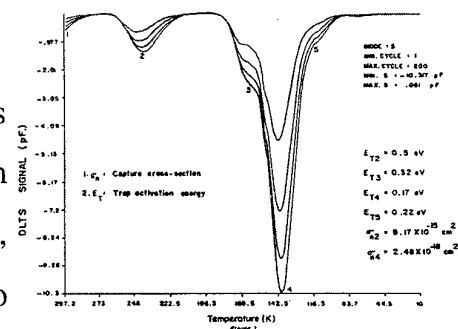
Crystal Growth Centre, Anna University, Chennai-600025, India.

Growth of GaAs and InP single crystals

Today's electronic field largely depends on compound semiconductors especially III-V compounds among which Gallium Arsenide and Indium Phosphide occupy the centre stage. The GaAs and InP crystals were grown using the High Pressure LEC puller (Cambridge Instruments). The ingots were pulled using either $\langle 100 \rangle$ or $\langle 111 \rangle$ oriented seed crystals from elemental and pre-synthesised charges with and without dopants. Flat shouldering and various cone angles have been tried to obtain twin free crystals. The thermal configuration of the system is effectively modified to improve the radial gradient by improving the heat shield capability and this in turn provided an improvement in the crystal quality. A non toxic alkaline-based slurry was developed during the work. The EPD was found to be between $10^3 - 10^4 \text{ cm}^{-2}$ for most of the crystals. Co-Doping of InP with CdTe was found to very much reduce EPD.

DLTS Studies:

The undoped GaAs samples were studied using this technique. The DLTS spectra obtained is depicted in figure.1. Two prominent peaks marked 2 and 4 in the figure, correspond to two electron traps. The arhenius plot for the two traps gives the activation energies as 0.5 eV and 0.17 eV which correspond to EL3 and EL10 respectively. The capture cross section for electrons measured are $\sigma_{n1} = 9.17 \times 10^{-15} \text{ cm}^2$ and $\sigma_{n2} = 2.48 \times 10^{-18} \text{ cm}^2$. Apart from these two prominent deep level signatures, two shoulders are also observed and the activation energy is computed using Urbach's rule and the activation energies are 0.32 eV and 0.22 eV which correspond to EL6 and EL9.

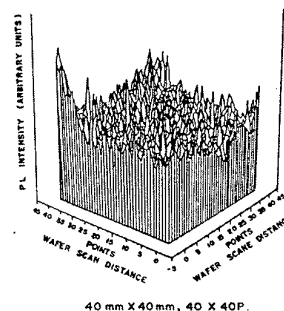


Photocapacitance measurements

The Photocapacitance measurements were carried out to confirm the prominent electron traps observed during the DLTS measurements. Experiments were done at 60 K with and without optical filling of hole traps in order to distinguish between electron and hole traps. Thresholds due to various electronic transitions are marked in the figure 2. The decreasing tendency at 1.15 eV is related to complementary transition from electron trap of $E_T=0.5$ eV, and the sharp decrease at 1.26 eV is similarly due to the electron trap having $E_T=0.17$ eV, identified by DLTS.

3-D PL mapping of 0.65 eV band on SI GaAs

We have studied the non-uniform distribution of EL2 level on our SI-GaAs using 3-D PL. 3-D PL maps of PL intensity are obtained at room temperature using an Argon Ion laser operating at 514.5 nm as the excitation source and PL from the sample was analysed using a Germanium Detector. Figure 3. shows the PL intensity plot made on the full 2 inch Diameter wafers and it can be observed that the PL intensity takes the well pronounced "W" pattern with respect to the "W" shaped dislocation density.



MESFET Fabrication

MESFET's were fabricated on our GaAs wafers (from bulk annealed ingots) and the threshold variation radially were measured and found to be uniform. The channel layer was grown by Silicon 28-ion implantation and the thickness of the n layer is 0.2 μm and the concentration was $1 \times 10^{17}/\text{cc}$. The gate length was 2 μm and gate width was 150 μm . The typical D.C. Characteristics of the MESFET's are

I_{DSS}	=	25-30 mA
V_{Ds}	=	2.5 Volts
$V_{pinchoff}$	=	-3.0 volts
C_{gs}	=	0.5 pF
Gain of the Device	=	8-9 ms

The results on Electrical, Structural characterisation will be presented in more detail.

III-V SEMICONDUCTORS: A STATUS REPORT ON THE R&D ACTIVITIES AT CENTRO RICERCHE VENEZIA

G.M. Guadalupi, F. Danieli, G. Tolomio, B. Molinas, M. Favaretto, L. Meregalli
ENIRISORSE Centro Ricerche Venezia

Via delle Industrie, 39 - 30175 Porto Marghera - Venezia - Italy

Tel: +39 (41) 5317322 Fax: +39 (41) 5316756 E-mail: cerive@port.venice.it

Since 1998, R&D activity on III-V Semiconductor Compounds at Centro Ricerche Venezia has been aimed at developing a prototype line for industrial scale production of state of the art substrate material. The lines for standard grade and epi-ready 2" wafer InP production and 3" GaAs wafer preparation are basically completed. 4" GaAs crystal growth process development has been lately concluded. III-V and II-VI Bulk Semiconductor Compounds (GaP, CdTe, ZnSe, etc.) synthesis activity is under development. The typical III-V Semiconductor Compound wafer production

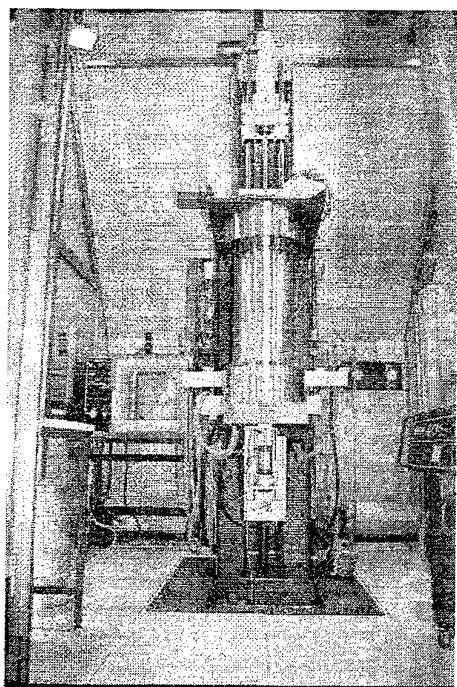


Fig. 1: Crystal puller equipment for growing up to 4-in ingots (LEC).

comprehends: synthesis, crystal growth, wafer and ingot thermal annealing, wafer processing, inspection and characterization. III-V polycrystal synthesis is performed at CERIVE using a proprietary method (VHPS) at high pressure. Polycrystalline ingots can be directly transferred to the growth chamber minimizing contamination and labor. Growth is performed using the Liquid Encapsulated Czochralski Method, which is the technique producing most of the commercial available material used today. A large capacity high pressure crystal puller, capable of producing single crystals up to 4"

in diameter, is used to grow, both manually and by on automatic controlled system, and the Thermal Wafer and Ingot Annealing is performed using a suitable horizontal high pressure furnace.

A complete line of wafer processing is capable of producing wafers in "pre-marketing" quantities. Such a line is divided into two sublimes, one for "as-cut" wafer (comprehensive of orientation determination, sampling for characterization, ingots and wafer grinding and final slicing) and one, installed in clean rooms Class 1000, for both single side lapping and double side polishing.

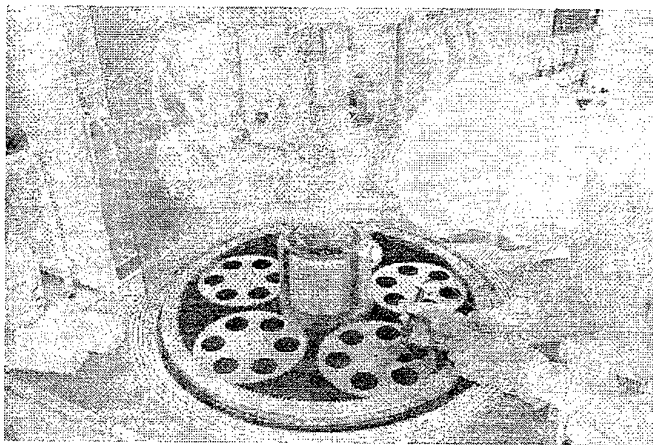


Fig. 2: Operator handling 2-in InP wafers at the double-side polishing machine.

A proprietary finishing process allow for the production of "epi-ready" quality. Inspection equipments (located in a Class 10

clean room) comprehend a wafer thickness non contact measuring system, a surface flatness analyser, a surface defect inspection and contamination detector.

Characterization covers Hall effect and resistivity measurement system, an Image

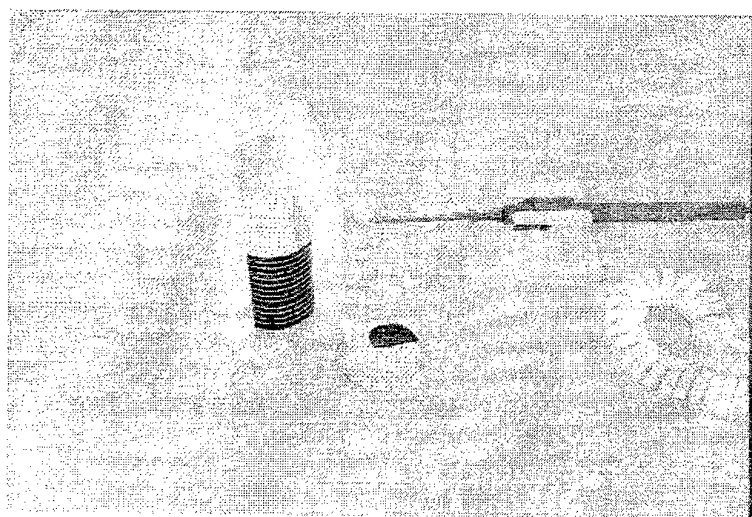


Fig. 3: 2-in InP mirror-like polished wafers

analyser for EPD measurement, an Atomic Force Microscopy for surface morphology mapping, a Photoluminescence unit with mapping facilities for compositional homogeneity checks and a Glow Discharge Mass Spectrometer (GDMS) for trace analysis.

Influence of different growth parameters and related conditions on the 6H-SiC crystal growth by the Modified Lely Method

H.-J. Rost, D.Siche, J.Dolle, D.Schulz, J.Wollweber, T.Müller, G.Wagner
Institute of Crystal Growth, Rudower Chaussee 6, D-12489 Berlin, Germany
Phone: +49 30 6392 3001 Fax: +49 30 6392 3003 e-mail: rost@ikz-berlin.de



To improve the yield of high quality large diameter 6H- SiC single crystals grown by the Modified Lely Method it is necessary to investigate the interaction of different growth parameters. Beside the quality of the seed crystal the stoichiometry of the vapour phase and the thermal conditions inside the growth chamber have to be carefully controlled.

Especially, the growth rate of the crystal is determined by the growth temperature, the temperature gradient, the distance between source and seed, the pressure inside the crucible, the stoichiometry and grain size of the SiC-source.

Crystals of about 1 inch diameter were grown in an inductive heated furnace in a temperature range of 2200-2400°C. The argon pressure varied between 5 and 100 mbar. The growth rate was investigated in dependence of the growth time, the seed temperature, the temperature difference between source and seed and

the system pressure. Using the method of marking the phase boundary by doping marks[1] the growth rate was determined for different pressures within one and the same growth run.

It was found that the growth rate strongly increases with the seed temperature and the temperature difference between seed and source while the growth rate decreases with the growth time. Furthermore, we found an anomalous behaviour of the growth rate in dependence of the pressure. It could be explained by an overcompensation of the pressure effect by the stoichiometry influence in the first part of the growth time.

- [1] S.G. Müller, R. Eckstein, D. Hofmann, E. Schmitt, W. Schoierer, A. Winnacker, W. Dorsch, H.P. Strunk, Mat. Science and Engineering B44 (1997) 392

T. Reichardt, B. Speit*

Schott ML GmbH, Göschwitzerstr. 20, 07745 Jena, GERMANY

*Schott ML GmbH, Wilh.-Th.-Römheld-Str. 32, 55130 Mainz, GERMANY

Optical Materials for Microlithography Applications

- **introduction**
- **i-line-glass**
 - **transmission, solarization**
 - **homogeneity**
- **fused silica**
 - **fluorescence spectra**
 - **193 nm marathon test**
- **calcium fluoride**
 - **stress birefringence**
 - **initial / induced absorption**
 - **homogeneity data**
- **summary**

Addresses of lecturers

Wilfried von Ammon: Dr.

Wacker Siltronic AG, Postfach 1140, 84479 Burghausen, Germany

Tel. +49-8677-83-2008

Fax +49-8677-83-7303

wilfried-ammon@wacker.de

Experiences: FZ, CZ / 14 years

Characterization of large Ø silicon (up to 150 kg), defects/growth parameters

Toshiaki Asahi: Engineer/Researcher

Japan Energy Corp., Mat. & Components Labs., 3-17-35 Niizo-Minami, Toda, 335-8502 Saitama, Japan

Tel. +81-48-433 2051

Fax +81-48-433 5400

asahi@j-energy.co.jp

Experiences: VGF/12 years

II-VI, III-V, 10 cm Ø, 5 kg

Vladimir Balitsky: Professor

Institute of Experimental Mineralogy, RAS, Chernogolovka 142432 Moscow Region, Russia

Tel. +7-095-913 2112

Fax +7-095-913 2112

balvlad@iem.ac.ru

Experiences: Hydrothermal/33 years,

70 domestic and international patents

Piezoelectrical and optical materials, Jewelry

Simon Brandon: Professor/Lecturer

Technion - Israel Institut of Technology, Dept. of Chemical Engineering, Haifa 32000, Israel

Tel. +972-4-8292822

Fax +972-4-8230476

CERSBSB@tx.technion.ac.il

Experiences: Numerical simulation of growth processes & solid-liquid interfaces

Ted Ciszek: Principal Scientist, Head Crystal Growth & Devices

National Renewable Energy Lab, SERF W/107, 1617 Cole Blvd., Golden, Co 80401-3393, USA

Tel. +1 303-384-6567

Fax +1 303-384-6531

ted_ciszek@nrel.gov

Experiences: CZ/2 years; FZ/32; VGF/3; Flux/3; LPE/3

15 patents

Si, Superconductors, Chalcopyrites; 6kg

Didier Cochet-Muchy: R&D Manager Optics

Crismatec S.A., 2, Rue des Essarts, 38610 Gières, France

Tel. +33-476-63-3405

Fax +33-476-44-1753

Experiences: 9 years

LNO/LTO/BGO/GGG/SGGG/YAG up to 15 cm Ø

Jeffrey J. Derby: Professor
University of Minnesota, Dept. of Chem. Eng. & Mat. Sci., 151 Amundson Hall, 421 Washington
Av., Minneapolis MN 55455-0132, USA

Tel. +1-612-625-8881
Fax +1-612-626-7246
derby@tc.umn.edu

Experiences: Modeling of CZ, Bridgman, aqueous solutions, Flux/16 years
Si, GaAs, II-VI; KDP, KTP

Francois Dupret: Professor
Université Catholique de Louvain, CESAME, 1384 Louvain-la-Neuve, Belgium

Tel. +32-10-472350
Fax +32-10-472180
fd@mema.ucl.ac.be

Experiences: Numerical Simulation & modelling, CZ, FZ, Bridgman, VGF

Robert Falster: Dr., Director of Research of MEMC international
MEMC Spa, Viale Gherzi 31, 28100 Novara, Italy

Tel. +39-321-334 394
Fax +39-321-691 000
rfalster@memc.com

Experiences: Defect control in Cz silicon

Tsuguo Fukuda: Professor, Director of Fukuda Research Laboratory at Institute of Materials
Research of the Tohoku University,
President of Japanese Project for Promotion of Science No. 161
Tohoku University, IMR, Sendai, 980-77, Japan

Tel. +81-22-215-2100
Fax +81-22-215-2101
fukuda@lexus.imr.tohoku.ac.jp

Experiences: many years crystal growth at Toshiba Ceramics, then director of crystal growth at
MITI Optoelectronics project, then joined Tohoku University
Research projects on various classes of materials and growth techniques, lately NLO
and laser oxides bulk & fibers

Alexander V. Gektin: Supervisor, Professor
Institute for Single Crystals, Lenin av. 60, 310001 Kharkov, Ukraine

Tel. +380-572-307981
Fax +380-572-321082
gektin@isc.kharkov.com

Experiences: Bridgman/15 years, CZ/10 years, Kyropoulos/20 years
Scintillators 50 cm Ø, 500 kg

Klaus Gillessen: Dr., Supervisor
TEMIC, Theresienstr. 2, 74072 Heilbronn, Germany

Tel. +49-7131-672602
Fax +49-7131-672399
Klaus.Gillessen@temic.de

Experiences: Crystal growth and LPE of III-V, LEDs

Ian Grant: Executive director

Wafer Technology Ltd. 34 Maryland Road, Tongwell, Milton Keynes MK 15 8HJ, England

Tel. +44-1908-210 444

Fax +44-1908-210 443

igrant@wafertech.co.uk

Experiences: LEC production & wafering of GaAs, GaP, InP

Charles Hauser: Dr., President of HCT Shaping Systems

HCT Shaping Systems S.A., Rte. de Genève 42, 1033 Cheseaux, Switzerland

Tel. +41-21-731-91-00

Fax +41-21-731-91-01

hauser@hct.ch

Experiences: Silicon wafering technology, development of commercial multiple wire saw

Michael Heuken: Supervisor/Manager, Professor

AIXTRON AG, Kackertstr. 15-17, 52072 Aachen, Germany

Tel. +49-241-8909-0

Fax +49-241-8909-40

ocs@aixtron.com

Experiences: MOCVD/CVD 13 years
II-VI, III-V, YBCO

Manabu Itsumi: Supervisor

NTT System Electr. Lab., 3-1 Morinosato Wakamiya, Atsugi-Shi, Kanagawa 243-0198, Japan

Tel. +81-462-40-2481

Fax +81-462-40-4321

itsumi@aecl.ntt.co.jp

Experiences: Electron microscopy, characterization of defects in Si

Leif Jensen: R & D Manager

TOPSIL Semiconductor Materials A/S, Linderupvej 4, 3600 Frederikssund, Denmark

Tel. +45-47311626

Fax +45-47314269

topsil@topsil.com

Experiences: FZ/12 years
Silicon 200 cm, 40 kg

Koichi Kakimoto: Professor

Kyushu University, 6-1, Kasuga-koen, Kasuga 816, Japan

Tel. +81-92-583-7836

Fax +81-92-583-7838

kakimoto@cm.kyushu-u.ac.jp

Experiences: CZ/12 years
Si, Ge, III-V, 5 cm Ø

Hiroaki Kakiuchi: Assistant Professor
Osaka University, Dept. of Precision Sci. & Tech., 2-1 Yamada-oka, Suita, Osaka 565-0871, Japan

Tel. +81-6-879-7270
Fax +81-6-879-7270
kakiuchi@prec.eng.osaka-u.ac.jp

Experiences: Precision Engineering

Juris P. Kalejs: Vice President Engineering
ASE Americas Inc., 4 Suburban Park Drive, Billerica MA 01821-3980, USA

Tel. +1-978-667-5900
Fax +1-978-663-7555
jpkasepv@aol.com

Experiences: EFG silicon ribbons and sheets/22 years
multiple hollow tubes 5 m long, 300 micron thick walls, 3 kg each

Shigeyuki Kimura: Dr., director of NIRIM Institute
NIRIM, Namaki 1-1, Tsukuba, Ibaraki 305, Japan

Tel. +81-298-55-3440
Fax +81-298-52-7449
kimura@nirim.go.jp

Experiences: Si (7.5 cm Ø), Oxide-lasers, Electro-optic crystals/30 years

Helmut Klapper: Professor, President crystal growth commission of IUCryst.
University Bonn, Mineralog. Institute, Poppelsdorfer Schloss, 53115 Bonn, Germany

Tel. +49-228-732 769
Fax +49-228-732 770
une110@ibm.rhrz.uni-bonn.de

Experiences: Crystal growth of inorganic salts & organic materials
X-ray topography including theoretical interpretation

Mikhail V. Korzhik: Professor
Institute for Nuclear Problems, 11 Bobryiskaya, 220050 Minsk, Belarus

Tel. +375-172-205844
Fax +375-172-265124
mikhail.korjik@cern.ch

Experiences: CZ/10 years, Bridgman/10 years
Oxide-scintillators, up to 20 kg

Krishan Lal: Director Grade Scientist
National Physics Lab, Hillside Road, New Delhi-110 012, India

Tel. +91-11-5813171
Fax +91-11-5752678
klal@csnpl.ren.nic.in

Experiences: CZ/17 years
Oxide and inorganic materials, up to 7 cm Ø

Michel Lebeau: Senior Mechanical Engineer
CERN, Division PPE, Rte. de Meyrin, 1211 Genève, Switzerland

Tel. +41-22-767-2044
Fax +41-22-767-8930
Michel.Lebeau@cern.ch

Experiences: Mechanical Processing of BGO, BaF₂, CeF₂, PbWO₄/15 years

Pei Jun Li: Professor
c/o CERN, Division PPE, Rte. de Meyrin, 1211 Genève, Switzerland

Tel.
Fax +41-22-767-8930
Pei.Jun.Li@cern.ch

Experiences: Bridgman/more than 20 years in Shanghai Institute of Ceramics
Scintillators

Leonid Lytvynov: Dr.
Institute for Single Crystals, Lenin av. 60, 310001 Kharkov, Ukraine

Tel. +380-572-307047
Fax +380-572-320019
lytvynov@isc.kharkov.ua

Experiences: Verneuil/10 years, EFG/10 years
Sapphire, Oxide-lasers, 90 cm

Shintaro Miyazawa: Senior Chief Researcher and deputy director
USHIO Research Institute of Technology, 1-90 Komakado, Gotenba-shi, Shizuoka 412-038, Japan

Tel. +81-550-87-5880
Fax +81-550-87-5887
miyazasn@mail.ushio.co.jp

Experiences: CZ, TSSG, LPE, PVD
LiNbO₃, LiTaO₃, TeO₂, BNN, SBN, BTO, LGO, III-V, 5 cm Ø x 15 cm length

Mikhail Moussatov: Professor
GOI (State Optical Institute), 36 Babushkina st. bld. 1, St.-Petersburg, 193171, Russia

Tel. +7-812-177-5709
Fax +7-812-560-1987

Experiences: Kyropoulos growth of large oxide crystals, sapphire 30 cm Ø

Georg Müller: Professor
University Erlangen, Martensstr. 7, 91058 Erlangen, Germany

Tel. +49-9131-857636
Fax +49-9131-858495
georg.mueller@ww.uni-erlangen.de

Experiences: CZ, VGF/25 years
Si, GaAs (3 kg, 7,5 cm Ø)
5 patents (melt growth)

Yashuhiro Nishida: Chief Corporate Representative R&D Group
Sumitomo Electric Industries, Ltd., 30 Dorset Square, London NW1 6QJ, UK

Tel. +44-171-723-0929

Fax +44-171-724-2102

dd720189@jnet.sei.co.jp

Experiences: VPE/7 years, Bridgman/5 years, MBE/3 years
GaAs (15 cm Ø, 25 kg)
1 US-patent, 16 Japanese patents

Tatau Nishinaga: Professor, President of International Organisation of Crystal Growth and of
Japanese Society of Applied Physics
Editorial board of Journal of Crystal Growth
President of National Projects on Surfaces and Growth Mechanisms
University of Tokyo, Dept. of Electrical Engineering, 7-3-1 Hongo, Bunkyo-ku, Tokyo 113, Japan

Tel. +81-3-3812-2111 ext. 6673

Fax +81-3-5684-3974

tatau@ee.t.u-tokyo.ac.jp

Experiences: Epitaxy growth mechanisms/surface diffusion, epitaxial lateral overgrowth

Jun-Ichi Nishizawa: President of Tohoku University, Professor emeritus, President of
Semiconductor Research Institute and Research Foundation
Semiconductor Research Institute, Kawauchi, Sendai 980, Japan

Tel. +81-22-223-7287

Fax +81-22-223-7289

Experiences: Numerous inventions in crystal growth and device technology including molecular
layer epitaxy, semiconductor lasers, high-speed transistors

Vyacheslav V. Osiko: Director of the Scientific Center, Academician and professor
General Physics Institute, RAS, Vavilov street 38, bld D, Moscow 117942, Russia

Tel. +7-095-135-7744

Fax +7-095-135-0270

osiko@ftt.gpi.ru

Experiences: Bridgman, CZ/ 36 years, skull-melting of zirconia etc.
Oxide-lasers, NLO, electro-optic (15 cm, 2 kg)

Vadim I. Polezhaev: Professor
Institute for Problems in Mechanics, RAS, Prospect Vernadskogo 101, Moscow 117526, Russia

Tel. +7-095-4343283

Fax +7-095-9382048

polezh@ipmnet.ru

Experiences: Modeling of crystal growth of Si, GaAs /20 years

Andrew Yeckel: Dr., research associate & lecturer
Dept. of Chem. Engng. and Mat. Science, Univ. of Minnesota, 421 Washington Ave SE,
Minneapolis MN 55455-0132, USA

Tel. +1-612-625-1313

Fax +1-612-626-7246

yeckel@cems.umn.edu

Experiences: Numerical simulation of crystal growth hydrodynamics

Peter Rudolph: Professor, Dr.

Institute for Crystal Growth, Rudower Chaussee 6, 12489 Berlin, Germany

Tel. +49-30-6392-3034

Fax +49-33-6392-3003

pr@ikz-berlin.de

Experiences: Phase relations & crystal growth technology of III-V and II-VI compounds, especially CdTe, ZnSe, GaAs, shaped crystal growth

Takatomo Sasaki: Professor

Osaka University, Dept. of Electrical Engineering, 2-1 Yamada-oka, Suita, Osaka 565-0871, Japan

Tel. +81-6-879-7706

Fax +81-6-879-7708

sasaki@pwr.eng.osaka-u.ac.jp

Experiences: Organic/Inorganic NLO, electro-optic/ 20 years
KDP: 45 x 45 x 70 cm³

Bernd Sauter: Dr., Supervisor

Wacker Siltronic AG, P.O. BOX 1140, 84479 Burghausen, Germany

Tel. +49-8677-83-2819

Fax +49-8677-83-4591

bernd.sauter@wacker.de

Experiences: Wafer development of 300 mm Si

Hans J. Scheel: Dr.-Ing., Head Crystal Growth Group/Cristallogenèse, member of IOCG executive committee

Cristallogenèse, Chemin de Bellerive 34, 1007 Lausanne, Switzerland

Tel. +41-21-693-4452

Fax +41-21-693-4750

Hans.Scheel@epfl.ch

Experiences: 40 years general experiences in crystal growth technology (Flux, CZ, vapor, LPE)
5 patents
Book of D. Elwell & HJS: "Crystal growth from high temperature solutions"
1975-1999
ACRT, and other new technologies

Frederick Schmid: President of Crystal Systems Inc.

Crystal Systems Inc., 27 Congress Street, Salem, MA, USA

Tel. +1-978-745-0088

Fax +1-978-744-5059

Experiences: Developed Heat Exchanger Method (1969), and Fixed Abrasive Slicing Technique (1975)
sapphire (33 cm, 65 kg), Ti:sapphire
multicrystalline Si for PV and optical applications (66 cm x 66 cm, 250 kg)

Shin'Ichiro Takasu: Senior Technology Advisor at SEMI
SEMI Japan, Kennwa Bld., 4-7-15 Kudan-minami, Chiyoda-ku, Tokyo 102-0041, Japan

Tel. +81-3-3222-5755
Fax +81-3-3222-5757
stakasu@semi.org

Experiences: Si (CZ: >30 cm Ø, > 100 kg), Ge, GaP, Diamond, YAG, LiNbO₃, TGS, Ferrite,
NaCl, CaWO₄, etc.
developed Si wafer design concept (thermal behavior of Si wafer, 1976-1980)
developed Cluster tool type MBE equipment (1980-1983)
developed hydrogen treated Si wafer production (1987-1992)

Kazutaka Terashima: Professor/Lecturer
Shonan Institute of Technology, 1-1-25 Tsujido-Nishikaigan, Fujisawa, Kanagawa 251, Japan

Tel. +81-466-34-4111
Fax +81-466-36-1594
terasima@mate.shonan-it.ac.jp

Experiences: CZ, CVD
Si, GaAs, GaN
7.5 cm Ø

Erich Tomzig: Dr.
Wacker Siltronic AG, P.O. BOX 1140, 84479 Burghausen, Germany

Tel. +49-8677-832084
Fax +49-8677-837303
erich.tomzig@wacker.de

Experiences: Silicon CZ & FZ growth technology

Robert Triboulet: Dr.
CNRS Bellevue, Lab. de Physique des Solides, 1, Place A. Briand, 92195 Meudon Cedex, France

Tel. +33-1-45 07 5088
Fax +33-1-45 07 5841
triboulet@cns-bellevue.fr

Experiences: Phase relations, crystal growth & physical characterization of II-VI compounds

Rowland Ware: Distinguished Fellow of Technology
M/A - COM Inc., 100 Chelmsford Street, Lowell MA 02090, USA

Tel. +1-978-656-2749
Fax +1-978-656-2800
warer@macom.com

Experiences: CZ, Bridgman, VPE / 39 years
Sapphire, GGG, FeSi₂, Si, II-VI, III-V
GaAs 24 kg

Günter Weimann: Professor Dr., Director IAP-FH Freiburg
Frauenhofer-Institute for Applied Physics, Tullastr. 12, 79108 Freiburg, Germany

Tel. +49-761-5159-410
Fax +49-761-5159-400
weimann@iaf.fhg.de

Experiences: MBE, semiconductor physics

Berndt Weinert: Dr., Director of R&D
Freiberger Compound Semiconductor Materials GmbH, Am Junger Löwe-Schacht 5,
09599 Freiberg, Germany

Tel. +49-3731-280 200
Fax +49-3731-280 106
weinert@fcm-germany.com

Experiences: 15 cm Ø GaAs by LEC

Helmut Wenzl: Professor Dr., director Institute for Material Development IFF,
KFA Jülich, 52425 Jülich, Germany

Tel. +49-2461-616664
Fax +49-2461-613916
h.wenzl@fz-juelich.de

Experiences: CZ, Bridgman, VGF, VAP / 25 years
Ge, Si, GaAs, EuO, FeO, Ni₃Al, Al-Pd-Mn-Quasicrystals, Cu As Au dislocation-free
up to 50 kg
Defect thermodynamics & phase equilibria in compound crystal growth processes,
Handbook of Crystal Growth, ed. D.T.J. Hurle
patent (1997)

Hirotohi Yamagishi: Manager
Super Silicon Crystal Research Institute Corp., Nakanoya 555-1, Annaka, Gunma 379-0125, Japan

Tel. +81-273-84-0550
Fax +81-273-84-0559
yama@super-si.co.jp

Experiences: CZ/17 years, FZ/5 years
Si (40 cm Ø, 300 kg)

Kazuuya Yamamura: Assistant Professor
Dept. of Precision Engineering, Osaka University, 2-1 Yamada-oka, Suita, Osaka 565-0871, Japan

Tel. +81-6-879-7286
Fax +81-6-879-7286
yamamura@prec.eng.osaka-u.ac.jp

Experiences: Precision Engineering

Kazuto Yamauchi: Associate Professor
Dept. of Precision Engineering, Osaka University, 2-1 Yamada-oka, Suita, Osaka 565-0871, Japan

Tel. +81-6-879-7285
Fax +81-6-879-7286
yamauchi@prec.eng.osaka-u.ac.jp

Experiences: Precision Engineering

Evgenii V. Zharikov: Professor, Lecturer
General Physics Institute, RAS, Vavilov str. 38, 117942 Moscow, Russia

Tel. +7-095-132-8352
Fax +7-095-496-6781
zharikov@lsg.gpi.ru

Experiences: Laser crystals, NLO (inorganic)
12 cm, 1 kg

List of participants

Takao	ABE	Shin-Etsu Handotai Co., Ltd.	J	ta.abe@seh.co.jp	66, 276
Haruko	ABE				
Artoush	ABGARIAN	Abgarian Group	RUS	007-95-921-5474/ 935-4866	751
Alexandre	ANNENKOV	BPTCP	RUS	007-08761 22359	
Toshiaki	ASAHI	Japan Energy Corp.	J	asahi@j-energy.co.jp	426
Willy	BACHMANN	WELL Walter Ebner	CH	0041-32-931-2336	
Vladimir	BALITSKY	Inst. of Exp. Mineralogy, RAS	RUS	balvlad@iem.ac.ru	658
Ludmila V.	BALITSKY				
Beatrix	BAUER				
Rosmarie	BAUMBERGER				
Hansjochen	BERNHARDT	Schott Spezialglas	D	0049-36691 624 33	
Andreas W.	BETT	FHG-ISE	D	andreas.bett@ise.fhg.de	
Cyrille	BEZENÇON	CTML - DMX, EPFL	CH	Cyrille.Bezencon@epfl.ch	
M.	BEZINGE	Comadur S.A.	CH	0041-26-684-8205	
Jean-Daniel	BOCHUD	Comadur S.A.	CH	0041-26-684-8205	
Nathalie	BOGAERT, VAN DEN	Univ. Catholique de Louvain	B	vdb@mema.ucl.ac.be	161, 747
Simon	BRANDON	Technion-Israel Inst. of Tech.	IL	cerbsb@technix.technion.ac.il	36
Tural	BRANDON				
Nicolas	BUCHER	N. Bucher AG	CH	nbucherag@swissonline.ch	
Marianne	BURRI				
Ted F.	CISZEK	NREL	USA	tciszek@nrel.nrel.gov	314
Dorothy	CISZEK				
Didier	COCHET-MUCHY	CRISMATEC	F	cochet-muchy.crismatec@wanadoo.fr	570
Mrs.	COCHET-MUCHY				
Ben	DEPUYDT	UM Electro-Optic Materials	B	ben.depuydt@um.be	
Maxim	DOROSHENKO	General Phys. Institute, RAS	RUS	dorosh@ftt.gpi.ru	
Peter	DRYBURGH	University of Edinburgh	UK	pmd@ee.ed.ac.uk	
François	DUPRET	Univ. Catholique de Louvain	B	fd@mema.ucl.ac.be	161, 747
Mrs.	DUPRET				
Dirk	EHRENTAUT	Cristallognèse-IMO, EPFL	CH	ehrenta@dpmail.epfl.ch	
Katsuyoshi	ENDO	Osaka University	J	endo@prec.eng.osaka-u.ac.jp	
Robert	FALSTER	MEMC Spa	I	rfalster@memc.com	258
Vladimir	FLEROV	Latvian Institute of Physics	LV	vflerov@sal.lv	
Tsuguo	FUKUDA	IMR, Tohoku University	J	fukuda@lexus.imr.tohoku.ac.jp	546, 769
Mineko	FUKUDA				

Mykola	GALUNOV	Institute for Single Crystals	UKR	galunov@isc.kharkov.com	777
Alexander V.	GEKTIN	Institute for Single Crystals	UKR	gektin@isc.kharkov.com	696
Klaus	GILLESSEN	TEMIC	D	0049- 7131-672399	534
Rengasamy	GOPALAKRISHNAN	Phys. Dept., Anna University	IN	gopalakrishnan65@hotmail.com	779
Ian	GRANT	Wafer Technology Ltd.	UK	igrant@wafertech.co.uk	414
Giuseppe	GUADALUPI	ENI, Centro Ricerche Venezia	I	guadalupi@port.venice.it	789
Kenji	HASEGAWA	IMR, Tohoku University	J	hase@lexus.imr.tohoku.ac.jp	769
Charles	HAUSER	HCT Shaping Systems S.A.	CH	hauser@hct.ch	204
Michael	HEUKEN	AIXTRON AG	D	ocs@aixtron.com	520
Karin	HOELDRICH				
Kanji	IIZUKA	Nippon Inst. of Technology	J	iizuka@nit.ac.jp	783
Marc	ILEGEMS	IMO - DP, EPFL	CH	ilegems@sdpdec9.epfl.ch	785
Valentin	IOV	Institute of Atomic Physics	ROM	viov@roifa.ifa.ro	773
Mitsuro	ISHII	Shonan Inst. of Technology	J	ishii@mate.shonan.it.ac.jp	767
Mine	ISHII				
Manabu	ITSUMI	NTT System El. Laboratories	J	itsumi@aecl.ntt.co.jp	144
Leif	JENSEN	TOPSIL Semiconductor Mat.	DAN	topsils@topsils.com	240
Koichi	KAKIMOTO	Kyushu University	J	kakimoto@cm.kyushu-u.ac.jp	172, 747
Hiroaki	KAKIUCHI	Osaka University	J	kakiuchi@prec.eng.osaka-u.ac.jp	753
Juris P.	KALEJS	ASE Americas Inc.	USA	jpkasepv@aol.com	326
Ruth	KESSLER				
Shigeyuki	KIMURA	NIRIM	J	kimura@nirim.go.jp	120
Mrs.	KIMURA				
Daisuke	KISHIMOTO	University of Tokyo	J	mercury@ee.t.u-tokyo.ac.jp	781
Helmut	KLAPPER	Universität Bonn	D	une110@ibm.rhrz.uni-bonn.de	46
Christine	KLEMENZ	Cristallogénese-IMO, EPFL	CH	Christine.Klemenz@epfl.ch	
Mikhail V.	KORZHIK	Institute of Nuclear Problems	B'rus	mikhail.korjik@cern.ch	672
Alexander	KUDIN	Institute for Single Crystals	UKR	amcrys-h@ovsharkov.ua	
Krishan	LAL	National Physics Laboratory	IN	klal@csnpl.ren.nic.in	108, 747
Michel	LEBEAU	CERN	CH	Michel.Lebau@cern.ch	230, 755
Nicolay	LEONYUK	Moscow State University	RUS	leon@geol.msu.ru	761, 763
Peijun	LI	CERN	CH	Pei.Jun.Li@cern.ch	686
Leonid	LYTVYNOV	Institute for Single Crystals	UKR	lytvynov@isc.kharkov.ua	712
Shintaro	MIYAZAWA	Ushio Research Inst. of Tech.	J	miyazasn@mail.ushio.co.jp	560
Kyoko	MIYAZAWA				
Yusuke	MORI	Osaka University	J	mori@pwr.eng.osaka-u.ac.jp	765

Georg	MÜLLER	Universität Erlangen	D	georg.mueller@ww.uni-erlangen.de	354
Hanne	MÜLLER				
Christian	MÜLLER				
Anne	NIELSEN	TOPSIL Semiconductor Mat.	DAN	topsil@topsil.com	
Yasuhiro	NISHIDA	Sumitomo Electric Ind., Ltd.	UK	dd720189@jnet.sei.co.jp	380
Tatau	NISHINAGA	University of Tokyo	J	tatau@ee.t.u-tokyo.ac.jp	496, 781
Jun-Ichi	NISHIZAWA	Semiconductor Research Inst.	J	0081-22-223-7289	460
Tomoya	OGAWA	Gakushuin University.	J	tomoya.ogawa@gakushuin.ac.jp	757
Atsumu	OHMURA	Geograph. Institute, ETH	CH	ohmura@geo.umnw.ethz.ch	
Mrs.	OHMURA				
Vyacheslav V.	OSIKO	General Phys. Institute, RAS	RUS	osiko@ftt.gpi.ru	580
Yasunao	OYAMA	OPTRON INC.	J	oyam@mb.infoweb.ne.jp	
Vadim I.	POLEZHAEV	Inst. for Probl. in Mech., RAS	RUS	polezh@ipmnet.ru	188
Torsten	REICHARDT	Schott ML GmbH	D	0049-36691 62433	793
Hans-Joachim	ROST	IKZ Berlin	D	rost@ikz-berlin.de	791
Peter	RUDOLPH	IKZ Berlin	D	pr@ikz-berlin.de	19, 368
Mieko	SAITO				
M.	SALODINI	WELL Walter Ebner	CH	0041-32-931-2336	
Yasuhisa	SANO	Osaka University	J	sano@prec.eng.osaka-u.ac.jp	218, 753
Parthasarathy	SANTHANARAGHAVAN	Cryst. Growth Ctr. Chennai	IN	psraghavan10@hotmail.com	787
Ana Maria do E.	SANTO	Cristallogénese-IMO, EPFL	CH	espirito@dpmail.epfl.ch	
Takatomo	SASAKI	Osaka University	J	sasaki@pwr.eng.osaka-u.ac.jp	632
Bernd	SAUTER	Wacker Siltronic AG	D	bernd.sauter@wacker.de	294
Hans J.	SCHEEL	Cristallogénese-IMO, EPFL	CH	Hans.Scheel@epfl.ch	86, 480, 753
Frederick	SCHMID	Crystal Systems Inc.	USA	001-978-744-5059	592
Kirill	SOUBBOTIN	General Phys. Institute, RAS	RUS	subbotin@llcg.mail.gpi.ru	
Svetlana I.	SOUBBOTINA				
Burkhard	SPEIT	Schott ML GmbH	D	spt@schott.de	793
Ulrich	STÄHLI	Meyer & Burger AG	CH	mub@swissonline.ch	
Pavel	STUDENIKIN	General Phys. Institute, RAS	RUS	PavelSt@physlab.msk.ru	771
Maryna	TABACHKOVSKA				
Shin'Ichiro	TAKASU	SEMI JAPAN	J	stakasu@semi.org	722, 732
Kazutaka	TERASHIMA	Shonan Institute of Tech.	J	terasima@mate.shonan-it.ac.jp	132
Erich	TOMZIG	Wacker Siltronic AG	D	erich.tomzig@wacker.de	158
Robert	TRIBOULET	CNRS Bellevue	F	triboulet@cnrs-bellevue.fr	436
Takuji	TSUZAKI		J	0081-742-51-2733	

Ivo	UTKE	IMO - DP, EPFL	CH	ivor.utke@epfl.ch	
Gerald	VUILLEUMIER	N. Bucher AG	CH	nbucherag@swissonline.ch	
Volker	WAGNER	IMO - DP, EPFL	CH	Volker.Wagner@epfl.ch	785
Rowland	WARE	M/A - COM Inc.	USA	warer@macom.com	402
Günter	WEIMANN	Fraunhofer-Inst. Phys.	D	weimann@iaf.fhg.de	508
Ingrid	WEIMANN				
Berndt	WEINERT	Freiberger Comp. Mat. GmbH	D	weinert@fcm-germany.com	392
Andreas	WEISLEDER	Schott Spezialglas GmbH	D	0049-36691 624 33	
Helmut	WENZL	KFA Jülich	D	HelmutFT.Wenzl@t-online.de	340
Mrs.	WENZL				
Thomas	WOLF	Forschungszentrum Karlsruhe	D	thomas.wolf@itp.fzk.de	
Hirotoishi	YAMAGISHI	Super Silicon Cryst. Res.Inst.	J	yama@super-si.co.jp	304
Kazuya	YAMAMURA	Osaka University	J	yamamura@prec.eng.osaka-u.ac.jp	218,753
Kazuto	YAMAUCHI	Osaka University	J	yamauchi@prec.eng.osaka-u.ac.jp	218,753
Kiyoshi	YASUTAKE	Osaka University	J	yasutake@prec.eng.osaka-u.ac.jp	
Andrew	YECKEL	University of Minnesota	USA	yeckel@cems.umn.edu	446
Akira	YOSHIKAWA	IMR, Tohoku University	J	yoshikaw@lexus.imr.tohoku.ac.jp	769
Yoshiko	YOSHIKAWA				
Evgenii V.	ZHARIKOV	General Phys. Institute, RAS	RUS	zharikov@lsk.gpi.ru	608, 624, 646
Tamara	ZHARIKOVA				